JOURNAL OF BIOLOGICAL REGULATORS & HOMEOSTATIC AGENTS
Volume 32, No. 4, July - August, 2018

CONTENTS

Editorials

B. Sposato, M. Scalese, M. Milanese, S. Masieri, C. Cavaliere, A. Ricci and P. Paggiaro. Should omalizumab be used in severe asthma/COPD overlap? 755

S.K. Kritas, C.E. Gallenga, C. D'Ovidio, G. Ronconi, Al. Caraffa, E. Toniato, D. Lauritano and P. Conti. Impact of mold on mast cell-cytokine immune response 763

Original articles

J.H. Lee and Y-Z. Jin. A rat osteoporosis model induced by ovariectomy and glucocorticoid 769

N. Yasuda and T. Yano. Concomitant assessment of DNA oxidation and bone resorption over a rapid body mass reduction period in female judokas 781

B. Perek, K. Kowalska, B. Kempisty, M. Nowicki, M. Dyszkiewicz-Konwińska, M. Puślecki, D. Ostalska-Nowicka, M. Jemielity, M. Jankowski, M.J. Nawrocki and A. Malińska. Gender and age-related variability of macrophage representation in the internal thoracic artery wall: does it matter? 791

M. Bobinac, T. Ćelić, I. Vukelić, J. Španjol, N. Rubinić and D. Bobinac. Nuclear factor erythroid 2-related factor 2 and choline acetyltransferase co-expression in rat spinal cord neurons after ischemia-reperfusion injury 803

C. Chen, RQ. Zheng, XC. Cao and GC. Zhang. Biological characteristics of osteoclast exosomes and their role in the osteogenic differentiation of somatic cells prior to osteogenesis 815

F. Xin, X.M. Ye, H.B. Liu, L.P. Liu, L.J. Yan and J. Hu. Differential expression and analysis of target regulation of microRNAs in alcohol-dependent rats 825

X-M. Bu, F-F. Xu, J. Ma and B. Jiang. The expression of circulating tumor cells in peripheral blood of patients with non-small cell lung cancer and its detection 843

F. Wang, B. Zhong and Z. Zhao. ACY 1215, a histone deacetylase 6 inhibitor, inhibits cancer cell growth in melanoma 851

Letters to the Editor

F. Hussain A. Irshad and M. Shahid. Study of selected therapeutic potentials of *Momordica charantia* fruit 859

S. Sharif, S. Rashid, A. Atta, A. Irshad, M. Riaz, M. Shahid and G. Mustafa. Phenolics, tocopherols and fatty acid profiling of wild and commercial mushrooms from Pakistan 863

L.B. Jia, L. Tang and Y. Cai. Comparison of nursing methods of pediatric epilepsy 869

T. Schnurrer-Luke-Vrbanić, V. Avancini-Dobrović, I. Sosa, O. Cvijanovic and D. Bobinac. Effect of radial shock wave therapy on long bone fracture repair 875

S. Mao, F. Liu, X-P. Wang, L-X. Wu and J-H. Zhang. Association between Ca/Mg/P status and suppurative tonsillitis in children 881

LH. Xia, YX. Sun, HW. Yan, Y. Meng and XX. Ma. Gastroscopy-guided placement of intranasal jejunum nutrient canal and analysis of nutrient absorption efficiency 887

G. Li, J. Li, CY. Hu, L. Tian, CA. Lv and LJ. Jin. Limb-salvage treatment of malignant tumors of the limbs 891

T. Siddique, A. Asghar, I. Pasha and M. Shahid. Evaluation of functional properties of zein extracted from various maize varieties 899

F. Li, J. Xu and W. Li. The role of color Doppler cardiac output index in the classification of heart disease 905

Y. Chen, S. Yu, H. Li, J.H. Yang and C.Y. E. A case of metastatic cutaneous melanoma to the liver 911

ZL. Hong, Q. Xu, YF. Mao, YZ. Ye, JG. Mao, MF. Wan and MY. Jiang. Polymorphism of the androgen receptor gene CAG repeat sequence and male climacteric syndrome 915

CF. Liu, J. Zhou, XR. Chen and J. Yu. Drug-loaded nanobubbles for ultrasound-mediated antitumor treatment 923

G. Kazdaglis, B. Molina-Moya, K. Manika, P. Ioannidis, D. Papaventsis, E. Vogiatzakis, M. Panopoulou, A. Melidou, J. Domínguez, N. Malisiovas and G. Gioula. Genetic diversity of *Mycobacterium tuberculosis* in Northern Greece 931

A. Goren, J. McCoy, M. Kovacevic, M. Situm, J. Chitalia, R. Dhurat, T. Naccarato and T. Lotti. The effect of topical minoxidil treatment on follicular sulfotransferase enzymatic activity 937

Y. Liu, L. Chen, Z-G. Liu and R-J. Li. Diagnosis and treatment of distal limb microcirculatory disturbance caused by steroid injection 941

JY. Xu and HY. Gao. Combined treatment of traditional Chinese medicine and Western medicine in the treatment of diabetic peripheral neuropathy 945

ZH. Wang, C. Qin, T. Ran, DQ. Yang and JH. Guo. Effects of astragalus glycoprotein on Th17/Treg cells in mice with collagen-induced arthritis 951

T. Wu, Y. Wang, S. Yin, YS. Cong and SH. Qi. Quantitative determination of endogenous cardiolipin in rat cerebral tissues by high-performance liquid chromatography using standard addition method 959

S.E. Aragona, G. Mereghetti and G. Ciprandi. Gastric reflux: the therapeutical role of Marial® 969

M. Bianchetti, S. Peralta, R. Nicita, S.E. Aragona, G. Ciprandi and the EMERGE Study Group. Emerging from gastroesophageal reflux (EMERGE): an Italian survey - I the viewpoint of the gastroenterologist 973

M. Bianchetti, S. Peralta, R. Nicita, S.E. Aragona, G. Ciprandi and the EMERGE Study Group. Emerging from gastroesophageal reflux (EMERGE): an Italian survey - II the viewpoint of the patient 983

M. Bianchetti, S. Peralta, R. Nicita, S.E. Aragona, G. Ciprandi and the EMERGE Study Group. Correlation between the Reflux Finding Score and the GERD Impact Scale in patients with gastroesophageal reflux disease 989

P. Vellante, M. Auriemma, P. Amerio, A. Carnevale and C. D'Ovidio. From new scientific knowledge on rosacea to its possible medico-legal consequences 995

G. De Marco, A. Lanza and F. Di Francesco. An innovative pick-up impression technique 1001

E. Dozio, E. Vianello, E. Grossi, L. Menicanti, G. Schmitz and M.M. Corsi Romanelli. Plasma fatty acid profile as biomarker of coronary artery disease: a pilot study using fourth generation artificial neural networks 1007

S. Taschieri, L. Karanxha, L. Francetti, R. Weinstein, A.B. Giannì and M. Del Fabbro. Minimally-invasive osteotome sinus floor elevation combined with short implants and platelet-rich plasma for edentulous atrophic posterior maxilla: a five-year follow-up prospective study 1015

G. Autieri, F. Mussano, M. Petruzzi, M. Carossa, T. Genova, M. Corsalini and S. Carossa. Proanthocyanidin may improve the shear bond strength at the composites/dentine interface 1021

L. Pacifici and A. Pacifici. Digital flow in medicine and dentistry: what's new? 1027

G. D'Addazio, L. Artese, T. Traini, C. Rubini, S. Caputi and B. Sinjari. Immunohistochemical study of osteopontin in oral squamous cell carcinoma allied to fractal dimension 1033

E. Anastasi, G. Gennarini, C. Del Monte, B. Colaprisca, S. Tartaglione, C. Di Segni and A. Angeloni. Perfomance assessment of a fully automated electro-chemiluminescence immunoassay system for serum S100B protein 1039

D. Tripodi, D. Martinelli, C. Ciaravino, D. Fulco, M. Tieri and S. D'Ercole. The use of casein in sport mouthguards: microbiological and ecological variations in oral cavity 1045

G. Ciprandi and A. Varricchio. The relevance of the mometasone furoate nasal spray in clinical practice 1051

EDITORIAL

SHOULD OMALIZUMAB BE USED IN SEVERE ASTHMA/COPD OVERLAP?

B. SPOSATO[1], M. SCALESE[2], M. MILANESE[3], S. MASIERI[4], C. CAVALIERE[4], A. RICCI[5] and P. PAGGIARO[6]

[1]Pneumology Department, "Misericordia" Hospital, Grosseto, Italy; [2]Institute of Clinical Physiology, CNR, Pisa, Italy; [3]Pneumology Department, "S. Corona" Hospital, Pietra Ligure (SV), Italy; [4]Otorhinolaryngology Clinic, Policlinico Umberto I, "Sapienza" University, Rome, Italy; [5]Division of Pneumology, Department of Clinical and Molecular Medicine, Sapienza University of Rome, AOU Sant'Andrea, Rome, Italy; [6]Cardio Thoracic and Vascular Department, Pathophysiology Unit, University of Pisa, Italy

Received February 1, 2018 – Accepted May 17, 2018

A large number of patients suffering from asthma or chronic obstructive pulmonary disease (COPD) can show overlapping features of both diseases. Several subjects affected by asthma-COPD overlap (ACO) may be at a severe stage, poorly responsive to triple therapy including inhaled corticosteroids, long-acting β2 agonists and muscarinic antagonists. This review tries to explore whether omalizumab can be used in poorly controlled severe ACO patients. According to the few studies available, omalizumab may improve asthma outcomes in ACO, although the magnitude of improvements may be lower in comparison to those obtained in subjects affected only by severe asthma. Omalizumab, by acting on IgE, might improve the eosinophilic pattern which is characteristic of the ACO asthma inflammation component. It can be hypothesized that a prevalence of Th1/Th17 airway inflammation pathways can modulate a lower response to anti-IgE while a Th2 pattern can lead to a higher effectiveness to omalizumab in ACO. High levels of IgE, FeNO and blood eosinophil count may be markers of a better response to omalizumab. In conclusion, on the basis of the few studies available, omalizumab could be effective in poorly-controlled severe ACO, although to a reduced extent in comparison to patients affected only by asthma.

Asthma and COPD seem to be a result of different mechanisms triggered by different pathogeneses and, although they show different features and symptoms of airway inflammation and obstruction, there are also patients with both asthma and COPD features. This disease association is generally known as asthma-COPD overlap syndrome (ACOS). However, the term "syndrome" that usually refers to an idiopathic pathology with common features (e.g. clinical symptoms, test findings etc.), is nowadays considered inappropriate in this context. As a result, GINA/GOLD guidelines have recommended that the term "syndrome" be abandoned and replaced with "asthma and COPD overlap (ACO)" (1, 2). As stated by the above said guidelines, ACO is characterized by persistent airflow limitation with several features usually associated with asthma and other characteristics which are typically connected with COPD. According to other authors (ERS definition), key ACO features include persistent airflow limitation in symptomatic

Keywords: *omalizumab, severe asthma, COPD, overlap, ACO, ACOS, treatment, effectiveness, phenotype*

Mailing address:
Dr Bruno Sposato,
U.O. Pneumologia,
Azienda Ospedaliera "Misericordia"
Via Senese 161, 58100 Grosseto, Italy
Tel.: +390564485454 - Fax: +390564485450
e-mail: bsposat@tin.it

0393-974X (2018)
Copyright © by BIOLIFE, s.a.s.
This publication and/or article is for individual use only and may not be further reproduced without written permission from the copyright holder.
Unauthorized reproduction may result in financial and other penalties
DISCLOSURE: ALL AUTHORS REPORT NO CONFLICTS OF INTEREST RELEVANT TO THIS ARTICLE.

individuals aged 40 years or more, a well-documented history of asthma in childhood or early adulthood and a significant exposure history to cigarette or biomass smoke (3). As a matter of fact, the term ACO refers to several phenotypes, such as eosinophilic COPD, severe asthma with incomplete airflow reversibility and asthma associated with smoking. In fact, some COPD patients have sputum eosinophilia and are more responsive to corticosteroids, whereas some asthmatic smokers have a neutrophilic pattern which can make the disease less responsive to ICS (4, 5).

It has been estimated that 15-50% of patients with obstructive airway diseases and aged over 50 years may show a combination of criteria for both asthma and COPD (1, 2). Other authors assert that asthma and COPD can overlap in 27-28% of asthmatics (6, 7), doubling in patients aged over 65 years (8). However, ACO frequency can vary from 11.9% to 48.3% according to the different diagnostic criteria used (9), thus highlighting the existence of divergent ACO definitions. Asthma and COPD overlapping can lead to a greater health impairment than that observed in individuals with either asthma or COPD. In fact, ACO is characterized by a lower lung function, more frequent exacerbations and hospitalizations, a worse health-related quality of life, more comorbidities and higher healthcare costs than asthma or COPD alone (6,7). Therefore, a multidrug treatment is necessary in ACO severe forms the asthmatic component of which indicates omalizumab as a possible further therapeutic option for these patients.

ACO TREATMENTS

The best ACO therapeutic approach is still debated. The coexistence of asthma and COPD is still an exclusion criterion to be included in clinical trials, therefore, the effects of COPD/asthma medications in ACO are unknown. Existing treatment suggestions for this disease are fundamentally given only by opinion leaders. Different COPD guidelines (Canadian, Finnish, Australian and Spanish) (4) suggest that, along with long-acting β2 agonists (LABA) and long-acting muscarinic antagonists (LAMA), inhaled corticosteroids (ICSs) should also be considered when COPD is associated with asthma. GINA/GOLD guidelines (1, 2) advocate the use of ICSs instead of LABA monotherapy, especially in patients showing mostly asthmatic features; whereas subjects with mainly COPD characteristics should be treated with LABAs and/or LAMAs ± ICSs but not with ICS alone. Consequently, ACO patients should be given either ICSs associated with LABAs, LAMAs, or both for symptomatic relief. In fact, one study has recently provided clinical evidence that ACO patients with mild-to-moderate airflow limitations show a greater lung function response after 3 months of ICS/LABA combination treatment in comparison to patients with only COPD (10). Another recent study, involving COPD patients with an asthma history - showing a persistent airflow limitation not fully reversible - also highlighted a significant response to budesonide alone after 6 months, confirming that ICS therapy is fundamental in ACO patients (11).

We have no clear indications about the treatment to be used in ACO at a severe stage and poorly responsive to triple therapy (LABA, LAMA and ICS). A recent research has categorized most subjects with ACO as GOLD grade B; only a low number of them has been classified as grade C or D, namely, at high risk for exacerbations and therefore with a possible greater disease severity (12). On the contrary, according to other authors, over 50% of ACO subjects may be at a severe stage (11) and may benefit from omalizumab. A further study has stated that approximately 39% of ACO patients, who smoked >10 pack years and had blood eosinophil counts >300 cells, showed an advanced form of the disease characterized by a greater number of serious exacerbations (13). As a result, ACO may be considered as a form of severe asthma. Only Spanish COPD guidelines, in case of poorly controlled ACO, suggest adding theophylline or PDE4 in case no control is obtained with a triple therapy (14). No mention of using omalizumab is made for these patients with an inadequately controlled disease, despite the use of ICSs and LABA/LAMA. Further guidelines do not give any indications on the possibility of using omalizumab in ACO. Omalizumab is a well-known monoclonal antibody blocking IgE recommended in severe persistent

allergic asthma, with a greater effectiveness in subjects with eosinophilic airway inflammation (15). It has shown to reduce exacerbation risks, to improve symptoms and quality of life both in trials and real-life studies (16). Omalizumab could also give the same results with ACO patients.

RATIONALE TO USING OMALIZUMAB IN ACO

Theoretically, adding omalizumab may further improve the outcomes in unstable severe asthma-COPD overlap by improving asthmatic/allergic aspects even if the association with COPD may lead to consider it as irreversible and untreatable.

Most ACO patients with a significant number of severe exacerbations were characterized by a smoking history ≥10 pack years and, above all, by blood eosinophil counts ≥300 cells (13). Fractional exhaled nitric oxide (FeNO), a noninvasive marker of eosinophilic airway inflammation, was higher also in patients with moderate/severe ACO than in the COPD group with the same disease severity (17). Furthermore, in a recent study, conducted on 127 subjects with ACO, FeNO levels, total serum IgE and induced sputum eosinophils were higher in patients with a greater ACO severity predicting an efficacy of ICS in the treatment of severe patients (11). These higher levels of asthma/eosinophilic inflammation (especially of IgE levels) would predict a positive response also to omalizumab in the above-mentioned patients. Therefore, anti-IgE therapy does have a role in treating severe ACO, showing a clear asthmatic inflammation and the inefficacy of all other treatments which were supposed to maintain a good disease control.

High levels of IgE, blood eosinophils and FeNO may be markers indicating a possible omalizumab treatment for severe uncontrolled ACO. Nowadays, total serum IgE levels associated with perennial allergen sensitizations guide omalizumab prescriptions (1). High levels of total IgE may be predictive of a better response to treatment (18). FeNO measurement is an easy, noninvasive, and sensitive method for differentiating ACO from COPD (17). Furthermore, in severe asthma, blood eosinophil counts are related to an increased response to omalizumab (15). Additionally, treating the eosinophilic COPD phenotype with a monoclonal antibody blocking interleukin-5 (such as mepolizumab, which is an anti-eosinophilic therapy) reduces the number of moderate/severe exacerbations (19). Therefore, blood eosinophils, IgE and FeNO, should be used to phenotype severe ACO and choose the most suitable therapy.

STUDIES ANALYZING OMALIZUMAB EFFECTIVENESS IN ACO

To date, very few studies have tested omalizumab effectiveness in ACO. Only four articles experimenting omalizumab were found in PubMed (Table I), one of which considered 10 patients characterized by airway obstruction partially reversible after bronchodilator, hyperinflation, clinical and laboratory findings suggestive of ACO (20). After 12 months of omalizumab treatment, patients showed an improvement in dyspnea, wheezing, bronchial hyperresponsiveness and a reduction of total serum IgE, FeNO, eosinophils, neutrophils, macrophages, eosinophil cationic peptide (ECP) values and serum IL-4 levels.

Other authors reported reduced asthma exacerbations and improved asthma control after a 1-year omalizumab treatment in 3 patients affected by ACO (21).

In further real-life studies, a long-term treatment (>30 months) proved to be effective also in 14 severe asthmatics with concomitant COPD, although the magnitude of the effect was lower when compared to a group of younger subjects (22). In particular, FEV_1 increased from 57.7% to 70% and ACT from 11 to 19. Furthermore, 35% of them did not show any exacerbations during the last year of treatment. Whereas, in younger subjects, ACT was approximately 24, 77% of whom did not experience any exacerbations after omalizumab.

Another recent research observed that a 6-month treatment led to a marked improvement of asthma control and of a health-related quality of life (HRQoL) in individuals with severe allergic asthma and overlapping COPD diagnosed by using different criteria (23). In fact, this significant improvement

was observed in subjects with a physician's previous ACO diagnosis (17 patients) when compared to the others. This was also observed in individuals with a post-bronchodilator FEV_1 <80% (55 patients) and even in smokers (11 subjects) compared to patients with post-bronchodilator FEV_1 >80% (17 subjects). However, according to this research, omalizumab treatment did not improve lung function (FEV_1, FVC or FEV_1/FVC ratio) in subjects with severe allergic asthma and overlapping COPD.

All these 4 studies (summarized in Table I), although carried out with a limited number of patients, seem to confirm a real-life anti-IgE treatment efficacy for these subjects, thus suggesting that this drug may be useful in the management of poorly controlled severe ACO.

POSSIBLE ACTIONS OF OMALIZUMAB IN ACO

In asthma-COPD overlap, the inflammatory pattern is characterized by a Th1- and Th17-driven processes with increased numbers of cytotoxic CD8+ lymphocytes, neutrophils, and TGF-β-induced fibrosis of the airways associated also with an increased number of eosinophils, Th2 or ILC2 cells (1). Therefore, a variable mixture of two main airway inflammatory patterns (Th1/Th17 and Th2) may characterize ACO subjects. As already

Table I. *Studies supporting omalizumab effectiveness in ACO.*

First Author	Study design	Number of patients	Months of follow-up	Main Results
Yalcin 2016 [20]	Observational retrospective study	10	12	↓Pulmonary symptoms (dyspnea, wheezing, bronchial hyperresponsiveness) ↓IgE, FENO, sIL-4, ECP, eosinophils, neutrophils
Tat 2016 [21]	Case reports (retrospective study)	3	12	↓Exacerbations ↓Hospitalizations ↑Asthma control
Sposato 2016 [22]	Observational retrospective study (compared to younger severe asthmatics)	14	39 (mean)	↑FEV_1% ↑ACT ↓Exacerbations
Maltby 2017 [23]	Multicenter non-interventional observational study (ACO, established with different criteria, compared to severe asthmatics)	17 (previous physician's diagnosis of asthma-COPD overlap) 55 (with post-bronchodilator FEV_1>80%) 11 (ever smokers with post-bronchodilator FEV_1>80%)	6	= FEV_1% ↑Asthma Control ↑Quality of life

stated, continuous smoking in asthma may lead to a progressive altered baseline airway inflammation with increased neutrophils (compared with non-smokers or younger patients) (5) overlapping/ covering the eosinophilic asthma pattern in time. A greater prevalence in neutrophilic inflammation can be responsible for an un-treatability or at least an under-responsitivity to anti-inflammatory treatment (2, 4, 5) and probably also to anti-IgE therapy. In fact, smokers with asthma showed a prevalent neutrophilic airway inflammation and cigarette smoking impaired the efficacy of ICS (5, 24). Furthermore, asthmatics with non-eosinophilic airway inflammation highlighted a reduced response to inhaled corticosteroids when compared to subjects with eosinophilic inflammation (25).

IgE plays a central role in allergic asthma, therefore omalizumab, by blocking IgE, is able to interfere/reduce Th2 cytokines production. Today, it has also become clear that omalizumab is more effective in patients with active eosinophilic airway inflammation (7). In fact, a retrospective analysis divided severe asthmatics into patients with and without type 2 inflammation based on median splits of blood eosinophil counts, serum periostin and FENO levels (26). Such analysis showed that patients with biomarker levels greater than the median had higher reductions in asthma exacerbations with Omalizumab therapy, compared with those with levels lower than median (26). Further studies highlighted an eosinophilic anti-inflammatory action of omalizumab showing that it could induce eosinophil apoptosis and down-regulation of some inflammatory cytokines such as IL-2 and IL-13 (27). Another paper highlighted that omalizumab reduced IgE-stimulated synthesis and secretion of pro-inflammatory cytokines (IL-6, IL-8 and tumor necrosis factor) synthesized by human airway smooth muscle cells (28). Furthermore, patients with moderate to severe allergic asthma, showed that circulating IL-13, IL-5, IL-8 and eosinophil count decreased significantly after 16 weeks of omalizumab treatment (29) which may act on the Th2 mediated airway asthmatic inflammatory component in ACO subjects. Depending on the prevalence of the neutrophilic or eosinophilic inflammatory pattern, omalizumab response may be more or less marked in ACO. In fact, in elderly asthmatics, whose neutrophil counts are higher (30), the anti-IgE showed a reduced response in comparison to younger subjects (22). Furthermore, in severe smoking asthmatics, who have a more important neutrophilic airway inflammation, omalizumab improves asthma control and quality of life but not lung function, contrarily to what has been observed in severe non-smoking asthmatics (23). Subjects with ACO showed a reduced clinical and functional response to omalizumab when compared to younger (18-39 years) severe asthmatics (22) whose eosinophilic inflammation may be higher.

CONCLUSION

According to the few studies in literature, omalizumab may have a role in treating severe ACO. Acting on IgE, it may improve ACO asthmatic component. Probably, a prevalence of Th1/Th17 airway inflammatory pathways can modulate a lower response to anti-IgE while a Th2 pattern can lead to a higher effectiveness to omalizumab in ACO. Therefore, a treatment with omalizumab may be efficient in poorly controlled severe ACO phenotypes, even if to a reduced extent in comparison to patients affected only by asthma. High levels of IgE, FENO and blood eosinophil count may be markers of a better response to omalizumab. Therefore, this treatment may be a further therapeutic opportunity to be considered for patients with poorly controlled severe asthma associated with COPD.

REFERENCES

1. Global Initiative for Asthma, Global Strategy for Asthma Management and Prevention Updated 2016, Available at: http://ginasthma.org/2018-gina-report-global-strategy-for-asthma-management-and-prevention/ [accessed March 2018].
2. Global Strategy for the Diagnosis, Management and Prevention of COPD. Updated 2017. Available at: www.goldcopd.org
3. Sin DD, Miravitlles M, Mannino DM, et al. What is asthma-COPD overlap syndrome? Towards a consensus definition from a round table discussion. Eur Respir J 2016; 48:664-73.

4. Reddel HK. Treatment of overlapping asthma-chronic obstructive pulmonary disease: Can guidelines contribute in an evidence-free zone? J Allergy Clin Immunol 2015; 136:546-52.
5. Nagasaki T, Matsumoto H. Influences of smoking and aging on allergic airway inflammation in asthma. Allergol Int 2013; 62:171-79.
6. Milanese M, Di Marco F, Corsico AG, et al. ELSA Study Group. Asthma control in elderly asthmatics. An Italian observational study. Respir Med 2014; 108:1091-99.
7. Alshabanat A, Zafari Z, Albanyan O, Dairi M, FitzGerald JM. Asthma and COPD overlap syndrome (ACOS): A systematic review and meta analysis. PLoS One 2015; 10:e0136065.
8. de Marco R, Pesce G, Marcon A, et al. The coexistence of asthma and chronic obstructive pulmonary disease (COPD): prevalence and risk factors in young, middle-aged and elderly people from the general population. Plos One 2013; 8:e62985.
9. Jo YS, Lee J, Yoon HI, Kim DK, Yoo CG, Lee CH. Different prevalence and clinical characteristics of asthma-chronic obstructive pulmonary disease overlap syndrome according to accepted criteria. Ann Allergy Asthma Immunol 2017; 118:696-703.
10. Lee SY, Park HY, Kim EK, et al. Combination therapy of inhaled steroids and long-acting beta2-agonists in asthma-COPD overlap syndrome. Int J Chron Obstruct Pulmon Dis 2016; 11:2797-803.
11. Feng JX, Lin Y, Lin J, He SS, Chen MF, Wu XM, Xu YZ. Relationship between Fractional Exhaled Nitric Oxide Level and Efficacy of Inhaled Corticosteroid in Asthma-COPD Overlap Syndrome Patients with Different Disease Severity. J Korean Med Sci 2017; 32:439-47.
12. Cosentino J, Zhao H, Hardin M, Hersh CP, Crapo J, Kim V, Criner GJ; COPD Gene Investigators. Analysis of asthma-chronic obstructive pulmonary disease overlap syndrome defined on the basis of bronchodilator response and degree of emphysema. Ann Am Thorac Soc 2016; 13:1483-89.
13. Joo H, Han D, Lee JH, Rhee CK. Heterogeinity of asthma-COPD overlap syndrome. Int J Chron Obstruct Pulmon Dis 2017; 12:697-703.
14. Miravitlles M, Soler-Cataluña JJ, Calle M, et al. Spanish Guidelines for Management of Chronic Obstructive Pulmonary Disease (GesEPOC) 2017. Pharmacological Treatment of Stable Phase. Arch Bronconeumol. 2017; 53(6):324-335.
15. Casale TB, Chipps BE, Rosén K, et al. Response to omalizumab using patient enrichment criteria from trials of novel biologics in asthma. Allergy 2018; 73:490-97.
16. Abraham I, Alhossan A, Lee CS, Kutbi H, MacDonald K. "Real-life" effectiveness studies of omalizumab in adult patients with severe allergic asthma: systematic review. Allergy 2016; 71:593-610.
17. Chen FJ, Huang XY, Liu YL, Lin GP, Xie CM. Importance of fractional exhaled nitric oxide in the differentiation of asthma-COPD overlap syndrome, asthma and COPD. Int J Chron Obstruct Pulmon Dis 2016; 11:2385-90.
18. Sposato B, Scalese M, Milanese M, et al. Factors reducing Omalizumab response in severe asthma. Eur J Int Med 2018; 52:78-85.
19. Pavord ID, Chanez P, Criner GJ, et al. Mepolizumab for eosinophilic chronic obstructive pulmonary disease. N Engl J Med 2017; 377:1613-29.
20. Yalcin AD, Celik B, Yalcin AN. Omalizumab (anti-IgE) therapy in the asthma-COPD overlap syndrome (ACOS) and its effects on circulating cytokine levels. Immunopharmacol Immunotoxicol 2016; 38:253-6.
21. Tat TS, Cilli A. Omalizumab treatment in asthma-COPD overlap syndrome. J Asthma 2016; 53:1048-50.
22. Sposato B, Scalese M, Latorre M, et al. Effects of omalizumab in severe asthmatics across ages: a real life Italian experience. Respir Med 2016; 119:141-9.
23. Maltby S, Gibson PG, Powell H, McDonald VM. Omalizumab treatment response in a population with severe allergic asthma and overlapping COPD. Chest 2017; 151:78-89.
24. Shimoda T, Obase Y, Kishikawa R, Iwanaga T. Influence of cigarette smoking on airway inflammation and inhaled corticosteroid treatment in patients with asthma. Allergy Asthma Proc 2016; 37:50-58.
25. Cowan DC, Cowan JO, Palmay R, Williamson A, Taylor DR. Effects of steroid therapy on inflammatory cell subtypese in asthma. Thorax 2010; 65:384-90.
26. Hanania NA, Wenzel S, Rosen K, et al. Exploring the effects of omalizumab in allergic asthma: an analysis

of biomarkers in the EXTRA study. Am J Respir Crit Care Med 2013; 187:804-11.
27. Noga O, Hanf G, Brachmann I, et al. Effect of omalizumab treatment on peripheral eosinophil and T-lymphocyte function in patients with allergic asthma. J Allergy Clin Immunol 2006; 117:1493-9.
28. Roth M, Tamm M. The effects of omalizumab on IgE-induced cytokine synthesis by asthmatic airway smooth muscle cells. Ann Allergy Asthma Immunol 2010; 104:152-60.
29. Noga O, Hanf G, Kunkel G. Immunological and clinical changes in allergic asthmatics following treatment with omalizumab. Int Arch Allergy Immunol 2003; 131:46-52.
30. Brooks CR, Gibson PG, Douwes J, Van Dalen CJ, Simpson JL. Relationship between airway neutrophilia and ageing in asthmatics and non-asthmatics. Respirology 2013; 18:857-65.

EDITORIAL

IMPACT OF MOLD ON MAST CELL-CYTOKINE IMMUNE RESPONSE

S.K. KRITAS[1], C.E. GALLENGA[2], C. D'OVIDIO[3], G. RONCONI[4], Al. CARAFFA[5], E. TONIATO[6], D. LAURITANO[7] and P CONTI[8]

[1]Department of Microbiology and Infectious Diseases, Aristotle University of Thessaloniki, Macedonia, Greece; [2]Department of Biomedical Sciences and Specialist Surgery, Section of Ophthalmology, University of Ferrara, Italy; [3]Section of Legal Medicine, Department of Medicine and Aging Sciences, "G. d'Annunzio" University of Chieti-Pescara, Italy; [4]UOS Clinica dei Pazienti del Territorio, Policlinico Gemelli, Rome, Italy; [5]Department of Pharmacology, University of Perugia, Perugia, Italy; [6]Department of Medical, Oral and Biotechnological Sciences, University "G. d'Annunzio" of Chieti-Pescara, Chieti, Italy; [7]University of Milano Bicocca, Milan, Italy; [8]Immunology Division, Postgraduate Medical School, University of Chieti-Pescara, Chieti, Italy

Received May 23, 2018 - Accepted July 18, 2018

Molds include all species of microscopic fungi, the spores of which are small molecules, ubiquitous, mostly found in soil with higher rainfall and high humidity, in the atmosphere of urban and rural settings and in decaying vegetation. They originate from pathogenic fungi and have a crucial role in inflammatory response, causing a broad range of diseases. Immune suppressed subjects may develop mycoses caused by opportunistic common pathogenic fungi. Mast cells (MCs) are immune cells involved in the pathophysiology of infected skin, lung, and organs, where there is an increase of angiogenesis. Airways fungi infections can induce allergic lung disease mediated by MCs and other immune cells. In addition, fungal infection may cause and/or aggravate asthma inflammation. Spores are able to navigate in the airways of the lung and can be recognized trough toll-like receptor (TLR) signaling by the innate immune cells including MCs. Activated MCs release preformed mediators including histamine, proteases (tryptase, chimase), pro-inflammatory cytokines/chemokines and they also generate arachidonic acid products. MCs activated by fungi provoke an increases of PGD2 levels and lead to hypersensitivity diseases which present signs such as irritation of the respiratory tract and eyes, recurrent sinusitis, bronchitis, cough and neurological manifestations including fatigue, nausea, headaches and brain fog. Therefore, fungi activate the innate immune response through the TLRs, leading to the release of myeloid differentiation factor 88 (MyD88) which, with a series of cascade reactions, induces the stimulation of AP-1 and NF-kB with subsequent activation of inflammatory IL-1 family members. Here, we report that fungi can activate MCs to secrete pro-inflammatory cytokines which may be inhibited by IL-37, a new anti-inflammatory IL-1 family member.

The vast majority of genes found in the human body are mainly microbes, such as bacteria, viruses and fungi. Molds are a large number of fungal species which appeared on our planet hundreds of millions of years ago before the appearance of animals that had to develop sophisticated mechanisms of defense against these infectious agents. Molds are a group of fungi called *Hyphomycetes* that play an important

Key words: mold, fungi, mast cell, cytokine, inflammation, IL-37

Mailing address:
Prof. Pio Conti,
Postgraduate Medical School,
University of Chieti, Viale Unità d'Italia 73,
Chieti, Italy
Tel./Fax: +39 0871 574136
e-mail: pconti@unich.it

0393-974X (2018)
Copyright © by BIOLIFE, s.a.s.
This publication and/or article is for individual use only and may not be further reproduced without written permission from the copyright holder.
Unauthorized reproduction may result in financial and other penalties
DISCLOSURE: ALL AUTHORS REPORT NO CONFLICTS OF INTEREST RELEVANT TO THIS ARTICLE.

role in the pathogenesis of plants, animals and humans, and are eukaryotic, saprophytic organisms. Mold exposure to immune compromised subjects may lead to an increased risk of lung infection, and the exposure to fungi during the first year of life may increase the risk of childhood asthma. Inhalation is considered the primary way that people are exposed to fungi, along with skin and diet. However, molds are generally not harmful to healthy humans. According to the Centers for Disease Control and Prevention, some of the most common indoor molds are *Cladosporium, Penicillium, Aspergillus, Alternaria, Stachybotrys chartarum.*

Aspergillus is the most common fungus group in our environment and can cause several pathological disorders; however, in individuals with normal functioning of the immune system, infections caused by *Aspergillus* are relatively unusual (1). *Conidies,* with aerodynamic properties, are structures capable of resisting adverse environments, allowing fungi to reproduce and settle in the airways. Therefore, fungi participate in the etiology of respiratory tract allergic disease (2). Subjects living in moldy environments show an increase of 30-40% of allergy and respiratory diseases.

In the United States, *Aspergillosis* is the second cause of fungi infection and includes more than 185 species (3). For examples, the most commonly isolated and pathogenic are: *A. fumigatus, A. flavus* and *A. niger*; while others are less pathogenic such as *A. clavatus, A. glaucus, A. nidulans, A. oryzae, A.* terreus, A. ustus and A. versicolor (4). After Candida, which causes opportunistic mycosis (and MCs are the first immune cells to recognize it), Aspergillus species can cause different clinical situations such as opportunistic infections, allergy, and toxicity. Aspergillus is the most commonly isolated in invasive infections (5).

Mold–induced asthma and allergy are characterized by an augmentation of MCs and eosinophils, which generate many inflammatory mediators demonstrating to be potential effectors cells in the pathogenesis of these disorders (6).

Epithelium Toll-like receptors (TLRs) react with fungi, generating inflammatory cytokine transcription and translation (7). The host responds to fungal invasions with self-defense mechanisms such as pattern recognition receptors (PRRs), pathogen-associated molecular patterns (PAMPs) and TLRs (8).

The Toll (which in German means extraordinary) gene was discovered by Jules Hoffmann (Nobel Prize) in the fruit fly (Drosophila melanogaster) and is essential for immune defenses. TLR-dependent pathways are very important for host defense against fungi and bacterial pathogens.

It is clear that phagocytes have a mechanism that can recognize mold on their surface, now known as PRRs, which have been reported to be involved in antifungal responses in immune cells. The PRR family consist of TLRs and several other molecules.

TLRs go from TLR1 to TLR13 proteins, most of which are externally expressed on the cell membrane; whereas TLR3, TLR7, TLR8, TLR9, TLR11, TLR12 and TLR13 are expressed intracellularly on endoplasmic reticulum, endosomes, phagosomes, and lysosomes. Excluding TLR3, all TLRs are involved in the activation of myeloid differentiation factor 88 (MyD88). Therefore, TLRs utilize MyD88 and the adaptor molecule IL-1 receptor-associated kinase (IRAK) complex to transduce intracellular signals.

The phosphorylation cascade engages IRAK4, TRAF6 and TAK which activate both NF- κB and MAPK, essential for cell proliferation and inflammation.

TLR, which was first described in fruit flies by Hoffman and Beutler (2011 Nobel Prize awarded in Physiology) is utilized by APC cells to initiate a bridge between innate and adaptive immunity. TLRs recognize the pathogens and begin the immune response by activating chemotherapeutic molecules and intervening in phagocytic cells and MCs that produce inflammation. TLRs are expressed by different human cells, including MCs and macrophages, and recognize microbes, mold, macromolecules and cytokines, leading to early detection of infections. TLR is an adjuvant for the stimulation of adaptive T-cell activity and regulation of CD8+ T cells. It behaves differently when they need to detect pathogen-associated molecules (PAMPs) and endogenous endocrine molecules (DAMPs) (9). For example, the stimulation of

TLR2 and TLR4 leads to an increase in the release of inflammatory cytokines and plays a major role in inflammatory disorders.

Therefore, pro-inflammatory TLR signaling pathway leads to the generation of inflammatory cytokines and chemokines, including TNF and interferon regulatory factors (IRFs), via NF-κB activation. TLR has been detected in many pathologies characterized by primary immune deficiency and infectious diseases. Mold infections, as well as bacterial infections, are associated with a defect of NF-κB and TLR3 deficiency which can lead to infection by herpes simplex.

Intracellular TLRs (excluding TLR3) recognize the invasion agent and amplify the signal through MyD88 which is important for the generation of cytokines and the elimination of infectious agents; while transmembrane TLRs (TLR4 and TLR2) recognize LPS and peptidoglycan (10). However, the inhibition of MyD88, IRAK4 and NF-κB may have a therapeutic effect on inflammatory diseases.

Cytokines and mold

Cytokines are a family of structurally- and functionally-related proteins that exhibit pleiotropic effects on the growth and function of a variety of cell types (11-12). Cytokines are key mediators of the host defense against mold provoking chronic inflammatory diseases (13). Cytokines play their biological effect through their trans-membrane receptors located on the cellular outer membrane triggering signal pathways.

Genetic factors, the environment and the characteristics of the fungus cause the allergic reaction, which may differ from one subject to another; this allergy is mediated by pro-inflammatory cytokines. Several mold diseases are favored by a type 1 cytokine profile associated with a type 2 cytokine. Fungi (such as *Aspergillus*, *Candidiasis*, etc.) can provoke allergy by increasing the levels of IgE and therefore the number of MCs involved in a bronchospasmic reaction with an increases of IL-4, IL-5, IL-1, IL-2 (modest production) and IFNγ; while IL-10 and IL-37 (of which we will speak below) released have a beneficial anti-inflammatory effect.

The interaction between human macrophages and MCs is of considerable interest since many macrophage products can potentially activate MCs and *vice versa*. The recruitment of MCs into fungus-infected tissue is a crucial feature of allergic inflammation where cytokines and chemokines are generated. Therefore, fungus are involved in allergic fungal asthma which is a relevant chronic disorder mediated by MCs and other cell types and causes fibrotic remodeling of bronchi, smooth muscle increase and inflammatory cell infiltration, causing long-term morbidity (14).

Epidemiological studies in industrialized countries have shown that some molds such as *Cladosporium herbarum,* are involved in severe and persistent asthma.

The most commonly studied fungus, such as *Aspergillus, Alternaria, Botrytis, Cladosporium, Epicoccum, Fusarium*, and *Penicillium* species, can cause an allergic reaction and in open environments more fungal spores of Ascomycota can be found. In addition, fungal proteins are the main adjuvant factors capable of inducing a Th2 response resulting in inflammation.

It is well documented that IL-1 plays an important role in host defense versus microbes and inflammation acting through two types of receptors: IL-1R1 (stimulatory type 1), and IL-1R2 (suppressive type 2). In general, mold has an interaction with the human immune system leading to the activation of innate immune cells following the release of pro-inflammatory cytokines including IL-1 family members.

IL-1 family members react against pathogens and promote an innate immune response, however, many of them are also highly inflammatory cytokines (15). IL-1 is found in individuals with mold inflammation and immunological disorders and is thought to contribute to leukocyte migration, tissue remodeling, pain, arachidonic acid cascade (thromboxane and PGE2 synthesis in macrophages) activation and inflammation (16-17).

IL-1 is mitogenic for mesangial cells in the kidney, and glial cells in the brain, and activates keratinocytes, osteoclasts and MCs, increases fibroblast proliferation, and the synthesis of collagens and glucosaminoglycans.

IL-1 also plays an important role in the TH1 response, and requires cleavage into an active mature

molecule by the intracellular cysteine protease called caspase-1 [also known as IL-1beta-converting enzyme (ICE)]. IL-1β shares with IL-18 significant primary amino acid sequences and induces gene expression and synthesis of TNF, Fas ligand, and several cytokines/chemokines (18). It has been reported that IL-1 activates MCs and promotes the generation of chemokines and therefore the cell recruitment influencing allergic mediator release (19).

MCs and mold

MCs have a complex immunomodulatory effect and their study has been increased in recent years. MCs develop and mature $CD34^+$ pluripotent progenitor cells under the influence of IL-3, IL-6 and SCF (20).

MCs respond to many different stimuli and are usually associated to immediate hypersensitivity and allergic disorders, as well as in certain protective immune responses to microbes and fungi which bind TLRs and lead to the production of de novo synthesis of pro-inflammatory cytokines.

MCs also generate growth factors, leukotrienes, prostaglandins, and NO. They can be activated by IL-1, IL-33, IL-9, tryptase, and certain neuropeptides; on the other hand, cytokines such as IL-33 and IL-1 may activate MCs without degranulation (21).

MCs are present in tissues, and particularly on the skin where they play the role of "sentinels" and come into contact with fungi, and participate in both the initial and the late immune phases producing cytokines and granular proteins.

MCs generate unique cellular responses through their receptor-mediated pathways. They express receptors for the chemokine family which signal through G-coupled receptors (GPCRs) on MC membrane (22).

Moreover, MCs activated with *Candida albicans in vitro* release IL-8 which is a chemokine that attracts neutrophils.

Therefore, MCs can generate IL-1 and TNF which may regulate the production of eotaxin which cannot be considered specific chemoattractant (23-24).

In the light of new research on inflammation, we propose IL-37, an inhibitor of the inflammatory IL-1 family members, as a cytokine that could help mold-induced disease therapies.

IL-37 as a potential inhibitor of inflammation induced by mold

We and other Authors recently reported that IL-37 may inhibit allergy, atherosclerosis and skin inflammation. Other authors published that IL-37 reduced the inflammatory reaction in arthritis, autoimmunity, and cancer. Inhibitors of inflammatory IL-1 family member activity, such as IL-37, may be useful as TH1 immunosuppressive agents (25-26).

In recent years, according to published international consensus, using IL-37 as an inhibitor has revealed a significant reduction of inflammation mediated by macrophages and other immune cells (27-29). IL-37 (or IL-1F7) exerts an anti-inflammatory effect by binding IL-18 receptor alpha (IL-18Rα) chain, and directly inhibits MyD88 (28).

IL-37 therapy is still in the embryonic stage, but we suggest that this interleukin, along with other appropriated therapies, may inhibit inflammatory Th1 cytokines in response to various stimulus including fungus and bacteria. This anti-inflammatory cytokine prevents inflammation induced by IL-1, IL-6, IL-18, IL-32 and IL-33, and it is involved in the improvement of inflammation due to *de novo* synthesis mediators generated by MC activation, reducing acute and systemic inflammatory diseases. IL-37 increases the anti-inflammatory IL-10 and owns pleiotropic effects, with significant reduction of inflammatory severity.

We propose IL-37 as a good candidate in clinical medicine to treat a broad spectrum of inflammatory diseases mediated by immune cells including macrophages and MCs, reducing the complications and mortality.

Here, we report for the first time that IL-37 can improve the physio-pathogenesis of inflammatory diseases mediated by molds, describing a new concept of inhibition and cure.

REFERENCES

1. Vacher G, Niculita-Hirzel H, Roger T. Immune responses to airborne fungi and non-invasive airway diseases. Semin Immunopathol 2015; 37(2):83-96.
2. Nazimek K, Bryniarski K, Askenase PW. Functions of exosomes and microbial extracellular vesicles in

allergy and contact and delayed-type hypersensitivity. Int Arch Allergy Immunol 2016; 171(1):1-26.
3. Schwartze VU, Jacobsen ID. Mucormycoses caused by Lichtheimia species. Mycoses. 2014; 57(Suppl 3):73-8.
4. Chrenkova V, Hubka V, Cetkovsky P, et al. Proven invasive pulmonary aspergillosis in stem cell transplant recipient due to Aspergillus sublatus, a cryptic species of A. nidulans. Mycopathologia 2017; 183(2):423-429.
5. Lopes JP, Stylianou M, Nilsson G, Urban CF. Opportunistic pathogen Candida albicans elicits a temporal response in primary human mast cells. Sci Rep 2015; 5:12287.
6. Kim HH, Lee S, Singh TS, Choi JK, Shin TY, Kim SH. Sparassis crispa suppresses mast cell-mediated allergic inflammation: Role of calcium, mitogen-activated protein kinase and nuclear factor-κB. Int J Mol Med 2012; 30(2):344-50.
7. Regan T, Nally K, Carmody R, Houston A, Shanahan F, Macsharry J, Brint E. Identification of TLR10 as a key mediator of the inflammatory response to Listeria monocytogenes in intestinal epithelial cells and macrophages. J Immunol 2013; 91(12):6084-92.
8. Taghavi M, Khosravi A, Mortaz E, Nikaein D, Athari SS. Role of pathogen-associated molecular patterns (PAMPS) in immune responses to fungal infections. Eur J Pharmacol 2017; 808:8-13.
9. Mortaz E, Adcock IM, Tabarsi P, Darazam IA, Movassaghi M, Garssen J, Jamaati H, Velayati A. Pattern recognitions receptors in immunodeficiency disorders. Eur J Pharmacol 2017; 808:49-56.
10. LeibundGut-Landmann S, Wüthrich M, Hohl TM. Immunity to fungi. Curr Opin Immunol 2012; 24(4):449-58.
11. Pennini ME, Perkins DJ, Salazar AM, Lipsky M, Vogel SN. Complete dependence on IRAK4 kinase activity in TLR2, but not TLR4, signaling pathways underlies decreased cytokine production and increased susceptibility to Streptococcus pneumoniae infection in IRAK4 kinase-inactive mice. J Immunol 2013; 190(1):307-16.
12. Gresnigt MS, Rösler B, Jacobs CW, et al. The IL-36 receptor pathway regulates Aspergillus fumigatus-induced Th1 and Th17 responses. Eur J Immunol 2013; 43(2):416-26.
13. Tang YJ, Dou HT, Zhang QH, Liu JJ, Yang XS. Expression of inflammatory cytokines in ovarian epithelial cancer and their correlation. J Biol Regul Homeost Agents 2017; 31(2):413-18.
14. Zidi S, Bediar-Boulaneb F, Belguendouz H, et al. Local pro-inflammatory cytokine and nitric oxide responses are elevated in patients with pterygium. Int J Immunopathol Pharmacol 2017; 30(4):395-405.
15. Amaral RC, Barbeiro DF, Koike MK, et al. Cytokine and chemokine levels in the heart tissue of aged rats following severe acute pancreatitis. Eur J Inflamm 2017; 15:102-6.
16. Morita H, Arae K, Unno H, et al. An interleukin-33-mast cell-interleukin-2 axis suppresses papain-induced allergic inflammation by promoting regulatory T cell numbers. Immunity 2015; 43(1):175-86.
17. Ma N, Liu Q, Hou L, Wang Y, Liu Z. MDSCs are involved in the protumorigenic potentials of GM-CSF in colitis-associated cancer. Int J Immunopathol Pharmacol 2017; 30(2):152-62.
18. Yang W-H, Liu Y-H, Liang J-L, et al. β-Patchoulene, isolated from patchouli oil, suppresses inflammatory mediators in LPS-stimulated RAW264.7 macrophages. Eur J Inflamm 2017; 15:136-41.
19. Garlanda C, Dinarello CA, Mantovani A. The interleukin-1 family: back to the future. Immunity 2013;39(6):1003-18.
20. Su C, Yang T, Wu Z, et al. Differentiation of T-helper cells in distinct phases of atopic dermatitis involves Th1/Th2 and Th17/Treg. Eur J Inflamm 2017; 15:46-52.
21. Taracanova A, Alevizos M, Karagkouni A, et al. SP and IL-33 together markedly enhance TNF synthesis and secretion from human mast cellsmediated by the interaction of their receptors. Proc Natl Acad Sci U S A 2017; 114(20):E4002-E4009.
22. Theoharides TC, Stewart JM, Tsilioni I. Tolerability and benefit of a tetramethoxyluteolin-containing skin lotion. Int J Immunopathol Pharmacol 2017; 30(2):146-151.
23. Galli SJ, Kalesnikoff J, Grimbaldeston MA, Piliponsky AM, Williams CM, Tsai M. Mast cells as "tunable" effector and immunoregulatory cells: recent advances. Annu Rev Immunol 2005; 23:749-86.
24. Kandere-Grzybowska K, Letourneau R, Kempuraj

D, Donelan J, Poplawski S, Boucher W. IL-1 induces vesicular secretion of IL-6 without degranulation from human mast cells. J Immunol 2003; 171(9):4830-36.

25. Galli SJ, Gaudenzio N. Human mast cells as antigen-presenting cells: When is this role important in vivo? J Allergy Clin Immunol 2017; 141(1):92-93.
26. Boraschi D, Lucchesi D, Hainzl S, et al. IL-37: a new anti-inflammatory cytokine of the IL-1 family. Eur Cytokine Netw 2011; 22(3):127-47.
27. Conti P, Carinci F, Lessiani G, Spinas E, Kritas SK, Ronconi G, Caraffa A, Theoharides TC. Potential therapeutic use of IL-37: a key suppressor of innate immunity and allergic immune responses mediated by mast cells. Immunol Res 2017; 65(5):982-86.
28. Conti P, Caraffa A, Ronconi G, et al. Impact of mast cells in depression disorder: inhibitory effect of IL-37 (new frontiers). Immunol Res 2018; doi: 10.1007/s12026-018-9004-9. [Epub ahead of print].
29. Conti P, Ronconi G, Kritas SK, Caraffa A, Theoharides TC. Activated mast cells mediate low-grade inflammation in type 2 diabetes: interleukin-37 could be beneficial. Can J Diabetes 2018. doi: 10.1016/j.jcjd.2018.01.008. [Epub ahead of print].
30. Zhan Q, Zeng Q, Song R, et al. IL-37 suppresses MyD88-mediated inflammatory responses in human aortic valve interstitial cells. Mol Med 2017; 23. doi: 10.2119/molmed.2017.00022.

A RAT OSTEOPOROSIS MODEL INDUCED BY OVARIECTOMY AND GLUCOCORTICOID

J.H. LEE[1,2,3] and Y-Z. JIN[1]

[1]Department of Orthopedic Surgery, College of Medicine, Seoul National University, Seoul, Korea;
[2]Department of Orthopedic Surgery, SMG-SNU Boramae Medical Center, Seoul, Korea;
[3]Institute of Medical and Biological Engineering, Seoul National University Medical Research Center, Seoul, Korea

Received October 28, 2017 – Accepted May 17, 2018

Osteoporosis is characterized by reduced bone mineral density (BMD) and changes in bone morphometry, which increases the risk of fracture. However, the lack of proper models of significant osteoporosis limits our study of related medications and fracture mechanisms. The objective of this study was to determine whether a combination of ovariectomy (OVX) and glucocorticoid injection was appropriate for establishing an osteoporosis animal model. Female Sprague-Dawley rats were divided into sham, an OVX group, a glucocorticoid injection osteoporosis (GIO) group, and an OVX + GIO group. All animals were sacrificed in their 26th week and their spines and bilateral femurs were harvested and analyzed. Their bone quality elements, including BMD, trabecular bone architecture, and cortical bone thickness were analyzed via micro-CT, and mechanical strength of the spines was measured with a Universal testing machine, TO-101G. Femur neck and total femur mean BMD (g/cm2) in the OVX + GIO group (0.307, 0.439) was significantly lower than the sham group (0.518, 0.644) and the GIO group (0.485, 0.587). Femur neck cortical bone thickness (cm) in OVX + GIO group (0.369) were significantly less than those in the OVX group (0.421) or the GIO group (0.510). Furthermore, the OVX + GIO group had significantly lower mechanical strength than the other groups in the spine. In conclusion, OVX combined glucocorticoid injection could induce significant bone loss that had poorer bone quality and less mechanical strength than simple OVX or glucocorticoid injection had, without significantly increased mortality. Therefore, OVX + GIO might be an appropriate osteoporosis animal model.

According to the criteria of WHO, human osteoporosis (OP) is defined as a bone mineral density that is 2.5 standard deviations (SD) or more under the average BMD of young female (1). The reduced BMD and weakened bone structure elevated the risk of osteoporotic femoral fracture and vertebral fracture that can lead to severe symptoms and increase mortality both in men and women (2). Therefore, increasing attention has been paid to the medications that prevent and treat OP (3, 4). To evaluate the efficacy of OP medications and analyze the fracture mechanisms, it is critical to use

Key words: osteoporosis, animal model, ovariectomy, glucocorticoid induced osteoporosis, bone mineral density

Mailing address:
Jae Hyup Lee, M.D., Ph.D.,
Department of Orthopaedic Surgery,
Seoul National University, College of Medicine,
Institute of Medical and Biological Engineering,
Seoul National University Medical Research Centre,
SMG-SNU Boramae Medical Centre, Boramae-ro 5-gil 20,
Dongjak-gu, Seoul 07061, Korea
Tel.: +82 2 870 2314 - Fax: +82 2 870 3863
e-mail: spinelee@snu.ac.kr

0393-974X (2018)
Copyright © by BIOLIFE, s.a.s.
This publication and/or article is for individual use only and may not be further reproduced without written permission from the copyright holder.
Unauthorized reproduction may result in financial and other penalties
DISCLOSURE: ALL AUTHORS REPORT NO CONFLICTS OF INTEREST RELEVANT TO THIS ARTICLE.

proper animal disease models.

Widely used OP models included immobilization model, ovariectomy (OVX) OP model and glucocorticoid-induced osteoporosis (GIO) model. OVX model has an advantage of reproducing postmenopausal OP to some extent but has limitations in inducing bone loss in long bones epiphysis, distal tibial metaphysis, and caud al vertebra (5). Moreover, the GIO model has a limited effect in inducing trabecular bone loss and requires a long injecting period (6). To establish an appropriate animal disease model, the feasibility of a combination of OVX and glucocorticoid injection in rats (7, 8), rabbits (9, 10) and sheep (11) have been probed in previous studies.

To further evaluate the efficacy and safety of this OP model, we induced OP in rats by injecting glucocorticoid steroid after OVX and compared their BMD, bone histomorphometry, and mechanical strength with the rats which received OVX or GIO only.

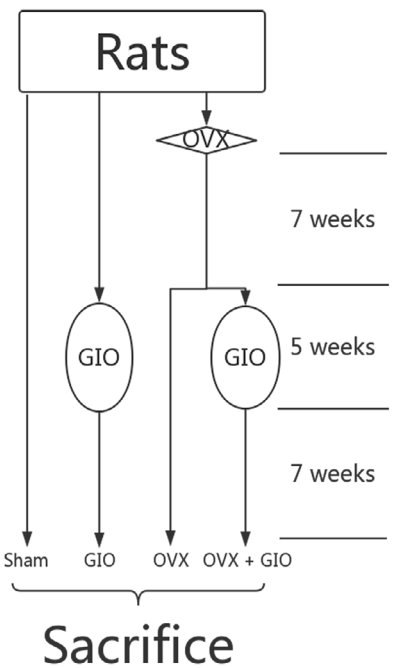

Fig. 1. *Flow chart of the experiment.*

MATERIALS AND METHODS

This study was carried out at the Preclinical Testing Laboratory in the Biomedical Research Institute of our institution after approval by the Seoul National University Institutional Animal Care and Use Committees. (IACUC No. 11-0216). A total of 48 7-week-old female Sprague-Dawley (SD) rats were divided into 4 groups: sham group, OVX group, GIO group, and OVX + GIO group. All rats were housed in a semi-Specific Pathogen Free animal facility. They had free access to solid compress feed and filtered tap water and were kept in cages under a controlled temperature (22±5°C) and humidity (50±5%) and an alternating 12-h light/dark cycle.

After one week of stabilization period in which the health conditions of the animal were evaluated and their microbe was monitored, 26 rats had bilateral OVX. After a rat was intraperitoneally anesthetized with 0.35 ml of diluted Zoletil (20 mg/kg) and 0.05 mL of Rompun (2 mg/kg) (12), its fur on the bilateral-dorsal area was shaved and the area was sterilized with 10% betadine solution. A skin incision of 1.5 cm was made on the dorsolateral surface to access to the peritoneal cavity. After exposing the ovary, a ligature was tied with silk at the medial side of the ovary with another vicryl ligature tied between the ovary and the silk ligature. The exposed ovary was carefully removed via electrocauterization between the two ligatures. The remaining uterine horn was placed back in the peritoneum, and the peritoneum, musculature, and skin were sutured layer by layer. The same procedure was performed on the contralateral side. In the sham group, only skin and fascia were incised without exposing ovary. Seven weeks after OVX, the remaining rats were randomly divided into an OVX group and an OVX + GIO group. The rats in the OVX + GIO group and GIO group were intramuscularly injected with diluted dexamethasone 0.125 mg/kg (dexamethasone 0.1 ml diluted in 0.5 ml of saline) on their thigh twice a week for 5 weeks. Meanwhile, no additional intervention was implemented on rats in the OVX group and sham group.

The operated animals were intramuscularly injected with metacam (Meloxicam 5mg/ml, Labiana Life Science S.A.) 0.3 ml and intraperitoneally injected with cefazolin (Cefazolin Sodium 1g) 0.5 ml after the operation. All animals were kept for additional 7 weeks after all interventions had been carried out and were sacrificed in their 26th week with CO_2 (Fig. 1).

Micro-CT analysis

After harvesting specimens including lumbar spine 1 to 5 and femurs from both sides, micro-CT (SkyScan 1173) images were taken for all specimens at 130 kV and 30 μA with an aluminum filter (1 mm). BMD values of lumbar vertebral bodies, femur neck, femur head, and trochanter were compared between groups. Additionally, bone morphological parameters including bone surface/volume ratio (BS/BV), percent bone volume (BV/TV), trabecular pattern factor (Tb.Pf), structure model index (SMI), trabecular thickness (Tb.Th), trabecular number (Tb.N), trabecular separation (Tb.Sp), and degree of anisotropy (DA) in the same regions were analyzed. To compare cortical bone thickness, the thickness in femur neck and proximal femur shaft were measured. In both regions, the first slice was chosen at the cross-section image that showed no cancellous bone, with two additional slices located distal to the first one. The three slices were separated from each other for 20 slices (Fig. 2). The average cortical bones thickness of the three slices was estimated as the mean value of a sample.

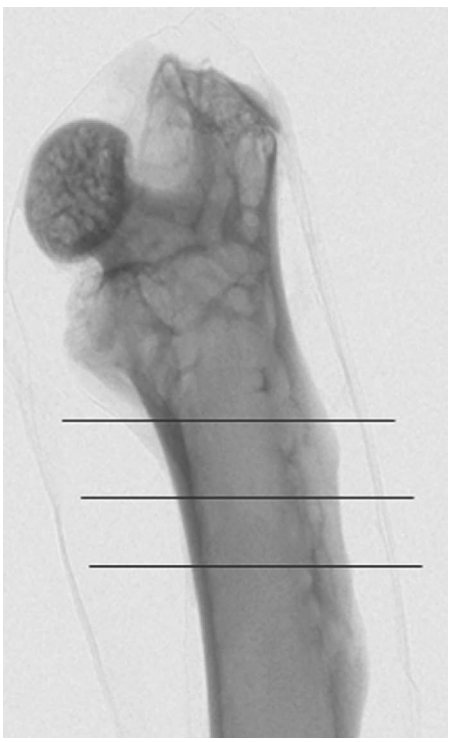

Fig. 2. *The measurement of the thickness of femur shaft.*

Histology

Specimens were organized to include the full spine or femur length and were fixed in formalin for 5 days. The sectioned tissues were dehydrated in 100% alcohol after 6 h of washing with water and were then stirred in methacrylate-based chemical curing resin for 2 days. These tissues were stirred and embedded in dissolved benzoyl peroxide. Embedded blocks were then trimmed. These blocks were cut along the specimen's longitudinal axis with EXAKT (Norderstedt, Germany; BS-3000N). Afterward, 4-mm thick sections were made along the sagittal plane to include the top and bottom parts of the specimen. These sections were then ground and attached to an acrylic slide using an EXAKT grinding machine (4110). After staining with hematoxylin and eosin, bone morphology was observed with a light microscope.

Biomechanical testing

After removing soft tissues, spinous processes, postzygapophyses, prezygapophyses and diapophyses from vertebrae, the remaining bodies were used for the biomechanical test. Biomechanical properties of vertebral bodies were detected with a material testing machine (Universal testing machine, TO-101G) at a crosshead speed of 1 mm/min and a cross-section area of 50.27 mm^2. The dorsal side of the vertebral body was kept upward.

Statistical analysis

One-way analysis of variance (ANOVA) was performed with the Bonferroni test for post hoc analysis if the four groups showed normal distribution. In the case of non-normal distribution, Kruskal–Wallis test was used. Statistical significance was considered when p-value was less than 0.05. All statistical analyses were performed with SPSS software (version 18.0, IBM)

RESULTS

Mortality

The mortality was 0% in the sham group and the GIO group. Two rats (2/13) in the OVX group and 3 rats (3/13) in the OVX + GIO group died before the terminal time point. Four of the 5 rats died immediately after surgery. The remaining rat died at 3 weeks after steroid injection. Accordingly, the steroid injection caused an additional mortality of 10%.

Micro-CT results

BMD. Using lumbar mean BMD of the sham group as a baseline, BMD values of the OVX, GIO, and OVX + GIO groups were 83%, 70.5%, and 67.5%, respectively. The OVX + GIO group and GIO group had significantly lower BMD values than the sham group and the OVX group (OVX + GIO vs sham, $p < 0.0001$; OVX + GIO *vs* OVX, $p < 0.0001$; GIO *vs* sham, $p < 0.0001$; GIO vs OVX, $p < 0.001$). The OVX group had significantly ($p < 0.0001$) lower BMD value than the sham group (Table I).

Using femur mean BMD of the sham group as a baseline, BMD values of the OVX, GIO, and OVX + GIO groups were 78.1%, 91.1%, and 68.2%, respectively. BMD value of femur in the OVX +GIO group was significantly lower than that of the sham group and the GIO group (both $p < 0.0001$). BMD value of the OVX group was significantly lower than that of the sham group ($p = 0.026$) and lower than the GIO group without statistical significance (p = 0.368) (Table II). Femur head BMD of the OVX + GIO group was significantly lower than that of other groups (all $p < 0.0001$). Femur head BMD of the OVX group was significantly lower than that of the sham group ($p = 0.005$). Femur neck BMD values of the OVX + GIO group and the OVX group were significantly lower than those of the sham group and the GIO group (all $p < 0.0001$). Femur trochanter BMD values of the OVX + GIO, OVX, and GIO groups were significantly lower than that of the sham group (all $p < 0.0001$). However, there was no significant difference in femur trochanter BMD among OVX + GIO, OVX, and GIO groups.

Bone histomorphometric analysis

Vertebrae. In lumbar spine, BV/TV of the OVX

Table I. *Bone mineral density of the lumbar spine.*

Group (n)	Bone mineral density (lumbar, g/cm^2) Mean (SD), %
Sham (21)	0.566 (0.072), 100
OVX (21)	0.470 (0.076), 83.0
GIO (33)	0.399 (0.063), 70.5*#
OVX + GIO (21)	0.384 (0.057), 67.8 *#

OVX: ovariectomy; GIO: glucocorticoid induced osteoporosis.
** p < 0.05, compared to sham group ; # p < 0.05, compared to OVX group*

Table II. *Bone mineral density of the femur.*

Group (n)	**Bone mineral density (g/cm^2), Mean (SD)**			
	Head	Neck	Trochanter	Total, %
Sham (10)	0.876 (0.101)	0.518 (0.036)	0.538 (0.052)	0.644 (0.18), 100
OVX (7)	0.768 (0.082)	0.317 (0.047)*	0.426 (0.087)	0.503 (0.21), 78.1
GIO (21)	0.819 (0.030)	0.485 (0.048)#	0.449 (0.043)	0.587 (0.17), 91.1
OVX + GIO (14)	0.605 (0.049)*#&	0.307 (0.064)*&	0.451 (0.067)	0.439 (0.13), 68.2*&

OVX: ovariectomy; GIO: glucocorticoid induced osteoporosis.
** p < 0.05 compared with sham group; # p < 0.05, compared to OVX group; & p < 0.05, compared to GIO group*

+ GIO group was significantly lower than that of the other three groups (all $p < 0.0001$). BV/TV of the OVX group and the GIO group were significantly lower than that of the sham group (both $p < 0.0001$) (Table III). Tb.N values were significantly lower in the OVX + GIO and OVX groups than those in the sham and GIO groups (all $p < 0.0001$). Tb.Sp value was significantly higher in the OVX group than that in the sham and GIO groups ($p = 0.035$, $p = 0.027$, respectively). Tb.Th values in GIO and OVX + GIO groups were significantly lower than those in sham and OVX groups.

BS/BV and Tb.Pf were significantly higher in the OVX + GIO and GIO groups than those of the

Table III. *Micro-CT results of lumbar spine.*

Group(N)	Sham (21)	OVX (21)	GIO (33)	OVX + GIO (21)
BV/TV (%)	54.4 (8.3)	37.0 (8.1)*	36.4 (6.6)*	25.7 (6.0)*#&
BS/BV (mm^{-1})	16.7 (2.9)	20.0 (3.6)*	27.3 (3.4)*#	26.2 (3.0)*#
Tb.Pf	-2.79 (2.5)	1.54 (2.6)*	4.81 (2.2)*#	5.0 (2.1)*#
SMI	0.59 (0.85)	1.47 (0.53)*	1.5 (0.24)*	2.0 (0.22)*#&
Tb.Th (mm)	0.195 (0.05)	0.178 (0.04)	0.128 (0.02)*#	0.139 (0.02)*#
Tb.N	2.84 (0.41)	2.11 (0.36)*	2.83 (0.28)#	1.84 (0.32)*&
Tb.Sp (mm)	0.253 (0.14)	0.338 (0.15)	0.259 (0.02)	0.328 (0.05)
DA	0.362 (0.15)	0.448 (0.15)	0.377 (0.11)	0.445 (0.09)

OVX: ovariectomy; GIO: glucocorticoid induced osteoporosis; BV/TV: percent bone volume; BS/BV: bone surface/volume ratio; Tb.Pf: trabecular pattern factor; SMI: structure model index; Tb.Th: trabecular thickness; Tb.N: trabecular number; Tb.Sp: trabecular separation; DA: degree of anisotropy.
** $p < 0.05$ compared with sham group ; # $p < 0.05$, compared to OVX group; ; & $p < 0.05$, compared to GIO group*
The data are presented as mean (SD).

Table IV. *Micro-CT results of femur head.*

Group (N)	Sham (21)	OVX (21)	GIO (33)	OVX + GIO (21)
BV/TV (%)	60.3 (4.8)	48.1 (8.0)*	56.3 (5.2)#	33.8 (4.4)*#&
BS/BV (mm^{-1})	27.1 (3.3)	29.3 (3.6)	26.7 (2.9)	36.3 (3.9)
Tb.Pf	-12.1 (6.7)	-5.7 (4.9)*	-6.9 (2.9)*	1.2 (1.9)*#&
SMI	-0.47 (0.64)	0.13 (0.69)	0.05 (0.63)	1.0 (0.21)*#&
Tb.Th (mm)	0.14 (0.01)	0.13 (0.01)	0.14 (0.01)	0.12 (0.01)*#&
Tb.N	4.41 (0.52)	3.63 (0.47)*	3.98 (0.28)*	2.84 (0.29)*#&
Tb.Sp (mm)	0.14 (0.01)	0.18 (0.02)*	0.15 (0.10)#	0.20 (0.03)*#&
DA	0.48 (0.07)	0.47 (0.07)	0.47 (0.07)	0.46 (0.08)

OVX: ovariectomy; GIO: glucocorticoid induced osteoporosis; BV/TV: percent bone volume; BS/BV: bone surface/volume ratio; Tb.Pf: trabecularpattern factor; SMI: structure model index; Tb.Th: trabecular thickness; Tb.N: trabecular number; Tb.Sp: trabecular separation; DA: degree of anisotropy.
** $p < 0.05$ compared with sham group ; # $p < 0.05$, compared to OVX group; ; & $p < 0.05$, compared to GIO group*
The data are presented as mean (SD).

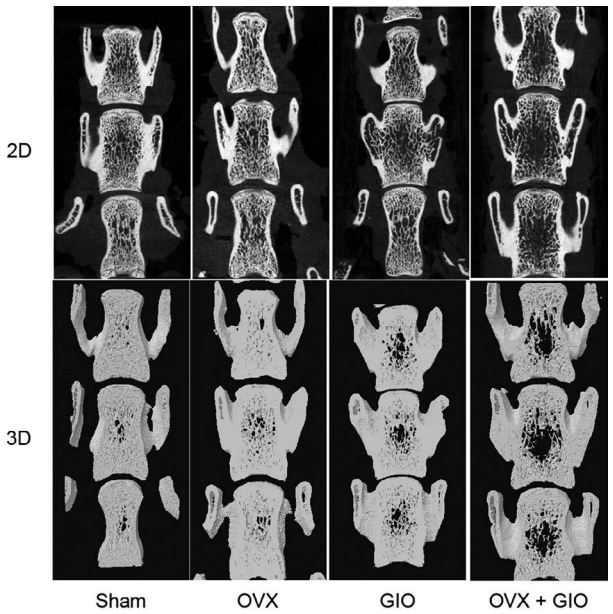

Fig. 3. *Reconstructed micro-CT images of lumbar spine. The OVX+GIO group showed significantly less trabecular bone volume, number, and connectivity with wider trabeculae separation in vertebral bodies than the other three groups. The GIO group showed significantly less trabecular bone in vertebral bodies than the sham group or the OVX group.*

sham group and the OVX group (all $p < 0.0001$). BS/BV and Tb.Pf of the OVX group were significantly higher than those of the sham group (BS/BV, $p = 0.008$; Tb.Pf, $p < 0.0001$). SMI was significantly higher in the OVX + GIO group than that in the other three groups ($p < 0.0001$, $p = 0.010$, $p = 0.008$, respectively).

As can be seen in the representative CT cross-sectional and 3D images of the spines, trabecular bone of the OVX + GIO group was also rare in the central portion of the vertebral body (Fig. 3).

Femur. In femur head, the OVX + GIO group had the lowest BV/TV, Tb.Th, and Tb.N, and the highest Tb.Sp, SMI, and Tb.Pf. No significant difference was observed among all groups in DA. (Table IV, Fig. 4)

In femur neck, OVX + GIO and OVX groups had significantly lower BV/TV and Tb.N than the other groups. (Table V, Fig. 4). However, DA in OVX + GIO group was significantly lower than sham and GIO groups. Femur neck cortical bone thickness was in the following order: sham group > GIO group > OVX group > OVX + GIO group, the differences between all groups were all significant (all $p < 0.0001$).

In femur trochanter, OVX + GIO group had the lowest BV/TV than the other three groups, but the differences between the three OP models were not significant. And OVX + GIO group had the lowest Tb.Th and Tb.Pf than the other two models (Table VI, Fig. 2).

Femur shaft cortical thickness of the OVX + GIO group was significantly thinner than that of the sham group and the GIO group (both $p < 0.0001$). The thickness of the OVX group was also significantly ($p = 0.008$) thinner than that of the sham group. But the difference between GIO and sham groups was not significant (Table VII).

In representative femur CT cross-sectional and 3D images, cortical bone thickness and trabecular bone connectivity were decreased the most in the OVX + GIO group, followed by OVX and GIO (Fig. 2).

Biomechanical results

In the vertical compression test for lumbar spine, the maximal compressive strength of the sham group and the GIO group were significantly higher than that of the OVX + GIO group (both $p < 0.0001$) and

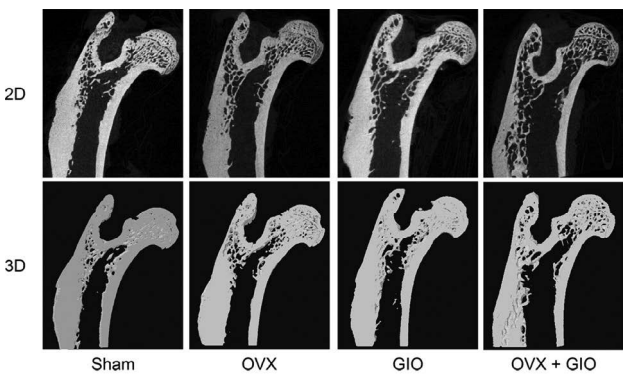

Fig. 4. *Reconstructed micro-CT images of femur. The OVX+GIO group and the OVX group showed significantly less trabecular bone volume, number, and connectivity with wider trabecular separation than the other three groups in trochanter, neck, and head. The OVX group and the GIO group showed significantly less trabecular bone than the sham group in trochanter.*

Table V. *Micro-CT results of femur neck.*

Group (N)	Sham (21)	OVX (21)	GIO (33)	OVX + GIO (21)
BV/TV (%)	24.0 (3.4)	11.8 (5.7)*	20.7 (4.4) $^{\#}$	9.5 (4.1)*$^{\&}$
BS/BV (mm^{-1})	44.4 (3.1)	46.6 (7.7)	44.0 (4.4)	53.2 (7.4)$^{*\&}$
Tb.Pf	9.77 (2.7)	17.3 (4.3) *	12.1 (3.2) $^{\#}$	17.2 (4.0) *$^{\&}$
SMI	1.69 (0.23)	2.30 (0.28) *$^{\&}$	1.95 (0.23) *	2.25 (0.20) *$^{\&}$
Tb.Th (mm)	0.10 (0.01)	0.11 (0.02)	0.11 (0.01)	0.097 (0.01) $^{\&}$
Tb.N	2.30 (0.29)	1.06 (0.38) *	1.88 (0.33) *$^{\#}$	0.96 (0.34) *$^{\&}$
Tb.Sp (mm)	0.23 (0.03)	0.31 (0.05) *	0.26 (0.33)	0.33 (0.05) *$^{\&}$
DA	0.64 (0.04)	0.60 (0.03)	0.64 (0.08)	0.54 (0.08) *$^{\&}$

OVX: ovariectomy; GIO: glucocorticoid induced osteoporosis; BV/TV: percent bone volume; BS/BV: bone surface/ volume ratio; Tb.Pf: trabecular pattern factor; SMI: structure model index; Tb.Th: trabecular thickness; Tb.N: trabecular number; Tb.Sp: trabecular separation; DA: degree of anisotropy.
** $p < 0.05$ compared with sham group; # $p < 0.05$, compared to OVX group; & $p < 0.05$, compared to GIO group*
The data are presented as mean (SD).

Table VI. *Micro-CT results of femur trochanter.*

Group (N)	Sham (21)	OVX (21)	GIO (33)	OVX + GIO (21)
BV/TV (%)	28.8 (3.0)	20.9 (4.1) *	21.4 (4.2) *	19.6 (2.8) *
BS/BV (mm^{-1})	30.4 (3.1)	30.5 (3.5)	30.0 (3.2)	35.6 (3.9) *$^{\&}$
Tb.Pf	4.91 (1.9)	6.77 (2.9)	6.77 (1.9)	9.78 (1.9) *$^{\&}$
SMI	1.37 (0.26)	1.66 (0.55)	1.70 (0.28)	1.94 (0.20) *
Tb.Th (mm)	0.13 (0.01)	0.14 (0.01)	0.14 (0.01)	0.13 (0.01) $^{\#\&}$
Tb.N	2.19 (0.35)	1.47 (0.37) *	1.53 (0.30) *	1.51 (0.16) *
Tb.Sp (mm)	0.29 (0.04)	0.35 (0.05)	0.34 (0.06)	0.39 (0.28)
DA	0.52 (0.09)	0.53 (0.10)	0.58 (0.08)	0.55 (0.08)*$^{\&}$

OVX: ovariectomy; GIO: glucocorticoid induced osteoporosis; BV/TV: percent bone volume; BS/BV: bone surface/ volume ratio; Tb.Pf: trabecular pattern factor; SMI: structure model index; Tb.Th: trabecular thickness; Tb.N: trabecular number; Tb.Sp: trabecular separation; DA: degree of anisotropy.
** $p < 0.05$ compared with sham group ; # $p < 0.05$, compared to OVX group; & $p < 0.05$, compared to GIO group*
The data are presented as mean (SD).

the OVX group ($p < 0.0001$, $p = 0.004$, respectively). However, there was no significant difference in maximal compressive strength between the GIO group and the sham group (Table VIII).

Histological results

Undecalcified histological sections of the lumbar spines showed that the OVX group had significantly less trabecular bone thickness, connectivity, and cortical bone thickness than the sham group. The GIO group showed thinner trabecular bone thickness and less connectivity than the sham group. However, there was no significant difference in cortical bone thickness between the two groups. The OVX + GIO group showed significant decreases in trabecular bone thickness, connectivity, and cortical bone thickness

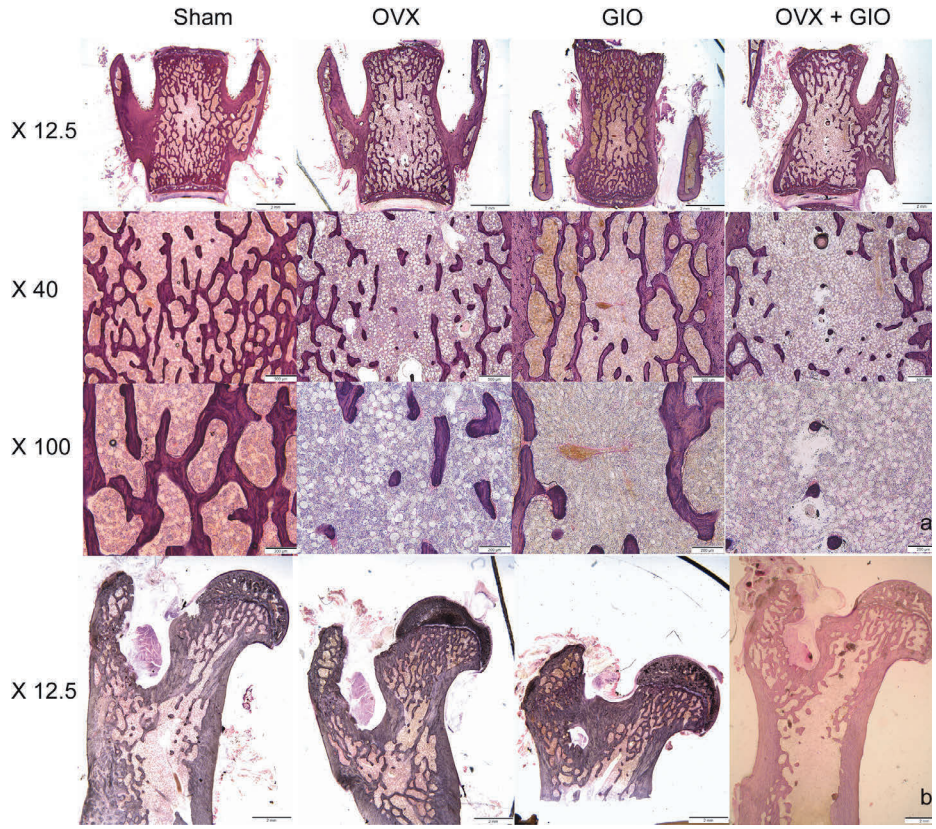

Fig. 5. ***a****) Hematoxylin and Eosin (H&E) stained sections prepared from undecalcified vertebral body and femur. The OVX group had significantly thinner trabecular and cortical bone than the sham group. The GIO group showed less connectivity in trabecular bone thickness compared to the sham group. The OVX + GIO group had significantly thinner trabecular and cortical bone thickness and less trabecular bone connectivity than the OVX and GIO groups.* ***b****) The OVX+GIO group and the OVX group showed significantly lower cortical bone thickness and lower trabecular bone connectivity than the GIO or sham group. The GIO group had no significant difference in cortical bone thickness compared to the sham group.*

Table VII. *Cortical thickness of femur.*

Group (n)	Cortical thickness, Mean (SD)	
	Neck (cm)	Shaft (cm)
Sham (10)	0.550 (0.023)	0.780 (0.057)
OVX (7)	0.421 (0.015) *	0.683 (0.060) *
GIO (18)	0.510 (0.025) *#	0.721 (0.050)
OVX + GIO (14)	0.369 (0.022) *#&	0.612 (0.054) *&

OVX: ovariectomy; GIO: glucocorticoid induced osteoporosis

** $p < 0.05$ compared with sham group; # $p < 0.05$, compared to OVX group; & $p < 0.05$, compared to GIO group. Femur neck cortical thickness was in the following order: sham group > GIO group > OVX group > OVX +GIO group (all $p < 0.05$). In femur shaft cortical thickness, the OVX + GIO group showed significantly lower value than the sham group and the GIO group (both $p < 0.0001$). The OVX group showed significantly lower value than the sham group ($p = 0.008$).*

Table VIII. *Biomechanical results.*

Group (n)	Vertical Compression Test, Mean (SD)	
	Load (N)	Compressive Strength (N/mm^2)
Sham (21)	175.8 (51.2)	3.50 (1.01)
OVX (21)	124.5 (53.2) *	2.48 (1.06) *
GIO (21)	188.9 (51.5) #	3.76 (1.02) #
OVX + GIO (21)	114.0 (28.8) *&	2.27 (0.57) *&

OVX: ovariectomy; GIO: glucocorticoid induced osteoporosis
** $p < 0.05$ comparedd with sham group; # $p < 0.05$, comparedd to OVX group ; & $p < 0.05$, comparedd to GIO group. The OVX + GIO group (both $p < 0.0001$) and the OVX group ($p < 0.0001$ and $p = 0.004$, respectively) had significantly lower maximal compressive strength than the sham group and the GIO group.*

compared to the other three groups (Fig. 5a).

Undecalcified histological sections of femur also showed that the OVX + GIO group had significant decreases in cortical bone thickness and trabecular bone connectivity compared to the other three groups. The OVX group showed less cortical bone thickness and trabecular bone connectivity than the sham group. However, the change in cortical bone thickness in the GIO group compared to that of the sham group was insignificant (Fig. 5b).

DISCUSSION

In OP studies, two methods were widely used to establish the OP animal model. One is via relatively increasing bone resorption, such as OVX, limb immobilization, and dietary calcium restriction. The other one is by relatively decreasing bone formation, such as the senile model and glucocorticoid injection (9, 13). OVX and glucocorticoid injection have their own mechanisms but both have limitations in their efficacy on inducing OP. OVX causes cancellous bone loss in proximal tibia (14), lumbar vertebra (15), and femoral head and neck (16, 17), but has limitations in inducing bone loss in long bone epiphyses, distal tibia metaphysis, and caudal vertebrae (5, 18, 19). Glucocorticoid injection induces bone loss via a dual mechanism, which decreases bone formation and increases bone resorption simultaneously (20). However, it took 90 days oral intake of prednisone to induce bone loss in lower limb cortical bone, without significant change in trabecular bone (6). Therefore, to establish an appropriate animal OP model that had significant BMD reduction and impaired bone structure, we combined the two methods and evaluated its feasibility.

The criteria of osteoporosis for rat is still absent, therefore, in this study we referred to a previous study that deemed a reduction of 25% of BMD as a criteria of osteoporosis (21). In our study, OVX only induced OP in femur neck, and glucocorticoid only induced OP in the lumbar spine. Compared to the treatments, OVX + glucocorticoid injections induced significant bone loss and OP in spine, femur neck, and total femur. Accordingly, simple OVX or glucocorticoid injection only induced osteopenia or mild OP while OVX + glucocorticoid injection induced significant bone loss and OP.

Besides decreased BMD, OP is also characterized by the alteration of trabecular bone architecture (22). Architecture changes in osteoporotic trabecular bone include decreases in BV/TV, Tb.N, Tb.Th and DA, and increases in Tb.Sp, Tb.Pf and SMI (23, 24) . In our study, OVX + GIO had the most delicate bone structure among the three models. It could be observed that bone structural change followed different patterns in different OP models. The GIO had thinner Tb.Th while significantly more Tb.N than the OVX model. OVX + GIO had similar Tb.Th to GIO and similar Tb.N to the OVX model, which

indicated OVX + GIO maintained the characteristics of both models and had significant OP. The characteristics obvious in vertebrae might be a result of vertebrae having a higher ratio of trabeculae than femur.

Cortical bone loss could be observed via measuring thickness of femur neck cortical bone, which was significantly lower in the OVX + GIO and OVX groups than that in the sham and GIO groups in our study. After OVX, endosteal bone resorption and periosteal bone formation can both increase and expand the bone marrow cavity and decrease bone thickness (25). Chronical use of glucocorticoid induces cortical porosity and endosteal thinning (26). In this study, the significantly thinner bone in OVX + GIO and OVX groups than that GIO indicated that OVX induced more severe cortical bone loss than GIO. The fractional cortical thinning in the GIO group could be explained by the relatively short injection period. It has been reported that four weeks of administration of high dose glucocorticoid could not induce significant cortical bone mass change, and 8 weeks of administration could only induce cortical osteopenia (27, 28). However, an overdose of glucocorticoid injection can cause subchondral bone necrosis and increase mortality (29, 30). Therefore, modulating the dosage and other factors, including classes of glucocorticoid, animal species and strains, administration route and period, is critical to optimize the animal model.

In the biomechanical test, the compressive strength was lowest in the OVX+ GIO group, followed by OVX group, and the GIO group showed the highest compressive strength. This might be related to the fact that one of the significant risk factors of fracture is an anisotropic trabecular structure (24) . According to the micro-CT results, OVX + GIO and OVX groups had significantly more anisotropic structure than the GIO group, which might be the reason for the GIO group having the highest compressive strength. However, it was somehow different from the results of previous studies, which showed GIO had higher fracture risk than primary osteoporosis, even though they had similar areal BMD (31). Such inconsistency might be attributed to the limited dosage and administration period of dexamethasone used in our study. Which also indicated the necessity of modulating the proper dosage.

In our study, we used skeletal immature rats that carry some confounding factors. However, performing OVX and prednisolone administration on skeletally immature rats could bring a low peak bone mass that is a high risk factor for human OP (5). Also, the combination of OVX and GIO brought significant bone loss that was presented in bone histomorphometry, BMD and mechanical strength. Therefore, this model might be more appropriate for studying endocrine, environmental and nutritional factors that influence the peak bone mass.(5)

One limitation in interpreting the results was the absence of a criteria of osteoporosis in rats. However, the BMD and bone architecture have been proved to be related to bone quality (32), and additionally, we observed a significantly reduced mechanical strength in rat vertebrae. Therefore, we believe the combination of OVX and GIO caused significant and substantial bone loss, which made the animal model appropriate for studying osteoporosis. Also, another limitation was that the intramuscularly injected volume (0.6 ml/rat) was higher than the recommended maximum volume (0.2 ml/site) (33), which should be noticed in further study.

Two previous studies also indicated the viability of inducing OP via the combination of OVX and glucocorticoid injection (34, 35). The dosages of dexamethasone in the studies were 0.3mg/kg and 0.6mg/kg, respectively, and the injections were implemented twice a week for 1 to 3 months. The dosage in our study was 0.125mg/kg and was injected for 5 weeks, which also induced significant OP in rat femur and lumbar. Therefore, 0.125 mg/kg might be also an applicable dosage for inducing OP in this model, without significantly increased mortality. Additionally, the results of our study indicated that even though no continuous glucocorticoid was injected, the bone loss did not recover during the resting period of 7 weeks. It allows testing efficacy of medications without or with minimal interference from glucocorticoid that was injected to induce OP, which was critical in pre-clinical studies.

In conclusion, compared to mild bone loss induced by simple OVX or glucocorticoid injection,

a combination of the two treatments could induce severe bone loss without significantly increased mortality. The dosage of dexamethasone used in this study seemed to be relatively safe and efficacious, but further research is still needed to optimize the dosage. The OVX + GIO model has advantages such as better control of steroid intake than oral prednisolone administration, easy manipulation, and inducing more certain and repeatable bone loss. Therefore, the OVX + GIO model could be considered as a safe and effective osteoporosis animal model.

ACKNOWLEDGEMENTS

This work was supported by Mid-career Researcher Program through an NRF grant funded by the Korean government (MSIP) (2016R1A2B3015048).

REFERENCES

1. Siris ES, Adler R, Bilezikian J, et al. The clinical diagnosis of osteoporosis: a position statement from the National Bone Health Alliance Working Group. Osteoporos Int 2014; 25:1439-43
2. Sadat-Ali M, Gullenpet AH, Al-Turki HA, et al. Are we missing osteoporosis-related vertebral fractures in men? Asian Spine J 2011; 5:107-10.
3. Seo J-B, Yoo J-S, Ryu J-W, Yu K-W. Influence of early bisphosphonate administration for fracture healing in patients with osteoporotic proximal humerus fractures. Clin Orthop Surg 2016; 8:437-43.
4. Kim TI, Choi JH, Kim SH, Oh JH. The adequacy of diagnosis and treatment for osteoporosis in patients with proximal humeral fractures. Clin Orthop Surg 2016; 8:274-79.
5. Lelovas PP, Xanthos TT, Thoma SE, Lyritis GP, Dontas IA. The laboratory rat as an animal model for osteoporosis research. Compar Med 2008; 58:424-30.
6. Lin S, Huang J, Zheng L, et al. Glucocorticoid-induced osteoporosis in growing rats. Calcif Tissue Int 2014; 95:362-73.
7. Ren H, Liang D, Shen G, et al. Effects of combined ovariectomy with dexamethasone on rat lumbar vertebrae. Menopause 2016; 23:441-50.
8. Govindarajan P, Khassawna T, Kampschulte M, et al. Implications of combined ovariectomy and glucocorticoid (dexamethasone) treatment on mineral, microarchitectural, biomechanical and matrix properties of rat bone. Int J Exp Pathol 2013; 94:387-98.
9. Wanderman NR, Mallet C, Giambini H, et al. An ovariectomy-induced rabbit osteoporotic model: a new perspective. Asian Spine Journal 2018; 12:12-17.
10. Oki Y, Doi K, Makihara Y, Kobatake R, Kubo T, Tsuga K. Effects of continual intermittent administration of parathyroid hormone on implant stability in the presence of osteoporosis: an in vivo study using resonance frequency analysis in a rabbit model. J Appl Oral Sci 2017; 25:498-505.
11. Yu Z, Wang G, Tang T, Fu L, Yu X, Zhu Z, Dai K. Long-term effects of ovariectomy on the properties of bone in goats. Exp Ther Med 2015; 9:1967-73.
12. Naples LM, Langan JN, Kearns KS. Comparison of the anesthetic effects of oral transmucosal versus injectable medetomidine in combination with tiletamine-zolazepam for immobilization of chimpanzees (Pan troglodytes). J Zoo Wildl Med 2010; 41:50-62.
13. Bonucci E, Ballanti P. Osteoporosis-bone remodeling and animal models. Toxicol Pathol 2014; 42:957-69.
14. Longo AB, Salmon PL, Ward WE. Comparison of ex vivo and in vivo micro-computed tomography of rat tibia at different scanning settings. J Orthopaed Res 2017; 35:1690-98.
15. Bahar H, Gallacher K, Downall J, Nelson CA, Shomali M, Hattersley G. Six weeks of daily abaloparatide treatment increased vertebral and femoral bone mineral density, microarchitecture and strength in ovariectomized osteopenic rats. Calcif Tissue Int 2016; 99:489-99.
16. Chen YJ, Wang SP, Cheng FC, et al. Intermittent parathyroid hormone improve bone microarchitecture of the mandible and femoral head in ovariectomized rats. BMC Musculoskelet Disord 2017; 18:171.
17. Kaczmarczyk-Sedlak I, Klasik-Ciszewska S, Wojnar W. Glabridin and glycyrrhizic acid show no beneficial effect on the chemical composition and mechanical properties of bones in ovariectomized rats, when administered in moderate dose. Pharmacoll Rep 2016; 68:1036-41.

18. Li M, Shen Y, Qi H, Wronski TJ. Comparative study of skeletal response to estrogen depletion at red and yellow marrow sites in rats. Anat Rec 1996; 245:472-80.
19. Miyakoshi N, Sato K, Abe T, Tsuchida T, Tamura Y, Kudo T. Histomorphometric evaluation of the effects of ovariectomy on bone turnover in rat caudal vertebrae. Calcif Tissue Int 1999; 64:318-24.
20. Sarinho ESC, Melo VMPP. Glucocorticoid-induced bone disease: mechanisms and importance in pediatric practice. Rev Paul Pediatr 2017; 35:207-15.
21. Lill CA, Gerlach UV, Eckhardt C, Goldhahn J, Schneider E. Bone changes due to glucocorticoid application in an ovariectomized animal model for fracture treatment in osteoporosis. Osteoporos Int 2002; 13:407-14.
22. Fields AJ, Keaveny TM. Trabecular architecture and vertebral fragility in osteoporosis. Curr Osteoporos Rep 2012; 10:132-40.
23. Campbell GM, Sophocleous A. Quantitative analysis of bone and soft tissue by micro-computed tomography: applications to ex vivo and in vivo studies. BoneKEy Reports 2014; 3:564.
24. Souzanchi MF, Palacio-Mancheno P, Borisov YA, Cardoso L, Cowin SC. Microarchitecture and bone quality in the human calcaneus: local variations of fabric anisotropy. J Bone Min Res 2012; 27:2562-72.
25. Komori T. Animal models for osteoporosis. Eur J Pharmacol 2015; 759:287-94.
26. Ilias IGH. Glucocorticoid-Induced Osteoporosis [Updated 2015 Jan 7]. In De Groot LJ CG, Dungan K, et al. (ed) Internet.
27. Iwamoto J, Seki A, Takeda T, Yamada H, Sato Y, Yeh JK. Effects of alfacalcidol on cancellous and cortical bone mass in rats treated with glucocorticoid: a bone histomorphometry study. J Nutr Sci Vitaminol (Tokyo) 2007; 53:191-97.
28. Iwamoto J, Seki A, Takeda T, Sato Y, Yamada H, Shen CL, Yeh JK. Preventive effects of risedronate and calcitriol on cancellous osteopenia in rats treated with high-dose glucocorticoid. Exp Anim 2006; 55:349-55.
29. Weinstein RS Glucocorticoid-induced osteonecrosis. Endocrine 2012; 41:183-90.
30. del Rincon I, Battafarano DF, Restrepo JF, Erikson JM, Escalante A. Glucocorticoid dose thresholds associated with all-cause and cardiovascular mortality in rheumatoid arthritis. Arthritis Rheumatol 2014; 66:264-272.
31. Briot K, Roux C. Glucocorticoid-induced osteoporosis. RMD Open 2015; 1:e000014.
32. Epstein S. The roles of bone mineral density, bone turnover, and other properties in reducing fracture risk during antiresorptive therapy. Mayo Clin Proc 2005; 80:379-88.
33. Diehl K-H, Hull R, Morton D, et al. A good practice guide to the administration of substances and removal of blood, including routes and volumes. J Appl Toxicol 2001; 21:15-23.
34. Govindarajan P, Khassawna T, Kampschulte M, et al. Implications of combined ovariectomy and glucocorticoid (dexamethasone) treatment on mineral, microarchitectural, biomechanical and matrix properties of rat bone. Intl J Expl Pathol 2013; 94:387-98.
35. Ren H, Liang D, Shen G, et al. Effects of combined ovariectomy with dexamethasone on rat lumbar vertebrae. Menopause 2016; 23(4):441-50.

CONCOMITANT ASSESSMENT OF DNA OXIDATION AND BONE RESORPTION OVER A RAPID BODY MASS REDUCTION PERIOD IN FEMALE JUDOKAS

N. YASUDA and T. YANO

Research Center in Sports Medicine and Science, Department of Physical Education, International Pacific University, Okayama, Japan

Received November 12, 2017 – Accepted May 2, 2108

The purpose of this study was to concomitantly determine oxidative DNA damage and bone resorption following a rapid body mass reduction in association with energy restriction and exercise training, considering 17β-estradiol level, in female collegiate judokas. Eighteen nationally ranked university female judokas were enrolled as participants in this study. All participants continuously managed to reduce their body mass 8 days just before a competition. To detect cumulative effects of oxidative DNA damage and bone resorption, urinary samples were collected in the morning on three different days (Day 1= the beginning of body mass reduction; Day 4=mid-term of body mass reduction; Day 7=the day before the competition) for the later analysis of 8-hydroxy-2'- deoxyguanosine (8-OHdG) as well as cross-linked N-terminal telopeptides of Type I collagen (NTx). Urinary 8-OHdG and NTx levels were determined with high performance liquid chromatography and enzyme-linked immunosorbent assay, respectively. No significant alterations were observed in urinary 8-OHdG or NTx levels over a rapid body mass reduction period. The findings of the present study indicate that female judokas appear to have relatively less oxidative DNA damage determined by quantification of 8-OHdG and bone resorption over a rapid body mass reduction period, potentially due to the enhanced endogenous defense responses (training adaptation). These data can provide athletes and coaches with valuable information in considering an optimal body mass management program to avoid detrimental physiological and biological conditions.

Female judokas who have 'weight class' manage to acutely reduce body mass (typically 5~10%, less than 5 days) based on rapid body mass loss procedures (1). In this regard, the important thing for the players is to reduce their body mass with no decrease of their fat-free mass to avoid the reduction of physical strength (1). Rapid body mass loss practices are most often combined with intense exercise training, including food and fluid restriction, exercise with rubber or plastic suits and even vomiting, which may lead to the negative effects on athletes' performance (2).

It has generally been accepted that high-intensity endurance and/or eccentric exercise, including unaccustomed exercise, appear to result in the alterations of the antioxidant defense systems followed by oxidative DNA damage (3). On the other hand, there may be protective effects of regular exercise training in association with the up-regulation of endogenous antioxidant defense and repair systems (4, 5), which is represented by previous data that trained athletes have less oxidative DNA damage than untrained individuals (4).

Key words: bone turnover, gluconeogenesis, hydration status, muscle mass, oxidative stress

Mailing address:
Nobuo Yasuda, Ph.D.
Department of Anesthesia, Critical Care and Pain Medicine,
Shriners Hospitals for Children - Boston,
Massachusetts General Hospital,
Harvard Medical School, 51 Blossom Street,
Boston, MA 02114-2601, U. S. A.
Tel.: +1 (617) 888 0140
e-mail: nobuoyasuda17@gmail.com

0393-974X (2018)
Copyright © by BIOLIFE, s.a.s.
This publication and/or article is for individual use only and may not be further reproduced without written permission from the copyright holder.
Unauthorized reproduction may result in financial and other penalties
DISCLOSURE: ALL AUTHORS REPORT NO CONFLICTS OF INTEREST RELEVANT TO THIS ARTICLE.

The 8-hydroxy-2'-deoxyguanosine (8-OHdG), which was originally introduced by Kasai and Nishimura in 1984, has been established as a sensitive biomarker of DNA damage induced by the hydroxyl radical attack at the C8 position of the nucleobase guanine or its nucleoside guanosine (6). Moreover, 8-OHdG has been recognized as a promutagenic lesion as this lesion induces G (guanine): C (cytosine) to T (thymine): A (adenine) transversion unless repaired prior to replication (3). In this respect, urinary 8-OHdG excretion has been considered to reflect the balance of oxidative DNA damage and repair from all cells *in vivo* (whole body level) (3).

Previous studies have reported effects of 17β-estradiol (one of the sex steroid hormones, a potential role of endogenous antioxidant to cell) on oxidative DNA damage, thus suggesting potential differences between follicular and luteal phases (7, 8). For instance, Kapiszewska et al. (7) have shown endogenous DNA damage in lymphocytes in association with the fluctuation of 17β-estradiol concentration in the follicular phase in healthy young women. Furthermore, Matsumoto et al. (8) observed increased tendency of urinary 8-OHdG levels during follicular phase, though statistical difference was not found. To sum up, it remains to be elucidated whether there are potential protective effects of 17β-estradiol concentration on oxidative DNA damage during a rapid body mass loss associated with acute caloric restriction and exercise training (9).

Judo, one of the weight bearing sports, has been recognized to increase bone formation (10). In contrast, acute and chronic body mass loss has been considered to increase bone resorption demonstrated by several biomarkers such as urinary cross-linked N-terminal telopeptides of Type I collagen (NTx) and urinary pyridinoline and deoxypyridinoline levels (11). As demonstrated by Zanker and Swaine (12), significant bone resorption may happen when a magnitude of energy restriction exceeds more than 50 % for 3 days. In line with the above-mentioned information, 17β-estradiol is a primary mediator of periosteal bone growth in women, which implies that 17β-estradiol may have an influence on bone strength and growth (13). Furthermore, 17β-estradiol concentration may have an influence on bone resorption during a rapid body mass reduction period (14). Moreover, Morris et al. (15) highlighted less exercise-induced osteogenic benefits in rowing training associated with low estrogen excretion.

Taken collectively, it remains inconclusive whether rapid body mass loss induced by caloric restriction combined with exercise training results in oxidative DNA damage determined by quantification of 8-OHdG and bone resorption, potentially in response to 17β-estradiol concentration. Accordingly, the purpose of this study was to concomitantly assess whole body DNA damage accounted for by 8-OHdG and bone resorption during a period of rapid body mass reduction in female judokas. It was hypothesized that female judokas would have less oxidative DNA damage determined by quantification of 8-OHdG and bone resorption over a rapid body mass reduction period due to potential impacts of training adaptation including endogenous steroid hormonal concentration.

MATERIALS AND METHODS

Experimental design for the problem

A critical barrier to make progress on physiological research in female judo athletes is the lack of a well-designed field study (the reality of the situation before a competition) that elucidates acute and chronic alterations in oxidative stress and bone turnover parameters in the athletes who are engaged in a body mass management program. Conducting such a field study could detect practical points of a body mass management on endogenous adaptive responses. Accordingly, a repeated measures design was used in the current research experiment for each participant over a rapid body mass reduction period as it controlled for all potential sources of variability, which was statistically effective and powerful (16).

Participants

Following a screening process, a total of eighteen female athletes were enrolled in the study and participated in a competition (September 2014). The inclusion criteria were that all participants had regular menstrual cycles (ranged from 25 to 34 days) without intake of any steroid contraceptives or major medical problems (i.e., endocrine

abnormality) at the time of the study. The participants who were nationally ranked university female judokas had a judo training (aerobic and anaerobic components) volume of 12 to 15 hours per week (≥ 7 years), having competitive experience in regional and national tournaments. The weight class for each participant ranged from 48 to 70 kilograms. The range of athletes' technical levels was between 1st and 2nd Dan black belt. At the beginning of the study, all participants provided urine samples (second voided urine), followed by anthropometric measurements (height, body mass and percent body fat). The physical characteristics of the eighteen participants are as follows; age: 19.9±1.4 years, height: 161.2±4.9 cm, body mass: 67.7±17.8 kg, body mass index: 25.8±5.5 kg/m^2, body fat: 28.1±6.9 %, body surface area: 1.708±0.209 m^2. Body mass and percent body fat were digitally measured with bioelectrical impedance analysis (InBody 270, Fujitex Corporation, Tokyo, Japan) on a calibrated scale with the participants barefooted and wearing underwear. All participants continuously managed to reduce their body mass 8 days prior to a competition. This study was conducted in accordance with the guidelines proposed in the declaration of Helsinki. The experimental procedures were approved by the University Research Ethics Committee. All participants gave their written informed consent before participating in this study.

Experimental procedures

A body mass reduction period had a total of 8 days, including 7 consecutive days of judo-specific exercise training. The exercise training lasted approximately 2.5 h per day. The training for each day (Days 1-6) consisted of 20 min warm-up, 60 min judo-specific skill training (*tachiwaza* and *newaza*), 40 min combat-simulated training (*randori*), and 20 min cool-down, including a rest interspersed over the training. On Day 7 all athletes headed to the competition venue and on the same day each athlete had approximately 30 to 60 min of preconditioning light exercise. The above-mentioned judo training was identical on each day except for Day 7. Day 8 was the day of competition. During the training period at the *dojo* (the place where judo athletes have exercise training), environmental conditions were recorded in the training place every 60 min with a combination of a thermometer, hygrometer and heat stress WBGT (Wet Bulb Globe Temperature) meter (WBGT-203A, Kyoto Electronics Manufacturing Co., Ltd., Tokyo, Japan) (17). Consequently, the averaged ranges in ambient temperature, relative humidity and WBGT were 27.1±2.1°C, 56.2±4.4% and 26.7±1.6°C, respectively. The average of the training load was determined on each day based on ratings of perceived exertion (RPE) along with a 6–20 scale (18), which resulted in 16.1±2.0 (mean ± SD) (range 14-19). While food restriction diet was self-selected, all participants were asked to use the similar dietary restriction procedures during the practice period prior to the competition. The participants were also instructed to record body mass and dietary intake as accurately as possible throughout the study. Percent energy restriction was consequently calculated between Day 1 and Day 7 on the basis of the athletes' total daily caloric intake. In the present study, the compliance rate of each participant was high throughout the observation period to carry out overall assessment.

In order to reduce the variability of excreted analyte induced by diurnal rhythms, the second voided morning urine samples were collected (19) on three different days (Day 1= the beginning of body mass reduction; Day 4= mid-term of body mass reduction; Day 7= the day before the competition) for later analysis of urinary 8-OHdG as well as urinary NTx excretion. The samples were stored at –80°C.

Quantification of urinary 8-OHdG level

Urinary 8-OHdG levels were quantified by using high performance liquid chromatography (HPLC) with electrochemical detection (ECD) based on a protocol described by Nakano et al. (20). In brief, the detection of urinary 8-OHdG was performed with the two-column-switching HPLC method. The HPLC system was set up by two pumps, an autoinjector, two analytic reversed-phase columns, a column oven, a valve unit, an electrochemical detector and an integrator. The electrochemical detector was activated at +370 mV *versus* an Ag-AgCl reference electrode. The main mobile phase was processed with 1000 ml of 30 mM phosphate buffer (pH 6.9) containing ethylenediamine tetraacetic acid, disodium salt (200 mg/l) and 20.8 ml of tetrahydrofuran. During the analyzing process, 400 µl of HPLC mobile-phase was added to 100 µl of urine, which was centrifuged at 10,000 rpm for 5 min, followed by 35 µl of the mixture injected into the HPLC system.

Determination of the level of urinary cross-linked N-terminal telopeptides of Type I collagen (NTx)

One of the valid bone resorption markers, which is urinary NTx, was determined with an enzyme-linked immunosorbent assay previously demonstrated by Hanson et al. (21). This assay was performed at the basis of a monoclonal antibody (MoAb) lHll which recognizes an epitope embodied in the N-telopeptide pyridino-line cross-linking domain of human type I collagen. The epitope is uniquely enriched in bone collagen in comparison with other tissue collagens. The peptide-antigen-coated microtiter plates were utilized in the inhibition assay with incubation of MoAb lHll with buffered urine samples in the wells, followed by a goat antimouse secondary antibody conjugated to horseradish peroxidase and tetramethylbenzidine as chromogenic substrate. This assay was calibrated with standard amounts of human bone collagen digested with bacterial collagenase. Consequently, the results were determined as nmol bone collagen equivalents per mmol creatinine.

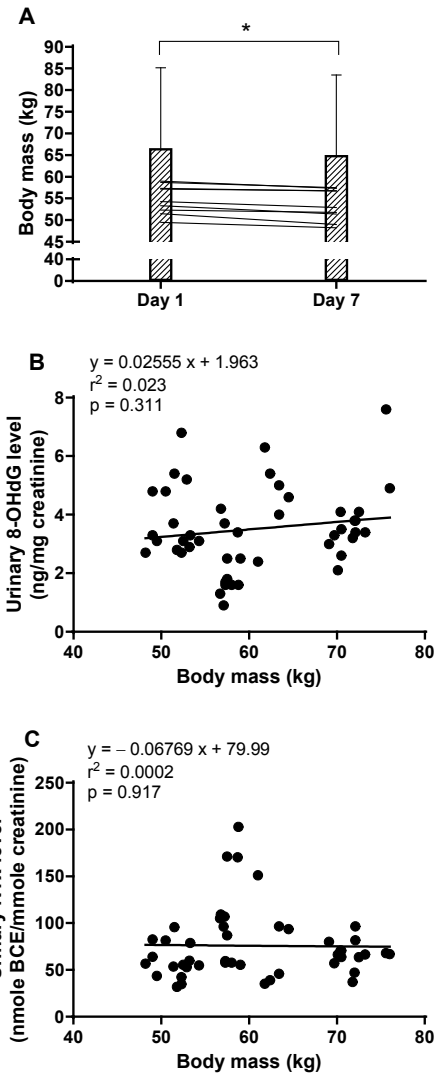

Fig. 1. *Change in body mass (kg) over an experimental period (*Significantly different from Day 1) (**A**). All data are expressed as mean ± SD. The relationship of body mass (kg) with urinary 8-OHdG (ng/mg creatinine) (**B**) and NTx (nmole bone collagen equivalents/mmole creatinine) (**C**) levels at all time points (Days 1, 4 and 7). (Day 1=the beginning of body mass reduction; Day 4=mid-term of body mass reduction; Day 7=the day before the competition)*

Measurement of 17β-estradiol level

Urinary 17β-estradiol was analyzed with radioimmunoassay as conducted by previous study (22). An aliquot of 0.5 ml of the spot urinary sample was hydrolyzed by heating with 0.075 ml of HCl for 60 min at 100°C. After 17β-estradiol were extracted with 4 ml of ether, the extract was washed with 0.5 ml of distilled water, evaporating to dryness under nitrogen. The dried extract was dissolved in 0.1 ml of benzenemethanol mixture, applying to a Sephadex LH-20 microcolumn. The column was eluted with the same solvent.

Assessment of hydration status

Urinary osmolality and specific gravity were assessed with an osmometer (OM-6060, ARKRAY, Inc., Kyoto, Japan) and a hand-held refractometer (Master-URC/Jα, ATAGO Co., Ltd., Tokyo, Japan), respectively.

Statistical analyses

A one-way analysis of variance (ANOVA) with repeated measures was used to explore any significant differences for all dependent variables by using a statistical package (Statistica V5.1, Statsoft, Tulsa, OK, USA). Moreover, a two-way repeated measure ANOVA was performed to detect any significances for percentage change in urinary biomarkers. Effect sizes for *t*-test and ANOVA were calculated with Cohen's *d* and omega-squared (ω^2), respectively. Interpretation of the effect size Cohen's *d* and ω^2 was as follows: $0.2 < d < 0.5$ = small effect, $0.5 < d < 0.8$ = medium effect, and $d > 0.8$ = large effect; $0.01 \leq \omega^2 < 0.06$ = small effect, $0.06 \leq \omega^2 < 0.14$ = medium effect, and $\omega^2 \geq 0.14$ = large effect, respectively

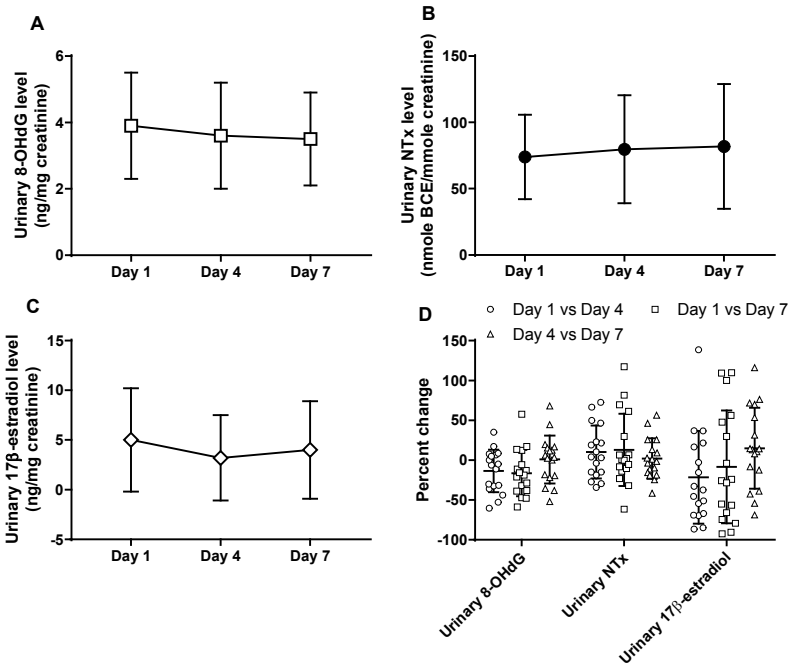

Fig. 2. *Urinary levels of 8-OHdG (ng/mg creatinine) (**A**), NTx (nmole bone collagen equivalents/mmole creatinine) (**B**) and 17β-estradiol (ng/mg creatinine) (**C**) at three different time points (Days 1, 4 and 7). The percent change in urinary 8-OHdG, NTx and 17β-estradiol levels (**D**) over a rapid body mass reduction period. All data are shown as mean ± SD. (Day 1=the beginning of body mass reduction; Day 4=mid-term of body mass reduction; Day 7=the day before the competition)*

(16). Pearson's correlation analysis was conducted between urinary 17β-estradiol, 8-OHdG and NTx levels. The overall alpha levels were set at $p < 0.05$. All data are shown as mean ± standard deviation (SD).

RESULTS

Significant reduction of body mass was observed between Day 1 and Day 7 [3.4±1.7% (mean ± SD)] with a result of relatively moderate energy restriction (< 30 %) and exercise training ($p < 0.001$, Cohen's $d = 0.12$, Fig. 1A). Regarding the relationship of body mass with urinary 8-OHdG and NTx levels, no significant correlations were found ($p = 0.311$, $r^2 = 0.023$, Fig. 1B; $p = 0.917$, $r^2 = 0.0002$, Fig. 1C, respectively).

A one-way ANOVA revealed no significant alterations in urinary 8-OHdG ($p = 0.115$, $\omega^2 = 0.13$, Fig. 2A) or NTx levels ($p = 0.427$, $\omega^2 = 0.01$, Fig. 2B) over the rapid body mass reduction period. Moreover, similar hormonal fluctuations concerning urinary 17β-estradiol levels (ng/mg creatinine) were detected ($p = 0.204$, $\omega^2 = 0.07$, Fig. 2C). With respect to percent change in urinary 8-OHdG, NTx and 17β-estradiol levels, a two-way ANOVA demonstrated no main effects for day ($p = 0.064$, $\omega^2 = 0.10$) and urinary biomarker ($p = 0.248$, $\omega^2 = 0.03$) or interaction ($p = 0.068$, $\omega^2 = 0.07$, Fig. 2D).

In terms of the relationship of urinary 17β-estradiol with urinary 8-OHdG and NTx levels, there were no significances ($p = 0.773$, $r^2 = 0.002$ for urinary 8-OHdG, Fig. 3A; $p = 0.560$, $r^2 = 0.007$ for urinary NTx, Fig. 3B, respectively). Furthermore, no significant relation was recognized between urinary 8-OHdG and NTx levels ($p = 0.917$, $r^2 = 0.033$, Fig. 3C).

Hydration status demonstrated by urinary osmolality and specific gravity was similar throughout the body mass reduction period ($p = 0.244$, $\omega^2 = 0.05$, Fig. 4A; $p = 0.248$, $\omega^2 = 0.05$, Fig. 4B, respectively). Significant correlations were noted between urinary osmolality and specific gravity in overall urine samples ($p < 0.001$, $r^2 = 0.537$, Fig.

4C). Additionally, no significant main effects for day ($p = 0.064$, $\omega^2 = 0.09$) and urinary hydration marker ($p = 0.405$, $\omega^2 = 0.01$) or interaction ($p = 0.075$, $\omega^2 = 0.09$, Fig. 4D) were represented concerning percent change in urinary osmolality and urinary specific gravity.

Practical applications

Regarding athletes' health issues, developing an appropriate body mass management program (e.g., considering 17β-estradiol concentration based on menstrual cycle phases) can result in better athletic performance (2, 13). In this regard, the results of the current study were preliminary data to explore whether the potential impact of 17β-estradiol on oxidative DNA damage and bone resorption was causative or an epiphenomenon, taking into consideration the optimal maintenance of skeletal muscle mass and bone mineral density. However, further comprehensive biochemical approaches could shed light on the effects of rapid body mass reduction associated with caloric restriction and exercise training on cellular and molecular mechanisms such as autophagy which relates to DNA oxidation accounted for by 8-OHdG output and contributes to gluconeogenesis, ß-oxidation of fatty acids and to ketone body formation during periods of energy deprivation. Accordingly, developmental cellular and molecular assessment of DNA and bone turnover in relation to oxidative stress based on biochemical markers to work in practice may offer the potential clues to advanced tactics for athletes and coaches to prepare for a competition with the practical body mass management program.

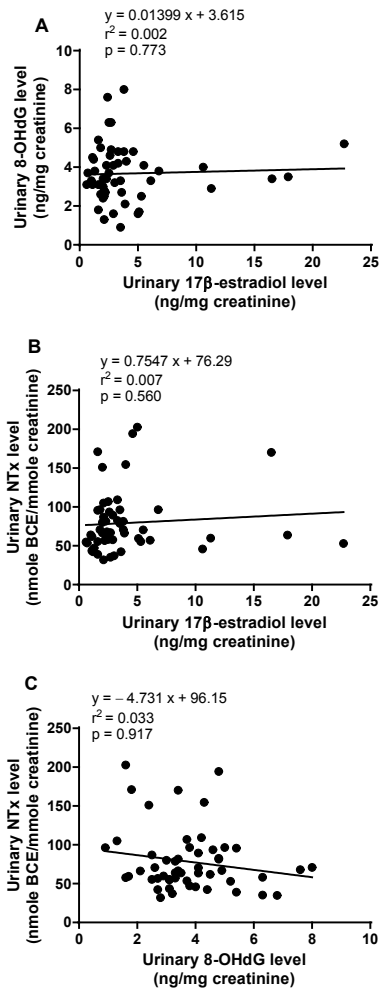

Fig. 3. *The relationship of urinary 17β-estradiol (ng/mg creatinine) with urinary 8-OHdG (ng/mg creatinine) (**A**) and NTx (nmole bone collagen equivalents/mmole creatinine) (**B**) levels and relation between 8-OHdG (ng/mg creatinine) and NTx levels (nmole bone collagen equivalents/mmole creatinine) (**C**) in urine at all time points (Days 1, 4 and 7). (Day 1=the beginning of body mass reduction; Day 4=mid-term of body mass reduction; Day 7=the day before the competition)*

DISCUSSION

The main findings of the present study were that no significant alterations were observed at the urinary 8-OHdG and NTx levels even when body mass was significantly decreased. Furthermore, urinary 17β-estradiol concentration was not significantly correlated with urinary 8-OHdG or NTx excretion. To our knowledge, this is the first study that has concurrently evaluated oxidative DNA damage determined by quantification of 8-OHdG and bone resorption, including the potential implication of 17β-estradiol levels, over a rapid body mass reduction period, combined with caloric restriction and exercise training in female judokas.

Most judokas try to restrict their diet and reduce fluid intake to fit into their weight class during short-term body mass reduction preceding their weigh-in as the weigh-in date gets closer (23). Previous data have represented a significant trend for higher-level judokas to be more aggressive in their body mass loss

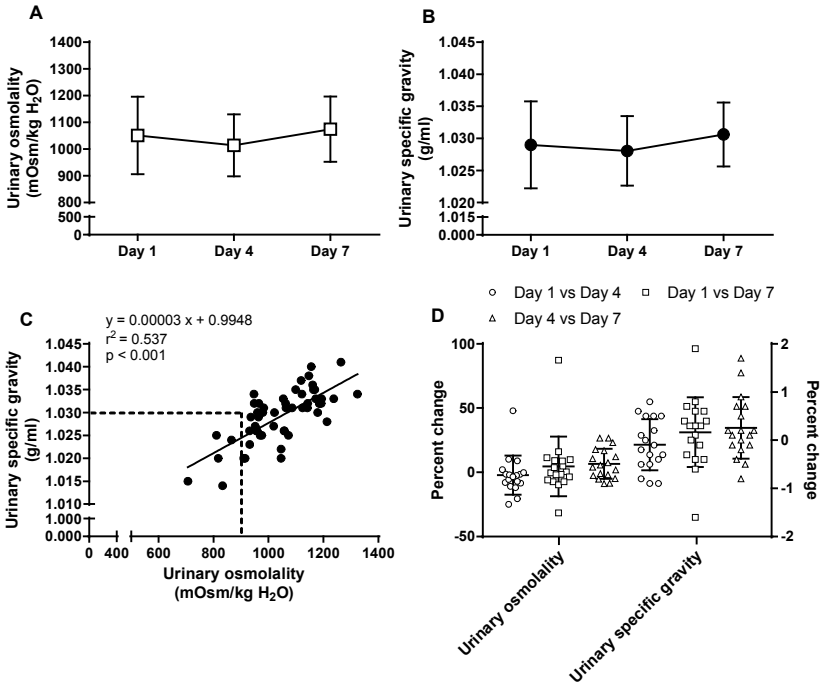

Fig. 4. *Urinary osmolality (mOsm/kg H_2O) (**A**) and urine specific gravity (g/ml) (**B**) at three different time points (Days 1, 4 and 7). All data are represented as mean ± SD. The correlation between urinary osmolality (mOsm/kg H_2O) and specific gravity (g/ml) (**C**) at all time points (Days 1, 4 and 7). The dotted lines show cutoff points for indication of adequate hydration status. The percent change in urinary osmolality and specific gravity (**D**) over a rapid body mass reduction period. (Day 1=the beginning of body mass reduction; Day 4=mid-term of body mass reduction; Day 7=the day before the competition)*

process (2). The findings of the present study also showed a significant body mass loss, which could be due to insufficient energy intake and dehydration (electrolyte losses) associated with exercise training observed in female judokas as shown by previous studies (2, 24, 25). In this respect, management of rapid body mass loss in female judokas has become a concern in considering health issues such as energy imbalance derived from eating disorders (2). Thus, the detailed eating patterns during a rapid body mass reduction period are needed to be monitored and characterized.

The mechanism by which body mass loss results in oxidative DNA damage has been unclear. For example, Lee et al. (26) found no effects of short-term fasting on oxidative stress-induced DNA damage accounted for by urinary 8-OHdG excretion in healthy women (average fasting period: 7.2 days, average percent loss of body mass: 6.3%). In addition to the aforementioned research, Finaud et al. (24) showed that energy restriction combined with intense exercise training may lead to body mass loss, increasing the antioxidant capacity of judokas before the beginning of the competition. Loft and Poulsen (27) demonstrated that body mass loss could be linked to oxidative DNA damage through increased mitochondrial production of reactive oxygen species in the cells, thereby resulting in greater magnitude of oxidative stress. The results of the current study did not show significant changes of urinary 8-OHdG excretion over a rapid body mass reduction period. It may have maintained the balance between oxidative damage and repair to DNA, which could be attributed to enhanced antioxidant defense system by a long-term judo training (aerobic and anaerobic components) as demonstrated by previous studies that regular exercise augments antioxidant capacity, upregulating antioxidative enzymes (3, 5). However, those phenomena cannot be concluded as it was not possible for us to conduct direct quantification of

any indicator of fitness level due to time and cost constraints in the present study. In this regard, the detailed relationship of antioxidant capacity with body mass reduction and exercise training is still inconclusive.

Previous data have demonstrated the effects of 17β-estradiol on oxidative DNA damage, thus implying potential disparity between follicular and luteal phases (7, 8). However, no significant relation between urinary 8-OHdG and 17β-estradiol were depicted in the present study, which is not in line with previous studies. For example, Kapiszewska et al. (7) observed endogenous DNA damage in lymphocytes with the alteration of 17β-estradiol concentration in the follicular phase in healthy young women. Moreover, Matsumoto et al. (8) noted increased trend of urinary 8-OHdG levels during the follicular phase, while there were no statistical differences. To some extent, those discrepancies with regard to the effects of 17β-estradiol on oxidative DNA damage may have been due to inter- and intra-individual variability regarding the status of endogenous antioxidant capacity. However, it remains unclear whether the potential impact of 17β-estradiol on oxidative DNA damage is causative or an epiphenomenon.

Body mass reduction has been demonstrated to result in acute as well as chronic increases in bone resorption (10). However, the certain mechanisms by which bone resorption augments remain to be determined. Because of the measurement, the cross-linked peptides largely stemmed from bone degradation, urinary NTx level, has been recognized as a more sensitive marker of bone resorption compared with previously demonstrated markers, such as hydroxyproline, pyridinoline and deoxypyridinoline (21). In addition, urinary NTx level has been shown as a more responsive marker to physical activity (11) compared to urinary pyridinoline and deoxypyridinoline levels (21). In the present study, no significant alterations were observed concerning urinary NTx level during a body mass reduction procedure with energy restriction and exercise training. One possible explanation for this phenomenon in the bone resorption marker could be due to relatively moderate energy restriction (< 30%) with the averaged percent change of –3.4±1.7 % (mean ± SD) in body mass. According to Zanker and Swaine (12), a greater magnitude of energy restriction (more than 50% for 3 days) may be needed to induce a significant bone resorption. Another plausible explanation is that the timing of urine sampling collection may not have been appropriate for detecting changes in the bone resorption markers (i.e., first or second voided morning urine *vs* 24 urine sampling). While the function of sex steroid hormones on bone remodeling balance has been demonstrated, little information about the effects of 17β-estradiol on urinary NTx is available (14). Though no significant correlations between urinary 17β-estradiol and NTx excretion were found during a rapid body mass reduction period in the present study, further investigation is warranted to explore potential mechanism to clarify.

In the current study, urinary specific gravity was significantly correlated with urinary osmolality, which was supported by previous results (28). As shown by the National Athletic Trainers' Association guidelines (29), the pre-exercise values for urine specific gravity implies that most athletes started training with the values between 1.021 and 1.030g/ml, which is regarded as a significant level of dehydration (equivalent to –3 to –5% body mass change). Some athletes initiated training in a state of serious dehydration, which is defined as urine specific gravity > 1.030g/ml, which is equal to a value for urine osmolality of more than 900 mOsm/kg H_2O (a cutoff point for indication of adequate hydration status) (29). Therefore, one possibility for the results of the current study could in part be due to a result of dehydration caused by insufficient fluid intake as a consequence of athletes' typical body mass loss practices (25). In light of the relationship between DNA oxidation and hydration status, there were significant correlations between urinary osmolality and 8-OHdG excretion in this study. However, precise causality cannot be ruled out, although dehydration condition may have led to DNA oxidation state or vice versa.

Concerning the technical considerations of the study, the second voided morning urine samples were collected to reduce the variability of excreted analyte induced by diurnal rhythms for the analysis

of oxidative stress and bone resorption in the current study (19), including hormonal and hydration status, as it was practical and feasible for the coaches, athletes and researchers (29). In line with those procedures, the application of the creatinine-adjustment has been recommended for physiological values in using spot urine compared to 12-h or 24-h urinary samples to reduce variability and avoid miscalculations (29). Especially, creatinine-adjustment for urinary 8-OHdG measurement of spot urine has been used as a valid method under certain circumstances (i.e., repeated measurements on the same individual). However, it should be considered doubtful when creatinine excretion can be thought to change in the same individual or in comparison with the different group (5). With respect to the above-mentioned information, Cheuvront et al. (30) have recently suggested the difficulty in evaluating hydration status based on spot urine concentrations. Thus, hydration condition was concurrently assessed with two urinary markers, urine specific gravity and urine osmolality, including body mass change, to establish a better determination of hydration status in the present study.

In conclusion, the results of the current study suggest that female judokas appear to have relatively less oxidative DNA damage determined by quantification of 8-OHdG and bone resorption regardless of 17β-estradiol levels during a rapid body mass reduction period, combined with energy restriction and exercise training. However, a degree of oxidative stress and bone turnover may depend on inter- and intra-individual variability related to energy deficiency, training adaptation and hormonal kinetics.

ACKNOWLEDGEMENTS

The authors express their very special thanks to all participants of the Women's Judo club at International Pacific University for their valuable collaboration and great compliance with this project. A part of the data was presented at the Integrative Biology of Exercise VII (2016 American Physiological Society Intersociety Meeting), Phoenix, Arizona, U. S. A. This work was supported in part by the International Pacific University Research Foundation (grant number 2015-09 to N. Y.) and Ryobi Teien Memorial Research Foundation (grant number 2016-I-20 to N. Y.).

REFERENCES

1. Kowatari K, Umeda T, Shimoyama T, Nakaji S, Yamamoto Y, Sugawara K. Exercise training and energy restriction decrease neutrophil phagocytic activity in judoists. Med Sci Sports Exerc 2001; 33:519-24.
2. Artioli GG, Gualano B, Franchini E, Scagliusi FB, Takesian M, Fuchs M, Lancha AH, Jr. Prevalence, magnitude, and methods of rapid weight loss among judo competitors. Med Sci Sports Exerc 2010; 42:436-42.
3. Radak Z, Zhao Z, Koltai E, Ohno H, Atalay M. Oxygen consumption and usage during physical exercise: the balance between oxidative stress and ROS-dependent adaptive signaling. Antioxid Redox Signal 2013; 18:1208-46.
4. 4. Pittaluga M, Parisi P, Sabatini S, et al. Cellular and biochemical parameters of exercise-induced oxidative stress: relationship with training levels. Free Radic Res 2006; 40:607-14.
5. Yasuda N, Bolin C, Cardozo-Pelaez F, Ruby BC. Effects of repeated bouts of long- duration endurance exercise on muscle and urinary levels of 8-hydroxy-2'-deoxyguanosine in moderately trained cyclists. J Sports Sci 2015; 33:1692-701.
6. Kasai H, Nishimura S. Hydroxylation of deoxyguanosine at the C-8 position by ascorbic acid and other reducing agents. Nucleic Acids Res 1984; 12: 2137-45.
7. Kapiszewska M, Kalemba M, Grzesiak A, Kocemba K. The level of endogenous DNA damage in lymphocytes isolated from blood is associated with the fluctuation of 17beta-estradiol concentration in the follicular phase of healthy young women. Acta Biochim Pol 2005; 52:535-39.
8. Matsumoto Y, Ogawa Y, Yoshida R, Shimamori A, Kasai H, Ohta H. The stability of the oxidative stress marker, urinary 8-hydroxy-2'-deoxyguanosine (8-OHdG), when stored at room temperature. J Occup Health 2008; 50:366-72.
9. Hofer T, Fontana L, Anton SD, Weiss EP, Villareal D, Malayappan B, Leeuwenburgh C. Long-term

effects of caloric restriction or exercise on DNA and RNA oxidation levels in white blood cells and urine in humans. Rejuvenation Res 2008; 11:793-99.
10. Prouteau S, Pelle A, Collomp K, Benhamou L, Courteix D. Bone density in elite judoists and effects of weight cycling on bone metabolic balance. Med Sci Sports Exerc 2006; 38:694-700.
11. Iwamoto J, Takeda T, Ichimura S. Relationships among physical activity, metacarpal bone mass, and bone resorption marker in 70 healthy adult males. J Orthop Sci 2002; 7:6-11.
12. Zanker CL, Swaine IL. Responses of bone turnover markers to repeated endurance running in humans under conditions of energy balance or energy restriction. Eur J Appl Physiol 2000; 83: 434-40.
13. Devlin MJ, Stetter CM, Lin HM, Beck TJ, Legro RS, Petit MA, Lieberman DE, Lloyd T. Peripubertal estrogen levels and physical activity affect femur geometry in young adult women. Osteoporos Int 2010; 21:609-17.
14. Balasch J. Sex steroids and bone: current perspectives. Hum Reprod Update 2003; 9:207-22.
15. Morris FL, Payne WR, Wark, JD. The impact of intense training on endogenous estrogen and progesterone concentrations and bone mineral acquisition in adolescent rowers. Osteoporos Int 1999; 10:361-68.
16. Kirk RE. Effect magnitude: a different focus. J Stat Plan Inference 2007; 137:1634-46.
17. Brake DJ, Bates GP. Fluid losses and hydration status of industrial workers under thermal stress working extended shifts. Occup Environ Med 2003; 60:90-96.
18. Borg G. Perceived exertion as an indicator of somatic stress. Scand J Rehabil Med 1970; 2:92-98.
19. Jung K. Enzyme activities in urine: how should we express their excretion? A critical literature review. Eur J Clin Chem Clin Biochem 1991; 29:725-29.
20. Nakano M, Kawanishi Y, Kamohara S, et al. Oxidative DNA damage (8-hydroxy- deoxyguanosine) and body iron status: a study on 2507 healthy people. Free Radic Biol Med 2003; 35:826-32.
21. Hanson DA, Weis MA, Bollen AM, Maslan SL, Singer FR, Eyre DR. A specific immunoassay for monitoring human bone resorption: quantitation of type I collagen cross-linked N-telopeptides in urine. J Bone Miner Res 1992; 7:1251-58.
22. Tominaga T, Tei N, Kitamura M, Taguchi T, Kudo Y. Urinary excretion of steroids by Japanese women with breast cancer. Gan 1975; 66:305-10.
23. Khodaee M, Olewinski L, Shadgan B, Kiningham RR. Rapid weight loss in sports with weight classes. Curr Sports Med Rep 2015; 14:435-41.
24. Finaud J, Degoutte F, Scislowski V, Rouveix M, Durand D, Filaire E. Competition and food restriction effects on oxidative stress in judo. Int J Sports Med 2006; 27:834-41.
25. Papacosta E, Nassis GP, Gleeson M. Effects of acute postexercise chocolate milk consumption during intensive judo training on the recovery of salivary hormones, salivary SIgA, mood state, muscle soreness, and judo-related performance. Appl Physiol Nutr Metab 2015; 40:1116-22.
26. Lee KH, Bartsch H, Nair J, Yoo DH, Hong YC, Cho SH, Kang D. Effect of short-term fasting on urinary excretion of primary lipid peroxidation products and on markers of oxidative DNA damage in healthy women. Carcinogenesis 2006; 27:1398-403.
27. Loft S, Poulsen HE. Cancer risk and oxidative DNA damage in man. J Mol Med 1996; 74:297-312.
28. Fernández-Elías VE, Martínez-Abellán A, López-Gullón JM, Morán-Navarro R, Pallarés JG, De la Cruz-Sánchez E, Mora-Rodriguez R. Validity of hydration non-invasive indices during the weightcutting and official weigh-in for Olympic combat sports. PLoS One 2014; 9: e95336.
29. Casa DJ, Armstrong LE, Hillman SK, et al. National athletic trainers' association position statement: fluid replacement for athletes. J Athl Train 2000; 35:212-24.
30. Cheuvront SN, Kenefick RW, Zambraski EJ. Spot urine concentrations should not be used for hydration assessment: a methodology review. Int J Sport Nutr Exerc Metab 2015; 25:293-97.

GENDER AND AGE-RELATED VARIABILITY OF MACROPHAGE REPRESENTATION IN THE INTERNAL THORACIC ARTERY WALL: DOES IT MATTER?

B. PEREK[1], K. KOWALSKA[2], B. KEMPISTY[2,3,4], M. NOWICKI[2], M. DYSZKIEWICZ-KONWIŃSKA[3], M. PUŚLECKI[1,5], D. OSTALSKA-NOWICKA[6], M. JEMIELITY[1], M. JANKOWSKI[3], M.J. NAWROCKI[3] and A. MALIŃSKA[2,7]

[1]Department of Cardiac Surgery and Transplantology, Poznan University of Medical Sciences, Poznan, Poland; [2]Department of Histology and Embryology, Poznan University of Medical Sciences, Poznan, Poland; [3]Department of Anatomy, Poznan University of Medical Sciences, Poznan, Poland; [4]Department of Obstetrics and Gynecology, University Hospital and Masaryk University, Brno, Czech Republic; [5]Department of Medical Rescue, Poznan University of Medical Science, Poznan, Poland; [6]Department of Pediatric Cardiology and Nephrology, Poznan University of Medical Science, Poznan, Poland; [7]Department of Anatomy and Histology, Faculty of Medicine and Health Sciences, University of Zielona Gora, Poland

Received March 9, 2018 – Accepted June 12, 2018

Some recent reports suggested that elderly and female patients did not benefit from implantation of the second internal thoracic artery (ITA) during coronary artery bypass surgery (CABG). Macrophages, among other cells, were described to be involved in both atherosclerosis and aortocoronary grafts failure. The aim of the study was to examine the age and gender association with different distribution of $CD68^+$ cells within the layers of ITA wall. This study involved 158 consecutive patients (95 male and 63 female), with the mean age of 64.5±9.5 years, who underwent elective CABG procedures. During surgery, the surplus distal segments of ITA were harvested for immunohistochemical analysis. The number and distribution of $CD68^+$ cells was calculated and plotted against the age and gender of the study participants. $CD68^+$ cells were present in all of the harvested ITA fragments (median 44), more in women (55) than in men (42) ($p<0.001$). However, this difference was of statistical significance exclusively in the *tunica intima*. Approximately 70% of macrophages were found in the tunica adventitia. The total number of $CD68^+$ cells the in arterial wall as well as in the *tunica intima* and *adventitia* correlated positively with the age of patients ($r=0.544$, $r=501$ and $r=0.462$, respectively). The lack of significant advantages of the use of two thoracic arteries, in elderly patients and women, might have resulted from the larger population of $CD68^+$ cells in their walls, especially the *tunica intima*. However, this result from immunohistochemical analysis needs validation in long-term clinical research on a larger cohort of patients.

Coronary artery bypass grafting (CABG) is a method of choice in treatment of diffuse coronary artery disease (CAD) to achieve alleviation of anginal pain and notable increase in functional capacity (1). Many years ago, it was established that the gold standard for CABG procedures was implantation of the left internal thoracic artery (LITA) to the left anterior descending artery (LAD) (2, 3). This strategy was proven to be optimal, in terms not only of clinical improvement, but also long-term, favorable angiographic outcome

Key words: coronary surgery, internal thoracic artery, macrophages, ageing, women

Mailing address:
Bartosz Kempisty, PhD,
Department of Histology and Embryology,
Department of Anatomy, Poznań University of Medical Sciences,
6 Święcickiego St., 60-781 Poznań, Poland
Tel./Fax: +48 61 8546418/8546440
e-mail: bkempisty@ump.edu.pl

0393-974X (2018)
Copyright © by BIOLIFE, s.a.s.
This publication and/or article is for individual use only and may not be further reproduced without written permission from the copyright holder.
Unauthorized reproduction may result in financial and other penalties
DISCLOSURE: ALL AUTHORS REPORT NO CONFLICTS OF INTEREST RELEVANT TO THIS ARTICLE.

(3). It is estimated that approximately 90% of those grafts function appropriately, many years after primary surgery (4–6). Thus, the next step was to find optimal grafts, to improve myocardial perfusion through the other coronary areas (7, 8). The natural clinical scenario was more common application of the second arterial graft (ie, right internal thoracic artery, RITA) (9). Interestingly, while outcomes of the observations, performed at several independent surgical centers, showed additional benefits from bilateral internal thoracic artery (ITA) implantation, an international, multicenter Arterial Revascularization Trial (ART) study failed to confirm previous findings (10, 11). Other reports stressed that the largest clinical beneficiaries of CABG procedures with bilateral ITA grafts were young and male patients (12, 13). Mohammadi et al. showed that the additional survival benefit of using a second ITA decreased gradually with age, and was lost after the age of 60 (12). Attia and colleagues proved that although bilateral ITA grafting was associated with better survival than single ITA grafting, it was less effective in women (13).

To date, many studies have been carried out to find cells and molecules, of paramount importance in atherosclerosis development in the grafts, eventually leading to their complete obstruction. The key pathogenic feature of lesions, at this early stage of atherosclerosis, is the maturation of monocytes, which migrate into arteries to form foam cells or lipid-laden macrophages (14). They can be identified by the expression of CD68, a glycoprotein that binds to low-density lipoprotein (15). Previously, our team proved that the patients with CD68- positive cells in the *tunica intima* of saphenous vein grafts had a significantly higher number of graft stenoses than the subjects without them in this vascular layer (16). Moreover, it was shown that arteries, even with ITA applied as aortocoronary grafts, undergo age-related changes that can be the cause of ongoing atherosclerosis, such as increase in thickness of the *tunica intima* as well as degeneration of the elastic skeleton (17). Pre-existing morphological changes in the ITA segment, prior to the implantation to the coronary artery of the recipient, may predispose to its preterm failure and unfavorable long-term outcome.

The main purpose of this study was to examine whether age and gender, that may have negative impact on long-term outcomes of CABG with ITA grafts, are associated with different distribution of $CD68^+$ cells within the layers of ITA wall.

MATERIALS AND METHODS

Patients

This study involved 158 consecutive patients [(95 male (60.1%) and 63 female (39.9%)] with the mean age of 64.5±9.5 years (range 41-86 years) with diffuse CAD who underwent elective CABG procedures in the years 2008 and 2010. The most important preoperative data are outlined in Table I. The study was approved by Local Bioethics Committee (No. 1201/08 and 385/12). Each study participant signed informed consent to donate a surplus distal segment of ITA harvested intraoperatively.

Material preparation

During CABG procedure, the surplus distal segments of ITA (approximately 1 cm long) were harvested with their surrounding tissue (a pedicle technique) for immunohistochemical analysis. All the vessel samples were fixed in Bouin's solution, embedded in paraffin and cut into 5-6 μm thin cross sections by semiautomatic rotation microtome (Leica RM 2145, Leica Microsystems, Nussloch, Germany).

Immunohistochemical analysis

All the immunohistochemical analyses employed the StreptABComplex/HRP method modified by addition of biotinylated tyramine (Dako Catalyzed Signal Amlification System, Peroxidase, K1500, Dako, Copenhagen, Denmark). The preparation for analyses was previously described in detail (16). Eventually, sections were incubated with monoclonal anti-CD68 antibody (dilution 1:100, M0814, Dako). Additionally, an eliminating assay with following specific antibodies for lymphocyte subpopulations such as anti-CD20cy (1:400 dilution, M0755, Dako), anti-CD3 (1:50 dilution, M7254, Dako), anti-CD8 (1:100 dilution, M7103, Dako) and anti-CD30 (1:40 dilution, M0751, Dako) was carried out.

Samples, prepared in that way, were observed, with their immunohistochemical reactions analyzed under brightfield microscope-Olympus BX 50 (OLYMPUS Optical Europe, Germany) equipped with Mirax-Midi

scanner (Carl Zeiss Microlmaging GmbH, Germany), coupled with Pannoramic Viewer, version 1.15.4, software (3DHISTECH Ltd., Budapest, Hungary).

Immunohistochemical expression of CD68, the macrophage specific protein, was analysed on transverse sections of the blood vessels. Firstly, the number of cells expressing this antigen throughout the vessel wall was analysed, followed by the analysis of specific sections, the *tunica intima,* the *tunica media and* the *tunica adventitia.* Additionally, the diameters of the $CD68^+$ cells were calculated using immersion magnification (100x). For every segment of ITA analysed, at least 10 sections were considered, with the results contributing to a sample average.

Immunohistochemical evaluation of protein expression was carried out by two experienced histologists, through blind sample analysis, based on encoded numbers corresponding to the basic rules of positive and negative control. The negative controls were carried out in the same way as in the experimental sample, with the exclusion of primary antibody, replaced with normal mouse serum or PBS.

Electron microscopy

For transmission electron microscopy (TEM), ITA samples were fixed in 2.5% glutaraldehyde in phosphate buffer (0.05 M, pH 7.4) and then prepared in steps described previously (16). Eventually, ultrathin sections were mounted on mesh nickel grids, counterstained with uranyl acetate and lead citrate and examined using a JEM-1010 (JEOL, Tokyo, Japan) transmission electron microscope. In TEM, typical ultrastructural features of macrophages were assessed. Special attention was paid to cell membrane and cytoplasmic organelles.

Postoperative period and assessment of clinical results

After surgery, patients were treated at the Intensive Postoperative Care Unit (IPCU) for 24-48 hours then they were referred to a surgical ward. In this period special attention was paid to any signs of ischemia in the electrocardiography and laboratory studies (creatine kinase isoenzyme MB (CK-MB), troponin I). Just before discharge, echocardiography was performed and new regional disturbances in regional myocardial contractility were recorded. Following hospitalization, CABG subjects were usually transferred to the rehabilitation centers.

All patients were followed-up in the outpatient clinic and regular clinical and electrocardiographic assessments were performed. If they reported recurrence or deterioration of coronary artery disease symptoms, they were transferred to the catheterization laboratory for the check-out coronary angiography. All native vessels and implanted aortocoronary bypass grafts were carefully analyzed.

Data management and statistical analysis

Before the analysis, continuous variables were tested with Shapiro-Wilk test, in order to determine their coherence to the normal distribution. If their distribution fitted the normal distribution criteria, they were presented as a mean ± standard deviation. Continuous variables, with distribution different than normal (e.g. percentage of $CD68^+$ cells in specific layers of vessels) were shown as a median (25^{th} percentile, 75^{th} percentile). Categorical variables (including dichotomic variables), were shown as numbers with their contribution in percentage (n %). They were compared (male *vs* female patients) by means of Yates corrected *chi*-squared test, whereas multiple range test was used to compare the number of $CD68^+$ cells in different ITA layers. Correlation of the brightfield analysis results and the age of patients undergoing the procedure, was tested with the Pearson correlation test (for continuous variables in normal distribution). The degree of correlation was interpreter with the use of a scale suggested by Salkin, where r value between 0.8 and 1.0 (or -0.8 and -1.0) indicated strong correlation, between 0.6 and 0.8 medium correlation and between 0.4 to 0.6 low, or no correlation. Probability of survival was estimated according to the Kaplan-Meier curves.

P value less than 0.05 was taken as statistically significant. The analysis was carried out with Statistica 10.0 Package for Windows (StatSoft, Inc., Tulsa, OK, USA).

RESULTS

Overall number of $CD68^+$ cells

Presence of $CD68^+$ cells was confirmed in all of the collected arterial samples, with their numbers between 4 and 95 (median 44 (24; 60). Morphological features of $CD68^+$ cells, such as a diameter exceeding 20 μm, as well as applied eliminating assay for lymphocytes (see Methods section) enabled to identify these cells as macrophages.

The study of correlation between patient age and total number of $CD68^+$ cells in transverse sections of ITA walls is directly proportionate, with intermediate correlation efficient (r=0.554) (Figs. 1 and 2). Moreover, median (25th percentile; 75th percentile) of $CD68^+$ cell number in transverse sections of female vessels [55 (41; 76)] was significantly higher than in those collected from males (42 (21; 50))($p<0.001$).

Distribution of $CD68^+$ cells

In the segments of ITA, approximately 70% of macrophages were found in the *tunica adventitia*.

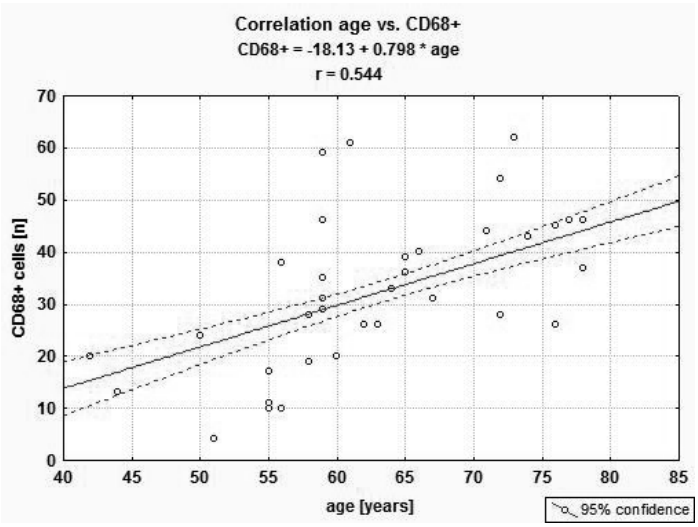

Fig. 1. *Correlation between the age of CABG patients and overall number of $CD68^+$ cells in the cross-sections of ITA.*

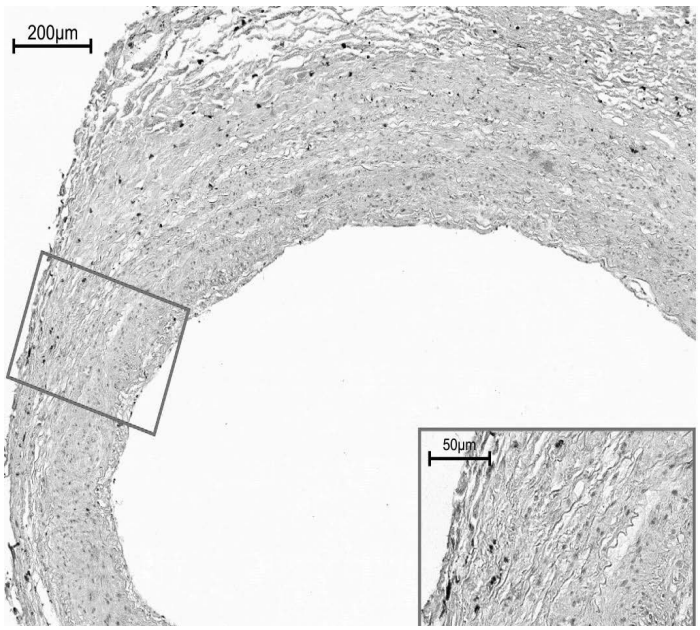

Fig. 2. *Cross-section showing CD68 immunostaining of ITA. The ITA segment was obtained from a 74-year-old man. $CD68^+$ cells were seen only in the tunica media and tunica adventitia.*

The detailed data regarding distribution of $CD68^+$ cells is outlined in Table II. Multiple range analysis showed that the number of cells was significantly lower in the *tunica intima* and *media*.

Closer analysis also showed that the sections in which there was no observable presence of $CD68^+$ cells in the inner membrane of IMA came from significantly younger patients (55.0±10.1 years old) than those samples harvested which exhibited the presence of $CD68^+$ cells (62.8±9.2 years old). The total number of cells in the *tunica intima* of IMA, showed significant correlation with the age of

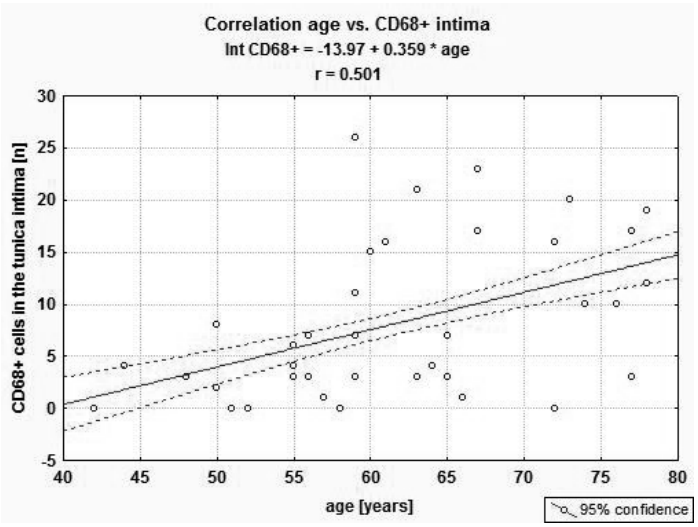

Fig. 3. *Correlation between age of CABG patients and the number of macrophages within the tunica intima of ITA.*

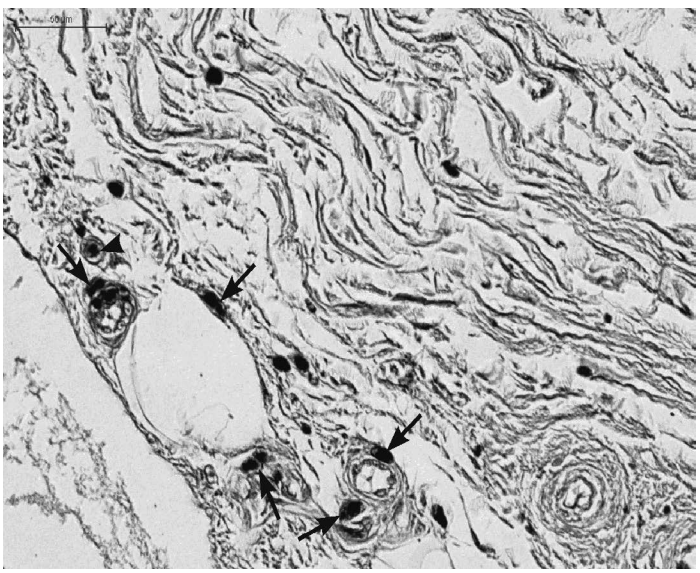

Fig. 4. *Typical localization of $CD68^+$ cells in the tunica adventitia of ITA. Most CD68-postitve cells were noted in the proximity of the tunica adventitia vessels (vasa vasorum, arrows) or within their lumen (arrowhead).*

patients (r=0.501; p<0.05) (Fig. 3).

CD68+ positive cells were present in the *tunica media* of 141 IMA transverse sections (89.2%). Patients who did not exhibit CD68+ cell presence were significantly younger (55.3±3.4 years old) than those who showed the presence of those cells (62.3±9.9 years old; p<0.001). Despite that, the analysis of age correlation showed very weak correlation between the number of CD68+ cells in the *tunica media* of IMA and the age of patients (r=0.208; Spearman R test)

CD68+ cells were present in all of the sample sections, in the region of the *tunica adventitia*. The biggest concentration of those cells occurred in the nearest proximity of *vasa vasorum* (Fig. 4). The absolute number of CD68+ cells in the *tunica*

Table I. *The most important preoperative data in male and female patients.*

Variable[1]	Males N=95	Females N=63
Obesity (BMI > 30)	**30 (31.6)**	**32 (50.8)***
Arterial hypertension	67 (70.5)	36 (57.1)
Diabetes treated with insulin	**18 (18.9)**	**23 (36.5)***
Hypelipidemia	38 (40.0)	25 (39.7)
Renal failure[2]	11 (11.6)	7 (11.1)
Neurological events before surgery[3]	10 (10.5)	2 (3.2)
Active smokers	50 (52.6)	30 (47.6)

** P < 0.05 females vs males*

[1]variables are expressed as the numbers (n) and percentages; [2]defined as glomerular filtration rate was below 60mL/min/1,73m²; [3] included transient ischemic attacks (TIAs) and central nervous system strokes. BMI: body mass index.

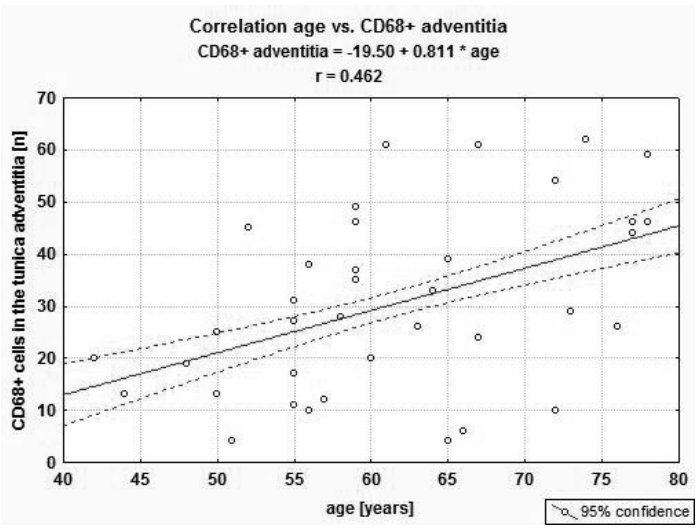

Fig. 5. *Correlation between the age of CABG subjects and the number of CD68+ cells in the tunica adventitia of ITA.*

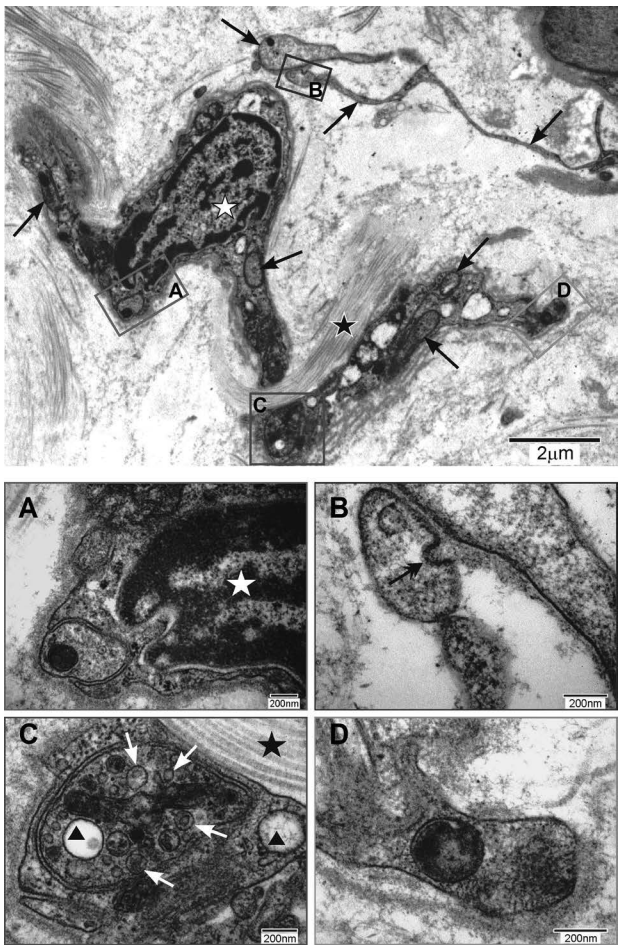

Fig. 6. *Microelectrophotography of the subendothelial layer of ITA. In the subendothelial layer of ITA, a cell of characteristics proprietary for macrophages is present. In numerous cytoplasmic protrusions (arrows), clathrin-coated vesicles, constructed from cellular membrane, can be observed (**B**, double headed arrow). Large nucleus of irregular outline is located centrally (white star). Cytoplasm, rich in polysomes, contains numerous vesicles of varying electron density (frame C-white arrows), as well as vacuoles (**C** – triangles). The presence of lysosomes (**A**) and phagocytic vacuoles (**D**) is an ultrastructural indicator of macrophages' phagocytic activity. Collagen fibres in longitudinal section were indicated by a black star.*

adventitia of IMA increased together with patient age (r=0.462; p<0.05) (Fig. 5).

CD68⁺ cell in female ITA segments

In all of the analysed vessels harvested from female patients, CD68⁺ cell presence was confirmed throughout the layers, with the biggest amount always present in the *tunica adventitia.* When comparing the number of those cells between the sexes, the only significant variation was observed in the *tunica intima* (Table III).

In the *tunica intima* and *tunica media*, there were cells equipped with ultrastructures typical for macrophages with pronounced phagocytic activity (Fig. 6). Folded cellular membrane with irregular outline forms various cytoplasmic protrusions, inside which numerous caveolae and clathrin-coated vesicles are present. The cytoplasm, rich in cellular organelles, contained both vesicles of varying electron density and non-membranous aggregations of electron-dense material. Lysosomes, both primary and mature, were also observed in the cytoplasm, showing significant heterogeneity of size and shape. Sizable phagocytic vacuoles were also present. Large, euchromatin nuclei of irregular outline were positioned centrally in the cytoplasm. In the nucleus, presence of one or two nucleoli was determined.

In-hospital and late outcomes

All patients enrolled in the study survived the early postoperative period. In 8 CABG subjects any symptoms and signs of myocardial ischemia were noted. However, in the emergent angiography no cases of left internal mammary occlusion or stenosis were diagnosed. Five of them had critical stenoses of non-bypassed coronary arteries while in the others venous aortocoronary grafts were occluded.

The mean follow-up lasted 6.5±1.7 years and was completed by 97.5% of patients (154/158). From those 154 subjects, in which the follow-up was completed, 12 (7.8%) died throughout this period, including seven because of cardiac reasons [acute coronary syndrome (n=5) and progressive congestive heart failure (n=2)]. The one-, three- and five-year probability of survival following CABG was 96.7±1.3%, 95.2±1.7% and 93.3±1.9%, respectively (Fig. 7).

Check-out coronary angiography was necessary in 22 patients whereas only in 3 of them significant lesions (obstructing more than 70% of the vessel lumen) in the ITA were found. Two of them were females (70 and 72 years old at the time of operation) and one a 77-year-old man. A total number and distribution of CD68⁺ cells are presented in Table IV. Due to a small

Table II. *Number and distribution of CD68⁺ cells in the layers of ITA.*

Vascular layers	Absolute number	Rate
Tunica intima	5 (3, 14)#	0.13 (0.03, 0.16)
Tunica media	4 (2, 9)	0.17 (0.06, 0.22)
Tunica adventitia	28 (18, 45)*	0.69 (0.56, 0.80)*

#variables are expressed as a median (25th percentile, 75th percentile); *p<0.001 *tunica adventitia vs tunica media/intima.*

Table III. *Number of CD68⁺ cells in the layers of ITA in men and in women.*

CD68⁺ cells number# Vascular layers	Men [n=95]	Women [n=63]
Tunica intima	**4 (3, 11)**	**10 (3, 17)***
Tunica media	4 (2, 9)	5 (2, 13)
Tunica adventitia	27 (17, 39)	35 (20, 42)

*#variables are expressed as a median (25th percentile, 75 percentile); *p<0.05 male vs female patients*

Table IV. *Total number and distribution of CD68⁺ cells in ITA segments harvested from patients who had ITA graft occlusion in check-out angiography.*

	Female, 70-y	Female, 72-y	Male, 77-y
Total number	64	72	61
Tunica intima [n (rate)]	16 (0.25)	20 (0.28)	18 (0.30)
Tunica media [n (rate)]	18 (0.28)	21 (0.29)	17 (0.28)
Tunica adventitia [n (rate)]	30 (0.47)	31 (0.43)	26 (0.42)

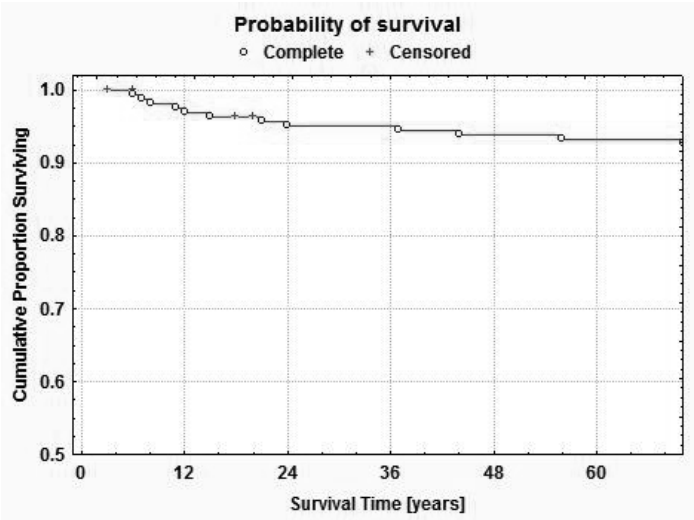

Fig. 7. *Probability of survival after CABG.*

number of patients with significant lesions in ITA, no statistical analysis was possible. However, a total number of CD68-postive cells as well as number and rate of them in the *tunica intima* and the *tunica media* were higher than medians for the whole group.

DISCUSSION

Macrophages located in the wall of blood vessels participate, though not alone, in the manufacturing processes of neointima and atherosclerotic plaques. It was previously proven in the SV studies, that their location in the inner membranes, not their total number, is a factor of the most unfavourable prognosis (16). The authors of the current study have found no reports of the number and placement of macrophages in the wall of ITA. The most important result of this study is that the age and sex correlate with the number and distribution of macrophages, which may account for the clinical results mentioned earlier (12, 13). The value of these findings would be even more significant, if they were used as a reference and related to clinical trials. However, in the case of ITA it is very difficult, as few of the bypasses that use this graft show the characteristics of atherosclerotic degeneration and, if so, they occur after many years. Therefore, to carry out such study is practically impossible as the present study was performed in just one cardiac surgical centre.

Monocytes and later macrophages can penetrate the vessel wall from the direction of the vessel lumen as well as *vasa vasorum*. One of the most characteristic features of the ITA which can affect its resistance to atherosclerosis, is the fact that its internal elastic lamina is tight and forms a barrier, much more difficult to overcome than that of other vessels routinely used in coronary bypass surgeries, such as the radial artery or the greater saphenous vein (18). On the other hand, *vasa vasorum* penetrate the medial venous vascular membrane while in the arteries they do not reach it (19).

Increase in the number of $CD68^+$ cells with ageing of CABG subjects is a novel observation of the current study. So, do older people (e.g. after the age of 70) with more $CD68^+$ cell population have a higher risk of failure of even such grafts as ITA? Today, there is no hard scientific evidence resulting from the analysis of clinical trials that could confirm the present observations, although there are individual indications that the elderly are not the beneficiaries of the use of two internal thoracic arteries (12). If, on the other hand, we assume that the macrophages in the vascular wall, regardless of the type of vessel, are a result of repeated microlesions (20), the fact that older people exhibit

higher number of $CD68^+$ cells should not be a surprise. This could explain why the number of $CD68^+$ cells in the *tunica media* correlated directly to the age of the patients. In addition, there is also scientific evidence from ITA autopsy studies which indicates an ageing-dependent change in its histological structure (21). Elastic laminae which are a barrier to migrant cells (22) are not overly persistent and are subject to age changes. With age, there are increasing numbers of fenestrations (seen in people over 60 years of age) with the mean number of elastic laminae decreasing (23). To date, very few cases of atherosclerosis in the wall of ITA have been described and, if it was present, was always accompanied by damage and fragmentation of the elastic laminae (24). Therefore, there are indications that the wall of ITA in the elderly becomes more permeable for cells and thus more susceptible to the formation of plaques. The current observation indicating a greater number of $CD68^+$ cells in the *tunica media* of the ITA with age may be a confirmation of the post-mortem research reports quoted above (21). Of course, the reference of this observation to clinical and angiographic results is very difficult, since after 20 years, more than 90% of the ITA grafts are still not obstructed. Hence, the obstruction of these kind of bypasses, even many years after the surgery, is not a common clinical problem. In addition, many older subjects of CABG do not survive (often not due to cardiac issues) long enough to exhibit possible obstruction of the ITA bypass.

Numerous clinical studies on the assessment of surgical CAD treatment indicate much worse results in women. This applies not only to survival in long-term observation but also to serious adverse events (13, 25, 26). This could be explained in many ways. Women treated with CABG are generally older than men (27). Moreover, they are a high-risk group with numerous co-morbidities (28). Presenting less common symptoms, CAD is often diagnosed and treated in its later stages (29, 30). Finally, it was proven that females had much smaller coronary arteries than males, even after taking mass, or surface of the body into account. It cannot be excluded that a larger representation of the $CD68^+$ cells in the wall of the bypass, especially in the inner membrane, before their implantation is one of the possible factors responsible for the earlier bypass failure and worse clinical outcomes in females. Furthermore, the fact that women subjected to CABG and qualified for the current study were older than men cannot be omitted. As previously mentioned, the number of $CD68^+$ cells in the wall of the ITA increases with age.

Our group's research has confirmed the validity of the current trend, that arterial bypasses, especially using the ITA, should be used commonly in CABG treatments, especially in young people (31, 32). The representation of macrophages, important cells involved in degenerative processes, is the smallest in the younger population, with their especially low population present in the *tunica intima*.

The aim of CABG surgery is a good, long-term, clinical result supported by imaging studies that show patency of the bypass several years after the operation. There are indications that this goal may be achieved with the use of ITA. Subjects with $CD68^+$ cells present only in the *tunica adventitia* of the ITA were not rare and were younger than those who exhibited presence of those cells in layers located closer to the lumen of the vessel. In the future, it would be ideal to trace the natural history in patients with and without the $CD68^+$ cells of the *tunica media* and *intima* of the ITA

We are aware of the limitations of our study. Either age- or gender-based results are univariate observations with their obvious disadvantages. It is possible that the observed differences in cell counts are also attributed to factors other than gender alone, but it would be difficult to prove this. Moreover, only 3 patients reached angiographic end-point (occlusion of ITA graft throughout the follow-up period). Thus, it was not possible to compare the results of histological study. Additionally, check-out coronary angiography was performed only on patients with obvious clinical deterioration. We cannot exclude that asymptomatic patients (ie., without anginal pain), particularly those with insulin-treated diabetes, had also exhibited ITA occlusion.

More abundant population of $CD68^+$ cells in

the walls of ITA, especially in the *tunica intima*, among women and elderly patients might be one of the causes for the lack of significant advantage of the use of that artery in CABG in these groups. However, this result of immunohistochemical analysis needs to be validated with long-term clinical studies on a larger cohort of patients

ACKNOWLEDGEMENTS

This study was supported by grant No. 5958/B/P01/2010/38 from the State Committee for Scientific Research, Poland,

REFERENCES

1. Banning AP, Westaby S, Morice M-C, et al. Diabetic and nondiabetic patients with left main and/or 3-vessel coronary artery disease. J Am Coll Cardiol 2010; 55(11):1067-75.
2. Lytle BW, Loop FD, Cosgrove DM, Ratliff NB, Easley K, Taylor PC. Long-term (5 to 12 years) serial studies of internal mammary artery and saphenous vein coronary bypass grafts. J Thorac Cardiovasc Surg 1985; 89(2):248-58.
3. Cooper GJ, Underwood MJ, Deverall PB. Arterial and venous conduits for coronary artery bypass. A current review. Eur J Cardiothorac Surg 1996; 10(2):129-40.
4. Chow MS, Sim E, Orszulak TA, Schaff H V. Patency of internal thoracic artery grafts: comparison of right versus left and importance of vessel grafted. Circulation 1994; 90(5 Pt 2):II129-32.
5. Gansera B, Schmidtler F, Angelis I, Kiask T, Kemkes B, Botzenhardt F. Patency of internal thoracic artery compared to vein grafts - postoperative angiographic findings in 1189 symptomatic patients in 12 years. Thorac Cardiovasc Surg 2007; 55(7):412-17.
6. Raza S, Blackstone EH, Houghtaling PL, et al. Influence of diabetes on long-term coronary artery bypass graft patency. J Am Coll Cardiol 2017; 70(5):515-24.
7. Cooper GJ, Underwood MJ, Deverall PB. The lima success story--whither other arterial grafts--are vein grafts obsolete? Br J Clin Pract 50(3):144-50.
8. Ura M, Sakata R, Nakayama Y, Arai Y, Saito T. Long-term patency rate of right internal thoracic artery bypass via the transverse sinus. Circulation 1998; 98(19):2043-48.
9. Bonacchi M, Battaglia F, Prifti E, Leacche M, Nathan NS, Sani G, Popoff G. Early and late outcome of skeletonised bilateral internal mammary arteries anastomosed to the left coronary system. Heart 2005; 91(2):195-202.
10. Kinoshita T, Asai T, Murakami Y, Hiramatsu N, Suzuki T, Kambara A, Matsubayashi K. Efficacy of bilateral internal thoracic artery grafting in patients with chronic kidney disease. Ann Thorac Surg 2010; 89(4):1106-11.
11. Taggart DP, Altman DG, Gray AM, Lees B, Gerry S, Benedetto U, Flather M: ART Investigators. Randomized trial of bilateral versus single internal-thoracic-artery grafts. N Engl J Med 2016; 375(26):2540-49.
12. Mohammadi S, Dagenais F, Doyle D, et al. Age cut-off for the loss of benefit from bilateral internal thoracic artery grafting . Eur J Cardio-Thoracic Surg 2008; 33(6):977-82.
13. Attia T, Koch CG, Houghtaling PL, Blackstone EH, Sabik EM, Sabik JF. Does a similar procedure result in similar survival for women and men undergoing isolated coronary artery bypass grafting? J Thorac Cardiovasc Surg 2017; 153(3):571-79.e9.
14. Angelovich TA, Hearps AC, Maisa A, Kelesidis T, Jaworowski A. Quantification of monocyte transmigration and foam cell formation from individuals with chronic inflammatory conditions. J Vis Exp 2017; (128). doi: 10.3791/56293.
15. Shashkin P, Dragulev B, Ley K. Macrophage differentiation to foam cells. Curr Pharm Des 2005; 11(23):3061-72.
16. Malinska A, Perek B, Buczkowski P, Kowalska K, Ostalska-Nowicka D, Witkiewicz W, Nowicki M. CD68 expression in aortocoronary saphenous vein bypass grafts. Histochem Cell Biol 2013; 140(2):183-88.
17. Borović ML, Borović S, Marinković-Erić J, et al. A comprehensive morphometric analysis of the internal thoracic artery with emphasis on age, gender and left-to-right specific differences. Histol Histopathol 2013; 28(10):1299-314.
18. Ruengsakulrach P, Sinclair R, Komeda M, Raman

J, Gordon I, Buxton B. Comparative histopathology of radial artery versus internal thoracic artery and risk factors for development of intimal hyperplasia and atherosclerosis. Circulation 1999; 100(19 Suppl):II139-44.
19. Hinojosa-Amaya JM, Villarreal-Silva EE, Elizondo-Omaña RE, et al. Conduits for myocardial revascularization grafts: The importance of morphology and imaging. Med Univ 2010; 12(12):115-19.
20. Brown RA, Shantsila E, Varma C, Lip GYH. Current understanding of atherogenesis. Am J Med 2017; 130(3):268-82.
21. Borović ML, Borović S, Perić M, et al. The internal thoracic artery as a transitional type of artery: a morphological and morphometric study. Histol Histopathol 2010; 25(5):561-76.
22. Sims FH. Discontinuities in the internal elastic lamina: a comparison of coronary and internal mammary arteries. Artery 1985; 13(3):127-43.
23. Reddy S, Kumar P, Prasad K. Histomorphometric and sympathetic innervation of the human internal thoracic artery. Clinics (Sao Paulo) 2011; 66(1):131-36.
24. Perrotta I, Sciangula A, Concistrè G, Mazzulla S, Aquila S, Agnino A. Internal mammary artery atherosclerosis: an ultrastructural study of two cases. Ultrastruct Pathol 2014; 38(3):199-203.
25. Schwann TA, Engoren M, Bonnell M, Clancy C, Habib RH. Comparison of late coronary artery bypass graft survival effects of radial artery versus saphenous vein grafting in male and female patients. Ann Thorac Surg 2012; 94(5):1485-91.
26. Fu S, Zheng Z, Yuan X, Zhang S, Gao H, Li Y, Hu S. Impact of off-pump techniques on sex differences in early and late outcomes after isolated coronary artery bypass grafts. Ann Thorac Surg 2009; 87(4):1090-96.
27. Wang J, Yu W, Zhao D, Liu N, Yu Y. In-hospital and long-term mortality in 35,173 Chinese patients undergoing coronary artery bypass grafting in Beijing: impact of sex, age, myocardial infarction, and cardiopulmonary bypass. J Cardiothorac Vasc Anesth 2017; 31(1):26-31.
28. Whayne TF, Mukherjee D. Unique coronary artery disease differences in women as related to revascularization. Curr Med Chem 2015; 22(31):3597-606.
29. Perek B, Jemielity M, Dyszkiewicz W. Why are the results of coronary artery bypass grafting in women worse? Asian Cardiovasc Thorac Ann 2003; 11(4):293-98.
30. Dodge JT, Brown BG, Bolson EL, Dodge HT. Lumen diameter of normal human coronary arteries. Influence of age, sex, anatomic variation, and left ventricular hypertrophy or dilation. Circulation 1992; 86(1):232-46.
31. Samak M, Fatullayev J, Sabashnikov A, et al. Total arterial revascularization: bypassing antiquated notions to better alternatives for coronary artery disease. Med Sci Monit Basic Res 2016; 22:107-14.
32. Fleissner F, Warnecke G, Cebotari S, Rustum S, Haverich A, Ismail I. Coronary artery bypass grafting in young patients - insights into a distinct entity. J Cardiothorac Surg 2015; 10(1):65.

NUCLEAR FACTOR ERYTHROID 2-RELATED FACTOR 2 AND CHOLINE ACETYLTRANSFERASE CO-EXPRESSION IN RAT SPINAL CORD NEURONS AFTER ISCHEMIA-REPERFUSION INJURY

M. BOBINAC[1], T. ĆELIĆ[2], I. VUKELIĆ[3], J. ŠPANJOL[4], N. RUBINIĆ[4] and D. BOBINAC[2]

[1]Department of Anesthesiology, Reanimatology and Intensive Care, Rijeka Clinical Hospital, University of Rijeka, Rijeka, Croatia; [2]Department of Anatomy, Medical Faculty University of Rijeka, Rijeka, Croatia; [3]Department of Chemistry and Biochemistry, Medical Faculty University of Rijeka, Rijeka, Croatia; [4]Department of Urology, Rijeka Clinical Hospital, University of Rijeka, Rijeka, Croatia

Received May 9, 2018 – Accepted June 18, 2018

Spinal cord ischemia-reperfusion injury (IRI) results in overproduction of reactive oxygen species leading to tissue oxidative stress which impacts the neuronal network in the spinal cord as well as glial cells. We investigated the expression of Nuclear factor erythroid 2-related factor 2 (Nrf2) in neurons and glial cells after occlusion of the abdominal aorta followed by IRI as well as the time-dependent expression of Nrf2 in the same cells. The experimental method of transient aortic occlusion was carried out on rats by cross-clamping of the abdominal aorta for 45 minutes. The animals used for this study were sacrificed 1 h, 6 h, and 48 h after reperfusion to determine time-related changes of Nrf2 expression, as well as changes of astrocyte activity in the spinal cord. Immunofluorescence results showed an increase in the staining intensity of Nrf2 expression in the neurons following ischemia with highest intensity 48 h post-reperfusion and an increase in a number of reactive astrocytes. Western blot analysis showed that Nrf2 protein expression increased in a cytoplasmic and nuclear fraction as early as 1 h after reperfusion and remained active 48 h after, resulting in increased expression of the main Nrf2 target gene HO-1. In conclusion, substances that enhance expression of Nrf2 may have the potential to prevent cellular damage to the spinal cord caused by IRI.

The spinal cord is exceptionally vulnerable to ischemic injury caused by a variety of abnormalities, such as thoracoabdominal aortic aneurysm, atherosclerosis, embolism, cardiac arrest and iatrogenic causes such as surgery (1). Aortic cross-clamping during thoracoabdominal aortic aneurysm surgery additionally causes spinal cord ischemia followed by reperfusion which finally leads to ischemia-reperfusion injury (IRI) of the spinal cord tissue. IRI impacts neurons and glial cells in the spinal cord causing reversible or even irreversible cell damage (2). Transient ischemia in the spinal cord, lasting more than 30 min, is manifested as alteration or loss of motor function of the lower extremity. Such severe and unpredictable neurological complications include diverse neurological disorders, such as paraparesis or even paraplegia (3).

Although the exact pathophysiological mechanism that underlies spinal cord ischemia-reperfusion injury

Key words: Nrf2, neurons, glia, spinal cord, ischemia-reperfusion injury

Mailing address:
Dr Tanja Ćelić,
Department of Anatomy,
Medical Faculty,
University of Rijeka, Rijeka, Croatia
Tel.: +385 916996969
e-mail: tanja.celic@medri.uniri.hr

0393-974X (2018)
Copyright © by BIOLIFE, s.a.s.
This publication and/or article is for individual use only and may not be further reproduced without written permission from the copyright holder. Unauthorized reproduction may result in financial and other penalties
DISCLOSURE: ALL AUTHORS REPORT NO CONFLICTS OF INTEREST RELEVANT TO THIS ARTICLE.

is not fully understood, it seems that oxidative stress and inflammatory response play a significant role in the progression of tissue damage. Spinal cord ischemia followed by reperfusion results in a sudden burst of reactive oxygen species (ROS) and reactive nitrogen species (RNS) that aggravate tissue injury. Overproduction of these compounds overcomes endogenous anti-oxidant defense in a state of oxidative stress, causing oxidative damage to lipids, proteins, and DNA, and thus disruption of standard cell functions (4, 5). Oxidative stress is accompanied with an inflammatory response characterized by infiltration of inflammatory cells (macrophages, lymphocytes, neutrophils) to the injured tissue, which produces more ROS and RNS (6, 7).

To maintain redox balance, synthesis of antioxidant enzymes is increased. This is under control of Keap1/Nrf2/ARE signaling pathway, and heme oxygenase 1 (HO-1) is one of the most studied downstream proteins activated by it. The three cellular components involved in this pathway at the transcriptional level are Kelch-like ECH-associated protein 1 (Keap1), nuclear factor erythroid 2-related factor 2 (Nrf2), and antioxidant response elements (ARE). Research indicates that the Keap1/Nrf2/ARE signaling pathway is responsible for "turning on" the adaptive response against oxidative stress (8). Recent studies have shown that the Nrf2 pathway plays an essential protective role in a state of IRI of the brain, but few data are published on Nrf2 and spinal cord IRI (9-11). Furthermore, the expression of Nrf2 in different cells of the spinal cord, as well as time-related expression of Nrf2 in acute happening (1 h post-ischemia reperfusion) and up to 48 h of reperfusion, are not well known.

This study aims to determine the localization and expression of Nrf2 in neurons and glial cells after occlusion of the abdominal aorta followed by IRI, as well as the time-dependent expression of Nrf2 in the same cells.

MATERIALS AND METHODS

Animals

Thirty-two male Wistar rats (10–12 weeks old) were used in accordance with the protocols approved by the Ethics Committee of the Faculty of Medicine, University of Rijeka. The rats were housed two per cage in controlled conditions of temperature and humidity, exposed to a 12-h light/dark cycle with free access to food and water. During procedures, all efforts were made to minimize the suffering of the animals.

Spinal cord ischemia-reperfusion injury procedure and study design

The abdominal aorta was cross-clamped for 45 min to produce transient spinal cord ischemia in lumbar segments. Animals were anesthetized with *ip* injections of ketamine hydrochloride (0.1 mg/g body weight) and xylazine hydrochloride (0.02 mg/g body weight). The *ip* injection of cephalosporin (10 mg/kg) was administered before skin incision. Postoperative analgesia was provided with tramadol for 12 h; 150 U/kg of heparin was administered *sc* to all animals immediately before the procedure (the detailed procedure is described in our previous work (12).

Rats were randomly divided into two groups: (1) ischemia-reperfusion injury (IRI) group and (2) control (sham) group. The IRI group included 24 rats which were divided into three subgroups based on time post-reperfusion as follows: 1 h, 6 h, and 48 h. Each subgroup consisted of 8 animals. The sham group included eight rats subjected to anesthesia and laparotomy without ischemia and served as control.

At 1 h, 6 h or 48 h post-reperfusion animals were anesthetized, perfused transcardially with 0.9% saline and 4% paraformaldehyde (PFA) in 0.1 M phosphate-buffered saline (pH 7.4), and sacrificed. The spinal cord was extracted whole, and lumbar regions were fixed in 4% PFA for 24 h followed by embedding in paraffin wax for immunofluorescence.

Immunofluorescence microscopy

Immunofluorescence staining was carried out on 3-μm thick formalin-fixed, paraffin-embedded spinal cord tissue sections. Following deparaffinization, the antigen retrieval was performed using citric acid (pH 6.6) for 15 min in water bath at 95°C. Following, the sections were rinsed with fluent water for 15 min. Non-specific binding sites were blocked using 3% bovine serum albumin (BSA) in phosphate-buffered saline (PBS). In the subsequent step, the sections were incubated with the primary antibodies shown in Table I. Incubation with suitable secondary antibodies followed, Alexa Fluor 488 goat anti-rabbit IgG (1:200, Invitrogen) and

Alexa Fluor 488 goat anti-mouse IgG (1:200, Invitrogen) were applied for 1 h at RT. The sections were washed using PBS 3 ×5 min after each step, and were then cover- slipped in fluorescence mounting media,

Microscopy and image analysis

Sections were observed under Olympus microscope BX51/BX52 (Tokyo, Japan) equipped with fluorescence and images captured using an Olympus camera. Images of the spinal cord ventral gray matter were analyzed by ImageJ software (National Institutes of Health, Bethesda, MD, USA). From each animal, every fifth consecutive serial section was studied to avoid the risk of double quantification of the same cell in adjacent sections. In every animal, five sections of lumbar spine region were studied. The mean density of the somata of labeled cells were measured using integrated density divided by the analyzed area of the cell. Images were adjusted on the same brightness set for all dual labeled images. The quantity of astrocytes was taken from each section and pooled.

From each sample, astrocytes number were counted on four fields of 280 ×280 μm area, and the cell area percentage was calculated for astrocyte activity analysis.

Western blot analysis of Nrf2 and HO1

Nuclear and cytoplasmic fractionation was performed by the spinal cord tissue trypsinization (50 μg total) and washing twice in ice-cold PBS. After that, the sample was lysed on ice for 15 min in 100 mL of cytoplasmic lysis buffer (10 mM HEPES pH 7.4, 10 nM KCl, 0.01 mM EDTA, 0.1 mM EGTA, 2 mM DTT, 5 mM Na2VO4, 20 mM sodium β-glycerophosphate, 0.1% and Protease inhibitor cocktail. Nuclei were sedimented by centrifugation and the supernatant containing the cytoplasmic fraction removed, to which Urea and SDS were added to a final concentration of 2 M and 2% respectively, and the samples were denatured by boiling for 5 min. The nuclei were then washed in 1 ml of cytoplasmic lysis buffer to remove any contaminating cytoplasm, and re-sedimented. The nuclei were then lysed in 100 μl of denaturing lysis buffer (2% SDS, 2 M urea, 8% sucrose, 20 mM sodium β-glycerophosphate, 1mM NaF, and 5 mM Na2VO4).

Ten μg of cytoplasmic and 10 μg nuclear extracts were loaded to 12% polyacrylamide gel, submitted to SDS-PAGE, and transferred to polyvinylidene difluoride (PVDF) membrane (Roche Diagnostics GmbH, Mannheim, Germany). After transfer, membranes were stained with Ponceau S dye, washed, and blocked with 5% non-fat dry milk in TBST buffer (50 mM Tris-HCl (pH 7.4), 150 mM NaCl, 0.05% Tween-20) for 1 h at RT. Membranes were further incubated overnight at 4°C with primary antibodies: rabbit polyclonal anti-heme oxygenase 1 (1:1000, Abcam,

Table I. *Primary antibodies used.*

Antibody	Species raised against	Manufacturer, catalog number	Antibody dilution
Nrf2 (nuclear factor erythroid 2 (NFE2)-related factor 2)	Rabbit polyclonal	Santa Cruz Sc-722	1:200
NeuN (neuronal nuclear antigen)	Mouse monoclonal	Milipore, MAB377	1:200
ChAT (Choline acetyltransferase)	Rabbit polyclonal	Abcam, ab6168	1:200
GFAP (glial fibrillary acidic protein)	Rabbit polyclonal	Abcam, ab7260	1:500
Iba1 (ionized calcium-binding adapter molecule 1)	Goat polyclonal	Abcam, ab5076	1:500
PLP1 (proteolipid protein 1)	Mouse polyclonal	Abcam ab9311	1:500
HO-1 (heme oxygenase 1)	Rabbit polyclonal	Abcam ab13243	1:1000
B-actin	Mouse monoclonal	Santa Cruz sc-47778	1:2000

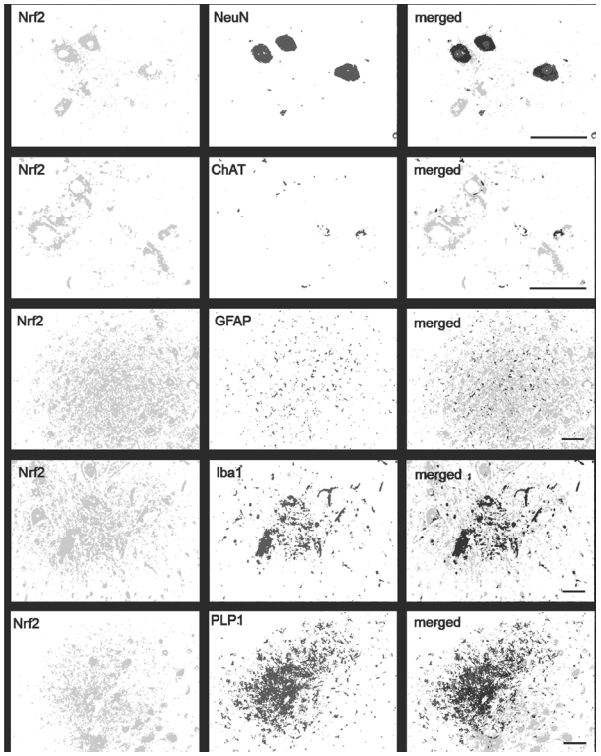

Fig. 1. *Double labelled (**A**) Nrf2 and NeuN, (**B**) Nrf2 and ChAT, (**C**) Nrf2 and GFAP, (**D**) Nrf2 and Iba1, (**E**) Nrf2 and PLP1 in cross sections of spinal cord lumbar region in control group and 1 h of IRI. Immunofluorescence images show co – expression of (A) Nrf2 and NeuN and (B) Nrf2 and ChAT in grey matter of spinal cord both in control and 1 h of IRI. The expression of Nrf2 is not observed in (C) GFAP, (D) Iba1 or (E) PLP1 positive cells. Although dark-field microscopy was used, images have been post-processed to enhance visibility. Scale bar = 50 and 100 μm.*

Cambridge, MA, USA), mouse monoclonal anti-β-actin (1:2000, Santa Cruz Biotechnology, Dallas, TX, USA) and rabbit polyclonal anti-Nrf2 (1:500, Santa Cruz Biotechnology, Dallas, TX, USA). The following day, membranes were washed and incubated for 1 h at RT with appropriate secondary antibodies: goat anti-mouse IgG-HRP (1:2000, Santa Cruz Biotechnology, Dallas, TX, USA), goat anti-rabbit IgG-HRP (1:2000, Santa Cruz Biotechnology, Dallas, TX, USA). The immunoblots were visualized by enhanced chemiluminescence using Amersham ECL Prime Western Blotting Detection Reagent (GE Healthcare, Buckinghamshire, UK) and quantified using ImageJ software. Band densities were normalized to β-actin for HO-1 and Ponceau S for Nrf2 and presented as relative densitometric units.

Statistical analysis

All statistical analyses were performed using Statistica software version 12 (StatSoft Inc., Tulsa, OK, USA). In densitometric analyses the values were expressed as relative optical densities of the related bands. Statistical significance for the Western blot data was calculated according to the one-way analysis of variance (ANOVA), followed by Duncan's multiple range post-hoc test. For the IF staining, the means of integrated density divided by analysed area of the cell were used for the Kruskal–Wallis analysis. Post-hoc group comparisons were accomplished utilizing the Mann–Whitney U test. Results are expressed as means ± SEM. In all comparisons, $P < 0.05$ was considered statistically significant.

All procedures were according to the ethical standards of the institutional and national responsible committee and with the Helsinki declaration of 1975, as revised in 2000.

RESULTS

Co-expression of Nrf2 and NeuN in the spinal cord after ischemia-reperfusion injury

NeuN and Nrf2 labeled cells were co-expressed

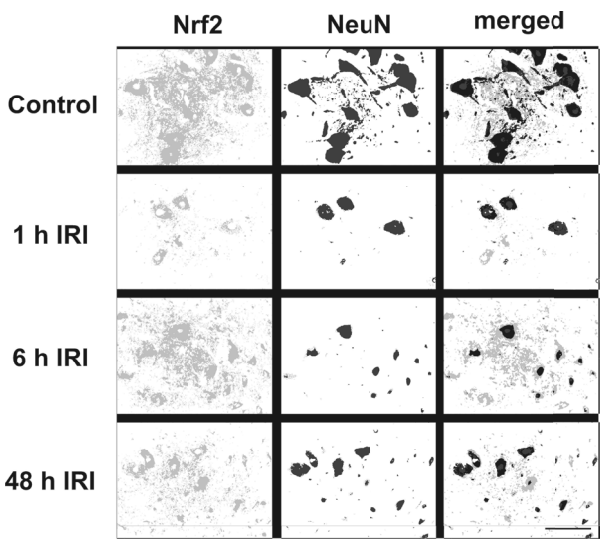

Fig. 2. *representative images of spinal cord sections stained with anti-nuclear factor erythroid 2-related factor 2 (nrf2) and the neuronal marker anti-neuronal nuclei (neun) by double-immunofluorescence labelling in control and at 1, 6 and 48 h after iri. although dark-field microscopy was used, images have been post-processed to enhance visibility. scale bar = 50 μm.*

in the grey matter of the spinal cord in control and IRI group. The co-expression was observed predominantly in the anterior horn and central part of the grey matter, while in the posterior horn of the grey matter only a few cells co-expressed NeuN and Nrf2. Immunoreactivity of Nrf2 was localized mostly in the cytoplasm or both cytoplasm and nucleus of neurons (Fig. 1). NeuN immunoreactivity was localized in the nucleus and peri-nuclear cytoplasm off all neurons in the grey matter, through the anterior, central and posterior horn. Neurons of the anterior horn were less immunoreactive for NeuN at 48 h of IRI, with mean density 45.2±11.7 A.U. (N = 8), however these values varied greatly ranging from 27A.U. to 86 A.U. (Fig. 2). Those variations may correspond to ischemic injury neurons suffered and consequent loss of NeuN reactivity.

Mean density of Nrf2 expression in cells co-

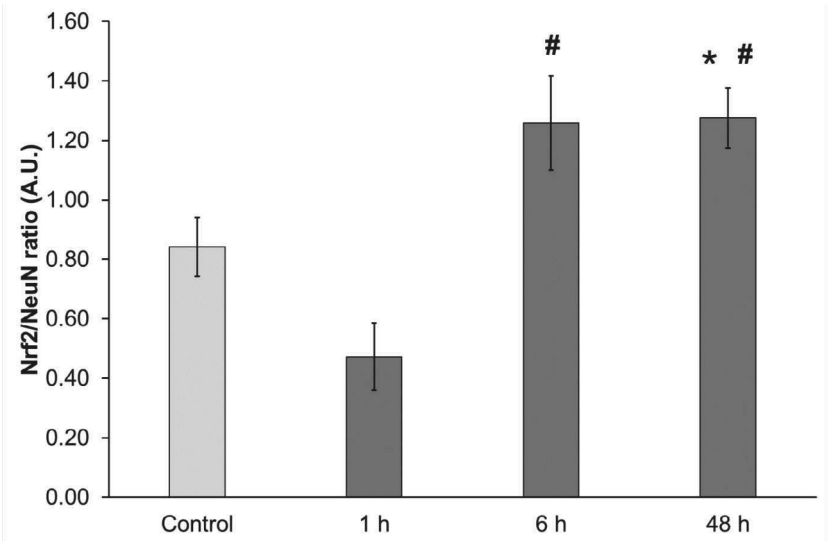

Fig. 3. *Nrf2/NeuN ratio (A.U.= arbitrary units) in control group and at 1h, 6 h and 48 h of IRI. control group; ischemia – reperfusion group (1 h, 6 h and 48 h). * p <0.005 vs control group; # p<0.005 vs 1 h of IRI. All data are expressed as average±SEM (N = 8)*

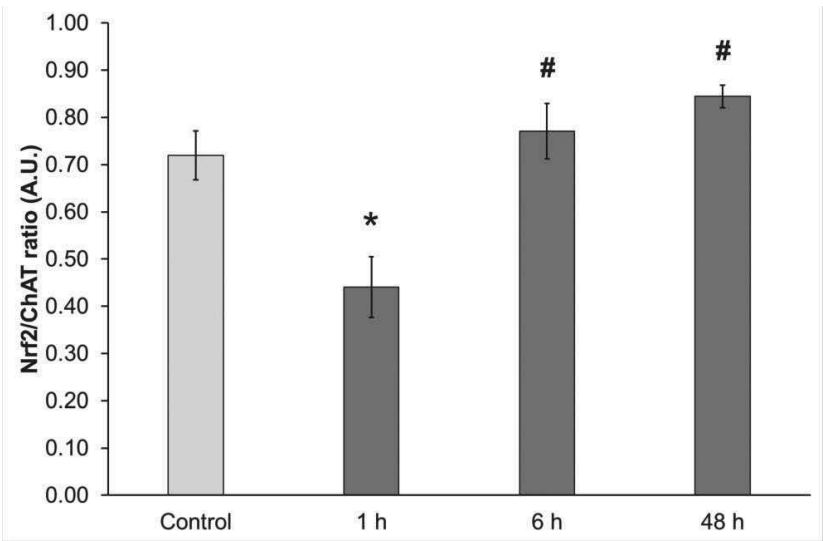

Fig. 4. *Nrf2/ChAT ratio (A.U.= arbitrary units) in control group and at 1 h, 6 h and 48 h of IRI. control group; ischemia – reperfusion group (1 h, 6 h and 48 h). * p <0.005 vs control group; # p<0.005 vs 1 h of IRI. All data are expressed as average±SEM (N = 8)*

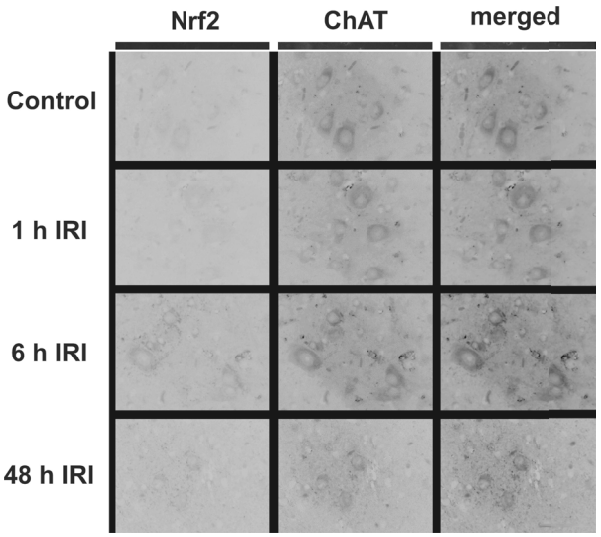

Fig. 5. *Representative images of spinal cord sections stained with anti-nuclear factor erythroid 2-related factor 2 (Nrf2) and the motor neuron marker anti-choline acetyltransferase (ChAT) by double-immunofluorescence labelling in control and at 1, 6 and 48 h after IRI. Although dark-field microscopy was used, images have been post-processed to enhance visibility. Scale bar = 50 μm.*

expressing NeuN was shown as Nrf2/NeuN mean intensity ratio in Fig. 3. In subacute time point, at 1 h of IRI, Nrf2/NeuN ratio was decreased compared to control group. The Nrf2/NeuN ratio at 6 h of IRI increased significantly compared to 1 h of IRI. The Nrf2/NeuN ratio at 6 h of IRI was significantly increased compared to 1 h of IRI. 48 h post-IRI Nrf2/NeuN ratio was significantly increased compared to control and 1 h of IRI.

Co-expression of Nrf2 and ChAT in the spinal cord after ischemia-reperfusion injury

Nrf2 and ChAT labeled cells were co-expressed in the grey matter of spinal cord in the control and IRI groups. All the cells expressing Nrf2 were ChAT-positive. The co-expression was observed in all motor neurons of the grey matter, mostly in the anterior and central horn, while in the posterior horn of the grey matter only a few cells co-expressed NeuN and Nrf2. Immunoreactivity of Nrf2 was localized mostly in the cytoplasm or in both cytoplasm and nucleus of neurons (Fig. 1). ChAT immunoreactivity was localised in cytoplasm and membrane of motor neuron bodies in mostly anterior and central horn, with few neurons positive in posterior horn. ChAT immunoreactivity had mean density 57.8±9.2 A.U. (N = 8) in controls, 41.5±14.2 A.U. (N = 8) at 1 h of IRI, 69.1±11.7 A.U. (N = 8) at 6 h of IRI, and 61.4±6.7 A.U. (N = 8) at 48 h of IRI.

Mean density of Nrf2 expression in cells co-expressing ChAT was shown as Nrf2/ChAT mean intensity ratio in Fig. 4. In subacute time point, at 1 h of IRI, the Nrf2/ChAT ratio was decreased compared to control group. The Nrf2/ChAT ratio at 6 h and 48 h of IRI increased significantly compared to 1 h of IRI.

Mean intensity of Nrf2 expression is increased in the spinal cord after ischemia-reperfusion injury

Immunoreactivity of Nrf2 was localized in the grey matter of spinal cord in the control and IRI groups. The localization of Nrf2 expression was observed in the cytoplasm, or both cytoplasm and nucleus of neurons, predominantly in the anterior and central horn of the spinal cord grey matter, but also in a few neurons of the posterior horn (Figs. 1, 2, 5).

The density of Nrf2 expression depended on the IRI time-point. After 1 h of IRI mean density of Nrf2 expression in neurons was decreased. After 6 h and 48 h of IRI Nrf2 expression in neurons was significantly increased compared to 1 h of IRI. Also at 48 h of IRI mean density of Nrf2 was significantly increased compared to the control group (Fig. 6.).

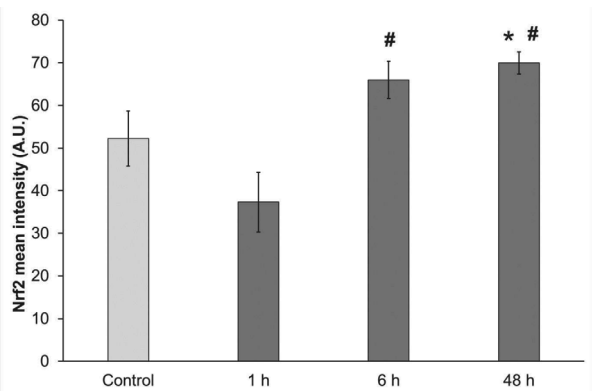

Fig. 6. *Nrf2 mean intensity (A.U.= arbitrary units) in control group and at 1 h, 6 h and 48 h of IRI. Control group; ischemia – reperfusion group (1 h, 6 h and 48 h). * p <0.005 vs control group; # p<0.005 vs 1 h of IRI. All data are expressed as average±SEM (N = 8)*

Co-expression of Nrf2 and GFAP, Iba1, PLP1 in the spinal cord after ischemia-reperfusion injury

To determine the possible expression of Nrf2 in GFAP, Iba1 or PLP1 positive cells in IRI of the spinal cord, we performed double labeled immunofluorescence. No double labeled Nrf2/GFAP, Nrf2/Iba1 or Nrf2/PLP1 expressions were observed in either grey or white matter of the spinal cord at 1, 6 and 48 h of IRI or in the control group (Fig. 1C-E).

Increase of astrocyte number and activity in white matter after IRI

During our experiments, we observed, in contrast to control animals, that animals in the IRI group exhibited an increase in GFAP positive cells in the spinal cord and also an increased percentage of GFAP positive cell area. The higher percentage of GFAP positive cell area confirms increased astrocyte activity. Analysis of GFAP positive cells number matter revealed moderate increase 6 h (627.2±27.4) after reperfusion and significant increase 48 h (784.3±21.2) after reperfusion compared to control animals (551±13.6). Analysis of GFAP positive area showed that astrocyte activity was increased in a lumbar segment of spinal cord 1 h (12%), 6 h (15%) and 48 h (17%) after reperfusion compared to control animals (8%) (Fig. 7).

nrf2 expression is increased in the spinal cord after IRI

To determine whether IRI induced activation of the Nrf2 transcription factor, we analyzed nuclear and cytoplasmic fractions of spinal cord lysates from IRI and sham animals for Nrf2 protein expression (Fig. 8). One hour after reperfusion, there was a decrease of the Nrf2 protein in the cytoplasmic and the nuclear fractions of IRI spinal cords. After 6 h of reperfusion Nrf2 protein levels increased in both cytoplasmic and nuclear fraction, while at 48 h after reperfusion Nrf2 protein expression stayed the same in cytoplasmic fraction and started to decline in nuclear fraction. Therefore, following IRI in the spinal cord, Nrf2 protein expression was significantly increased after 6 h and 48 h of reperfusion in the cytoplasm of cells followed by translocation into the nucleus.

IRI induces increased protein expression of Nrf2 signaling target HO-1

Fig. 9 shows the expression of Nrf2 regulated signaling protein HO-1 in sham-operated animals

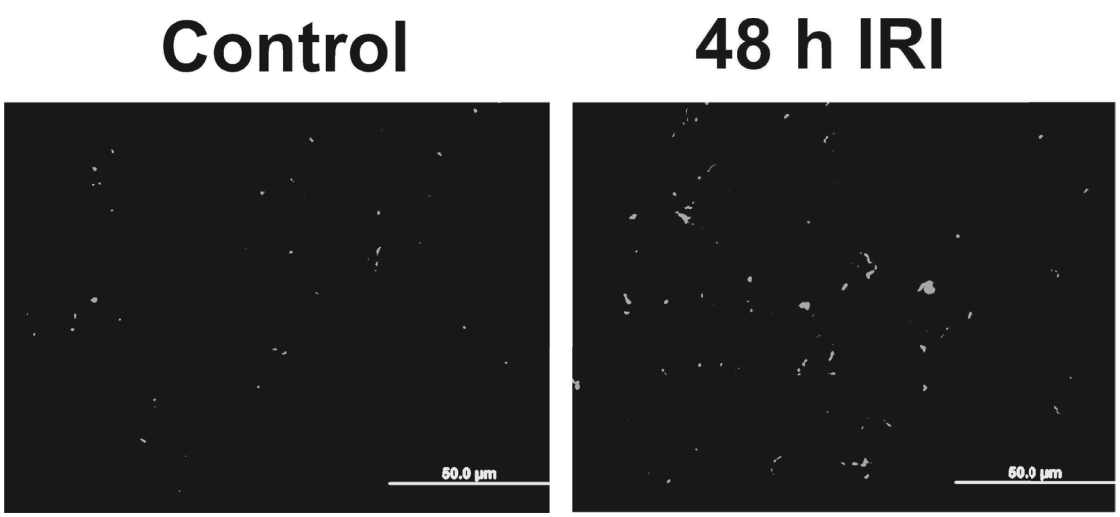

Fig. 7. *Representative images of spinal cord sections stained with anti- astrocyte marker glial fibrillary acidic protein (GFAP). Scale bar = 50 µm. At 48 h of IRI astrocyte number and activity is increased compared to control group.*

and animals that underwent IRI for 1 h, 6 h, and 48 h of reperfusion. After 6 h of reperfusion, there was a significant increase in the levels of HO-1 in spinal cord lysates and the level continued to increase 48 h after IRI compared to sham animals. Therefore, IRI induced increased protein expression of Nrf2 signaling target HO-1.

DISCUSSION

The present study demonstrated the expression of Nrf2 in neurons, an increase in the staining intensity of Nrf2 expression in the neurons following ischemia at all time-points of reperfusion and an increase in some reactive astrocytes. Ischemia followed by 1 hour of reperfusion decreased the level of Nrf2 expression in neurons but 6 hours after reperfusion the expression of Nrf2 was recovered and we observed an increase of Nrf2 expression in motoneurons. Astrogliosis was manifested as an increase in some GFAP positive cells as well as an increase in cellular volume.

Moreover, our data showed that Nrf2 protein expression increases in cytoplasm and nucleus of spinal cord lysates 6 h post-reperfusion and remains active 48 h after, resulting in increased expression of the main Nrf2 target gene HO-1.

We used NeuN antibody to identify all neurons, ChAT to identify motoneurons, Iba1 to identify microglia, GFAP to identify reactive astrocytes and PLP1 to identify oligodendrocytes.

The spinal cord is extremely vulnerable to ischemic injury which could be caused by a variety of abnormalities (1). However, ischemia of the nervous tissue followed by reperfusion causes secondary injury manifested as neuronal apoptosis, inflammation, and astrogliosis (2). Although the exact pathophysiologic mechanism that underlies spinal cord I/R injury is not fully understood, it seems that oxidative stress (imbalance between reactive species and endogenous anti-oxidative defenses) plays an important role and contributes to spinal cord oxidative damage (3). Thoracoabdominal aortic aneurysm surgery may cause spinal cord ischemia-reperfusion injury because of transient aortic cross-clamping. Such scenario is consistent with the anatomy of the spinal cord blood supply. Except by anterior and posterior spinal arteries, the spinal cord from Th8 to the conus medullaris is supplied by segmental (radicular) arteries. The dominant segmental artery for supplying the lumbar and sacral part of the spinal cord is the artery of Adamkiewicz, which commonly arises from the posterior branch of the last intercostal artery or a lumbar artery which arises from the thoracic or abdominal aorta, respectively. In clinical practice, transient aortic cross-clamping may cause reversible or even irreversible spinal cord neuronal damage, manifested as alteration or loss of neurological motor function.

Nrf2 is ubiquitously expressed antioxidant transcription factor (13) which, under normal conditions (reduced intracellular conditions), is stabilized through binding to Keap-1 in the cytoplasm. During enhanced ROS formation, the cysteine residues in Keap-1 are modified or oxidized, causing the dissociation of Nrf2 and its translocation to the nucleus where it binds to ARE and, depending

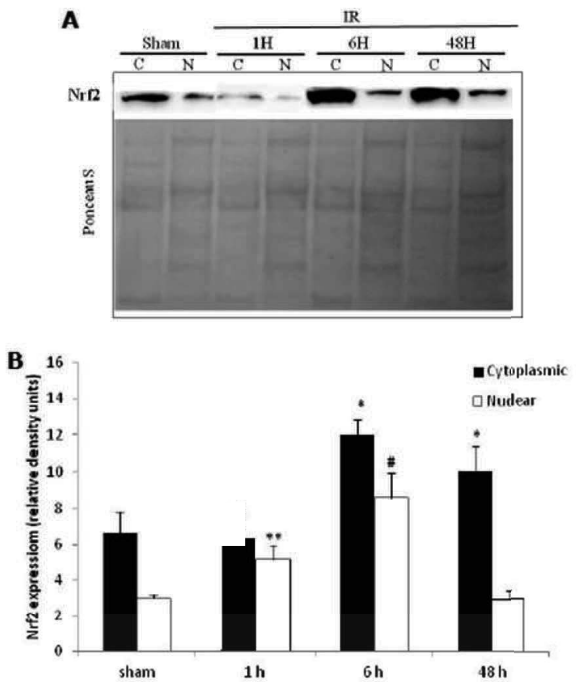

Fig. 8. *Ischemia reperfusion injury (IRI) induces expression of Nrf2 in cytoplasmic ■ (C) and nuclear □ (N) fractions of spinal cord. Representative immunoblots are shown. Data are presented as relative density units normalized to Ponceau S and expressed as mean±SEM. *p<0.05, **p<0.01 compared to sham; n= 8 per group.*

upon the binding site, the different antioxidant genes are induced, including HO-1, NQO-1, SOD, GPx (9-11). Our results are in agreement with this, showing that IRI induces increased cytoplasmic and nuclear Nrf2 expression in the spinal cord after 6 h of reperfusion. Also Nrf2 expression stays elevated in both cellular compartments after 48 h of reperfusion. Data presented in this paper are the first showing Nrf2 activation in early phases of IRI in the spinal cord. The function of the Nrf2/ARE signaling pathway is important for protection in states of increased oxidative stress due to ischemia because enhanced ROS production induces activation of Nrf2 (14, 15). Therefore, increased expression of Nrf2 in the motoneurons after IRI may be implicated as a viable strategy for the promotion of neurological function recovery and a strategic target for IRI therapies (16).

The cell biology of the response to IRI is not well understood and the roles played by different cell types at different time-points in the progression of secondary degeneration during IRI are not well defined. Therefore, in the current study, we focused on identifying the cell types in the spinal cord for the expression of Nrf2 molecules and whether I/R injury affects the expression of the Nrf2 protein as a common antioxidative signaling pathway. We detected the expression of Nrf2 in the neurons in the gray matter of the spinal cord in the control group and after I/R injury. Nrf2 expression was significantly higher after 6 and 48 hours after IRI compared with the levels detected in the control group, thus implying the activation of the Nrf2 signaling pathway. Most of the neurons expressing Nrf2 molecules were motoneurons in the anterior horn and central part of the gray matter. IRI caused an increase in the density of Nrf2 expression in motoneurons after 6 and even more after 48 hours after reperfusion. Nrf2 expression was not detected in other cell types. Park et al. reported human neuronal cell protection by elevated Nrf2 activity and its downstream molecules HO-1 and NQO1, against oxygen-glucose deprivation/ reoxygenation (17). Dai et al. found that isoquercetin attenuates oxidative stress and neuronal apoptosis after ischemia-reperfusion injury via Nrf2 inhibiting NFκB inflammatory pathway (18). Li et al. showed that suppression of neuronal injury caused by oxygen-glucose deprivation/reoxygenation is achieved by activating Brg1/Nrf2/ARE signaling pathway via suppression of microRNA – 144 – 3p (19). Xun et al. reported that only overexpression of nuclear factor of activated T cells 5 (NFAT5) could protect astrocytes against oxidative damage by promoting the nuclear transport of Nrf2 from cytoplasm to cell nucleus, or NFAT regulates Nrf2 pathway in astrocytes (15). Other reports showed that the level of Nrf2 expression could also be increased in neurons, microglia, and astrocytes after treatment by some drugs (20).

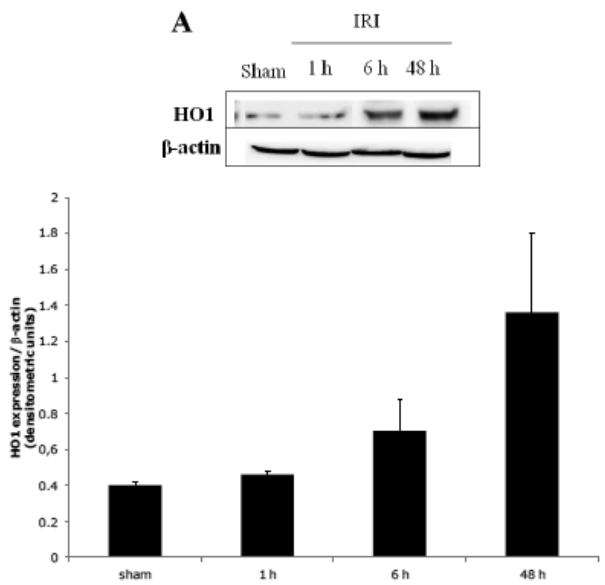

Fig. 9. *IRI induces increased protein level of the Nrf2 main signalling target HO-1. Immunoblots indicate that levels of HO-1 start to increase 6 h after reperfusion and continue to increase at 48 h. Data are presented as relative density units normalized to β-actin and expressed as mean±SEM; n= 8 per group.*

Reactive astrocytosis, increasing GFAP positive cells, was a prominent feature of the cellular response to IRI. We found that astrocytes exhibit the expression of the glial fibrillary acid protein, hypertrophy, process extension and cell division. IRI induced an increase in the number of GFAP positive cells during the first 48 hours. Scar tissue formed by reactive astrocytes has long been implicated as a significant impediment to neuronal tissue repair after SC injury, however, a report by Faulkner et al.

showed that reactive astrocytes restrict inflammation, protect neurons and oligodendrocytes and preserve motor functions after SCI (21).

Our results suggested that ischemia of the spinal cord followed by reperfusion increased the level of Nrf2 expression in neurons, did not cause Nrf2 expression in other cell types and induced reactive astrocytosis.

Moreover, we demonstrated that IRI enhances activation of Nrf2 as well as its target gene HO-1 in the early phase after reperfusion, probably as a protective mechanism from oxidative stress.

REFERENCES

1. Crawford ES, Crawford JL, Safi HJ, Coselli JS, Hess KR, Brooks B. Thoracoabdominal aortic aneurysms: preoperative and intraoperative factors determining immediate and long-term results of operations in 605 patients. J Vasc Surg 1986; 3:389-404.
2. Svensson LG, Crawford ES, Hess KR, Coselli JS, Safi HJ. Experience with 1509 patients undergoing thoracoabdominal aortic operations. J Vasc Surg 1993; 17:357-68.
3. Coselli JS, LeMaire SA, Miller CC, Curling PE. Mortality and paraplegia after thoracoabdominal aortic aneurysm repair: a risk factor analysis. Ann Thorac Surg 2000; 69:409-14.
4. Ege E, Ilhan A, Gurel A, Akyol O, Ozen S. Erdosteine ameliorates neurological outcome and oxidative stress due to ischemia/reperfusion injury in rabbit spinal cord. Eur J Vasc Endovasc Surg 2004; 28:379-86.
5. Ilhan A, Yilmaz HR, Armutcu F, Gurel A, Akyol O. The protective effect of nebivolol on ischemia/reperfusion injury in rabbit spinal cord. Prog Neuropsychopharmacol Biol Psychiatry 2004; 28:1153-60.
6. Zhu P, Li J, Fujino M, Zhuang J, Li XK. Development and treatments of inflammatory cells and cytokines in spinal cord ischemia-reperfusion injury. Mediators Inflamm 2013; 2013:701970.
7. Fan L, Wang K, Shi Z, Die J, Wang C, Dang X. Tetramethylpyrazine protects spinal cord and reduces inflammation in a rat model of spinal cord ischemia-reperfusion injury, J Vasc Surg 2011; 54:192-200.
8. Yamazaki H, Tanji K, Wakabayashi K, Matsuura S, Itoh K. Role of the Keap1/Nrf2 pathway in neurodegenerative diseases. Pathol Int 2015; 65:210-19.
9. Yang C, Zhang, X Fan H, Liu Y. Curcumin upregulates transcription factor Nrf2, HO-1 expression and protects rat brains against focal ischemia. Brain Res 2009;1 282:133-41.
10. Wang X, de Rivero Vaccari JP, Wang H, Diaz P, German R, Marcillo AE, Keane RW. Activation of the Nuclear Factor E2-Related Factor 2/antioxidant response element pathway is neuroprotective after spinal cord injury. J Neurotrauma 2012; 29:936-45.
11. Huang Y, Li W, Su ZY, Kong AN. The complexity of the Nrf2 pathway: beyond the antioxidant response. J Nutr Biochem 2015; 26:1401-13.
12. Celic T, Spanjol J, Bobinac M, et al. Mn porphyrin-based SOD mimic, MnTnHex-2-PyP(5+), and non-SOD mimic, MnTBAP(3-), suppressed rat spinal cord ischemia/reperfusion injury via NF-κB pathways. Free Radic Res 2014; 48:1426-42.
13. Taguchi K, Motohashi H, Yamamoto M. Molecular mechanisms of the Keap1–Nrf2 pathway in stress response and cancer evolution. Genes Cells 2011; 16:123-40.
14. Ding Y, Chen M, Wang M, Li Y, Wen A. Posttreatment with 11-Keto-β-Boswellic acid ameliorates cerebral ischemia-reperfusion injury: Nrf2/HO-1 pathway as a potential mechanism. Mol Neurobiol 2015; 52:1430-39.
15. Xia X, Qu B, Li YM, et al. NFAT5 protects astrocytes against oxygen-glucose-serum deprivation/restoration damage via the SIRT1/Nrf2 pathway. J Mol Neurosci 2017; 61:96-104.
16. Wang L, Yao Y, He R, et al. Methane ameliorates spinalcord ischemia-reperfusion injury in rats: Antioxidant, anti-inflammatory and anti-apoptotic activity mediated by Nrf2 activation. Free Radic Biol Med 2017; 103:69-86.
17. Park SY, Choi YW, Park G. Nrf2-mediated neuroprotection against oxygen-glucose deprivation/reperfusion injury byemodin via AMPK-dependent inhibition of GSK-3β. J Pharm Pharmacol 2018; 70:525-35.
18. Dai Y, Zhang H, Zhang J, Yan M. Isoquercetin attenuates oxidative stress and neuronal apoptosis after ischemia/reperfusion injury via Nrf2-mediated

inhibition of the NOX4/ROS/NF-κB pathway. Chem Biol Interact 2018; 284:32-40.

19. Li Y1, Zhao Y2, Cheng M1, Qiao Y1, Wang Y1, Xiong W3, Yue W4.Suppression of microRNA–144-3p attenuates oxygen–glucose deprivation/reoxygenation-induced neuronal injury by promoting Brg1/Nrf2/ARE signaling J Biochem Mol Toxicol 2018; 32:e22044.
20. Zhou Z, Liu C, Chen S, et al.Activation of the Nrf2/ARE signaling pathway by probucol contributes to inhibiting inflammation and neuronal apoptosis after spinal cord injury. Oncotarget 2017; 8:52078-93.
21. Faulkner JR, Herrmann JE, Woo MJ, Tansey KE, Doan NB, Sofroniew MV.Reactive astrocytes protect tissue and preserve function after spinal cord injury. J Neurosci 2004; 24:2143-55.

BIOLOGICAL CHARACTERISTICS OF OSTEOCLAST EXOSOMES AND THEIR ROLE IN THE OSTEOGENIC DIFFERENTIATION OF SOMATIC CELLS PRIOR TO OSTEOGENESIS

C. CHEN, RQ. ZHENG, XC. CAO and GC. ZHANG

Department of Orthopaedics, General Hospital of Jinan Military Command, Jinan, Shandong Province, China

Received April 24, 2018 – Accepted June 18, 2018

This study aimed to investigate the biological characteristics of osteoclast exocrine bodies and their role in the differentiation of somatic cells, so as to find out the key factors involved in osteoclast exosomatic growth and osteogenesis. RANKL (Receptor Activator for Nuclear Factor-κ B Ligand) induced factor was used to induce the osteoclast differentiation of Raw 264.7 cells, and TRAP(Tartrate resistant acid phosphatase) staining was employed to identify induced cells. Ultra-filtration centrifugation was used to separate OC-exosomes from osteoclast supernatant, while Western blot was employed to detect the expression characteristics of exosomal proteins CD9 and CD63. PKH67 labeled exosomes were observed to target kusao cells, which were divided into 3 groups, i.e., the complete medium group (group A), the osteoblast induced group (group B), and the osteogenesis induced liquid + OC-exosomes group (group C). The medium was changed on the next day and after 14-day culture. Using Western blot, alizarin red staining and Von Kossa silver staining, the role of OC-exosomes in the differentiation of kusao cells was clarified. Results showed that TRAP staining showed osteoclasts as irregular and TRAP positive giant cells with a red multicore and a large volume. Microcapsule membrane structures with a uniform size were detected in osteoclast supernatant, and the expression of CD9 and CD63 proteins was confirmed by Western blot. In addition, the Western blot results showed that the expression of RUNX2 (Runt-related transcription factor 2) protein in group B was 1.254 times of that in group A and 2.636 times of that in group C. Furthermore, alizarin red staining showed that the ratios of calcium salt deposition area to the total area in group A, group B and group C were 0.208%, 3.469%, and 20.724%, respectively. Von Kossa silver staining showed that the ratios of calcium salt deposition area to the total area in group A, group B and group C were 0.064%, 2.636%, and 20.872%, respectively. To sum up, OC-exosomes can promote the osteogenic differentiation of osteoblast cells (kusao cells).

Osteoporosis (OP) is a type of systemic and metabolic bone disease characterized by reduced bone masses and the destruction of bone microstructures, which can lead to the increased fragility of bones and the tendency of bone fracture (1, 2). The pathogenic mechanism of OP is closely related to a negative bone balance, which is caused by the higher rate of bone degradation by osteoclasts (OC) and the lower rate of bone formation by osteoblasts (OB) (3). As membrane vesicles with

Key words: OC-exosomes, osteogenic precursor cells, osteogenic differentiation, biological characteristics

Mailing address:
Dr Guichun Zhang,
Department of Orthopaedics,
The General Hospital, Jinan Military Command,
No. 25 Shifan Road, Tianqiao Square,
Jinan 250031, Shandong Province, China
e-mail: drzhangguichun@yeah.net

0393-974X (2018)
Copyright © by BIOLIFE, s.a.s.
This publication and/or article is for individual use only and may not be further reproduced without written permission from the copyright holder.
Unauthorized reproduction may result in financial and other penalties
DISCLOSURE: ALL AUTHORS REPORT NO CONFLICTS OF INTEREST RELEVANT TO THIS ARTICLE.

a diameter of about 60-100nm, exosomes are released to the extracellular matrix after fusing with multivesicular body (MVB) and cell membrane (4, 5). According to this study, exosomes mainly act on target cells through endocrine or paracrine mechanisms. In addition, exosomes are capable of clearing the intracellular wastes (6), participating in antigen presentation and immune response (7, 8), and mediating the transmission of intercellular signals (9). A recent study showed that exosomes also played an important role in osteosarcoma, myeloma and other bone related diseases. In a study on the exosomes of osteosarcoma cells, Kuniaki Ota (10) found that the TGF-β in osteosarcoma exosomes could directly or indirectly regulate the secretion of factor ligand 16 (CXCL16) from osteoclasts, thus regulating the transformation between osteoblasts and osteosarcoma cells. In a study on multiple myeloma (MM), Raimondi et al. (11) found that the exosomes derived from MM cells played an important role in promoting the differentiation of osteoclasts by regulating the function of osteoclasts. Therefore, in this study, the biological characteristics of OC-exosomes and their mechanism in osteogenic differentiation were investigated to understand the role of osteoclasts in different metabolic bone diseases, such as osteoporosis and osteosclerosis.

MATERIALS AND METHODS

Cell culture

The Raw 264.7 cells (Shanghai Gefan Biology Technology Co., Ltd., Shanghai, China) and kusao cell strains (Shanghai Bogu Biology Technology Co., Ltd., Shanghai, China) in the liquid nitrogen tank were taken out, rapidly placed in a 37°C water tank, and after thawing, the suspension of cells was aspirated into a 5 ml glass centrifuge tube with a 1 ml sterile pipette tip and centrifuged at 1200 rpm for 3 min. The supernatant was discarded and the cells were gently blown and resuspended in 1 ml of pre-warmed α-MEM complete medium. The suspension was transferred to a 25 cm^2 flask and an appropriate amount of preheated α-MEM complete medium (approximately 3 ml) was added. The flasks were gently shaken and the cells were evenly distributed in the flasks. After being observed by an inverted microscope (Shanghai Yiyuan Optical Instrument Co., Ltd., Shanghai, China), they were placed in a 5% CO^2 incubator (Shanghai Simpson experimental instrument Co., Ltd., Shanghai ,China) at 37°C. After 24-h cultivation, the α-MEM complete medium was replaced, and the growth condition of the cells was observed under an inverted microscope and then the cells were further cultured in a 5% CO^2 incubator at 37°C. When the cells grew to approximately 85% of the flask area, the culture medium in the culture flask was aseptically discarded, and the cells were washed three times with 1 × PBS (Beijing Solarbio Technology Co., Ltd., Beijing, China) and 400 μl of 0.25% trypsin (Gibco Co., Ltd., USA) was added. The flask was shaken gently to allow the pancreatin to fully contact and digest the cells. When the cells became round, wrinkled, and the gap increased, most of the cells floated and the digestion was considered complete. The digestion of trypsin was terminated by adding 1 ml of pre-warmed α-MEM complete medium and the tube was repeatedly pipetted with 1 ml sterile pipette tip. The suspension was pipetted into a 5 ml glass centrifuge tube and centrifuged at 1200 rpm for 3 min. The supernatant was discarded and the cells were gently blown and resuspended in 1 ml of pre-warmed α-MEM complete medium. In which Raw 264.7 cells were resuspended in a ratio of 1:3 to 3 new flasks, and 4 ml of preheated α-MEM complete medium was added to each flask; the kusao cells were pipetted with a 10 μl resuspended cell suspension into a cell counting plate with a sterile pipette and the number of cells was counted under an inverted microscope. They were seeded into 12-well plates at a density of 0.5×10^5 cells, and 2 ml of pre-warmed α-MEM complete medium was added to each well. The subcultivation flasks and inoculated flasks and the 12-well plate were gently shaken so that the cells were evenly distributed therein. The cells were observed in an inverted microscope and cultured in a 5% CO^2 incubator at 37°C. Raw 264.7 cells and kusao cells were cultured in an osteogenic supplemented medium (OS). After 24 h, the medium of kusao cells was replaced by α-MEM complete culture fluid (group A), osteogenic induction medium (group B), or osteogenic induction medium + OC-exosomes (group C). The cells of each group were cultured in 4 wells of a 12-well plate. After every other day, the media were changed. After 14-day culture, the proteins in the media were harvested.

Osteoclast induction

When the cells reached 90% confluency as observed under an inverted microscope, the cells were rinsed 3 times by 1x PBS and trypsinized using 500 μL of 0.25% trypsin. During trypsinization, the culture plate was gently shaken until all cells became round and detached. Subsequently, 1 mL preheated α-MEM complete medium was added into the culture flask to terminate trypsin digestion. Using a 1 mL aseptic pipette, the cells were dispersed into a uniform suspension, which was then loaded into a 5 mL glass centrifuge tube and centrifuged at 1200 rpm for 3 min. After discarding the supernatant, the cells were re-suspended in 1mL preheated α-MEM complete medium and 10μL of the suspension was loaded onto a cell counting plate to calculate the density of the cells under an inverted microscope. Subsequently, cells at a density of 2.5×10^5 cells/ml were inoculated into a $25cm^2$ culture flask containing 4mL of preheated α-MEM complete medium. The cells were cultured in 5% CO_2 and 37°C for 24 h before the medium was replaced with 4 mL of preheated α-MEM complete medium containing 4 μL of RANKL inducer (Gibco Co., Ltd., USA) at a final concentration of 100ng/mL. After 48-hour culture, the medium was replaced to serum-free α-MEM complete medium and the morphological changes of the cells were observed under the inverted microscope. Finally, the cell supernatant in the culture flask was collected 24 h later.

Collection of exosomes

Raw 264.7 cells and osteoclasts were cultured in a serum-free medium for 24 h before the supernatant was collected. The collected supernatant was then filtered through a 0.22 μm filter and subjected to ultra-filtration using a 0.06 μm filter. The filtrate was then concentrated by centrifugation at 10,000 rpm and 4°C for 10 min to obtain the exosomes.

TRAP staining

After 48-hour RANKL induction, the supernatant was discarded and the cells were washed 3 times with 1x PBS before they were fixed in a proper amount of polyoxymethylene at room temperature for 30min. Subsequently, the polyoxymethylene was removed and the cells were washed again for 3 times with 1x PBS, followed by the addition of a proper amount of TRAP staining dye (Beijing Reagan Biotechnology Co., Ltd., Beijing, China) in the culture flask and incubation for about 30 min at 37°C. Finally, the TRAP staining dye was removed, and the cells were washed with 1x PBS and air dried at room temperature.

Determination of protein concentration

The protein concentration of prepared protein samples was measured by Bradford assay. In brief, 10, 15, 10, 0, 0, 0, 0, and 0 μL of standard BSA solution (2mg/mL) was added into 8 EP labels, respectively, followed by the addition of 5 μL double distilled water in the No. 2 tube. After mixing, 10 μL of the solution in the No. 2 tube was transferred into the No. 4 tube. In the next step, 10 μL of double distilled water was added into the No. 3 tube.

Table I. *Protein concentration measured by Bradford assay.*

EP tube number	1	2	3	4	5	6	7	8
Volume of standard solution	10 μL							
Source of standard solution	2mg/mL stock	2mg/mL stock	2mg/mL stock	No. 2 tube	No. 3 tube	No. 5 tube	No. 6 tube	-
Volume of dilute /μL	0	5	10	10	10	10	10	10
Final concentration /mg·mL^{-1}	2	1.5	1	0.75	0.5	0.25	0.125	0

After mixing, 10 μL of the solution in the No. 3 tube was transferred into the No. 5 tube. In the next step, 10 μL of double distilled water was added into the No. 4 tube. After mixing, 10 μL of the solution in the No. 4 was removed. In the next step, 10 μL of double distilled water was added into the No. 5 tube. After mixing, 10 μL of the solution in the No. 5 tube was transferred into the No. 6 tube. In the next step, 10 μL of double distilled water was added into the No. 6 tube. After mixing, 10 μL of the solution in the No. 6 tube was transferred into the No. 7 tube. In the next step, 10 μL of double distilled water was added into the No. 7 tube. After mixing, 10 μL of the solution in the No. 7 tube was removed. Finally, 10 μL of double distilled water was added into the No. 8 tube, and the concentration of proteins in these tubes was 2, 1.5, 1, 0.75, 0.5, 0.25, 0.125, and 0mg/mL, respectively, as shown in Table I. The above concentrations of BSA standard were used to plot the standard curve. During the measurement of protein samples, 10μL of the samples were added into each EP tube and mixed with 0.5 mL of Bradford reagent (Bio-Rad Co., Ltd., USA). Subsequently, 100 μL of mixed solution was added into each well of a 96-well plate and each sample was measured in triplicate. The actual concentration of each sample was calculated by comparing its OD value, which was measured using a multifunctional plate reader (Promega Co., Ltd., USA), with the standard curve.

Western blot detection

The protein samples were loaded onto a 10% SDS-PAGE gel (Bio-Rad Co., Ltd., USA) according to the concentration of the protein samples. Subsequently, the proteins were separated by electrophoresis and then blotted onto a PVDF membrane pre-soaked in methanol. During the 45 min of blotting, the voltage was set to 20V. After the blotting was completed, the PVDF membrane was blocked for 1 h at room temperature using 15 mL of 1× TBST containing 5% skimmed milk. Subsequently, according to the molecular weight of target proteins and reference standards, the membrane was cut into several strips and incubated with 2 mL of 1× TBST containing 5% skimmed milk and rabbit polyclonal anti-CD9 antibodies (1:1000 dilution). Similarly, other membrane strips were also incubated with 2 mL of 1× TBST containing 5% skimmed milk and rabbit polyclonal anti-CD63 antibodies, rabbit polyclonal anti-RUNX2 antibodies, rabbit polyclonal anti-MMP9 antibodies, rabbit polyclonal anti-β-actin antibodies, and rabbit polyclonal anti-α-Tubulin antibodies. The incubation was carried out overnight at 4°C. After rinsing 3 times with 10 mL of 1× TBST, the membrane strips were incubated for 1h at room temperature with 2 mL of 1× TBST containing 5% skimmed milk and HRP-conjugated goat anti-rabbit IgG antibodies (1:3000 dilution). After rinsing 3 times with 10mL of 1× TBST, the protein bands were visualized using an ECL reagent.

PKH67 labeling of exosomes in target kusao cells

Exosomes in 1 mL of diluted suspension were precipitated and stained with a PKH67 dye at the concentration of 4×10^{-6}mol/L. The staining was carried out by incubating the exosomes with the PKH67 dye for 2-5min at room temperature. At the end of incubation, an equal amount of 1% BSA solution was added to the stained exosomes to terminate the staining reaction, followed by centrifugation at 10,000 rpm for 70 min. After removing the supernatant, 1 mL of serum-free culture medium was added into the precipitated exosomes, which were then cultured with kusao cells for 6 h. Finally, after 4-h DAPI(4', 6-diamidino-2-phenylindole) staining, the intake of exosomes by kusao cells was analyzed under a fluorescence microscope.

Alizarin red staining

There were 4 holes for each group in the 12 orifice plate. On the next day, the liquid was changed. After 14 days of culture, the supernatant was removed. After cleaning with 1× PBS, it was given to 4% polyformaldehyde at room temperature for 20 min. The fixed liquid was removed and washed 3 times with a proper amount of 1× PBS. At room temperature, 1% alizarin red dye was used for staining for 5 min, and it was then rinsed with distilled water, and stored at room temperature after drying.

Von kossa silver staining

On a 12-well plate, there were 4 wells for each group. On the next day, the culture medium was changed. After 14 days of culture, the supernatant was removed and the cells were rinsed with 1×PBS, followed by fixation in 4% polyformaldehyde at room temperature for 20 min. Subsequently, polyformaldehyde was removed and the cells were rinsed with 1×PBS for 3 times. Under good illumination of sunlight or under ultraviolet light, the cells

were then stained in a 2% silver nitrate solution for 60 min and rinsed with distilled water for 5 min. Subsequently, the cells were incubated with a 5% sodium thiosulfate solution for 2 min and rinsed with tap water for 5 min, followed by staining with 0.1% nuclear fast red for 2 min and rinsing with distilled water for 5-10 s and air dried at room temperature.

Statistical analysis

In images of cells which underwent alizarin red and Von kossa silver staining, the amount of calcium salt deposition was quantitatively analyzed by Image Pro Plus 6 software. In addition, the gray value of protein bands in Western blotting was semi quantitatively analyzed by Image Lab 5.2.1 software. All results were tested by *t*-tests using SPSS 19 statistical software. The data were expressed as $\bar{x} \pm s$ and $P<0.05$ indicated that the difference was statistically significant.

RESULTS

Identification of osteoclasts by TRAP staining

The anti-tartaric acid phosphatase (TRAP) staining forms a specific insoluble and red precipitate by the enzyme of the zeol ASBI phosphate in the TRAP dye. TRAP staining is the most common and intuitive method for the identification of osteoclasts. TRAP positive cells with 3 or more than 3 nuclei can be identified as osteoclasts. In the TRAP staining experiments of this study, many TRAP positive giant cells were identified as osteoclasts, which were red, multinucleated (>3), of large dimension and irregular shape. Therefore, the successful induction of Raw264.7 cells into osteoclasts was confirmed (Fig. 1).

Western blot detection of CD9 and CD63 protein expression

The protein concentration of the samples was measured by the Bradford method. The equation of the standard curve was y=5.091×-0.975 and the protein concentration of osteoclast exosomes was 1876.65μg/mL. In particular, since CD9 and CD63 are specific markers of exocrine bodies, they are often used to identify exosomes. In this study, the exosomes isolated from the samples were evaluated using Western blot analysis. The results showed that the molecular weight of CD9 protein was 20kD, and the molecular weight of CD63 protein was 43kD. The molecular weight of these two proteins was expected, thus confirming that the isolation of exosomes was successful (Fig. 2).

Uptake of osteoclast exosomes by kusao cells

PKH67 is a special membrane protein dye that can specifically bind to the membrane protein and emit a green fluorescence to mark the membrane protein. The results of this study showed that upon PKH67 staining, green fluorescence signals were observed around the nucleus (marked as blue by DAPI staining) of kusao cells, consistent with the characteristics of typical exosomes after assimilation (Fig. 3).

Western blot analysis on the expression of nuclear transcription factor RUNX2 during osteogenic differentiation

The protein concentration of the samples was determined by the Bradford method. The equation of the standard curve was y=6.336×-1.730 and the protein concentrations in group A, group B and group C were 1376.52μg/mL, 1389.21μg/mL and 1358.69μg/mL, respectively. RUNX2 is a member of the RUNXX family and plays an important role in the formation and reconstruction of bone tissues. It is the most specific marker gene during the process of bone formation. Western blot analysis on the three groups of protein samples showed that the molecular weight of RUNX2 protein was 57kD, while the molecular weight of reference protein β-actin was 43kD. The molecular weight of these two proteins was expected, indicating that RUNX2 was present in all 3 groups of protein samples, although its expression in different groups was different. By analyzing the gray values of RUNX2 and β-actin bands, the results showed that the expression of RUNX2 protein in group B was 1.254 times higher than that in group A and 2.636 times higher than that in group C (Table II).

Alizarin red staining

In the alizarin red staining experiment, no red

Table II. *Protein expression analysis of RUNX2.*

Groups	Group A	Group B	Group C
RUNX2	67,771.33	87,236.26	36,574.24
β-actin	1,724,724.45	1,770,342.15	1,953,691.41
RUNX2/β-actin	0.0393	0.0493	0.0187
Odds ratio	2.102(A/C)	1.254(B/A)	2.636(B/C)

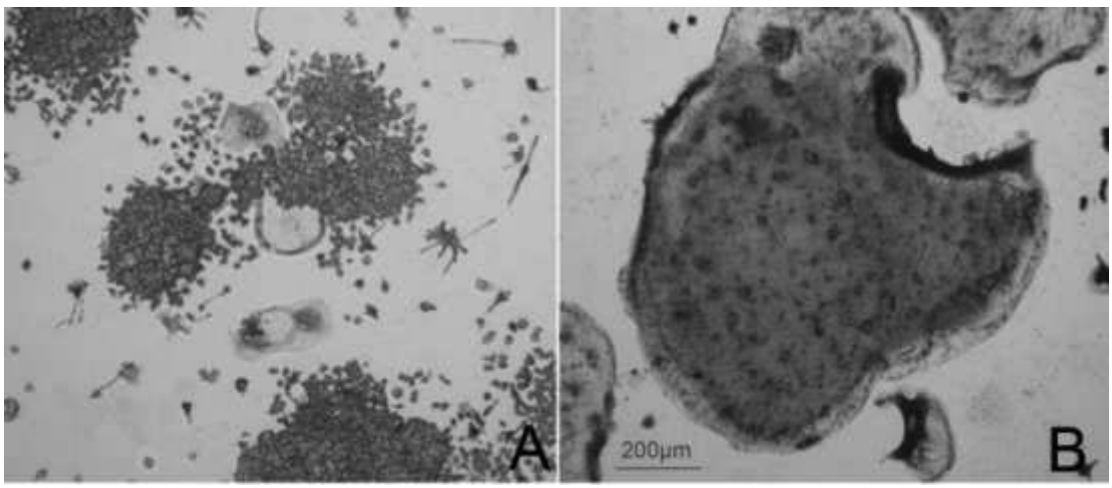

Fig. 1. *TRAP staining results (×100).*

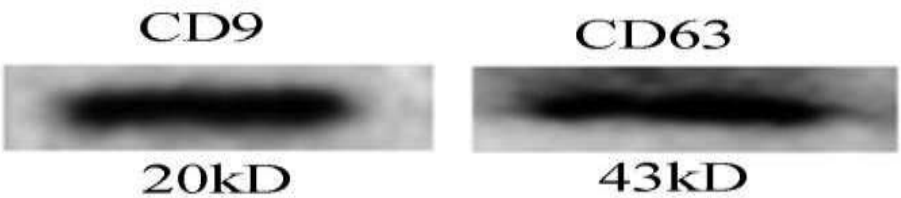

Fig. 2. *Western blot detection of CD9 and CD63 protein expression.*

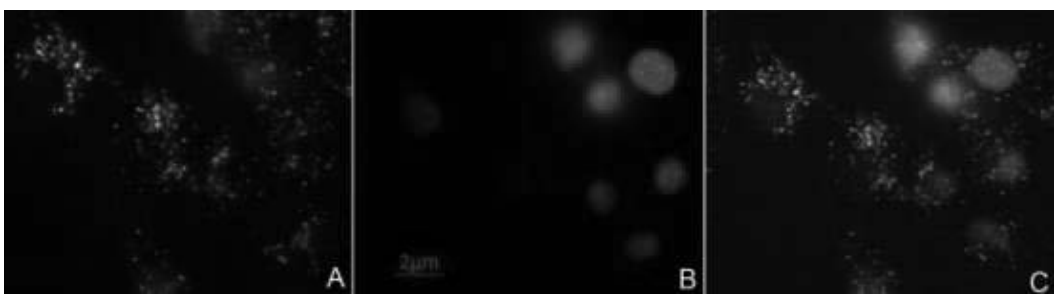

Fig. 3. *PKH67 labeled exosomes in kusao cells.*

calcium deposition was found in group A, while little red calcium deposition was found in group B. However, a large number of red calcium deposits were found in group C. The ratios of calcium deposition area to the total area in the 3 groups were 0.208%, 3.469% and 20.724%, respectively (Fig. 4).

Von kossa silver staining

Von kossa silver staining is commonly used in the identification of osteogenic differentiation of cells. In the Von Kossa silver staining experiment performed in this study, no black calcium deposition was observed in group A, while a small amount of black calcium deposition was observed in group B. However, a large number of black calcium deposits were observed in group C. The ratios of calcium deposition area to the total area of 3 groups were 0.064%, 2.636% and 20.872%, respectively.

DISCUSSION

The identification of exosomes mainly depends on morphological observation and protein analysis (12). During protein analysis, Western blot is commonly used to detect the protein composition of exosomes and to measure the expression of characteristic marker proteins such as CD63 and CD9. In this study, the exosomes obtained by ultrafiltration centrifugation were evaluated by Western blot, and the presence of CD9 and CD63 in these exosomes was confirmed. In addition, the results also showed that ultrafiltration centrifugation could extract bioactive exosomes from osteoclast supernatant and effectively obtain extracellular osteoclasts with biological activity.

In alizarin red staining, the sulfuric acid group and light radical group of alizarin red S structure react with calcium ions to form red or orange complexes. Therefore, alizarin red staining can be used to identify calcium compounds in tissues or cells (13). During Von kossa silver staining, silver or silver carbonate can be produced by mixing the silver nitrate solution with calcium phosphate or carbonate (14, 15), and hence the black deposits indicate the deposition of calcium salt in mineralized tissues. The change of calcium salt content is one of the markers for the osteogenesis potential of bone tissues as well as the proliferation and differentiation of osteoblasts. The above two staining methods are commonly used in the identification of osteogenic differentiation of cells (13, 15). In the alizarin red staining and Von kossa silver staining of this experiment, the ratio of calcium salt deposition area to the total area in group C was significantly larger than that in group A and group B, indicating the mineralization level in group C was high and osteoclast exosomes could promote the osteoblastic differentiation of kusao cells.

RUNX2 is one of the specific transcription factors for osteogenic differentiation. RUNX2 has the ability to regulate the transcription of various proteins related to the mineralization of preosteoblasts and chondrocytes, as well as the differentiation of these cells to osteoblasts (16, 17). Both *in vitro* and *in vivo* experiments have shown that RUNX2 acts as a key factor in the osteogenesis of bone marrow mesenchymal stem cells (MSCs) and bone development (18, 19). In this study, the results

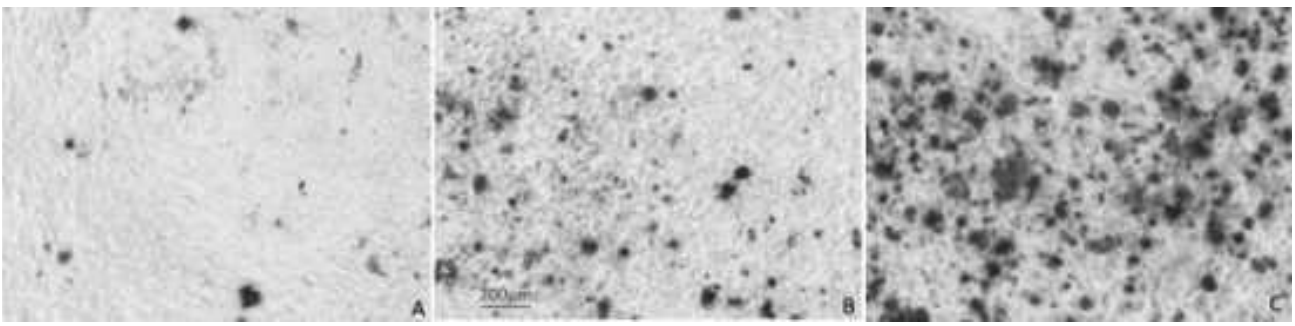

Fig. 4. *Alizarin red staining results (×100).*

of Western blot analysis showed that the osteogenic differentiation process in group C was faster than that in group B, indicating that the exosomes of osteoclasts accelerated the osteogenic differentiation process of kusao cells. In fact, after being cultured for 14 days, the kusao cells in group C were found to be in the late stage of cell differentiation. Since RUNX2 and SPP1 are both products of early osteoblast differentiation, the expression of these two genes in group C was significantly reduced after 14 days of cell culture. In contrary, since the cells in group B were still in the early stage of osteoblastic differentiation, the expression of RUNX2 and SPP1 in group B was still high after 14 days of cell culture, indicating that osteoclast exosomes promoted the osteogenic differentiation of kusao cells. However, it is not clear which substance in the osteoclast exosomes promoted the osteogenic differentiation of the cells. In addition, the underlying mechanism of such substance during osteogenic differentiation remains unclear.

REFERENCES

1. Jacques RM, Boonen S, Cosman F, Reid IR, Bauer DC, Black DM, Eastell R. Relationship of changes in total hip bone mineral density to vertebral and nonvertebral fracture risk in women with postmenopausal osteoporosis treated with once-yearly zoledronic acid 5 mg: the HORIZON-Pivotal Fracture Trial (PFT). J Bone Miner Res 2012; 27(8):1627-34.
2. Yesil Y, Ulger Z, Halil M, Halaçli B, Yavuz BB, Yeşil NK, Kuyumcu ME, Cankurtaran M, Ariogul S. Coexistence of osteoporosis (OP) and coronary artery disease (CAD) in the elderly: it is not just a by chance event. Arch Gerontol Geriatr 2012; 54(3):473-76.
3. Bonnelye E, Chabadel A, Saltel F, Jurdic P. Dual effect of strontium ranelate: Stimulation of osteoblast differentiation and inhibition of osteoclast formation and resorption in vitro. Bone 2008; 42(1):129-38.
4. Nagashima S, Jirintai S, Takahashi M, et al. Hepatitis E virus egress depends on the exosomal pathway, with secretory exosomes derived from multivesicular bodies. J Gen Virol 2014; 95(10):2166-75.
5. Wei T, Hibino H, Omura T. Release of Rice dwarf virus from insect vector cells involves secretory exosomes derived from multivesicular bodies. Commun Integr Biol 2009; 2(4):324-26.
6. Géminard C, de Gassart A, Vidal M. Reticulocyte maturation: mitoptosis and exosome release. Biocell 2002; 26(2):205-15.
7. Théry C, Ostrowski M, Segura E. Membrane vesicles as conveyors of immune responses. Nat Rev Immunol 2009; 9(8):581-93.
8. Escudier B, Dorval T, Chaput N, et al. Vaccination of metastatic melanoma patients with autologous dendritic cell (DC) derived-exosomes: results of the first phase I clinical trial. J Transl Med 2005; 3(1):10.
9. Kate K, Vivian B. Exosomes go with the Wnt. Cell Logist 2012; 2(3):169-73.
10. Ota K, Quint P, Weivoda MM, et al. Transforming growth factor beta 1 induces CXCL16 and leukemia inhibitory factor expression in osteoclasts to modulate migration of osteoblast progenitors. Bone 2013; 57(1):68-75.
11. Raimondi L, De Luca A, Amodio N, et al. Involvement of multiple myeloma cell-derived exosomes in osteoclast differentiation. Oncotarget 2015; 6(15):13772-89.
12. Mccready J, Sims J D, Chan D, Jay DG. Secretion of extracellular hsp90α via exosomes increases cancer cell motility: a role for plasminogen activation. BMC Cancer 2010; 10(1):294.
13. Cheng SL, Shao JS, Behrmann A, Krchma K, Towler DA. Dkk1 and MSX2-Wnt7b signaling reciprocally regulate the endothelial-mesenchymal transition in aortic endothelial cells. Arterioscler Thromb Vasc Biol 2013; 33(7):1679-89.
14. Chae IH, Kwon HJ, Kim EK, Moon HJ, Yoon JH, Lee HS, Kwak JY. Value of additional von Kossa staining in thyroid nodules with echogenic spots on ultrasound. Pathol Res Pract 2016; 212(5):415-20.
15. Martin TJ, Allan EH, Ho PW, et al. Communication between EphrinB2 and EphB4 within the osteoblast Lineage. Adv Exp Med Biol 2010; 658:51-60.
16. Lecka-Czernik B, Gubrij I, Moerman EJ, Kajkenova O, Lipschitz DA, Manolagas SC, Jilka RL. Inhibition of Osf2/Cbfa1 expression and terminal osteoblast differentiation by PPARγ2. J Cell Biochem 1999; 74(3):357-71.
17. Park JS, Chu JS, Tsou AD, Diop R, Tang Z, Wang A, Li

S. The effect of matrix stiffness on the differentiation of mesenchymal stem cells in response to TGF-β. Biomaterials 2011; 32(16):3921-30.
18. Saito T, Ogawa M, Hata Y, Bessho K. Acceleration effect of human recombinant bone morphogenetic protein-2 on differentiation of human pulp cells into odontoblasts. J Endod 2004; 30(4):205-8.
19. Komori T. Regulation of osteoblast differentiation by transcription factors. J Cell Biochem 2006; 99(5):1233-39.

DIFFERENTIAL EXPRESSION AND ANALYSIS OF TARGET REGULATION OF microRNAs IN ALCOHOL-DEPENDENT RATS

F. XIN[1], X.M. YE[1], H.B. LIU[2], L.P. LIU[3], L.J. YAN[4] and J. HU[1]

[1]The First Affiliated Hospital of Harbin Medical University, Harbin, Heilongjiang, China; [2]College of Bioinformatics Science and Technology, Harbin Medical University, Harbin, Heilongjiang, China; [3]Harbin First Specialist Hospital, Heilongjiang, China; [4]The Fourth Affiliated Hospital of Harbin Medical University, Harbin, Heilongjiang, China

Received April 12, 2018 – Accepted June 8, 2018

This study analyzed the differential expression of miRNAs related to alcohol dependence in rats undergoing continued consumption and withdrawal. Furthermore miRNAs were sought and evaluated for potential use as biomarkers for diagnosis. This study used Exiqon miRCURY™ LNA miRNA microarray on alcohol-dependent and normal rats for the expression of microRNAs in perfluorinated compounds, and the stem-loop qPCR method to validate its expression in brain tissue. We forecast the relevant target genes of differentially expressed miRNA and drew the regulatory network. Comparison of the differential expression between brain tissue and plasma was carried out and the correlation and analyzed.65 miRNA with differential expression with threshold of 1.5 were screened out; among them, most miRNA with differential expression in the dependent group had relatively high expression values. The target genes were found with great confidence: PIK3CA, MAPK, NTF, BDNF, NGFR, IGF-1, and the pair consisting of miRNA- mRNA. Among the three groups, the expression levels of miR-101b ($F=8.12$, $P<0.05$) showed significant difference; no significant difference was found in the expression levels of miRNA in plasma among the groups ($F=1.23$, $P>0.05$). No consistency was shown in the changing trend of miRNA in PFC and plasma ($r= -.004$, $p>0.05$). The genetic regulatory network of neurotrophic factors, its receptors and the protein kinases that influence metabolism may mediate the incidence of alcohol-dependence. There is a lack of conformity between the expression of miR-101b in the prefrontal cortex and the plasma.

Alcohol dependence is currently one of the important public health problems in the world; its incidence is closely related to genetic and environmental factors (1). It has been found that chronic consumption of alcohol induces long-term changes in brain gene and protein expression, which allow brain cells to adapt through homeostatic alterations in distinct signaling pathways (2). MicroRNAs are short, non-coding RNAs that utilize sequence complementarity to bind RNA transcripts, thus modifying their expression. A single microRNA can simultaneously alter expression of numerous genes, while multiple microRNAs can act in a coordinated fashion to precisely control the expression of a single gene (3). Recently, microRNAs (miRNAs) have been proposed as regulators in the various processes involved in alcohol intake, and there is growing evidence that they may play an important regulatory role. There are multiple differential expressions of miRNA existing in alcohol

Key words: alcohol dependence, withdrawal, microRNA, target gene, prefrontal cortex, plasma

Mailing address:
Dr Jian Hu,
Mental Health Institute, First Affiliated Hospital
Harbin Medical University, 23 Youzheng Street,
Nangang District, Harbin, Heilongjiang 150001, PR China
Tel.: +86 451 53674442 - Fax: +86 451 53670428.
e-mail: hujianhj0451@126.com

0393-974X (2018)
Copyright © by BIOLIFE, s.a.s.
This publication and/or article is for individual use only and may not be further reproduced without written permission from the copyright holder. Unauthorized reproduction may result in financial and other penalties
DISCLOSURE: ALL AUTHORS REPORT NO CONFLICTS OF INTEREST RELEVANT TO THIS ARTICLE.

dependence but, due to certain characteristics of miRNA, many studies have differing conclusions (4-6). In three studies using miRNA microarrays with the brain tissue of alcohol-dependent mammals, an overlap of only 2 miRNAs was found the expression of which was altered following alcohol dependence both in rats and humans: miR-7, miR-101 (7-9). Interestingly, some of the common differentially expressed genes change in opposite directions when the human and animal models are compared, with a majority of differentially expressed genes being upregulated in the ethanol-treated animal brains but downregulated in the brains of alcoholics. This may be related to the timing of miRNA expression, and is consistent with the results of the *in vitro* experiments. This fully illustrates the differences in the role of miRNA at the different stages of alcohol dependence.

Mounting evidence revealed that miRNAs play a key role in the effects of alcohol on brain function (7-12), although the complex regulatory mechanisms governing these changes are not fully understood. Research has shown that miRNA exists in circulatory biofluids, such as blood and its components (which in our case consists of serum and plasma), and that it has great stability. For example, the miRNA content can remain relatively stable at room temperature for as long as 24 h after 8 repeated freezes and thaws. It can, moreover, even remain stable under a variety of adverse circumstances, such as exposure to strong acids, strong bases, DNA enzymes and RNA enzymes. Thus, it is convenient to set reference values for detection and comparison. In addition, since there are no significant individual differences in the expression of miRNA in serum and plasma, miRNA can be detected by the extraction of serum or plasma in clinical practice, which can be regarded as a biological marker for diagnosis of disease. At present, brain-specific miRNAs have been identified in the blood, and it has been suggested that they may provide an opportunity for evaluating ongoing changes in the CNS upon the initiation of neurodegeneration. For example, in Alzheimer's disease, miRNAs that are associated with neuropathological changes in post-mortem brain tissue have been detected in blood sera of subjects meeting ante-mortem criteria for the disease, albeit at lower basal levels. MiRNAs are a promising biomarker for monitoring the pathogenesis of neurodegenerative disease, particularly in its pre-symptomatic and initial phases (13). To date, no report has been published on the detection of changes in serum levels of miRNA in alcohol-dependent patients. Furthermore, no research has ever been conducted on the consistency of miRNA expression in tissues and bodily fluids.

In respect to the circumstances and (academic) reasons mentioned above, a comparative/contrastive study was carried out in order to evaluate the expression profiles of miRNAs in the prefrontal cortex of rats with alcohol-dependent non-withdrawal and with alcohol withdrawal. In addition, bioinformatics technology was used to predict target genes related to miRNAs with differential expression, and a regulatory network map was constructed at the same time with the expectation of improving and working towards a comprehensive understanding of the mechanism of alcohol dependence. At the same time, expression levels of miR-101 expressed differentially in the prefrontal cortex was detected in the plasma, followed by a correlation analysis with the expression level in brain tissues. The present study achieved its goals/aims in terms of laying a theoretical foundation for further analysis of the role of miRNAs in the pathogenesis of alcohol dependence and helping to promote the search for biomarkers for the diagnosis of alcohol dependence.

MATERIALS AND METHODS

Animals

Adult male Wistar rats (Qualified number: SCXK (ji) - 2011-0004) were 6–8 weeks old and weighed 200 ~ 250 g at the outset of the experiment. The animals were housed 10 per cage and acclimated to the colony room for at least one week, and lights were on a reversed 12-h light/dark cycle in a temperature-controlled (21±1°C) and humidity-controlled (55±10%) environment, with food and water available ad libitum. The rats were then randomly divided into an alcohol-dependent non-withdrawal group (n=20), a withdrawal group (n=20) and a control group (n=10). The procedure was approved by the ethics committee on animal experiments of the Harbin medical University in

accordance with international regulations on the care and use of laboratory animals.

Chronic ethanol administration

In accordance with the literature of Braconi and Gilpin et al., an alcohol-dependent animal model was established by modified repeated gavage administration with alcohol (14). An ethanol solution was allocated with distilled water and anhydrous ethanol. Gavage administration was provided for 1 week with the initial concentration of the volume ratio of alcohol and distilled water at 5% (V/V), followed by 10% (V/V) in the 2nd week and 20% (V/V) in the 3rd week, which was then maintained at 40% (V/V) beginning in the 4th week. A dose of 10 ml/kg/d was used 2 times a day for gavage administration, with an interval of 10 h at a time, and a total duration of 8 weeks. Furthermore, 12 h after gavage administration on the 8th weekend in the process of modeling, experimental rats were given a withdrawal score to determine the success of modeling. Rats in the control group were fed with equal amounts of glucose solution.

Alcohol was withdrawn 24 h before the sample was taken in the withdrawal group. In the alcohol-dependent non-withdrawal group, rats were decapitated and 2 ml of blood taken from the abdominal aorta, after which brain tissues were quickly collected following intraperitoneal injection of 0.3ml/100g 10% chloral hydrate for anesthesia 1 h after the last administration of alcohol. Additionally, the bilateral prefrontal cortex was separated on a surface of saline ice. Blood samples were collected in tubes containing EDTA as anticoagulant and centrifuged for 10 min at 3,000 rpm and -4°C to obtain plasma supernatant. The tissue and plasma specimens were preserved in cryogenic vials and frozen under liquid nitrogen. All rats were treated according to the above-described methods.

RNA extraction and microarray expression profiling

Total RNA was isolated using TRIzol (Invitrogen) and an miRNeasy Serum/Plasma Kit (QIAGEN) according to the manufacturers' instructions, which efficiently recovered all RNA species, including miRNAs. RNA quality and quantity was measured using a nanodrop spectrophotometer and RNA integrity was determined by gel electrophoresis.

Random selection was using 3 subsamples of each sample for microRNA microarray analysis. After having passed RNA quantity measurement using the NanoDrop 1000, the samples were labeled using the miRCURY™ Hy3™/Hy5™ Power labeling kit and hybridized on the miRCURY™ LNA Array (v.18.0). Following the washing steps the slides were scanned using the Axon GenePix 4000B microarray scanner. Scanned images were then imported into the GenePix Pro 6.0 software (Axon) for grid alignment and data extraction. Replicated miRNAs were averaged and miRNAs with intensities>=30 in all samples were chosen for calculating the normalization factor. Expressed data were normalized using median normalization. After normalization, significantly differentially expressed miRNAs were identified through volcano plot filtering. Hierarchical clustering was performed using the MEV software (v4.6, TIGR).

Reverse transcription and validation by real-time PCR analysis

According to the results of the miRNA chip, combined with previous related literature (4, 6, 15, 16), four miRNAs were selected for stem-loop RT-PCR detection. The primers were synthesized by Harbin BOSCH company. Reference instructions for cDNA synthesis steps, 20 ul reaction system, total RNA1000 ng (Promega A3500). Reaction conditions 25°C, 10 min; 42°C, 60 min; 95°C, 5 min. The synthetic cDNA was temporarily stored at 4°C and then at -80°C for long-term storage.

Real-time quantitative PCR (qPCR) analysis of brain tissue and circulating microRNAs was performed as previously reported. miR-101b-RT:CTCAACTGGTGTCGTGGAGTCGGCAATTCAGTTGAGGCATCGGT,F:ACACTCCAGCTGGGTCGGTTATCATGGTA-3,R:TGGTGTCGTGGAGTCG. miR-34c-5p-RT:GTCGTATCCAGTGCGTGTCGTGGAGTCGGCAATTGCACTGGATACGACGCAATC, F:GAGGCAGTGTAGTTAGCT, R:GGCAATTGCACTGGATAC. miR-10b-3p-RT:GTCGTATCCAGTGCGTGTCGTGGAGTCGGCAATTGCACTGGATACGACTTCCC, F:GGGGACAGATTCGATTCTAG, R:TCGGCAATTGCACTGGATAC. miR-16-3p-RT:CTCAACTGGTGTCGTGGAGTCGGCAATTCAGTTGAGAAGCAG,F:ACACTCCAGCTGGGACCAATATTATTGTG,R:TGGTGTCGTGGAGTCG. U6 by internal reference, U6-RT:GTCGTATCCAGTGCAGGGTCCGAGGTATTCGCACTGGATACGACAAAAATAT,F:G

CGCGTCGTGAAGCGTTC,R:TGGTGTCGTGGAGTCG. Real-Time PCR was performed in 25μl with 2.5μl of cDNA, 1μl of each primer, and 12.5μl of Fast Start Universal SYBR Green Master (Rox) under the following conditions: 95°C for 10min, 40 cycles of 95°C for 30s, and 58°C for 60s in MX3005p (Agilent). QPCR assays were performed in duplicate for each sample, and the mean value was used for the calculation of microRNA expression levels.

MiRNA target prediction and gene list functional enrichment analysis

The experiment confirmed miRNA target genes within *Rattus norvegicus* species, including 285 miRNA-target gene pairs, all obtained through the miRTarBase database. Moreover, 171 miRNA-target gene pairs were obtained from miRecords, and both were combined to obtain a total of 418 miRNA-target gene pairs. The functional enrichment of these target genes was analyzed by DAVID (http://david.abcc.ncifcrf.gov/home.jsp). Pathway annotation was performed on the target genes regulated by differential miRNAs in order to ascertain all the pathways. In addition, the significance level (P value) and false discovery rate (FDR) of pathways were calculated using the Fisher's exact test and *chi*-squared test to screen the significant pathway-involved targets genes. The screening criteria for significant results were P value<0.001 and FDR<0.05. In such way, the significant target genes were screened out. The control network diagram of the relationship between miRNAs and target genes was constructed.

Statistical analyses

All analyses were performed using IBM SPSS Statistics version 20 (IBM Corporation). The normal distribution of the data and the homogeneity of variances were tested using the Shapiro-Wilk and Levene's tests, respectively. Analysis of relative gene expression data was conducted using real-time quantitative PCR and the $2^{\Delta\Delta CT}$ method. Comparison of miRNA expression in each group was made using the Cruskal-Wallis rank sum test. Spearman correlation analysis was used to compare the correlation between the expression of miR-101 in brain tissue and in plasma. The threshold for statistical significance was set at $P<0.05$. Extreme values, which were defined as potential outliers using the box-plot function from SPSS software, are denoted in the figure legends and were excluded from the analyses.

RESULTS

Sample RNA quality control data

The integrity of RNA can be assessed by electrophoresis on a denaturing agarose gel. Intact total RNA run on a denaturing gel will have sharp 28S and 18S rRNA bands. The intensity of the upper band should be about twice that of the lower band. This is depicted in Fig. 1.

Differentially expressed miRNAs

To screen differentially expressed miRNA among the three groups, the maximum and minimum values were calculated for each miRNA

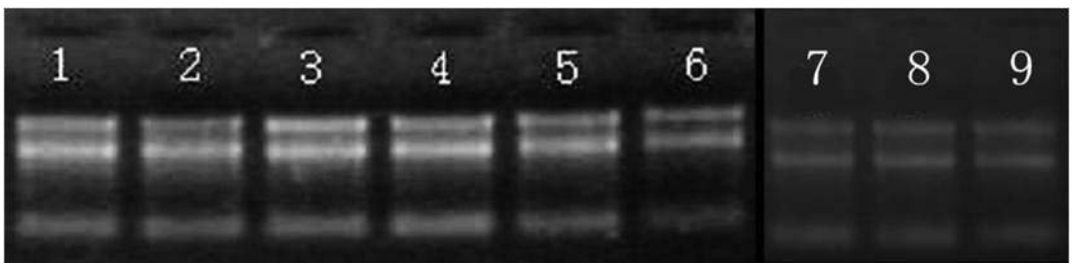

Fig. 1. *Denaturing agarose gel electrophoresis. The 28S and 18S ribosomal RNA bands should be fairly sharp, intense bands. The intensity of the upper band should be about twice that of the lower band. Smaller, more diffuse bands representing low molecular weight RNAs (tRNA and 5S ribosomal RNA) may be presented.*

expressed in the three groups. MiRNAs with a maximum value - minimum value >1.5 were differentially expressed miRNA. Based on this threshold, a total of 65 differentially expressed miRNA were screened among the three groups of samples. Of these, most miRNA with differential expression in the dependent group had relatively high expression value. Compared with the control group, in the dependent group there were 42 upregulated miRNA genes, and 8 downregulated miRNA genes (Table I). Compared with the control group, in the abstinent group there were 4 upregulated miRNA genes, and 6 downregulated miRNA genes (Table II).

Functional enrichment analysis of target genes of differential expression miRNA

Target genes of differentially expressed miRNA were obtained based on miRNA target genes information provided by the miRDB database (http://mirdb.org/miRDB/). In 65 differentially expressed miRNA, 17 miRNA target genes (2,087 in total) were found with high confidence. DAVID (http://david.abcc.ncifcrf.gov/home.jsp) was applied for

Table I. *The differential expression of miRNA and its low confidence target gene between the dependence group and the control group.*

Name	Fold change	low confidence target gene
miR-412-5p	4.183↑	Xpo1/ Dhx15/ Hn1l
miR-3574	3.699↑	Htr2c/ Map2k6/ Aldh1a3/ Aldh1b1/ Bcl2/ Gabrr1/
miR-295-5p	3.514↑	Aldh7a1/Aldh18a1/ Nxph1/ Aldh1a3/ Aldh5a1/ Aldh1a1/ Aldh3a2/ Aldh16a1/ Aldh4a1/ Bcl2/Bdnf/ Casp2/ Cdc42se2/ Cdc42se1Nf1/ Nptxr/ Prkca
miR-101b-5p	3.489↑	Aldh2/Bdnf
miR-3546	3.377↑	Adh5/Cdc42ep4
miR-547-3p	3.336↑	Aldh8a1/ Aldh1b1/ Aspa/ bdnf/ Igf1
miR-365-5p	3.284↑	Aldh7a1/ Aldh18a1/ Aldh16a1/ Aldh1l1/ Bcl2/ Igf1/ Ngb/ Nptxr/ Ntrk3/ Ntrk2/ Nxph1/ Nxph4/ Per2/ Pik3c3/ Pik3ip1/ Pik3c2g/ Pik3r5/ Pik3r2/ Pik3cg/ Prkca

miR-3548	3.011↑	Adh6-ps1/ Adh6b/ Adh6a/ Aldh3b1/ Aldh3a2/ Aldh7a1/ Aldh6a1/ Aldh5a1/ Aldh2/ Aldh1a1/ Aspa/ bdnf/Cacna1c/ Cacna1b/ Cdc42ep1/Igf1r/ Igf2r/ Map3k / Nf1/ Ntrk3/ Nxph3/ Nxph1/ Pik3r3/ Pik3c2a/ Pik3cg/ Pik3cb/ Plp1/ Prkcg/ Tph1
miR-429	3.011↑	Aldh1a1/ Bcl2/ Cacna1c/ Egr3 / Map3k/ Ntf3/ Nxph1/ Pik3ca/ Pik3cb/ Prkca
miR-326-5p	2.792↑	Cacna1c/ Calb2/ Calb1/ Cdc42ep1/ Cdc42bpb / Cdc42se1/ Cdc42bpa/ Cdc42ep2/ Egr3/Mapk3/ Ngfr/ Nptxr/ Ntrk2/ Ntrk3/ Nxph4/ Nxph1/ Pik3cd/ Pik3c2b/ Pik3r5/ Pik3r2/ Prkca
miR-17-2-3p	2.713↑	Aldh3b2/ Aldh2/ Aldh1b1/ Aldh1a3/ Aldh5a1/ Aldh3a2/ Aspa/ bdnf/ B Bcl2/ Cacna1b/ Cacna1c/ Cdc42se2/ Cdc42bpa/ Drd5/ Drd4/ Egr3/ Fos/ Htr2c/ Igf1/ Map2k/ Ngfr/ Ntrk3/ Nxph1/ Nxph3/ Per2/ Pik3ap1/ Pik3cd/ Prkca/ tph1
miR-489-3p	2.688↑	Bdnf
miR-150-3p	2.566↑	Adh4/ Aldh4a1/ Aldh1b1/ Aldh4a1/ Aldh1b1/ Aspa/ bdnf/ Calb/ Cdc42ep3/ Drd2/ Egr3/ Igf1/Igf1/ Ntrk3/ Nxph1/ Per2/ Pik3r4/ Pik3r3/ Pik3c2a/ Pik3cg/ Pik3c2b/ Plp1
miR-216b-5p	2.538↑	Ntrk3
miR-296-5p	2.522↑	Bcl2/ Pik3ip1
miR-298-3p	2.512↑	Adh6-ps1/ Aldh1b1/ Aldh3a2/ Aldh1a1/ Arc/ bdnf/ Bcl2/ Ccdc42/ Nf1/ Nptxr/ Ntrk3/ Nxph1/ Nxph4/ Pik3cg/ Pik3r1/ Pik3c2b/ Pik3cd/ Pik3r2/ Plp1/ Prkca/ tph1
miR-871-5p	2.453↑	Adh6a/ Adhfe1/ Aldh9a1/ Aldh7a1/ Aldh3b1/ Aldh4a1/ Aldh1a1/ Aldh1l1/ Bcl2/ Cdc42ep4/ Igf1/ Ngfr/ Ntrk2/ Ntrk3/ Nxph1/ Pik3ip1/ Pik3ca/ Pik3r5/ Pik3ap1/ Pik3cg/ Pik3cb/ Pik3r1/ Prkca
miR-3593-5p	2.423↑	Aldh1b1/ Aldh3a2/ Aldh5a1/ Aldh4a1/ Aldh1l1/ bdnf/ Cdc42se2/ Egr4/ Igf1/ Nf1/ Nptxr/ Ntrk2/ Ntrk3/ Nxph3/ Pik3r6/ Pik3r3/ Pik3r2/ Prkca

miR-673-5p	2.377↑	Adhfe1/ Aldh1a2/ Aldh18a1/ Aldh5a1/ Aldh3b2/ Aldh1b1/ Aldh1l1/ Aldh2/ Aspa/ bdnf/Bcl2/ Cdc42se2/ Cdc42ep2/ Cdc42bpb/ Drd5/ Egr1/ Igf1/ Nf1/ Ngfr/ Nptxr/ Ntrk2/ Ntrk3/ Nxph1/ Nxph4/ Pik3r3/ Pik3cb/ Pik3c2b/ Pik3r1/ Pik3r6/ Pik3cg/ Pik3ca/ Pik3cd/ Prkca/ Slc12a2
miR-293-5p	2.357↑	Cdc42se1/ Pik3c2b
miR-653-5p	2.307↑	Cacna1c/ Nxph1
miR-632	2.247↑	Adh7/ Adh5/ Aldh1l2/ Aldh4a1/ Aldh5a1/ Aldh1a1/ Aldh1b1/ Aldh1l1/ Arc/ Aspa/ bdnf/ Bcl2/ Cacna1c/ Cdc42se1/ Cdc42se2/ Ccdc42/ Cdc42ep3/ Egr4/ Igf1/ Map2k2/ Ntrk3/ Ntrk2/ Nxph1/ Per2/ Pik3r5/ Pik3c2a/ Pik3cg/ Pik3cd/ Plp1/ Prkca/ Sstr2/ Tph1
miR-666-3p	2.233↑	Adh6a/ Aldh3b2/ Aldh7a1/ Aldh1b1/ Aldh1l2/ Aldh3a2/ Aldh4a1/ Aldh1l1/ bdnf/ Bcl2/ Cacna1c/ Cdc42ep4/ Cdc42bpg/ Cdc42ep3/ Cdc42bpa/ Cdc42se2/ Cdc42bpb/ Egr2/ Igf1/ Nf1/ Nptxr/ Ntrk3/ Ntrk2/ Nxph1/ Pik3c2b/ Pik3c2a/ Pik3r1/ Pik3r5/ Pik3ap1/ Pik3r2/ Pik3ca/ Plp1/ Prkca
miR-10b-3p	2.216↑	Aldh3b1/ Aldh18a1/ Aldh4a1/ Aldh3b2/ Aldh1l2/ Aldh6a1/ Aldh3a2/ Aldh1a1/ Aldh1l1/ bdnf/ Bcl2/ Cacna1b /Cacna1c/ Calb1/ Cdc42ep4/ Comt/ Comtd1/ Drd2/ Egr1/ Egr4/ Igf1/ Ngfr/ Ntrk3/ Per2/ Pik3c2a/ Pik3ca/ Pik3r1/ Pik3r6/ Pik3ap1
miR-219-1-3p	2.196↑	Aldh1a3/ Aldh5a1/ Aldh18a1/ Aldh1a1/ Aldh16a1/ Aldh1l1/Egr4/ Fosb/ Nptxr/ Ntrk3/ Ntrk2/ Nxph2/ Nxph1/ Pik3cb/ Pik3ca
miR-871-3p	2.085↑	Aldh7a1/ Aldh1a2/ Aldh1a1/ Aldh5a1/ Aldh4a1/ Aldh16a1/ Aldh1l1/ Aldh1a7/ Aldh3a2/ Arc/ Aspa/ Bcl2 / Cdc42se2/ Ccdc42/ Cdc42ep2/ Cdc42bpa/ Drd2/ Egr3/ Igf1/ Ntrk3/ Ntrk2/ Per2/ Pik3cd/ Pik3r2/ Pik3r1/ Pik3r6/ Slc6a4/ Snca/ Tph1
miR-188-3p	1.969↑	Adh6-ps1/ Adh4/ Aldh3b1/ Aldh1a3/ Aldh16a1/ Aldh1l1/ Aspa/ Bcl2/ Cacna1c/ Cdc42ep4 / Cdc42ep2/ Comt/ Gabarapl1/ Gabarap/ Htr2c/ Nf1/ Ngb/ Ntrk2/ Nxph3/ Nxph1/ Pik3r3/ Pik3ap1/ Pik3ip1/ Pik3cb/ Pik3r6/ Pik3ca/ Prkca

miR-135b-3p	1.961↑	Adh7/ Adh6-ps1/ Aldh1a1/ Aldh1a7/ Aldh18a1/ Aldh4a1/ Aldh3a2/ Aldh1a1/ Aldh2/ Bcl2l1/ Bcl2l13/ Bcl2/ Calb1/ Cdc42bpb/ Ccdc42/ Cdc42ep3/ Igf1/ Ntrk2/ Ntrk3/ Pik3r6/Pik3cg/ Pik3c2b
miR-203b-3p	1.877↑	Adh6-ps1/ Adh6a/ Aldh1l2/ Aldh6a1/ Aldh18a1/ Aldh3a2/ Aspa/ Cacna1c/ Ccdc42/ Cdc42ep3/ Egr3/ Fosb/ Igf1/ Nptxr/ Ntrk3/ Ntrk2/ Nxph2/ Nxph1/ Per2/ Pik3r3/ Pik3c2a/ Pik3cb/ Pik3r1/ Plp1/ Slc12a2/ Syn2
miR-3570	1.792↑	Adh6-ps1/ Adh4/ Aldh1b1/ Aldh3a2/ Aldh1a3/ Aspa/ Bcl2/ Cacna1c/ Cdc42ep5/ Cdc42se2/ Cdc42bpa/ Drd1a/ Egr1 / Htr2c/ Igf1/ Ngfr/ Nxph1/ Nxph2/ Pik3r5/ Pik3c2a/ Pik3r2/ Pik3ca/ Pik3r1/ Pik3c3/ Slc12a2/ Sstr2/ Syn2
miR-133a-5p	1.735↑	Adh6-ps1/ Aldh1a1/ Aldh8a1/ Aldh6a1/ Aldh1a3/ Aldh5a1/ Arc/ bdnf/ Bcl2/ Ccdc42b/ Ccdc42/ Cdc42ep2/ Drd2/ Egr3/ Nf1/ Ntrk1/ Ntrk2/ Ntrk3/ Pik3cg/ Pik3r3/ Pik3r1/ Pik3cd/ Pik3ca/ Slc12a2/ Tph1
miR-421-5p	1.733↑	Adh5/ Aldh3a2/ Aldh7a1/ Aldh1a7/ Aldh1b1/Bcl2 / Cacna1b/ Cacna1c/ Calb1/ Cdc42bpa/ Cdc42se2/ Cdc42ep2/ Nptxr/ Ntrk3/ Nxph2/ Per2/ Pik3r3/ Pik3r5/ Pik3cb/ Pik3r1/ Pik3ca/ Pik3ap1/ Pik3r6/ Pik3ca/ Prkca
miR-184	1.726↑	Cdc42bpg
miR-16-3p	1.721↑	Adh7/ Aldh4a1/ Aldh8a1/ Aldh1a7/ bdnf/ Bcl2/ Cacna1c/ Cdc42ep2/ Egr1/ Egr2/ Fosb/ Gabarapl2/ Nptxr/ Ntrk3/ Nxph1/ Pik3ap1/ Pik3c2b/ Pik3ca
miR-196c-5p	1.633↑	Igf1/ Pik3r6
miR-223-5p	1.661↑	Adh6-ps1/ Adh7/ Adh6b/ Adh5/ Aldh1l2/ Aldh9a1/ Aldh5a1/ Aldh2/ Aldh1a7/ Aspa/ Bcl2/Cacna1b/ Ccdc42/ Cdc42ep3/ Drd1a/ Egr3/ Htr2c/ Igf1/ Nf1/ Ntrk3/ Nxph1/ Pik3r1/ Pik3r5/ Pik3c2g/ Pik3c2a/ Pik3r3/ Pik3c2b/ Pik3cg/ Pik3r6/ Pik3cd/ Plp1/ Slc12a2/ Syn2
miR-382-3p	1.612↑	Cacna1c/ Egr3/ Htr2c/ Ntrk3
miR-351-3p	1.585↑	Adh4/ Aldh18a1/ Aldh8a1/ Aldh6a1/ Aldh5a1/ Cacna1c/ Calb2/ Cdc42ep3/ Comtd1/ Drd2/ Egr3/ Fosb/ Gabarapl2/Ntrk3/ Ntrk2/ Nxph1/ Pik3ap1/ Pik3ip1/ Pik3r3/ Pik3r6/ Pik3r1/ Pik3ca/ Plp1/ Slc12a2/ Tph1

miR-615	1.544↑	Adhfe1/ Aldh1l1/ Aldh1a1/ Aldh1a3/ Aldh5a1/ Arc/ Aspa/ Cacna1c/ Cdc42se2/ Cdc42ep1/ Cdc42ep4/ Cdc42bpa/ Drd2/ Fosb/ Htr2c/ Igf1/ Map2k2/ mapk3/ Ngfr/ Ntrk2/ Ntrk3/ Pik3r2/ Pik3c2b/ Prkca/ Tph1
miR-20b-3p	1.502↑	Aldh1a1/ Aldh3a2/ Aldh1a2/ Aldh1l2/ Aldh1a3/ Aldh5a1/ Aldh1l1/ Aldh2/ Bcl2/ Cacna1c/ Calb1/ Cdc42ep4/ Cdc42se1/ Comtd1/ Comt/ Egr2/ Egr4/ Fosb/ mapk3/ Nf1/ Nptxr/ Ntrk3/ Nxph1/ Pik3cd/ Pik3c2a/ Pik3r3/ Pik3ca/ Pik3r1/ Pik3ap1/ Pik3c3
miR-1188-5p	1.500↑	Aldh18a1/ Aldh3a2/ Aldh8a1/ Aldh1l2/ Aldh1l1/ Arc/ Bcl2/ Cacna1c/ Cdc42ep2/ Cdc42bpa/ Cdc42bpb/ Comt/ Drd5/ Egr2/ Egr3/ Htr2c/ Igf1/ Nptxr/ Ntrk2/ Ntrk3/ Nxph3/ Nxph1/ Pik3c2g/ Pik3ca/ Pik3r1/ Pik3ip1/ Prkca/ Sstr2
miR-34c-5p	1.707↓	Bcl2/Htr2c/ Ntrk3/
miR-34b-5p	1.769↓	Slc12a2/ Syn2/Bcl2/Htr2c/ Ntrk3/ Slc12a2/ Syn2
miR-222-3p	1.804↓	Aldh1a1/Ntf3/ Nxph1/ Pik3r1
miR-221-3p	2.051↓	Aldh1a1/Ntf3/ Nxph1/ Pik3r1
miR-211-5p	2.081↓	Adh6-ps1/ Aldh16a1/ Bcl2/ Nxph4/ Nxph1/ Pik3ip1/ Pik3cb
miR-1912-5p	2.465↓	Adh4/ Adh7/ Aldh4a1/ Aldh1l2/ Aldh5a1/ Aldh2/ Aldh3b2/ Aldh1l1/ bdnf/ Cacna1c/ Cdc42se1/ Cdc42bpg/ Egr4/Igf1/ Ntrk3/ Nxph1/ Pik3ca/ Pik3cg/ Sstr2
miR-448-3p	3.654↓	Bcl2/ Cacna1b/ Cacna1c/ Igf1/ Ntrk3/ Pik3r1
miR-1298	3.824↓	-

Table II. *The differential expression of miRNA and its low confidence target gene between the withdrawal group and the control group.*

Name	Fold change	Low confidence target gene
miR-3546	1.891↑	Adh5/Cdc42ep4/Comtd1/ Htr2c/Nxph1
miR-1912-5p	1.849↑	Adh4/ Adh7/ Aldh4a1/ Aldh1l2/ Aldh5a1/ Aldh2/ Aldh3b2/ Aldh1l1/ bdnf/ Cacna1c/ Cdc42se1/ Cdc42bpg/ Egr4/ Gabarapl1/ Igf1/ Ntrk3/ Nxph1/ Pik3ca/ Pik3cg/ Sstr2
miR-365-5p	1.642↑	Aldh7a1/ Aldh18a1/ Aldh16a1/ Aldh1l1/ Aspa/ Bcl2/Comtd1/ Drd2/ Gabarapl2/ Htr2c/ Igf1/ Ngb/ Nptxr/ Ntrk3/ Ntrk2/ Nxph1/ Nxph4/ Per2/ Pik3c3/ Pik3ip1/ Pik3c2g/ Pik3r5/ Pik3r2/ Pik3cg/ Prkca
miR-764-5p	1.634↑	Adh4/ Aldh1l1/ Aldh3a2/ Aldh1a1/ Aldh4a1/ bdnf/Cacna1c/Cdc42se2/ Cdc42se1/ Cdc42bpa/ Cdc42ep3/ Drd2/ Egr2/Ngfr/ Nptxr/ Ntrk3/ Ntrk2/ Nxph1/ Pik3r3/ Pik3c3/ Plp1/ Prkca/ Slc12a2/ Tph1
miR-18a-5p	1.726↓	Igf1
miR-96-5p	2.009↓	PIK3C2A/PIK3R1/CDC42BPB/EGR3/BCL2/NF1/CDC42BPA/ PIK3CA/CACNA1B/CACNA1C
miR-196a-5p	2.255↓	Igf1/ Pik3r6
miR-181b-2-3p	2.316↓	Adh7/Adh6a/Aldh7a1/ Aldh1a1/ Aldh1b1/ Aldh1l1/ Arc/ Bcl2/ Cacna1c/ Calb1/ Cdc42se1/ Ccdc42b/ Cdc42ep2/ Cdc42bpa/ Cdc42/ Cdc42ep3/ Comtd1/ Egr2/ Igf1/Ngfr/Ntrk3/ Nxph1/ Per2/ Pik3c2a/ Pik3r1/ Pik3cb/ Pik3r3/ Prkca/ Slc12a2/ Snca/ Syn2
miR-203a-5p	2.316↓	Adh7/ Aldh3b2/ Aldh6a1/ Aldh1l2/ Aldh3a2/ Aldh16a1/ Aspa/ bdnf/ Bcl2l1/ Bcl2/ Drd2/ Egr2/ Htr2c/ Igf1/ Ngfr/ Nptxr/ Ntrk2/ Ntrk3/ Pik3c2g/ Pik3cd/ Pik3cb/ Pik3ca/ Pik3ap1/ Pik3r2
miR-19b-1-5p	3.285↓	Adh6-ps1/ Aldh8a1/ Aldh1a1/ Aldh1l2/ Aldh3b1/ Aspa/ bdnf/ Cacna1b/ Cdc42ep4/ Cdc42bpa/ Egr2/ Igf1/Nptxr/ Ntrk3/ Ntrk2/ Nxph2/ Nxph1/ Per2/ Pik3r1/ Pik3ip1/ Pik3ca/ Pik3r3/ Pik3c2a/ Pik3cd/Prkca/ Slc12a2/ Snca/ Tph1/ Syn2

functional enrichment analysis of these target genes. The results showed that these genes were significantly enriched in 67 functional classes (Benjamini $p<0.05$), including transcriptional regulation, neural differentiation, neuron development and other biological processes (Fig. 2).

According to the target genes of miRNAs, which have been reported to be related to psychiatric disorders, there were 23 miRNAs with differential expression in reverse selection. Among them, 4 miRNAs (rno-miR-17-2-3p, rno-miR-184, rno-miR-219-1-3p, and rno-miR-429) had target genes with high confidence, targeting 628 genes. Functional enrichment analysis in target genes of these four miRNAs revealed that these genes were significantly enriched in 6 functional classes (Benjamini $p<0.05$) (Fig. 3).

A total of 23 differential expressions were determined, and 4803 target genes reported to be related with psychiatric disease were found, among which 2,265 were identified as Rat genes in the DAVID database. Functional enrichment analysis of these 2265 genes discovered that they were significantly enriched in 55 biological pathways,

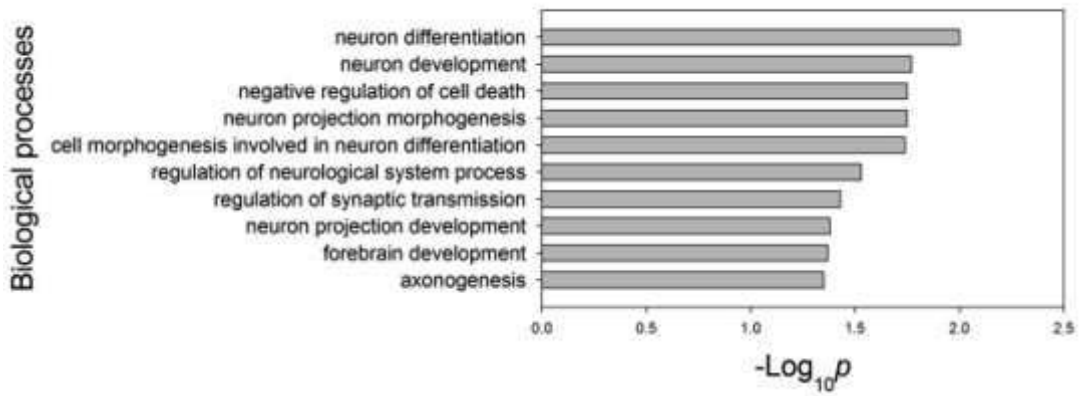

Fig. 2. *Functional enrichment analysis of target genes with high confidence.*

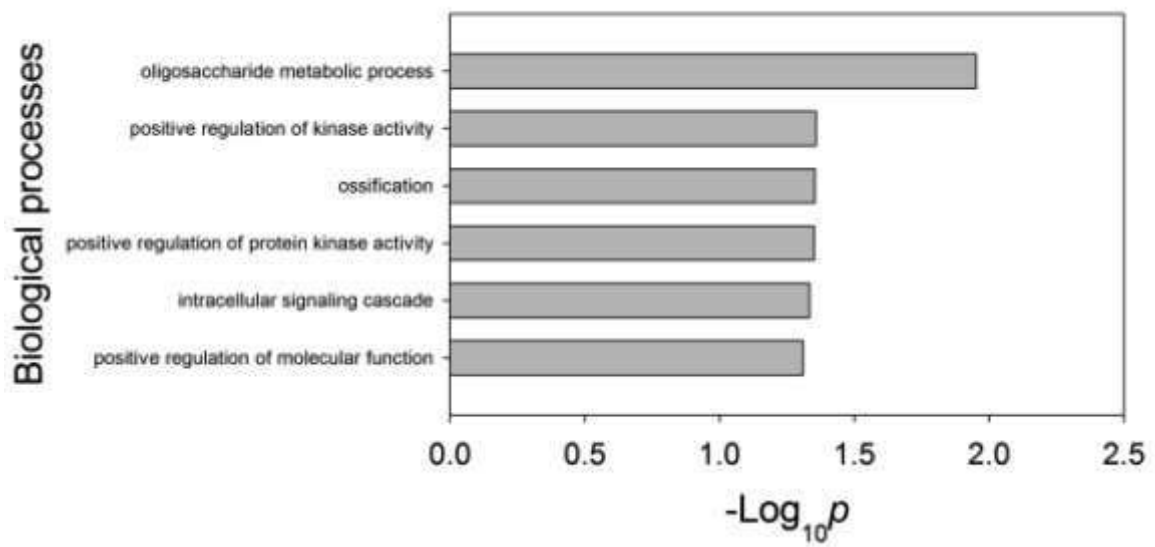

Fig. 3. *Analysis of functional enrichment of miRNA target genes with high confidence that has been reported in literature.*

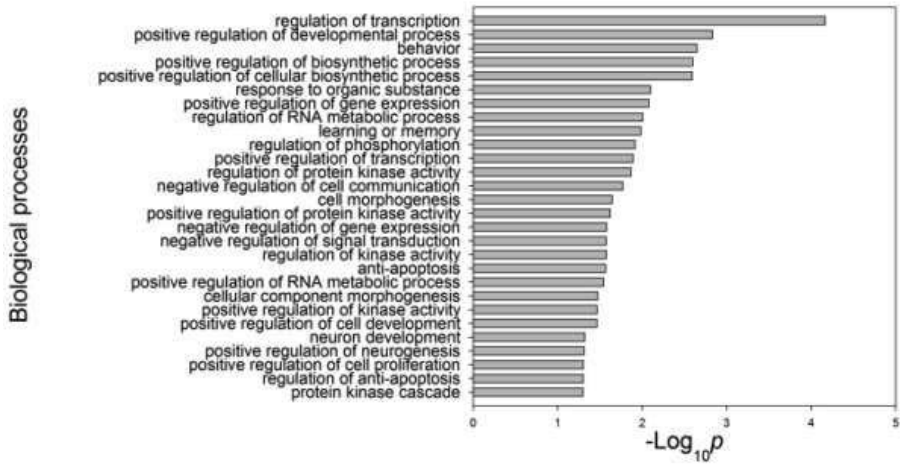

Fig. 4. *Analysis of functional enrichment of miRNA target genes with low confidence that has been reported in literature.*

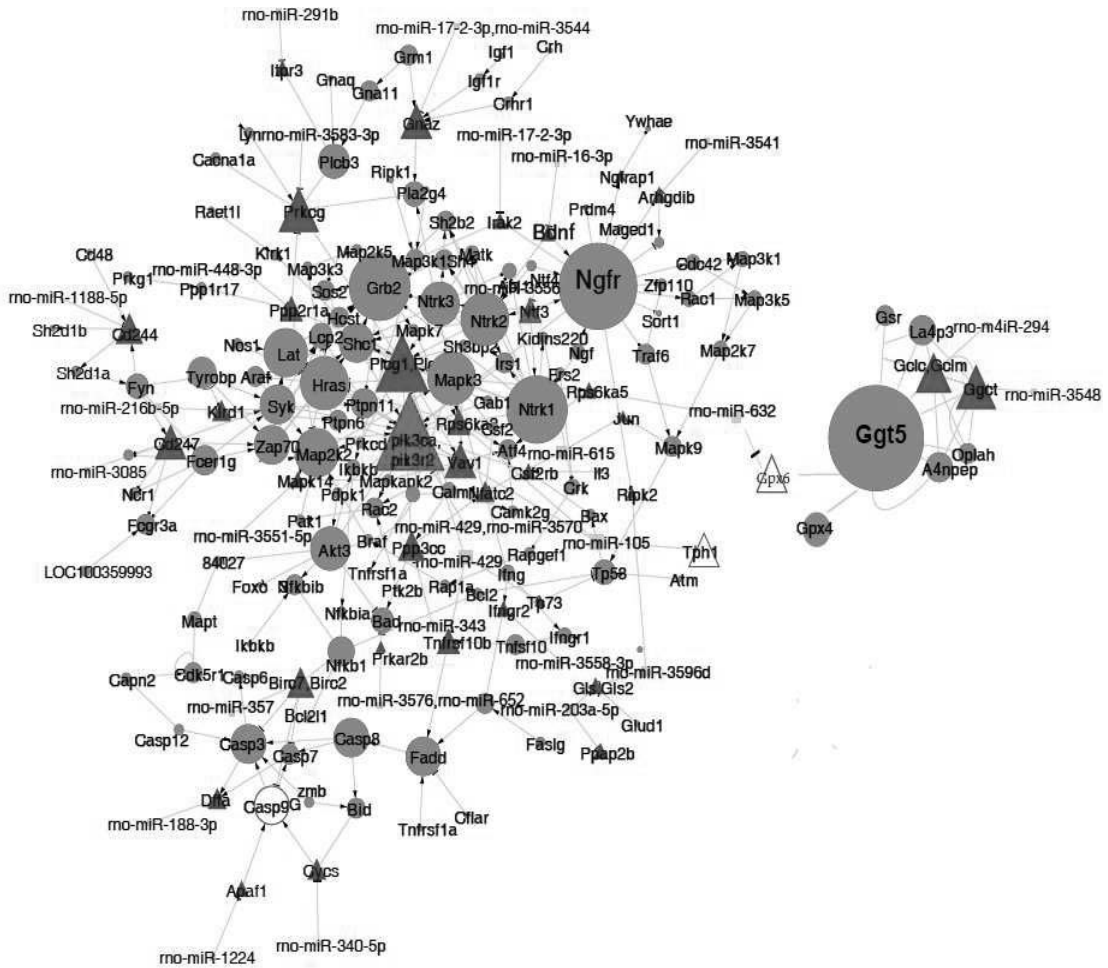

Fig. 5. *KEGG network of target genes of Differential expression miRNA with low confidence. The spots represent miRNA; target genes of differential expression miRNA with low confidence are shown as triangles. The spots show genes associated with above-mentioned target genes in the KEGG pathway, and their size indicates the relationship between the gene and other genes. Different edges represented different relationships between the two genes (arrow: activation; vertical line: inhibition; spots: interaction). The KEGG network of target genes of differential expression miRNA with low confidence is also shown in the figure with high definition.*

including regulation of transcription, positive regulation of developmental process, neuron development and so on (Fig. 4).

KEGG function analysis of target genes of Differential expression miRNA with low confidence

In the functional analysis based on DAVID illustrated above, target genes of Differential expression miRNA with low confidence were significantly enriched in several KEGG pathways. Genes involved in these pathways were obtained and the relationship (including activation, inhibition, interaction, etc.) among these genes was determined afterwards. Moreover, the KEGG network of target genes of Differential expression miRNA with low confidence was plotted by the Cytoscape software (Fig. 5).

Detection of miRNA expression by RT-PCR method

SYBR Green real-time quantitative PCR the method was used to verify miRNA with differential expression. Four miRNAs were chosen with relatively significant differentiation (miR-34c-5p, miR-101b-5p, miR-10b-3p and miR-16-3p). Among the three groups, the expression levels of miR-101b showed a significant difference, but the expression levels of miR-34c-5p and miR -10b-3p and miR-16-3p showed no significant differences (Table III).

The relative expression of miR-101b-5p in brain tissue and plasma was analyzed by Spearman correlation (r = -.004, p=0.977). There was no correlation between the expression of miR-101b-5p in brain tissue and plasma.

DISCUSSION

In this study, expression profiles of miRNAs were analyzed in the prefrontal cortex of alcohol-dependent rats 24 h after non-withdrawal and withdrawal, and 65 differentially expressed miRNAs were eventually screened among the three groups. Most of the differentially expressed miRNAs had

Table III. *Comparison of relative expression of miRNA in each group.*

miRNA	Grade mean of dependence group (n=20)	Grade mean of withdrawl group (n=20)	Grade mean of control group (n=10)	F	*p*
miR-101b-5p	32.45*	22.10	18.40	8.00	0.02*
miR-34c-5p	25.70	24.65	26.80	0.15	0.93
miR-10b-3p	25.05	25.12	25.05	0.06	0.97
miR-16-3P	27.45	23.65	25.30	0.68	0.71
miR-101b-5p in plasma	28.27	23.93	23.10	1.23	0.54

Note: compared with the two groups, the relative expression of miR-101b-5p after Bonferroni correction of the P value, there was a significant difference between the control group and the dependence group, P<0.05.

high expression values in the alcohol-dependent non-withdrawal group, which was in line with most of the research results (16). Previous studies have documented that there were significant differences in expression levels of miRNAs in different brain regions (17, 18). Moreover, differentially expressed miRNAs were the most abundant in the prefrontal cortex. Three miRNA expressions were consistent with previous studies (6, 7, 9): miR-10, miR-17 and miR-101. Only miR-101 was found to have a differential expression after further intersection with studies involving alcoholics. Alcohol could induce higher expression of miR-10 and miR-219 in the fetal brain. This study also discovered that alcohol dependence could lead to higher expression levels of miR-10 and miR-219.

After alcohol withdrawal, the expression of miRNAs showed a decreasing trend, but a few were still higher than those of the control group. The results showed that with the cessation of alcohol intake, the effect of increased miRNAs on protein was decreased, leading to reduced brain tissue damage. In this study, miRNAs with differential expression in the prefrontal cortex during alcohol dependence significantly outnumbered those during alcohol withdrawal, a finding which was consistent with those of Melendez et al. (19). Additionally, miRNAs were also different during alcohol withdrawal from those during alcohol dependence, indicating that alcohol withdrawal has a unique mechanism here. Prior research confirmed that the mechanism of alcohol-dependent withdrawal was not the same as that of non-withdrawal (11).

Chronic alcohol consumption may induce gene expression alterations in brain reward regions such as the prefrontal cortex (PFC). MiRNA can affect hippocampal synaptic plasticity, learning and memory (20, 21), as well as addiction behavior (22) and tolerance. miRNAs are involved in regulation of ethanol neurotoxicity and inhibit alcohol-induced brain inflammation (23). As for the results of target gene predictions in the study, the target genes that were differentially expressed by miRNA were mainly correlated with cell apoptosis, cell adhesion, nervous system development, learning and memory, and signal transduction between cells, which were related to neurogenesis and neurological disease.

In accordance with the KEGG network map of target genes that were differentially expressed by miRNA with low confidence, some genes reported to be related to alcohol dependence in previous studies were found, including PIK3CA, NTF3, BDNF and TPH1. Coding for the catalytic subunit p110 of class I phosphatidylinositol 3-kinases (PI3Ks), PIK3CA possesses many functions, such as regulating cell increment, differentiation, and survival. In the phosphatidylinositol signalling pathway, the extracellular signal molecules are combined with the cell-surface G protein coupled receptor to activate phospholipase C (PLC-β) in the plasma membrane. This, in turn, promotes the hydrolysis of phosphatidylinositol 4,5-bisphosphate (PIP2) in the plasma membrane into two second messengers of inositol 1,4,5-trisphosphate (IP3) and diacylglycerol (DG). Furthermore, Ca^{2+} can activate calmodulin (CaM) and CaM-Kinase. CaM-Kinase II is present in high numbers in synapses of mammalian brain neurons and is associated with memory formation. Phosphatidylinositol 3-phosphate promotes GABAergic neurotransmission at inhibitory postsynaptic sites (24). It was also found in the present study that rats of the alcohol-dependent non-withdrawal group showed a great increase in miR-200, miR-429, miR-203, miR-10 and miR-3570, which synergistically assist in inhibiting the expression of PIK 3CA and play their biological effect to the fullest. The protein encoded by NTF3 gene is a member of the neurotrophin family, which controls survival and differentiation of mammalian neurons. This protein is closely related to both nerve growth factor and brain-derived neurotrophic factor. It may be involved in the maintenance of the adult nervous system, and may affect development of neurons in the embryo when it is expressed in the human placenta. Furthermore, it was found that miR-222, miR-221, miR-200, miR-429 and miR-3356 all worked on NTF3 in both synergistic and antagonistic manners.

Expression of brain-derived neurotrophic factor (BDNF) is developmentally regulated in prefrontal cortex (PFC). BDNF has a well-documented role in synaptic plasticity and alcohol dependence (25).

Some research has shown that BDNF is significantly down-regulated in PFC tissue and serum (26). Other studies have demonstrated that the BDNF pathway within the dorsolateral striatum controls the level of ethanol self-administration. Furthermore, neuronal overexpression of miR-30a-5p resulted in down-regulation of the BDNF protein. Together, these data support a role for BDNF in the modulation of ethanol intake. Our results showed that expression levels of miR-16, miR-10 and miR-101 were significantly up-regulated to inhibit the expression of BDNF (27, 28), which was consistent with the results of previous research. Therefore, it was speculated that miRNA might cooperate with the common target gene of BDNF, thus inhibiting its expression. Tryptophan hydroxylase is the rate-limiting enzyme in the biosynthesis of the neurotransmitter, serotonin.

These data identify a role for micro-RNAs as epigenetic intermediaries, which permit teratogens to shape complex, divergent developmental processes, and additionally demonstrate that coordinately-regulated miRNAs exhibit both functional synergy and antagonism toward each other. Accordingly, it can be concluded that alcohol induced differential expression of miRNAs, which intervened in the abnormal expression of target genes and hence mediated the alcohol dependence event.

Another important discovery in this study was that, as verified by RT-PCR, the expression of miR-101 was up-regulated in brain tissues, which was consistent with the results reported by Nunez, et al. (9). It was also the most consistent result of the current studies on alcohol dependence. Unfortunately, differential expression of miR-101 was not detected in peripheral plasma, and no correlation was found with that in brain tissues. MiR-101 is a specific miRNA of vertebrates. The length of mature miR-101 is about 23 nt, and its mature sequence is highly conserved among all species. Mature miR-101 is also in serum or plasma (29). MiR-101 is highly expressed in brain tissue, and plays an important role in brain development, aging and neurodegenerative processes (30-32). Furthermore, miR-101 can exert a protective role in Alzheimer's disease by inhibiting the expression of hippocampal neuron-regulated amyloid precursor protein. MiR-101 can also promote apoptosis by promoting the overexpression of histone methyltransferase EZH2.

Long-term alcohol intake destroys the blood-brain barrier (BBB) (33) and causes some of the larger molecules to enter the brain from circulating blood through the BBB. In addition, a number of studies have shown that microbubbles containing miRNA can be released into the peripheral blood through the BBB. Exosomes have the potential to cross the BBB through transcytosis; hence, they can easily pass through endothelial cellular layers and circulate in biofluids, which is important in brain-related disorders (34). All of the above interpretations suggest that miRNA is a meaningful and feasible biomarker for the diagnosis of alcohol dependence. However, results related to differential expression of miR-101 have not been identified and concluded in the plasma of alcohol-dependent rats, which may be related to the low level of miR-101 expression in the plasma. The experimental methods used in this study are not sufficiently accurate. There is still great room for further improvement in the methods in determining whether miR-101 can be used as a biological marker for alcohol dependence. It may also be related to miR organization and species specificity (35). Secondly, it may also be correlated with the tissue and species specificity of miRNAs. Thirdly, alcohol can also cause damage to other organs (36) and induce differential expression of miR-101 (37), which will then enter the circulating blood, thereby affecting the expression of miRNA within the circulating blood. Although differential expression of plasma miR-101 has not been found in this study, multiple studies have confirmed that alcohol can induce the expression of miR-101, and that it is related to the function of the nervous system. Besides, miR-101 is a promising biomarker and therapeutic target.

In summary, the key role of miRNAs in the development of alcohol dependence represent a major research interest and direction for the next steps in this area. It is believed that it will be possible for miRNA to serve as a highly useful new biological marker for the diagnosis of disease. This would not only make the molecule a drug target, but also contribute to providing a new means for treatment of

human diseases through simulation of the molecule for development of new drugs.

ACKNOWLEDGEMENTS

This study was supported by grants from the National Natural Science Foundation of China (81271471), innovation research project of Graduate Student in Heilongjiang Province (YJSCX2012-236HLJ); Research project in Health and Family Planning Commission Heilongjiang Province (2017-013).

REFERENCES

1. Heath AC, Whitfield JB, Madden PA, et al. Towards a molecular epidemiology of alcohol dependence: analysing the interplay of genetic and environmental risk factors. Br J Psychiatry Suppl 2001; 40(2):s33-40.
2. Osterndorff-Kahanek EA, Becker HC, Lopez MF, et al. Chronic ethanol exposure produces time- and brain region-dependent changes in gene coexpression networks. PLoS One 2015; 10(3):e0121522.
3. Bartel DP. MicroRNAs: genomics, biogenesis, mechanism, and function. Cell 2004; 116(2):281-97.
4. Mamdani M, Williamson V, McMichael GO, et al. Integrating mRNA and miRNA weighted gene co-expression networks with eQTLs in the nucleus accumbens of subjects with alcohol dependence. PLoS One 2015; 10(9):e0137671.
5. Gorini G, Nunez YO, Mayfield RD. Integration of miRNA and protein profiling reveals coordinated neuroadaptations in the alcohol-dependent mouse brain. PLoS One 2013; 8(12):e82565.
6. Wang F, Gelernter J, Zhang H. Differential expression of miR-130a in postmortem prefrontal cortex of subjects with alcohol use disorders. J Addict Res Ther 2013; 4(155).
7. Tapocik JD, Solomon M, Flanigan M, et al. Coordinated dysregulation of mRNAs and microRNAs in the rat medial prefrontal cortex following a history of alcohol dependence. Pharmacogenomics J 2013; 13(3):286-96.
8. Lewohl JM, Nunez YO, Dodd PR, Tiwari GR, Harris RA, Mayfield RD. Up-regulation of microRNAs in brain of human alcoholics. Alcohol Clin Exp Res 2011; 35(11):1928-37.
9. Nunez YO, Truitt JM, Gorini G, Ponomareva ON, Blednov YA, Harris RA, Mayfield RD. Positively correlated miRNA-mRNA regulatory networks in mouse frontal cortex during early stages of alcohol dependence. BMC Genomics 2013; 14:725.
10. Pietrzykowski AZ, Friesen RM, Martin GE, et al. Posttranscriptional regulation of BK channel splice variant stability by miR-9 underlies neuroadaptation to alcohol. Neuron 2008; 59(2):274-87.
11. Sinirlioglu ZA, Coskunpinar E, Akbas F. miRNA and mRNA expression profiling in rat brain following alcohol dependence and withdrawal. Cell Mol Biol (Noisy-le-grand) 2017; 63(2):49-56.
12. Most D, Leiter C, Blednov YA, Harris RA, Mayfield RD. Synaptic microRNAs coordinately regulate synaptic mRNAs: perturbation by chronic alcohol consumption. Neuropsychopharmacology 2016; 41(2):538-48.
13. Kumar S, Reddy PH. Are circulating microRNAs peripheral biomarkers for Alzheimer's disease? Biochim Biophys Acta 2016; 1862(9):1617-27.
14. Gilpin NW, Richardson HN, Lumeng L, Koob GF. Dependence-induced alcohol drinking by alcohol-preferring (P) rats and outbred Wistar rats. Alcohol Clin Exp Res 2008; 32(9):1688-96.
15. Wang LL, Zhang Z, Li Q, et al. and teratogenic effects which can be suppressed by folic acid supplementation. Hum Reprod 2009; 24(3):562-79.
16. Nunez YO, Mayfield RD. Understanding alcoholism through microRNA signatures in brains of human alcoholics. Front Genet 2012; 3:43.
17. Ponomarev I, Wang S, Zhang L, Harris RA, Mayfield RD. Gene coexpression networks in human brain identify epigenetic modifications in alcohol dependence. J Neurosci 2012; 32(5):1884-97.
18. Osterndorff-Kahanek EA, Tiwari GR, Lopez MF, Becker HC, Harris RA, Mayfield RD. Long-term ethanol exposure: Temporal pattern of microRNA expression and associated mRNA gene networks in mouse brain. PLoS One 2018; 13(1):e0190841.
19. Melendez RI, McGinty JF, Kalivas PW, Becker HC. Brain region-specific gene expression changes after chronic intermittent ethanol exposure and early withdrawal in C57BL/6J mice. Addict Biol 2012; 17(2):351-64.
20. Capitano F, Camon J, Licursi V, et al. MicroRNA-

335-5p modulates spatial memory and hippocampal synaptic plasticity. Neurobiol Learn Mem 2017; 139:63-68.

21. Lambert TJ, Storm DR, Sullivan JM. MicroRNA132 modulates short-term synaptic plasticity but not basal release probability in hippocampal neurons. PLoS One 2010; 5(12):e15182.
22. Tapocik JD, Luu TV, Mayo CL, et al. Neuroplasticity, axonal guidance and micro-RNA genes are associated with morphine self-administration behavior. Addict Biol 2013; 18(3):480-95.
23. Yu Z, Guangkuan W, Zhiyong D, Qingjie Z. miR-339-5p inhibits alcohol-induced brain inflammation through regulating NF-κB pathway. Biochem Biophys Res Commun 2014; 452(3):450-56.
24. Papadopoulos T, Rhee HJ, Subramanian D, et al. Endosomal phosphatidylinositol 3-phosphate promotes gephyrin clustering and GABAergic neurotransmission at inhibitory postsynapses. J Biol Chem 2017; 292(4): 1160-77.
25. Grzywacz A, Samochowiec A, Ciechanowicz A, Samochowiec J. Family-based study of brain-derived neurotrophic factor (BDNF) gene polymorphism in alcohol dependence. Pharmacol Rep 2010; 62(5):938-41.
26. Huang MC, Chen CH, Liu HC, Chen CC, Ho CC, Leu SJ. Differential patterns of serum brain-derived neurotrophic factor levels in alcoholic patients with and without delirium tremens during acute withdrawal. Alcohol Clin Exp Res 2011; 35(1):126-31.
27. Schratt GM, Tuebing F, Nigh EA, Kane CG, Sabatini ME, Kiebler M, Greenberg ME. A brain-specific microRNA regulates dendritic spine development. Nature 2006; 439(7074):283-89.
28. Xu Y, Xu L, Zheng J, Geng L, Zhao S. MiR-101 inhibits ovarian carcinogenesis by repressing the expression of brain-derived neurotrophic factor. Febs Open Bio 2017; 7(9):1258-66.
29. Ignacio C, Hicks SD, Burke P, Lewis L, Szombathyne-Meszaros Z, Middleton FA. Alterations in serum microRNA in humans with alcohol use disorders impact cell proliferation and cell death pathways and predict structural and functional changes in brain. BMC Neurosci 2015; 16:55.
30. Liu D, Tang H, Li XY, et al. Targeting the HDAC2/HNF-4A/miR-101b/AMPK pathway rescues tauopathy and dendritic abnormalities in Alzheimer's disease. Mol Ther 2017; 25(3):752-64.
31. Vilardo E, Barbato C, Ciotti MT, Cogoni C, Ruberti F. MicroRNA-101 regulates amyloid precursor protein expression in hippocampal neurons. J Biol Chem 2010; 285(24):18344-51.
32. Lee Y, Samaco RC, Gatchel JR, Thaller C, Orr HT, Zoghbi HY. miR-19, miR-101, and miR-130 co-regulate ATXN1 levels to potentially modulate SCA1 pathogenesis. Nat Neurosci 2008; 11(10):1137-39.
33. Haorah J, Schall K, Ramirez SH, Persidsky Y. Activation of protein tyrosine kinases and matrix metalloproteinases causes blood-brain barrier injury: novel mechanism for neurodegeneration associated with alcohol abuse. Glia 2008; 56(1):78-88.
34. Grasso M, Piscopo P, Confaloni A, Denti MA. Circulating miRNAs as biomarkers for neurodegenerative disorders. Molecules 2014; 19(5):6891-910.
35. Sempere LF, Freemantle S, Pitha-Rowe I, Moss E, Dmitrovsky E, Ambros V. Expression profiling of mammalian microRNAs uncovers a subset of brain-expressed microRNAs with possible roles in murine and human neuronal differentiation. Genome Biol 2004; 5(3):R13.
36. Natarajan SK, Pachunka JM, Mott JL. Role of microRNAs in alcohol-induced multi-organ injury. Biomolecules 2015; 5(4):3309-38.
37. Zhao X, Wang K, Liao Y, et al. MicroRNA-101a inhibits cardiac fibrosis induced by hypoxia via targeting TGFβRI on cardiac fibroblasts. Cell Physiol Biochem 2015; 35(1):213-26.

THE EXPRESSION OF CIRCULATING TUMOR CELLS IN PERIPHERAL BLOOD OF PATIENTS WITH NON-SMALL CELL LUNG CANCER AND ITS DETECTION

X-M. BU[1], F-F. XU[1], J. MA[2] and B. JIANG[3]

[1]Department of Pathology, Jining No.1 People's Hospital, Jining City, Shandong, China;
[2]Department of Oncology, Jining No.1 People's Hospital, Jining City, Shandong, China;
[3]Department of Thoracic Surgery, Affiliated Hospital of Jining Medical University, Jining City, Shandong, China

Received February 22, 2018 - Accepted June 26, 2018

This study aimed to investigate the expression of circulating tumor cells (CTCs) in peripheral blood and relevant detection methods as well as the clinical values of determination of CTCs for the diagnosis of non-small cell lung cancer (NSCLC). Peripheral blood specimens were acquired from the patients with NSCLC who came to the Thoracic Surgery Department of Jining No.1 People's Hospital, Shandong, China for the first visit between January 2015 and November 2016. Whether there was metastasis of CTCs or not was determined by detecting the number of epithelial cell adhesion molecules (EpCAM) which had expression in the CTCs of the peripheral blood with fluorescence polymerase chain reaction. Moreover, the correlation between the expression level of EpCAM of patients with NSCLC during postoperative adjuvant treatment and the efficacy of adjuvant therapy was initially explored. The expression level of EpCAM of the NSCLC patients was remarkably different to that of the patients with benign lung diseases. The expression level of EpCAM of the patients with NSCLC was notably different with that of the healthy volunteers. The expression level of EpCAM of the patients with NSCLC was much higher than that of patients with benign lung diseases and the volunteers. Moreover, the expression level of NSCLC at stages I, II and IIIA had significant differences; the expression level of EpCAM tended to increase as the stage of NSCLC developed. The expression level of EpCAM in CTCs of peripheral blood can be regarded as a reference for the early diagnosis and detection of NSCLC before and after surgery.

The incidence of lung carcinoma has increased rapidly in recent years. To cope with the increase of incidence and mortality of lung carcinoma, hospitals should make response and adjustment to the diagnosis of lung carcinoma. The diagnosis of lung carcinoma mainly relies on imaging; however imaging is poor in promptness and efficiency. Circulating tumor cells is a hotspot in recent studies concerning the diagnosis of cancer and has values in early diagnosis. Some Chinese and foreign experiments have carried out relevant studies deeply. Wu et al. (1) directly isolated circulating tumor cells (CTCs) from the whole blood of patients with lung adenocarcinoma using microcirculation-based immunomagnetic separation, and found that the method was applicable to the *in vitro* amplification of CTCs, and pointed out that the analysis on the genome, proteomics and metabolism of CTCs could guide the precise treatment of carcinoma. Wang et al. (2) found that immunomagnetic bead technique

Key words: circulating tumor cells, epithelial cell adhesion molecules, expression, clinical values

Mailing address:
Jiang Bo,
Affiliated Hospital of Jining Medical University,
No. 89, Guhuai Road, Rencheng District,
Jining City, Shandong,
272029, China
e-mail: bojjnmc@yeah.net

0393-974X (2018)
Copyright © by BIOLIFE, s.a.s.
This publication and/or article is for individual use only and may not be further reproduced without written permission from the copyright holder.
Unauthorized reproduction may result in financial and other penalties
DISCLOSURE: ALL AUTHORS REPORT NO CONFLICTS OF INTEREST RELEVANT TO THIS ARTICLE.

could effectively enrich the CTCs in peripheral blood of patients with lung carcinoma and was valuable in evaluating prognosis and guiding treatment. Dorsey et al. (3) used an adenoviral probe to detect the telomerase activity which almost existed in all cancer cells in the peripheral blood obtained from the patients with non-small cell lung cancer (NSCLC) and determined the effectiveness of the assay with secondary tumor-specific markers. Saucedozeni et al. (4) functionalized a structured medical Seldinger guidewire and found that it could be a vital tool to enrich CTCs for supervising the progress of cancer and the effectiveness of anti-tumor therapy. This study analyzed the detection methods of expression of CTCs in peripheral blood through comparing the lung carcinoma group, the benign lung diseases group and the healthy volunteers group and moreover verified the values of detecting expression of CTCs in the diagnosis of NSCLC.

MATERIALS AND METHODS

Research subjects

Lung carcinoma group. Patients who were pathologically diagnosed as NSCLC and treated in the Department of Thoracic Surgery of Jining No. 1 People's Hospital, Shandong, China, between January 2015 and November 2016 were selected. Patients who had previously undergone radical treatment and were pathologically diagnosed with NSCLC at TNM stage IA ~ IIIA (5) were included. Those who were diagnosed with other categories of lung carcinoma, had previously undergone other anti-tumor treatment, previously received organ transplant, and were unwilling to cooperate in the study were excluded. This study included 120 patients with NSCLC, including 67 males and 53 females, aged from 34 to 73 years (median 56 years). 66 patients had adenocarcinoma and 54 patients had squamous carcinoma; there were 18 cases of stage IA, 32 of stage IB, 26 of stage IIA, 30 of stage IIB and 14 of stage IIIA.

Benign lung diseases group. Patients who were pathologically diagnosed with benign lung diseases and were admitted to the Department of Thoracic Surgery of Jining No. 1 People's Hospital, Shandong, China, between January 2015 and November 2016 were selected. Patients without tumors in other areas of the body were included, while those who had history of tumor diseases were excluded. Fifty patients with benign diseases who satisfied the criteria were included, including 23 patients with tuberculosis, 15 with hamartoma and 12 with pulmonary cyst.

Healthy volunteer group. People who underwent physical examination in our hospital from January 2015 were selected. People who had no history of tumor diseases were included, while those who had level of white blood cells higher than 4.0×10^9/L or lower than 10.0×10^9/L or had blood system diseases were excluded. Finally, 30 healthy volunteers who satisfied the criteria were included.

All the subjects were aged from 18 to 69 years old and signed informed consent on a voluntary basis. The study protocol was approved by the medical ethics committee of the hospital.

Instruments and reagents

The instruments included electronic balance, ultraviolet spectrophotometer, polymerase chain reaction (PCR) amplifier, CK40 inverted phase contrast microscope, millipore, Ethylene Diamine Tetraacetic Acid (EDTA) anticoagulant tube (6), clean bench, incubator (37°C), high-speed refrigerated centrifuge, ordinary centrifuge and fluorescence quantitative PCR amplifier.

The reagents included chloroform, 95% ethyl alcohol, sodium hydroxide, red blood cell lysate, fluorescence quantitative PCR kit, Rnasin (RNA) inhibitor, 0.1% diethyl pyrocarbonate solution and phosphate buffer solution (PBS).

Collection of peripheral blood specimens

Two mL of peripheral venous blood was extracted at the median position of the elbow of the patients with NSCLC using an EDTA anticoagulant tube twice on the seventh day before and after surgery. The first tube of blood was discarded, and the second tube was reserved.

Detection procedures of expression level of epithelial cell adhesion molecules in circulating tumor cells

All the operations were performed in ice bath. All the liquids and instruments were processed by 0.1% diethyl pyrocarbonate solution. Moreover, new sterile Eppendorf (EP) tubes were used. The operators wore gloves and masks during surgery.

Extraction of RNA from EpCAM

The peripheral venous blood was processed by centrifugation at 500 rpm for 10 min, and red blood cell lysate was added after the plasma at the upper layer was removed (7). Then it was processed by ice bath for 8 min and centrifuged at 2500 rpm for 15 min. After the addition of 10 ml of PBS, the mixture was vibrated mildly and resuspended twice. Then it was centrifuged at 3200 rpm, and 20 min later the supernate was removed, and the sediment was reserved. 1 ml of Trizol was added into the sediment. Nucleic acid-protein compound was completely separated from the mixture by 5 min of incubation at room temperature and then transferred to an EP tube. Then it was processed by centrifugation at 12,000 rpm at 4°C. There were three layers; the upper layer which contained RNA was transferred to a new EP tube, and the white membrane at the boundary phase should be kept away. Then ethyl alcohol at a concentration of 75% and 1 ml of Trizol were added to wash the sediment; then it was centrifuged at 12,000 rpm at 4°C. The supernate was removed after 10 min, the EP tube was inverted on a piece of clean filter paper for 10 min to volatilize the residual ethyl alcohol. Then 30 μl of RNA-free water was added to dissolve RNA. The content of RNA was detected using an ultraviolet spectrophotometer (8). The content between 1.8 and 2.0 indicated good purity; if the content was lower than 1.8 or higher than 2.0, RNA should be re-extracted.

Before the experiments for acquiring complementary DNA (cDNA) by RNA reverse transcription and fluorescent PCR detection, relevant primers and probe were designed (9). The reverse transcription primer was 5'-GAGCTAGGACAGCGTAGCCGACG-3'.The forward primer was '-GAATGCAGATGCGCCCCCATTCGGTTCC-3', the reverse primer was 5' TAAGCGGATACGCGCCCCATGCCGAACGG-3', and the fluorescence quantitative probe was 5'-FAM-CAGTTGAGGGTTC-MGB-3'.

Acquisition of cDNA

1 μg of RNA, 10 μg of forward primer (10) and 2 μg of reverse primer were taken and processed at 42°C for 10 min, 30°C for 20 min, 99°C for 5 min and 4°C for 5 min using RT-PCR to obtain cDNA.

Fluorescent PCR detection

15.0 μL of cDNA was mixed with 1 μL of double-labeled probe. Then the experiment was performed at 50°C for 2 min, 95°C for 10 min and 1 min for 60 min, for forty cycles. Finally the result was observed using a PCR amplifier.

Statistical processing

Data were analyzed using SPSS ver. 18.0; *t*-test was used in the intra-group comparison. Difference was statistically significant if $p < 0.05$. The results were expressed as mean±standard deviation or median and quartile.

RESULTS

Electrophoretic result of EpCAM amplification

After total RNA extracted from the peripheral venous blood was amplified using EpC-01 and EpC-02 and amplified using PCR with primers EpC-1/2 and EpC-3/4, gel electrophoresis was performed, and the results are shown in Fig. 1. In Fig. 1, M

Table I. *PCR detection of the expression of EpCAM.*

	Patients with NSCLC	**Patients with benign lung diseases**	**Healthy subjects**
Number of cases/ n	120	50	30
The expression level of EpCAM in the CTCs (copies/2 mL)	18469±19502**	376±263**	318±153**

** *statistically significant difference between the patients with NSCLC and patients with benign lung diseases and between the patients with NSCLC and healthy volunteers ($p < 0.01$).*

Table II. D*etermination of the expression level of EpCAM.*

	Expression level of EpCAM		
	≥ 777 copies/2 mL (positive)	< 777 copies/2 mL (negative)	Total
Patients with NSCLC	114	6	120
Patients with benign lung diseases	2	48	50
Healthy volunteers	0	30	30

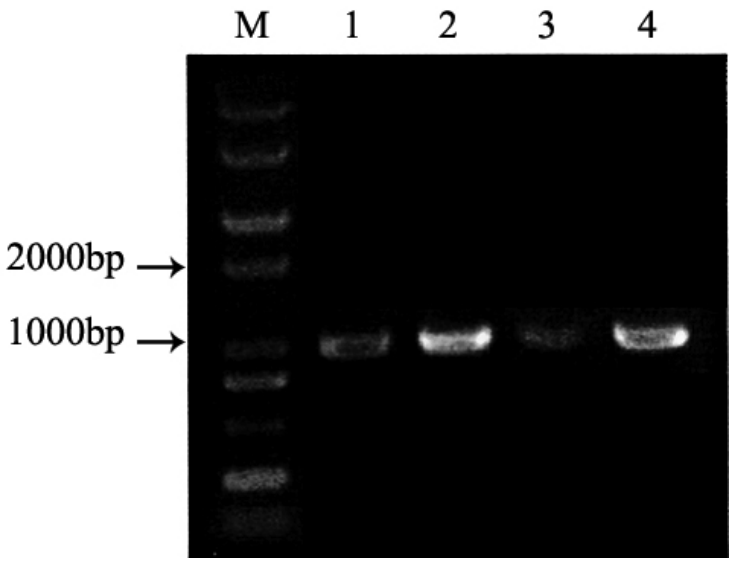

Fig. 1. *The gel electrophoretogram of EpCAM which were processed by PCR amplification using EpC-01, EpC-02, EpC-1/2 and EpC-3/4.*

stands for blank control, 1 stands for the amplified band of the samples after amplification using EpC-01 and EpC-1/2, 2 stands for the amplified band of the samples after amplification using EpC-02 and EpC-1/2, 3 stands for the amplified band of the samples after amplification using EpC-01 and EpC-3/4, and 4 stands for the amplified band of the samples after amplification using EpC-02 and Epc-3/4.

It can be noted from Fig. 1 that 1000 bp band could be seen in the sample 1 which was obtained by amplifying RNA using EpC-01 and EpC-1/2 and sample 2 which was obtained by amplifying EpC-02 and EpC-3/4. The amplified band of sample 2 was bright; therefore sample 2 was selected, i.e., RNA which was amplified using EpC-02 was taken for subsequent experiment.

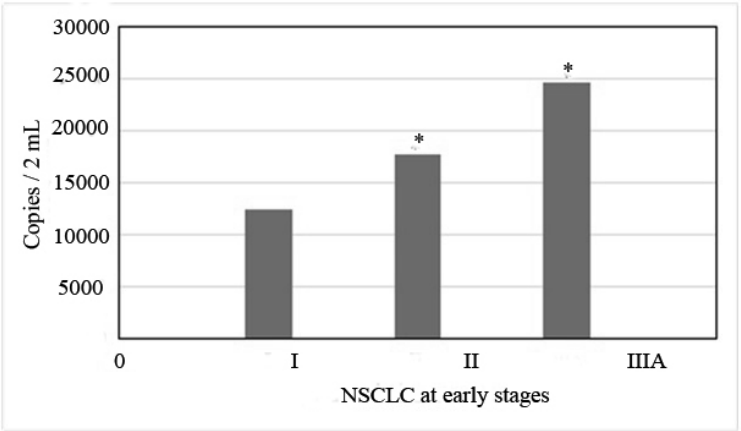

Fig. 2. *The expression level of EpCAM in the CTCs. * indicated that the difference between NSCLC at stages I and II in the expression level of EpCAM in the CTCs of the peripheral blood specimens had statistical significance ($p < 0.05$); the differences between NSCLC at stage IIIA and NSCLC at stage I and II were statistically notable ($p < 0.05$).*

Expression of EpCAM

The expression level of EpCAM in the CTCs of the peripheral blood of the patients with NSCLC and benign lung diseases before surgery and that of the healthy volunteers are shown in Table I.

The expression level of EpCAM of the 120 patients with NSCLC and 50 patients with benign lung diseases was 18469±19502 copies/2 mL and 376±263 copies/2 mL respectively, before surgery. The expression level of EpCAM of the healthy volunteers was 318±153 copies/2 mL.

The differences of the EpCAM level between the patients with NSCLC and benign lung diseases and between the NSCLC patients and the healthy volunteers were statistically significant ($p < 0.01$).

The determination results of the expression level of EpCAM

The positive threshold of the expression level of EpCAM was determined using TaqMan probe based fluorescence quantitative PCR detection. The expression level of EpCAM of the 30 healthy volunteers was 318±153 copies/2 mL. The positive threshold value was calculated using enzyme-linked immunosorbent assay (ELISA), 318+153×3=777 copies/2 mL (Table II).

Table II demonstrates that the expression level of EpCAM of 114 patients with NSCLC was not lower than 777 copies/2 mL, suggesting a positive result, and that of the remaining 6 patients was lower than 777 copies/2 mL, indicating a negative result; the expression level of EpCAM of 2 patients with benign lung diseases were not lower than 777 copies/2 mL, indicating a false positive result, while that of the remaining 48 patients with benign lung diseases was lower than 777 copies/2 mL, indicating a negative result; the 30 healthy volunteers had a negative result. The sensitivity and specificity of fluorescence PCR assay of EpCAM in the diagnosis of NSCLC were 95% and 97.5%.

The expression level of EpCAM of NSCLC at stage I, II and IIIA

As shown in Fig. 2, the expression level of EpCAM of NSCLC at stage I was 12472±14329 copies/2 mL; that of NSCLC at stage II was 17649±18762 copies/2 mL; that of NSCLC at stage IIIA was 24587±25679 copies/2 mL. The expression level of EpCAM increased greatly with the stage increase of NSCLC. The differences between NSCLC at stages I, II and IIIA in the expression level of EpCAM had statistical significance ($p < 0.05$).

DISCUSSION

NSCLC, which accounts for a large percentage in lung cancer, has strong invasiveness and metastases. Diagnosis of lung cancer usually relies on imaging

techniques such as computed tomography (CT); however lung cancer usually has transferred when being diagnosed, which brings huge difficulties to the treatment. Moreover, the specificity of the diagnosis is low. Hence a reference indicator which can reflect the metastasis of NSCLC early is needed. CTC (11-13) is considered as such a target, and it is vital in the metastasis process of lung cancer. Dynamic monitoring of CTCs in peripheral blood is greatly beneficial to the early diagnosis, detection and metastasis determination of NSCLC.

EpCAM is a kind of molecule which has a high expression in CTCs (14, 15) and a low expression or even no expression in healthy people and patients with benign lung diseases. A large content of EpCAM in peripheral blood can indicate the existence of CTCs and the migration of tumor.

This experiment firstly established EpCAM TaqMan probe for acquiring the special mRNA of EpCAM. Then corresponding cDNA was obtained through reverse transcription. Finally fluorescence quantitative PCR was performed on cDNA using a PCR amplifier to detect EpCAM in the CTCs. The experiment suggested that the determination of EpCAM was of high sensitivity and specificity in the diagnosis of NSCLC at the early or middle stage. The detection of EpCAM in CTCs in peripheral blood can be applied to detect the metastasis intensity of CTCs in peripheral blood and tumor cells, which is beneficial to the timely discovery of lung carcinoma and the arrangement of surgery and adjuvant treatment.

REFERENCES

1. Wu Z, Wang Z, Wang Y, Deng Q. Fast isolation and ex vivo culture of circulating tumor cells from the peripheral blood of lung cancer patients. Hereditas 2017; 39(1):66.
2. Wang B, Wang B, Zhang D, Guo H, Zhang L. Clinical test on circulating tumor cells in peripheral blood of lung cancer patients, based on novel immunomagnetic beads. Artif Cell Nanomed Biotech 2016; 44(3):892.
3. Dorsey JF, Kao GD, Macarthur K, et al. Tracking viable circulating tumor cells (CTCs) in the peripheral blood of non–small cell lung cancer (NSCLC) patients undergoing definitive radiation therapy: Pilot study results. Cancer 2015; 121(1):139.
4. Saucedozeni N, Mewes S, Niestroj R, Gasiorowski L, Murawa D. A novel method for the in vivo isolation of circulating tumor cells from peripheral blood of cancer patients using a functionalized and structured medical wire. Int J Oncol 2012; 41(4):1241.
5. Goldstraw P, Chansky K, Crowley J, Rami-Porta R, Asamura H. The IASLC Lung Cancer Staging Project: Proposals for Revision of the TNM Stage Groupings in the Forthcoming (Eighth) Edition of the TNM Classification for Lung Cancer. J Thorac Oncol 2016; 11(1):39-51.
6. Du S, Krämer S, Giese C, Weiss C, Wehling M. Chromogenic assays for measurement of rivaroxaban from EDTA anticoagulated plasma samples. Thromb Haemost 2015; 113(5):1149-51.
7. Winkler TE, Ben-Yoav H, Kelly DL, Ghodssi R. Osmotic erythrocyte lysis for chemical- and label-free impedance cytometry. Transd-Int Confer Solid-state Sens 2015; 351-54.
8. Miura T, Masago Y, Sano D, Omura T. Development of an effective method for recovery of viral genomic RNA from environmental silty sediments for quantitative molecular detection. Appl Environm Microbiol 2011; 77(12):3975-81.
9. Earnshaw DJ, Gait MJ. Modified oligoribonucleotides as site-specific probes of RNA structure and function. Biopolymers 2015; 48(1):39-55.
10. Cutolo A, D'Apice C, Manzo R. An integrated, valveless system for microfluidic purification and reverse transcription-PCR amplification of RNA for detection of infectious agents. Lab on A Chip 2011; 11(5):957.
11. Vansteenkiste J, Crinò L, Dooms C, Douillard JY, Faivrefinn C. 2nd ESMO Consensus Conference on Lung Cancer: early-stage non-small-cell lung cancer consensus on diagnosis, treatment and follow-up. Ann Oncol Offic J Eur Soc Med Oncol 2014; 25(8):1462-74.
12. Punnoose EA, Atwal S, Liu W, Raja R, Fine BM. Evaluation of circulating tumor cells and circulating tumor DNA in non-small cell lung cancer: association with clinical endpoints in a phase II clinical trial of pertuzumab and erlotinib. Clin Cancer Res: Offic J Am Assoc Cancer Res 2012; 18(8):2391.
13. Lecharpentier A, Vielh P, Perezmoreno P, Planchard

D, Soria JC. Detection of circulating tumour cells with a hybrid (epithelial|(sol)|mesenchymal) phenotype in patients with metastatic non-small cell lung cancer. Br J Cancer 2011; 105(9):1338-41.

14. Amato R J, Melnikova V, Zhang Y, Liu W, Saxena S. Epithelial cell adhesion molecule-positive circulating tumor cells as predictive biomarker in patients with prostate cancer. Urology 2013; 81(6):1303-7.
15. Song Y, Zhu Z, An Y, Zhang W, Zhang H. Selection of DNA aptamers against epithelial cell adhesion molecule for cancer cell imaging and circulating tumor cell capture. Analyt Chem 2013; 85(8):4141.

ACY 1215, A HISTONE DEACETYLASE 6 INHIBITOR, INHIBITS CANCER CELL GROWTH IN MELANOMA

F. WANG[1*], B. ZHONG[2*] and Z. ZHAO[3]

[1]Plastic Surgery Department, Daqing Oilfield General Hospital, Daqing, P.R.China; [2]Ophthalmology Department, Daqing Oilfield General Hospital, Daqing, P.R.China; [3]The Eastern Division Plastic and Cosmetic Surgery Department, The First Hospital of Jilin University, Changchun, P.R.China

Received September 29, 2017 – Accepted April 27, 2018

[*]These Authors contributed equally to this work

Histone deacetylase 6 (HDAC6) plays critical roles in dozens of malignant cancers, including melanoma. Therefore, inhibition of HDAC6 can be a potential strategy of targeting melanoma. ACY 1215 (ricolinostat), a selective HDAC6 inhibitor, is currently being clinically trialed in multiple cancers but not in melanoma. In this study, we tested the pre-clinical efficacy of ACY 1215 in melanoma cell lines. First, we found higher HDAC6 expression in melanoma cell lines than in an epidermal melanocyte cell line. Then, we observed the dose- and time-dependent reduction of cell proliferation caused by ACY 1215 treatment. Proliferation inhibition by ACY 1215 was associated with accumulation of acetylated tubulin but did not affect histone H3K9 acetylation. In addition, ACY 1215 induced cell apoptosis and G0/G1 cell cycle arrest. Finally, we show that ACY 1215 reduced tumor burden and increased survival in an *in vivo* mouse cell line xenograft model. All of these pre-clinical data indicate that HDAC6 is a potential target in melanoma, and that targeting HDAC6 in melanoma using ACY 1215 may be translationally relevant.

Malignant melanoma is a common type of skin cancer characterized by poor survival and high mortality. In recent years, targeted therapy and immune checkpoint blockade have made major advancements in treating melanoma (1-4). However, novel strategies still need to be developed as resistance to previous therapies have frequently emerged. Recent data reveals that epigenetic gene regulation might play an important role in melanoma, providing potential targets for treating the disease (5, 6). One group of epigenetic regulators are histone deacetylases (HDACs), consisting of a family of 18 enzymes. Most HDACs reside in the nucleus and form mass complexes with other proteins to regulate gene transcription (7). These 18 members can be divided into 4 categories: classes I, II, III and IV (8). Class I has four isoforms (HDAC1-3 and HDAC8); Class II is subdivided into IIa (HDAC4, 5, 7 and 9) and IIb (HDAC6 and 10); Class III contains seven HDAC isoforms but are referred to as sirtunins (Sirt1-7); and Class IV has one isoform (HDAC11). HDACs can modify histone proteins directly or deacetylate non-histone proteins (9). HDAC6 belongs to Class IIb and localizes in the cytoplasm in contrast to most other HDAC isoforms (7). HDAC6 possesses two catalytic domains but only one is

Key words: HDAC6, melanoma, ACY 1215, preclinical, apoptosis

Mailing address:
Fang Wang,
Plastic Surgery Department, Daqing Oilfield General Hospital,
No. 9, Zhongkang Street, Daqing, 163000, Heilongjiang, P.R.China
Tel./Fax: +86 459 5805826
e-mail: zhongwang2011@163.com

0393-974X (2018)
Copyright © by BIOLIFE, s.a.s.
This publication and/or article is for individual use only and may not be further reproduced without written permission from the copyright holder. Unauthorized reproduction may result in financial and other penalties
DISCLOSURE: ALL AUTHORS REPORT NO CONFLICTS OF INTEREST RELEVANT TO THIS ARTICLE.

well characterized for its enzymatic activity (10). Given HDAC6 is predominantly distributed in the cytoplasm, most of its physiological substrates are cytoplasmic proteins. One substrate of HDAC6 is the cytoskeletal protein α-tubulin which dimerizes with β-tubulin to form microtubules (11). HDAC6 has been reported to be up-regulated in multiple cancer types, such as breast cancer (12), B-cell lymphoma (13), multiple myeloma (14) and melanoma (15-17). In melanoma, targeting HDAC6 exhibits dual anti-cancer effect: enhanced antitumor immunity and impaired cell proliferation (17, 18). Playing a role in immune modulation, HDAC6 also regulates PD-L1 expression by recruiting and activating STAT3 (19). Therefore, targeting HDAC6 can ameliorate negative pathways affecting the T-cell response against cancer. HDAC6 facilitates tumor growth and metastasis by multiple pathways, such as activation of Ras, PI3K and MAPK or interaction with HSP90 (20, 21). Targeting HDAC6 by small molecular inhibitors resulted in reducing cell proliferation *in vitro* and delayed tumor growth *in vivo* (17).

ACY 1215 is a selective HDAC6 inhibitor which has shown great single agent and combinational efficacy in several types of cancer (22-25). However, most studies were conducted on multiple myeloma or B-cell lymphoma, and no study reported the efficacy of ACY 1215in melanoma treatment. Therefore, we tested the efficacy of ACY 1215 in melanoma both *in vitro* and *in vivo*. We show that ACY 1215 inhibits cell proliferation, induces both apoptosis and cell cycle arrest *in vitro*, and also reduces tumor burden and increases survival *in vivo*. The results suggest that targeting HDAC6 using ACY 1215 could be a potential therapy in melanoma.

MATERIALS AND METHODS

Reagents and cell culture

HDAC6 inhibitor ACY 1215 was purchased from Selleck Chemicals. The human epidermal melanocyte cell line PIG1 was maintained in medium 254 supplemented with 10% FBS and human melanocyte growth supplement. Human melanoma cell lines SK-MEL-5, Hs-695T and CHL-1 were cultured in medium RPMI 1640 supplemented with 10% FBS.

RNA isolation and real-time RT-PCR

2×10^6 cells for each cell line were used for RNA isolation by RNeasy Mini Kit (Qiagen) according to the manufacturer's instruction. Reverse transcriptions were performed by using iScript Advanced cDNA Synthesis Kit (Bio-Rad) following the manufacturer's instruction. Quantitative PCR was conducted by using SYBR® Green Real-Time PCR Master Mixes (Thermo Fisher Scientific) on a real-time PCR machine (Bio-Rad). The primer sequences of HDAC6 were: forward, 5'-TATCTGCCCCAGTACCTTCG-3' and reverse, 5'-GGACATCCCAATCCACAATC-3'. The human GAPDH served as internal control and primer sequences were: forward, 5'-CATCTTCCAGGAGCGAGA-3' and reverse, 5'-CTGCTTCACCACCTTCTTGAT-3'. The relative expression ratio was calculated by the $2^{-\Delta\Delta CT}$ method.

Cell viability assay

Cells were digested by trypsin and diluted to 1×10^5 cells per mL. In a dose-dependent assay, 100 μL cells were seeded in a 96-well plate containing 8 serial doses of ACY 1215: 20, 10, 5, 2.5, 1.25, 0.63, 0.31, 0 μM. Cells were incubated for 72 h and cell viability was tested by CellTiter-Glo™ luminescent cell viability assay (Promega) according to manufacturer's instruction. In the time-course study, cells were treated with 4 μM ACY 1215 for 6, 12, 18, 24 and 48 h, respectively, and cell viability assay followed the same protocol as the dose-dependent assay. Each treatment was carried out in triplicate withvDMSO as a negative control.

Annexin v cell apoptosis assay

Hs-695T and CHL-1 cells were treated with 0, 1, 2 and 4 μM ACY 1215 for 24 h. After treatment, cells were collected and washed twice by PBS. Certain amount of Annexin v (Thermo Fisher Scientific) and PI were added and incubated at room temperature for 15 min. Apoptosis was detected by using a BD Fortessa flow machine and data were analyzed by FlowJo V10. Both Annexin v^+ PI^- and Annexin v^+ PI^+ populations were calculated as apoptotic cells.

Cell cycle arrest assay

Hs-695T and CHL-1 cells were treated with 4 μM ACY 1215 for 24 h. Cells were digested by trypsin and washed twice with PBS. Then cells were fixed with 70%

ethanol for 30 min and RNaseA was then added. After washing twice with PBS, cells were resuspended in 0.05 mg/ml PI and data were analyzed by flow cytometry.

Western blot

2×10^6 cells of 4 parental cell lines and 1×10^6 cells of drug treated samples (treated with 0, 1, 2 and 4 μM ACY 1215 for 24 h) were collected and lysed by RIPA lysis buffer (Thermo Fisher Scientific) with proteinase inhibitors. Protein concentrations were determined by BCA Protein Assay Kit (Bio-Rad). Primary antibodies HDAC6, GAPDH, Ac-α-tub, α-tub, Ac-H3K9, Histone H3, cleaved PARP, cleaved caspase 3 and cleaved caspase 9 were purchased from Cell Signaling. Anti-rabbit IgG and anti-mouse IgG, HRP-linked secondary antibodies were also purchased from Cell Signaling. GAPDH served as an internal control.

Animal studies

Thirty BALB/c nude mice were purchased from Beijing Vital River Laboratory Animal Technology. All procedures complied with recommendations of the Guide for Care and Use of Laboratory Animals. 1×10^6 cells of each cell line were subcutaneously injected into the right flank of 4-week-old mice (n=5). Treatments were initiated one week after cancer cell transplantation. 5mg/g and 10mg/g ACY 1215 were orally administered once daily, 5 days a week, for three consecutive weeks for each cell line. Tumor volumes and body weights were measured every three days throughout the three-week treatment. Tumor volume = $1/2(\text{length} \times \text{width}^2)$.

Statistical analysis

In vitro experiments such as cell viability assay were performed in triplicate and repeated 3 times. The statistical differences were determined by using a one-way ANOVA test or Student's *t*-test between the two groups. Differences in tumor volume were determined by *p* values obtained by performing a one-way ANOVA at the final tumor measurement time point. All statistical analyses were performed using Prism v6.3 software.

RESULTS

HDAC6 is highly expressed in melanoma cell lines

It is reported that HDAC6 is highly expressed in melanoma and plays important roles in cancer proliferation and metastasis(15, 26, 27). To confirm these results, we tested HDAC6 expression in one human epidermal melanocyte cell line PIG1 and three melanoma cell lines by real-time RT-PCR and Western blot. Compared with PIG1, the three melanoma cell lines have higher HDAC6 mRNA and protein (Fig. 1 A, B). These results indicate that HDAC6 could be a potential target in melanoma.

ACY 1215 induced cytotoxicity in melanoma cells

ACY 1215 is being actively tested in several phase 1 and 2 clinical trials in multiple cancer types (NCT02787369, NCT02632071, NCT02091063, NCT02088398 and NCT01997840). To test whether ACY 1215 can inhibit melanoma cell proliferation, a 72-h cell viability assay was conducted in PIG1 and three melanoma cell lines. All data were normalized to the negative DMSO control. In both a dose-dependent assay (Fig. 1C) and time-dependent assay (Fig. 1D), ACY 1215 inhibited cell proliferation in three melanoma cell lines but not in PIG1 cells. The inhibition efficiency was positively correlated with HDAC6 expression among different cell lines.

ACY 1215 induced accumulation of acetylated tubulin in melanoma cells

As reported previously, HDAC 6 inhibitors could induce accumulation of Ac-α-tubulin (28). To confirm the result, we treated both Hs-695T and CHL-1 cells in a dose-dependent and time-dependent manner. In the dose-dependent assay, ACY 1215 induced Ac-α-tubulin accumulation without increasing histone H3K9 acetylation (Fig. 2A). In the time-dependent assay, ACY 1215 also induced the accumulation of Ac-α-tubulin but did not change histone H3K9 acetylation status (Fig. 2B). This result indicates that ACY 1215 induced accumulation of acetylated Tubulin without changing H3 acetylation status.

ACY 1215 induced apoptosis in melanoma cells

To investigate whether ACY 1215 inhibits melanoma cell proliferation by inducing cell apoptosis, we treated two cell lines, Hs-695T and CHL-1, using different doses of ACY 1215 and performed Annexin ν apoptosis assay and Western blot. In Annexin ν apoptosis assay, ACY 1215 induced

cell apoptosis in a dose-dependent manner (Fig. 3 A, B). In Western blot assay, ACY 1215 activated caspase 3, caspases 9 and PARP in a dose-dependent manner (Fig. 3C). We can conclude that ACY 1215 both inhibits cell proliferation and induces apoptosis in melanoma.

ACY 1215 arrested G0/G1 phase in melanoma cells

Cell apoptosis is also correlated with cell cycle arrest in many cancers. To test whether inhibition of HDAC6 by ACY 1215 can induce cell cycle arrest, both Hs-695T and CHL-1 cells were treated with 4 μM ACY 1215 for 24 h. ACY 1215 arrested both cell lines in G0/G1 phase (Fig. 3 D, E).

ACY 1215 reduced tumor burden and increased survival in vivo

Finally, we tested whether ACY 1215 could reduce tumor growth *in* vivo. Two cell lines Hs-695T and CHL-1 were transplanted into nude mice and two different doses of ACY 1215 were administered orally for three consecutive weeks. In both cell line models, ACY 1215 reduced tumor burden compared to the vehicle control (Fig. 4 A, B).The drug showed minimal toxicity as evidenced by stable body weight throughout treatment (Fig.C-D). Moreover, ACY 1215 increased survival in both animal models (Fig. 4 E,F).

DISCUSSION

Melanoma is one of the most aggressive skin cancers, characterized by rapid proliferation and metastases. This abnormal growth is due to the imbalance between oncogenes and tumor suppressors, such as the up-regulation of HDAC6. HDAC6 has been found up-regulated in many cancer types including melanoma and can induce oncogenesis, promote cancer development and progression, and enhance tumor invasion and metastasis by different mechanisms (20, 29, 30). Therefore, targeting HDAC6 could be an effective strategy in melanoma. To confirm our hypothesis, we confirmed the expression level of HDAC6 in

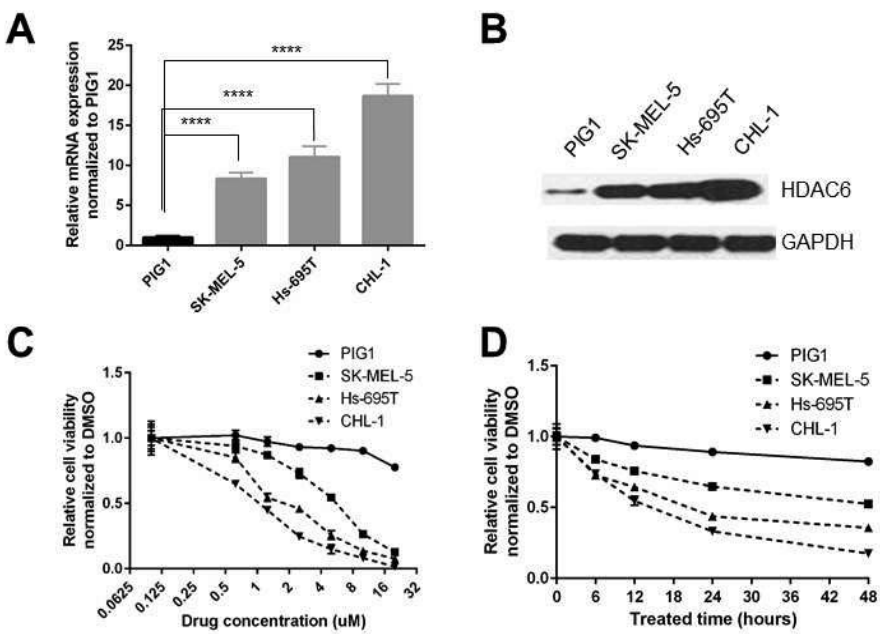

Fig. 1. *ACY 1215 reduced cell growth in melanoma cells with high HDAC6 expression.* ***A-B****) real-time RT-PCR and Western blot quantification of HDAC6 expression in melanoma cell lines. Total RNA and protein from 1 human epidermal melanocyte cell line and 3 melanoma cell lines were isolated as mentioned in the methods section. Real-time PCR and Western blot were conduct as previously reported.* ***C-D****) Dose- and time-dependent cell viability assay of ACY 1215 in melanoma cell lines. 72-hour cell viability assay with 8 drug dose and 5 time-point cell viability assay with 4 μM ACY 1215 were conducted in 4 cell lines. Each experiment for real-time RT-PCR and cell viability assay was carried out in triplicate.*

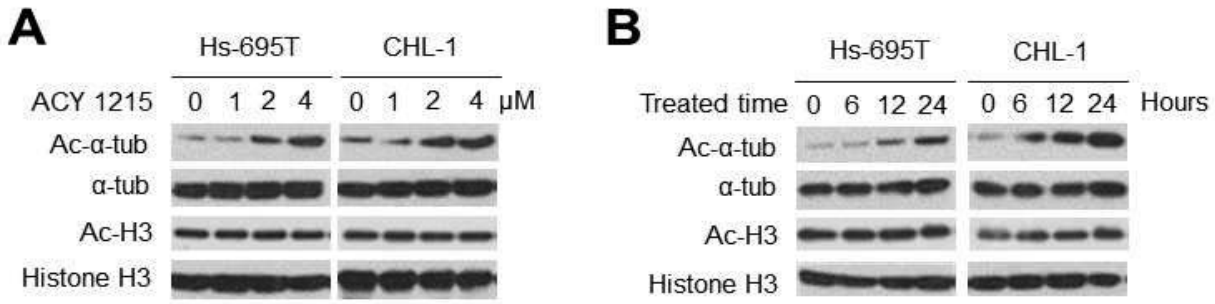

Fig. 2. *ACY 1215 deacetylates α-tubulin in melanoma cells.* ***A****) Dose-dependent assay: two melanoma cell lines were treated with 4 different doses of ACY 1215 for 24 h and cells were collected for Western blot.* ***B****) Time-dependent assay: two melanoma cell lines were treated with 4 μM ACY 1215 for 4 different time-points and cells were collected for Western blot.*

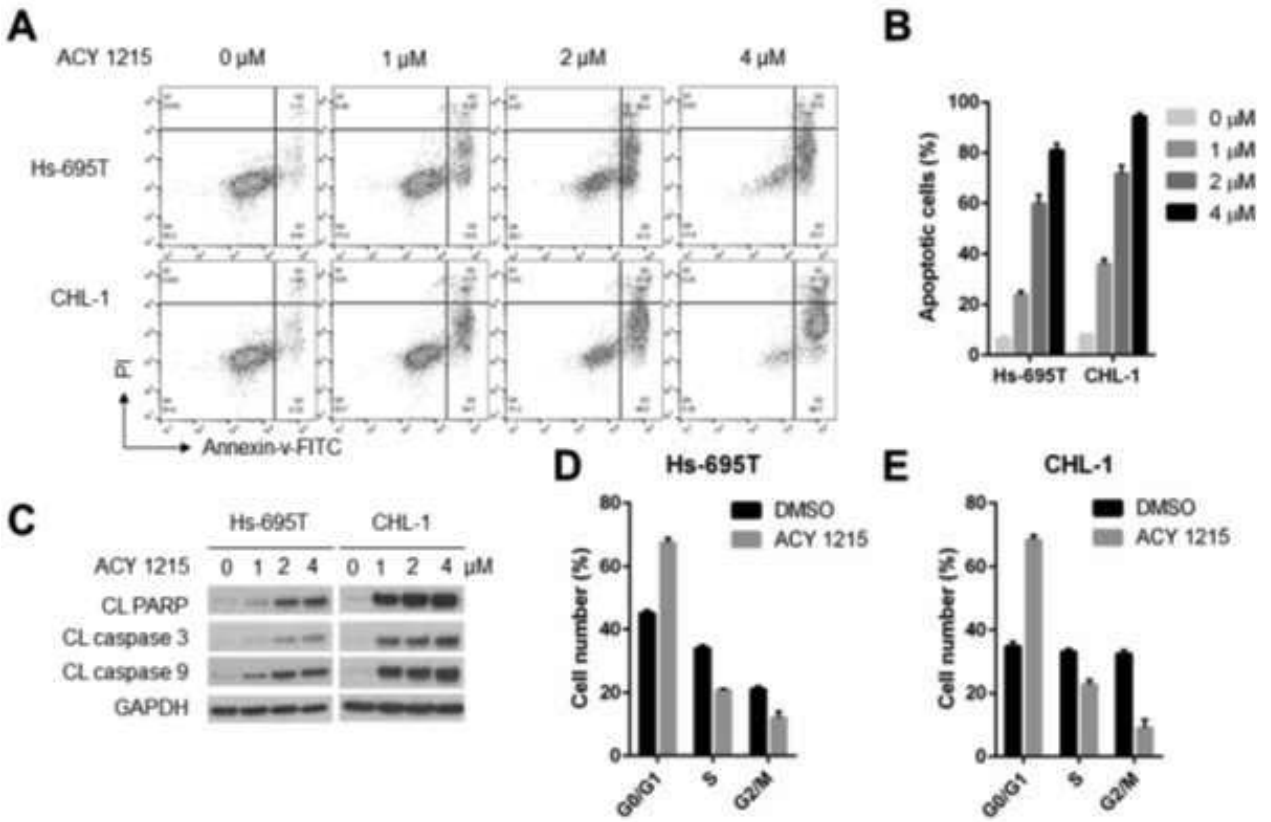

Fig. 3. *ACY 1215 induces apoptosis and arrests G0/G1 phase in melanoma cells.* ***A****) Two melanoma cell lines were treated for 4 different doses of ACY 1215 and apoptosis was tested by Annexin v/PI staining.* ***B****) Quantitative data for Annexin v/PI staining assay.* ***C****) Cells with same treatment as apoptosis assay were collected and cleaved caspases and PARP were detected by Western blot.* ***D-E****) Hs-695T and CHL-1 cells were treated with 4 μM ACY 1215 for 24 h and cell cycle arrest was tested by PI staining flow cytometry.*

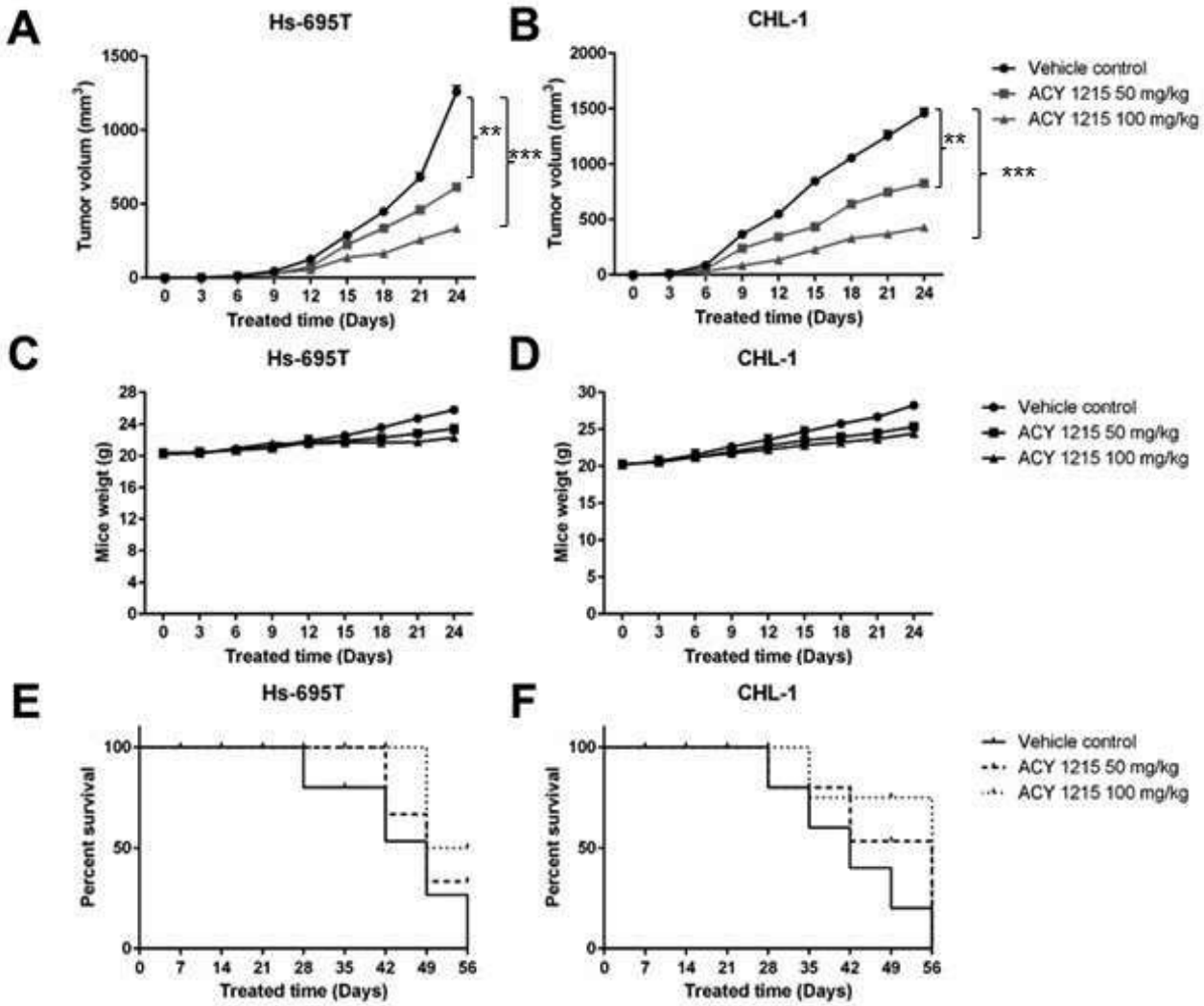

Fig. 4. *In vivo efficacy of ACY 1215 in melanoma. 1 × 10⁶ cells of two cell lines (Hs-695T and CHL-1) were injected into BALB/c nude mice. Two doses of ACY 1215 (50 mg/kg and 100 mg/kg) were orally administered daily. ACY 1215 reduces tumor burden (**A-B**), increases survival (**E-F**) but does not affect body weight (**C-D**) in two animal models. PBS was used as vehicle control and each group with 5 mice. Survival curves of individual groups of mice were evaluated using Kaplan-Meier analysis from the first day of treatment until sacrifice.*

melanoma cells. As expected, both HDAC6 RNA and protein expression levels were elevated compared to the human epidermal melanocyte cell line, PIG1 (Fig. 1 A, B). The result indicates that HDAC6 could be a therapeutic target in melanoma.

Targeting HDAC6 demonstrates dual functions in cancers: upregulation in the expression of tumor associated antigens, and inhibition of cancer cell growth with concomitant induction G0/G1 cell cycle arrest (17). In our study, we looked at the direct cytotoxic effect of a HDAC inhibitor, ACY 1215. This agent has been studied in many cancers, especially in multiple myeloma and non-Hodgkin lymphoma (NHL), with great success (22, 31). In addition, multiple clinical trials are ongoing among different cancers. However, no study of the drug has been performed in melanoma. To test whether ACY 1215 can also be used for targeting melanoma, we conducted both dose-dependent and time-dependent cell viability assays in three melanoma cell lines and

PIG1. As expected, ACY 1215 only inhibited cell growth in the melanoma cell lines with high HDAC6 expression but not in PIG1 (Fig. 1 C, D). Inhibition of tumor proliferation and differentiation by ACY 1215 may be due to FOXO1-dependent pathways, which are transcription factors involved in autophagy. The results suggest that ACY 1215 specifically targets melanoma cells with high HDAC6 expression. One biomarker for HDAC6 inhibition is α-tubulin acetylation (28). HDAC6 deacetylates lysine residue 40 on α-tubulin. To test the mechanistic effect of ACY 1215 in melanoma, we treated two cell lines with different drug doses and time points. We demonstrate ACY 1215 treatment increases levels of acetylated α-tubulin but not acetylated H3K9 (Fig. 2). The results indicated that ACY 1215 exerts its function by deacetylation of α-tubulin as reported previously.

To verify whether ACY 1215 can induce apoptosis in melanoma, we treated two cell lines with three different doses of drugs. Both Annexin v/PI apoptosis assay and Western blot showed ACY 1215 induces caspase activation and apoptosis (Fig. 3A, C). HDAC inhibitors have been reported to induce apoptosis through valproic acid (VPA), which also inhibits angiogenesis and induces G1 phase cell cycle arrest. Also, HDAC inhibitors can enhance apoptosis with up-regulation of BIM, BAX and BIK and down-regulation of Bcl-XL and XIAP. In addition, ACY 1215 arrested cell lines in G0/G1 phase(Fig. 3 D, E). ACY 1215 induced G1 phase arrest is not well studied, but may due to the elongation of p27 half-life or down-regulation of TbX2.These data show that ACY 1215 induces apoptosis and arrests cell cycling in melanoma.

In vivo efficacy is the gold standard for preclinical study of new drugs. Animal study will provide a closer analog for clinical application (32). As ACY 1215 has been going through clinical trials in diverse cancers, a successful animal study provides credence for the clinical application of ACY 1215 in melanoma. ACY 1215 reduced tumor burden and increased survival but did not affect body weight in nude mice transplanted with melanoma cell lines (Fig. 4). In conclusion, ACY 1215 exerts great efficacy in inhibiting melanoma cell growth both *in vitro* and *in vivo*. These first pre-clinical findings in melanoma support the potential use of ACY 1215 in a melanoma clinical trial.

REFERENCES

1. Robert C, Thomas L, Bondarenko I, et al. Ipilimumab plus d acarbazine for previously untreated metastatic melanoma. N Engl J Med 2011; 364:2517-26.
2. Hamid O, Robert C, Daud A, et al. Safety and tumor responses with lambrolizumab (anti–PD-1) in melanoma. N Engl J Med 2013; 369:134-44.
3. Bollag G, Hirth P, Tsai J, et al. Clinical efficacy of a RAF inhibitor needs broad target blockade in BRAF-mutant melanoma. Nature 2010; 467:596-99.
4. Falchook GS, Lewis KD, Infante JR, et al. Activity of the oral MEK inhibitor trametinib in patients with advanced melanoma: a phase 1 dose-escalation trial. Lancet Oncol 2012; 13:782-89.
5. Sarkar D, Leung EY, Baguley BC, Finlay GJ, Askarian-Amiri ME. Epigenetic regulation in human melanoma: past and future. Epigenetics 2015; 10:103-21.
6. Greenberg ES, Chong KK, Huynh KT, Tanaka R, Hoon DS. Epigenetic biomarkers in skin cancer. Cancer Lett 2014; 342:170-77.
7. Batchu SN, Brijmohan AS, Advani A. The therapeutic hope for HDAC6 inhibitors in malignancy and chronic disease. Clin Sci (Lond) 2016; 130:987-1003.
8. Hornig E, Heppt MV, Graf SA, Ruzicka T, Berking C. Inhibition of histone deacetylases in melanoma—a perspective from bench to bedside. Exp Dermatol 2016; 25:831-38.
9. Dokmanovic M, Clarke C, Marks PA. Histone deacetylase inhibitors: overview and perspectives. Mol Cancer Res 2007; 5:981-89.
10. Liu Y, Peng L, Seto E, Huang S, Qiu Y. Modulation of histone deacetylase 6 (HDAC6) nuclear import and tubulin deacetylase activity through acetylation. J Biol Chem 2012; 287:29168-74.
11. Hubbert C, Guardiola A, Shao R, et al. HDAC6 is a microtubule-associated deacetylase. Nature 2002; 417:455-58.
12. Chang Y, Tseng C, Wang M, et al. Deacetylation of HSPA5 by HDAC6 leads to GP78-mediated HSPA5

ubiquitination at K447 and suppresses metastasis of breast cancer. Oncogene 2016; 35:1517-28.
13. Amengual JE, Johannet PM, Zullo K, Lombardo M, O'Connor OA. Development and characterization of two lymphoma cell lines resistant to the selective HDAC6 inhibitor ricolinostat (ACY-1215) as a tool to better understand the biology of HDACs on lymphoma. Blood 2014; 124:1777.
14. Hideshima T, Qi J, Paranal RM, et al. Discovery of selective small-molecule HDAC6 inhibitor for overcoming proteasome inhibitor resistance in multiple myeloma. Proc Natl Acad Sci U S A. 2016; 113:13162-67.
15. Liu J, Gu J, Feng Z, Yang Y, Zhu N, Lu W, Qi F. Both HDAC5 and HDAC6 are required for the proliferation and metastasis of melanoma cells. J Transl Med 2016; 14:7.
16. Bai J, Lei Y, An G-l, He L. Down-regulation of deacetylase HDAC6 inhibits the melanoma cell line A375. S2 growth through ROS-dependent mitochondrial pathway. PLoS One 2015; 10:e0121247.
17. Woan K, Lienlaf M, Perez-Villaroel P, et al. Targeting histone deacetylase 6 mediates a dual anti-melanoma effect: Enhanced antitumor immunity and impaired cell proliferation. Mol Oncol 2015; 9:1447-57.
18. Cheng F, Lienlaf M, Wang H-W, et al. A novel role for histone deacetylase 6 in the regulation of the tolerogenic STAT3/IL-10 pathway in APCs. J Immunol 2014; 193:2850-62.
19. Lienlaf M, Perez-Villarroel P, Knox T, et al. Essential role of HDAC6 in the regulation of PD-L1 in melanoma. Mol Oncol 2016; 10:735-50.
20. Lee Y-S, Lim K-H, Guo X, et al. The cytoplasmic deacetylase HDAC6 is required for efficient oncogenic tumorigenesis. Cancer Res 2008; 68:7561-69.
21. Murphy PJ, Morishima Y, Kovacs JJ, Yao T-P, Pratt WB. Regulation of the dynamics of hsp90 action on the glucocorticoid receptor by acetylation/deacetylation of the chaperone. J Biol Chem 2005; 280:33792-99.
22. Santo L, Hideshima T, Kung AL, et al. Preclinical activity, pharmacodynamic, and pharmacokinetic properties of a selective HDAC6 inhibitor, ACY-1215, in combination with bortezomib in multiple myeloma. Blood 2012; 119:2579-89.
23. Vogl DT, Raje NS, Jagannath S, et al. Ricolinostat (ACY-1215), the first selective HDAC6 inhibitor, in combination with bortezomib and dexamethasone in patients with relapsed or relapsed-and-refractory multiple myeloma: phase 1b results (ACY-100 study). Blood 2015; 126:1827-27.
24. Amengual JE, Johannet P, Lombardo M, et al. Dual targeting of protein degradation pathways with the selective HDAC6 inhibitor ACY-1215 and bortezomib is synergistic in lymphoma. Clin Cancer Res 2015; 21:4663-75.
25. Huang S, Nastoupil LJ, Guo H, et al. Pre-Clinical Evaluation of the PI3K-p110β/δ inhibitor KA2237 in mantle cell lymphoma. Hematology Am Soc Hematol Educ Program, 2016.
26. Wickström SA, Masoumi KC, Khochbin S, Fässler R, Massoumi R. CYLD negatively regulates cell-cycle progression by inactivating HDAC6 and increasing the levels of acetylated tubulin. EMBO J 2010; 29:131-44.
27. Aldana-Masangkay GI, Sakamoto KM. The role of HDAC6 in cancer. Biomed Res Int 2010; 2011.
28. Dhanyamraju PK, Holz PS, Finkernagel F, Fendrich V, Lauth M. Histone deacetylase 6 represents a novel drug target in the oncogenic Hedgehog signaling pathway. Mol Cancer Ther 2015; 14:727-39.
29. Zhang X, Yuan Z, Zhang Y, et al. HDAC6 modulates cell motility by altering the acetylation level of cortactin. Mol Cell 2007; 27:197-213.
30. Mak AB, Nixon AM, Kittanakom S, et al. Regulation of CD133 by HDAC6 promotes β-catenin signaling to suppress cancer cell differentiation. Cell Rep 2012; 2:951-63.
31. Dasmahapatra G, Patel H, Al-Khafaji JT, Fisher RI, Friedberg JW, Grant S. The irreversible proteasome inhibitor carfilzomib interacts synergistically with the selective HDAC6 inhibitor ACY1215 in ABC- and GC-DLBCL and mantle cell lymphoma sensitive or resistant to bortezomib. Blood 2012; 120:2765-65.
32. Zhang L, Nomie K, Zhang H, et al. B-cell lymphoma patient-derived xenograft models enable drug discovery and are a platform for personalized therapy. Clin Cancer Res 2017: 23(15):4212-23.

LETTER TO THE EDITOR

STUDY OF SELECTED THERAPEUTIC POTENTIALS OF *MOMORDICA CHARANTIA* FRUIT

F. HUSSAIN, A. IRSHAD and M. SHAHID

Clinico-Medical Biochemistry Laboratory, Department of Biochemistry, Faculty of Sciences, University of Agriculture, Faisalabad, Pakistan

Received September 30, 2017 – Accepted April 27, 2018

M. charantia **extract partitioned in different solvents was assessed for antioxidant (2, 2-diphenyl l-picrylhydrazyl), total phenolic contents (TPC), total flavonoid contents (TFC), antiglycation, alpha amylase and acetylcholinesterase inhibitory activities along with cytotoxic, thrombolytic and antibiofilm potentials. Most effective antioxidant fraction was *n*-hexane with TPC and TFC, highest in *n*-butanol and ethanol fractions, respectively. Ethyl acetate fraction showed maximum glycation and alpha amylase inhibitions and optimum acetylcholinesterase inhibition was by ethanol fraction. Fractions exhibited significant hemolytic and thrombolytic efficacies and bacterial growth restraint. The present research reveals some medicinal potency of *M. charantia*.**

To the Editor,

Momordica charantia fruits have been used in treatment of various ailments, such as obesity, acquired immune deficiency syndrome, cancer, diabetes, malaria, jaundice, fever and scabies, due to containing vitamins, minerals, glycosides, saponins, phenolics, essential oils, alkaloids, reducing sugars, resins and free acids. *M. charantia* prevents oxidative disorders and possesses anti-diabetic potential due to charantin, an insulin-like peptide and anthocyanins. Current investigation is designed to assess antioxidant, antibiofilm, antidiabetic, thrombolytic and cytotoxic potentials of the *M. charantia* fruit.

MATERIALS AND METHODS

M. charantia fruit methanol extract, fractioned into *n*-hexane, *n*-butanol, ethanol, ethyl acetate, chloroform and aqueous solvents was tested for antioxidant (i), antidiabetic (ii), cytotoxic (iii) properties along with fibrinolytic and antibiofilm activities (iv).

RESULTS

The results of all assessments are shown in Table I. Highest TPC and TFC were found in *n*-butanol and ethanol fractions, respectively. Highest DPPH scavenging activity was of *n*-hexane fraction, although it was quite lower than that reported earlier (5). Optimal antiglycation and alpha amylase inhibition action was of ethyl acetate fraction. Previously, antiglycation activity of *M. charantia* fruit was 67-75% (6), results analogous to another study (7). Ethanol extract showed highest inhibition of acetylcholinesterase. Previously, leaf extract of *M. charantia* showed 77.6% inhibition (8). Maximum antimicrobial activity was shown by aqueous fraction against *P. multocida* and by methanol extract against *S. aureus* (Fig. 1). Least damage to

Key words: Momordica charantia, therapeutic properties, 2, 2-diphenyl l-picrylhydrazyl

Mailing address:
Dr Fatma Hussain,
Department of Biochemistry,
Faculty of Sciences, University of Agriculture,
Faisalabad, 38040, Pakistan
Tel.: +92 41 9200161 170, Ext. 3313
e-mail: fatmauaf@yahoo.com

0393-974X (2018)
Copyright © by BIOLIFE, s.a.s.
This publication and/or article is for individual use only and may not be further reproduced without written permission from the copyright holder.
Unauthorized reproduction may result in financial and other penalties
DISCLOSURE: ALL AUTHORS REPORT NO CONFLICTS OF INTEREST RELEVANT TO THIS ARTICLE.

Table I. *Antioxidant, antidiabetic, thrombolytic, hemolytic and antibiofilm activities.*

Activities	**Fractions**							
Antioxidant profile	**Methanol**	**Ethyl acetate**	***n*-hexane**	**Chloroform**	**Ethanol**	***n*-butanol**	**Aqueous**	**control**
TFC	14±0.013	17±0.023	24±0.010	16±0.024	33±0.028	20±0.026	24±0.011	-
TPC	10±0.035	14±0.021	8±0.015	9±0.016	11±0.023	15±0.019	9 ±0.014	-
DPPH (IC_{50})	22	6	40	3	12	25	28	90
Antidiabetic profile (% inhibition)								
Glycation	47	53	23	38	44	47	45	32
Alpha amylase	15	47	40	34	22	25	33	27
AChE	7	2	2	17	78	4	1	59.5
Thrombolytic	30.5	31	26	42	32	30	24	48
Hemolytic	27	30	20	8	14	32	17	87.13
Biofilm assay (% inhibition)								
P. multocida	22.7	45.3	16.3	6.31	5.57	21.6	49.1	83.79
S. aureus	60.2	27.5	22.1	1	41.6	34.6	43.8	82.2

Data expressed as (mean ± SD) or percentage.

TPC: total phenolic contents expressed g gallic acid equivalent /100 g dry weight; TFC: total flavonoid contents expressed as g catechin equivalents/100 g dry weight; DPPH: 2, 2-diphenyl l-l-l-picrylhydrazyl. Control: BHT; butylated hydroxy toluene (antioxidant), metformin (antiglycation), glucobay (alpha amylase inhibition), physostigmine (AChE inhibition), Triton-X (hemolytic assay), streptokinase (thrombolytic assay), ampicillin (biofilm assay).

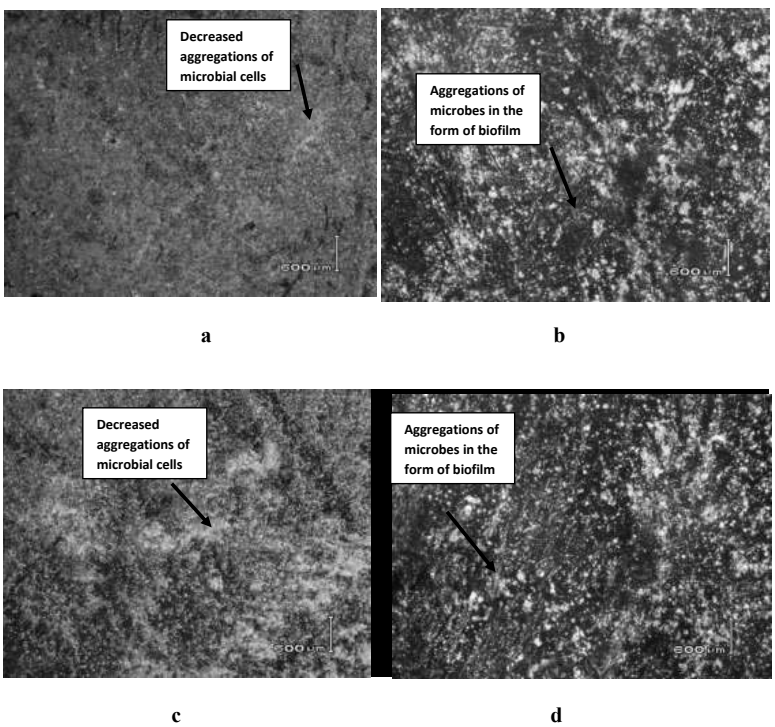

Fig. 1. *Biofilm assay micrographs. Highest and lowest growth inhibitions.* ***a, b)*** *P. multocida.* ***c, d)*** *S. aureus.*

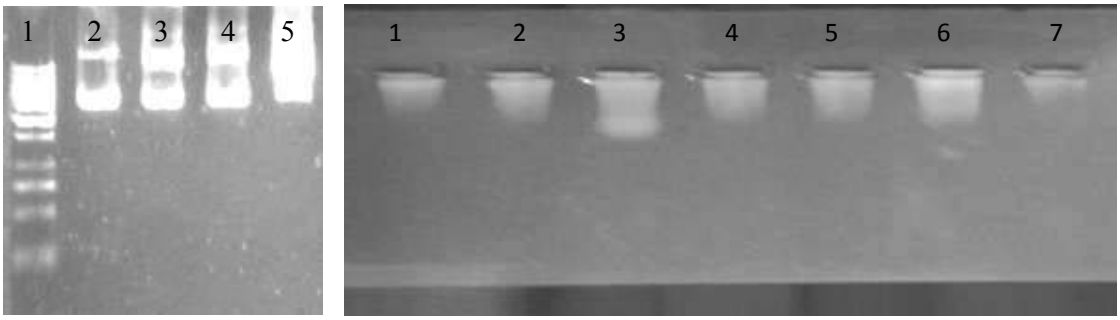

a **b**

Fig. 2. *Electrophoretic analysis of DNA-damage protection assay.* ***a)*** *Controls. 1: ladder, 2: positive control, 3: negative control ($FeSO_4$), 4 and 5: negative control (H_2O_2).* ***b)*** *Samples: 1: methanol treated, 2: ethanol treated, 3: ethyl acetate treated, 4: chloroform treated, 5: n-hexane treated, 6: n-butanol treated, 7: aqueous treated.*

RBCs was done by *n*-butanol fraction in accordance with earlier reported 23.61% hemolytic activity (9). Maximum thrombolytic response was of chloroform fraction while previously, ethanolic extract showed anticoagulation in the range 2.16±0.72-5.18±1.69% (10). DNA remained intact (Fig. 2) by antioxidant ability of fractions. In previous investigation, aqueous fraction prevented oxidative DNA impairments during carcinogenesis (11).

DISCUSSION

M. charantia is a medicinal plant that is popularly used for the treatment of many ailments such as cancer, diabetes and many more. Current research exposed some diverse therapeutic abilities of *M. charantia* fruit that warrant further clinical trials.

ACKNOWLEDGEMENTS

The authors are grateful to the Higher Education Commission, Pakistan for funding the current research.

REFERENCES

1. Siddique, NA, Mujeeb M, Najmi AK, Akram M. Evaluation of antioxidant activity, quantitative estimation of phenols and flavonoids in different parts of *Aegle marmelos*. Afr J Plant Sci 2010; 4**:**001-005.
2. Matsuura, N, Aradate T, Sasaki C, Kojima H, Ohara M, Hasegawa J, Ubukata M. Screening system for the maillard reaction inhibitor from natural product extracts. J Health Sci 2002; 48:520-26.
3. Ruma, K, Kumar S, Prakash HS. Anti-oxidant, anti-inflammatory, anti-microbial and cytotoxic properties of fungal endophytes from Garcinia species. Int J Pharm Sci 2013; 5:889.
4. Dheepa, M, Rashme VL, Appalaraju B. Comparison of biofilm production and multiple drug resistance in clinical isolates of *Acinetobacter baumanii* from a tertiary care hospital in South India. Int J Pharm Biomed Sci 2011; 2:103-7.
5. Aljohi, A, Nasri SM, Ahmed N. Antiglycation and antioxidant properties of *Momordica charantia*. PLoS ONE 2016; 10:1-14.
6. Ghous, T, Aziz N, Mehmood Z, Andleeb S. Comparative study of antioxidant, metal chelating and antiglycation activities of *Momordica charantia* flesh and pulp fractions. Pak J Pharm Sci 2015; 28:1217-23.
7. Poovitha, S, Parani M. *In vitro* and *in vivo* alpha-amylase and alpha-glucosidase inhibiting activities of the protein extracts from two varieties of bitter gourd (*Momordica charantia* L.). BMC Complement Altern Med 2016; 16:1-15.

8. Nagarani, G, Abirami A, Siddhuraju P. A comparative study on antioxidant potentials, inhibitory activities against key enzymes related to metabolic syndrome and anti-inflammatory activity of leaf extract from different *Momordica* Species. Food Sci Human Wellness 2014; 3:36-46.
9. Umukoro, S, Ashorobi RB. Evaluation of anti-inflammatory and membrane stabilizing property of aqueous leaf extract of *Momordica charantia* in rats. Afr J Biomed Research 2006; 9**:**119-24.
10. Das, A, Dewan SMR, Ali MR, Billah MM. Investigation of *in vitro* thrombolytic potential of ethanolic extract of *Momordica charantia* fruits: an anti-diabetic medicinal plant. Der Pharmacia Sinica 2013; 4:104-8.
11. Ganguly, C, De S, das S. prevention of carcinogen-induced mouse skin papilloma by whole fruit aqueous Extract of *Momordica charantia*. Eur J Cancer Prev 2000; 9:238-83.

LETTER TO THE EDITOR

PHENOLICS, TOCOPHEROLS AND FATTY ACID PROFILING OF WILD AND COMMERCIAL MUSHROOMS FROM PAKISTAN

S. SHARIF[1], S. RASHID[2], A. ATTA[3], A. IRSHAD[2], M. RIAZ[4], M. SHAHID[2] and G. MUSTAFA[5]

[1]College of Biosystem, Engineering and Food Science, Zhejiang University, China; [2]Department of Biochemistry, University of Agriculture, Faisalabad, Pakistan; [3]Department of Biochemistry, Bahauddin Zakariya University Multan, Pakistan; [4]Department of Allied Health Sciences, Sargodha Medical College, University of Sargodha, Pakistan; [5]Department of Biochemistry, Government College University, Faisalabad, Pakistan

Received March 12, 2018 – Accepted May 2, 2018

Mushrooms can be used as nutraceutical or functional foods to maintain and promote good health. In the present study, wild *Ganoderma lucidum* and four commercial mushrooms, *Pleurotus ostreatus, Volvariella volvacea, Hericium erinaceus* and *Lentinus edodes,* collected from Pakistan were screened for phenolics, tocopherols and fatty acid contents. High performance liquid chromatography analysis of phenolic acids showed that chlorogenic acid, ferulic acid, gallic acid, p-Coumaric and caffeic acids were observed in selected mushrooms. *H. erinaceus* contained high amounts of chlorogenic acid (11.49±0.1 µg/g of dry weight) and ferulic acid (7.84±0.7 µg/g of dry weight). γ-tocopherol and lutein were present in all studied mushrooms. Lutein contents were higher in *H. erinaceus* (2.42±0.087 µg/g of DW) followed by *V. volvacea* > *P. ostreatus* > *L. edodes*. γ-tocopherol was observed in the range of 74.25±3.01 to 29.65±1.2 µg/g of dry weight. GC/MS analysis of fatty acids showed that linoleic acid (18':2n6c), oleic acid (18':1n9c), palmitic acid (C16:0), stearic acid (C18:0), linolenic acid (18':3n3) and nonadecanoic acid (C19-0), were the main fatty acids found in selected mushrooms. The unsaturated fatty acids were predominated over saturated fatty acids. It is concluded that selected mushrooms are good sources of antioxidant compounds and unsaturated fatty acids.

To the Editor,

The use of natural antioxidants, particularly phenolics, flavonoids, tocopherols and carotenoids in foods, as well as therapeutic and preventive medicines, are gaining recognition because of their health-improving qualities (1). Recent epidemiological studies have showed that natural antioxidants, such as polyphenols, flavonoids and vitamin C, from edible mushrooms are correlated with reduced incidence of chronic diseases, cancer and cardiovascular diseases. Synthetic antioxidants have been widely used for preventing oxidation and enhancing shelf life of foods. However, the use of synthetic antioxidants in food is discouraged due to their perceived carcinogenic potentials (2). Mushrooms are also considered as significant and potent sources of phytoconstituents including tocopherols, flavonoids, ascorbic acid, β-carotene,

Key words: fatty acid, γ-tocopherols, lutein, phenolics, mushrooms

Mailing address:
Dr Ghulam Mustafa,
Department of Biochemistry,
Government College University,
Faisalabad, 38060, Pakistan
Tel.: +92(41)9330047
e-mail: drghulammustafa@gcuf.edu.pk

0393-974X (2018)
Copyright © by BIOLIFE, s.a.s.
This publication and/or article is for individual use only and may not be further reproduced without written permission from the copyright holder. Unauthorized reproduction may result in financial and other penalties
DISCLOSURE: ALL AUTHORS REPORT NO CONFLICTS OF INTEREST RELEVANT TO THIS ARTICLE.

glycosides, saponins, alkaloids and tannins that vary among different species renowned for their pharmaceutical properties (3, 4).

Generally, lipid contents of mushrooms are low. It is reported that the lipid proportion per 100 grams of dried mushrooms ranges from 1.75–15.5%, since the fresh mushrooms contain high amounts of water. Many wild edible mushroom species are also known to have high amounts of unsaturated fatty acids. Lipids are the least studied components in mushrooms since their overall contents are rarely higher than 6–8% of the dry weight. However, low lipid content is one of the advantages of mushrooms as healthy nutrients. Therefore, it is necessary to investigate wild and commercial mushrooms for their fatty acid contents. In the present study, one wild and four commercial types of mushrooms were analyzed to evaluate their phenolics, tocopherols, carotenoids and fatty acid profiles.

MATERIALS AND METHODS

Mushroom collection

The wild local *Ganoderma lucidum* (Fr.) P. Karst. was collected from the stem of a *Salmalia malabarica* plant from Jinnah Garden, Faisalabad, Pakistan. Indigenously cultivated commercial *Pleurotus ostreatus* (Jacq. Ex. Fr.) Kumm. and *Volvariella volvacea* (Bull, ex. Fr.) Sing were collected from the Horticulture Department, University of Agriculture Faisalabad, Pakistan, and exotic commercially available mushrooms *Lentinus edodes* (Berk.) Sing. and *Hericium erinaceus* (Bull.) Pers. (imported from China) were collected from local markets of Faisalabad, Pakistan. The specimen of each species was immediately ground in a domestic blender and reduced to fine powder and stored at 4°C.

Analysis of phenolic acids by HPLC

Sample extraction and preparation. Freeze dried mushroom powder (0.20 g) was extracted with 2 mL of 0.1% formic acid/methanol and sonicated for 20 min. The mixture was centrifuged at 3,000 rpm for 10 min. Residues were re-extracted twice and extracts were combined and evaporated to dryness under vacuum. Samples were re-dissolved in 0.1% formic acid/ water and filtered through a 0.20 µm disposable LC filter disk prior to HPLC analysis.

Instrumentation and chromatography. Samples were injected in a Waters 2695 separations module equipped with a Waters Xterra reverse phase C_{18} 3.5 µm 2.1 × 100 mm column in a heated chamber set at 35°C. Elution was performed by a linear biphasic gradient with a flow rate of 0.30 mL/min with mobile phase A (2% formic acid in MS grade water) and mobile phase B (0.1% formic acid in acetonitrile). At 0, 10, 30, and 31 min, the solvent composition used was 95, 90, 75 and 95%, respectively, of mobile phase A. The flow was split so that half of it went to a Waters 2996 photodiode array detector and half to a Waters Micromass ZQ mass spectrometer (5).

Tocopherols analysis of selected mushrooms

Sample preparation. Tocopherol contents were determined following a procedure previously optimized and described by L Barros et al. (6). Butyl hydroxyl toluene (BHT) solution in *n*-hexane (10 mg/mL; 100 µL) and IS solution in *n*-hexane (tocopherol; 2.0 µg/mL; 250 µL) were added to the sample prior to the extraction procedure. The sample (500 mg) was homogenized with methanol (4 mL) using a vortex mixer (1 min). Subsequently, *n*-hexane (4 mL) was added and again vortexed for 1 min. Then, saturated aqueous solution of NaCl (2 mL) was added, the mixture was homogenized (1 min) and centrifuged (5 min, 4000 g). The clear upper layer was carefully transferred to a fresh vial. Sample was re-extracted twice with *n*-hexane. The combined extracts were dried under a nitrogen stream, re-dissolved in 5 mL of ethyl acetate, 0.5 mL of methanol, filtered through a 0.22 µm disposable LC filter disk, transferred into a dark injection vial and analyzed by HPLC.

HPLC analysis. Carotenoid and tocopherol analyses were completed with a Hewlett-Packard model 1090A HPLC system equipped with a model 79880A diode array detector. Separations were achieved using a YMC carotenoid reversed phase (2.0 × 250 mm) polymeric C_{30} column with a guard column containing the same stationary phase (Waters Corp., Milford, MA, USA). A gradient elution profile based on a binary mobile phase system consisting of methanol/1 M ammonium acetate (98:2 v/v) in phase A and ethyl acetate in phase B was used. A flow rate of 0.37 mL/min was utilized with initial conditions set at 100% A with a linear gradient to 80:20 A/B over 6 min. The gradient was held for 2 min followed by a 3 min linear gradient back to 100% A and equilibration at initial

conditions for 3 min for a total analysis time of 14 min. Detection and tentative identification of carotenoids and tocopherols were accomplished using inline diode array data between 250 and 600 nm.

Fatty acid analysis of selected mushrooms

Extraction. The sample (200 mg) was weighed and transferred to a 12 cm × 1.5 cm tube. 1 mL of absolute chloroform and 3 mL of fresh 5% methanolic HCl (prepared by slowly adding 10 mL of acetyl chloride to 100 mL of anhydrous methanol) were added. Tubes were capped and mixed slowly using a vortex mixer for 1 min and heated at 100°C for 1 hr. After cooling to room temperature, 5 mL of 6% K_2CO_3 and 4 mL of chloroform were added and again mixed using a vortex mixer for half minute and centrifuged at 2,500 rpm for 10 min. Different layers were formed and the bottom organic layer was removed with pasture pipette and washed with 4 mL of chloroform to completely remove the organic compounds. It was dried under nitrogen and re-suspended in 2 mL of *n*-hexane and 4 mL of KCL (0.88%). Two layers were formed and the upper layer was transferred to a GC vial for gas chromatography analysis (7).

Instrumentation and chromatography.

Chromatographic separation of fatty acid methyl esters was accomplished with a Hewlette-Packard (Wil-mington, DE) model 6890 GC equipped with electronic pneumatics control, a model 7683 automatic liquid sampler, and a flame ionization detector. The sample (2 µL) was introduced by split injection (50:1 ratio) onto a WCOT fused silica, chemically bonded capillary column (Chrompack CP-select CB for FAME, 100 m long, 0.25 mm inside diameter, 0.39 mm outside diameter, 0.25-µm film thickness; Varian Walnut Creek, CA). Helium 3 mL was used as carrier gas. The temperature gradient (70-250°C) consisted of the following steps: 70°C for 1 min; increased to 135°C at 90°C min^{-1}, hold for 1 min; increased to 160°C at 1.5°C min^{-1}; hold for 0.5 min, increased to 185°C at 1°C min^{-1}, hold for 0.5 min, increased to 195°C at 60°C min^{-1}, hold for 5.5 min, increased to 250°C at 90°C/min, hold for 3 min, total run time was 54.7 min. Injector temperature was 280°C; detector temperature was 300°C. Fatty acids were identified according to their retention times using reference standard GLC-63B, Nu-Check- Prep, Elysian, MN) and quantified using a Hewlette-Packard Chem station data system. Fatty acids quantified on dry matter basis were lauric (C12:0), myristic (C14:0), palmitic (C16:0), palmitoleic (C16:1), stearic (C18:0), oleic (C18:1), linoleic (C18:2) and α-linoleic (C18:3). Heptadecanoic acid (C17:0, 0.4 mg/mL in *n*-hexane; Matreya, pleasant Gap, PA) was used as an internal standard.

Table I. *HPLC analysis of phenolics (µg phenolics/g DW) in selected mushrooms (mean±SD).*

Phenolics (µg/g)	*H. erinaceus*	*L. edodes*	*V. volvacea*	*P. ostreatus*	*G. lucidum*
Chlorogenic acid	11.49±0.1	ND	6.63±0.09	ND	4.81±0.09
Ferulic acid	7.84±0.7	1.41±1.9	1.41±1.9	ND	0.91±0.03
p-Coumaric acid	3.18±0.2	ND	ND	ND	ND
Gallic acid	0.77±0.1	ND	0.13±0.1	ND	ND
Caffeic acid	0.75±0.04	0.38±0.01	0.14±0.1	6.51±8.7	0.031±0.01

Table II. *γ-Tocopherol and lutein composition (µg/g DW) of the mushrooms (mean±SD).*

Mushrooms Compounds	*H. erinaceus*	*L. edodes*	*V. volvacea*	*P. ostreatus*	*G. lucidum*
γ-tocopherol	57.99±0.5	39.22±1.1	74.25±3.01	49.21±2.03	29.65±1.2
Lutein	2.42±0.08	1.27±0.04	2.26±0.1	1.50±0.07	1.64±0.05

Table III. *Fatty acid chemical finger print of selected mushrooms (mg/g DW).*

Fatty acids	*H. erinaceus*	*L. edodes*	*V. volvacea*	*P. ostreatus*	*G. lucidum*
16':0	4.229	2.321	3.809	2.671	1.24
18':0	1.193	0.128	0.979	0.413	0.25
18':1n9c	6.075	0.253	2.0103	3.544	1.17
18':2n6c	7.547	7.865	16.013	10.257	1.42
19':00	0.487	0.442	0.482	0.491	0.45
18':3n3	0.196	ND	0.036	0.0202	0.03
Total fatty acids	19.73	11.01	23.33	17.40	4.58
SFA	30.33	27.96	20.77	24.65	48.7
MUFA	28.64	1.53	7.77	18.26	5.85
PUFA	37.31	63.86	62.51	54.06	30.5

Palmitic acids (C16:0), stearic acid (c18:0), linoleic (18':2n6c), oleic (18':1n9c), linolenic (18':3n3) and nonadecanoic acid (C19-0)

ND: Not Detected; C:carbon atoms; SFA: saturated fatty acids; MUFA: mono unsaturated fatty acids; PUFA: poly unsaturated fatty acids

Statisticala analysis

Minitab software was used for computation and analysis of different parameters. Differences were analyzed by considering $p<0.01$ statistically significant. The collected data was analyzed by means and standard deviation.

RESULTS

The results showed that *H. erinaceus* had the highest concentration of phenolic acids. *P. ostreatus* contains the highest amount of caffeic acid 6.51±8.7 µg/g of DW, whereas the other studied mushrooms have low caffeic acid contents (i.e. 0.031-0.75 µg/g of DW). *V. volvacea* and *H. erinaceus* contain chlorogenic acid 6.63 and 11.49 µg/g, respectively. Chlorogenic acid, p-Coumaric acid and Gallic acid were not detected in *L. edodes* and *P. ostreatus* whereas ferulic acid was not found in *P. ostreatus* (Table I).

The analysis showed that *V. volvacea* had the highest contents of γ-tocopherol 74.25 µg/g of DW. The order for γ-tocopherol in selected mushroom species was *V. volvacea* > *H. erinaceus* > *P. ostreatus* > *L. edodes* > *G. lucidum* (Table II).

On the fatty acid analyses identified over 25 different FAs; linoleic acid (18':2n6c), oleic acid (18':1n9c), palmitic acid (C16:0), stearic acid (C18:0), linolenic (18':3n3) and nonadecanoic acid (C19-0) were the main fatty acids found in selected mushrooms. The results for fatty acid composition, total saturated fatty acids (SFAs), monounsaturated fatty acids (MUFAs) and polyunsaturated fatty acids (PUFAs) in selected mushrooms are shown in Table III. Linoleic acid was found in the highest concentration in *V. volvacea* 16.013 mg/g followed by *P. ostreatus* (10.257 mg/g), *L. edodes* (7.547 mg/g) and *H. erinaceus* (7.865 mg/g) on dry weight basis.

DISCUSSION

Our findings are in accordance with the previous study on phenolic composition from different mushrooms (8). Our findings can also be compared with the study of AZ Woldegiorgis et al. (9), who reported two cultivated and five wild mushrooms contained caffeic acid in the highest concentration (7.80 µg/g) in *P. ostreatus*, chlorogenic acid (4.55 µg/g) in *T. letestui* and p-Coumaric acid (15.8 µg/g) in *T. microcarpus*. The specific and characteristic

composition of each mushroom may be associated with the environmental factors of their harvest conditions and their species.

The interest in natural antioxidants is growing for their potential to prevent oxidative stress-induced diseases. Synthetic antioxidants are being questioned because of their carcinogenic activities (10). Carotenoids can be classified in two categories i.e. carotenes (carotene or lycopene) and xanthophylls (lutein and cryptoxanthin). It is concluded that *V. volvacea* and *H. erinaceus* are very good sources of γ-tocopherol and lutein as compared to *L. edodes* and *P. ostreatus*.

The main fatty acids in selected mushrooms were linoleic acid > oleic acid > palmitic acid which are in accordance with previous study (11). Our results are also in agreement with the previous report that many mushroom species have high proportions of unsaturated fatty acids (linoleic acid) in *P. ostreatus* (65.29%), *L. salmonicolor* (59.44%) and in *F. velutipes* (40.87%) (12). As unsaturated fatty acids are essential in human diet, the current finding of a high proportion of unsaturated fatty acids and especially high percentage of linoleic acids in these mushrooms is a significant factor in regarding mushrooms as healthy food.

ACKNOWLEDGEMENTS

The Authors are highly thankful to Higher Education Commission (HEC), Islamabad, Government of Pakistan for providing funding for IRSIP and Nutrition Science Department of Purdue University, USA for conducting all analyses.

REFERENCES

1. Barros L, Baptista P, Correira DM, Casa S, Oliveira B, Ferreira ICFR. Fatty acid and sugar compositions and nutritional value of five wild edible mushrooms from Northeast Portugal. Food Chem 2007; 105(1):140-45.
2. Ren L, Hemar Y, Perera CO, Lewis G, Krissansen GW, Buchanand PK. Antibacterial and antioxidant activities of aqueous extracts of eight edible mushrooms. Bio Act Carb Diet Fiber 2014; 3:41-51.
3. Egwim ECR, Elem C, Egwuche RU. Proximate composition, phytochemical screening and antioxidant activity of ten selected wild edible Nigerian mushrooms. Amer J Food Nut 2011; 1(2):89-94.
4. Unekwu HR, Audu JA, Makun MH, Chidi EE. Phytochemical screening and antioxidant activity of methanolic extract of selected wild edible Nigerian mushrooms. Asian Pac J Trop Dis 2014; 4(1):153-57.
5. Song BJ, Sapper TN, Burtch CE, Brimmer K, Goldschmidt M, Ferruzzi MG. Photo- and thermodegradation of anthocyanins from grape and purple sweet potato in model beverage systems. J Agri Food Chem 2013; 61:1364-72.
6. Barros L, Correia DM, Ferreira ICFR, Baptista P, Santos-Buelga C. Optimization of the determination of tocopherols in *Agaricus sp*. Edible mushrooms by a normal phase liquid chromatographic method. Food Chem 2008; 110: 1046-50.
7. Clapham MW, Foster JG, Neel JPS, Fedders JM. Fatty acid composition of traditional and novel forages. J. Agri. Food Chem 2005; 53:10068-10073.
8. Barros L, Duenas M, Ferreira ICFR, Baptista P, Santos-Buelga C. Phenolic acids determination by HPLC-DAD-ESI/MS in sixteen different Portuguese wild mushrooms species. Food Chem Toxic 2009; 47:1076-79.
9. Woldegiorgis AZ, Abate D, Haki DG, Ziegler GR. Antioxidant property of edible mushrooms collected from Ethiopia. Food Chem 2014; 157:30-36.
10. Barros L, Cruz T, Baptista P, Estevinho LM, Ferreira ICFR. Wild and commercial mushrooms as source of nutrients and nutraceuticals. Food Chem Toxic 2008; 46:2742-47.
11. Wang X. The analysis of the fatty acid compositions in the fruit body and the mixture barley and mycelium of *Pleurotus eryngii*. J Huaiyin Teach Coll (Natural Science Edition) 2004; 3:61-63.
12. Shao S, Hernandez M, Kramer JKG, Rinker DL, Tsao R. Ergosterol profiles, fatty acid composition and antioxidant activities of button mushrooms as affected by tissue part and developmental stage. J Agri Food Chem 2010; 58:11616-25.

LETTER TO THE EDITOR

COMPARISON OF NURSING METHODS OF PEDIATRIC EPILEPSY

L.B. JIA[1], L. TANG[2] and Y. CAI[3]

[1]Department of Neurology, Xuzhou Children's Hospital, Xuzhou, Jiangsu, China; [2]Intensive Care Unit, Xuzhou Children's Hospital, Xuzhou, Jiangsu, China; [3]Department of Nursing, Xuzhou Children's Hospital, Xuzhou, Jiangsu, China

Received August 21, 2017 – Accepted April 24, 2018

We evaluated a modified clinical nursing procedure applied in pediatric epilepsy treatment. A total of 120 sick children were randomly selected and evenly divided into control and observation groups. The control group was treated with a conventional epilepsy nursing protocol, while the observation group was treated with a modified clinical nursing protocol including establishment of a nursing care quality control group, designing a standardized nursing workflow using unified tables, adjusting nursing intensity according to different types of epilepsy, and extension of nursing care post-hospitalization. The clinical effects of the two groups were compared. The cure rate of epilepsy in the observation group was significantly higher than that in the control group (P<0.05). The duration of treatment was shortened and the incidence of complications was reduced in the observation group compared to the control group with statistical significance (P<0.05). The satisfaction for nursing care and treatment compliance were significantly improved in the observation group compared with controls (P<0.05). In conclusion, a relevant clinical nursing method can significantly enhance pediatric epilepsy therapy through improvement of nursing care quality.

To the Editor,

The frequency of occurrence of pediatric epilepsy is different from adult epilepsy (1-2) as children possess relatively undeveloped nervous systems. As such, pediatric epilepsy is easily recurrent, but also easily cured. Pediatric epilepsy is often caused by preterm birth and perinatal asphyxia; its onset time is short and may be accompanied by loss of consciousness. It can cast continuous negative impacts on the nervous system, spirit, cognition, and patient emotions. To date, the mechanism of epilepsy is not well understood and treatment compliance is poor. Therefore, the treatment effects display substantial diversity, especially for pediatric epilepsy as it is closely related to parental supervision. In China, approximately 400,000 new pediatric epilepsy cases occur each year and, following standard treatment, about 70-80% of occurrence could be under control, eventually progressing to cessation of drug treatment within 3 to 5 years (3). A good care model will not only improve the rate controlling epilepsy onset, but also play a significant role in the development of the central nerve system and emotional cognition of the afflicted children (4). The traditional epilepsy nursing model only emphasizes disease intervention, but neglects the importance of environment, psychology, and parental involvement. It only focuses intensive intervention in-hospital and ignores the necessity of education post hospitalization (within the family and community). Finally, the nursing barely

Key words: clinical nursing procedure, pediatric epilepsy, clinical effect

Mailing address:
Dr Ying Cai,
Department of Nursing,
Xuzhou Children's Hospital,
18 Sudibei Road, Xuzhou,
Jiangsu, 221002, China
e-mail: caiying791029@163.com

0393-974X (2018)
Copyright © by BIOLIFE, s.a.s.
This publication and/or article is for individual use only and may not be further reproduced without written permission from the copyright holder.
Unauthorized reproduction may result in financial and other penalties
DISCLOSURE: ALL AUTHORS REPORT NO CONFLICTS OF INTEREST RELEVANT TO THIS ARTICLE.

relays on treatment of drugs without introducing a comprehensive therapy according to the type and severity of the epilepsy present (2, 5). The procedure designed for clinical nursing care in this study was generated based on our clinical practice over several years and standardized as concise tables. In this way, the practical operation to control and cure pediatric epilepsy can be better handled and correctively modified upon receiving the true feedback from sick children and their parents as well as medical care staff. This study aimed to evaluate a modified procedure of clinical nursing care accompanied with pediatric epilepsy treatment.

A total of 120 children diagnosed with epilepsy for the first time at the Xuzhou Children's Hospital were selected between January 2012 and January 2016. Subjects possessing brain developmental abnormalities, dementia, and/or genetic metabolic diseases were excluded. Patients were confirmed after portable EEG monitoring for 24 h and were evenly divided into control and observation groups by a computerized randomized method. The control group consisted of 32 males (M) and 28 females (F) aged from 3 to 12 years old (average: 6.6±2.4), of whom 33 were cases of partial epileptic seizures and 27 of generalized epileptic seizures. The observation group was composed of 35 M and 25 F with an age range of 2.5-13 years old (average: 6.5±2.7), of whom 31 were cases of partial epileptic seizures and 29 of generalized epileptic seizures. The baseline data were comparable between two groups. The study was approved by the Ethics Committee of Xuzhou Children's Hospital. Written informed consent was obtained from the legal guardians of the children.

According to the recommendations of epilepsy guidelines, all subjects in both groups received various drugs and associated treatment based on epilepsy type, seizure frequency, and duration and severity of accompanying clinical symptoms. Medication included sodium valproate, phenobarbital, and carbamazepine as antiepileptic drugs, and diazepam as sedative drug. In addition, nerve factor implantation, hyperbaric oxygen, and surgical treatments were also adopted.

The control group was treated with the conventional procedure for epilepsy nursing care and the observation group was treated with our modified method for clinical nursing care. The nursing process in the control group included monitoring of vital signs, making emergency preparations for epileptic seizures, imparting correct knowledge of epilepsy prevention and first aid to children and parents, giving diet and psychological guidance, conducting medication supervision, and providing support for various treatments. Moreover, the nursing process in the observation group followed four steps: establishing the strict standards of quality-control for nursing care, designing and standardizing the nursing care procedure and summarizing as concise tables, adjusting nursing intensity according to epilepsy type, and extending nursing care post-hospitalization. In order to set up quality-control standard, four people were employed as head nurses from the department of nursing management or nurse supervisors from the department of neurology responsible for quality improvement, operation assessment, and staff training. To standardize the procedure for epilepsy nursing workflow, all possible operating steps were collected and summarized as an effective and unified process into a concise table after experts' demonstration, repeatedly practiced by nurses, and feedback received. Each operating

Table I. *Comparison of control rate and cure rate of epilepsy [Cases (%)].*

Group	Cases	Control rate	Cure rate
Control	60	43 (71.7)	23 (38.3)
Observation	60	52 (86.7)	35 (58.3)
χ^2		4.093	4.805
P		0.043	0.028

step was confirmed by the responsible nurse upon his or her authorized signature. The procedure was formed mainly based on epilepsy types. Partial seizures, main symptom of epilepsy, included simple partial seizures, complex partial seizures, and partial seizures secondary to generalized seizures, whereas generalized seizures were composed of tonic-clonic seizures, myoclonic seizures, atonic seizures, and absence seizures.

The similarities between the control and observation groups were environment and regulations, education on health and disease, diet, medical and psychological guidance, and follow-up observation, while the differences were treatment program and supporting nursing operations. The ward was maintained quiet with fresh air, with 2-3 patients suffering from the same type of epilepsy per room. Bedside guardrails were used to prevent falling from bed; vital signs and mood changes were monitored every other hour. Health education was taught to the children and their parents, in which the causes and types of seizures, treatments, precautions, and preventive measures were vividly expounded through videos, pictures, and other media. Knowledge regarding epilepsy in children and their parents was investigated aiming at enhancement of education in order to improve prevention and control of seizures. The diets for patients were mainly kept light and easily digested and daily urination and defecation was recorded. Adequate sleep, relaxation, normal work and study were ensured..

Guidance regarding medication was the top priority. A small dose of drug was administered to the patient for initial treatment with a gradual increase in dosage. The patients and their parents were also instructed to closely observe if any adverse reaction of drug occurred and to never miss a dose or overdose. During acute epileptic seizures, patients were instructed to calm down, keep the respiratory tract unobstructed, and avoid fall or bite injury. During intermission periods, it was suggested to intensively evaluate neurological, mental, and cognitive function of patients in order to reduce adverse effects on growth and intelligence development.

For partial seizures, the doctors focused on finding the possible triggers. Most of the cases with partial seizures exhibited no significant disturbance of consciousness and their neurological and cognitive impairments were relatively less. Triggers may include incorrect nutrition, mood disorders, and lack of sleep therefore carefully observation of lifestyle care may effectively reduce the frequency of epileptic seizures. For generalized seizures,

Table II. *Comparison of course of treatment and complications.*

Group	Cases	Treatment course (months)	Cerebral injury	Growth and intelligence development disorders	Disability	Lethal	Complication occurrence rate (%)
Control	60	6.5±1.7	3	2	5	3	13 (21.7)
Observation	60	4.7±1.2	1	2	1	1	5 (8.3)
t/χ^2		4.628					4.183
P		0.027					0.041

doctors should focus on nursing management during acute seizures. The patients require an intensive care management by building up confidence, strengthening preventive measures, incorporating a variety of treatment methods, and paying close attention to follow-up visits. For patients with continuous or refractory epileptic seizures, experts should be actively and closely looking for potential organic lesions, at which point the operations can be conducted to remove or repair the lesions. Scientific and reasonable perioperative nursing management is important for successful operations. Nerve factor implantation has been proven safe and effective. Through a minimally invasive 2 mm incision, a JY-24 computer stereotactic positioning detector can conduct an in-depth exploration for lesion locations presenting abnormal brain neural activities, and can precisely and effectively implant nerve factors. The principles of operation, preparation, the main operating processes, postoperative possible complications, and treatment methods should be expounded in detail so as to improve treatment compliance of the patients and their family members.

After 12-month follow-up visits, difference in epilepsy control and cure rates, course of treatment and complications, and nursing satisfaction and patient compliance were compared between the two groups. In accordance with records of epileptic seizures in sick children, if attack frequency was reduced by ≥50% and the duration of epilepsy shortened, the epilepsy was deemed to be under control. If the attack frequency was reduced by ≥90% and the duration of epilepsy shortened by ≥80%, the epilepsy was deemed to be cured. Nursing satisfaction was investigated in the form of questionnaires and completed by patients and their parents. Opinions on 25 items, including epilepsy control condition, nursing attitude, nursing level, problem solving condition during hospitalization, and follow-up attention were scored on a scale from Grade 0 to Grade 4. A total score was compiled from the individual component scores, with higher scores indicating higher care satisfaction. Patient compliance was investigated using a life experience survey, which examined extent of knowledge on epilepsy, medication regularity, lifestyle management, and follow-up visit inspection. Again, 25 items were examined and ranked from Grade 0 to 4, with higher scores indicating higher compliance. Individual component scores were summed to generate a total score.

SPSS 20.0 software (Chicago, IL, USA) was used for statistical analysis. Measurable data were presented as mean ± standard deviation and comparisons between the two groups were checked with independent samples *t*-test; count data was presented as the number or percentage of cases and comparisons between groups were tested using χ^2. The difference was statistically significant if $P < 0.05$.

The control and cure rates of epilepsy in the observation group were significantly higher than those of control group ($P < 0.05$, Table I). In the observation group, the duration of treatment was shortened and the incidence of complication was

Table III. *Comparison of nursing satisfaction degree and compliance (Score).*

Group	Satisfaction degree	Compliance
Control group	72.3±13.5	68.5±11.4
Observation group	85.6±12.7	79.8±12.2
t	5.324	5.569
P	0.013	0.010

decreased with statistical significance ($p < 0.05$, Table II). The nursing satisfaction and patient compliance were significantly increased in the observation group ($p < 0.05$, Table III).

Optimized clinical nursing procedures are extremely important for treatment and nursing of many diseases. Manifestations of children with epilepsy could exhibit in multiple forms, for which many treatments exist. For an effective treatment, participation of both patients and their parents is essentially required. These facts increase difficulty in managing this disease. Most sick children cannot express themselves clearly, so there is a need for nursing staff with professional knowledge and experience to conduct a comprehensive judgment (6). Nursing procedures based on evidence-oriented medicine can formulate tables with treatment guidance depending on epilepsy type and onset characteristics. After continuous learning and assessment, the mastery of operating processes is of significant meaning for the improvement of nursing quality and satisfaction (7).

Our data indicate the clinical outcomes were significantly improved upon applying an optimized nursing care procedure. An epileptic control effect was the center of clinical treatment and nursing work. The predominant nursing methods enabled sick children and parents to be familiar with the entire nursing process, and put forward more reasonable and targeted nursing requirements in light of actual individual needs (8). For pediatric epilepsy, there is a need to attach an importance to the assessment of growth and mental development, establish the correct treatment of disease concepts, and adapt to normal life and learning (9). Comprehensive treatment and vital signs management should be guaranteed for sick children with generalized seizures (10). Compliance is another important factor affecting treatment effect, so emphasizing seamless integration of in-hospital and out-of-hospital nursing is practical for improving compliance (11). Accepting and treating diseases with the correct attitude, as well as an increased emphasis on social support, play important roles in the treatment and prevention of epilepsy (12).

In summary, optimized clinical nursing methods can significantly improve pediatric epilepsy treatment as well as the quality of nursing. Constantly improving clinical nursing methods are an important aspect for managing pediatric epilepsy.

REFERENCES

1. Chong L, Jamieson NJ, Gill D, et al. Children's experiences of epilepsy: a systematic review of qualitative studies. Pediatrics 2016; 138(3).
2. Cross JH. Epilepsy in the WHO European region: fostering epilepsy care in Europe. Epilepsia 2011; 52(7):187-88.
3. Vaewpanich J, Reuter-Rice K. Continuous electroencephalography in pediatric traumatic brain injury: seizure characteristics and outcomes. Epilepsy Behav 2016; 62(8):225-30.
4. Dayapoğlu N, Tan M. Clinical nurses' knowledge and attitudes toward patients with epilepsy. Epilepsy Behav 2016; 61(8):206-9.
5. Helde G, Bowim G, Brathen G, Brodtkorb E. A structured, nurse-led intervention program improves quality of life in patients with epilepsy: a randomized, controlled trial. Epilepsy Behav 2005; 7(7):451-57.
6. Chomba EN, Haworth A, Atadzhanov M, Mbewe E, Birbeck LG. Zambian health care workers' knowledge, attitudes, beliefs, and practices regarding epilepsy. Epilepsy Behav 2007; 10(5):111-19.
7. Atadzhanov M, Chomba E, Haworth A, Mwewe E, Birbeck G. Knowledge, attitudes, behaviors and practices (KABP) regarding epilepsy among Zambian clerics. Epilepsy Behav 2006; 9(5):83-88.
8. Kinnunen UM, Kivekäs E, Paananen P, Kälviäinen R, Saranto K. Testing of triggers by data mining of epilepsy patients' structured nursing records. Stud Health Technol Inform 2016; 225(5):461-65.
9. Kivekäs E, Kinnunen UM, Paananen P, Kälviäinen R, Haatainen K, Saranto K. Functionality of triggers for epilepsy patients assessed by text and data mining of medical and nursing records. Stud Health Technol Inform 2016; 225(4):128-32.
10. Davidson GT, Eaton M, Paul SP. Childhood epilepsy: a clinical update. Community Pract 2016; 89(4):25-29.
11. DeVries-Rizzo M, Canadian Epilepsy Nursing Group. A description of Canadian epilepsy monitoring units: an initial step toward developing

nursing practice consensus guidelines. Epilepsy Behav 2016; 57(Pt A):145-50.
12. Akbarbegloo M, Valizadeh L, Zamanzadeh V, Jabarzadeh F. The relationship between self-efficacy and psychosocial care in adolescents with epilepsy. Epilepsy Res Treat 2015; 2015:756849.

JOURNAL OF BIOLOGICAL REGULATORS & HOMEOSTATIC AGENTS Vol. 32, no. 4, 875-879 (2018)

LETTER TO THE EDITOR

EFFECT OF RADIAL SHOCK WAVE THERAPY ON LONG BONE FRACTURE REPAIR

T. SCHNURRER-LUKE-VRBANIĆ[1], V. AVANCINI-DOBROVIĆ[1], I. SOSA[2], O. CVIJANOVIC[3] and D. BOBINAC[3]

[1]University Hospital Centre Rijeka, Department of Physical and Rehabilitation Medicine, Rijeka, Croatia; [2]University of Rijeka, Medical Faculty, Department of Forensic Medicine and Criminalistics, Rijeka, Croatia; [3]University of Rijeka, Medical Faculty, Department of Anatomy, Rijeka, Croatia

Received February 1, 2018 – Accepted May 9, 2018

Nowadays, various diseases of the locomotor system are treated by extracorporeal shock wave therapy (ESWT) for instance: acute fracture and pseudoarthrosis, nonunion, chronic tendinitis. Unfocused (radial) pressure wave therapy (RPWT) primarily affects superficial tissues, so justifiability of its medicinal employment is uncertain. We aimed to observe time sequence of the long bone fracture healing using RPWT. Forty-eight female Wistar rats were divided into an RPWT group (n=36) and a control group (n=12). The RPWT group had the largest cross-sectional area (CSA) of the bone trabeculae compared to controls. Post-hoc analyses revealed the largest cross-sectional area (CSA) of the bone trabeculae (1.7 mm^2) and the smallest CSA of the cartilage (0.04 mm^2) of the RPWT group on the 22nd day. Conclusively, long bone fracture repair is enhanced by RPWT, suggesting that it strongly stimulates the processes of callus ossification.

To the Editor,

Bone, exposed to a biophysical stimulation delivered by different instruments, exhibits improved repair during fracture healing (1). Extracorporeal shock wave stimulation (ECSW) causes bone microfractures and neovascularization, which can be demonstrated by osteoblast and fibroblast activity (2, 3). Therefore it is used in the treatment of various diseases of the locomotor system, for instance, acute fracture, pseudoarthrosis, nonunion or chronic tendinitis (4, 5). As in any wound, the bone in fracture repair, is healed – regenerated in order to sustain mechanical loads. Inflammation, chemotaxis, proliferation, and differentiation are events in fracture repair that culminate in conversion to a mechanical construction able to sustain loads (1). Among these events, the most pivotal is probably the penetration of capillaries in the callus, which afterwards blends to the calcified cartilage (3). Furthermore, ECSW promotes the production of growth factors by stimulating proliferation of the bone marrow cells. Moreover, blood flow delivers osteoblasts, and they produce bone morphogenetic proteins (BMPs) further stimulating activity of osteoblasts (6). Basically, fracture repair is a unique form of wound healing in which bone is regenerated to accept mechanical loads. During fracture repair, a series of events which begin with inflammation, chemotaxis, proliferation,

Key words: extracorporeal shock wave therapy, cross-sectional area, bone morphogenetic proteins

Mailing address:
Dr. sc. Ivan Sosa, PhD, MD
University of Rijeka, Medical Faculty,
Department of Forensic Medicine and Criminalistics,
Brace Branchetta 20, Rijeka, Croatia
Tel/GSM: 00385916996969
e-mail: ivan.sosa@medri.uniri.hr

0393-974X (2018)
Copyright © by BIOLIFE, s.a.s.
This publication and/or article is for individual use only and may not be further reproduced without written permission from the copyright holder.
Unauthorized reproduction may result in financial and other penalties
DISCLOSURE: ALL AUTHORS REPORT NO CONFLICTS OF INTEREST RELEVANT TO THIS ARTICLE.

and differentiation, culminates in a stage where the healing tissue is converted to a mechanically competent structure.

Using immunohistochemistry and other methods such as Western blot or reverse transcription polymerase chain reaction, studies have investigated differences in expression of the specific factors: angiogenic, oxidative and osteogenic. On the other hand, as in other studies, histomorphometry, micro-CT, callus measurement, densitometry and biomechanical tests, assessments were performed to compare ESWT group and controls. Recent studies have employed a more comprehensive approach, but whichever research method was applied, the conclusion was that ESWT enhances acute bone fracture healing (1, 3, 7).

Bearing in mind its mainly superficial effect, it is logical that only a few types of research were conducted to observe the effect RPWT in the experimental model of long bone fracture repair. Thus, we conducted a temporal sequence monitoring of the callus ossification during bone fracture repair induced by ESWT and compared it to spontaneous bone fracture repair.

MATERIALS AND METHODS

Experimental model

Forty-eight three-month-old female Wistar rats with an average weight of 250 g were used in this study.

Rats were administered 3.6% chloral hydrate, and the fibula was approached from the lateral side. The body (1 mm in diameter) of the fibula was fractured by scissors. Bone fragments were not fixed after fracture, so the healing was not additionally stimulated.

For shock wave therapy we used a SWISS DUOCLAST (EMS- Electro Medical systems) device and its DOLORCLAST applicator for radial shock waves. The treated area was 3 cm in diameter.

Animals were divided into experimental and control groups. The experimental group consisted of 36 animals, divided into 3 subgroups of 12 animals each treated with radial shock waves with three different pressures: 1.6; 2.2; 3.0 bar, 500 shocks per application, of 5 Hz. An applicator 15 mm in diameter was used. Shock waves were applied the 3rd, the 8th and the 13th day from surgery. Six animals from each subgroup were sacrificed on the 15th day and the remaining animals on the 22nd day. The control group consisted of 12 animals, which were

Table I. *Means and 95% confidence intervals as function of the cross-sectional area.*

CSA (mm^2)	Control 15th day	Control 22nd day	RPWT 15th day	RPSWT 22nd day	p value
Cartilage	0.58±0.23	0.31±0.1	0.45±0.12	0.04±0.02	P < 0.001
Mineralized cartilage	0.52±0.12	0.33±0.15	0.3±0.11	0.08±0.01	P < 0.001
Bone trabeculae in cartilage	0.57±0.22	0.52±0.11	0.38±0.13	0.36±0.12	P < 0.001
Bone trabeculae	0.63±0.17	0.96±0.21	1.39±0.21	1.7±0.24	P < 0.001
Callus	2.31±0.18	1.63±0.14	2.62±0.22	2.17±0.3	P < 0.001

RPWT - unfocused pressure wave therapy

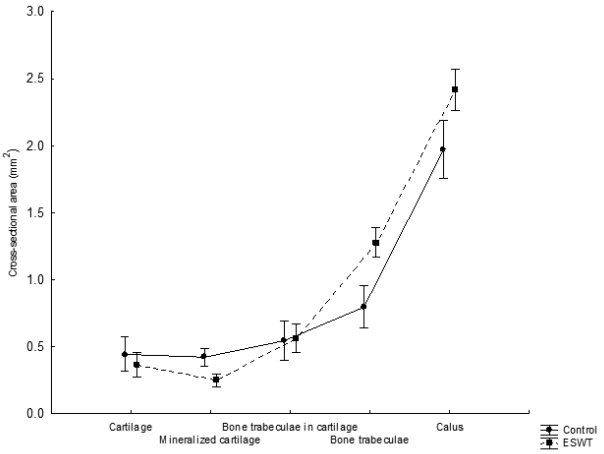

Fig. 1. *Means as function of the ESWT and control.*

subjected to a fracture of the fibula but were not treated with shock waves. Six animals were sacrificed on the 15th day, and the remaining six on the 22nd day.

Methods

After sacrificing the animals, the segment of the body of the fibula on the fracture point was approached.

The bone fragment was decalcinated in Osteodek for 5 days (Biooptika). Tissue samples were fixed in 4% paraformaldehyde and embedded in paraffin. All samples were cut to 5 mm serial cuts a stained by Toluidinee blue. The five visual fields of the bone fracture healing samples were examined by an Olympus microscope (Olympus, Tokyo, Japan) and photographed at a magnification of 100x using a Sony video camera (SONY SSC-DC58AP, Japan) connected to a personal computer.

The photographic images were analyzed using an image analysis system that employed ISSA v.2.5. Software (V.A.M.S., Zagreb, Croatia). The cross-sectional area (CSA) of the cartilage, mineralized cartilage, bone trabeculae in cartilage, bone trabeculae and callus were measured and expressed in mm^2 (8).

Cross-sectional areas (CSA) were analyzed at time intervals and expressed as follows: (i) control group on the 15th day; (ii) control group on the 22nd day; (iii) RPWT group on the 15th day; (iv) RPWT group on the 22nd day (Figs. 1 and 2).

Statistical analyses

Statistica 8.1 (StatSoft) computer software (StatSoft Inc., Tulsa, USA) was used for statistical analyses. For each of the above-given parameters, differences between the controls and ESWT group, as well as differences between the fESWT and UDWT methods were explored on the 15th and 22nd day, respectively. The Fisher Highly Significant Difference test was used post hoc to identify specific differences between the groups.

Ethical disclosure

All procedures followed were according to the ethical standards of the institutional and national responsible committee and with the Helsinki declaration of 1975, as revised in 2000.

RESULTS

No differences between different pressures of 1.6, 2.2, and 3.0 bars applied by UDWT were observed during the experiment.

Cross-sectional area variations on 15th and 22nd days of the bone fracture healing

Results showed that the CSA measured for the cartilage, mineralized cartilage, bone trabeculae in cartilage, bone trabeculae, and callus, had significant differences ($F_{(4,\ 144)} = 176$; $P<0.001$) (Fig. 1).

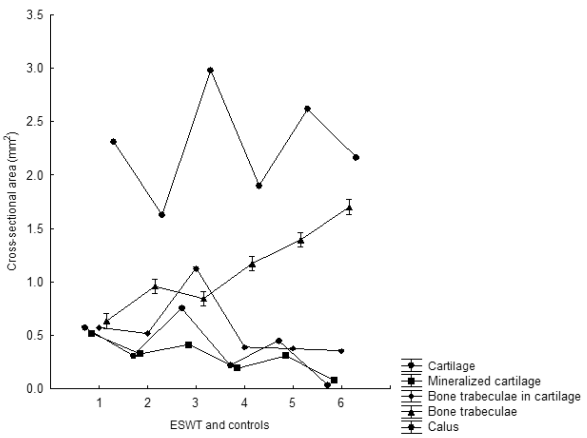

Fig. 2. *Means as function of the cartilage, mineralized cartilage, bone trabeculae in cartilage, bone trabeculae and callus.*

Variations were observed on the 15th and 22nd day between the RPWT group and the control group ($F_{(5, 35)} = 579.51$; $P < 0.001$).

The general trend showed that CSA of the callus was the largest on the 15th day in the fESWT group, while the smallest was the CSA of the cartilage on the 22nd day of the UDWT group.

The smallest cross-sectional area of the cartilage (CSA = 0.04 mm^2), and the the smallest CSA of the callus (CSA = 2.17 mm^2) were found on the 22nd day of the UDWT group, which significantly differed to those of the 15th day, fESWT groups and controls, ($P<0.001$), respectively (Table I). The largest CSA of the mineralized cartilage was observed in the control group on the 15th day (CSA = 0.52 mm^2), which significantly differed to the 22nd day, fESWT groups and UDWT groups, ($P<0.001$), respectively (Table I). The highest value for the bone trabeculae in cartilage was measured on the 15th day of the fESWT group (CSA = 1.13 mm^2), which significantly differed to the 22nd day, controls, and UDWT groups, ($P<0.001$), respectively (Table I). The highest value of the bone trabeculae was measured on the 22nd day of the UDWT group (CSA = 1.7 mm^2), which significantly differed to the 15th day, fESWT groups and controls, ($P<0.001$), respectively (Table I).

DISCUSSION

The larger cross-sectional area of the bone trabeculae in the ESWT group, compared to controls (Fig. 1), suggests that long bone fracture repair was enhanced in the ESWT group (1, 3, 8). According to our findings, UDWT resulted with the smallest CSA of the cartilage on the 22nd day, and the largest CSA of the bone trabeculae on the 15th and 22nd days, which suggests that this method was the most efficient during long bone fracture repair in mice.

Mechanical signals such as pressure or shear stress affect osteocytes and interstitial fluid flow in lacunar-canalicular meshwork. Thus, when transmitted on other, adjacent structures (for instance osteocytes, osteoblasts and osteoclasts) those signals penetrate more deeply, causing microfractures in cortical and trabecular compartments, simply put - regulate bone remodeling (1, 3).

UDWT was applied in the experimental model of long bone fracture repair. In the RPWT group, the

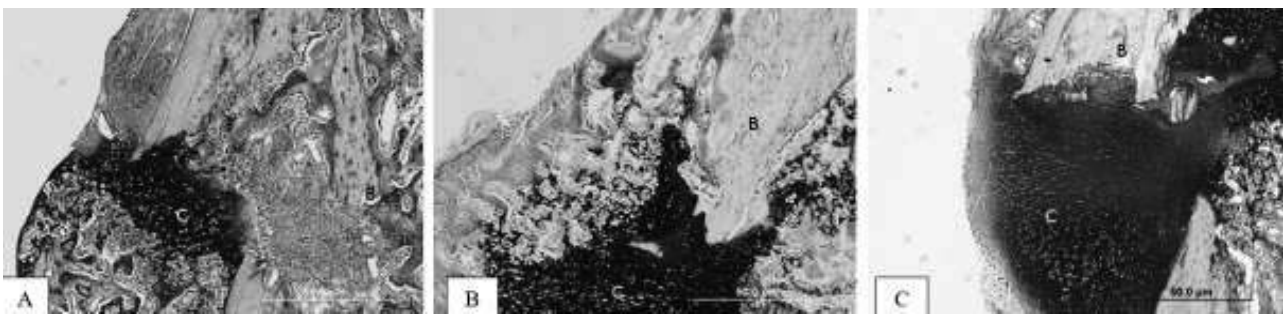

Fig. 3. *Histological findings on 15th day. **A)** fESWT; **B)** UDWT; **C)** Control. C: cartilage; B: bone. Toluidine blue x 100*

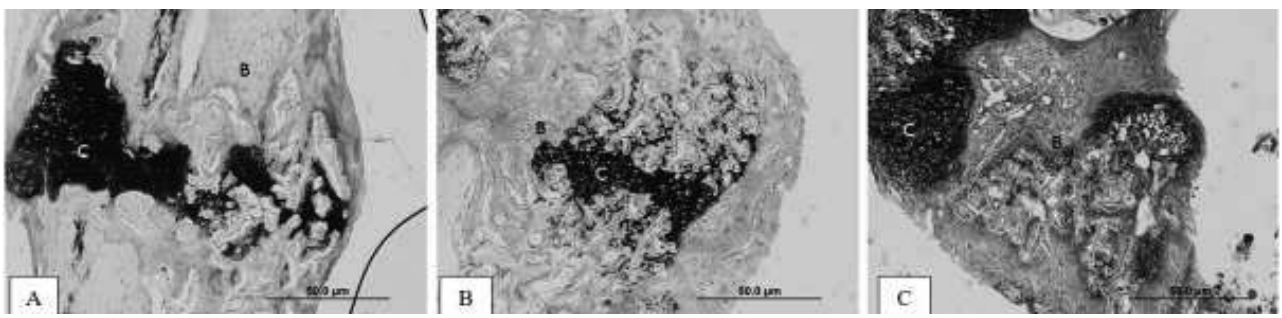

Fig. 4. *Histological findings on 22nd day. **A)** fESWT; **B)** UDWT; **C)** Control. C: cartilage; B: bone. Toluidine blue x 100.*

largest CSA of the bone trabeculae was measured on the 15th day (CSA = 1.39 mm^2) (Fig. 3A-C), and 22nd day (CSA = 1.7 mm^2) (Fig. 4A-C), while the smallest CSA of the cartilage was measured on the 22nd day (CSA = 0.04 mm^2) (Fig. 4B).Our results suggest that UDWT enhances bone tissue formation spatially and temporally, leading to complete bone fracture healing (9). One could say that UDWT indirectly acce e rat fibula. During the experimental procedure, animals treated by UDWT were badly injured, and the surrounding superficial tissue was bleeding. This significantly limits the applicability of this method in experimental animals.

UDWT can improve vascularisation and hyperemia in the superficial tissues; however, in osteoporosis and old bone, microfractures accumulate in the cortical and trabecular compartment, therefore, sites of minor bone quality prone to fracturing should be preferentially treated by UDWT (1, 3, 7).

REFERENCES

1. Padilla F, Puts R, Vico L, Guignandon A, Raum K. Stimulation of bone repair with ultrasound. Adv Exp Med Biol 2016; 880:385-427.
2. d'Agostino MC, Craig K, Tibalt E, Respizzi S. Shock wave as biological therapeutic tool: From mechanical stimulation to recovery and healing, through mechanotransduction. Int J Surg 2015; 24:147-53.
3. Izadifar Z, Babyn P, Chapman D. Mechanical and biological effects of ultrasound: a review of present knowledge. Ultrasound Med Biol 2017; 43(6):1085-104.
4. MC DA, Frairia R, Romeo P, et al. Extracorporeal shockwaves as regenerative therapy in orthopedic traumatology: a narrative review from basic research to clinical practice. J Biol Regul Homeost Agents 2016; 30:323-32.
5. Romeo P, Lavanga V, Pagani D, Sansone V. Extracorporeal shock wave therapy in musculoskeletal disorders: a review. Med Princ Pract 2014; 23:7-13.
6. Glass GE, Jain A. Cochrane corner: bone morphogenetic protein (BMP) for fracture healing in adults. J Hand Surg Eur Vol 2013; 38:447-9.
7. Rinella L, Marano F, Paletto L, et al. Extracorporeal shock waves trigger tenogenic differentiation of human adipose-derived stem cells. Connect Tissue Res 2018; 1-13.
8. Wu YT, Ke MJ, Chou YC, et al. Effect of radial shock wave therapy for carpal tunnel syndrome: A prospective randomized, double-blind, placebo-controlled trial. J Orthop Res 2016; 34:977-84.
9. Gerdesmeyer L, Schaden W, Besch L, et al. Osteogenetic effect of extracorporeal shock waves in human. Int J Surg 2015; 24:115-9.

LETTER TO THE EDITOR

ASSOCIATION BETWEEN Ca/Mg/P STATUS AND SUPPURATIVE TONSILLITIS IN CHILDREN

S. MAO, F. LIU, X-P. WANG, L-X. WU and J-H. ZHANG

Department of Pediatrics, Shanghai Jiao Tong University Affiliated Sixth People's Hospital, Shanghai, China

Received October 9, 2017 – Accepted May 2, 2018

Suppurative tonsillitis (ST) is a common respiratory disease in children. This study aims to investigate the association between calcium (Ca)/magnesium (Mg)/phosphorus (P) and the risk of onset of suppuration in tonsillitis in children. Seventy children with ST and 61 age- and sex-matched children with non-ST were enrolled in this study. The association between Ca/Mg/P and suppuration risk in tonsillitis was investigated. The relationship between Ca/Mg/P and the potential risk factors for ST were also studied. White blood cell (WBC), platelet (PLT), c-reactive protein (CRP) and erythrocyte sedimentation rate (ESR) levels were significantly higher in the ST group than those in the non-ST group ($p<0.05$). Mg and P levels were significantly lower in the ST group than those in the non-ST group ($p<0.05$). There was no obvious difference in Ca level between the ST group and the non-ST group ($p=0.762$). A significantly negative association between P and PCT was noted ($r=-0.236$, $p=0.035$). The results indicated that Mg/P disorder may be associated with the susceptibility to suppuration in children with tonsillitis, inflammatory indexes may reflect this risk.

To the Editor,

Tonsillitis, a common respiratory disease in children, is likely to occur in cases with low immunity (1). Suppuration often occurs in severe tonsillitis cases, which may aggravate the prognosis and result in lower respiratory infection. However, some subjects with suppurative tonsillitis (ST) rarely seek doctoral consultation due to the atypical symptoms, particularly for younger children. Sometimes suppurative cases do not show fever or typical sore throat (2). On the other hand, severe ST cases may complicate with peritonsillar abscess, which may lead to the spread of infection (3). Of note, recurrent tonsillitis may lead to kidney injury, such as IgA nephropathy (4). Hence, early diagnosis and treatment are imperative for ST to prevent the onset of suppuration during the course of tonsillitis is of significant importance.

Many tonsillitis patients are likely to present with suppuration at the onset of the disease. By contrast, some tonsillitis patients are likely to present without suppuration Notably, many ST cases present without typical symptoms. It is hypothesized that certain factors may affect the formation of suppuration. Because of the harm which may be caused by suppuration, it is imperative to identify the risk factors or indicators for its onset in tonsillitis patients.

Previous studies showed that an age >35 years and serum C-reactive protein (CRP)>15.5mg/dl were associated with higher risk of abscess during tonsillitis (3). Group A streptococcus carrier state

Key words: suppurative tonsillitis, risk factors, children, Ca, Mg, P

Mailing address:
Dr Liangxia Wu,
Department of Pediatrics,
Shanghai Jiao Tong University,
Affiliated Sixth People's Hospital,
600 Yishan road, Shanghai, China
e-mail: wlxmed@sina.com

0393-974X (2018)
Copyright © by BIOLIFE, s.a.s.
This publication and/or article is for individual use only and may not be further reproduced without written permission from the copyright holder.
Unauthorized reproduction may result in financial and other penalties
DISCLOSURE: ALL AUTHORS REPORT NO CONFLICTS OF INTEREST RELEVANT TO THIS ARTICLE.

(5) was not associated with recurrent tonsillitis. Another study (6) showed that the serum levels of selenium and zinc were significantly lower in chronic tonsillitis compared to healthy controls. However, specific investigation regarding the risk factors for suppuration in early stage tonsillitis remains rare, and whether the common elements, such as Ca, Mg and P are associated with the risk factors of suppuration after tonsillitis remains elusive.

To have an in-depth understanding of the role of Ca/Mg/P for the susceptibility to ST, we compared laboratory findings between tonsillitis with and without suppuration, and also investigated the association between Ca/Mg/P and the potential risk factors for the onset of suppuration after tonsillitis in children.

MATERIALS AND METHODS

Patient population

The study population was chosen from children diagnosed with tonsillitis in the pediatric department of Shanghai Sixth People's Hospital from April 2014 to April 2016. ST was diagnosed when tonsillitis was complicated with suppuration. The patients were excluded if they were with other systemic diseases or lower respiratory diseases. The guardians of all the enrolled subjects gave informed written consent.

Data collection

The clinical and laboratory findings of the patients were studied at the initial diagnosis. Demographic and clinical data were reviewed respectively for age, gender, birth weight, white blood cell (WBC), platelet (PLT), c-reactive protein (CRP), hemoglobulin (Hb), mycoplasma (MP), albumin (ALB), alanine aminotransferase (ALT), calcium (Ca), phosphorus (P), magnesium (Mg), procalcitonin (PCT), and erythrocyte sedimentation rate (ESR).

Statistical analysis

Categorical variables were expressed as cases/total, OR (odds ratio) was used to compare the differences of categorical variables between tonsillitis with and without suppuration. Continuous variables were expressed as means±standard deviation (SD),

The analyses were performed using SPSS software.

Table I. *Baseline characteristics of tonsillitis with and without suppuration*

	Tonsillitis with suppration（70）	Tonsillitis without suppration (61)	P
Age (years)	**5.11±2.67**	**4.98±2.90**	**0.789**
Male/female ratio	**39/31**	**36/25**	**0.843**
Birthweight (Kg)	**3.25±0.83**	**3.29±0.64**	**0.691**
WBC ($X10^9$/L)	**7.89±3.19**	**6.65±3.07**	**0.030**
PLT($X10^9$/L)	**232.09±81.12**	**205.71±55.28**	**0.036**
CRP	**26.50±28.48**	**13.79±15.86**	**0.006**
Hb (g/L)	**129.78±10.67**	**129.47±10.57**	**0.875**
MP (n)	**23**	**16**	**0.544**
ALB (g/L)	**43.96±3.03**	**44.62±2.59**	**0.296**
ALT	**11.40±5.42**	**12.67±4.64**	**0.261**
Ca	**2.36±0.10**	**2.35±0.13**	**0.762**
P	**0.92±0.07**	**0.95±0.08**	**0.009**
Mg	**1.32±0.10**	**1.50±0.34**	**0.048**
PCT	**0.54±0.60**	**0.34±0.37**	**0.085**
ESR	**31.85±20.78**	**16.27±16.10**	**$<10^{-4}$**

WBC: white blood cell; PLT: platelet; CRP: c-reactive protein; Hb: hemoglobulin; MP: mycoplasm; ALB: albumin; ALT: Alanine aminotransferase; Ca: calcium; P: phosphorus; Mg: magnesium; PCT: procalcitonin; ESR: erythrocyte sedimentation rate.

Table II. *Association between P/Mg and WBC/CRP/PCT/ESR in tonsillitis children.*

Index	Index	R	P
P	WBC	-0.173	0.124
P	CRP	-0.175	0.173
P	PCT	-0.236	0.035
P	ESR	-0.213	0.061
P	PLT	0.026	0.819
Mg	WBC	-0.113	0.318
Mg	CRP	-0.054	0.678
Mg	PCT	-0.070	0.539
Mg	ESR	-0.131	0.253
Mg	PLT	0.059	0.595

WBC: white blood cell, PLT: platelet, CRP: c-reactive protein, Ca:calcium, P: phosphorus, Mg: magnesium, PCT: procalcitonin, ESR: erythrocyte sedimentation rate.

The independent sample *t*-test was used to compare the differences of various indexes between tonsillitis with and without suppuration. The Pearson correlation coefficients were used to analyse the relationship between Ca/Mg/P and potential risk factors for the onset of suppuration after tonsillitis.

RESULTS

Tonsillitis cases with and without suppuration

A total of 131 tonsillitis (70 with suppuration, 61 without suppuration) cases were enrolled in the study. The mean age was 5.11±2.67 and 4.98±2.90 years for tonsillitis with and without suppuration, respectively. No marked differences of age, male/female ratio, birth weight, Hb, MP, ALB, ALT, Ca, and PCT were observed between tonsillitis with and without suppuration (Table I). Patients with ST had markedly higher levels of WBC, PLT, CRP, and ESR compared those without suppuration (Table I). Patients with ST had markedly lower levels of Mg and P than those without suppuration (Table I).

Association between Mg/P and WBC/CRP/PCT/ESR inchildren with tonsillitis

Mg was not significantly associated with WBC (r=-0.113, p=0.318, Table II), CRP (r=-0.054, p=0.678, Table II), PCT (r=-0.070, p=0.539, Table II), ESR (r=-0.131, p=0.253, Table II) and PLT (r=0.059, p=0.595, Table II). P was negatively associated with PCT markedly (r=-0.236, p=0.035, Table II, Fig. 1). P was insignificantly associated with ESR (r=-0.213, p=0.061, Table II, Fig. 2). P was not obviously associated with WBC (r=-0.173, p=0.124, Table II), CRP (r=-0.175, p=0.173, Table II) and PLT (r=0.026, p=0.819, Table II).

DISCUSSION

The findings indicated that the disorder of Mg/P and inflammation may be involved in the suppuration onset in tonsillitis cases. Ca performs several functions, such as intracellular signal transduction (7). Ca status is also closely associated with the levels of certain trace elements, such as lead and iron (8). Vitamin D, which promotes the absorption of Ca, can not lower the risk of respiratory diseases (9). Mg regulates glucose and insulin action, and plays a role in the development of diabetes (10). Mg

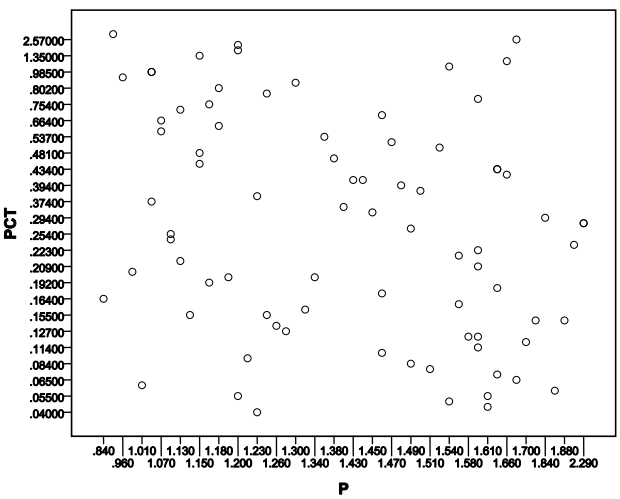

Fig. 1. *Association between P and PCT in tonsillitis children.*

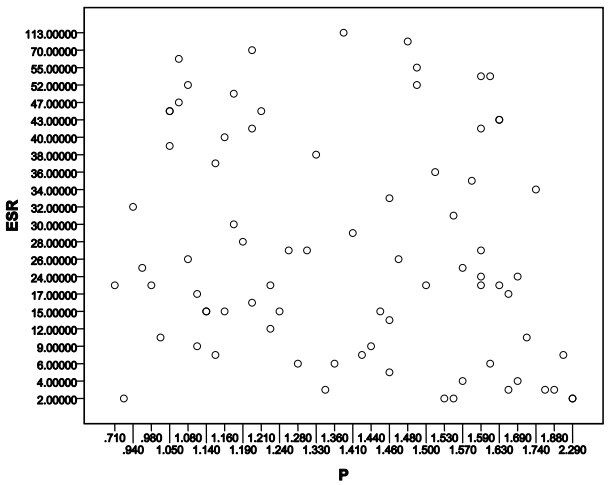

Fig. 2. *Association between P and ESR in tonsillitis children.*

dysregulation is closely associated with oxidative stress and inflammation, which is involved in the risk of respiratory diseases. A null association between Mg and WBC/CRP/PCT/ESR/PLT was noted in tonsillitis cases, which may be due to the fact that the test of indexes was during the first three days of the course. P, an important element for the signal transduction of cells and energy production (11), is the most important component of ATP. Lower P status is likely to lead to lower ATP production, which is important for the energy requirements of the body. P depletion is likely to induce insulin resistance and glucose intolerance (12). Lower levels of P were also involved in impaired chemotaxis, phagocytosis, oxidative stress, and bactericidal activity of macrophages, which indicated that P status affected inflammation. Of note, P was not obviously related with WBC, CRP and ESR, which are all inflammatory indexes. Higher status of PLT contributes to the activation of systemic and local inflammatory processes.

Taken together, our investigation suggested that Mg/P disorder may be associated with the susceptibility to suppuration in children with tonsillitis, and inflammatory indexes may reflect this risk.

ACKNOWLEDGEMENTS

This study was supported by a Grant from the National Natural Science Foundation of China (grant number 81600578) and weak discipline construction of Shanghai health and family planning commission (grant number 2016ZB0102-03).

REFERENCES

1. Hu L, Yang J. Immune function alteration in children after tonsillectomy and (or) adenoidectomy. Lin Chung Er Bi Yan Hou Tou Jing Wai Ke Za Zhi 2016; 30:418-23.
2. Di Muzio F, Barucco M, Guerriero F. Diagnosis and treatment of acute pharyngitis/ tonsillitis: a preliminary observational study in general medicine. Eur Rev Med Pharmacol Sci 2016; 20:4950-54.
3. Gahleitner C, Hofauer B, Stark T, Knopf A. Predisposing factors and management of complications in acute tonsillitis. Acta Otolaryngol 2016; 136:964-68.
4. Liess BD, Mytyk C, Calhoun KH, Whaley-Connell AT. Tonsillectomy for the treatment of tonsillitis-induced immunoglobulin A nephropathy. Am J Otolaryngol 2010; 31:485-88.
5. Pontin IP, Sanchez DC, Di Francesco R. Asymptomatic Group A Streptococcus carriage in children with recurrent tonsillitis and tonsillar hypertrophy. Int J Pediatr Otorhinolaryngol 2016; 86:57-59.
6. Michalska-Mosiej M, Socha K, Soroczyńska J, Karpińska E, Łazarczyk B, Borawska MH. Selenium, zinc, copper, and total antioxidant status in the serum of patients with chronic tonsillitis. Biol Trace Elem Res 2016; 173:30-34.
7. Davis FM. The ins and outs of calcium signalling in lactation and involution: Implications for breast cancer treatment. Pharmacol Res 2016; 116:100-4.
8. Lal CS, Kumar S, Ranjan A, et al. Comparative analysis of serum zinc, copper, magnesium, calcium and iron level in acute and chronic patients of visceral leishmaniasis. J Trace Elem Med Biol 2013; 27:98-102.
9. Vuichard Gysin D, Dao D, Gysin CM, Lytvyn L, Loeb M. Effect of Vitamin D3 supplementation on respiratory tract infections in healthy individuals: a systematic review and meta-analysis of randomized controlled trials. PLoS One 2016; 11:e0162996.

10. Barbagallo M, Dominguez LJ, Galioto A, et al. Role of magnesium in insulin action, diabetes and cardio-metabolic syndrome X. Mol Asp Med 2003; 24:39-52.
11. Marzan LW, Shimizu K. Metabolic regulation of Escherichia coli and its phoB and phoR genes knockout mutants under phosphate and nitrogen limitations as well as at acidic condition. Microb Cell Fact 2011; 10:39.
12. Sciacqua A, Perticone M, Cimellaro A, et al. Multiplicative effect of serum phosphorus levels and insulin resistance on hypertensive vascular stiffness. Thromb Haemost 2016; 115:227-29.

LETTER TO THE EDITOR

GASTROSCOPY-GUIDED PLACEMENT OF INTRANASAL JEJUNUM NUTRIENT CANAL AND ANALYSIS OF NUTRIENT ABSORPTION EFFICIENCY

LH. XIA[1], YX. SUN[2], HW. YAN[3], Y. MENG[4] and XX. MA[5]

[1]Section of Gastroscopy, Central Hospital of Linyi City, Shandong Province, China; [2]Division of Emergency, Center Hospital of Binzhou City, Shandong Province, China; [3]Section of Thyroid and Breast Surgery, Center Hospital of Binzhou City, Shandong Province, China; [4]Department of Medicine, Center Hospital of Binzhou City, Shandong Province, China; [5]Section of Gastroscopy, Centre Hospital of Ji'nan City, Shandong Province, China

Received August 21, 2017 – Accepted May 17, 2018

This study investigated and analyzed using both a pair of clamping pliers to place intranasal-jejunum nutrient canal under the guidance of gastroscope and using a guide wire to place the canal under the guidance of gastroscope. Ninety critically ill patients were randomly divided into a control (n=45) and an observation (n=45) group. The observation group had the intranasal-jejunum nutrient canal placed under the guidance of gastroscope by using a pair of clamping pliers while patients in the control group had the same canal placed under the guidance of gastroscope but using the guide wire. An intergroup comparison was conducted on the success rate of intranasal-jejunum nutrient canal placement and the incidence of complications. The results showed that the comparison yielded no significant difference in the success rate between observation (95.56 %) and control (97.78 %) groups (P□0.05). When compared with control group, the A/G ratio and BMI level in the observation group increased significantly (P□0.05). The intergroup comparison also yielded no significant difference in the incidence of complications. It was concluded that the method of gastroscopy-guided placement of intranasal jejunum nutrient canal produced better clinical results. The operating steps were simple and it had very low incidence of complications, therefore this method can be widely promoted for clinical practices.

To the Editor,

Due to long-term fasting and food deprivation, critically ill patients may experience symptoms such as athrepsia and acceleration in body metabolism (1-2). The use of intranasal jejunum nutrient canal is a major technique for feeding these patients. This method is characterized by a low incidence of complications, easy operating and efficient absorption of nutrients (3). Previous studies have shown the gastroscopy-guided placement of intranasal-jejunum nutrient canal is an efficient way to guarantee patient's nutrient absorption (4). In this study, the method of placing an intranasal-jejunum nutrient canal using clamping pliers under the guidance of a gastroscope was investigated.

The study was approved by the Ethics Committees of the Authors' hospitals and registered as a clinical trial. Ninety critically ill patients admitted to hospital from January 2013 to September 2014 were randomly divided into a control (n=45) and an observation (n=45) group. Twenty-three males (M) and 22 females (F) aged from 45 to 65 years (mean:

Key words: gastroscope, nasointestinal tube, jejunum nutrient canal, research value

Mailing address:
Dr Xiaoxia Ma,
No.105 Jiefang Road,
Ji'nan City, Shandong Province,
250013, China
Tel.: +86 053185695138
e-mail: em1h63@163.com

0393-974X (2018)
Copyright © by BIOLIFE, s.a.s.
This publication and/or article is for individual use only and may not be further reproduced without written permission from the copyright holder. Unauthorized reproduction may result in financial and other penalties
DISCLOSURE: ALL AUTHORS REPORT NO CONFLICTS OF INTEREST RELEVANT TO THIS ARTICLE.

Table I. *Intergroup comparison in the success rate of intranasal jejunum nutrient canal placement.*

Group	Case (n)	Number of patients with operation failure	Number of patients with successful operation	Success rate (%)
Control group	45	1(2.22)	44(97.78)	44(97.78)
Observation group	45	2(4.44)	43(95.56)	43(95.56)
χ^2 value	-	0.3448	0.3448	0.3448
P value -		0.5571	0.5571	0.5571

[n (%)]

Table II. *Intergroup comparison in relevant indices of patient's nutritional status.*

Group Control group	Case (n) 45	Albumen (g/L) 44.44±8.1	Globulin (g/L) 23.8±0.6	Hemoglobin (g/L) 9.3±2.8	A/G ratio 1.2±0.6	BMI (kg/m^2) 19.7±0.8
Observation group	45	42.8±7.7	24.3±1.8	9.9±1.5	2.0±0.8	22.1±1.2
χ^2 value	-	0.3448	0.5728	0.3448	8.4728	12.7836
P value	-	0.5571	0.4672	0.5571	0.0182	0.0017

51.39±5.38) were in the observation group, of whom, 12 cases were of pancreatitis, 25 of infectious shock, and 8 of brain trauma. Twenty-one M and 24 F, aged from 42 to 66 years (mean: 53.29±3.92) were in the control group, of whom, 10 cases were of pancreatitis, 25 of infectious shock, and 10 of brain trauma. The two groups exhibited no statistical difference in the patient basic data ($P > 0.05$).

Informed consent forms were obtained from all patients and they all agreed to a regimen of gastroscopy-guided placement of intranasal jejunum nutrient canal. For the observation group, a proper nasointestinal tube was chosen and the upper end of the nasal tube (17-20 cm long) was inserted into the nostril after lubrication. When the nasal tube entered the nostril by about 25 cm, a gastroscope was pushed into the nasointestinal tube until the gastric cavity was reached. The nasointestinal tube with its head clamped using a pair of clamping pliers was slowly pushed to the descending part of the duodenum and fixed After the gastroscope was pushed into place, the nasointestinal tube with gastroscope was further pushed to the descending part of duodenum for a second and a third time, and the pair of clamping pliers was withdrawn. After withdrawal of the gastroscope, the guide wire was also removed from the patient's nostril. For the control group, we used a superfine gastroscope which was inserted through the nostril until the descending part of the duodenum was touched and the guide wire was released into that part of the duodenum through the fine tubing fixed along with the flexible optic fiber of the gastroscope. Subsequently, the superfine gastroscope was withdrawn and the nasointestinal tube was further

Table III. *An intergroup comparison in the incidence rate of complications of intranasal jejunum nutrient canal placement.*

Group Control group	Case (n) 45	Massive hemorrhage 2 (4.44)	Digestive tract perforation 2 (4.44)	Incidence rate of complications (%) 5 (8.88)
Observation group	45	1 (2.22)	2 (4.44)	3 (6.66)
χ^2 value	-	0.3448	0.0000	0.5488
P value	-	0.5571	1.000	0.4588

[n (%)].

inserted to the descending part of duodenum along with the guide wire. Patient's nutrient absorption was monitored and recorded.

Criteria for efficacy judgment (4): Successful operations were those where patients could effectively absorb nutrients without any adverse reaction such as post-operative massive hemorrhage and digestive tract perforation. Failed operations were those where patients had insignificant nutrient absorption, or experienced the adverse reactions such as post-operative mass hemorrhage and digestive tract perforation. . Success rate = 1 – (number of patients with operation failure) / (total number of patients) 100%.. Intergroup comparison of incidence of complications, such as massive hemorrhage and digestive tract perforation was conducted.

We used SPSS19.0 (SPSS Inc., IL, USA) for our statistical assessments. Qualitative data were analyzed using the analysis of variance (ANOVA), *t*-test and *Chi*-squared test. In patients who failed to satisfy the conditions, the four-fold table data were tested using the Fisher exact probability method. Quantitative data were compared and tested using the analysis of variance (ANOVA). $p<0.05$ meant that the difference was statistically significant.

The intergroup comparison yielded no statistically significant difference in the success rate of intranasal jejunum nutrient canal placement between observation (95.56 %) and control (97.78 %) groups ($P > 0.05$) (Table I). For the relevant indexes of patients' nutritional status, A/G ratio and BMI level in the observation group were significantly higher than controls ($P < 0.05$, Table II). For the incidence of complications following intranasal jejunum nutrient canal placement, the intergroup comparison yielded no significant difference ($P > 0.05$, Table III).

Due to incapability of eating, critically ill patients often experience symptoms such as athrepsia, acceleration in body metabolism functions, and severe loss of protein and fat (4). Traditional methods providing nutrients using parenteral nutrition can aggravate the injuries in the patient's intestinal tract and may cause infection in the digestive tract. Currently, the nutritional methods for critically ill patients mainly include (i) enteral nutrition and (ii) parenteral nutrition. Parenteral nutrition provides nutrients and energy mainly by intravenous infusion of a nutrient solution containing multiple essential amino acids, microelements, vitamins and essential fatty acids. Nevertheless, venous catheterization (mainly through subclavian vein) for parenteral nutrition is frequently complicated by infection and is harmful for the patient's gastrointestinal function. Although enteral nutrition is still the primary nutritional method for critically ill patients, it may disturb the microbial population of the intestinal tract (5-6). Results obtained from previous studies suggested that gastroscopy-guided placement of an intranasal-jejunum nutrient canal could reduce the gastrointestinal tract injuries and maintain the balance of gut flora. It was also indicated this method had a high success rate and was efficient for nutrient absorption (7-9).

In the present study, the intergroup comparison yielded no significant difference in the success rate between the observation group and the control group, nor difference in the incidence rate of complications. There are two main methods for the gastroscopy-guided placement of intranasal-jejunum nutrient canal to provide nutrients to patients: the use of gastroscopy-guided placement of an intranasal jejunum nutrient canal and the use of gastroscopy-guided placement of the nutrient canal along with a guide wire. Our study indicated both methods were easily handled with rare complications as intergroup comparison yielded no significant difference in the success rate and incidence of complications between observation and control groups.

The intranasal-jejunum nutrient canal method can effectively inhibit the growth and propagation of digestive tract bacteria and minimize the risk of digestive tract infection. This method could accelerate the recovery through helping patients to regain their normal digestive functions by maintaining gastrointestinal integrity (10). Furthermore, the use of an intranasal-jejunum nutrient canal can promote protein and fat synthesis, slow down metabolism, and improve immunity. Moreover, this method is very efficient and easy to handle with shorter operating time (11). The traditional methods may induce digestive tract infection and gastrointestinal injuries and are more complicated, and their efficiency is not as good as the intranasal-jejunum nutrient canal method (12).

It was concluded that the method of gastroscopy-guided placement of intranasal-jejunum nutrient canal yielded good clinical outcome. The operating steps are simple with very low incidence of complications, therefore this method should be widely promoted in clinical practices.

REFERENCES

1. Afaneh C, Gerszberg D, Slattery E, Seres DS, Chabot JA, Kluger MD. Pancreatic cancer surgery and nutrition management: a review of the current literature. Hepatobiliary Surg Nutr 2015; 4:59-71.
2. Zhu J, Zhao Y, Sun T. Clinical observation of the nasojejunal tube placement by transnasal gastroscope. Med J Liaoning 2010; 24:13-15.
3. Boyer N, McCarthy MS, Mount CA. Analysis of an electromagnetic tube placement device versus a self-advancing nasal jejunal device for postpyloric feeding tube placement. J Hosp Med 2014; 9:23-28.
4. Crosby J, Duerksen DR. A prospective study of tube- and feeding-related complications in patients receiving longterm home enteral nutrition. J Parenter Enteral Nutr 2007; 31:274-77.
5. Jain R, Maple JT, Anderson MA, et al. The role of endoscopy in enteral feeding. Gastrointest Endosc 2011; 74:7-12.
6. Kurien M, Leeds JS, Delegge MH, et al. Mortality among patients who receive or defer gastrostomies. Clin Gastroenterol Hepatol 2013; 11:1445-50.
7. Chadha KS, Thatikonda C, Schiff M, Nava H, Sitrin MD. Outcomes of percutaneous endoscopic gastrostomy tube placement using a T-fastener gastropexy device in head and neck and esophageal cancer patients. Nutr Clin Pract 2010; 25:658-62.
8. Lai CW, Barlow R, Barnes M, Hawthorne AB. The operation techniques and clinical applications of placing nasointestinal feeding tube under X-ray examination. Ningxia Med J 2014; 36:488-90.
9. Holzinger U, Brunner R, Miehsler W, et al. Jejunal tube placement in critically ill patients: A prospective, randomized trial comparing the endoscopic technique with the electromagnetically visualized method. Crit Care Med 2011; 39:73-77.
10. McClave SA, Codner P, Patel J, Hurt RT, Allen K, Martindale RG. Should we aim for full enteral feeding in the first week of critical illness? Nutr Clin Pract 2016; 31(4):425-31.
11. Kar A, Rao V, Datta A, Ahmed A. Causes of interruption in enteral nutrition in CCU patients - experience from an Indian hospital. Intensive Care Med Exp 2015; 3(Suppl 1):A580, 2015.
12. Uozumi M, Sanui M, Komuro T, et al. Interruption of enteral nutrition in the intensive care unit: a single center survey. Intensive Care Med Exp 2015; 3(Suppl 1):A289.

LETTER TO THE EDITOR

LIMB-SALVAGE TREATMENT OF MALIGNANT TUMORS OF THE LIMBS

G. LI[1], J. LI[1], CY. HU[2], L. TIAN[1], CA. LV[3] and LJ. JIN[2]

[1]Orthopedic Department, Affiliated Hong Qi Hospital of Mu Dan Jiang Medical University, Mudanjiang City, China; [2]Anesthesiology Department, Affiliated Hong Qi Hospital of Mu Dan Jiang Medical University, Mudanjiang City, China; [3]ICU Department, Affiliated HongQi Hospital of Mu Dan Jiang Medical University, Mudanjiang City, China

Received February 20, 2018 – Accepted April 16, 2018

The aim of this study was to explore the clinical efficacy of limb-salvage therapy for malignant bone tumors of the limbs using two surgical methods. This investigation presents a retrospective study of malignant bone tumors of the limbs in 42 patients. Participants were divided into two groups: group A of 25 patients who were treated with artificial prosthesis replacement, and group B of 17 patients treated with bone inactivation. By collection of clinical data, the survival rate, surgical complications, quality of life, pain relief and postoperative limb function following artificial prosthesis replacement and tumor inactivation were comprehensively evaluated in patients with malignant bone tumors of the limbs. Group A had significantly higher Karnofsky quality of life scores compared to group B after six months (P=0.027). The Enneking scores of limb functions in group A were significantly higher than those of group B (P =0.022). In group A the postoperative limb function score was good and excellent in 92% and in group B in 64.7%. There were significantly more postoperative complications in group B compared with group A (P=0.027), but no significant difference in the recurrence rate in the two group (P=0.976). The study results can provide reference for surgical treatment of the patients with malignant bone tumors.

To the Editor,

Malignant bone tumor of the limbs has high fatality and mutilation rates, and is one of the most common diseases that endanger human health. Before 1970s, amputation was the only way to treat these malignant bone tumors, which not only did not improve survival rates, but also severely affected the quality of life of the patients (1). Advances in neo-adjuvant chemotherapy, imaging diagnosis, pathological diagnosis and therapeutic approaches for malignant bone tumors of the limbs have changed from amputation to comprehensive treatment based on limb-sparing surgery (2). Reports in the past 20 years showed that about 80% of patients with malignant bone tumors had chosen limb salvage surgery (3). Limb salvage includes methods that preserve limb functions as much as possible based on the complete removal of tumor tissues. Limb salvage treatment of limb malignant bone tumors has gained increased interest in bone tumor research (4). However, lack of methods to safely and effectively repair bone defects and reconstruct limb functions remains a limitation factor.

This study compares the effect of prosthetic replacement and replantation of bone as two surgical methods used for malignant bone tumor patients through a follow-up analysis of preoperative and postoperative pain relief, improvement of quality of life, limb function and prognosis, surgical complications,

Key words: bone tumor, limb salvage, prosthesis replacement, inactivated replantation

Mailing address:
Dr Lianjin Jin,
TongXiang Road No 5
Affiliated Hong Qi Hospital
Mu Dan Jiang Medical University,
Mudanjiang City, Hei Longjiang Province, China
e-mail: dr_jinlianjinjlj@126.com

0393-974X (2018)
Copyright © by BIOLIFE, s.a.s.
This publication and/or article is for individual use only and may not be further reproduced without written permission from the copyright holder.
Unauthorized reproduction may result in financial and other penalties
DISCLOSURE: ALL AUTHORS REPORT NO CONFLICTS OF INTEREST RELEVANT TO THIS ARTICLE.

etc. comprehensively, to provide reference for surgical treatment of patients.

MATERIALS AND METHODS

Clinical information

From May 2010 to May 2017, 63 patients with malignant bone tumors of the limbs were observed at the Affiliated Hong Qi Hospital of Mu Dan Jiang Medical University. The study was approved by the Ethics Committee of the Hospital and all patients signed informed consent. Clinical data were collected to comprehensively evaluate the survival rate, surgical complications, quality of life, pain relief and postoperative limb function of artificial prosthesis replacement and tumor inactivation in patients with malignant bone tumors of the limbs. Among these patients, full access to clinical data was available only for 42 patients, including 23 males and 19 females. Their age range was 18 to 67 years, average 47.4 years. Patients were requested to participate in the telephone survey to complete the questionnaire. In this survey, patients were followed-up for 6 to 70 months. The average follow-up time was 36.5 months, and the follow-up rate was 66.7%.

Patient grouping

The patients were divided into two groups: group A which included 25 cases of the artificial prosthesis replacement, accounting for 59.5% (25/42); and group B (segment inactivated reimplantation) which included 17 cases of bone inactivation, accounting for 40.5% (17/42). Of these subjects there were 13 cases of osteosarcoma, 9 cases of chondrosarcoma, 6 cases of malignant giant cell tumor, 5 cases of malignant fibrous histiocytoma (MFH), 4 cases of fibro sarcoma, 1 case of ameloblastoma, and 4 cases of metastatic tumor. Enneking staging of 38 patients with primary bone tumor: 7 cases were in stage I B, 14 in stage II A, and 17 in stage II B. Incidence site: 6 cases of upper humerus, 5 of middle humerus, 4 of proximal femur, 7 of middle femur, 7 of distal femoral, 4 of proximal tibia, and 5 of middle tibia. The patients included 4 cases of metastatic tumor pathological diagnosis: 2 of breast cancer, 1 of prostate cancer, 1 of indeterminate primary metastatic lesions, and 4 cases of proximal femur.

Inclusion criteria

Primary tumor: (i) primary tumor without distant metastasis or metastases which can be completely cleared, such as: stage I A, I B and II A of Enneking and stage II B sensitive to radiotherapy and chemotherapy; (ii) after tumor resection, there is sufficient soft tissue to cover the prosthesis, and the important blood vessels and nerves are not involved. Metastatic tumor: (i) pathological fractures cause severe cancer pain, patients need long-term oral or intramuscular strong analgesics, which seriously affects the quality of life of patients. The expected survival of more than 3 months; (ii) The patient's imaging data shows that the diameter of the metastatic bone tumor lesion is more than 2.5 cm (more than 50% of the cortical bone is destroyed). Mirels long bone pathological fracture score system ≥ 9 points.

Surgical methods and postoperative treatment

All the surgical specimens were examined and the cancer diagnosis was confirmed by a pathologist. Based on the sensitivity of tumor cells to chemotherapy, preoperative chemotherapy was performed. For tumors with abundant blood supply, digital subtraction angiography (DSA) was performed before embolization of tumor vessels. Imaging studies were used to determine the various parts of the tumor and to establish the safety margin The scope of surgical resection includes tumor entities, pseudocapsules, reaction zones and surrounding normal tissues. In general, they are removed between 3-5cm from the tumor, and 1-3 cm from the soft tissue outside of the reaction zone. In group A there were 8 cases with hip tumor prostheses, 11 with knee prostheses, and 6 with shoulder prostheses. The hip prosthesis used was a standard prosthesis, and the knee and shoulder prostheses were custom-made. During the operation, the focus was on the repair of the main dynamic structures around the joints.

In patients in group B, tumor bone inactivation replantation was used, which is one of the methods of limb salvage surgery for malignant bone tumors of the limbs based upon bone reconstruction after inactivation of tumorous bone. The inactivation replantation method can be divided into external inactivation replantation and internal inactivation. External inactivation replantation regards removing the tumor bone and tumor tissue, and using low temperature liquid nitrogen, high temperature boiling, chemical drugs, irradiation and other methods to inactivate the tumor cells. Then, the bone is put back in place, and fixed with a steel plate or intramedullary pin. Internal inactivation is exposing the malignant tumor tissue,

without cutting the tumor bone to radiation or microwaves and other methods for killing tumor cells. Then, the outgrowth bone is removed, to restore its natural shape. The treated tumor tissue is put back in the tumor cavity, and autogenous bone or allogeneic bone filling is used. Finally, it is fixed with steel screws or intramedullary nails.

Karnofsky Performance Scale (KPS)

KPS is one of the indicators used primarily to assess the patient's health status. Scoring is positively related to the patient's health, which indicates that patients can better tolerate the adverse reactions caused by the treatment.

Evaluation of limb function after limb salvage by Enneking scoring system

The scoring system consists of six aspects, namely, three common items (pain, function, emotion) and three special items for upper and lower limbs (upper limb: hand position, dexterity and lift function; lower limbs: walking ability and gait). Each project has six levels, 0 to 5, where 0, 1, 3 and 5 are specific values, and all have clear connotations, 2 and 4 are intermediate values, that is, when the check results are between the specific values, the checker determines the fill value.

Kaplan-Meier method

Kaplan-Meier method was used for the survival analysis, and the survival rate was estimated in 1 year, 3 years and 5 years. Log-rank test was used to determine whether there was a significant difference between the two groups.

Statistical analysis

SPSS statistical software (version19.0) was used to analyze the results, and *chi*-squared was used for comparisons in count and rate. Measurement indexes were expressed as (mean ± standard deviation). The differences between groups were analysed by Student's *t*-test for continuous data and χ^2 test. $P < 0.05$, was considered statistically significant. For survival analysis the Kaplan-Meyer survival curves were conducted and the differences between the curves were tested using the Log-rank test.

RESULTS

All patients safely underwent surgery. Clinical data was available in 42 out of 63 patients, and the follow-up rate reached 66.7% (42/63). Follow-up time: 6 to 70 months, average time 36.5 months.

Postoperative patient evolution and quality of life assessment.

Six months after the operation, the quality of life of 42 patients was improved to some extent compared to before surgery. In patients from group A the healing rate was 92% (23/25). 3 patients in the postoperative period (at 13 and 24 months) developed local recurrence and one patient developed prosthetic loosening, so amputation was performed. The limb salvage rate was 84.2%. The Karnofsky score was increased from preoperative average (44.6±10.5) to (59.7±10.1) (P=0.027).

Table I. *Patient parameters before and after surgery.*

Parameters	Group A (n=25)	Group B (n=17)	P
Preoperative Karnofsky score	44.6±10.5	44.8±10.2	0.951
Postoperative Karnofsky score	59.7±10.1	51.9±11.8	0.027*
Postoperative Enneking score	23.7±2.1	22.1±2.2	0.022*
Healing rate	92.0%	88.2%	0.666
Excellent/good postoperative function rate	92.0%	64.7%	0.027*
Limb salvage rate	84.2%	82.4%	0.877

* *P<0.05*

In patients from group B the clinical healing rate was 88.2% (15/17). Amputation was performed on 3 patients because of infection in 1 case and tumor recurrence in 2 cases. Reoperation was performed on 2 patients because of the delayed healing and non-union. After about 1 year after surgery, in 2 cases of bone inactivated replantation inactivated bone fracture occurred. The limb salvage rate was 82.4%. 70.6% of patients scored good or excellent score for postoperative limb function. Six months after the operation, the Karnofsky score of patients from group B increased from (44.8±10.2) preoperatively to (51.9±11.8) (P=0.027) (Table I and Fig. 1A).

Evaluation of limb function after limb surgery

Six months after surgery, the Enneking score for limb function was (23.7±2.6) for patients in group A. Fourteen patients were evaluated as excellent, 9 as good, 2 as fair, and 1 as poor. The rate of excellent or good assessment was 92%. For patients in group B the Enneking score for limb function was (22.1±2.2). Eight patients were evaluated as excellent, 3 as good, 3 as fair, and 3 as poor. The rate of excellent and good assessment was 64.7%.

After surgery, the rate of excellent and good for limb function for patients in group A was higher than that of patients in group B (P=0.027). The results showed that the postoperative limb function in group A was increased compared with group B (Table I and Fig. 1B).

Postoperative complications

Compared with amputation, limb salvage treatment for malignant bone tumors was relatively high. Therefore, difficulty in preventing and treating the complications of limb salvage surgery is a major limitation of the surgery success. Of 42 patients, postoperative complications occurred in 8: 2 (8%) in group A, and 6 in group B (35.3%). Through the χ^2 test, we compared the incidence of postoperative complications in the two patient groups and the difference was statistically significant (P 0.027) (Table II).

Postoperative tumor recurrence

From the 42 patients that were followed up, a total of 5 presented local recurrence after surgery: 3 (12%) patients in group A, and 2 (11.7%) in group B. The difference between the two groups was not statistically significant (P=0.976) (Table II).

Survival analysis

From the 25 patients in group A with artificial prosthesis replacement, 7 died after 3 years and

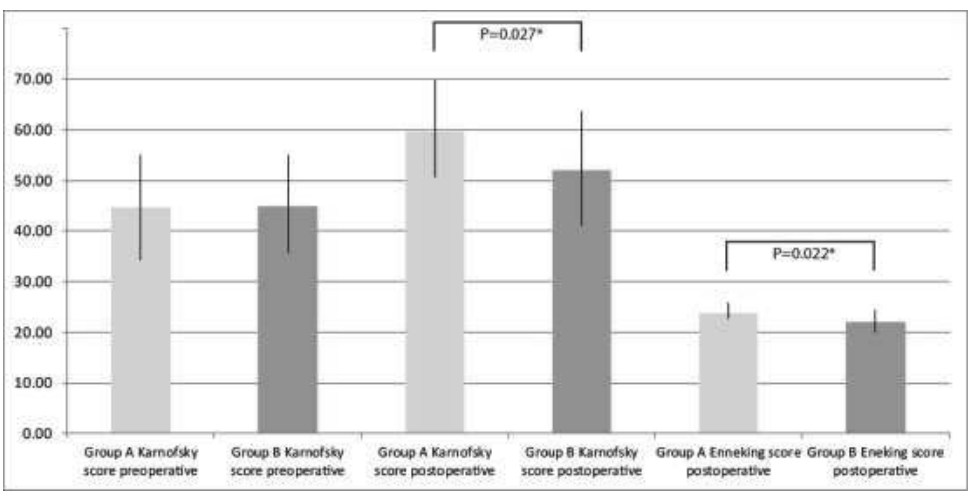

Fig. 1. *Comparison between Karnofsky score between and after surgery and Enneking score after surgery between the two groups (* P<0.05 compared with group A).*

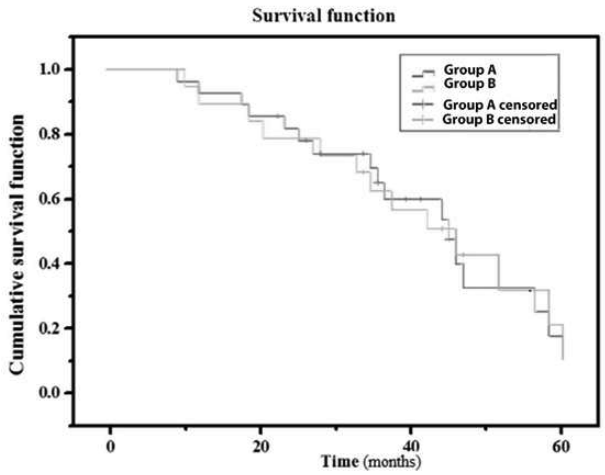

Fig. 2. *Kaplan-Meier survival curve (censored: excluding patients lost to follow-up).*

15 died in 5 years following surgery. From the 17 patients in group B, 6 died after 3 years and 11 died in 5 years after surgery. The patients died either of tumor metastasis or from various other causes related to the oncologic disease. The postoperative mortality and survival rates are shown in Table III.

After surgery, the 3- and 5-year survival rates of the artificial prosthesis replacement group were 72% and 40%, respectively. The 3- and 5-year survival rates of the inoculation group were 64.7% and 35.3%, respectively. Log-rank was used to test the survival rates of the two groups, $\chi^2 = 0.18$, P=0.893 >0.05. There was no significant difference in the survival curves between the two groups (Fig. 2).

Table II. *Comparison of two groups of patients with postoperative local recurrence.*

Parameter	Group A	Group B	P
Postoperative recurrence	3	2	
			0.976
The recurrence rate	12%	11.7%	
Number of postoperative complications	2	6	0.027*

* *P<0.05*

Table III. *Mortality and survival rate in two groups.*

	Group A (n=25)	Group B (n=17)	P
Postoperative mortality in 6 months to1 year (case)	1	1	
Postoperative mortality in 1 year to1.5 year (case)	1	1	
Postoperative mortality in 1.5 year to 2 year (case)	2	2	
Postoperative mortality in 2 year to 3 year (case)	3	2	
Postoperative mortality in 3 year to 4 year (case)	5	3	
Postoperative mortality in 4 year to 5 year (case)	3	2	
3-year survival rate	72%	64.7%	0.6155
5-year survival rate	40%	35.3%	0.7582

DISCUSSION

Infection is one of the main reasons for the failure of prosthesis replacement (5). Types of infection include early infection and delayed infection with germs difficult to eradicate such as *Staphylococcus aureus*, *Klebsiella*, or fungus from *Fusarium* or *Aspergillus* species (6, 7). The main reason for early infection is that the soft tissue weakness after tumor resection is often related to the decrease of body resistance after chemotherapy. The presence of foreign bodies is beneficial to the reproduction of bacteria, and increases the chance and severity of infection (8). Local recurrence is one of the most common causes of the failure of limb salvage surgery, mainly due to the lack of radical scavenging (9). The local recurrence rate of tumor after tumor prosthesis replacement is generally reported between 4 and 14% (10) which is in accordance with our results. Generally, *in situ* microwave inactivation plus tumor prosthesis replacement can retain more bone mass without increasing the chance of local recurrence (11). To a certain extent, it can reduce the postoperative long-term prosthesis loosening rate (12). It is reported that the application of coating prosthesis and porous prosthesis can prevent the occurrence of prosthesis loosening (13). Inactivated tumor cells can be used as antigens to stimulate the immune system and improve the immune ability of the body (14).

In conclusion, limb salvage treatment of malignant bone tumor could not change the outcome of the disease, but it significantly improved postoperative limb function and quality of life of the patients. There were no significant differences in postoperative metastasis rate and recurrence rate between the prosthetic replacement and tumor inactivation replantation. However, the functional recovery was better after tumor prosthesis replacement.

REFERENCES

1. Groundland JS, Binitie O. Reconstruction after tumor resection in the growing child. Orthop Clin North Am 2016; 47(1):265-81.
2. Rod Fleury T, Miozzari HH, Hoffmeyer PJ. Management of malignant bone tumors around the knee. Rev Med Suisse 2014; 10(455):2403-6.
3. Chen Y, Yu XC, Xu SF, Xu M, Song RX. Impacts of tumor location, nature and bone destruction of extremity osteosarcoma on selection of limb salvage operative procedure. Orthop Surg 2016; 8(2):139-49.
4. Zoccali C, Anelli V, Chichierchia G, Erba F, Biagini R. The use of engineered biomaterial Bone Plexur M® in benign epiphyseal tumors: our experience at 20 months of follow-up. J Biol Regul Homeost Agents 2014; 28(1):65-71.
5. Leckenby JI, Grobbelaar AO, Aston W. The use of a free vascularised fibula to reconstruct the radius following the resection of an osteosarcoma in a paediatric patient. J Plast Reconstr Aesthet Surg 2013; 66(3):427-29.
6. Ungureanu A, Zlatian O, Mitroi G, et al. Staphylococcus aureus colonisation in patients from a primary regional hospital. Mol Med Rep 2017; 16(6):8771-80.
7. Călina D, Docea, AO, Roşu L et al. Antimicrobial resistance development following surgical site infections. Mol Med Rep 2017; 15(2): 681-688.
8. Niimi R, Matsumine A, Hamaguchi T, Nakamura T, Uchida A, Sudo A. Prosthetic limb salvage surgery for bone and soft tissue tumors around the knee. Oncol Rep 2012; 28(6):1984-90.
9. Müller DA, Beltrami G, Scoccianti G, Cuomo P, Capanna R. Allograft-prosthetic composite versus megaprosthesis in the proximal tibia—What works best? Injury 2016; 47(Suppl 4):S124-30.
10. Xu S, Yu X, Xu M, et al. Limb function and quality of life after various reconstruction methods according to tumor location following resection of osteosarcoma in distal femur. BMC Musculoskelet Disord 2014; 15:453.
11. Yang J, Zhu B, Fu K, Yang Q. The long-term outcomes following the use of inactivated autograft in the treatment of primary malignant musculoskeletal tumor. J Orthop Surg Res 2015; 10:177.
12. Galliera E, Marazzi MG, Vianello E, et al. Circulating sRAGE in the diagnosis of osteolytic bone metastasis. J Biol Regul Homeost Agents 2016; 30(4):1203-8.
13. Nikitovic D, Kavasi RM, Berdiaki A, et al. Parathyroid hormone/parathyroid hormone-related peptide regulate osteosarcoma cell functions: Focus on the

extracellular matrix . Oncol Rep 2016; 36(4):1787-92.
14. D'Adamio S, Cazzato G, Ziranu A, Sgambato A, Rosa MA, Maccauro G. Soft tissue adhesion patterns over Trevira tube on modular endoprosthesis for malignant bone tumours: an in vitro study. J Biol Regul Homeost Agents 2017; 31(4 suppl 1):37-42.

LETTER TO THE EDITOR

EVALUATION OF FUNCTIONAL PROPERTIES OF ZEIN EXTRACTED FROM VARIOUS MAIZE VARIETIES

T. SIDDIQUE[1], A. ASGHAR[1], I. PASHA[1] and M. SHAHID[2]

[1]National Institute of Food Science and Technology, University of Agriculture, Faisalabad, Pakistan; [2]Department of Biochemistry, University of Agriculture, Faisalabad, Pakistan

Received February 8, 2018 – Accepted May 18, 2018

Zein is the major storage protein of maize and was identified initially on the basis of solubility in aqueous alcohol solution. It is comprised of 45-50% grain portion and has a wide range of application as a functional ingredient in the food industry. In the current study, five different maize varieties were analyzed and compared for the physicochemical, mineral and functional characteristics. Zein protein was extracted at different concentrations of ethanol and was further characterized for its antioxidant and functional properties. Significant variations in the characteristics were observed in different varieties related to their mineral and chemical composition. Likewise, antioxidant properties of zein extracted from Agaiti-2002 variety were 32.61% and minimum value (30%) was observed in the Pearl variety. Zein protein has the potential to be used as encapsulating material for controlled release of different bioactive compounds.

To the Editor,

Maize (*Zea Mays*) is an important industrial crop with almost half of the world production in USA. The endosperm and germ are the major parts of maize kernel containing most of the oil and starch. Zein is a protein found in maize and has long been applied in food and pharmaceutical industries because of its film-forming ability and superior biodegradable properties. Zein protein plays an important role in the hardness of the grain. Its endosperm portion contains about 75% of the protein while the rest is distributed between the germ and bran portions. Maize processing involves different techniques and the protein byproduct from corn wet milling is corn gluten which has protein contents of 6-12% on dry basis in different varieties.

Zein protein is hydrophobic in nature and is considered a safe food ingredient by the Food and Agriculture Organization (FAO). About 50% residues of hydrophobic amino acids are present in zein which results in hydrophobic nature (1). Zein has both hydrophobic and hydrophilic zones which can form diverse bonds to encapsulate (1). It is a byproduct of maize processing and is of great scientific interest. The essential amino acids, such as lysine and tryptophan, are deficient in zein which make it a nutritionally poor product. Upon hydrolysis with the enzyme thermolysin, zein produces angiotensin-converting enzyme (ACE)-inhibitory peptides (2). Zein has potential use as a functional ingredient for flavor encapsulation and controlled release of different biologically active ingredients (3). In the present work, the major objectives were to study the major physicochemical, mineral properties and

Key words: zein, maize, extraction, encapsulation, antioxidant, functional properties

Mailing address:
Ali Asghar, Ph.D.,
National Institute of Food Science & Technology,
Faculty of Food, Nutrition and Home Sciences,
University of Agriculture, Faisalabad, Pakistan
Tel.: +92 41 9200008 - Fax: +92 41 9201645
e-mail: ali.asghar@uaf.edu.pk

0393-974X (2018)
Copyright © by BIOLIFE, s.a.s.
This publication and/or article is for individual use only and may not be further reproduced without written permission from the copyright holder.
Unauthorized reproduction may result in financial and other penalties
DISCLOSURE: ALL AUTHORS REPORT NO CONFLICTS OF INTEREST RELEVANT TO THIS ARTICLE.

composition of zein protein extracted from various maize varieties and their effects on functional and antioxidant behaviors.

MATERIALS AND METHODS

Raw materials

Five locally grown maize varieties named Sadaf, Sahiwal 2002, Agaiti 2002, Pearl and MMRI-Yellow were obtained from Ayyub Agriculture Research Institute (AARI), Faisalabad. Chemicals were purchased from Sigma Aldrich, USA and Merck, Germany while other raw materials used in the research were procured from the local market.

Physical and chemical analysis of maize

Grain size and thousand kernel weights of hundred grams of clean, sound and unbroken kernels of all varieties were determined. Proximate analysis (moisture content, ash, fat, fiber and protein content) of all five varieties were determined according to their standard methods (4).

The mineral contents i.e., Na, Mg, K, P, Cu, Fe, Zn and Manganese were determined by Atomic Absorption Spectrophotometer (AA 240 Varian K, Australia) on an acetylene air flame.

Zein was extracted from corn gluten meal after wet milling process according to the method of Shukla and Cheryan, 2011. Gluten meal was treated with different concentrations of ethanol i.e. 60%, 75% and 90% to extract zein from different maize varieties (2).

Functional characterization of zein protein

Zein extracted from different maize varieties were characterized for the functional properties according to their standard methods and antioxidant activity was measured for free radical scavenging ability by DPPH and FRAP methods (5, 6).

Statistical analysis

The results obtained in this study were analyzed statistically to determine the level of significance through

Table I. *Chemical and physical characteristics of maize kernel.*

Treatment	Moisture%	Ash%	Fat%	Fibre %	Protein%	NFE	Size (mm)	Weight (g)
Agaiti-2002	$10.54^{b}\pm0.14$	$0.44^{a}\pm0.02$	$4.55^{bc}\pm0.19$	$3.01^{a}\pm0.1$	$12.29^{a}\pm0.4$	$69.17^{a}\pm2.84$	$7.97^{c}\pm0.29$	$253.04^{a}\pm8.9$
Sahiwal-2002	$12.18^{a}\pm0.17$	$0.45^{a}\pm0.02$	$4.29^{cd}\pm0.18$	$2.84^{ab}\pm0.11$	$9.66^{d}\pm0.8$	$70.58^{a}\pm3.04$	$9.03^{b}\pm0.31$	$241.90^{a}\pm8.5$
Sadaf	$11.95^{a}\pm0.15$	$0.36^{c}\pm0.01$	$5.20^{a}\pm0.23$	$2.73^{b}\pm0.09$	$10.97^{bc}\pm0.2$	$68.79^{a}\pm3.03$	$7.53^{c}\pm0.26$	$181.80^{c}\pm6.4$
MMRI-Yellow	$11.59^{ab}\pm0.17$	$0.40^{b}\pm0.02$	$3.78^{d}\pm0.17$	$2.96^{ab}\pm0.08$	$10.09^{cd}\pm0.3$	$71.18^{a}\pm3.27$	$9.03^{b}\pm0.31$	$127.93^{d}\pm4.5$
Pearl	$12.07^{a}\pm0.19$	$0.43^{ab}\pm0.02$	$4.87^{ab}\pm0.21$	$2.86^{ab}\pm0.13$	$11.74^{ab}\pm0.6$	$68.03^{a}\pm2.86$	$10.03^{a}\pm0.35$	$218.83^{b}\pm7.6$

Mean value table represent means ± standard deviation; Tukey's HSD all-pairwise comparison tests

the analysis of variance techniques according to the respective methods.

RESULTS

Physicochemical analysis

The results related to the physicochemical properties of different maize cultivars are presented in Table I. The results revealed that grain size values ranged from 7.53±0.26 mm to 10.03±0.35mm, while the values of thousand kernels weights varied from 127.93±4.5g to 253.04±8.9g (7). Similarly, maximum value for fat was 5.20±0.23% in the Sadaf variety while minimum value was observed in the MMRI-Yellow variety 3.78±0.17% (8). The results related to the protein content were also affected significantly and maximum mean values 12.29±0.4% were observed in the Agaiti-2002 maize variety while the minimum value of 9.66±0.8% was observed in the Sahiwal-2002 variety.

Zein extraction

Ethanol is generally used for the extraction of zein from maize, and the highest extraction was observed with 90% concentration from Agaiti-2002 variety (10). The highest percent values in the present study were 4.48 (w/v)% with 90% ethanol, 3.25 (w/v)% with 75% ethanol and 2.03 (w/v)% with 60% ethanol concentration. 1.6% zein was found by using 70% ethanol at laboratory scale from fresh milled maize. A difference of yield and composition among maize zein extracts and maize gluten were noted earlier and the laboratory method gave only 5-6% yield of zein (2, 3).

Functional and antioxidant properties of zein

Foaming and emulsification properties of extracted zein were determined by calculating the foaming stability and foaming capacity. The maximum value for foam stability and foam capacity was observed in zein extracted from the Agaiti-2002 maize variety (Fig. 2).

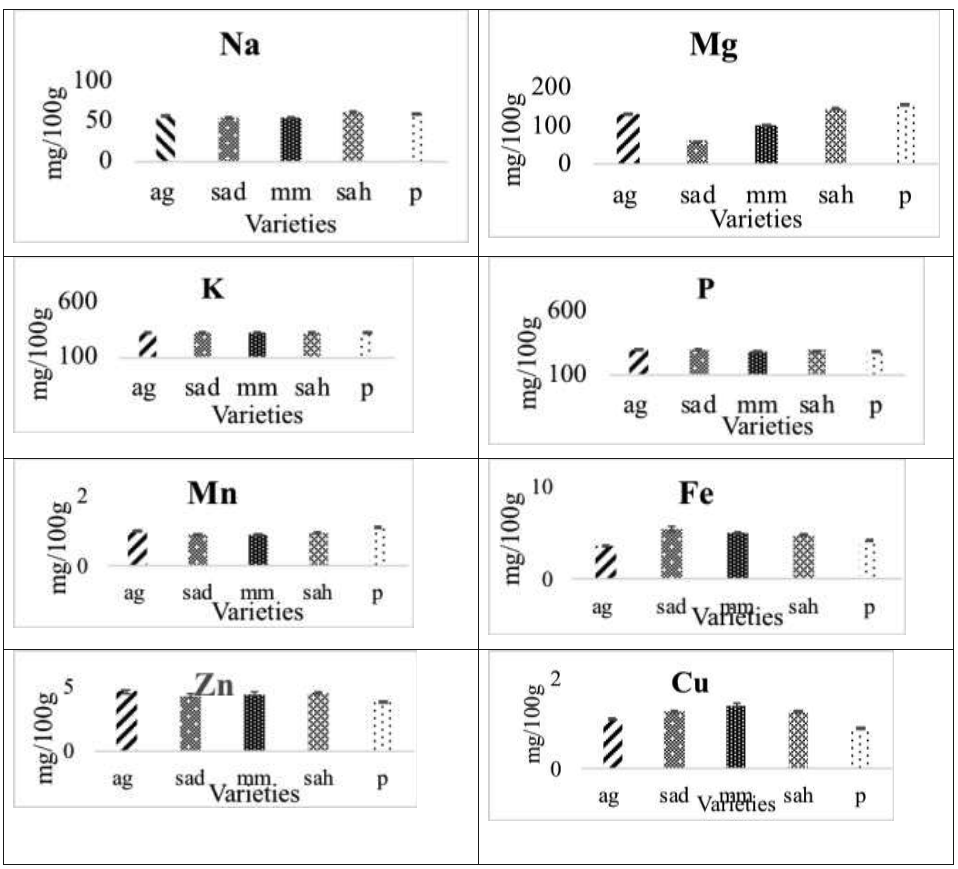

Fig. 1. *Minor minerals present in different maize varieties ag: Agaiti-2002; sad: Sadaf; mm: MMRI-Yellow; sah: Sahiwal; p: Pearl*

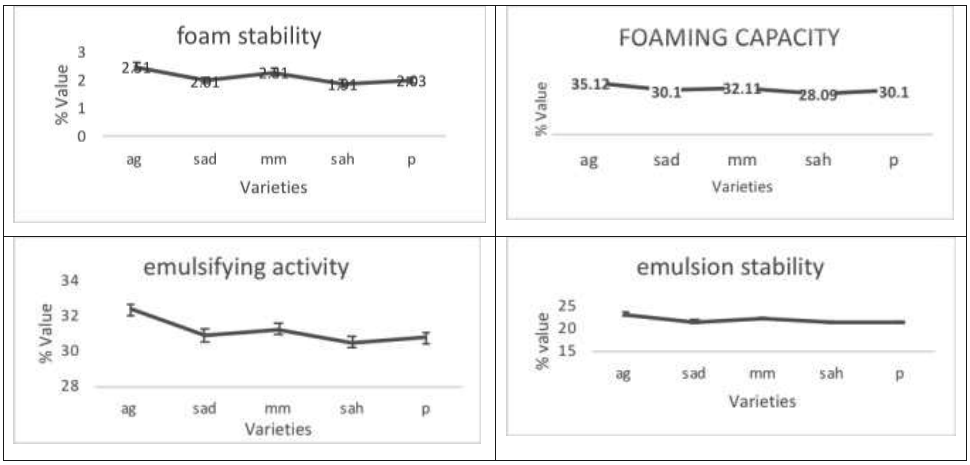

Fig. 2. *Functional properties value in percent of different maize varieties. Agaiti: Agaiti-2002. sad: Sadaf. MMRI: MMRI-Yellow. sah: Sahiwal. P: Pearl*

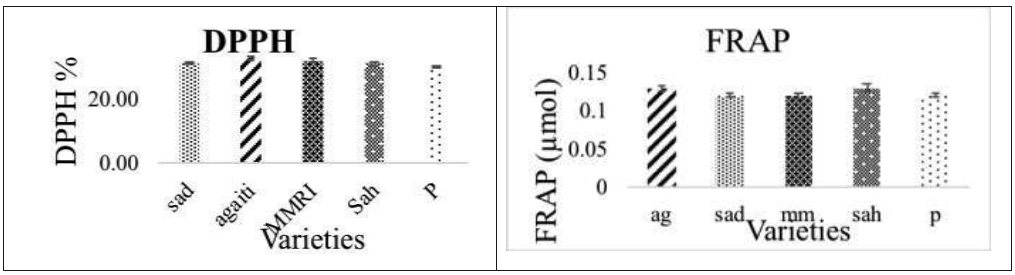

Fig.3. *Antioxidant value in percent of different maize varieties. Agaiti: Agaiti-2002; sad: Sadaf; MMRI: MMRI-Yellow; sah: Sahiwal; P: Pearl*

Likewise, emulsion characteristics were determined by calculating emulsifying activity and emulsion stability of zein. The maximum value for both emulsifying activity and emulsion stability was observed in zein extracted from the Agaiti-2002 variety. The present findings are in accordance with Xue et al. who found emulsifying activity of zein 32.83% and emulsion stability 23.26% (5).

Zein also exhibited excellent antioxidant potential, and DPPH and FRAP tests were used to determine the free radical scavenging ability and total antioxidant capacity. The results revealed that the maximum value (32.61%) of DPPH was observed in zein extracted from the Agaiti-2002 variety while the minimum (30%) was observed in the Pearl variety (Fig. 3). The outcome of the present study was in accordance with previous findings in which DPPH value up to 31.5% was observed (11). A little antioxidant capacity of zein was observed up to 25% DPPH which was reduced after 24 hours (11). Values obtained for FRAP are shown in Fig 3. The maximum value was observed in zein extracted from Agaiti-2002 and the minimum value was observed in the Pearl variety of maize, and the values ranged between 0.12 to 0.13 µmol, respectively.

DISCUSSION

Zein is alcohol-soluble maize protein dissolved in 70–80% aqueous ethanol solution before dispersion to precipitate as nanoparticles. It forms tough, glossy, hydrophobic and greaseproof coatings that are resistant to microbial attack. Due to these excellent flexibility and compressibility properties, there has been substantial interest of

commercial processors since its discovery. It is a completely natural, biodegradable and food grade source for production of useful colloidal structures. The grain size and thousand kernels weights are affected significantly in different maize varieties, the main reason for this being the difference in genetic background, agronomic and natural conditions. It was noticeable from the present results that varietal difference was one of the main factors which contributed to the overall characteristics. Mineral contents of different maize varieties indicated that sodium and magnesium were found significant as compared to phosphorus and potassium and the major factors affecting the mineral conformation of maize includes type of cultivar, soil, application of fertilizers and climate. It was also observed that zein protein extraction rate was directly proportional to the concentration of ethanol. Similarly, foaming is an important parameter, and high foam stability is provided by proteins because of their hydrophobic nature. This is due to the conformational rearrangements that permit quick adsorption at air/water interface which results in development of flexible adsorbed layer (12). Zein exhibited good foaming stability due to its hydrophobic nature. Emulsion characteristics of proteins are dependent on the interface of oil and water, while the destabilization process is opposed by structural, mechanical and electrostatic energy barriers which are produced by the interfacial layer (4). Zein proteins presented little difference among varieties regarding antioxidant potential (6). With the growing realization of the uniqueness of zein as an industrial polymer, there are more potential commercial ventures to explore in the future.

REFERENCES

1. Zhang, B, Luo, Y, Wang, Q. Effect of acid and base treatments on structural, rheological, and antioxidant properties of a-zein. Food Chem 2011; 124:210-20.
2. Shukla R, Cheryan M. Zein: the industrial protein from corn. Indus. Crops and Prod 2001; 13:171-92.
3. Lawton JW. Zein: a history of processing and use. Cereal Chem 2002; 79:1-18.
4. Vega-Rojas LJ, Padilla MC, Londono NR, Lopez AR, Garcia RML, Rojas NP, Vollbrecht E, Sigmon B. Amazing grass: developmental genetics of maize domestication. Biochem Soc Transact 2005; 33**:**1502-6.
5. Xue F, Li C, Liu Y, Zhu X, Pan S, Wang L. Encapsulation of tomato oleoresin with zein prepared from corn gluten meal. J Food Eng 2013; 119:439-45.
6. Li KK, Yin SW, Yin YC, Tang CH, Yang XQ, Hong S. Preparation of water-soluble antimicrobial zein nanoparticles by a modified anti solvent approach and their characterization. J Food Eng 2013; 119:343-52.
7. Sandhu KS, Singh N, Malhi NS. Some properties of corn grains and their flours: Physicochemical, functional and chapatti-making properties of flours. Food Chem 2007; 101:938-46.
8. Ullah I, Ali M, Farooqi A. Chemical and nutritional properties of some maize (*Zea mays* L.) varieties grown in NWFP, Pakistan. Pak J Nutrition 2010; 9:1113-17.
9. Shah HU, Thomas J, Simpson, Alam S, Khattak KF, Perveen S. Mold incidence and mycotoxin contamination in maize kernels from Swat Valley, North West Frontier Province of Pakistan. Food Chem Toxic 2010; 48:1111-16.
10. Wang Q, Yin L, Padua GW. Effect of hydrophilic and lipophilic compounds on zein microstructures. Food Biophysic 2008; 3:174-81.
11. Wu Y, Luo Y, Wang Q. Antioxidant and antimicrobial properties of essential oils encapsulated in zein nanoparticles prepared by liquid-liquid dispersion method. LWT-Food Sci Technol 2012; 48:283-90.
12. Foegeding, EA, Luck PJ, Davis JP. Factors determining physical properties of protein foams. Food Hydrocolloids 2006; 20:284.

LETTER TO THE EDITOR

THE ROLE OF COLOR DOPPLER CARDIAC OUTPUT INDEX IN THE CLASSIFICATION OF HEART DISEASE

F. LI[1], J. XU[2] and W. LI[1]

[1]CT Department, Xinxiang Central Hospital, Xinxiang, Henan Province, China; [2]Ultrasonic Department, Xinxiang Central Hospital, Xinxiang, Henan Province, China

Received June 24, 2017 – Accepted April 23, 2018

This study aims to investigate the relationship between the value of cardiac output index (COI) and pathological Gleason score of heart disease by color Doppler. The dynamic contrast-enhanced color Doppler data of 312 patients with heart disease were collected. Multi-parameter oxygen concentration images based on color Doppler were used to detect the COI of heart disease. Multi spin relaxation time editing sequence and weak diffusion model were used to estimate the oxygen saturation level and pO2. The biological behavior and prognosis of the patients were determined according to the haematoxylin and eosin staining of the cardiac pathological tissues and Gleason score, and the relationship between the COI and Gleason score level of heart disease was evaluated. Of the 312 patients, 28 cases had a Gleason score 10, 112 had score 9, 56 had score 8, and 116 had score ≤ 7. According to the degree of differentiation, they were divided into middle-high differentiation group (Gleason scores ≤ 7) and low differentiation group (Gleason scores 8-10). Multi-parameter oxygen concentration images based on color Doppler were successfully built, the COI was measured, and the Gleason scores and classification for the patients were made. There was a positive correlation between the value of COI and Gleason score (r_s=0.349, P<0.05). There was significant difference in the value of COI between the middle-high differentiation group and the low differentiation group (P<0.05). In conclusion, the value of COI is positively associated with Gleason score; COI values may be used to evaluate the classification of heart disease and the prognosis of patients.

To the Editor,

Treatment options for heart disease are often based on the classification (1). Currently, Gleason classification is the most widely used method for evaluation of a heart attack (2). Ultrasound combined with heart biopsy can not only diagnose heart disease, but can also be used for pathological grading. However, the utility of ultrasonic combined with Gleason classification in the diagnosis and prognosis evaluation of heart disease remains to be further explored.

Color Doppler has been widely used in the diagnosis and classification of heart diseases (3). Previous studies have shown that color Doppler can detect the distribution of contrast agents in different tissues and organs by adding a contrast agent in the body, which can not only distinguish between heart disease and benign heart disease, but can also open up an important non-invasive method for diagnosis (4). However, the contrast

Key words: heart disease, nuclear magnetic resonance, cardiac output index values, Gleason score

Mailing address:
Dr Feng Li,
CT Department, Xinxiang Central Hospital,
No. 56 Jinsui Avenue, Weibin District,
Xinxiang 453000, Henan Province, China
Tel.: +86 0373 2048907
e-mail: lifenglf6@163.com

0393-974X (2018)
Copyright © by BIOLIFE, s.a.s.
This publication and/or article is for individual use only and may not be further reproduced without written permission from the copyright holder.
Unauthorized reproduction may result in financial and other penalties
DISCLOSURE: ALL AUTHORS REPORT NO CONFLICTS OF INTEREST RELEVANT TO THIS ARTICLE.

agent often causes a variety of complications, such as sepsis, infection, etc. A better noninvasive way without complications is therefore urgently need needed.

Currently, color Doppler combined with cardiac output index (COI) value has been used in detecting heart disease and its pathology classification. However, its utility has not been well established. In this study, we aim to evaluate the classification of heart disease and prognosis of patients by using color Doppler combined with COI value, and measure the COI value by color Doppler dynamic scanning around the heart, as well as its correlation with Gleason score.

MATERIALS AND METHODS

Study subjects

Color Doppler dynamic contrast-enhanced data of 312 patients (aged 43-81 years; mean age 0.3±7.2 years) with heart disease, diagnosed in our hospital from August 2013 to August 2015 were enrolled in the study. All subjects gave informed consent to participate in the study.

Inclusion criteria: (i) definitive diagnosis with complete clinical data; (ii) underwent Color Doppler enhanced scanning with full scan data; (iii) no surgical treatment, hormone therapy or radiation therapy, and chemotherapy before color Doppler scanning; (iv) The interval between the color Doppler scanning and surgery was no more than 30 days. Exclusion criteria: (i) clinical data was not complete; (ii) scan data was not complete; (iii) had undergone surgical treatment, hormone therapy or radiation therapy, and chemotherapy before color Doppler scanning; (iv) The interval between the color Doppler scanning and surgery was more than 30 days.

Color Doppler

Color Doppler scanning was performed in accordance with the conventional method (5). GE 1.5T and 5.0T Signa Twin Speed scanner and phased array coils with 16 channels were used for color Doppler scanning. Bandage fixed scanning coil was also used in order to reduce the influence of respiration on the results. The scanning process of color Doppler enhanced scanning in the local area of the heart were as previously reported (6).

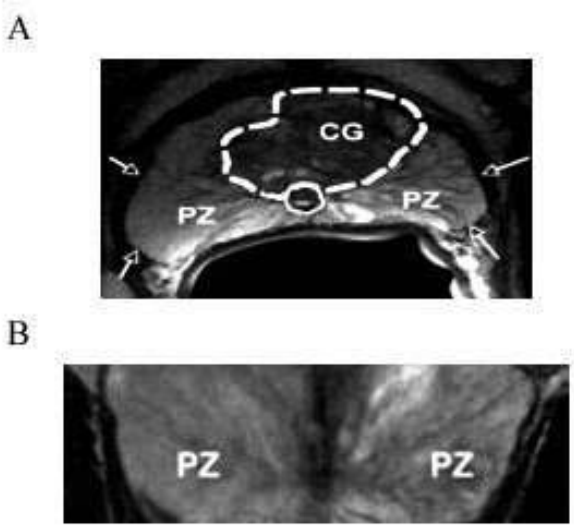

Fig. 1. *Images of a 60-year-old healthy male volunteer. **A**) An axial T2 weighted image (the heart cross-section) showed high signal intensity in the peripheral zone (PZ). But the signal intensity of central gland (CG, dashed line) was lower than the peripheral zone. A clear heart sac was observed (as shown by the arrow). **B**) Coronary T2W images through the heart. Around the peripheral zone, there were urethral distal and ejaculatory product. Seminal vesicle (SV) was a tubular structure with high signal strength and fluid filled.*

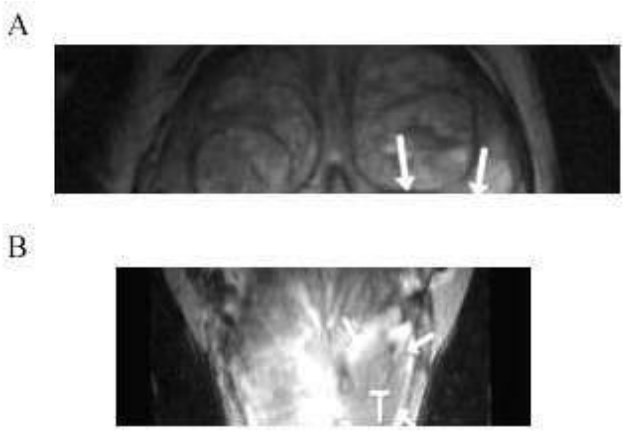

Fig. 2. *Images of a 60-year-old male patient with heart disease. Peripheral zone showed color Doppler scan images of heart disease in stage T3. T2 weighted (**A**) axial images and coronal image (**B**) showed that the peripheral area of the left side was the heart cross-section and the signal strength of heart disease was lower (arrow). Heart disease nodules produced swelling and irregular capsules, which indicated that the patient was at a stage of penetration.*

Heart biopsy

According to the conventional methods (7), the heart biopsy was performed under the guidance of rectal ultrasound. The samples fixed in formaldehyde were then used for HE staining (8), the results were evaluated with Gleason score system.

Color Doppler scanning image analysis

Color Doppler scanning images or enhanced scanning images were analyzed by a COI computing system developed by the Academy for Advanced Interdisciplinary Studies of Peking University. The running environment of software was MATLAB R2009a. All the DCE-color Doppler materials and data were input into this system (9). According to the puncture results of pathology of the heart, COI value was measured in the target area. Furthermore, according to this computer software, the mean value of COI in the selected area, color of COI value of ROI heart disease, gray-time curve in selected area, mean Kep value and the time-concentration curve of contrast agent for the control vessels were calculated and measured.

Statistical analysis

All the statistical analyses in this study were performed with SPSS 16 software. The numerical variables were expressed as mean ± standard deviation. One-way ANOVA was used for the comparison of COI value among different groups. Spearman correlation analysis was used for analyzing the correlation between Gleason score and the value of COI. $P \leq 0.05$ was considered as statistically significant.

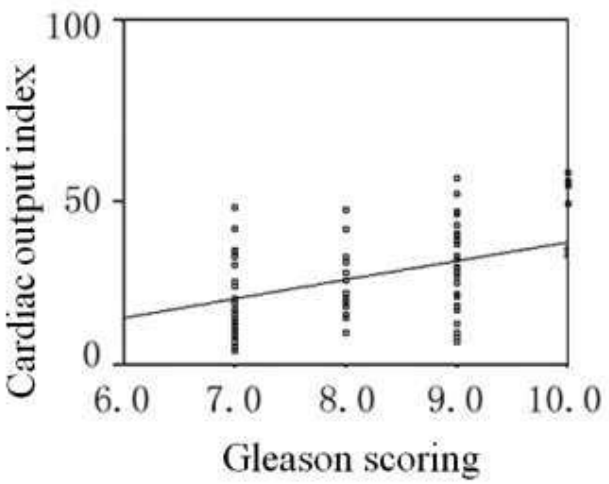

Fig. 3. *The comparison results of cardiac output index value of heart disease patients with color Doppler scanning in different Gleason scoring groups.*

Table I. *Color Doppler cardiac output index value.*

Gleason score	PICCO cardiac output index value
≤ 7	1.02±0.16 × 10(-3) mm(2)
8	0.86±0.05 × 10(-3) mm(2)
9	0.63±0.17 × 10(-3) mm(2)
10	0.43±0.04 × 10(-3) mm(2)

RESULTS

Pathological results of heart disease biopsy

According to the Gleason scoring system, 28 cases had a score of 10, 112 cases had 9, 56 cases had 8, and 116 cases had a score ≤ 7. According to the degree of differentiation, they can be divided into a middle-high differentiation group (Gleason scores ≤ 7) including 116 cases and a low differentiation group (Gleason scores 8-10) including 196 cases.

With the gradual increase of Gleason score the value of COI also demonstrated an increasing trend. Among the 4 different Gleason score groups, the value of the COI had obvious overlap. The difference was significant in the value of the COI among different Gleason score groups (F=2.928, P<0.05). There was significant difference in the values of the COI between the group with Gleason score ≤ 7 and the group with Gleason score of 9-10 (P<0.05). However, there was no significant difference in other comparisons (all P<0.05) (Fig. 3).

Diagnostic accuracy of COI value of heart disease patients adopting color Doppler

The diagnostic accuracy of COI value of heart disease patients adopting color Doppler are as follows: The

accuracy rate of color Doppler COI value which Gleason score was ≤ 7, 8, 9 and 10 were 91/116 (78.5%), 47/56 (83.9%), 98/116 (87.5%) and 22/28 (78.6%), respectively. The accuracy was closely to 80%, and the average accuracy rate was 82.3%. Table I shows the concrete values of the color Doppler COI value, which suggest that the color Doppler COI value may be a potential indicator of heart disease.

Analysis of the correlation between the COI value with color Doppler dynamic enhanced scanning and the Gleason score

The results showed that there was significant correlation between the COI value in cardiac ward and the Gleason score (r_s = 0.342, P<0.05).

DISCUSSION

Gleason classification has now become the first choice for evaluation of the heart attack. However, this method requires biopsy. Although color Doppler is widely used in the detection, location and evaluation of prognosis of heart disease, the introduction of the contrast agents often causse a variety of clinical complications, such as sepsis, and infection, (10). Therefore, there is an urgent need for more effective and less toxic side effect methods for heart disease diagnosis and classification.

In the present study, based on the low oxygen environment of the heart disease micro-environment, we diagnosed and graded heart disease by color Doppler from the point of COI. We successfully established a multi-parameter oxygen concentration image based on color Doppler, measured the COI of heart disease, and found a positive correlation between the COI value and the Gleason score. Our results suggest that the COI value may be used to evaluate the classification of heart disease and the prognosis of patients.

Previous study (11) has shown that the use of color Doppler can quantitatively determine the ADC value. Further study showed that the ADC value has negative correlation with the Gleason score, which suggests that we can determine the value of ADC to evaluate the classification of heart disease and the prognosis of patients. This is consistent with the results of the current study. There are also some reports that a positive correlation exists between Gleason score and heart disease. In addition, there was a significant positive correlation between the Gleason score and the ratio of Cho+Cr/Cit in the cardiac ward measured by color Doppler, which further supports the viewpoint of our study.

In conclusion, this study shows that there is a positive correlation between the Gleason score and the COI value for cardiac subjects, therefore COI values may be used to evaluate the classification of heart disease and the prognosis of patients.

REFERENCES

1. Hansson EM, Lendahl U. Regenerative medicine for the treatment of heart disease. J Intern Med 2013; 273(3):235-45.
2. Egevad L, Samaratunga H, Srigley JR, Delahunt B. New Gleason grading system: Statement from the editors of 6 journals. Urol Oncol 2016; 34(11):479-80.
3. Sandor GG. Echocardiographic tests of left ventricular function in pediatric cardiology: are we searching for the Holy Grail? Can J Cardiol 2016; 32(10):1186-92.
4. Zhao Y, Ji L, Liu J, et al. Intensity of left atrial spontaneous echo contrast as a correlate for stroke risk stratification in patients with nonvalvular atrial fibrillation. Sci Rep 2016; 6:27650.
5. Gerster JC, Landry M, Dufresne L, Meuwly JY. Imaging of tophaceous gout: computed tomography provides specific images compared with magnetic resonance imaging and ultrasonography. Ann Rheum Dis 2002; 61(1):52-54.
6. Okuda S, Kikinis R, Geva T, Chung T, Dumanil H, Powell AJ. 3D-shaded surface rendering of gadolinium-enhanced MR angiography in congenital heart disease. Pediatr Radiol 2000; 30(8):540-45.
7. Yu CM, Sanderson JE, Marwick TH, Oh JK. Tissue Doppler imaging a new prognosticator for cardiovascular diseases. J Am Coll Cardiol 2007; 49(19):1903-14.
8. Taylor DO, Edwards LB, Aurora P, et al. Registry of the International Society for Heart and Lung Transplantation: twenty-fifth official adult heart transplant report--2008. J Heart Lung Transplant 2008; 27(9):943-56.

9. Dagvasumberel M1, Shimabukuro M, Nishiuchi T, et al. Gender disparities in the association between epicardial adipose tissue volume and coronary atherosclerosis: a 3-dimensional cardiac computed tomography imaging study in Japanese subjects. Cardiovasc Diabetol 2012; 11:106.
10. Seo WK, Choi CW, Kim CK, Oh K. Contrast-enhanced color-coded Doppler sonography in Moyamoya disease: a retrospective study. Ultrasound Med Biol 2018; 44(6):1281-85.
11. Zhu FP, Luo S, Wang ZJ, Jin ZY, Zhang LJ, Lu GM. Takayasu arteritis: imaging spectrum at multidetector CT angiography. Br J Radiol 2012; 85(1020):e1282-92.

LETTER TO THE EDITOR

A CASE OF METASTATIC CUTANEOUS MELANOMA TO THE LIVER

Y. CHEN[1], S. YU[2], H. LI[3], J.H. YANG[2]* and C.Y. E[2]*

[1]Department of Hepatobiliary and Pancreas Surgery, The Second Hospital of Jilin University, Changchun, China; [2]Department of Neurology, China-Japan Union Hospital of Jilin University, Changchun, Jilin, P.R. China, Changchun, China; [3]Department of Cerebral Surgery, Jilin Cancer Hospital, Changchun, Jilin, China

Received March 6, 2018 – Accepted April 19, 2018

*These Authors contributed equally to this study

Cutaneous melanoma (CM) with liver lesions is uncommon in Asia and found in only 14-20% of all cases. Here, we report the case of a 70-year-old male patient with cutaneous melanoma with metastases to the liver. Computerized tomography (CT) revealed multiple hepatic cystic lesions, and hepatic puncture biopsy was used for definitive diagnostics. The primary lesion was found on the patient's scalp. We briefly reviewed the literature to summarize the recent progress in diagnosis and treatment of metastatic cutaneous melanoma. Examination of pathology data is still considered the gold standard of diagnosis, while imaging is used to detect metastases, assess the stage of disease and monitor the patients. Metastasectomy, whenever possible, may benefit most patients. Systemic therapies remain the mainstay of the treatment, with some important breakthroughs reported in the recent years. New treatments, such as adult-to-adult living donor liver transplantation, are still in the early stages.

To the Editor,

Here we report the case of a 70-year-old man who was admitted to the Department of Hepatobiliary and Pancreatic Surgery of China-Japan Union Hospital (Jilin University, Changchun, Jilin Province, China) in December 2014 complaining of abdominal distension and pain lasting for about 3 weeks. Written consent for publication of this case was obtained from the patient. Abdominal ultrasound examination in a local hospital revealed multiple hepatic cysts. Physical examination showed that the liver was palpable 7 cm below the xiphoid with tenderness of the right upper quadrant. The spleen was not palpable. Liver function tests demonstrated the elevated levels of aspartate aminotransferase (AST) (115.6 U/L, normal range < 40 U/L), alanine aminotransferase (ALT) (85.5 U/L, normal range < 40 U/L), lactate dehydrogenase (LDH) (1423 U/L, normal range < 248 U/L), and γ-glutamyltransferase (γ-GTP) (1301 U/L, normal range < 57 U/L). Serum tumor markers of alpha-fetoprotein (AFP), carcinoembryonic antigen (CEA) and cancer antigen 199 (CA199) were all normal, but cancer antigen 125 (CA125) was elevated (120.80 U/mL, normal range < 35 U/mL). Other laboratory tests, including those for hepatitis B surface antigen (HBsAg) and anti-hepatitis C virus (HCV) antibody, were normal. CT scans revealed multiple hepatic cystic lesions

Key words: cutaneous melanoma, liver metastasis, tumor of liver, diagnosis, physical examination

Mailing address:
Dr. Changyong E,
Department of Hepatobiliary and Pancreatic Surgery,
China-Japan Union Hospital, Jilin University,
No. 126 of Xiantai Street, Changchun, Jilin
130021, P.R. China
e-mail: echangyong@yahoo.com

0393-974X (2018)
Copyright © by BIOLIFE, s.a.s.
This publication and/or article is for individual use only and may not be further reproduced without written permission from the copyright holder.
Unauthorized reproduction may result in financial and other penalties
DISCLOSURE: ALL AUTHORS REPORT NO CONFLICTS OF INTEREST RELEVANT TO THIS ARTICLE.

with uneven density, ill-defined margins, and rim enhancement the cystic walls of which displayed nodular or speckled enhancement (Fig. 1). We used hepatic puncture biopsy guided by ultrasound to get a definite diagnosis. Immunohistochemical stainingsfor Melan-A, HMB45, andS-100 were positive (Fig. 2), which suggested a serious possibility of metastatic melanoma to the liver. Finally, we found the primary lesion at the patient's scalp. Unfortunately, the patient refused further treatment and left the hospital after remission of symptoms. Later we learned that he died soon after.

DISCUSSION

As in the case presented here, patients often see their doctors with abdominal symptoms caused by occult primary lesions. Clinical signs and symptoms on physical examinations are often nonspecific, so imaging plays an important role in the diagnosis. When melanoma is confirmed, imaging is typically used to detect metastases, evaluate clinical stage and monitor the progress of the disease (1, 2). Due to its documented high sensitivity in the detection of skin and lymph node metastases, MRI has been proposed as the standard imaging modality for staging high-risk patients (3). The use of MRI is often considered because this method avoids exposure to radiation. It is, however, more expensive and does not allow the coverage in the same timely manner as CT (4). For this reason, the use of single portal venous phase imaging by CT is advocated for staging and routine surveillance of patients with metastatic CM. Dual phase CT increases radiation dose without significant diagnostic benefits. MRI is also useful when the diagnosis of hepatic metastatic disease by CT is inconclusive, as MRI could detect additional extrahepatic metastases (5).

The diagnosis of our patient was mainly confirmed by pathologic results. However, melanoma has a wide spectrum of histological features that mimic epithelial, hematologic, mesenchymal and neural tumors (6). Fine-needle aspiration (FNA) biopsy is the first-line diagnostic option in patients with a mass clinically suspicious for metastatic melanoma. We used this

Fig. 1. *CT scans revealing multiple hepatic cystic lesions with uneven density, ill-defined margins, and rim enhancement the cystic walls of which displayed nodular or speckled enhancement.*

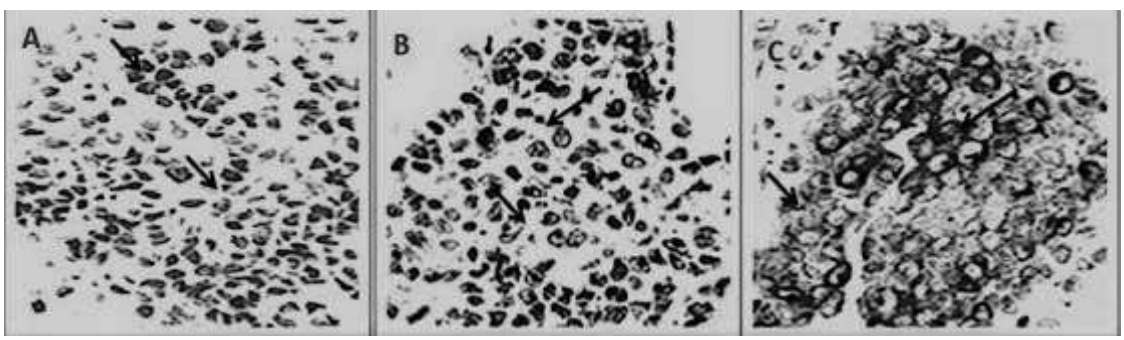

Fig. 2. *Immunohistochemical staining showing positive reaction to Melan-A, HMB45, and S-100:* ***A****) subcellular fraction for Melan-A;* ***B****) membranous and cytoplasmic fractions for HMB45;* ***C****) nucleus and cytoplasmic fractions for S100.*

technique to confirm the diagnosis in our case. FNA provides several advantages over other pathological methods. These advantages include low cost of procedure, minimal risk of harm to the patient, and rapid turnaround time (7).

Currently, surgery seems to be the only way to successfully treat melanoma with liver metastases, even though this approach remains controversial. Theoretically, liver metastases signify systemic disease involvement. No randomized controlled studies have been performed to date to explicitly demonstrate the benefits of surgery. Only 2-7% of patients with liver metastases from melanoma are offered surgery (8). It is important to set the standards for selecting patients who can gain benefits from surgery, as most of them are not considered suitable for surgical treatment. For these patients, systemic therapy or localised therapy are the available alternatives.

At present, the main approach to the treatment of malignant melanoma is systemic therapy which include chemotherapy, with single agents such as dacarbazine (DTIC), temozolomide and fotemustine; combination therapies such as CVD (cisplatin, vinblastine and DTIC), CVD in combination with IL-2 and IFN-α, and immunotherapy using cytokines (IL-2, IFN-α), immune checkpoint inhibitors such as CTLA-4 blocking agents (ipilimumab) and PD-1 blocking agents (pembrolizumab, nivolumab). In addition, tumor-targeted therapeutics such as BRAF inhibitors (vemurafenib, dabrafenib) and MEK inhibitors (trametinib) can be used.

The common methods of localised therapy include hepatic arterial infusions (HIA), chemoembolization, and isolated or percutaneous hepatic perfusions. Fotemustine and melphalan are the most common agents for HIA and hepatic perfusions, respectively. Although melanoma is generally considered a relatively radio-resistant tumor (9), the applications of radiotherapy for treating melanoma continue to be investigated. Stereotactic radio-surgery and stereotactic body RT have been confirmed to be effective in patients with non-resectable local recurrent or metastatic disease that produces bone pain, epidural spinal cord compression, and central nervous system dysfunction (10).

In conclusion, we present here a case of CM with metastases to the liver, as very few cases of this kind have been previously reported in Asia. The disease is not difficult to confirm by imaging and pathologic methods, but early detection still remains a problem. Liver resection may benefit most patients whenever possible, while systemic therapy remains the most common approach to the treatment of this condition.

REFERENCES

1. Trotter SC, Sroa N, Winkelmann RR, Olencki T, Bechtel M. A global review of melanoma follow-up guidelines. J Clin Aesthet Dermatol 2013; 6:18-26.
2. Hong H, Sun J, Cai W. Anatomical and molecular imaging of skin cancer. Clin Cosmet Investig Dermatol 2008; 1:1-17.
3. Ghanem N, Altehoefer C, Högerle S, et al. Detectability of liver metastases in malignant melanoma: prospective comparison of magnetic resonance imaging and positron emission tomography. Eur J Radiol 2005; 54:264-70.
4. Winkler N, Rezvani M, Heilbrun M, Shaaban A. Utility of dual phase liver CT for metastatic melanoma staging and surveillance. Eur J Radiol 2013; 82:2189-93.
5. Balasubramanya R, Selvarajan SK, Cox M, Joshi G, Deshmukh S, Mitchell DG, O'Kane P. Imaging of ocular melanoma metastasis. Br J Radiol 2016; 89:20160092.
6. Ohsie SJ, Sarantopoulos GP, Cochran AJ, Binder SW. Immunohistochemical characteristics of melanoma. J Cutan Pathol 2008; 35:433-44.
7. Murali R, Thompson JF, Uren RF, Scolyer RA. Fine-needle biopsy of metastatic melanoma: clinical use and new applications. Lancet Oncol 2010; 11:391-400.
8. Agarwala SS, Eggermont AM, O'Day S, Zager JS. Metastatic melanoma to the liver: a contemporary and comprehensive review of surgical, systemic, and regional therapeutic options. Cancer 2014;120:781-89.
9. Strojan P. Role of radiotherapy in melanoma management. Radiol Oncol 2010; 44:1-12.
10. Mahadevan A, Patel VL, Dagoglu N. radiation therapy in the management of malignant melanoma. Oncology 2015; 29:743-51.

LETTER TO THE EDITOR

POLYMORPHISM OF THE ANDROGEN RECEPTOR GENE CAG REPEAT SEQUENCE AND MALE CLIMACTERIC SYNDROME

ZL. HONG, Q. XU, YF. MAO, YZ. YE, JG. MAO, MF. WAN and MY. JIANG

Department of Urinary Surgery, The First People's Hospital of Tonglu, Tonglu, Zhejiang Province, China

Received March 29, 2018 – Accepted May 3, 2018

The aim of this study was to analyze the association between polymorphism of the androgen receptor (AR) gene CAG repeat sequence and the climacteric syndrome in men. The study was performed in 103 males with climacteric syndrome and 111 males without the clinical syndrome of climacteric, aged between 40 and 70 years. DNA sequencing of the CAG repeat sequence in the N-terminal domain of the first exon of the AR gene was analyzed. The AR allele length ranged from 18-34 CAG repeats in males with climacteric syndrome. The average value of CAG repeat was 24.71 ± 2.58. However, the corresponding values ranged from 15-24 CAG repeat in control group and the average value of CAG repeat was 21.25±2.63. There was a significant difference of the number of CAG repeat between the two groups. The occurrence of male climacteric syndrome was related to the CAG repeat number of androgen receptor gene, and the male patients with more CAG repeats had higher risk of clinical syndrome of climacteric. The detection of CAG repeat number of AR gene might be helpful for the prediction of clinical syndrome of climacteric.

To the Editor,

Male climacteric syndrome (MCS) is a common health problem in males of middle and old age all over the world. With the coming of the aging society, it has attracted more and more attention in recent years. MCS characteristics include different types of neurological dysfunction, depression, memory loss, lack of concentration, fatigue, insomnia, sweating and sexual dysfunction which seriously affect the quality of life of patients (1). Usually, MCS has a long incubation period before symptoms appear. Therefore, early detection and early intervention therapy can effectively reduce its incidence and severity. Testosterone replacement therapies have been tried, but hepatic adverse effects limit its administration, especially if there are liver diseases such as hepatitis or non-alcoholic fatty liver (2). The diversity of the clinical symptoms limits the development of diagnostic methods, and current approaches are too expensive and difficult to apply in large-scale screening (3). Therefore, it is essential to find specific biomarkers for early diagnosis.

Androgen receptor (AR) is a steroid receptor, a member of the nuclear receptor superfamily, which mediates many cellular processes, including cell proliferation, differentiation and apoptosis. The encoding gene is located at Xq11-12, with a total length of approximately 90 KB, containing 8 exons and 7 introns. The first exon of AR gene contains polymorphic structures, in which poly (CAG) n trinucleotide sequence and transcriptional activation of AR are related. It has been found that AR gene

Key words: male climacteric syndrome, androgen receptor gene, CAG repeat, polymorphism

Mailing address:
Dr Mingyou Jiang,
Department of Urinary Surgery,
The First People's Hospital of Tonglu,
No.338 Xuesheng Road, Tonglu county 311500,
Hangzhou City, Zhejiang Province, China.
e-mail: jiangmingyouus@163.com

0393-974X (2018)
Copyright © by BIOLIFE, s.a.s.
This publication and/or article is for individual use only and may not be further reproduced without written permission from the copyright holder.
Unauthorized reproduction may result in financial and other penalties
DISCLOSURE: ALL AUTHORS REPORT NO CONFLICTS OF INTEREST RELEVANT TO THIS ARTICLE.

(CAG) n repeat sequence mutations are related to diseases, including including prostate cancer, breast cancer, bladder cancer, acne, male infertility, male patients with acute myocardial infarction, rheumatoid arthritis, coronary heart disease and late-onset hypogonadism (LOH), which reflects the AR wide (4-6) biological effect. This study explores the correlation of polymorphisms in AR gene (CAG) n repeat sequence with MCS e clinical relations, enriching the understanding of gene polymorphism and clinical syndrome.

MATERIALS AND METHODS

Patients

A total of 214 men, aged 40-70 years were randomly selected from local communities. One hundred three male climacteric clinical group patients were selected from male outpatients for urinary concerns and other male outpatients. The exclusion criteria included: patients with prostate cancer, breast cancer, bladder cancer, acne, male infertility, male acute myocardial infarction, rheumatoid arthritis, coronary heart disease and delayed hypogonadism. These patients were divided into an experimental group of 103 cases aged 40-70 years (average 55.3±9.6 years), and a control group of 111 cases aged 40-69 years (average 54.1±9.3 years). The study was approved by the Ethics Committee of the The First People's Hospital of Tonglu and all the patients included in the study signed an inform consent to participate in the study.

Patient grouping

The use of "MCS questionnaire" rating scale (including physical symptoms, vasomotor symptoms, physical and mental symptoms and sexual dysfunction symptoms analysis; see Table I), is combined with the "Self-assessment of MCS" (Table II) for the screening of community survey, to determine males with clinical symptoms of climacteric syndrome. If the total physical symptoms with vasomotor symptoms is more than 5, or the psychological symptoms scores more than 4, or the sexual dysfunction symptom score is greater than 8, it is classified with male climacteric clinical syndrome. If there were 4 or more than 4 points in the self-assessment table, it was also classified in the MCS group. According to the above criteria, subjects in the climacteric clinical syndrome group were included in the clinical syndrome group, and the others in the control group. There was no kinship between the selected people and no difference between age.

Sample collection

After 12 h fasting, 4 mL blood samples were taken from the elbow vein at 7:30~8:30 a.m. The time of blood collection was chosen because the concentrations of testosterone are maximum in the morning. EDTA was used for anticoagulation and blood samples were stored at -80C° until analysis of AR gene (CAG) n repeat number.

Detection of AR gene (CAG) n repeat sequence

Genomic DNA Extraction Kit from Hangzhou Jian Biologic Technology Co., Ltd. was used to extract genomic DNA from the blood samples. PCR was used to amplify the amino terminal transcriptional regulatory region 700 bp fragment of the AR gene exon 1, the upstream primer was F:5 -CAGTTAGGGCTGGGAAGGGTCTA-3', and the downstream primer was R:5 'TGGCGTTGTCAGAAATGGTCGAA-3'. The PCR reaction volume was 20 μL: including genomic DNA 10 ng, 10 x buffer (including $MgCl_2$) 2 μL, 10mmol/L dNTP 1.6 μL, upstream and downstream primers each is 0.8 μL, Taq Pfu DNA 0.5 μL, adding sterilized deionized water to 20 μL. PCR amplification reaction program: 94°C predenaturation for 4 min, 94°C denaturation for 30 s, 60°C annealing for 30 s, 72°C extension for 45 s, 32 cycles, 72°C extension for 10 min. The PCR product of 2 μL was used and separation in 1% agarose gel by ethidium bromide staining, 30 min electrophoresis was performed under 80 voltage. The results were observed under ultraviolet light and the system was imaged by 2500 gels. The PCR products were recovered by Biotechnology (Shanghai) Co., Ltd. for Sanger sequencing reaction of all PCR recovered fragments. The sequencing primers were 5 CTCAGGATGTCTTTAAGGTCAGCG-3', the sequencing machine used was ABI3730XL. After the sequencing of PCR amplification products was completed, the results were analyzed by blind method, which was read by more than two professional molecular biology professionals to determine the number of CAG repeats.

Statistical analysis

Data were collected in the Excel database. SPSS 13 software was used for statistical analysis. The

Table I. *Male climacteric syndrome questionnaire.*

Name _____ Age__ Contact_____Address_____

Physical condition				
	Lethargic	Insomnic	Lack of appetite	Bone and joint pain
Highly frequently (3 points)				
Always (3 points)				
Occurs at times (1 point)				
Never (0 zero)				
Total points				
Vasomotoricity				
	Hectic fever	Night sweat	Palpitation	Forgetfulness
Highly frequently (3 points)				
Always (3 points)				
Occurs at times (1 point)				
Never (0 zero)				
Total point				
Psychological condition				
	Attention deficit	A sense of fear	Become jumpy	Lost interest in things used to like
Highly frequently (3 points)				
Always (3 points)				
Occurs at times (1 point)				
Never (0 zero)				
Total point				

Sexual dysfunction					
	Lost desire for sex	Get no feeling at all	No more erection in the morning	Failed when attempted	Failed to erect at sexual intercourse
Highly frequently (3 points)					
Always (3 points)					
Occurs at times (1 point)					
Never (0 zero)					
Total point					

Table II. *Self-assessment of male climacteric syndrome.*

Have the following related symptoms appeared during last year	Yes (√) No (×)
Myopic lens does not help in reading anymore and it is easier to read without. This is a sign of aging	
Eye fatigue, suffer from headache and dizziness after reading	
Less sleep than previously, start to keep early hours	
Drink less	
Hearing loss	
Teeth get loose and have to shut hard to bite food. People who have dentures need to change them frequently	
A change of in the taste of food: like to eat sweet, sour, spicy, salty and other heavy flavors, indicating a decline in taste	
Weakness for snacks, especially confections, which is associated with a diminished taste.	
Diminished sexual desire	
Memory impairment	
Constantly haunted by childhood memories	
Performance in work and study is not as satisfying, even though you aspire for the better	

experimental data were tested by *t*-test with mean standard deviation, and the difference was considered significant if $p< 0.05$. In cases where $p> 0.05$, then it has no significant statistical significance. These methods were used to determine the difference between the experiment group and the control group.

RESULTS

Demographic analysis

The results of independent sample *t*-test showed that there was no statistical difference between the two groups ($t =-1.003$, $p=0.317$) regarding age and sex of the patient distribution.

Electrophoretic results of PCR products in the 1NH2 terminal transcriptional regulation area of the AR exon and sequencing results of 1.3 AR gene exon 1 (CAG) n repeat sequence

The first exon (CAG) n of AR microsatellite gene amplification result is shown in Fig. 1A. The PCR band is single and specific, and the size of the amplified fragment is about 700 BP, which is consistent with the expected molecular weight.

The results of reverse sequencing of the first exon (CAG) n of AR were analyzed by blind method. As depicted in Fig. 1, B and C, the (CAG) n sequence concentration, a strong sequencing signal produced a clear judgment of repetitive sequence.

Polymorphism analysis of 1.4 AR gene (CAG) n repeat sequence

In the control group with 111 cases, the shortest AR gene (CAG) n repeats was 15 and the longest was 24, the average length 21.25±2.63. In cases of MCS in the clinical group, the shortest AR gene (CAG) n repeats was 18, the longest was 34, the average length was 24.71±2.58. Using Fisher's Exact non-parametric test (CAG) n repeats for analysis, results showed that among the two groups (CAG) there were significant differences in the number of n repeats ($p=1.26402E-18$, $p<0.001$), the clinical syndrome of male climacteric group AR gene (CAG) n repeat number was significantly higher than the normal control group ($P < 0.001$) (Table III).

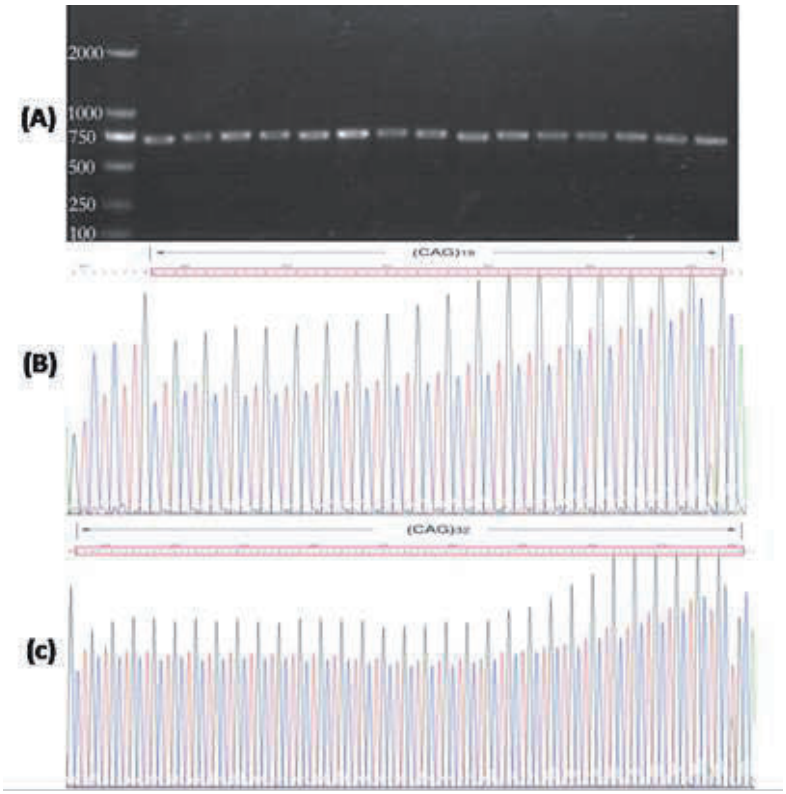

Fig. 1. ***A****)Electrophoresis results of PCR products of AR gene exon 1 CAG repeat sequences (incomplete data);* ***B****) AR gene NH2- end (CAG) 19 reverse sequencing peak map;* ***C****) AR gene NH2- end (CAG)32 reverse sequencing peak map.*

Table III. *Comparison of the number of AR gene (CAG) n repetitions in the male climacteric experimental group and the control group.*

	Control group (n=111)	Experiment group (n=103)
(CAG)n shortest	15	18
(CAG)n longest	24	34
(CAG)n average	21.25 ± 2.63	24.71±2.58
t-test	1.26402E-18	
p	0.0005	

DISCUSSION

Male climacteric is a transitional period from mature male into older age. Even if the majority of the men do not manifest clinical symptoms, in some cases the symptomatology is similar to the female climacteric group, which has adverse effects on multiple organ function, reducing the quality of life (7).

The current study showed that the minor regulation of AR transcriptional activity was negatively correlated with the length of the (CAG) n sequence. Previous studies have shown that the decrease of androgen levels may be the cause of clinical climacteric syndrome in middle-aged and old men (8). The biological effects of androgens are shown via the AR. Studies showed that the repeat length of AR gene exon in 1 N-terminal transcriptional regulatory region (CAG) is closely related with AR expression and transcriptional activity. The polymorphism of (CAG) n repeats of AR gene is closely related to elderly MCS (9, 10, 11). To our knowledge, this is the first study that uses DNA sequencing to study the relationship between the number of n repeats and clinical MCS. The results showed that in the 111 cases in the control group of male AR gene (CAG) the average length of n is 21.25±2.63, and 103 cases of the MCS group male AR gene (CAG) the average length of n is 24.71±2.58, compared with the normal male, MCS group AR gene (CAG) n repeat pole increased significantly. The transcriptional activity of AR and (CAG) n was negatively related to the length of the sequence, increasing the number of n repeats (CAG). The aging process can determine a decrease in AR level and sensitivity (12 and the specific mechanism needs to be further investigated.

In conclusion, there is a significant correlation between AR gene (CAG) n repeat polymorphism and the occurrence of male climacteric clinical syndromes, suggesting that it may be a new risk factor for male climacteric clinical syndromes.

ACKNOWLEDGEMENTS

This work was supported by Hangzhou Science and Technology Foundation of Zhejiang province (NO.20150633B77).

REFERENCES

1. Tirabassi G, Delli Muti N, Corona G, Maggi M, Balercia G. Androgen receptor gene CAG repeat polymorphism independently influences recovery of male sexual function after testosterone replacement therapy in postsurgical hypogonadotropic hypogonadism. J Sex Med 2014; 11(5):1302-8.
2. Brawer MK. Testosterone replacement in men with andropause: an overview. Rev Urol 2004; 6(Suppl 6):S9-S15.
3. Delli Muti N, Agarwal A, Buldreghini E, Gioia A, Lenzi A, Boscaro M, Balercia G. Have androgen receptor gene CAG and GGC repeat polymorphisms an effect on sperm motility in infertile men? Andrologia 2014; 46(5):564-69.
4. L'Eplattenier H, Teske E, Van Sluijs F, Mol JA. CAG-repeats in the androgen receptor gene relate with plasma androgen levels in the Bouvier Des Flandres. In Vivo 2014; 28(6):1051-55.
5. Francomano D, Greco EA, Lenzi A, Aversa A. CAG repeat testing of androgen receptor polymorphism: is this necessary for the best clinical management of hypogonadism? J Sex Med 2013; 10(10):2373-81.
6. Tirabassi G, Delli Muti N, Corona G, Maggi M, Balercia G. Androgen receptor gene CAG repeat polymorphism regulates the metabolic effects of testosterone replacement therapy in male postsurgical hypogonadotropic hypogonadism. Int J Endocrinol 2013; 2013:816740.
7. Delli Muti N, Agarwal A, Buldreghini E, Gioia A, Lenzi A, Boscaro M, Balercia G. Have androgen receptor gene CAG and GGC repeat polymorphisms an effect on sperm motility in infertile men? Andrologia 2014; 46(5):564-69.
8. Huang G, Shan W, Zeng L, Huang L. Androgen receptor gene CAG b repeat polymorphism and risk of isolated hypospadias: results from a meta-analysis. Genet Mol Res 2015; 14(1):1580-8.
9. Mosaad YM, Shahin D, Elkholy AA, Mosbah A, Badawy W. CAG repeat length in androgen receptor gene and male infertility in Egyptian patients. Andrologia 2012; 44(1):26-33.
10. Zhang C, Guo M, Pei L, et al. Polymorphisms of (CAG) n and(GGN)n repeats of androgen receptor gene among ethnic Hui and Han Chinese from Ningxia. Zhonghua

Yi Xue Yi Chuan Xue Za Zhi 2013; 30(3):365-69.

11. Sampson ER, Yeh SY, Chang HC, Tsai MY, Wang X, Ting HJ, Chang C. Identification and characterization of androgen receptor associated coregulators in prostate cancer cells. J Biol Regul Homeost Agents 2001; 15(2):123-29.
12. Kamilos MF, Borrelli CL. New therapeutic option in genitourinary syndrome of menopause: pilot study using microablative fractional radiofrequency. Einstein Sao Paulo 2017; 15(4):445-51.

LETTER TO THE EDITOR

DRUG-LOADED NANOBUBBLES FOR ULTRASOUND-MEDIATED ANTITUMOR TREATMENT

CF. LIU[1], J. ZHOU[2], XR. CHEN[2] and J. YU[3]

[1]Ultrasonic Department, The affiliated Hongqi Hospital of Mudanjiang Medical University, Mudanjiang, China; [2]Ultrasonic Department, The Second affiliated Hospital of Mudanjiang Medical University, Mudanjiang, China; [3]Outpatient Clinic, Affiliated Hongqi hospital of Mudanjiang Medical University, Mu Danjiang, China

Received February 25, 2018 – Accepted May 9, 2018

Polylactic acid (PLA) bubbles that can act both as ultrasound contrast agents and drug carriers have the disadvantage of low encapsulation efficiency and do not allow effective extravasation into the tumor tissue. In this regard, PLA and lecithin are considered drug carriers. The present study used a modified ultrasonic double emulsion-solvent evaporation technology in order to prepare paclitaxel-loaded PLA-lecithin nanobubbles. X-ray diffraction analysis (XRD) was used to investigate the state of the drug in the bubbles, whereas the tumor weight and the inhibition rate of tumor bearing mice in the ultrasound-mediated function were further examined. The results indicated that the nanobubbles prepared with a mass ratio of PLA and lecithin at 50:250 were characterized as inner hollow. The size of these particles was approximately 615 nm, and the drug loading and encapsulation reached 8.34±0.67% and 91.42±5.48%, respectively. Paclitaxel was distributed in the shell of the bubbles in an amorphous state, and the *in vitro* drug release was characterized by sustained release, zero release and ultrasound mediated drug release. The injection of H22 hematoma-bearing mice with ultrasound-mediated drug-loaded PLA-lecithin nano-scaled bubbles could reduce the toxicity and increase the antitumor efficacy compared with paclitaxel.

To the Editor,

Currently, ultrasound contrast agents exhibit potent contrast enhancement function and are widely used in gene therapy, drug delivery, thrombolytic therapy, cancer treatment and other fields (1). However, the ultrasound contrast agent exhibits limited drug release to the tumor target due to its low drug loading rate and larger particle size (2). The ultrasound contrast agent currently exists in the form of soft film bubbles packaged with high density inert gases (3). The average particle size of the bubbles is between 200 and 500 nm, which is less than that of red blood cells (4). The ultrasound contrast agent can pass through the pulmonary circulation freely, but not through the blood vessels (5). It is a blood pool imaging agent, which limits the diagnosis and treatment of extravascular diseases. The Nano-scaled contrast agent (ultrasound contrast agent with a diameter of less than 1000 nm) has a strong penetration force, compared to the conventional contrast agents (6). A previous study indicated that the vascular endothelial space of the diseased tissue (such as tumor tissue) expanded and could eventually allow the particles with diameter of less than 700 nm

Key words: ultrasound contrast agent, nano-scaled bubbles, poly lactic acid-lecithin, paclitaxel

Mailing address:
Dr Jing Yu,
Outpatient Clinic, Affiliated Hongqi Hospital
Mudanjiang Medical University,
Taiping Road No.1,MuDanjiang City,
Heilongjiang Province, China
e-mail: dr_yujingyj@163.com

0393-974X (2018)
Copyright © by BIOLIFE, s.a.s.
This publication and/or article is for individual use only and may not be further reproduced without written permission from the copyright holder.
Unauthorized reproduction may result in financial and other penalties
DISCLOSURE: ALL AUTHORS REPORT NO CONFLICTS OF INTEREST RELEVANT TO THIS ARTICLE.

to pass through (7).

In the present study, PLA and soybean lecithin were mixed with shell material for bubbles. We prepared paclitaxel-loaded nano-scaled bubbles using the modified ultrasound double emulsion method, and controlled the bubble size and drug loading rate by the content of lecithin and the time required for ultrasonic treatment. In addition, we investigated the bubble characteristics and the drug release properties following ultrasonic treatment, and further examined the antitumor effects of drug-loaded bubbles on mice with hematoma malignancies.

MATERIALS AND METHODS

Materials

DL-PLA (Viscosity Molar mass of 10,000 g/mol) was from Shandong Kaiyuan Biological Material Co., Ltd; dichloromethane from pure analysis, Beijing Chemical Reagent Factory; soybean lecithin from Guangdong Wankai Microbial Technology Co., Ltd; Bo Losham from German BASF Co., Ltd; Rhoda mine B from Tianjin Fine Chemical Industry Research Institute; and paclitaxel (purity 99.9%) from Shenyang Tianfeng Bioengineering Technology Co., Ltd.

XL-30 environmental scanning electron microscope was from Philips; JEM- 2100 transmission electron microscope from Hitachi; and laser confocal microscope from Leica. The Nan (-ZS Nano particle size Zeta potential analyzer) was purchased from Malven, whereas the high performance liquid chromatography instrument was from Waters. The X-pert type powder X ray diffraction was obtained from Panalytical Analysis Instrument Company; the ultrasonic cell crusher from Ningbo Scientz Biological Technology Co., Ltd; and the ultrasound imaging diagnostic instrument from CHISON (600AG-type).

Animals

Kunming mice were provided by the animal center of the Xiamen University School of Medicine. The mice were kept under a 14-hour light/10-hour dark cycle, at a temperature of 18-23°C with 40-60% humidity. The animals were approximately 6-7 weeks old with a body mass of about 20 g. Subsequently, they were implanted with the mouse hepatoma H22 cell line (provided by the animal center of the Xiamen University School of Medicine) subcutaneously in the forelimb armpit. The Mouse Cultured Liver H22 was preserved at the Mudanjiang Medical University's Center for Type Culture Collection. The H22 cell line was cloned and the well developed cells were selected. Then the selected tumor cells were allowed to grow to a diameter of approximately 0.8 cm, and 49 nude mice were selected as the experimental model with no spontaneous bleeding necrosis, and peritumoral lesions in the absence of infection. The present study was approved by the medical Ethics Committee of the affiliated Hongqi hospital of the Mudanjiang Medical University.

Preparation of bubble contrast agent

Ultrasound contrast agent with blank PLA bubbles was prepared by ultrasound multiple emulsion solvent evaporation technique. A total of 1 mL of 0.01 g/mL sodium bicarbonate solution was selected as the internal phase (W_1) and was mixed with 10 mL dichloromethane at a different ratio of PLA and lecithin (oil phase, O). A total of 200 W ultrasonic bursts were used for 100 s in order to form water in oil (W_1/O) colostrum. The colostrum was subsequently injected into 0.01g/mL poloxamer solution (external water phase, W_2) with a volume fraction of 1% in the same ultrasonic irradiation in order to form water in the oil water (W_1/O/W_2) emulsion. The double emulsion was slowly stirred for 10 h in order to vaporize the organic solvent and produce a solidified organic phase. The mixture was centrifuged at 8,000 r/min and washed twice in order to collect the precipitate. Subsequently, 2 mL of 0.05g/mL of mannitol was added. The bubbles (one or two) with paclitaxel-loaded and fluorescent dye rhodamine B were added in the organic phase in the process of bubble preparation at a paclitaxel concentration of 3 mg/mL.

Characterization of drug-loaded bubbles

Scanning electron microscope and transmission electron microscope were used for the observation of the external morphology and the internal structure of bubbles, respectively. Confocal microscopy was used for blank PLA-lecithin bubbles loaded with rhodamine B in order to reflect the internal structure of bubbles with the distribution of Rhodamine B. Nanoparticle size Zeta potential analyzer was used to detect and investigate the particle size of bubbles that were dispersed in the water. In addition, we detected the presence of drugs in bubbles by X-ray powder diffraction.

Determination of drug-loaded amount and entrapment efficiency

The determination of paclitaxel drug-loaded amount and entrapment efficiency was performed using high performance liquid chromatography (HPLC). The chromatographic column was a symmetry C18 column (250 mm x 4.6 mm 5 μm) and the mobile phase consisted of a solution containing methanol and water at a ratio of 75:25. The flow rate was 1.0mL/min, the column temperature 25°C and the detection was performed at a wavelength of 227 nm. A total of 15 μL of each paclitaxel standard sample was loaded on the column at a concentration range of 1 to 100 μg/mL. The peak area (Y) was estimated for the regression of the standard solution concentration (X) and a standard curve was obtained. We accurately weighed freeze-dried bubble powder (10 mg) and placed it in a 5 mL centrifuge tube. The powder was mixed with 0.5 mL dichloromethane and subjected to ultrasound in order to dissolve the bubbles. Subsequently, we added 2.5 mL methanol and the solution was vortexed for 10 min. The solution was then centrifuged at 8,000 r/min for 10 min and the supernatant (15 μL) was collected. The peak area was measured and the standard curve was used in order to estimate the concentration of paclitaxel. The drug loading content (DC) and drug entrapment efficiency (EE) were calculated according to the following formula:

$$DC = \frac{\text{Paclitaxel quality}}{\text{Bubbles quality}} \times 100\% \quad \text{(i)}$$

$$EE = \frac{\text{Actual drug loading content}}{\text{Theoretical drug loading content}} \times 100\% \quad \text{(ii)}$$

The PLA-bubbles and PLA-lecithin drug-loaded bubbles were used for the *in vitro* drug release experiments and the effects of ultrasound on the two types of bubble *in vitro* drug release were investigated. A total of 50 mg of each sample was weighed, placed in a 30 mL centrifuge tube and mixed with 10 mL of release medium (containing 1% volume fraction, and phosphate buffer solution with 1% volume fraction methanol and a pH value of 7.4). The solution was vortexed for 1 min and centrifuged at 37°C at 75±5 r/min oscillation conditions in a predetermined period of time. An additional centrifugation was conducted at 8,000 r/min for 10 min, all the supernatants were removed and the released drug concentration was measured by high performance liquid chromatography. The solution was replaced with fresh medium, and the oscillation was carried out after vortexing for an additional 1 min. An ultrasound diagnostic instrument of 3.5 MHz R60 convex array was used, and the ultrasound was carried out for 10 min with an acoustic intensity of 22.57 mW/cm^2, and then placed into the thermostat box for concussion. We determined the concentration of paclitaxel by HPLC and estimated the cumulative drug release curve, while concomitantly comparing the effects of ultrasound on the release kinetics.

Animal experiments

The mice were randomly divided into 7 groups as follows: i) saline control group; ii) paclitaxel injection solution group; iii) blank PLA-lecithin bubble injection group; iv) paclitaxel PLA bubble group; v) paclitaxel PLA bubble/ultrasound group; vi) paclitaxel PLA-lecithin bubble group; and vii) paclitaxel PLA-lecithin bubble ultrasound group. Each group was injected with a dose equivalent to a paclitaxel dose of 20 mg/kg into the tumor surrounding tissues, 3 times a week for a total period of 2 weeks. Following administration of the agents to the ultrasound group, the hairs around the mice were removed and they were coated with an ultrasonic coupling agent. The samples were sonicated for 1 min by an ultrasonic probe with diameter of 1.5 cm (V306, 2.25 MHz) for the injection areas. Following 20 days of treatment, the animals were sacrificed by cervical dislocation. The adipose tissues, the skin and the blood were removed. The tumor tissues were weighed by electronic scales, and the inhibition rate (IR) was calculated.

$$IR = \left(1 - \frac{\text{Average body quality in the treatment group}}{\text{Average tumor quality in the control group}}\right) \times 100\%$$

The experimental data were analyzed using SPSS 16.0 version statistical software for analysis of variance. The data were expressed as mean ± standard deviation (X ± s) and $p<0.05$) was considered significantly different.

RESULTS

Effect of lecithin content on particle size and drug loading content of bubbles

The concentration of lecithin exhibited a positive effect both on bubble size and drug loading content (DC). Initially, we observed that the increase of the

proportion of lecithin enhanced the dissolution rate and facilitated the dispersion of the freeze-dried bubbles. Fig. 1 indicated the morphology of the particles that were prepared when the quality ratio of lecithin and PLA was 0:300, 50:250 and 300:0, respectively. Fig. 1 indicated that the addition of a small amount of lecithin increased the dispersion effect of the bubbles, whereas the size of the bubbles size was decreased. However, when the lecithin content increased to 100%, the bubbles disappeared and were replaced by nanoparticles with a surface roughness diameter of approximately 111 nm (Fig. 1). According to the particle size distribution (Fig. 1), the increase in the levels of lecithin, decreased the particle size of the bubbles, and the particle size polydispersity. This was mainly reflected in PLA bubbles that did not contain lecithin and had a particle size distribution of 200 nm to 2 μm. Using a quality ratio of lecithin and PLA that increased from 50: 250 to 150: 150, resulted in a shift in the detection wavelength of the particle size of the bubbles to 615 nm, and in a reduction in the distribution range, indicating that lecithin was important in stabilizing the Nano-scaled bubbles.

In addition, the content of lecithin exhibited significant effects on the drug entrapment efficiency (EE) of the bubbles. A small amount of lecithin could improve the drug EE, whereas when the lecithin content was higher than a certain threshold, the drug EE was reduced. When the quality ratio of lecithin and PLA was 50:250, the drug EE reached (91.42±5.48)% (Fig. 1). This effect was significantly higher than that of the PLA bubbles EE (79±8.23)%. When the dosage was 10% of the total organic phase, the DC reached (8.34±0.67)%.

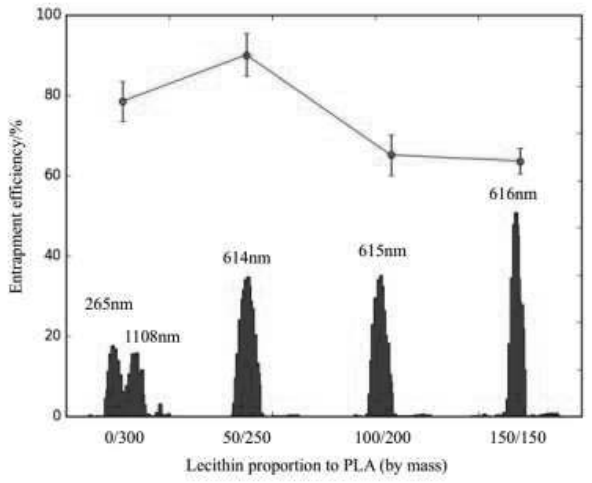

Fig. 1. *Variation of EE (curve) and bubble size distribution as determined by intensity (bar) corresponding to different lecithin proportion to PLA of the bubble component.*

Lecithin contains lipid compositions and hydrophilic phosphate and choline, which are amphiphilic molecules. In the preparation process of the double emulsion, a small amount of lecithin was distributed in the interface of the internal water and oil phases, and paclitaxel was capable of forming hydrogen bonds with lecithin. In the bubbles, lecithin was distributed in the inner shell. As a result, a small amount of lecithin could enhance the drug EE, whereas an excessive amount of lecithin following the saturation of the interface of double emulsion of the internal water phase to the oil phase, would drain the external water phase. Alternatively this formulation could self-assemble into nanoparticles (Fig. 1), and paclitaxel would further be lost to the external water phase, suggesting that the drug EE would be reduced.

Presence state of drugs in bubbles

The powder crystal diffraction analysis indicated that paclitaxel existed in bubbles in an amorphous state. Fig. 2 shows the XRD atlas of paclitaxel crystals, blank bubbles and paclitaxel bubbles.

Paclitaxel crystals had characteristic peaks when 2θ was at 5.14 degrees, 8.82 degrees and 12.38 degrees, while the peaks disappeared in the PLA-lecithin bubbles (Fig. 2). This suggested that paclitaxel existed in an amorphous state, which was conducive for paclitaxel to be dissolved in a buffer solution and subsequently be released from the bubbles.

Drug release kinetics analysis

The paclitaxel bubble *in vitro* cumulative release curve is shown in Fig. 3. The drug release characteristics of the drug-loaded PLA-lecithin bubbles and the drug-loaded PLA bubbles were similar. In the absence of ultrasound stimulation, the data were indicative of a zero-order release and no burst release behavior was noted. Additionally, the

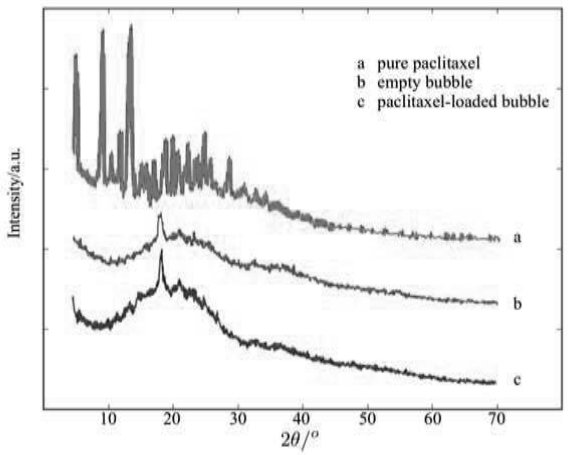

Fig. 2. *XRD diagrams of pure paclitaxel, empty bubbles and paclitaxel-loaded bubbles.*

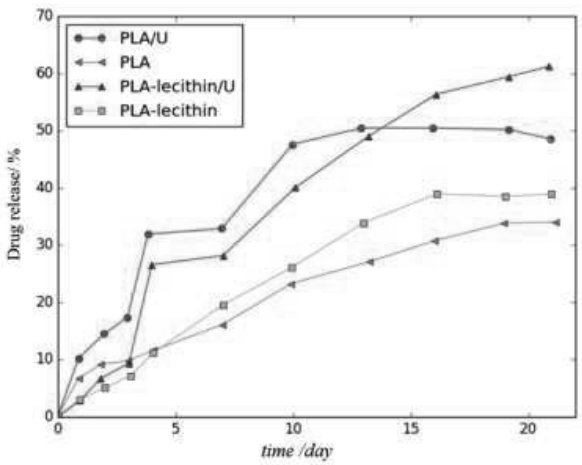

Fig. 3. *Ultrasound triggered/without release profile of drug-loaded PLA/PLA-lecithin bubbles.*

drug release rate was 30.86% and 38.45% on the sixteenth day of the drug release effect. Following ultrasound, the drug release of the two types of bubbles was significantly increased, and at the sixteenth day period, it reached 56.47% and 49.88%, respectively.

On the first, fourth, and eighth day following the release of the drugs, the ultrasound that was diagnostic for this effect was used for 10 min (Fig. 3). A total of two samples suddenly released drugs following ultrasonic stimulation, which indicated that ultrasonic waves could promote the bubble release drug effect. The results were of great significance for the bubble release system carrying out timing drug release in the body. Moreover, it has been widely studied that ultrasound has targeted transfer effects on drug-loaded particles. As a result, the *in vitro* ultrasound-mediated-drug-loaded bubbles were expected to result in a new timing and designated drug release system.

Therapeutic effect of drug-loaded bubbles in liver cancer mice

The average tumor weights and IR of each animal are shown in Table I. We performed a comparison among the factors affecting the experiment. This included the comparison between each group and the saline group, the comparison between other paclitaxel carrier groups and the paclitaxel injection group, the comparison between the ultrasound group and the group devoid of ultrasound, and the comparison between the PLA-lecithin group and the group that had no lecithin. The specific analysis is shown hereunder.

The c, d, e and g groups with the exception of the blank PLA-lecithin bubble control group, that contained paclitaxel (c, d, e, g group) exhibited decreased tumor mass compared with the saline group ($p<0.05$). This result demonstrated that paclitaxel had a certain antitumor effect on the tumor bearing H22 liver cancer mice. Concomitantly, the effects of blank PLA-lecithin bubble group were investigated with regard to the tumor growth. The tumor in this group increased compared with the saline group, although there was no significant difference ($p>0.05$).

The paclitaxel injection group exhibited greater side effects due to the direct effects of the drug on the assembly of the bubbles. The mice indicated a curling up phenomenon following the injection, and the stripped tumor revealed severe ulcer, leading to a decrease in tumor weight. In the other groups, the ulcer was not apparent. The Paclitaxel PLA-lecithin bubble ultrasound group IR was 74.27%, higher than that (64.70%) of the paclitaxel injection group. However, the IR of the e, f, and g groups was not higher than that of the paclitaxel injection group. This was notably observed for the f group (paclitaxel-loaded PLA bubbles group) and its IR was only 12.82%. The tumor weight of the aforementioned

Table I. *H22 tumor weight and inhibition rate in mice (n= 7).*

	Groups	Tumor mass/g	IR/%
a	The saline group	1.3145±0.6151	-
b	The blank PLA-lecithin bubbles group	1.1286±0.7312	-
c	The paclitaxel injection group	0.4872±0.3121*	64.70
d	The paclitaxel PLA-lecithin bubbles	0.7542±0.2345*	44.32
e	The paclitaxel PLA-lecithin bubbles ultrasound group	0.3024±0.4862*	74.27
f	The paclitaxel PLA bubbles group	1.1852±0.4852*#	12.82
g	The paclitaxel PLA bubbles ultrasound group	0.6752± 0.2853*	46.14

** Statistically significant compared to group a # statistically significant compared to group g.*

groups exhibited a significant difference compared with the paclitaxel injection group.

DISCUSSION

A previous study demonstrated that an altered expression of extracellular matrix molecules ultimately affects all biological processes including inflammation (8). In addition, a similar study indicated that amphiphilic poly-N-vinylpyrrolidone nanoparticles could be considered as potential carriers for novel, highly efficient, injectable drug delivery systems that can be used for hydrophobic drugs such as indomethacin (9). *In vitro* drug release studies have indicated a slow release effect of the prepared bubbles (10). In tumors that were developed from subcutaneous injection of cancer cells, the bubbles degraded slowly (11). A similar study indicated that the amount of PLA that remains in the tumor could cause the tumor mass to increase (12). These findings are consistent with the results presented in the current study.

However, the results provided in this study suggested that the drug-loaded PLA-lecithin bubbles had sustained release effect *in vitro*. The ultrasound-treated bubbles could accelerate the drug release. The PLA-lecithin drug-loaded bubbles combined with ultrasound positioning had higher antitumor effect *in vivo* compared to the paclitaxel drug loaded bubbles alone, while no ulcer or other side effects were present. The results confirmed that the treatment has a good prospect

REFERENCES

1. Xie F, Li ZP, Wang HW, et al. Evaluation of liver ischemia-reperfusion injury in rabbits using a nanoscale ultrasound contrast agent targeting ICAM-1. PLoS One 2016; 11(4):e0153805.
2. Liu HL, Fan CH, Ting CY, Yeh CK. Combining microbubbles and ultrasound for drug delivery to brain tumors: current progress and overview. Theranostics 2014; 4(4):432-44.
3. Xing Z, Wang J, Ke H, Zhao B, Yue X, Dai Z, Liu J. The fabrication of novel nanobubble ultrasound contrast agent for potential tumor imaging. Nanotechnology 2010; 21(14):145607.
4. Wu H, Rognin NG, Krupka TM, et al. Acoustic

characterization and pharmacokinetic analyses of new nanobubble ultrasound contrast agents. Ultrasound Med Biol 2013; 39(11):2137-46.
5. Martinez HP, Kono Y, Blair SL, et al. Hard shell gas-filled contrast enhancement particles for colour Doppler ultrasound imaging of tumors. Medchemcomm 2010; 1(4):266-70.
6. Min KH, Min HS, Lee HJ, et al. pH-controlled gas-generating mineralized nanoparticles: a theranostic agent for ultrasound imaging and therapy of cancers. ACS Nano 2015; 9(1):134-45.
7. Lima-Tenório MK, Pineda EA, Ahmad NM, Fessi H, Elaissari A. Magnetic nanoparticles: In vivo cancer diagnosis and therapy. Int J Pharm 2015; 493(1-2):313-27.
8. Zhang J, Liang YC, Lin X, et al. Self-monitoring and self-delivery of photosensitizer-doped nanoparticles for highly effective combination cancer therapy in vitro and in vivo. ACS Nano 2015; 9(10):9741-56.
9. Liang PC, Chen YC, Chiang CF, Mo LR, Wei SY, Hsieh WY, Lin WL. Doxorubicin-modified magnetic nanoparticles as a drug delivery system for magnetic resonance imaging-monitoring magnet-enhancing tumor chemotherapy. Int J Nanomedicine 2016; 11:2021-37.
10. Yildirim A, Chattaraj R, Blum NT, Goldscheitter GM, Goodwin AP. Stable encapsulation of air in mesoporous silica nanoparticles: fluorocarbon-free nanoscale ultrasound contrast agents. Adv Healthc Mater 2016; 5(11):1290-98.
11. Nomikou N, Curtis K, McEwan C, O'Hagan BMG, Callan B, Callan JF, McHale AP. A versatile, stimulus-responsive nanoparticle-based platform for use in both sonodynamic and photodynamic cancer therapy. Acta Biomater 2017; 49:414-421.
12. Miyoshi N, Kundu SK, T, Yasui K, Shimada I, Ito Y. Combination of sonodynamic and photodynamic therapy against cancer would be effective through using a regulated size of nanoparticles. Nanosci Nanoeng 2016; 4(1):1-11.

LETTER TO THE EDITOR

GENETIC DIVERSITY OF *MYCOBACTERIUM TUBERCULOSIS* IN NORTHERN GREECE

G. KAZDAGLIS[1*], B. MOLINA-MOYA[2*], K. MANIKA[3], P. IOANNIDIS[4], D. PAPAVENTSIS[4], E. VOGIATZAKIS[4], M. PANOPOULOU[5], A. MELIDOU[1], J. DOMÍNGUEZ[2**], N. MALISIOVAS[1**] and G. GIOULA[1**]

[1]Microbiology Department, Medical School, Aristotle University of Thessaloniki, Greece; [2]Microbiology Laboratory, University Hospital Germans Trias i Pujol, Institute of Investigation Germans Trias i Pujol, Badalona, Autonomous University of Barcelona, CIBERES, Spain; [3]Pulmonary Department, Aristotle University of Thessaloniki, G. Papanikolaou Hospital, Greece; [4]Microbiology Laboratory and National Reference Center for TB, Sotiria Chest Diseases Hospital, Athens, Greece; [5]Microbiology Department, Medical School, Democritus University of Thrace, Greece

Received April 12, 2018 – Accepted May 15, 2018

*These authors contributed equally to this work ** Co-senior authors

The aim of the present study was to describe the genetic diversity of *Mycobacterium tuberculosis (M.tuberculosis)* strains circulating in the region of Northern Greece. A total of thirty-seven *M. tuberculosis* clinical isolates were analysed by the spoligotyping method. According to the results, six clusters comprising seventeen strains were detected, and the remaining twenty strains showed unique patterns. The *M.tuberculosis* families according to SITVITWEB were distributed as follows: Haarlem (H) (27.0%); T (24.3%); Beijing (13.5%); Latin-America and Mediterranean (LAM) (5.4%) and S (2.7%). The remaining isolates (27%) did not match any isolates within the database and they were characterized as orphans. Regarding GenoType MTBDR*plus* results, two strains (5.4%) were Multi-Drug-Resistant, four strains (10.8%), were isoniazid monoresistant, while the remaining thirty-one strains (83.8%) were susceptible. In conclusion, in the region of Macedonia-Thrace (Northern Greece), there was high phylogenetic diversity among *M. tuberculosis* isolates. Molecular tools used and data presented can have regional and national impact on tuberculosis control.

To the Editor,

Local gradients in the prevalence of particular bacterial lineages and sub-lineages may reflect different events in the past history of the human host. Europe as a whole and the Balkans in particular used to be and still are at the crossroad of human migrations, thereby transmitting human pathogens across the continent. Greece represents a link between Europe and Asia and is always in front of these migrations. Tuberculosis (TB) remains one of the most prevalent infectious diseases, and the percentage of cases due to resistant strains is increasing worldwide (1). One of the greatest concerns of TB control programs is the emergence and spread of drug-resistant, and especially MDR, isolates (the latter being defined by combined resistance to isoniazid-INH and rifampicin-RIF) (1). In Greece, the case notification rate in 2014 was 4.7 cases per 100.000 of population, while the proportion of multidrug resistant *Mycobacterium tuberculosis* strains was 2.4% (2). However, underreporting is an important issue for TB control in Greece, as it is estimated to be 77-81% (3). Various limitations in the national TB monitoring system, access limitations

Mailing address:
Dr. Georgios Kazdaglis,
Specialist Microbiologist,
Linköping University Hospital,
581 85 Linköping, Sweden
Tel.: +46 729268885
e-mail: georgioskazdaglis@live.com

0393-974X (2018)
Copyright © by BIOLIFE, s.a.s.
This publication and/or article is for individual use only and may not be further reproduced without written permission from the copyright holder. Unauthorized reproduction may result in financial and other penalties
DISCLOSURE: ALL AUTHORS REPORT NO CONFLICTS OF INTEREST RELEVANT TO THIS ARTICLE.

and migration from regions with high TB incidence (such as Former Soviet Union countries) possibly leads to further underestimation of the TB burden and facilitates further spread of the disease. (1). Studies of genotyping diversity of *M. tuberculosis* isolates from infected individuals can provide useful information about the origin and transmission of these strains (4) as well as those drug-resistant (5).

Recent advances in molecular techniques have enabled development of a variety of genotyping methods for the differentiation of clinical isolates of *M. tuberculosis*. The chromosomal locus, containing a large number of direct repeats (DRs) interspersed with unique spacer sequences, is the target of spoligotyping (i.e., spacer oligonucleotide typing) technique. This method has been widely applied to study the molecular epidemiology and evolutionary genetics of TB (6).

The aim of the present study was to describe the genetic diversity of *M. tuberculosis* strains circulating in the region of Macedonia-Thrace in Northern Greece.

MATERIALS AND METHODS

In total, thirty-seven *M. tuberculosis* strains were isolated from clinical samples from newly diagnosed symptomatic patients with a diagnosis of pulmonary tuberculosis during 2011-2012. Our samples were collected from the Pulmonary Department of G. Papanikolaou Hospital in Thessaloniki, which is the main hospital for TB management in the Macedonia region in Greece, and the University Hospital of Thrace. All patients were informed and signed consent to participate in the study. In the case of deceased, informed written consent was given by the family. The ages of the patients ranged from twenty to eighty-three years, with a mean age of forty-six years. Twenty-four out of the thirty-seven patients (65%) were male and thirteen (35%) were female. According to their country of origin, twenty-eight patients were Greek (76%), and nine (24%) were born in foreign countries: 4 from Georgia, 2 from Russia, 1 from Romania, 1 from China and 1 from Africa.

After microscopic examination with Ziehl-Neelsen staining, clinical samples were simultaneously tested by two methods: conventional culture method on Löwenstein-Jensen (LJ) slants for 8 weeks (at 37°C) and molecular typing method Genotype MTBDR plus (Hain-Lifescience). The cultures were subjected to phenotypic identification based on growth and colony characteristics, pigment production and biochemical tests. Conventional drug susceptibility testing was determined on LJ, by the proportion method with resistance ratio. The susceptibility of *Mycobacteria* was analysed for the two major anti-tuberculosis agents, isoniazid (INH) and rifampicin (RMP). DNA extraction from LJ cultures was performed with the QIAamp DNA Mini Kit (Qiagen, Germany), according to the manufacturer's instructions. The confirmation of the existence of *M. tuberculosis* DNA was performed by Real time PCR, using Artus *M. tuberculosis* RG PCR Kit (Sacace Biotechnologies), where detection is based on the amplification of specific regions of the mycobacterial genome (DNA fragments of IS 6110 insertion). Molecular detection of RIF and INH resistance was performed by the line probe assay GenoType MTBDR *plus* (Hain Lifescience, Germany) following the manufacturer's instructions. This assay detects the specific mutations in the *rpoB* genes 531, 526, and 516, associated with RIF resistance (coding the β-subunit of the RNA polymerase) and the *katG* gene 315 and the *inhA* promoter region positions -15 and -8, associated with INH resistance (coding for the the NADH enoyl ACP reductase). Moreover, Human Immunosuppressive Virus (HIV) 1 and 2 testing was performed to all patients (Architect HIV Ag/Ab Combo). All of the used methodologies are recommended by the World Health Organization (WHO). They were performed at the Greek National Reference Laboratory for *Mycobacteria* (NRLM), Sotiria Chest Disease Hospital, which is quality assured for these molecular techniques. The Phylogenetic analysis of the strains was performed by spoligotyping (Ocimum Biosolutions, India) following the manufacturer's instructions. This assay is based on the polymorphism of the clustered regularly interspaced short palindromic repeats (CRISPR) locus. Spoligotyping International type (SIT) and clade were identified according to the International Spoligotyping Database SITVITWEB (http://www.pasteur-guadeloupe.fr:8081/SITVIT_ONLINE/).Statistical analysis was performed using Pearson's *chi*-squared test or Fischer's exact test, and $p<0.05$ was considered statistically significant (SPSS 15.0, Chicago, Illinois, USA).

RESULTS

A total of thirty-seven *M. tuberculosis* clinical isolates originating from the Macedonia and Thrace regions of Greece were analysed by spoligotyping.

Regarding GenoType MTBDR*plus* results, two strains (5.4%) were MDR, four strains (10.8%) were INH monoresistant, while the remaining thirty-one strains (83.8%) were sensitive. Available phenotypic DST results were concordant with MTBDR*plus* results. Resistance results were similar to the resistance profile of *M. tuberculosis* in the rest of the country (3). According to the spoligotyping results, six clusters comprising seventeen strains were detected, and the remaining twenty strains showed unique patterns (Fig. 1); thus, there were twenty-six different patterns, and the Hunter and Gaston discriminatory index of spoligotyping was 0.9745. The *M. tuberculosis* families according to SITVITWEB (7) were distributed as follows: Haarlem (H), n=10 (27.0%); T, n=9 (24.3%); Beijing, n=5 (13.5%); Latin-America and Mediterranean (LAM), n=2 (5.4%); and S, n=1 (2.7%). The remaining 10 isolates (27%) did not match any isolates within the database and they were characterised as orphans (Fig. 1).

Four out of the five Beijing strains were isolated from patients coming from Georgia and Russia, while the two LAM strains were isolated from one Greek and one patient from Africa. The Haarlem strains were isolated from eight Greek patients and two foreign ones, from China and Georgia, while T strains were isolated from eight Greek and one Romanian patient. It is worth mentioning that all strains isolated from patients coming from Thrace, which is Greece's geographical part closest to Turkey,

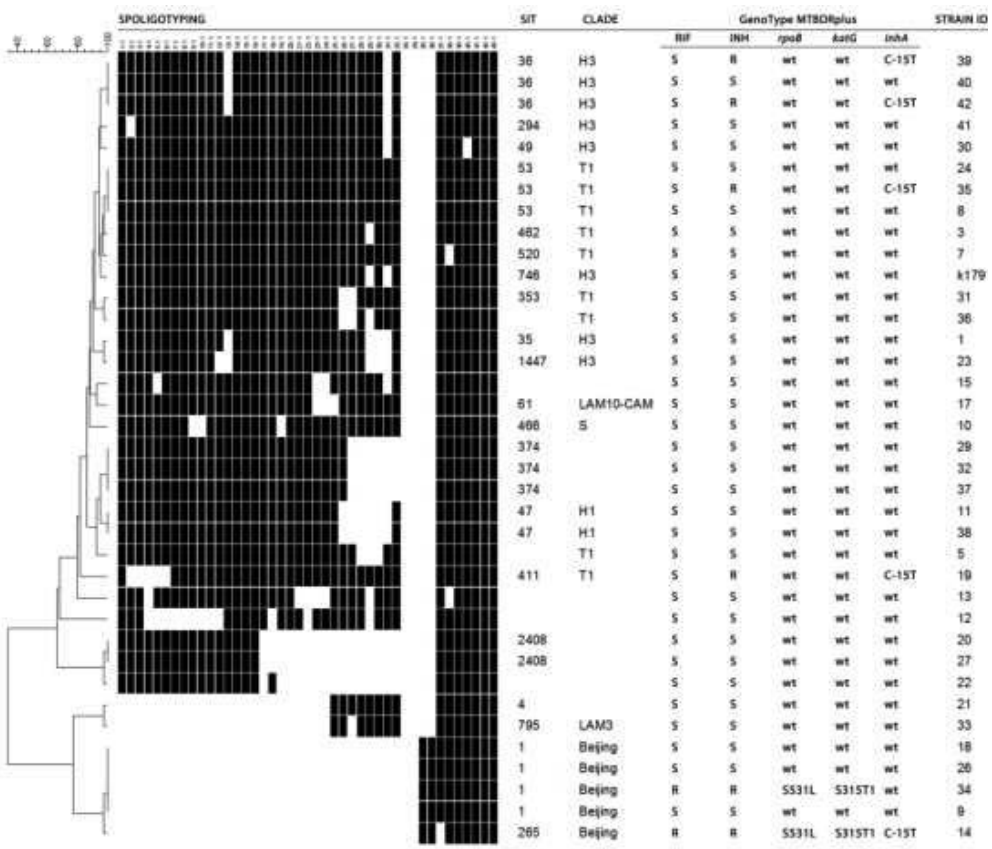

Fig. 1. *Phylogenetic tree based on spoligotyping patterns obtained for the 37 M. tuberculosis complex strains included in this study. SIT and clade were identified according to the International Spoligotyping Database SITVITWEB (http://www.pasteur-guadeloupe.fr:8081/SITVIT_ONLINE/). Molecular drug resistance and mutations detected by GenoType MTBDRplus are shown.*

were classified as Haarlem family. Moreover, all the above patients were of Greek origin.

In respect to drug resistance, both the two MDR-TB strains of our study belonged to Beijing family. The first one was isolated from a 64-year-old Greek patient who presented with radiographic findings in both lungs and was suffering from stomach cancer, while the second one was isolated from an immigrant whose country of origin was Russia. Two out of the total four INH-resistant strains, were classified as Haarlem and the remaining two as T lineage.

Statistical analysis

Statistical analysis demonstrated that there was no statistically significant difference between either the patients' sex (p=0.868) or resistance (p=0.567) with the *M. tuberculosis* family.

Moreover, data regarding the country of origin revealed that nine patients were non-Greeks. Regarding their *M. tuberculosis* family, four strains were classified as Beijing, two as Haarlem, one belonged to T family and one strain was classified as LAM. It is worth mentioning that three out of the four patients whose strains belonged to Beijing family came from Georgia. Clinical samples obtained from Greek patients were mostly classified as Haarlem family (30, 8%). Statistical relationship between *M. tuberculosis* family and patients' origin was not found statistically significant (p=0.540).

DISCUSSION

Tuberculosis remains a great public health concern in Greece, as well as in many countries in Europe and worldwide. The genetic diversity of *M. tuberculosis* strains can be linked to human demographic and migratory events, which indicates that the current increases in human population, urbanization and global travel, combined with the population genetic characteristics of *M. tuberculosis*, could contribute to the emergence and spread of drug-resistant tuberculosis (8).

In the present study, according to the results, six clusters comprising seventeen strains were detected, and the remaining twenty strains showed unique patterns. The majority of the clinical isolates belonged to Haarlem, T and Beijing family. In the Macedonia region of Northern Greece, and during the study period, there was no predominant lineage, but a high phylogenetic diversity among *M. tuberculosis* isolates was observed. In the Thrace region, all five strains belonged to the Haarlem lineage, but as the size sample was small and not representative of the area population, more studies are needed in order to confirm such dominance of Haarlem strain. Thrace, on the other hand, is the part of Greece nearest to Turkey. Many studies conducted in neighbouring countries revealed a genetic diversity both among sensitive and drug-resistant strains of *M. tuberculosis*. An interesting fact is that a high proportion of the sub-lineage LAM7-TUR was present in many geographical areas of Turkey, but this sub-lineage is not yet identified in Northern Greece (9). Moreover, one study investigating the distribution of spoligotyping defined genotypic lineages among drug-resistant *M. tuberculosis* isolates in Turkey, revealed that Haarlem family was the dominant one, followed by LAM7-TUR lineage (9). This may suggest a probable transmission and distribution of this family in the specific geographical area due to population exchange and movement over past years and also possibly explain the dominance of Haarlem family in Thrace.

All MDR strains in the present study belonged to the Beijing lineage. In addition, a not negligible proportion of drug resistance was detected. Moreover, data regarding the country of origin revealed that clinical samples obtained from Greek patients were mostly classified as Haarlem family, while clinical isolates from four out of the eight patients, who were non-Greeks, belonged to Beijing family.

A previous study conducted in Greece, from MTB isolates from patients with pulmonary drug-resistant tuberculosis (DR-TB), in order to determine whether there is an association between the prevalent genotypes and drug resistance, demonstrated that the most prevalent lineages among drug-resistant strains according to mycobacterial interspersed repetitive units typing were first Beijing, followed by Haarlem, and LAM family. Moreover, Greek patients were more likely to have Mono-resistant and MDR-TB with the most prevalent isolates belonging to the

Haarlem family. Among non-Greek patients with MDR-TB, the most prevalent genotypes belonged to the Beijing family (10). These results are in accordance with the results of the present study.

Observation of similar studies from other neighbouring countries may provide useful information on the circulating strains and explain their presence in a particular geographical area at a specific time. A large proportion of *M. tuberculosis* strains isolated from TB patients in Bulgaria revealed that the majority of the studied strains belonged to spoligotype subfamily T1, which is a worldwide-distributed type. This family was also present in our study in a high proportion in Greeks, as well Turks, but not in Russians. This may lead to a hypothesis that these Bulgarian strains were likely brought to the country due to the Balkan intraregional movement, or even long before that, and their importation was a result of the medieval expansion of the Ottoman Empire. Haarlem family was also present in the above study, as well as LAM7_TUR subfamily, which is phylogenetically specific to Turkey. Haarlem family was the dominant type in our study, but LAM7_TUR isolates have been rarely described in Greece or other neighbouring countries, such as Romania, so perhaps this subfamily has not yet penetrated these countries in significant proportions (11).

Another study conducted in Albania revealed a high level of genetic diversity, as well as the presence of Bulgarian and Turkish types in the country. Moreover, the finding of the Beijing genotype family strains, which were not found in Bulgaria or Romania, but were present in Northern Greece, is another feature characteristic of the country and may be evidence of strains exchange between Albania and Greece. In Albania, Beijing family strains came from MDR-TB cases and although they were not present in Bulgaria or Romania, they were transmitted to Russia, where it is suggested that current transmission of MDR-TB is greatly influenced by the ongoing dissemination of the Beijing family strains (12).

In our study, the Beijing family strains were isolated from patients whose origins were mostly from Georgia. Moreover, both in the present study, as well as in a previous Greek study, all MDR-TB strains belonged to Beijing family. All these may be evidence of the continuous circulation of *M. tuberculosis* between Former Soviet Union countries and Greece.

Indeed, the unravelling of the effect of the genetic variability of *M. tuberculosis* on the presentation of the disease remains a challenging, poorly investigated issue, which consists in understanding why a strain may become prevalent in certain communities.

In the present study, we have demonstrated heterogeneity of the Greek *M. tuberculosis* population that appears to be dominated by several, worldwide-distributed and Balkan-specific, spoligotypes. These results should, however, be confirmed in more exhaustive studies.

Moreover, these data and the molecular tools used can have regional and national impact on TB control, by helping the National Tuberculosis Control Program intensify its intervention strategies to achieve early detection of micro-epidemics and outbreaks and timely establishment of treatment, given that the delay in treatment is a key factor for disease transmission.

A coordinated approach in the notification of *M. tuberculosis* surveillance of genetic lineages and bacterial resistance will aid in setting more efficient prevention and control policies in Greece.

ACKNOWLEDGEMENTS

The authors are grateful to all microbiology laboratories contributing to *M. tuberculosis* strain collection. We would also like to thank the Microbiology Laboratory and National Reference Center for TB, Sotiria Chest Diseases Hospital for performing the line probe assay GenoType MTBDR*plus* and for their excellent technical assistance. Sofia Samper, Alicia Lacoma, and Oriol Martos are acknowledged for their invaluable help.

J. Domínguez is funded by the "Miguel Servet" program of the Instituto de Salud Carlos III (Spain).

REFERENCES

1. World Health Organization. Global tuberculosis report. 2015 (WHO/HTM/TB/2015.22). Geneva Switzerland.

2. Hellenic Centre for Diseases Control and Prevention (KEELPNO). Latest epidemiological data on tuberculosis in Greece. 2015.
3. Lytras T, Spala G, Bonovas S, Panagiotopoulos T. Evaluation of tuberculosis underreporting in Greece through comparison with anti-tuberculosis drug consumption. PLoS One 2012; **7:**e50033.
4. Kanduma E, McHugh TD, Gillespie SH. Molecular methods for Mycobacterium tuberculosis strain typing: a users guide. J Appl Microbiol 2003; 94:781-91.
5. Lacoma A, Garcia-Sierra N, Prat C, Ruiz-Manzano J, Haba L, Roses S, Maldonado J, Dominquez J. GenoType MTBDRplus assay for molecular detection of rifampin and isoniazid resistance in Mycobacterium tuberculosis strains and clinical samples. J Clin Microbiol 2008; 46**:**3660-67.
6. Brudey K, Driscoll JR, Rigouts L, et al. Mycobacterium tuberculosis complex genetic diversity: mining the fourth international spoligotyping database (SpolDB4) for classification, population genetics and epidemiology. BMC Microbiol 2006; 6:6:23.
7. Demay C, Liens B, Burguiere T, et al. SITVITWEB--a publicly available international multimarker database for studying Mycobacterium tuberculosis genetic diversity and molecular epidemiology. Infect Genet Evol 2012; 12:755-66.
8. Hershberg R, Lipatov M, Small PM, et al. High functional diversity in Mycobacterium tuberculosis driven by genetic drift and human demography. PLoS Biol 2008; 6:e311.
9. Kisa O, Tarhan G, Gunal S, et al. Distribution of spoligotyping defined genotypic lineages among drug-resistant Mycobacterium tuberculosis comlex clinical isolates in Ankara, Turkey. PLoS One 2012; **7**:e30331.
10. Rovina N, Karabela S, Constantoulakis P, Michou V, Konstantinou K, Sgountzos V, Roussos C, Poulakis N. MIRU-VNTR typing of drug-resistant tuberculosis isolates in Greece. Ther Adv Respir Dis 2011; 5**:**229-36.
11. Valcheva V, Mokrousov I, Rastogi N, Narvskaya O, Markova N. Molecular characterization of Mycobacterium tuberculosis isolates from different regions in Bulgaria. J Clin Microbiol 2008; 46:1014-18.
12. Tafaj S, Zhang J, Hauck Y, Pourcel C, Hafizi H, Zoraqi G, Sola C. First insight into genetic diversity of the Mycobacterium tuberculosis complex in Albania obtained by multilocus variable-number-tandem-repeat analysis and spoligotyping reveals the presence of Beijing multidrug-resistant isolates. J Clin Microbiol 2009; 47:1581-84.

LETTER TO THE EDITOR

THE EFFECT OF TOPICAL MINOXIDIL TREATMENT ON FOLLICULAR SULFOTRANSFERASE ENZYMATIC ACTIVITY

A. GOREN[1,2], J. MCCOY[1], M. KOVACEVIC[2], M. SITUM[3], J. CHITALIA[4], R. DHURAT[4], T. NACCARATO[1] and T. LOTTI[2]

[1]Applied Biology, Inc., Irvine, CA, USA; [2]Department of Dermatology and Venereology, University of Rome "G. Marconi", Rome, Italy; [3]Department of Dermatology and Venereology, University Hospital Center "Sestre milosrdnice", Zagreb, Croatia; [4]Department of Dermatology, LTM Medical College & Hospital Sion, Mumbai, India

Received May 1, 2018 – Accepted June 11, 2018

Minoxidil is the only US FDA-approved topical drug for the treatment of female and male pattern hair loss. Previously, it was demonstrated that topical minoxidil is metabolized to its active metabolite, minoxidil sulfate, by sulfotransferase enzymes located in the outer root sheath of hair follicles. The expression of sulfotransferase in the scalp varies greatly between individuals, and this difference in expression explains the varied response to minoxidil treatment. Previously, we have demonstrated the clinical utility of detecting sulfotransferase in plucked hair follicles to predict minoxidil response in pattern hair loss patients. Typically, exogenous exposure to substrates affects the expression of the enzymatic system responsible for their metabolism. For example, Phase I metabolizing enzymes, such as the cytochrome P450 family of enzymes, are known to be up-regulated in the presence of xenobiotic substrates. However, it is not known if Phase II metabolizing enzymes, such as the sulfotransferase family of enzymes, are similarly affected by the presence of substrates. In this study, we recruited 120 subjects and analyzed their sulfotransferase enzymatic activity before and after treatment with topical minoxidil. Adjusting the results for biologic (within subject) variability, we discovered that the sulfotransferase enzymatic system expression is stable over the course of minoxidil treatment. To the best of our knowledge, this is the first study to demonstrate the stability of sulfotransferase, a Phase II metabolizing enzyme, over the course of minoxidil treatment.

To the Editor,

Xenobiotics are extrinsic chemical substances (e.g., drugs), which may be present in human body (1). They are included into specific metabolic pathways evolved to mitigate toxicity to an organism. Xenobiotic metabolism includes several pathways designed to modify chemical structure and decrease the toxicity of the compounds. Although, in some instances, the intermediates in xenobiotic metabolism may themselves cause toxic effects (2). Xenobiotic metabolism is divided into 3 phases, organized to modify lipophilic compounds into hydrophilic conjugates that can more readily be excreted. In Phase I, lipophilic xenobiotic molecules are metabolized by enzymes such as cytochrome P450 oxidases, which introduce

Key words: sulfotransferase, minoxidil, pattern hair loss

Mailing address:
Andy Goren, MD
Applied Biology, 17780 Fitch,
Suite 192, Irvine, CA 92614, USA
Tel.: +1 949 387 4526
e-mail: andyg@appliedbiology.com

0393-974X (2018)
Copyright © by BIOLIFE, s.a.s.
This publication and/or article is for individual use only and may not be further reproduced without written permission from the copyright holder. Unauthorized reproduction may result in financial and other penalties
DISCLOSURE: ALL AUTHORS REPORT NO CONFLICTS OF INTEREST RELEVANT TO THIS ARTICLE.

polar groups and provide sites for downstream conjugation reactions. Phase I reactions are mainly localized in the liver. In Phase II, conjugating enzymes interact with metabolites produced by Phase I enzymes and eliminate them through both passive and active transport. Conjugating enzymes include a large group of broad-specificity transferases, with glutathione S-transferases as the most important representatives (3). After conjugation, any xenobiotic conjugates or their metabolites not eliminated in Phase II are further processed and eliminated in Phase III by transporter proteins (4, 5).

Pharmacological action of lipophilic drugs is dependent on the duration of its metabolism, i.e., drugs that are slowly metabolized can have longer action. Thus, all factors that decrease clearance rate can increase the duration or intensity of the drug action. On the other hand, if an enzyme is responsible for metabolizing a pro-drug into its active form, changes in metabolism can have the opposite effect. Apart from chemically active substances, many physiological and pathological factors can affect drug metabolism. Some examples are dose, route of administration, frequency, tissue distribution, and protein sequestering of drug via binding. Finally, physiological factors including sex differences, nutrition, intestinal flora and enterohepatic circulation, as well as, pathological conditions of liver, kidney, or heart are related to metabolic differences (1).

Several Phase I and II metabolizing enzymes are known to be inducible by both endogenous and xenobiotic molecules. The most widely studied drug-metabolizing enzyme, by far, is the cytochrome P450 family. Many of the members of the cytochrome P450 family are inducible via nuclear receptor mediated induction. For example, cytochrome family 1 genes are up-regulated by the aryl hydrocarbon receptor (AhR) after it binds aromatic hydrocarbon ligands (6, 7). Similarly, sulfotransferases have been demonstrated to be regulated by endogenous hormones (8) and xenobiotics (9).

Minoxidil is a pro-drug converted to its active form, minoxidil sulfate, by sulfotransferase enzymes (10). Minoxidil sulfate is required for both the promotion of hair regrowth and the vasodilatory effects of minoxidil. Sulfotransferase enzymes are located in both the skin and the liver and are important Phase II xenobiotic metabolizing enzymes for a number of phenolic molecules in addition to minoxidil (11). In previous works we have demonstrated a simple enzymatic test that measures sulfotransferase activity in plucked hair follicles (12). As such, we were interested to study how prolonged exposure to minoxidil would effect the expression of sulfotransferase enzymes in hair follicles. This determination is important first to assess the benefits of continued minoxidil use and second to confirm the validity of enzymatic testing as a predictor of minoxidil efficacy for persons already using minoxidil.

MATERIALS AND METHODS

Patients

The study was conducted over a period of 12 weeks at three independent sites (United States, China, and India). One hundred fifty subjects, 18 years of age or older with clinically diagnosed patterned hair loss were included in the study. The ethnicities included Asian (Chinese), Indian, Caucasian, and African Americans. All subjects provided informed, signed consent to participate in the study. A total of 60 men and 90 women were recruited. Eight to ten hair samples were plucked with tweezers from the border between the most prominent area of thinning and non-thinning at the vertex/mid-scalp and inspected visually for an intact bulb. Suitable anagen hairs were sent for sulfotransferase activity determination (Applied Biology, Inc., Irvine, California, USA). Three replicate measurements were obtained to study biologic (within-subject) variability of the testing procedure. Further, to determine the treatment effect on the hair sulfotransferase enzyme expression, 120 subjects, 18 years of age or older with clinically diagnosed patterned hair loss were recruited. All subjects were treated with 5% topical minoxidil for a period of at least 8 weeks. 96 subjects successfully completed the study. After a minimum of 8 weeks of minoxidil treatment, eight to ten hair samples were collected and analyzed for sulfotransferase activity. The samples were analyzed within 7 days of collection.

Sulfotransferase activity determination and statistical model

Suitable anagen hairs were trimmed to a length of ~1 cm and immersed, bulb first, in 100 µL of the assay solution previously reported (12). Hairs were allowed to react with the solution for 24 hours at room temperature. After incubation, hairs were removed and the optical absorbance of the solution at 405 nm was determined with a spectrophotometer (Shimadzu UV-1700, Kyoto, Japan) using a single scan and 1 cm path length. The raw data for the cohort was tabulated and analyzed with statistical software (MedCalc Version 18).

RESULTS

Repeated measure ANOVA corrected using Huynh-Feldt was used to determine the within-subjects effect. The analysis of the dataset yielded $F(1.93, 287.87) = 0.19$, $p = 0.823$; therefore, the null hypothesis is not rejected and we conclude that there was no significant difference in the sulfotransferase activity (as determined by the MRT test) between the 3 repeated measurements per subject. The within-subject variability was determined to be 0.197 absorbance units (AU). We determined the quantitative effect of minoxidil treatment on sulfotransferase enzymatic activity using a paired sample t-test. 3 subjects from the pool of 96 that completed the study were determined to be outliers using the generalized ESD test (alpha-level 0.05). The histogram of differences in the AU (Δ AU) values recorded before and after minoxidil use for all 96 patients is shown in Fig. 1, the outliers are labeled in grey. Removing the 3 subjects from the dataset restored normality ($p=0.2766$) and the paired sample t-test yielded $t(92)=-0.445$, $p=0.6577$ indicating that the null hypothesis was not rejected; hence, we conclude that there was no significant difference in sulfotransferase enzyme activity before or after minoxidil treatment. The 95% confidence interval for the difference in means is $-0.07871 \leq \mu_b - \mu_a \leq -0.04992$ with the best estimate being the mean difference = -0.014; hence, we can conclude that treatment with 5% topical minoxidil did not alter the sulfotransferase enzymatic activity.

DISCUSSION

Minoxidil is a pro-drug, converted to its active form in the outer root sheath of the hair follicle. Sulfotransferase enzyme activity in the hair follicle

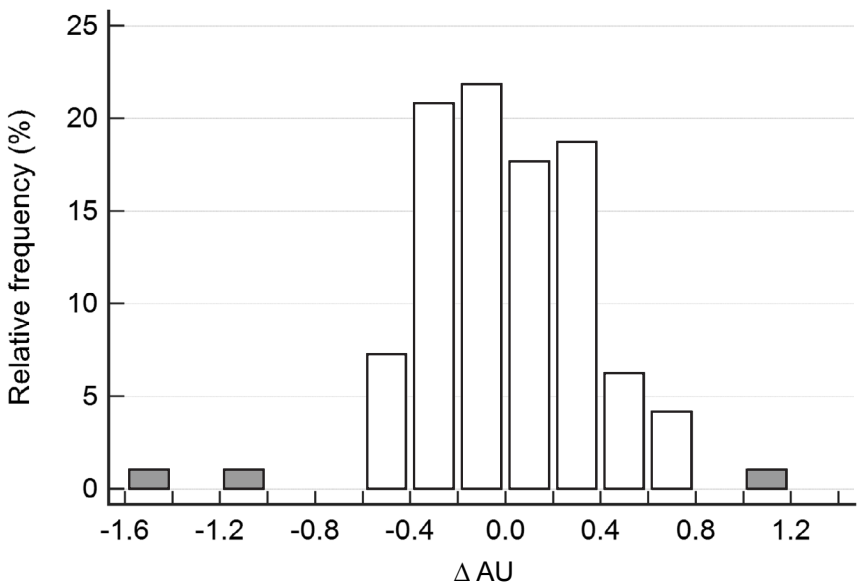

Fig. 1. *Histogram of the difference (Δ) in measured AU before and after minoxidil treatment. Patients determined to be outliers using the generalized ESD test (alpha-level 0.05) are shown in gray.*

is an important predictor of minoxidil efficacy for the treatment of hair loss. Prolonged daily exposure to topical minoxidil does not alter the activity of the sulfotransferase enzymes responsible for its metabolism. As such, minoxidil will be beneficial to patients, whom it is predicted to be effective, as a long-term treatment for hair loss. Additionally, the enzymatic activity assay used to predict minoxidil efficacy will be valid whether or not a person has used minoxidil prior to the test. To the best of our knowledge this is the first report to explore the response of follicular sulfotransferase enzyme activity to chronic exposure to minoxidil.

REFERENCES

1. Croom E. Metabolism of xenobiotics of human environments. Prog Mol Biol Transl Sci 2012; 112:31-88.
2. Bunchorntavakul C, Reddy KR. Acetaminophen (APAP or N-Acetyl-p-Aminophenol) and Acute liver failure. clinics in liver disease 2018; 22(2):325-346.
3. Jakoby WB, Ziegler DM. The enzymes of detoxication. J Biol Chem 1990; 265(34):20715-18.
4. König J, Nies AT, Cui Y, Leier I, Keppler D. Conjugate export pumps of the multidrug resistance protein (MRP) family: localization, substrate specificity, and MRP2-mediated drug resistance. Biochim Biophys Acta 1999; 1461(2):377-94.
5. Commandeur JN, Stijntjes GJ, Vermeulen NP. Enzymes and transport systems involved in the formation and disposition of glutathione S-conjugates. Role in bioactivation and detoxication mechanisms of xenobiotics. Pharmacol Rev 1995; 47(2):271-330.
6. Hankinson O, Brooks BA, Weir-Brown KI, et al. Genetic and molecular analysis of the Ah receptor and of Cyp1a1 gene expression. Biochimie 1991; 73(1):61-66.
7. Gonzalez FJ, Liu SY, Yano M. Regulation of cytochrome P450 genes: molecular mechanisms. Pharmacogenetics 1993; 3(1): 51-57.
8. Runge-Morris M, Kocarek TA, Falany CN. Regulation of the cytosolic sulfotransferases by nuclear receptors. Drug metabolism reviews 2013; 45(1):15-33.
9. Runge-Morris M, Kocarek TA. Regulation of sulfotransferases by xenobiotic receptors. Curr Drug Metab 2005; 6(4):299-307.
10. Buhl AE, Waldon DJ, Baker CA, Johnson GA. Minoxidil sulfate is the active metabolite that stimulates hair follicles. J Invest Dermatol 1990; 95(5): 553-77.
11. Nimmagadda D, Cherala G, Ghatta S. Cytosolic sulfotransferases. Indian J Exp Biol 2006; 44(3):171-82.
12. Goren A, Shapiro J, Roberts J, et al. Clinical utility and validity of minoxidil response testing in androgenetic alopecia. Dermatol Ther 2015: 28(1):13-16.

LETTER TO THE EDITOR

DIAGNOSIS AND TREATMENT OF DISTAL LIMB MICROCIRCULATORY DISTURBANCE CAUSED BY STEROID INJECTION

Y. LIU, L. CHEN, Z-G. LIU and R-J. LI

Department of Hand Surgery, The First Hospital of Jilin University, Changchun, Jilin, China

Received March 8, 2018 – Accepted June 2018

Corticosteroid is commonly used for the clinical treatment of pain. It is safe, reliable and a simple procedure with other advantages. However, a possible potential catastrophic complication of corticosteroid injections in distal limbs (e.g., the wrist) is acute radial artery ischemia due to the injection into the radial artery. This may result from spasm attributed to the steroids. While the complication of corticosteroids in the wrist is rare, ischemia of the hand caused by corticosteroid injections in radial artery has been reported in several articles. We treated five patients with microcirculation disturbance of distal limb caused by corticosteroid treatment. Here, we report the two different treatment strategies adopted according to the severity of the disease which achieved good therapeutic effects.

To the Editor,

Case study

A total of five female patients were selected for the study. The ages of the patients varied from 49-59 years. One patient had humeral epicondylitis (left) and the four other cases were radial styloid process of tenosynovitis stenosis (left in 1 and right in 3 cases). The drug injection given to patients was a mixture of corticosteroid and lidocaine. In a short period of time after corticosteroid injection, all five patients exhibited obvious microcirculation disturbances in the hand, of which two patients had finger-tip necrosis and were treated by interception, the other two showed obvious improvement after conservative treatment and one patient was cured by surgery and recovered well after the operation.

Case 1. A 52-year-old female patient was admitted to our hospital five days after steroid injection for the treatment of left lateral humeral epicondylitis. The patient exhibited low temperature and ecchymosis on the forearm skin at the time of admission. She reported that she had been treated at a local hospital about a week previously for lateral pain in the left elbow which was diagnosed as left lateral humeral epicondylitis. She was given steroid injections using a mixture of corticosteroid (specific drug name unknown) and lidocaine for the treatment. The patient felt severe pain, whitening, numbness and swelling immediately after injection in the left hand. The local hospital treated her with medication to improve the circulation (specific treatment of unknown drugs). However, even after several days the symptoms did not improve significantly.

We performed physical examination and found that the left elbow distal skin exhibited ecchymosis. Skin temperature was low and the results of nail bed capillary refill test were acceptable. The tingling sensation at the distal forearm was decreased. Her left handgrip decreased, and radial artery and ulnar artery was palpable (Fig. 1a). We also performed auxiliary

Key words: radial artery, ischemia, corticosteroid injection, diagnosis

Mailing address:
Dr. Rui-Jun Li,
Department of Hand Surgery,
The First Hospital of Jilin University,
71 Xinmin Street, Changchun 130021,
Jilin, China
e-mail: mrsruijun_li@yahoo.com

0393-974X (2018)
Copyright © by BIOLIFE, s.a.s.
This publication and/or article is for individual use only and may not be further reproduced without written permission from the copyright holder.
Unauthorized reproduction may result in financial and other penalties
DISCLOSURE: ALL AUTHORS REPORT NO CONFLICTS OF INTEREST RELEVANT TO THIS ARTICLE.

examination and found that arterial ultrasound of the left upper extremity showed no significant thrombosis. Electromyography (EMG) of the left upper extremity median nerve, ulnar nerve, and radial nerve exhibited no clear electrophysiological abnormalities. Clinical diagnosis after admission was microcirculation disturbance at the distal left elbow. The patient was given anticoagulant to improve microcirculation, and a baking light was used to keep the distal left elbow warm. Two days later, the left forearm and left-hand skin ecchymosis was significantly improved. The incidence and extent of pain was significantly reduced (Fig. 1b). After 4 days, the left forearm and left-hand ecchymosis were significantly reduced, to a lesser degree, with a marked reduction in the degree of swelling and a good tingling of the left hand (Fig. 1c). After discharge, the patient continued to be given anticoagulant drugs to improve circulation. After two weeks, the left forearm and left-hand ecchymosis disappeared completely. The blood supply returned to normal, the pain and numbness disappeared and the left handgrip recovered.

Case 2. Another female aged 49 years was admitted to our hospital due to localized finger pain with bruising approximately 8 hours after corticosteroid injection for the treatment of the right after being diagnosed with radial styloid de Quervain tenosynovitis. The patient reported that she had been treated at a local clinic about six months previously. She received corticosteroid injections using a mixture of prednisolone acetate suspension and lidocaine (unknown dose). Due to the injections, sever bleeding occurred and she was immediately given local pressurized hemostasis. The patient immediately experienced a cooling sensation, swelling, pain in the right thumb, and gradual skin discoloration (turning purple). In order to receive further treatment, she was admitted to our hospital.

On examination, the skin exhibited diffuse purple on the right palm and right thumb ring, especially in the nail bed area. She suffered from hand swelling, low skin temperature, low nail bed refill, weak radial artery pulsation, negative Allen's test, and significantly weak central finger pulsation. After admission, the clinical diagnosis was right wrist radial synovial stenosing tenosynovitis and vascular injury after steroid injection. She was given anticoagulant, antispasmodic and thrombolysis treatment to improve microcirculation within 24 hours after admission. However, no significant improvement was seen. The following day, we decided to perform right-sided surgical exploration under anesthesia. During surgical exploration, the dorsal carpal tunnel was examined at the radial cord to explore the radial artery (1) which showed good continuity, the puncture was healed, and there was no obvious bleeding at the radial artery patency. Then, *via* Z-shaped incision, the palm of the hand was explored. The superficial patellar pulsed well, and there was no existence of substances along the distal branches. The dorsal metacarpophalangeal artery at the "Y" structure and its proximal end were then explored, and found the presence of white emboli in the lumen, which blocked the arterial blood supply. The white embolus was about 1.0 ~ 1.5 cm long (Fig. 2a). A longitudinal incision was made of the arterioles at the formation of emboli under 10×microscope, and micro-instruments were used

Fig. 1. ***A)*** *Left forearm and left-hand ecchymosis at admission.* ***B)*** *Left forearm and left-hand ecchymosis 2 days after admission.* ***C)*** *Left forearm and left-hand ecchymosis 4 days after admission.*

to gently remove the emboli followed by urokinase solution rinse and micro-vascular suture. The emboli were observed under a microscope and found that it was cylindrical, thick in the middle, thin at both ends, with some flexibility and toughness (Fig. 2b), and not soluble in saline solution. After the original treatment and close observation of the affected hand blood supply situation, the patient's hand skin temperature was significantly improved after one week. Her skin bruising color was gradually reduced after two weeks, and she was completely relieved from pain in the hand. The blood supply of thumb and finger rings was good, exhibited normal capillary refilling and finger shape and function were satisfactory.

Both patients provided informed, signed consent for publishing the details of these cases.

DISCUSSION

Corticosteroid injection is widely used for pain management originating from local anesthesia. The basic method of operation is to inject a mixture of local anesthetics and steroids into the site of pain. Corticosteroid injection has both anti-inflammatory and analgesic effects. It is commonly used for the treatment of acute or chronic soft tissue injury, non-suppurative inflammation, such as frozen shoulder, epicondyelodynia, tenosynovitis, myofascitis, etc. While surgery may be considered for patients with early improper treatment, a history of illness and stubborn symptoms, corticosteroid injection treatment is an effective treatment for early symptoms of humeral epicondylitis or tenosynovitis (2, 3). Although corticosteroid injection therapy has its advantages in clinical application in recent years, it has been found to have a potential to cause microcirculation disturbance of the distal limbs, which may lead to the risk of amputation in severe cases. (4, 5).

As for the pathogenesis of microcirculation disturbance caused by treatment of corticosteroid injection, we believe that the following two aspects may be the major contributors. Firstly, sympathetic dysfunction: corticosteroid injections may stimulate the sympathetic nervous system. When sympathetic nervous activity in patients is high, small artery resistance is increased due to the reaction to the

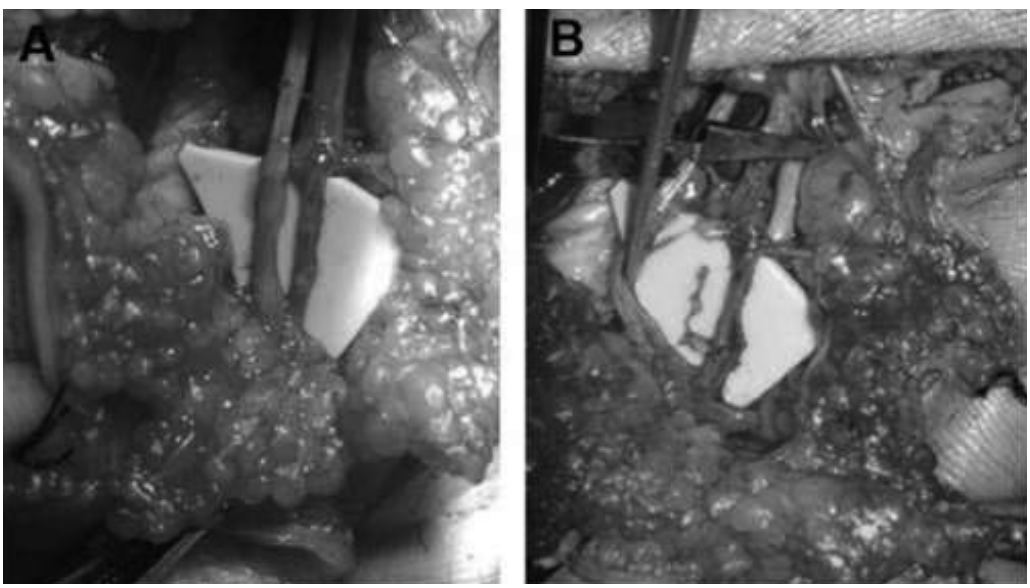

Fig. 2. ***A)*** *The presence of white emboli in the lumen of the carotid artery. The black tip refers to the location of the embolus.* ***B)*** *Arterial incision exposed white emboli, which was cylindrical, thick in the middle, and thin at both ends. The black tip refers to the partial removal of the emboli.*

sympathetic nervous system, leading to intractable vaso-occlusive crisis, manifested as large-scale skin ecchymosis, numbness and pain. When using anti-coagulation to improve microcirculation, nourishing nerves and other symptomatic treatment, the corticosteroid injection crisis can be gradually lifted and the symptoms can be gradually reduced to disappear. Therefore, the causes of microcirculation disturbance may be caused by abnormal sympathetic excitement. Secondly, if the operator is not familiar with anatomy and the operation is not standardized, steroids may be injected into important arteries, resulting in micro-thrombosis and microcirculation disturbances. In the present case no. 2, the presence of white emboli was found in the lumen of the dorsal metacarpophalangeal artery at the "Y" structure. We postulated that the emboli were the formation of drugs in the blood vessel. After removing the emboli, the blood supply of the affected hand was significantly improved. The location of the drug emboli may be related to the molecular size of the drug molecule and its solute consistency.

Apart from these two circumstances, other reasons may include vascular anatomical variation (6) and mismatched drugs.

Thus, we have developed the following preventive measures:

i. The familiarity with anatomical landmarks and standardized operation (7). During corticosteroid injection treatment, when the needle is inserted into the skin, it is critical to ensure that there is no access to the blood vessels after local injection.

ii. The choice of corticosteroid drug treatment. It is possible to select water soluble drugs without precipitation to reduce the incidence of vascular embolism.

iii. Being cautious of sympathetic sensitivities, such as patients with Reynolds syndrome. If necessary, the corticosteroid injection can be injected twice with a time interval of 10-15 minutes. If abnormal reaction or microcirculation disorder occurs, injection should be stopped, and treatment given immediately.

iv. Early detection and treatment. If microcirculation disorder occurs, anticoagulant can be given to improve microcirculation and nourish nerves. Baking light can be used to keep the local area warm. If the symptoms do not improve or become further aggravated, surgical intervention should be carried out to avoid limb distal necrosis.

Corticosteroid treatment is a simple and effective method for the treatment of pain widely used in clinical practice. However, it may lead to microcirculation disturbance of distal limbs, therefore this should be brought to the attention of clinicians. Early detection and early treatment should be carried out to avoid adverse consequences.

REFERENCES

1. Sachin AC, Karen V, Achilleas T. Ischemia of the hand secondary to radial artery thrombosis: A report of three cases. Can J Plast Surg 2003; 11(3)145-8.
2. Akram M, Shahzad ML, Farooqi FM, Irshad M, Kumar Sah R, Awais SM. Results of injection corticosteroids in treatment of De Quervain's Tenosynovitis. J Pak Med Assoc 2014; 64(12 Suppl 2):S30-3.
3. Schubert C, Hui-Chou HG, See AP, Deune EG. Corticosteroid injection therapy for trigger finger or thumb: a retrospective review of 577 digits. Hand (NY) 2013; 8(4):439-44.
4. Taweepoke P, Frame JD. Acute ischaemia of the hand following accidental radial artery infusion of depo-medrone. J Hand Surg Br 1990; 15B:118-20.
5. Swindells MG, Tehrani H, Goodwin-Walters A, Sassoon EM. Acute radial artery ischemia following therapeutic steroid injection. Ann Plast Surg 2007;58(4):461-62.
6. Green DP, Hotchkiss RN, Pederson WC. Green's Operative Hand Surgery. 4th ed. Philadelphia: Churchill Livingstone; 1999:2036.
7. Coleman SS, Anson BJ. Arterial patterns in the hand based upon a study of 650 specimens. Surg Gynecol Obstet 1961; 113:409-24.

LETTER TO THE EDITOR

COMBINED TREATMENT OF TRADITIONAL CHINESE MEDICINE AND WESTERN MEDICINE IN THE TREATMENT OF DIABETIC PERIPHERAL NEUROPATHY

JY. XU and HY. GAO

Department of Traditional Chinese Medicine, Binzhou City Center Hospital, Binzhou, China

Received November 21, 2017 – Accepted May 24, 2018

Diabetic peripheral neuropathy (DPN), a common complication of diabetes, has a high morbidity, and currently there is no effective therapy. To investigate the clinical effect of traditional Chinese medicine in combination with Western medicine, 88 patients with early DPN who were admitted to Binzhou City Center Hospital, Shandong, China, between November 2015 and November 2016, were selected as the research subjects and were randomly divided into a control group and an observation. Patients in the control group were treated by conventional Western medicine, while patients in the observation group were treated by traditional Chinese medicine in addition to conventional Western medicine. The clinical effect was compared between the two groups. The results demonstrated that the overall effective rate of the observation group was much higher than that of the control group, and the difference was statistically significant (P<0.05). The vibration perception threshold (VPT) of nervus peroneus communis, nervus suralis and posterior tibial nerve of the two groups significantly declined after treatment (P<0.05), however, the decreae in the observation group was more obvious (P<0.05). The improvement of glycosylated hemoglobin (HbAlc) and blood glucose of the observation group was superior to that of the control group, and the difference had statistical significance (P<0.05). In conclusion, traditional Chinese medicine in combination with Western medicine has a remarkable effect in the treatment of DPN and can effectively relieve vital signs and clinical symptoms of patients and significantly improve nerve conduction velocity. The therapy is worth clinical application and promotion.

To the Editor,

Diabetic peripheral neuropathy (DPN), a common complication of diabetic patients, has a morbidity of 50-80%. It manifests as paresthesia, such as numbness of limb, stinging and burning pain in the extremities of limbs (1, 2). DPN, which is difficult to cure, is the major risk factor inducing diabetic foot ulcer, infection and gangrene. It can severely affect the living quality of patients besides bringing an economic burden on the patient's family, hence effective treatment is extremely important (3).

The basic treatment measures for DPN are to strictly control blood glucose and give drug or non-drug treatment based on effective controlling of blood glucose (4, 5). Currently, many chemical drugs, including vasodilation, neurotrophic drugs, antioxidants and drugs which can improve neural microcirculation can be used for treating DPN, and their action mechanisms are different in treating DPN. Although the drugs are effective, the effects are not satisfactory. Mecobalamine, a frequently used drug for treating DPN, has functions of controlling

Key words: diabetic peripheral neuropathy, traditional Chinese medicine in combination with Western medicine, vibration perception threshold

Mailing address:
Dr Jianyong Xu,
No.108 Huancheng South Road,
Department of Traditional Chinese Medicine,
Binzhou City Center Hospital,
Binzhou, Shandong, 251700, China
e-mail: xujianx0543@163.com

0393-974X (2018)
Copyright © by BIOLIFE, s.a.s.
This publication and/or article is for individual use only and may not be further reproduced without written permission from the copyright holder.
Unauthorized reproduction may result in financial and other penalties
DISCLOSURE: ALL AUTHORS REPORT NO CONFLICTS OF INTEREST RELEVANT TO THIS ARTICLE.

disease development and relieving limb dysfunction, but its clinical treatment has limitations. Tripple et al. (6) found that mecobalamine could not relieve the feeling of numbness and of piercing pain in patients. Alprostadil, which is a prostaglandin vasodilator agent, can significantly improve microcirculation; however its half-life period is short, usually between 5 and 10 min, and most patients cannot tolerate 24 h of intravenous administration because of multiple adverse reactions (7). In the present study, 88 patients with DPN were treated with conventional Western medicine only or with Western medicine combined with traditional Chinese medicine, and the comparison of the clinical effects were statistically significant.

MATERIALS AND METHODS

General data

Eighty-eight patients with DPN who were admitted to Binzhou City Center Hospital, Shandong, China, between November 2015 and November 2016, were selected as research subjects. They were randomly divided into an observation group and a control group, 44 in each group. In the observation group, there were 25 males and 19 females aged between 50 and 77 years (average 60.5±5.3 years). In the control group, there were 24 males and 20 females aged between 51 and 78 years (average 61.7±6.8 years). The differences of age and gender between the two groups had no statistical significance ($p>0.05$); therefore the results were comparable. This study was approved by the ethics committee of our hospital, and all the patients signed informed consent.

Criteria for inclusion and exclusion of research subjects

Patients who satisfied the diagnostic criteria of DPN stipulated in Diagnostic Classification Criteria of Diabetes released by WHO in 1999 (8) and had vital signs and symptoms of polyneuropathy and hypoesthesia and multifocal motor neuropathy, such as numbness of limb, formication, burning sensation and stabbing pain on admission, were included.

Patients who had neuropathy induced by other reasons including neurotoxic drugs, drinking, deficiency of vitamin B1 and B12, renal diseases, chronic inflammatory demyelinating polyneuropathy, hereditary neuropathy and vasculitis were excluded.

Treatment

Patients in the control group were treated with conventional Western medicine. Oral hypoglycemic drugs such as insulin and metformin were used for controlling the blood glucose level of patients; the level of fasting blood glucose was controlled below 7.0 mmol/L, and the level of blood glucose 2 h after a meal was controlled below 10.0 mmol/L. 500 μg of mecobalamine was was mixed with 250 ml of NaCl solution (0.9%), and then the patients were intravenously injected with the mixture, once each day, for three weeks. Patients in the observation group were given Buyang Huanwu decoction besides conventional Western medicine. Buyang Huanwu decoction was composed of 15 g of *Radix paeoniae rubra*, 15 g of *lumbricus*, 15 g of *Angelica sinensis*, 15 g of *Ligusticum wallichii*, 25 g of *Astragalus membranaceus*, 10 g of red flower and 10 g of peach kernel. If the upper limbs were the main diseased part, then 20 g of *Ramulus mori* was added. If the lower limbs were the main diseased part, then 15 of *Achyranthes bidentata* was added. The aforementioned drugs were decocted with water. The patient took 300 ml of decoction each day, in the morning and evening, for three weeks.

Observation indexes

The clinical effects, VPT and blood glucose levels were observed and compared between the two groups. The evaluation criteria were as follows. Treatment was considered as remarkably effective if VPT recovered to normal value, the clinical symptoms disappeared, and tendon reflex was obviously relieved. Treatment was considered as effective if VPT decreased, the clinical symptoms were obviously relieved, and tendon reflex was relieved slightly. Treatment was considered as ineffective if VPT, the clinical symptoms and tendon reflex had no improvement. The computational formula of the overall effective rate was: overall effective rate = (cases of significantly effective treatment + cases of effective treatment) * 100%.

VPT was measured using a digital vibrance threshold tester (Beijing Laxons Times Science and Technology Co., Ltd., China). After 10 min of rest, the patient took a supine position on the examination bed. The VPT of nervus peroneus communis, nervus suralis and posterior tibial nerve was measured. The average value was taken as the final result.

The level of fasting blood glucose and the level of

blood glucose 2 h after a meal were measured. Blood glucose was measured using a fully automatic biochemical analyzer based on the glucose oxidase method. Glycosylated hemoglobin (HbAlc) was measured using the latex agglutination method (transmission endpoint method).

Statistical analysis

All the data were processed using SPSS ver. 20.0 software. Data were expressed as mean ± standard deviation. Comparison between groups was performed using paired *t*-test. Enumeration data were processed by *Chi*-squared test. Difference was considered as statistically significant if $P<0.05$.

RESULTS

Comparison of curative effect between the two groups

The overall effective rate of the observation group was 93.3%, which was significantly higher than that of the control group (75%) ($\chi^2=8.273$; $P<0.05$; Fig. 1).

Comparison of VPT between the two groups before and after treatment

The VPT of nervus peroneus communis, nervus suralis and posterior tibial nerve of the two groups had no remarkable difference before treatment ($P>0.05$). The VPT of both groups had an obvious decrease after treatment ($P<0.05$). The decrease in the observation group was more remarkable than that of the control group ($P>0.05$; Table I).

Comparison of blood glucose level between the two groups

The levels of HbAlc, fasting blood glucose and blood glucose 2 h after meal of the two groups had no remarkable difference before treatment ($P>0.05$). The levels of HbAlc, fasting blood glucose and blood glucose 2 h after meal decreased after treatment, and the decline of the observation group was more obvious than that of the control ($P<0.05$; Table II).

DISCUSSION

The pathogenesis of DPN is not yet clearly known, and is extensively considered as the result of multiple factors. It was reported that the occurrence and development of DPN was in a close association with glucose metabolism disorder (9, 10), abnormal protein kinase c activity, insufficiency of nerve growth factor, insufficiency of γ- linolenic acid and

Table I. *Comparison of VPT between the two groups before and after treatment.*

Group		Observation group	Control group
Before treatment	Nervus peroneus communis	31.23± 2.71	30.18±3.22
	Nervus suralis	30.33±3.26	29.27±3.67
	Posterior tibial nerve	29.35±2.16	28.88±4.10
After treatment	Nervus peroneus communis	15.62±2.69*#	19.23±3.54*
	Nervus suralis	13.28±3.26*#	18.25±3.18*
	Posterior tibial nerve	12.65±3.33*#	17.59±3.35*

*(Mean±standard deviation, V) * $P<0.05$ compared to before treatment; # indicated $P<0.05$ compared to the control group.*

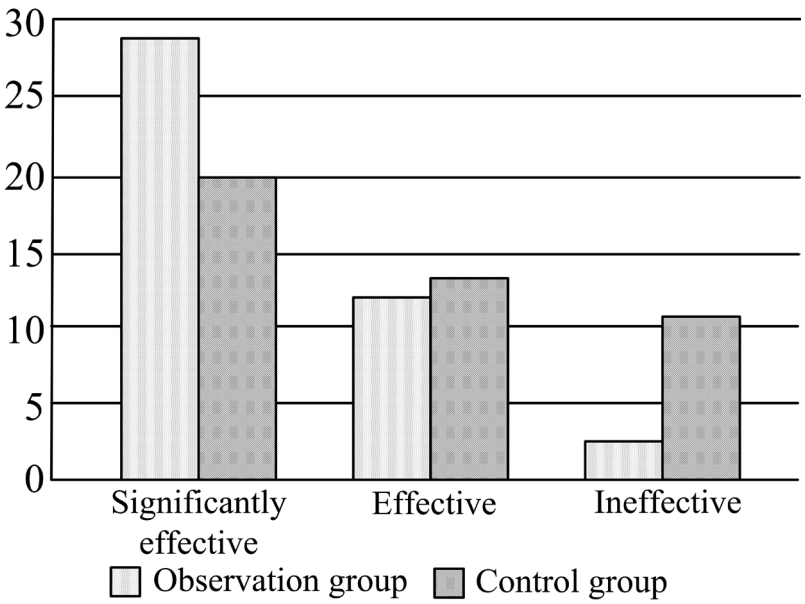

Fig. 1. *Comparison of curative effects between the two groups after treatment.*

Table II. *Comparison of level of HbAlc and blood glucose between the two groups.*

Group	Before treatment			After treatment		
	HbA1c	Fasting blood glucose	Blood glucose 2 h after meal	HbA1c	Fasting blood glucose	Blood glucose 2 h after meal
Observation group	10.4±2.2	26.4±1.3	16.6±2.8	6.7±1.2*#	9.2±1.1*#	7.1±0.2*#
Control group	10.2±2.5	26.3±1.2	16.4±2.4	8.4±2.6*	19.4±4.3*	10.3±2.2*

*(mean ± standard deviation, mmol/L). * $P < 0.05$ compared to before treatment; # indicated that $P < 0.05$ compared to the control group.*

immune abnormality. Traditional Chinese medicine considered that DPN belonged to the category of flaccid paralysis and arthromyodynia and that DPN was induced by deficiency of yin, stagnancy of energy, blood stasis, blocking of main and collateral channels, muscular malnutrition and imbalance of yin and yang.

Buyang Huanwu decoction developed by Qingren Wang, a famous doctor in the Qing dynasty, was used in this study according to years of experience of the authors. *Astragalus membranaceus* can reinforce Qi and nourish Yin; peach kernel, *Carthamus tinctorious*, *radix paeoniae rubra*, *Ligusticum wallichii* and *Angelica sinensis* can activate blood, remove stasis, stimulate the circulation of the blood, and cause the muscles and joints to relax; lumbricus can dredge collaterals. In the prescription, tonifying qi combined with nourishing yin, activating blood was implemented along with dredging collaterals (11). Modern studies concerning pharmacology

of traditional Chinese medicine demonstrated that *Carthamus tinctorious* injection could significantly reduce the content of endothelin and thromboxane, i.e., improve vascular endothelial cell function, through reducing levels of fasting blood glucose and HbAlc and significantly improve the content of 6-Keto-PG F1a (12). Lumbricus can resist coagulation and thrombogenesis. Herbs which have functions of activating blood and removing stasis can expand blood vessels, inhibit platelet aggregation, reduce blood viscosity, and increase the microcirculation perfusion of peripheral nerve tissues, which can help relieve ischemia and anoxia. The results of the present study demonstrated that the overall effective rate of the observation group was much higher than that of the control group after treatment; the decline of VPT of nervus peroneus communis, nervus suralis and posterior tibial nerve and the improvement of blood glucose level of the observation group was significantly superior to that of the control group. The results indicate that Buyang Huanyang decoction could improve the effect of mecobalamine in treating DPN. The reason might be the different action mechanisms of the two drugs and the synergistic effect of combined use of drugs.

In conclusion, traditional Chinese medicine in combination with Western medicine has a significantly better effect in treating DPN, therefore it is worth application and promotion. However, the study also had limitations, such as the small sample size and short follow-up period. Multi-center tests with a large sample size remain to be carried out to further study the effects of traditional Chinese medicine combined with Western medicine on the long-term survival quality of DPN patients.

REFERENCES

1. Adams AS, Parker MM, Moffet HH, et al. Communication barriers and the clinical recognition of diabetic peripheral neuropathy in a diverse cohort of adults: the distance study. J Health Commun 2016; 21(5):544-553.
2. Patil PR, Wolfe J, Said Q, Thomas J, Martin BC. Opioid use in the management of diabetic peripheral neuropathy (DPN) in a large commercially insured population. Clin J Pain 2015; 31(5):414-424.
3. Fernando M, Crowther R, Lazzarini P, Sangla K, Cunningham M, Buttner P, Golledge J. Biomechanical characteristics of peripheral diabetic neuropathy: A systematic review and meta-analysis of findings from the gait cycle, muscle activity and dynamic barefoot plantar pressure. Clin Biomech 2013; 28(8):831-845.
4. Galuppo M, Giacoppo S, Bramanti P, Mazzon E. Use of natural compounds in the management of diabetic peripheral neuropathy. Molecules 2014; 19(3):2877-2895.
5. Gupta M, Singh J, Sood S, Arora B. Mechanism of antinociceptive effect of nimodipine in experimental diabetic neuropathic pain. Methods Find Exp Clin Pharmacol 2003; 25(1):49-52.
6. Trippe BS, Barrentine LW, Curole MV, Tipa E. Nutritional management of patients with diabetic peripheral neuropathy with L-methylfolate-methylcobalamin-pyridoxal-5-phosphate: results of a real-world patient experience trial. Curr Med Res Opin 2016; 32(2):219-227.
7. Wu QP. Influence of epalrestat in combination with alprostadil on homocysteine and nerve function in patients with diabetic peripheral neuropathy. Int Med Health Guid News 2016; 22(2):248-251.
8. Vileikyte L, Peyrot M, Gonzalez JS, et al. Predictors of depressive symptoms in persons with diabetic peripheral neuropathy: a longitudinal study. Diabetologia 2009; 52(7):1265-1273.
9. Javed S, Petropoulos IN, Alam U, Malik RA. Treatment of painful diabetic neuropathy. Ther Adv Chronic Dis 2015; 6(1):15-28.
10. Mustapa A, Justine M, Mohd MN, Jamil N, Manaf H. Postural control and gait performance in the diabetic peripheral neuropathy: a systematic review. Biomed Res Int 2016; 2016:9305025.
11. Ning LN. Comparison of curative effects of Mudan granule, lipoic acid and mecobalamine in treating DPN. World Latest Med Inform 2015; 15(43):29.
12. Stavniichuk R, Shevalye H, Lupachyk S, Obrosov A, Groves JT, Obrosova IG, Yorek MA. Peroxynitrite and protein nitration in the pathogenesis of diabetic peripheral neuropathy. Diabetes Metab Res Rev 2014; 30(8):669-78.

LETTER TO THE EDITOR

EFFECTS OF ASTRAGALUS GLYCOPROTEIN ON Th17/TREG CELLS IN MICE WITH COLLAGEN-INDUCED ARTHRITIS

ZH. WANG[1*], C. QIN[1*], T. RAN[1*], DQ. YANG[2] and JH. GUO[3]

[1]Department of Orthopedics and Ttraumatology, Traditional Chinese Medicine Hospital, Dianjiang, Chongqing, China; [2]Department of Cardiovascular, Traditional Chinese Medicine Hospital, Dianjiang, Chongqing, China; [3]Department of Traumatology Center, Traditional Chinese Medicine Orthopaedic Hospital, Chongqing, China

Received April 11, 2018 – Accepted May 21, 2018

* These authors contribute equally to this work

In this study of Th17/Treg cells, the therapeutic effect of Astragalus glycoprotein on collagen-induced arthritis in mice (CIA) was explored, and a basis for the clinical treatment of rheumatoid arthritis is provided. Sixty mice were selected for the establishment of a CIA mouse model, and were then randomly divided into a CIA model group, a hydrocortisone control group, a low, medium, and high dose group of Astragalus glycoprotein, respectively. The same number of control groups with same number of mice was established and after basic immunization, intraperitoneal injections were given once daily for two weeks in the treatment. At the end of the treatment, the mice in each group were selected and the proportion of Th17/Treg cells was detected by flow cytometry. The expression and positive expression of RORγt, Foxp3, P-STAT3 and P-STAT5 protein were detected by Western blot and immunohistochemistry. Astragalus glycoprotein was shown to potentially improve the diet and mental state, reduce the arthritis index score and improve the pathological state of synovial membranes in the mice. Moreover, flow cytometry results showed that, compared with the CIA model group, the proportion of Th17 cells in the four other groups of mice decreased, while the proportion of Treg cells increased. This difference was statistically significant ($P<0.05$). From the experiment, the following conclusions were drawn: Astragalus glycoprotein can reduce Th17 cells and their transcription factors in the peripheral blood of CIA mice, up-regulate Treg cells and their transcription factors, and correct the balance of Th17/Treg cells so as to achieve an effective of treatment for CIA mice.

To the Editor,

Rheumatoid arthritis (RA) is a common autoimmune disease. It can seriously affect the quality of life of patients (1-2). At present, the pathogenesis of RA is not yet clear, but immune dysfunction, especially the immune imbalance of CD4+ T cell subsets is the main pathogenesis of RA (3-4). For example, Moon et al. (5) found that biological inhibitors against the interferon and retinoic acid-induced apoptosis-related gene (GRIM-19) can improve the symptoms of joint inflammation in CIA mice through down-regulation of IL-17 expression, up-regulation of Treg expression, and other pro-inflammatory cytokines. The discovery of a pattern of an imbalance of Th17/Treg cells has complemented and expanded the traditional mechanism of Th1/Th2

Key words: yellow glycoprotein, collagen-induced arthritis, Th17/Treg cells, transcription factors

Mailing address:
Dr Jianhua Guo,
Department of Traumatology Center,
Traditional Chinese Medicine Orthopaedic Hospital,
No. 489 Xinhua Road, Chongqing, China
e-mail: drguojianhua@163.com

0393-974X (2018)
Copyright © by BIOLIFE, s.a.s.
This publication and/or article is for individual use only and may not be further reproduced without written permission from the copyright holder.
Unauthorized reproduction may result in financial and other penalties
DISCLOSURE: ALL AUTHORS REPORT NO CONFLICTS OF INTEREST RELEVANT TO THIS ARTICLE.

imbalance in RA, and has opened up new avenues for further exploration of the mechanism behind the treatment of RA. In addition, discovery of the Th17/Treg cell imbalance mode has not only built on and broadened the traditional mechanism of Th1/Th2 imbalance in RA, but has supplied new strategies for further investigating its mechanism and treatment.

Astragalus membranaceus is an effective traditional Chinese medicine for tonifying qi. It has a variety of pharmacological effects, such as immune regulation, and obvious liver and kidney toxicity has not been found (6-7). Liu et al. (8) found that astragalus flavonoids can protect the OPG/RANKL/NF-κB pathway of adjuvant arthritic rats. However, the mechanism of interaction between Astragalus membranaceus and the active components of RA, as well as that between its components, has not yet been completely elucidated, and further in-depth study is needed. A CIA mouse model was established to investigate the efficacy and possible mechanism of the effects of astragalus glycoprotein on CIA mice. This research was conducted in order to provide an experimental basis for the clinical treatment of RA with *Astragalus membranaceus*.

MATERIALS AND METHODS

Eighty BALB/c male mice (60 mice were ised in the study and the remaining 20 were for standby), weighing 20±2g, were purchased from Beijing Weitong Lihua Experimental Animal Technology Co., Ltd, China. Before the experiment, all mice were placed in a clean room with a relative humidity of 50% at a room temperature of 22±2°C and fed with common chow for one week. During this period, the mice were given free access to chow and water. The study was approved by Ethics Committee of Traditional Chinese Medicine Hospital.

The main equipment used: flow cytometry, Becton Dickinson, USA; protein electrophoresis system, Beijing Junyi Eastern Electrophoresis Equipment Co., Ltd., China; optical microscopy, Olympus Optical, Japan; paraffin slicer, Leica, Germany; exhibition machine, Shanghai Yi Huai Instrument Co., Ltd., China; low-temperature high-speed centrifuge, Shanghai Aiyi Electronic Technology Co., Ltd., China; electric blast drying oven, Shenzhen Huade Weikang Technology Co., Ltd., China.

The main experimental reagents were: astragaloside provided by the laboratory of Henan College of Traditional Chinese Medicine. Hydrocortisone was purchased from Tianjin Biochemical Pharmaceutical Co., Ltd, China. Freund's complete adjuvant was purchased from Beijing Gaoke Henghui Technology Development Co., Ltd, China. Collagen type II (bovine) was purchased from Sigma. Formaldehyde, anhydrous ethanol, xylene, paraffin wax, and neutral gum were all purchased from China National Pharmaceutical Group Chemical Reagent Co., Ltd. Decalcification solution, hematoxylin dye solution, eosin staining solution, hydrochloric acid-diethanol differentiation solution, coverslip, and anti-offset glass slides were purchased from Beijing Zhongshan Jinqiao Biotechnology Co., Ltd, China.

Preparation of CIA mouse model

Sixty Balb/c mice were subcutaneously injected in the abdomen, back and tail root with 0.1 ml of prepared emulsifier (a mixture of equal volumes of bovine type II collagen and Freund's complete adjuvant). The basic immunization was performed on the first day of injection and the same method was used for boosting on the 21st day. The Polyarthritis index (PI) was used to evaluate whether the mouse model was replicated successfully. For evaluation, the same laboratory staff observed the pathological limb changes in the mice every 3 days.

Grouping

The mice of the successful model were randomly divided, with 12 in each group, into a CIA model group, a hydrocortisone control group, and low, medium, and high dose astragalus glycoprotein groups, respectively. On the 41st day after injection the 5 groups of mice were treated with drugs: in the hydrocortisone control group, the mice were intraperitoneally injected with hydrocortisone (HC) 10 mg/kg, while the mice in the low, medium, and high dose groups were intraperitoneally injected with 0.5 mg/kg, 1.0 mg/kg, and 2.0 mg/kg astragalus glycoprotein, respectively. The mice in the CIA model group were intraperitoneally injected with 0.4 ml/20 g saline. The medication was administered once a day for a total of two weeks.

The next day, the mice's knee joints were taken and placed in decalcification solution at room temperature, and 1 ml of the blood from an eyeball of each of the mice

was collected and placed in a refrigerator at 4°C. The mice were subsequently euthanized, after which the spleen was removed and divided into three parts and labeled. Two of these were placed in liquid nitrogen and one in a 10% formaldehyde solution for later use.

Experiment

HE staining was used to observe the pathological damage of the mice's knee joints. First, the decalcified mouse joints were removed, washed and dehydrated; they were then cleared in xylene, wax immersed, and embedded in paraffin; the wax blocks were sliced, spread, filleted and baked. The HE staining was performed on the wax pieces, and after the treatment was completed, they were naturally air-dried for observation under the light microscope.

Flow cytometry was used to detect the proportion of Th17/Treg cells in the peripheral blood of the mice.

Western blotting was used to detect the expression of RORγt, Foxp3, P-STAT3, and P-STAT5 in the spleen tissue of the mice. Lysates were prepared and proteins were extracted and stored at -20°C. Protein concentration was determined according to the protein quantification kit instructions. SDS-PAGE gel electrophoresis was performed at 100 V constant pressure wet transfer for 75 min. Blocking treatment was performed for one hour. Primary and secondary antibodies were incubated. The film was developed and fixed and then canned, and Quantity One software was used to analyze the light density value.

The expression of RORγt, Foxp3, P-STAT3, and P-STAT5 protein in the spleen of mice was detected by immunohistochemistry. After the paraffin section was prepared, it was dewaxed, hydrated, washed, ruptured, incubated, and antigen-repaired. The bovine serum albumin and primary antibody were added dropwise, and the secondary antibody was added dropwise after rewarming to room temperature. The color was developed with a developer, and the dehydration and xylene were again rinsed. Finally, the sealing was performed and the image was analyzed and processed under a 400-fold field of view with a light microscope.

Statistical analysis

SPSS 22.0 statistical software was used to process the data, and the measurement data was expressed as the mean standard deviation ($\bar{x}\pm s$). If the data was in a normal distribution and the variance was equal, one-way analysis of variance was used. Comparison between the groups was performed using the LSD test. If the normal distribution or variance was not met, then the Rank sum test was used. The cutoff value for a statistically significant difference was $P<0.05$.

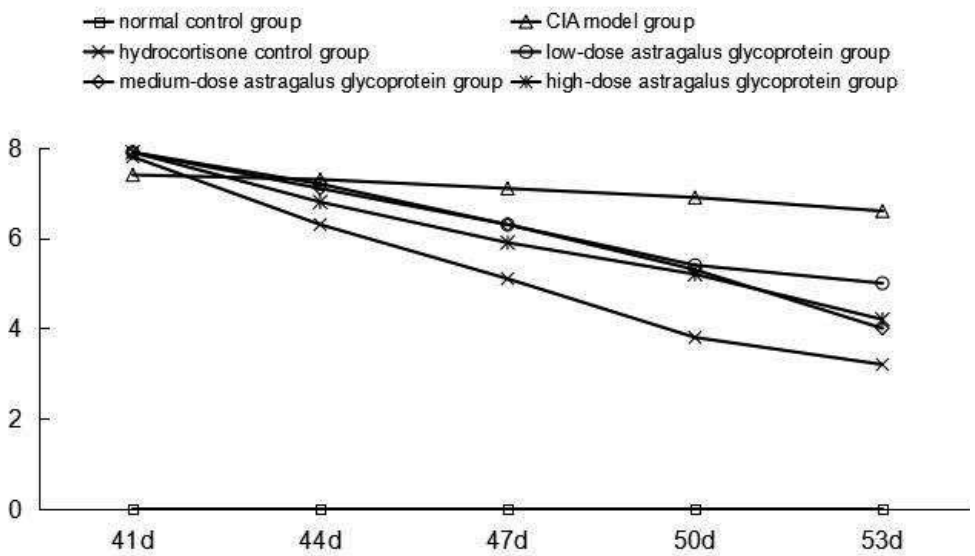

Fig. 1. *Changes in the influence of astragalus glycoprotein on the arthritis index of CIA mice.*

RESULTS

Establishment of CIA mouse model and its PI situation

Compared with normal mice, the model mice developed typical reactions, including redness and swelling of the joints on the 21st day after immune injections. The swelling first appeared in the toe joints of the mice and, with the passage of time, it gradually increased, reaching a peak on the 41st day. Upon reaching this peak, the mean arthritis index scores of the model mice all achieved the model standard (PI>=4). With continuous administration of the drug in each drug group, the PI value continuously decreased. In the hydrocortisone control group, the arthritis index was the lowest, and the PI value was significantly lower than that in the CIA model group ($P<0.01$). The PI values of different dose groups of the astragalus glycoprotein group were all different from that of the model group.

Pathological damage of knee joints in CIA mice

Pathological lesions of the knee joints of CIA mice are shown in Fig. 2. In the CIA model group, the typical pannus was found, developing towards the articular cavity and cartilage. The articular cartilage surface was rough, uneven, defective and stripped, and there was severe destruction of articular cartilage and bone. In the hydrocortisone control group, the joint structure of the mice was intact, and the formation of pannus reduced. In addition, the articular cartilage surfaces of this group were relatively smooth, while cartilage and bone destruction was significantly reduced. In the low dose astragalus glycoprotein group, there was still obvious vascular exclusion of surface generation. The surface of the articular cartilage appeared rough and flaky, with some papillary bulges on parts of the cartilage. In the medium-dose and high-dose astragalus glycoprotein groups, the generation of pannus decreased, while the articular cartilage surfaces were slightly rough with intact structures. In these groups, there was no obvious damage to cartilage or bone tissue.

Proportion of Th17/Treg cells in peripheral blood of mice

Flow cytometry results are shown in Table I. It can

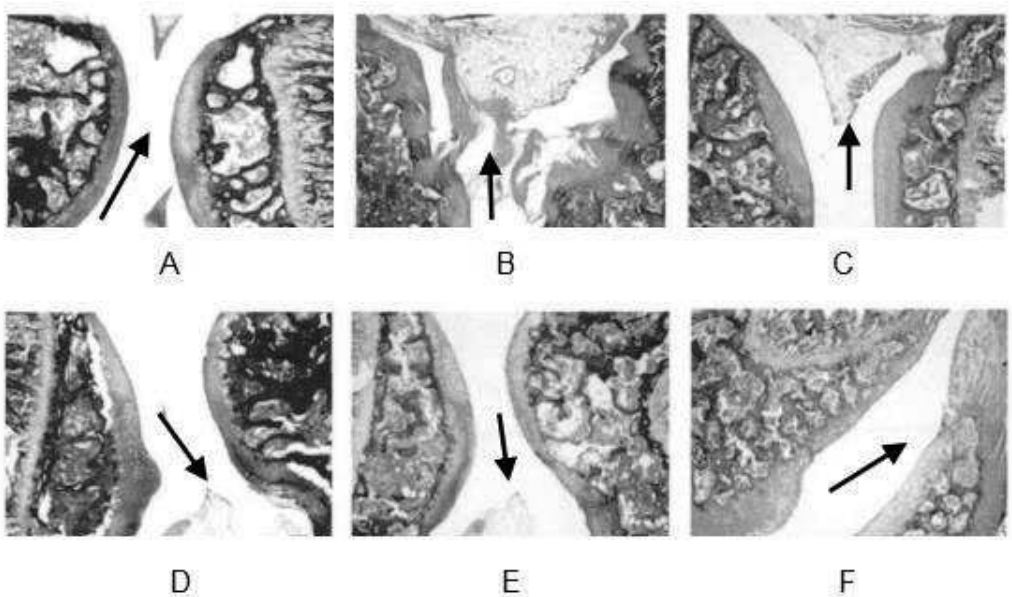

Fig. 2. *Effect of astragalus glycoprotein on pathological joint damage in CIA Mice (100×) **A**) Normal control group; **B**) CIA model group; **C**) hydrocortisone control group; **D**) low-dose astragalus glycoprotein group; **E**) medium-dose astragalus glycoprotein group; F. high-dose astragalus glycoprotein group)*

be seen from the data therein that, compared with the CIA model group, the proportion of Th17 cells in the hydrocortisone control group and the various doses of the astragalus glycoprotein groups decreased to differing extents. In addition, the proportion of Treg cells increased, and the difference was statistically significant (P<0.05).

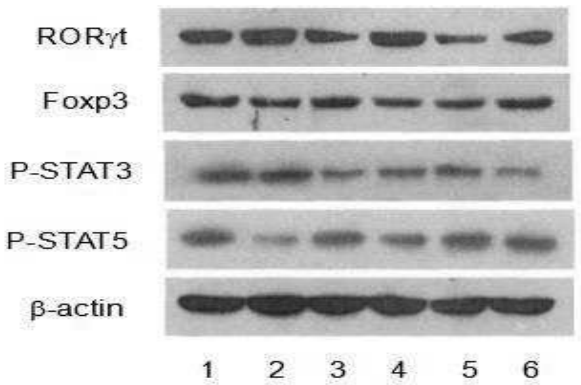

Fig. 3. *Effect of astragalus glycoprotein on the expression of RORγt, Foxp3, P-STAT3 and P-STAT5 protein in spleen tissue of CIA mice (Note: Lanes 1-6 are: the normal control group; the CIA model group; the hydrocortisone control group; the low-dose astragalus glycoprotein group; the medium-dose astragalus glycoprotein group; and the high-dose astragalus glycoprotein group, respectively)*

Expression of RORγt, Foxp3, P-STAT3 and P-STAT5 protein in spleen tissue of mice

Western blot test results showed that, compared with the CIA model group, the expression of RORγt and P-STAT3 decreased in the hydrocortisone control group, the medium-dose astragalus glycoprotein group and the high-dose astragalus glycoprotein group, while the expression of Foxp3 and P-STAT5 increased in these groups. The differences were statistically significant (P<0.05), as shown in Fig. 3 and Table I.

Protein expression distribution of RORγt, Foxp3, P-STAT3 and P-STAT5 in the spleen tissue of mice

The expression and distribution of RORγt, Foxp3, P-STAT3 and P-STAT5 proteins in the spleen tissue of the mice were detected by immunohistochemical analysis. It was found that four proteins were in the

Table I. *The effect of Astragalus glycoprotein on the proportion of peripheral blood Th17/Treg cells in peripheral blood of CIA mice, expression of RORγt, Foxp3, P-STAT3, P-STAT5 protein in CIA mice and the expression and distribution of RORγt, Foxp3, P-STAT3, P-STAT5 protein in spleen tissue (n=12, $\bar{x}\pm s$)*

	Normal control group	CIA model group	Hydrocortisone control group	Astragaloside low dose group	Baicalin glycoprotein intermediate dose group	Astragaloside high dose group
Th17 cell ratio	0.389±0.051	0.972±0.219#	0.532±0.084*	0.725±0.10**	0.593±0.194*	0.611±0.165*
Treg cell ratio	2.059±0.078	1.058±0.127#	1.830±0.171*	1.572±0.112**	1.899±0.213*	1.802±0.130.339±0.008**9*
RORγt/β-actin protein expression	0.324±0.018	0.436±0.011##	0.310±0.061**	0.419±0.022	0.291±0.086**	0.339±0.008**
Foxp3/β-actin protein expression	0.523±0.014	0.326±0.029##	0.461±0.037**	0.359±0.009	0.428±0.058**	0.450±0.025**
P-STAT3/β-actin protein expression	0.323±0.025	0.401±0.012##	0.227±0.013	0.302±0.016**	0.291±0.017**	0.254±0.028**
P-STAT/β-actin protein expression	0.464±0.012	0.288±0.011##	0.481±0.023	0.356±0.010**	0.543±0.015**	0.457±0.045**
RORγt positive cells	52.786±13.638	84.232±8.891#	47.454±5.741*	73.509±18.523	55.972±5.349*	64.233±8.874*
Foxp3 positive cells	167.893±28.676	78.937±14.675#	154.368±14.320*	86.733±12.473	131.831±12.925*	142.098±17.021*
P-STAT3 positive cells	31.135±7.902	42.973±3.098#	14.760±3.163*	34.175±5.104	25.287±4.972*	19.575±2.809*
P-STAT positive cells	41.693±4.762	18.480±3.142#	46.276±8.704*	23.691±4.242	47.018±4.395*	40.782±5.076*

*Note: Compared with the normal control group, #P<0.01, ##P<0.05; compared with the CIA model group, *P<0.01, **P<0.05*

spleen lymphocytes. Specifically, RORγt, Foxp3 and P-STAT5 were located in the nucleus and P-STAT3 was located in the nucleus and cytoplasm. All positive particles were brown or tan. Compared with the normal group, the positive expression of RORγt and P-STAT3 in the spleen tissue of the CIA model group increased significantly ($P<0.01$), and the positive expression of Foxp3 and P-STAT5 decreased significantly ($P<0.01$). In comparison with the CIA model group, the positive expressions of RORγt and P-STAT3 decreased to varying degrees in the spleen tissue of the hydrocortisone control group and all of the astragalus glycoprotein treatment groups. Specifically, the positive expression of RORγt and P-STAT3 decreased significantly in both the hydrocortisone control group and the medium-dose astragalus glycoprotein group ($P<0.01$). On the other hand, the positive expression of Foxp3 and P-STAT5 increased to varying degrees: the positive expression of Foxp3 as well as P-STAT5 increased significantly in both the hydrocortisone control group and the medium-dose astragalus glycoprotein group ($P<0.01$), as shown in Table I.

DISCUSSION

Th17 cells can induce the occurrence and progress of autoimmune diseases such as RA. Treg cells can reduce the autoimmune inflammatory response caused by the former, thereby maintaining the body's immune balance (9-10).

RORγt and STAT3 are the key transcription factors of Th17 cells. Loss of STAT3 leads to a decrease in the number of Th17 cells. Foxp3 is a specific transcription factor for Treg cells, and its activation depends on the STAT5 signaling pathway. The deletion of STAT5 inhibits the differentiation of Treg cells. The balance of RORγt/Foxp3 and STAT3/STAT5 can fundamentally affect the balance of Th17/Treg cells and eventually affect the development of autoimmune diseases like RA.

The results of the present study show that Th17/Treg cell imbalance exists in peripheral blood of CIA mice, however, after treatment with intraperitoneal injection of astragalus glycoprotein, the percentage of Th17 cells in the peripheral blood decreased and the proportion of Treg cells increased. Correspondingly, the expression of the RORγt and P-STAT3 proteins decreased while the expression of the Foxp3 and P-STAT5 proteins increased in mouse spleen tissues, which was statistically significant compared with the model group ($P<0.01$).

In summary, the effect of astragaloside on improving joint inflammation in CIA mice may be achieved by correcting the balance of RORγt/Foxp3 and STAT3/STATS signaling pathway proteins and correcting Th17/Treg cell balance.

REFERENCES

1. Cross M, Smith E, Hoy D, et al. The global burden of rheumatoid arthritis: estimates from the Global Burden of Disease 2010 study. Ann Rheum Dis 2014; 73(7):1316-22.
2. Tanaka Y. Human mesenchymal stem cells as a tool for joint repair in rheumatoid arthritis. Clin Exp Rheumatol 2015; 33(4 Suppl 92):S58-62.
3. Aterido A, Palacio C, Marsal S, Avila G, Julià A. Novel insights into the regulatory architecture of CD4+ T cells in rheumatoid arthritis. PLoS One 2014; 9(6):e100690.
4. Niu Q, Cai B, Huang ZC, Shi YY, Wang LL. Disturbed Th17/Treg balance in patients with rheumatoid arthritis. Rheumatol Int 2012; 32(9):2731-36.
5. Moon YM, Lee J, Lee SY, et al. Gene-associated retinoid-interferon-induced mortality 19 (GRIM-19) attenuates autoimmune arthritis by regulation of Th17 and Treg cells. Arthritis Rheumatol 2014; 66(3):569-78.
6. Zhang P, Guo M, Xing Y, et al. Immunomodulatory effect of Huangqi glycoprotein on mice with experimental autoimmune encephalomyelitis. Xi Bao Yu Fen Zi Mian Yi Xue Za Zhi 2016; 32(1):54-58.
7. Yang B, Xiao B, Sun T. Antitumor and immunomodulatory activity of Astragalus membranaceus polysaccharides in H22 tumor-bearing mice. Int J Biol Macromol 2013; 62:287-90.
8. Liu XY, Xu L, Wang Y, et al. Protective effects of total flavonoids of Astragalus against adjuvant-induced arthritis in rats by regulating OPG/RANKL/NF-κB pathway. Int Immunopharmacol 2017; 44:105-14.
9. Aterido A, Palacio C, Marsal S, Avila G, Julià A.

Novel insights into the regulatory architecture of CD4+T cells in rheumatoid arthritis. Plos One 2014; 9(6): e100690.

10. Littman D R, Rudensky A Y. Th17 and regulatory T cells in mediating and restraining inflammation. Cell 2010; 140(6):845-58.

LETTER TO THE EDITOR

QUANTITATIVE DETERMINATION OF ENDOGENOUS CARDIOLIPIN IN RAT CEREBRAL TISSUES BY HIGH-PERFORMANCE LIQUID CHROMATOGRAPHY USING STANDARD ADDITION METHOD

T. WU[1], Y. WANG[1], S. YIN[2], YS. CONG[1] and SH. QI[1]

[1]Department of Anesthesiology, The Fourth Affiliated Hospital, Harbin Medical University, Harbin, PR China; [2]Department of Pharmacy, The Fourth Affiliated Hospital, Harbin Medical University, Harbin, PR China

Received April 12, 2018 – Accepted May 30, 2018

Cardiolipin is an important cellular component, and its normal level is a key prerequisite for maintaining the structure and function of mitochondria. To accurately quantify endogenous cardiolipin content in mitochondria, a standard addition method (SAM) was developed to establish a high-performance liquid chromatographic (HPLC) technique that is both reliable and accurate. Increasing amounts of cardiolipin standards were added to a constant amount of isolated mitochondria prior to the extraction procedure, and the two were extracted together. By limiting the interference effects that occur to within an acceptable range in an analytical system examined, this procedure ensures an ideal match of the sample composition in the standards, even if the composition is extremely complex or completely unknown. Then, the desired results can be obtained by extrapolation. As such, the authentic content of the endogenous cardiolipin can be obtained with greater accuracy than with classical detection methods, e.g. external standard calibration (ESC) and internal standard calibration (ISC). This method provides an excellent means of quantifying endogenous substances in living cells. The authors expect this method to be useful for researchers working on mitochondria-related mechanisms, cell survival-related mechanisms and similar topics.

To the Editor,

Cardiolipin is a special phospholipid that was first found and isolated from the bovine heart in 1942 (1). As an organelle marker, cardiolipin can be used to estimate the quantity of mitochondria in a given tissue (2). Cardiolipin plays a crucial part in ATP synthesis and resisting oxidative stress during interactions with reactive oxygen species (ROS) (3). In a previous study, the present Authors found that mitochondria swell after ischemia-reperfusion as a result of the destruction of mitochondrial membrane potential and the generation of excessive ROS (4). Thus, cardiolipin is likely responsible for the irreversible nerve damage induced by cerebral ischemia-reperfusion injuries (5). Cardiolipin is also involved in the optimal function of numerous mitochondrial proteins and biochemicals and plays multiple roles in the complicated process of apoptosis to control a cell's fate (6). Cardiolipin is therefore of great significance to mitochondria and

Key words: endogenous cardiolipin, standard addition method, high-performance liquid chromatography, rat cerebral tissue, mitochondria

Mailing address:
Professor Sihua Qi,
Department of Anesthesiology,
The Fourth Affiliated Hospital
Harbin Medical University, NO. 37, Yiyuan Street
Nangang District 150001, Harbin, China
Tel.: +86 451 82576626 - Fax: +86 451 82576624
e-mail: sihuaqi2012@126.com

0393-974X (2018)
Copyright © by BIOLIFE, s.a.s.
This publication and/or article is for individual use only and may not be further reproduced without written permission from the copyright holder.
Unauthorized reproduction may result in financial and other penalties
DISCLOSURE: ALL AUTHORS REPORT NO CONFLICTS OF INTEREST RELEVANT TO THIS ARTICLE.

cells, and changes in its levels affect the function of both. Therefore, developing an effective and accurate method for quantifying cardiolipin content in biological tissue is valuable.

HPLC is used most frequently to quantify cardiolipin (3), external standard calibration (ESC), internal standard calibration (ISC) and standard addition method **(**SAM) are all basic alternative HPLC assay methods (7). ESC and ISC can be applied only when certain prerequisite conditions are fulfilled, such as simple preparation of the sample for ESC and analyte-free matrix for ISC. They all have substantial limitations to quantify endogenous cardiolipin. SAM is a classical calibration approach for instrumental analysis that can compensate for the shortages of ESC and ISC for its characteristics, and it is more suitable to quantify endogenous cardiolipin (24).

In this paper, a novel reliable and sensitive HPLC method using SAM with methodological details for quantification of endogenous cardiolipin are provided. This study provides a valuable reference for the determination of other endogenous substances.

MATERIALS AND METHODS

All procedures were performed according to NIH guidelines and were approved by the Committee on the Guidelines for Animal Experiments of Harbin Medical University. All rats (Vital River Laboratory Animal Technology Co., Ltd., Beijing, China) were healthy, of the same age, and housed in a climate-controlled room (temperature 25-28°C with a relative humidity of 60±5%) with a 12-h light/dark cycle. The animals were housed in groups of 4 per cage and had access to food and water ad libitum. The animals were quarantined for at least 3 days before the study. LiChrosorb Si60 normal column was supplied by Merck & Co, Inc. (Darmstadt, Germany) and 20-mL Dounce homogenizer was purchased from KIMBLE Co. (Vineland, NJ, USA).

Reference standard of cardiolipin was obtained from Avanti Co. (Alabaster, Alabama, USA). Hexane, 2-propanol, and anhydrous ethanol were of HPLC grade and were purchased from Merck & Co, Inc. (Darmstadt, Germany). All other reagents were of analytical grade and were obtained from commercial sources.

Preparation of reagents

2.5 mL of cardiolipin standard (10 mg/mL) was transferred to a 5-mLdark-brown volumetric flask, and the volume was brought to 5 mL by adding chloroform, thus preparing a 5 mg/mL cardiolipin solution. The stock solution was maintained at −20°C until use.

Three series of standard working solutions including series A, series B and series C were obtained by gradual dilution of the stock solution with chloroform. The final concentrations of cardiolipin were 5, 10, 20, 50, 100, 250, 500 and 1000 μg/mL in series A; 0, 200, 500 and 1000 μg/mL in series B; and 60, 150 and 300 μg/mL in series C. The working solutions were kept at −20°C in dark-brown volumetric flasks.

Liquid chromatography was performed on a Waters HPLC instrument (Waters, Milford, MA, USA) coupled with a UV spectrometer. Chromatographic separations were achieved on an LiChrosorb Si60 column (5 μm, 250 mm × 4.0 mm) at 35°C with an isocratic mobile phase of hexane/2-propanol/25 mM dipotassium phosphate (pH 7.0)/anhydrous ethanol/glacial acetic acid (441:490:62:20:0.6, by vol) at a flow rate of 1.0 mL/min, a column pressure of approximately 130~140 bar and a UV detection wavelength of 206 nm. The sample injection volume was 10 μL.

Preparation of quality control samples (QCs)

Rat brain tissue homogenate. All manipulation processes during this step were performed on ice in ice-cold isolation buffer (IB; 320 mM sucrose, 1 mM EGTA, and 10 mM Tris-Base, pH 7.4). The rats were euthanized at the beginning of the study using an overdose of 5% sevoflurane via inhalation and decapitated with a small animal guillotine. The brain was quickly removed within 60 s and placed into a pre-chilled brain slice template to obtain a coronal slice (4 mm thick) between the forebrain and cerebellum. The required cortical subregion from 1 o'clock to 3 o'clock of the cerebral cortex (approximate weight: 40 mg) was dissected from the slice using a sharp scalpel. The mixed tissue was manually homogenized in IB (10%; wt/vol) using a 20-mL Dounce homogenizer, and mixed cerebral tissue homogenate was obtained.

The homogenate was transferred to a chilled tube and centrifuged at 2,000 g for 3 min at 4°C. The supernatant fluid was transferred to a new chilled tube and centrifuged at 2,000 g for 3 min at 4°C. The supernatant fluid was then transferred to a third chilled tube again and centrifuged at

10,000 g for 10 min at 4°C to obtain a crude mitochondrial sediment pellet (8). This mitochondrial pellet was resuspended in 400 μL of IB and incubated on ice for further analyses.

The standard addition method was applied in the extraction procedure (9). 30 μL working solution series B (0, 200, 500 and 1000 μg/mL) was added to four new tubes and evaporated to dryness under nitrogen to obtain a cardiolipin standard gradient for Series B. The mitochondrial suspensions (400 μL) were divided equally into the four tubes (100 μL per tube) containing the cardiolipin standard gradient, followed by vortexing for 60 s to mix thoroughly. 1 mL of lipid extraction solvent (chloroform/methanol = 2:1, by vol) was added to each of the four tubes containing the mitochondrial suspensions (100 μL) in the proportion of 10:1 (by vol). The tubes were mixed thoroughly by vortexing for 60 s and incubated on ice for 20 min. The tubes were then centrifuged at 1,000 g for 3 min at 4°C, and the lower phase was carefully collected and transferred to four new tubes. Next, 200 μL of 0.05 mol/L $CaCl_2$ was added to each tube with a ratio of 1:5 (by vol) and mixed thoroughly. The four tubes were centrifuged at 1,000 g for 10 min at 4°C. The lower chloroform phase containing the lipids was carefully transferred to four new tubes, and the chloroform was evaporated to dryness under nitrogen. Finally, the lipids were redissolved in 100 μL of lipid diluent (hexane:2-propanol = 3:4, by vol) and vortexed for 10 s, then the quality control samples (QCs) were obtained. The samples were stored at −80°C until HPLC analysis.

Ten μL aliquots of working solution series A (5, 10, 20, 50, 100, 250, 500, and 1000 μg/mL), series C (60, 150 and 300 μg/mL) and QCs were injected into HPLC system for analysis, respectively. The peak areas of cardiolipin were recorded to prepare the standard and calibration curves.

Data analysis

The calibration curve was prepared using Origin 8.6 (OriginLab) Data Analysis and Graphing software. The primary endogenous cardiolipin concentration was calculated by extrapolation. Each calibration curve was elongated oppositely to intersect the negative axis of the abscissa. The value of the intercept is the primary endogenous cardiolipin concentration in each sample. The final results are presented as the quantity ratio (μg/mg) of cardiolipin and cerebral tissue.

Method validation

Selectivity is the ability of an analytical method to differentiate and quantify the analytes in the presence of other components in the sample. The selectivity was ascertained by comparing homologous spectra of the sample containing the cardiolipin standard and the QCs at the same retention time in both chromatograms. The sample contained 300 μg/mL cardiolipin standard, and the QCs contained 0 μg/mL cardiolipin standard. After separately injecting these two samples into the HPLC system for analysis, each pair of chromatograms and homologous spectra for cardiolipin were recorded to validate the selectivity.

Linearity of the lower limit of quantification

The standard curve was constructed by plotting the peak areas versus the concentrations of the cardiolipin standard with a weighted ($1/X^2$) least square linear regression using seven concentrations of the standard samples (10, 20, 50, 100, 250, 500, and 1000 μg/mL of standard working solutions series A). The LLOQ was defined as the lowest concentration of the cardiolipin standard that resulted in a signal-to-noise ratio of 10:1.

Linearity was determined by constructing calibration curves. The calibration curve for cardiolipin was prepared according to the principles of SAM. The calibration curve was constructed using the peak areas of the total cardiolipin versus the final concentrations of cardiolipin standard in QCs with a weighted ($1/X^2$) least square linear regression and the linear regression equations and correlation coefficients were obtained. An independent calibration curve should be established for each sample.

Both the inter-day and intra-day accuracy and precision were evaluated by determination of QCs at three concentration levels (60, 150 and 300μg/mL) in six replicates on the same day and on three different days, respectively. The accuracy was defined as RE and the precision was defined as RSD.

The recovery of standard addition method was standard addition recovery and the recoveries at three concentration levels (60, 150 and 300μg/mL) were measured with the formula below:

$$R = \frac{M_2 - M_1}{M} \times 100\%$$

where R represents standard addition recovery, M_2

represents the measured value of sample with standard addition, M_1 represents the measured value of sample without standard addition, M represents the amount of standard addition. The extraction efficiency of cardiolipin was determined by analyzing the QCs at three concentration levels (60, 150 and 300μg/mL) in six replicates.

The stability of the cardiolipin standard working solution and QCs, including freeze–thaw stability (three freezes at −20°C and thaws at ambient temperature cycles), long-term stability (storage for 30 days at −20°C), short-term stability (storage for 4 h at ambient temperature and for 0, 3, 6, 12 and 24 h at 4°C), was tested at three concentration levels (60, 150 and 300μg/mL) with five replicates at each level. The results of all of the stability tests were assessed by comparing the mean responses to the responses of freshly prepared standard samples.

The method described above was applied to assay endogenous cardiolipin content in study samples (Ss) in ten healthy adult rats.

RESULTS

A representative pair of chromatograms and homologous spectra of cardiolipin are shown in Fig. 1. The chromatogram and homologous spectra of cardiolipin standard and QCs are shown in Fig. 1, A and B, respectively. The retention time of the analytes in both samples was 8.61±0.03 min, and the shapes of the spectral curves for the analytes in each chromatogram for each sample were the

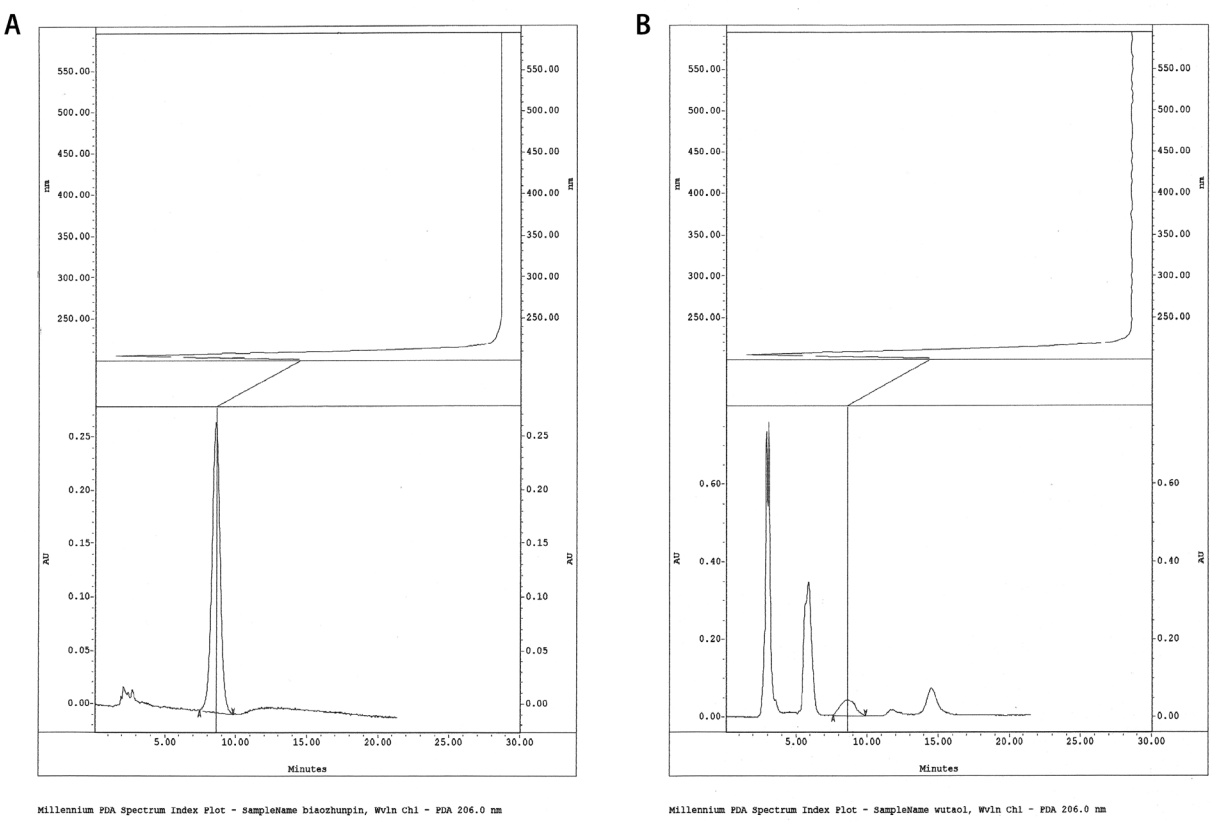

Fig. 1. *Chromatograms and homologous spectra of cardiolipin. **A)** Chromatogram and homologous spectra of cardiolipin standard sample (300 μg/mL). **B)** Chromatogram and homologous spectra of the QCs containing 0 μg/mL cardiolipin standard. The retention time of the analyte in both samples was 8.61±0.03 min. The shapes of the spectral curves for the analytes corresponding to each chromatogram in each sample were the same, indicating that the cardiolipin standard and endogenous cardiolipin in the samples were the same substance. There were no interfering peaks from endogenous compound at the retention time of cardiolipin.*

same, indicating that the cardiolipin standard and the endogenous cardiolipin in the sample were the same substance. There were no interfering peaks of endogenous compounds at the retention time of cardiolipin. Cardiolipin was easily differentiated and quantified in the presence of other components in the sample, and the cardiolipin peak areas were reproduced in multiple samples.

Linearity and lower limit of quantification

The standard curve and representative calibration curve for cardiolipin method validation are shown in Fig. 2, A and B, respectively. The typical regression equation of standard curve was: Y =3784.22 + 9811.40X, the correlation coefficient (R^2 = 0.9998), linearity ranges was 10-1000μg/mL and the LLOQ was 10μg/mL. The regression equations, the correlation coefficients and X-intercepts of the calibration curves of QCs are shown in Table I. All of the correlation coefficients were greater than 0.9960. An excellent correlation was observed between the peak area and cardiolipin concentration.

The calibration curve intercepted the negative axis of the abscissa, and the absolute value of the intercept represented the concentration of endogenous cardiolipin. The slopes of the curves all ranged from approximately 8300 to 8600. The discrepancy between the slope of the calibration curve obtained during method validation and the standard curve was less than 20%.

The accuracy and precision for cardiolipin in QCs at three concentration levels (60, 150 and 300 μg/mL) are shown as RSD and RE. The intra-day relative standard deviation (RSD) did not exceed 8%, and the inter-day RSD was less than 7%. The relative error (RE) ranged from 3% to 7% (data was not shown). The accuracy and precision were in conformity with relevant biological sample analysis method guidelines.

The recoveries of cardiolipin in QCs at three concentration levels (60, 150 and 300 μg/mL) all ranged from 74% to 89% (data not shown); thus, the extraction method used in the study showed good and stable extraction efficiency.

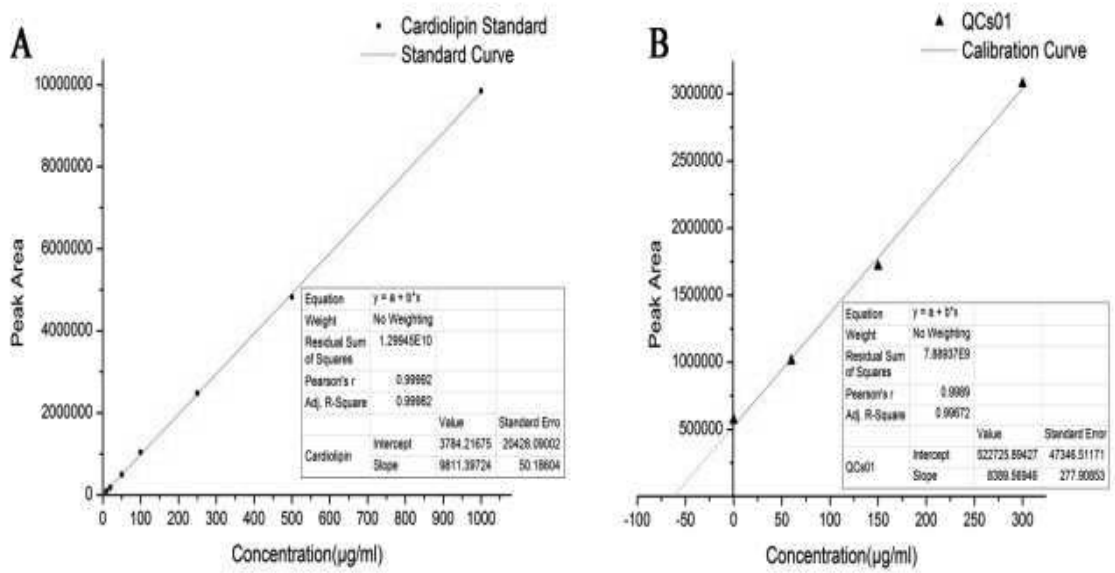

Fig. 2. *Standard curve and all six calibration curves for cardiolipin of QCs in method validation.* ***A)*** *Standard curve, the correlation coefficient (R^2) was 0.9999 and the slope was 9811.* ***B-G)*** *six calibration curves of QCs, the correlation coefficients (R^2) for calibration curves were all greater than 0.9970. The slopes of the curves all ranged from approximately 8300 to 8600. The discrepancy between two slopes was less than 20%.*

Table I. *The regression equations, X-intercepts of calibration curves of endogenous cardiolipin in QCs (n=6) and Study samples (Ss)(n=10).*

Number	Y =a+ bX	R^2	X-Intercept	concentration (μg/mL)	content (μg/mg)
QCs 1	Y =522725.89 + 8389.57X	0.9978	-62.31		
QCs 2	Y =543856.84 + 8319.30X	0.9993	-65.37		
QCs 3	Y =553137.41 + 8456.75X	0.9985	-65.41		
QCs 4	Y =546367.95 + 8431.21X	0.9982	-64.80		
QCs 5	Y =543384.29 + 8591.09X	0.9981	-63.25		
QCs 6	Y =558637.70 + 8327.64X	0.9991	-67.08		
Ss 01	Y =545735.54 + 8580.59X	0.9989	-63.60	63.60	6.36
Ss 02	Y =533040.75 + 8561.08X	0.9988	-62.26	62.26	6.23
Ss 03	Y =569548.11 + 8505.82X	0.9991	-66.96	66.96	6.70
Ss 04	Y =526263.11 + 8416.59X	0.9986	-62.72	62.72	6.27
Ss 05	Y =551866.07 + 8475.18X	0.9981	-65.12	65.12	6.51
Ss 06	Y =537156.44 + 8375.05X	0.9981	-64.14	64.14	6.41
Ss 07	Y =551052.35 + 8368.61X	0.9988	-65.85	65.85	6.59
Ss 08	Y =542406.47 + 8639.56X	0.9982	-62.78	62.78	6.28
Ss 09	Y =555680.48 + 8424.02X	0.9986	-65.96	65.96	6.60
Ss 10	Y =547025.73 + 8307.73X	0.9984	-65.85	65.85	6.59
Mean (%)				64.52	6.45
SD (%)				1.64	0.17
RSD (%)				2.55	2.55

The stability of cardiolipin standard and QCs at three concentration levels (60, 150 and 300 μg/mL) under various conditions is shown in Table II. The percentage differences were all less than 5%, indicating that cardiolipin was stable at ambient temperature for 4 h, at 4°C for 24 h, and at -20°C for 30 d, as well as after three freeze-thaw cycles.

Endogenous cardiolipin content in normal rat cerebral tissue

The standard curve and representative calibration curve for cardiolipin application are shown in Fig. 3, A and B, respectively. The concentrations of endogenous cardiolipin in cerebral tissues from ten rats are shown in Table I. The endogenous cardiolipin

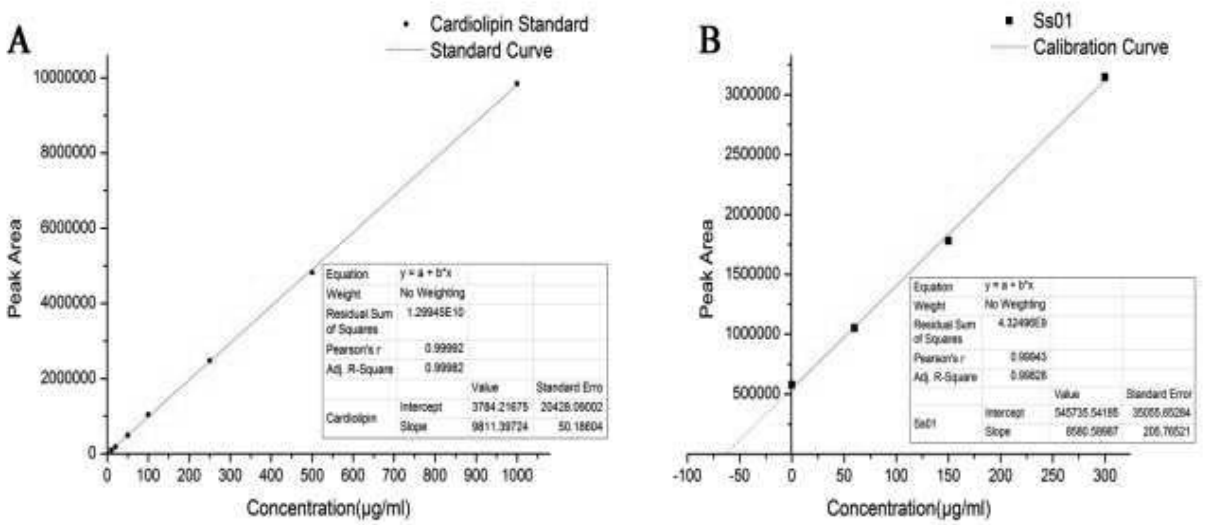

Fig. 3. *Standard curve and all ten calibration curves for cardiolipin of Ss in application. **A**) Standard curve, the correlation coefficient (R^2) was 0.9999 and the slope was 9811. B-L, ten calibration curves of Ss, all correlation coefficients (R^2) for the calibration curves were greater than 0.9970. The slopes of the curves ranged from approximately 8300 to 8700. The discrepancy between two slopes was less than 20%. The intercepts on the abscissa axis ranged from approximately -60 to -70 μg/mL.*

Table II. *The stability of cardiolipin standard and QCs at three concentration levels under various conditions (n=6).*

Standard Concentration (μg/mL)	Cardiolipin Standard				QCs			
	Short-term stability RE (%)		Long-term stability RE (%)	Freeze-thaw stability RE (%)	Short-term stability RE (%)		Long-term stability RE (%)	Freeze-thaw stability RE (%)
	ambient temperature	4°C			ambient temperature	4°C		
60	-2.46	-1.69	2.86	-2.28	1.32	2.64	3.28	-3.03
150	-3.28	-1.82	2.95	2.74	-2.67	2.69	3.68	2.82
300	-4.13	-2.80	3.61	1.48	-3.89	-2.81	-3.84	3.28

content calculated using the formula is also shown in Table I. The RSD was less than 3%.

DISCUSSION

The quantitative determination of endogenous compounds in biological samples is complicated, both analytically and from a validation point of view (10). To obtain cardiolipin-free samples of the authentic biological matrix or samples with accurately-known cardiolipin concentrations is often difficult in practice because cardiolipin is tightly binding to the mitochondrial inner membrane (4) and difficult to be eliminated while leaving other components intact.

In ISC, the calibration curve should be established by analyzing a series of concentrations of the standard in a blank (cardiolipin-free) matrix, and thus a synthetic or cardiolipin-stripped matrix is required (7, 11). So, it is barely possible to apply ISC under this circumstance as the sample preparation of cardiolipin is so complicated and the extraction efficiency cannot reach 100%. Once ESC is applied, the calibration curve is artificially replaced by a standard curve with a different slope, such that the authentic content of endogenous cardiolipin cannot be obtained. ESC should not therefore be used as an accurate result cannot be achieved. The crucial task for endogenous cardiolipin quantification is the ability to compensate for interference effects (12). In marked contrast to ISC and ESC, SAM procedure consists of the addition of known amounts of cardiolipin standard into a sample containing an unknown amount of endogenous cardiolipin and undergoing the same pre-treatment and does not require an analyte-free matrix. Then the total cardiolipin in each portion is measured, and the calibration dependence is able to be reconstructed only over the original cardiolipin concentration by extrapolation (12). Therefore, SAM provides the opportunity to compensate for potential interference effects to obtain an analytical result with greater accuracy.

In the present paper, a detailed HPLC methodology using SAM was established for the quantification of the endogenous cardiolipin content in cerebral tissues from healthy adult rats.

ACKNOWLEDGEMENTS

We are grateful to Professor Bing Li and Fujun Qu from the Second Affiliated Hospital of Harbin Medical University for research assistance with this study.

This study was supported by National Natural Science Foundation of China (NSFC) (No. 81271456) and also by Science and Technique Foundation of Educational Commission of Heilongjiang Province of China (No. 11531120). The funding agencies had no role in the study design, data collection and analysis, decision to publish, or preparation of the manuscript.

REFERENCES

1. Pangborn MC. Isolation and Purification of a Serologically Active Phospholipid from Beef Heart. J Biol Chem 1942; 143(1):247-56.
2. Schlame M. Assays of cardiolipin levels. Methods Cell Biol 2007; 80:223.
3. Schlame M, Rua D, Greenberg ML. The biosynthesis and functional role of cardiolipin. Prog Lipid Res 2000; 39(3):257-88.
4. Li J, Ma XS, Yu W, Lou ZQ, Mu DL, Wang Y, Shen BZ, Qi SH. Reperfusion Promotes Mitochondrial Dysfunction following Focal Cerebral Ischemia in Rats. PloS ONE 2012; 7(9):e46498.
5. Lin MT, Beal MF. Mitochondrial dysfunction and oxidative stress in neurodegenerative diseases. Nature 2006; 443(7113):787-95.
6. Choi SY, Gonzalvez F, Jenkins GM, et al. Cardiolipin deficiency releases cytochrome c from the inner mitochondrial membrane and accelerates stimuli-elicited apoptosis. Cell Death Differ 2007; 14(3):597-606.
7. Cuadros-Rodríguez L, Bagur-González MG, Sánchez-Viñas M, González-Casado A, Gómez-Sáez AM. Principles of analytical calibration/quantification for the separation sciences. J Chromatogr A 2007; 1158(1–2):33-46.
8. Mattiasson G, Friberg H, Hansson M, Elmer E, Wieloch T. Flow cytometric analysis of mitochondria from CA1 and CA3 regions of rat hippocampus reveals differences in permeability

transition pore activation. J Neurochem 2003; 87(2):532-44.
9. Bligh EG, Dyer WJ. A rapid method of total lipid extraction and purification. Can J Biochem Physiol 1959; 37(8):911-17.
10. Van de Merbel NC. Quantitative determination of endogenous compounds in biological samples using chromatographic techniques. Trends Anal Chem 2008; 27(10):924-33.
11. Mircioiu I, Aldea A, Anuta V, Neagu O, Miron D, Radulescu F, Enache F. Internal standard versus external standard in bioanalytical assay for bioequivalence studies. Farmacia 2007; LV(5):569-79.
12. Kościelniak P, Kozak J. Review of univariate standard addition calibration procedures in flow analysis. Crit Rev Anal Chem 2006; 36(1):27-40.

JOURNAL OF BIOLOGICAL REGULATORS & HOMEOSTATIC AGENTS Vol. 32, no. 4, 969-972 (2018)

LETTER TO THE EDITOR

GASTRIC REFLUX: THE THERAPEUTICAL ROLE OF MARIAL®

S.E. ARAGONA[1], G. MEREGHETTI[1] and G. CIPRANDI[2]

[1]Center of Regenerative Medicine, Humanitas Mater Domini, Castellanza (VA), Italy; [2]Ospedale Policlinico San Martino, Genoa, Italy

Received April 6, 2018 – Accepted April 19, 2018

The worldwide relevance of gastroesophageal reflux disease (GERD) has had a considerable increase in recent years. The guidelines for the diagnosis and treatment of GERD are well consolidated and continuously updated. Recently, the extra-esophageal manifestations of reflux have been considered from a multidisciplinary point of view, so the symptoms of the laryngo-pharyngeal reflux (LPR) have been precisely defined. At present, a new Medical Compound (Marial®) has the indication for the treatment of both GERD and LPR. Clinical experience has initially confirmed its effectiveness in both disorders.

To the Editor,

Gastric reflux is a physiological phenomenon that may become complicated, such as gastro-esophageal reflux disease (GERD). GERD has showed a considerable epidemiological increase worldwide. This issue has therefore attracted the attention of the scientific community, especially for clinical and pharmacological research. The phenomenon of reflux involves numerous aspects, i.e. anatomical, functional, biochemical, and hormonal, that are in turn closely linked together. Therefore, the approach to GERD management should be multidisciplinary and join the various skills in knowing the pathogenic and the pathophysiological mechanisms as well as the possibility of identifying new therapeutic strategies for the patient wellbeing (1-6).

Frequently, patients with GERD may present not well-defined symptoms, whereby the prescribed medications could be ineffective. This failure usually encourages the patient to search alternative therapeutic solutions which are often not found or, if found, may often be ineffective. Moreover, there are patients who present atypical symptoms, frequently underestimated or even overestimated by doctors. As a consequence, physicians tend to prescribe medications without a pathophysiological rationale and appropriate diagnostic work-up. In particular, these patients with reflux show symptoms concerning the upper or the lower airways. If the reflux material involves upper airways tissues, it causes symptom occurrence, i.e. laryngo-pharyngeal reflux (LPR). From a clinical point of view, LPR patients present throat symptoms, including mainly hoarseness, clearing, dysphagia, and irritating cough.

A new medical compound (Marial®) is the first compound (at present) with the indication for treating both GERD and LPR.

Reflux pathophysiology

The defined causes of GERD and LPR are multiple, but the main mechanism is the reflux of the gastric gas and/or liquid/solid material, containing hydrochloric acid and pepsin that create a condition of acute or sub-acute inflammation of the esophageal

Key words: gastric reflux, esophagus, E-Gastryal®, magnesium alginate

Mailing address:
Giorgio Ciprandi, M.D.
Largo R. Benzi 10,
16132 Genoa, Italy
Tel.: +39 10 35331820
Fax: +39 10 3538664
e-mail: gio.cip@libero.it

0393-974X (2018)
Copyright © by BIOLIFE, s.a.s.
This publication and/or article is for individual use only and may not be further reproduced without written permission from the copyright holder.
Unauthorized reproduction may result in financial and other penalties
DISCLOSURE: ALL AUTHORS REPORT NO CONFLICTS OF INTEREST RELEVANT TO THIS ARTICLE.

and extra-esophageal mucosal tissues, potentially with consequent epithelial lesions. Thus, the mechanisms of clearance and defense, including defensive enzyme (carbonic anhydrase III, CAIII) and epithelial mucin, become defective. The impaired protective layer determines an exposure of the mucosa to injuries from the chemical corrosive agents. The ultrastructural lesions, the defect of E-Cadherine (molecule of epithelial adhesion), and the defect of mucins and CAIII determined by pepsin, cause a structural upheaval of the mucosal epithelium sustained by a cascade of inflammatory events. An initial acute inflammation may evolve to chronic inflammation characterized by an alteration of the cellular structure blocking the collagen production useful for the regenerative processes (6,7).

The inflammatory process and the alteration of the cellular structure

Usually, the inflammatory process is envisaged as a negative event in view of the possible structural damage. On the contrary, a new line of thought has been proposed; regenerative medicine that considers the inflammatory process as a potential protective event and not only harmful (1-5).

Understanding the intimate neuro-immuno-endocrine mechanisms of these biological pathways, the cellular populations that characterize the various stages of wound healing, the current attention on biomaterials and growth factors used in regenerative medicine, together with the use of bioengineered tissues, turned the spotlight on the correct interpretation of the process of healing of epithelial lesions, allowing the possibility to recreate a tissue as much as possible similar to the original tissue, such as before the damage (1).

Some mechanisms, involved in tissue repairing, have been identified: it allows to apply new therapeutic approaches in daily clinical practice. The modulation of the inflammatory process, also stimulating specific cell lines, promotes and supports the reparative mechanisms. In this regard, the healing process takes place through three complex steps: i) inflammation; ii) cell proliferation (in excess or in defect); and iii) remodeling (mainly concerning the extracellular matrix (ECM) deposition) (4). The repairing of the epithelial lesion is characterized by an incomplete regeneration of the original tissue with a hyper-production of organized collagen, that can lead to the production of a new tissue, up to 80% similar to the original tissue (2). However, an abnormal progression of this process causes a fibro-proliferative response, which leads to the production of scar tissue.

The mucosal homeostasis, necessary for the barrier function, is ensured by the synergic cross-talk among numerous cellular populations, including keratinocytes, dendritic cells, T lymphocytes, fibroblasts, mast cell, and macrophages. When the mucosal tissue is damaged by acute or chronic harm, a series of pro-inflammatory cytokines and mediators are released, so starting the process of amplification of the inflammatory response. These pro-inflammatory cytokines, produced by the cell populations involved in wound healing, are able to trigger, promote, and govern the repairing phenomena acting on the inflammatory cells (4).

The role of the matrix metalloproteases (MMPs), enzymes degrading the extracellular matrix, balanced by their inhibitors (TIMPs), has been well clarified in recent years. In particular, the attention has been focused on TNF-α and on gelatinase MMP9, significantly over-expressed in conditions of both endothelial inflammation and alteration of the venous wall (5). The endothelium plays an important role in the initial repairing phase by its ability to stimulate the inflammatory process as endothelial cells produce large quantities of TNF-α, measurable and quantifiable through the intercellular adhesion molecule expression [molecule of intracellular adhesion, targeted also to the endogenous hyaluronic acid, (HA)]. Indeed, endogenous HA reduces the production of TNF-α by a down-regulation mechanism. At the same time, the restoration of endothelial function by HA occurs through different steps: recovery of endothelial glycosaminoglycan (GAG), reduction of MMP9, and blocking of MMPs (3). These events depend on the hydrodynamic activity of the natural HA that, by increasing the body water flow, allows the lock of zinc atom, core of MMPs, priming the repairing and the regeneration of damaged tissues.

During the inflammatory phase of the mucosal injury, the reduced production of TNF-α by M1 macrophages, the inhibition of monocytes, and the proliferation of fibroblasts associated with the deposition of specific collagen, stimulated by endogenous HA, induce the switch M1-M2 and start the repairing and regeneration phenomena (1).

E-Gastryal®: its rationale as a biological regulator and homeostatic agent

The knowledge of the inflammatory events caused by physical and chemical stimuli, the symptom polymorphism of the patients with reflux, and the pathogenic role of some molecules involved in the healing process have given rise to two questions: i) how to associate in a synergic way the agents of anti-inflammatory response, and ii) how to make this synergy accessible to patients with LPR (8).

The homeostatic agents, physiologically active in resolving the inflammatory phenomena, indirectly operate on the scenario so that endogenous HA and GAGs promote hydration of the damaged tissues (by hygroscopic capacity) and, at the same time, determine the modulation of the reconstitution of the ECM (by plastic capacity).

To attract water molecules, at the level of the inflamed tissues, seems like a paradox because of the presence of edema. However, molecules with high hygroscopic activity, such as HA and mucopolysaccharides, create intense water replacement and eliminate toxic substances from the matrix, thus rebooting the gel phase of EMC. Consequently, a recovery of tissue alkalinity occurs and the reparative process begins induced by fibroblasts (9-12). Therefore, the research of a new medical compound has addressed some important aspects as it should be able to i) recreate the natural scenario of the anti-inflammatory response (stimulating the tissue repair), ii) induce a rapid relief of symptoms (inhibiting the acid exposure), and iii) protect the mucosa (amplifying the biological response). A new compound, named E-Gastryal®, has been produced combining hyaluronic acid, hydrolyzed keratin mucoproteins, glycoproteins such as fibronectin, meso glycans and integrins, and viscous agents (as thickener). This compound has been proved to effectively relieve the discomfort caused by gastric reflux, preventing and alleviating the injury to mucous membranes. In fact, this compound is able to actively regenerate the damaged tissue by repairing and regenerative properties on mucous membranes and by muco-adhesive and film-forming characteristics that allow to prolong the contact time with the mucous membranes and consequently to improve the effectiveness (1). Hydrolyzed keratin significantly enhances the regeneration process of the desmosomes, of which it is a fundamental component.

The effectiveness of hyaluronic acid (with MW of 1500 KDa) and hydrolyzed keratin is enhanced and optimized by its combination with two thickener agents: Tara gum and Xanthan gum. It allows the formation of a film on the mucosal surface. Such mixture guarantees an optimal and easy swallowing to the patient (1).

After the formulation of E-Gastryal®, research focused on the role of magnesium alginate in contrasting gastroesophageal reflux disease. Magnesium alginate is highly effective in GERD patients as it creates a raft in the gastric dome, so inhibiting the reflux of gastric content. The concentration of magnesium alginate was defined to avoid HA degradation by low pH level.

A new medical compound has been introduced on the market: Marial®. Marial® is the combination of E-Gastryal plus magnesium alginate.

Marial® is effective in the treatment of gastroesophageal reflux disease and also of laryngo-pharyngeal reflux. Marial® has a biological versatility that goes from the modulation of the inflammatory process both directly and indirectly, by acting with the properties of hyaluronic acid or its salt to the modulation of the process of re-epithelialization of the mucosa, thanks to the action of the keratin and hyaluronic acid or its salt, and preventing the backflow with the action of the magnesium alginate.

REFERENCES

1. Aragona SE, Mereghetti G, Bianchetti M, at al. Regenerative Medicine in the treatment of gastro-esophageal reflux disease an laryngo-pharyngeal

reflux. From research to cure. J Biol Regul Hom Agents 2017; 31:1-4.
2. Gelardi M, Ciprandi G. Focus on gastroesophageal reflux (GER) and layngopharyngeal reflux (LPR): new pragmatic insights in clinical practice. J Biol Regul Hom Agents 2018; 32:1-5.
3. Zhao R, Liang H, Clarke E, Jackson C, Xue M. Inflammation in chronic wounds. Int J Mol SCI 2016; 17(12):2085.
4. Serban MA, Skardal A. Hyaluronan chemistries for three-dimensional matrix applications. Matrix Biol 2018; 10:11-16.
5. Iwakiri K, Kinoshita Y, Habu Y, et al. Evidence-based clinical practice guidelines for gastroesophageal reflux disease 2015. J Gastroenterol 2016; 51:751-67.
6. Seo SI, Bang CS, Kang HS, et al. Evaluation of treatment pattern and symptom control in patients with gastroesophageal re ux disease: multihospital questionnaire survey on the current situation in Korea. Dis Esophagus 2017; 30:1-8.
7. Yadaplati R, Kahrilas PJ. When is proton pump inhibitor use appropriate? BMC Medicine 2017; 15:36.
8. Internal Clinical Guidelines Team (UK). Dyspepsia and Gastro-Oesophageal Reflux sease: Investigation and Management of Dyspepsia, Symptoms Suggestive of Gastro-Oesophageal Reflux Disease, or Both. London: National Institute for Health and Care Excellence (UK); 2014 Sep.
9. Davies I,Burman-Roy S, Murphy MS; Guideline Development Group. Gastroesophageal reflux disease in children: NICE guidance. BMJ 2015; 350:g7703.
10. Caruso AA, Del Prete S, Ferrara L, Serra R, Telesca DA, Ruggiero S, Russo T, Sivero L. Relationship between gastroesophageal reflux disease and Ph nose and salivary: proposal of a simple method outpatient in adults. Open Med (Wars) 2016; 11:381-86.
11. Johnston N, Dettmar PW, Strugala V, Allen JE, Chan WW. Laryngopharyngeal reflux and GERD. Ann N Y Acad Sci 2013; 1300:71-79.
12. Laczkó D, Wang F, Johnson FB, et al. Modeling esophagitis using human three-dimensional organotypic culture system. Am J Pathol 2017; 187:1787-99.

LETTER TO THE EDITOR

EMERGING FROM GASTROESOPHAGEAL REFLUX (EMERGE): AN ITALIAN SURVEY - I THE VIEWPOINT OF THE GASTROENTEROLOGIST

M. BIANCHETTI[1], S. PERALTA[2], R. NICITA[3], S.E. ARAGONA[4], G. CIPRANDI[4] and the EMERGE STUDY GROUP*

[1]Gastroenterologia - Humanitas Mater Domini, Castellanza (VA), Italy; [2]Endoscopia Digestiva – Policlinico P. Giaccone, Università di Palermo, Palermo, Italy; [3]Gastroenterologia - ASP 5, Reggio Calabria, Italy; [4]Center of Regenerative Medicine - Humanitas Mater Domini, Castellanza (VA), Italy; [5]Ospedale Policlinico San Martino, Genoa, Italy

**EMERGE Study Group: A. Arrigoni, D. Artuso, M. Astegiano, C. Azzinnari, E. Battaglia, C. Belcari, E. Bendia, P. Benedicenti, M. Bianchetti, G. Brandimarte, I. Buoncompagni, M. Cabras, S. Camilleri, G. Capece, S. Caronna, C. Cassieri, F. Castaldo, T. Catalano, C. Citarella, F. D'amore, G. D'alia, F. D'arpa, A. Dattola, N. De Bortoli, A. De Medici, S. Di Marzo, R. Di Mitri, A. Di Napoli, V. D'onofrio, L. Dughera, W. Elisei, G. Errico, L. Familiari, P. Familiari, R. Frasca, A. Frunzio, M. Gatti, S. Genova, S. Grosso, R. Gullotta, D.R. Iannuzziello, G. Indennitate, G. Leonardi, C. Luigiano, B. Macchiarella, T. Maisto, M.G. Mancino, A. Mancino, G. Manes, R. Marin, G.R. Mastinu, A. Moi, L.M. Montalbano, N. Monterosso, A. Morabito Loprete, L. Morlando, R. Nicita, C. Ogliari, N. Paiano Primaldo, G. Paliani, A.P. Palieri, D. Pardocchi, A. Pati, G. Pedretti, S. Peralta, A. Pisani, P. Plomaritis, A.C. Privitera, R. Pumpo, F. Quatraro, D. Raimondo, G. Rivellini, L. Rizzo Giovanni, M. Romano, R. Salerno, E. Savarino, G. Scarpulla, E. Sinagra, M. Soncini, G. Tammaro, C. Trovato, R. Vassallo, M. Vinti, C.M.P. Virgilio*

Received April 6, 2018 - Accepted April 23, 2018

Gastroesophageal reflux disease (GERD) is defined as a "disease that develops when the reflux of stomach contents induces troublesome symptoms and/or complications". From a therapeutic point of view, many options have been proposed, including proton pump inhibitors (PPI), antihistamines (H2-receptor antagonists), antacid chemical compounds, antireflux barrier (using alginates), prokinetics, inhibitors of gastric sphincters, protection of mucosal tissue, neuromodulators, nociceptor antagonists, lifestyle modification, and surgery. A new medical compound has been recently launched in Italy: Marial® (manufactured by Aurora, Milan, Italy) containing magnesium alginate and E-Gastryal®. The aim of this survey was to analyse the patients' characteristics and the prescriptive approach considering both the past or current treatments and clinical features during a visit in 56 gastroenterological centers, distributed in the whole of Italy. One thousand eight hundred forty-nine patients (46.5% males, and 53.5% females, mean age 48.59 years) were visited. Patients with positive reflux symptoms index (RSI^+) had higher GIS scores than RSI^- subjects. PPIs (both as monotherapy or plus add-on) were the most common medication prescribed before the visit. There was a significant change of prescription to Marial® at the visit. More precisely,, Marial® was preferentially prescribed to about a quarter of the patients,

Key words: gastroesophageal reflux, gastroenterologist, diagnosis, treatment

Mailing address:
Giorgio Ciprandi, M.D.
Largo R. Benzi 10,
16132 Genoa, Italy
Tel.: +39 10 35331820
Fax: +39 10 3538664
e-mail gio.cip@libero.it

0393-974X (2018)
Copyright © by BIOLIFE, s.a.s.
This publication and/or article is for individual use only and may not be further reproduced without written permission from the copyright holder.
Unauthorized reproduction may result in financial and other penalties
DISCLOSURE: ALL AUTHORS REPORT NO CONFLICTS OF INTEREST RELEVANT TO THIS ARTICLE.

particularly to those with lower GIS score, whereas PPI plus add-on option was preferred for patients with higher GIS score. In conclusion, the current experience demonstrated that GERD may be managed considering a patient-centred work-up by using the GIS questionnaire. GIS score may be able to define the medication choice that includes also the new medical compound Marial®.

To the Editor,

Gastroesophageal reflux (GER) has to be considered as a physiological phenomenon that usually occurs during and after meals. On the contrary, gastroesophageal reflux disease (GERD) is defined as a "disease that develops when the reflux of stomach contents induces troublesome symptoms and/or complications" (1). This umbrella definition was devised to encompass the broad spectrum of GERD, including endoscopically evident disease (esophagitis, stricture, Barrett's metaplasia, and adenocarcinoma), troublesome esophageal symptoms without endoscopically evident disease (heartburn, regurgitation, and chest pain), and potential extra-esophageal manifestations, including asthma, cough, and laryngopharyngeal reflux. Although the GERD definition, widely referred to as the Montreal definition is adequate in fusing the potential manifestations of GERD by the common element of stemming the reflux of gastric content into the esophagus, it also implies some clinically relevant practical problems. In particular, the appropriate diagnostic work-up, the (over)use of proton pump inhibitors (PPIs), and the approach to alternative therapeutic strategies.

GERD is classified into ''erosive GERD'' with esophageal mucosal break and ''non-erosive GERD'' (NERD) with symptoms alone. In addition, GER is classified into ''acidic-GER'' and ''non-acidic (weakly acidic, alkaline) GER'' (1). From a diagnostic point of view, if GERD is suspected, the patient should be clinically evaluated by a questionnaire and the PPI test. The typical symptoms of GERD are heartburn and regurgitation, but patients may not necessarily accurately perceive their symptoms (2). Thus, in addition to questions regarding the typical symptoms of GERD, a careful interview with different expressions may be helpful. GER may cause not only typical symptoms but also extraesophageal symptoms (chronic cough, bronchial asthma, discomfort of the pharyngolarynx, pharyngalgia, and non-cardiac chest pain) (2). Since extraesophageal symptoms may be the only symptoms of GER, it is important to take them into consideration when diagnosing GERD. In particular, laryngopharyngeal reflux (LPR) is a disorder involving upper airways as a consequence of gastric refluxate in these tissues (3). In practice, if GERD is highly suspected, two types of algorithms are proposed: (i) administration of standard-dose PPI, which is the first-line treatment option of GERD, is started first without endoscopy (therapy at clinics without endoscopy equipment), such as an empiric trial on the basis of the ex juvantibus criteria; and (ii) upper digestive endoscopy is performed first before PPI therapy (4, 5). If symptomatic resolution was obtained with PPI before endoscopy, they are regarded as transient symptoms, and treatment should be discontinued. If the symptoms persist or are relapsed, endoscopy needs to be performed. However, if the PPI test is started before endoscopy, erosive GERD and non- erosive-GERD cannot be differentiated by the endoscopy even if it is carried out afterward. Other diagnostic tests include pH-manometry, imaging, pepsin assay, and the pH-measurement with 24h-monitoring. However, PPI test is usually performed as the first step in common practice (1). Nevertheless, as PPI test may be not conclusive in a large quote of patients and may be not reasonable, mainly concerning the prescriptive applicability, an alternative diagnostic strategy could be based on asking the patients to fill in a validated questionnaires. The most commonly used are: Reflux Symptoms Index (RSI) and gastroesophageal reflux disease impact scale (GIS), both of which are quick, self-completed, validated, and reliable (3, 4).

From a therapeutic point of view, many options have been proposed, which include: neutralization of acid gastric content (using PPI, antihistamines (H2-receptor antagonists), antacid chemical compounds), antireflux barrier (using alginates), prokinetics, inhibitors of gastric sphincters, protection of mucosal

tissue, neuromodulators, nociceptor antagonists, lifestyle modification, and surgery (6). It is to note that many medications are over the counter compounds, and self-medication is the prevalent approach by the patients. Medical prescriptions usually include PPI, alginates, and antacids. PPI class is very effective and has changed the therapeutic strategy, however, there is an increasing new trend of thought that is reluctant for the enthusiastic use of PPI, mainly concerning the potential side effects (5-7). Therefore, new interest has been directed to alginates, as they offer different positive mechanisms of action and are safe (8-10), thus alginates may represent a fruitful therapeutic option in the treatment of both GERD and LPR. In this regard, a new medical compound has been recently launched in Italy: Marial® (manufactured by Aurora, Milan, Italy) containing magnesium alginate and E-Gastryal®. For this reason, an Italian survey explored the pragmatic approach of a group of gastroenterologists in the management of GERD. The aim of this survey was to analyse the patient characteristics and the prescriptive approach, considering both the past or current treatments and clinical features during a specialistic routine visit.

MATERIALS AND METHODS

The current survey was conducted in 56 gastroenterological centers, distributed in the whole of Italy, thus assuring a wide and complete national coverage. The gastronterologists endorsed to the Project EMERGE (Emerging from RGE), and were asked to recruit all consecutive patients visited because of GERD. Patients were visited and completed the GIS and RSI questionnaires.

GIS was evaluated according to the protocol proposed by Jones (6). Items are analytically reported in Table I. Briefly, the GIS comprises nine questions regarding the frequency of the following over the previous week: acid-related symptoms, chest pain, extra-esophageal symptoms, the impact of symptoms on sleep, work, meals and social occasions, and the use of additional non-prescription medication. Four response options are provided to describe frequency over the previous 2 weeks: 'none of the time' (1), 'a little of the time' (2), 'some of the time' (3) and 'all of the time' (4).

RSI was evaluated according to the protocol proposed by Belafsky (5). Items are analytically reported in Table II. RSI was considered positive if the score was >13.

Past or current treatment was recorded and analyzed. As several possible combinations of treatment regimens could be prescribed, an arbitrary restriction was decided where 3 main options were considered: PPI alone, PPI plus add-on treatment (limited to antacids/alginates), and alginates alone. The same subdivision was adopted for new treatments prescribed during the visit. As the survey was based on a real-world practice, doctors had the complete liberty of choosing the medications on the basis of the best practice.

Demographic and clinical characteristics were described using means with SDs for normally-distributed continuous data (i.e. age) or medians with lower and upper quartiles for not normally-distributed data (i.e. for RSI or GIS) or as absolute frequency and percentages for categorical data (i.e. frequency of patients' RSI+ or RSI-).

Any statistically significant difference in the mean values or in the median values of each continuous variable between normal and pathological patients (as defined in the RSI or GIS questionnaire) was evaluated with the Unpaired *t*-test or Mann-U Whitney test, respectively. When more than two groups were compared, Kruskal Wallis test, followed by Dunn's test, was used.

Comparison of frequency distributions was made by means of the *chi*-squared test or Fisher's exact test in case of expected frequencies <5. Statistical significance was set at $p < 0.05$, and the analyses were performed using GraphPad Prism software, GraphPad Software Inc, CA, USA and MedCalc.

RESULTS

Globally, 1,839 patients (46.5% males, and 53.5% females, mean age 48.59 years) were visited in the 56 Italian gastroenterological centers. Interestingly, 47% of the patients had a previous GERD diagnosis. The percentage of patients with recognized GERD increased according to age (data not shown). In addition, most patients with diagnosis of GERD were visited and assessed within the previous year.

The GIS questionnaire was completed by all patients, whereas 785 patients filled in the RSI questionnaire.

RSI values for each single symptom are

analytically reported in Fig. 1A. The symptom with the highest score was heartburn, whereas cough, dyspnea, difficulty in swallowing, and hoarseness had the lowest score.

GIS values for each single sign are analytically reported in Fig. 1B. The signs with the highest score were burning sensation in the chest or behind the breastbone, regurgitation or acid taste in the mouth, or pain or burning in the upper stomach.

A total of 594 (75.7%) patients had positive RSI score; the total RSI score was 16 (14-20) in the whole population and 18 (15-22) in RSI^+ patients and 12 (11-13) in RSI^- patients, respectively ($p<0.0001$), as shown in Fig. 3. The total GIS score was 19 (16-23) in the whole population and 20 (17-24) in RSI^+ patients and 17 (13-20) in RSI^- patients, respectively ($p<0.001$), as reported in Fig. 2.

Fig. 3A shows the distribution of the patients considering the treatments: past, current or never: 1005 patients (57%) were treated: 426 (25%) in the past and 579 (33%) currently, whereas 718 (42%) patients were still untreated at the visit.

The different types of treatments prescribed in the past or currently used are reported in Fig. 3B, respectively. We considered 3 subgroups: monotherapy with PPI, PPI plus add-on, and Miscellany. Add-on therapy included anti-acidic or anti reflux treatment, alginates or prokinetics. Miscellany included anti-acidic or anti-reflux treatment, alginates or prokinetics. There was no

Table I. *GERD Impact Scale (GIS).*

	none of the time 1	a little of the time 2	some of the time 3	all of the time 4
In the past week				
1.How often have you had the following symptoms				
a. Pain in chest/behind the breastbone?				
b. Burning sensation in your chest or behind the breastbone?				
c. Regurgitation or acid taste in your mouth?				
d. Pain or burning in upper stomach?				
e. Sore throat or hoarseness that is related to your heartburn or acid reflux?				
2. How often have you had difficulty in getting a good night's sleep because of your symptoms?				
3. How often have your symptoms prevented you from eating or drinking any of the foods you like?				
4. How often have your symptoms kept you from being fully productive in your job or daily activities?				
5. How often do you take additional medication other than what the physician told you to take (such as Gaviscon, Maalox)?				

relevant difference among groups with regard to the frequency of the different therapeutic options.

Fig. 4 shows changes in the distribution of the different medications options: Marial as monotherapy, PPI as monotherapy, or PPI plus add-on in current treatments (Fig. 4A), and in new prescribed treatments (i.e. prescription made during the visit) (Fig. 4B). PPI as monotherapy was the most frequent current treatment (71%). After the visit, a significant change in the drug prescription was observed ($p<0.0001$): about one-fourth of patients (24.6%) received Marial® as monotherapy, whereas PPI plus add-on were prescribed to almost two-thirds of the patients. PPI alone was prescribed to about 7%. No statistically significant difference was detected in RSI among the three treatment groups ($p=0.55$) (Fig. 4C); differently, GIS values differed among the three groups ($p=0.01$) being significantly different in Marial® as monotherapy and in PPI as add-on treated patients ($p<0.05$).

Comparison between the distribution of Marial® as monotherapy, PPI as monotherapy, or PPI plus add-on in past treatments (Fig. 4D) and in new prescribed treatments (i.e. prescription made during the visit) (Fig. 4E) are reported in Fig. 7. As for current treatment, also for past treatment, PPI as monotherapy was administered to most of the patients (62.5%). Again, after the visit, a significant change in the drug prescription was observed ($p<0.0001$): prescription of Marial as monotherapy was tripled and that of PPI plus add-on was doubled. Less than 15% of patients received PPI in monotherapy. Patients who received PPI only as prescription had a significantly lower RSI than those who received PPI plus add-on ($p<0.05$) (Fig. 4F). GIS was significantly lower in patients who received as prescription Marial® as monotherapy than in those who received PPI as monotherapy or PPI plus add-on ($p<0.05$, each comparison).

Finally, the new prescribed treatments (i.e.

Table II. *Reflux Symptom Index.*

Within the last month, how did the following problems affect you?	0 = no problem 5 = severe problem					
1. Hoarseness or a problem with your voice	0	1	2	3	4	5
2. Clearing your throat	0	1	2	3	4	5
3. Excess throat mucus or postnasal drip	0	1	2	3	4	5
4. Difficulty swallowing food, liquids, or pills	0	1	2	3	4	5
5. Coughing after you ate or after lying down	0	1	2	3	4	5
6. Breathing difficulties or choking episodes	0	1	2	3	4	5
7. Troublesome or annoying cough	0	1	2	3	4	5
8. Sensation of something sticking in your throat or a lump in your throat	0	1	2	3	4	5
9. Heartburn, chest pain, indigestion, or stomach acid coming up	0	1	2	3	4	5
RSI > 13 = Abnormal	Total					

Abbreviation: RSI, reflux symptom index

prescription made during the visit) in the whole population (1,653 patients) were: 1,118 (67.6%) patients were treated with PPI alone, 425 (25.7%) with Marial® as monotherapy, and less than 7% (110) received PPI as monotherapy.

DISCUSSION

GERD is a very common disorder and, being a chronic illness, significantly impairs quality of life, therefore long-term treatment is often needed in most patients (11). However, GERD definition and GERD diagnosis may be inconsistent between them. So, in clinical practice the diagnosis may be commonly based on a symptom assessment without testing, and, as a general rule, the extent of diagnostic testing should be limited to tests which guide management decisions, detect alternate diagnoses, and/or protect the patient from the risk of an inappropriate treatment. Therefore, the use of easy and reliable questionnaires, such as GSI and RSI, represents a clinically relevant approach also based on the patient's perception of the disease severity. The management approach could depend on an assessment of the risk that complications exist, the history and success of previous treatment trials, whether or not a potentially morbid therapy such as anti-reflux surgery is under consideration, and the history of prior testing. The treatment has therefore been mainly focused on acid suppression, and PPIs are the mainstay of GERD treatment. However, there is a considerable number of clinical failures despite their high degree of efficacy, and PPI failure in GERD has become a common dilemma in clinical practice (12). Several factors have been postulated as possibly contributing to the continuation of GERD symptoms despite PPI therapy. Poor compliance, delayed gastric emptying, visceral hypersensitivity, drug metabolism, *H. pylori* infection status, and emotional stress have

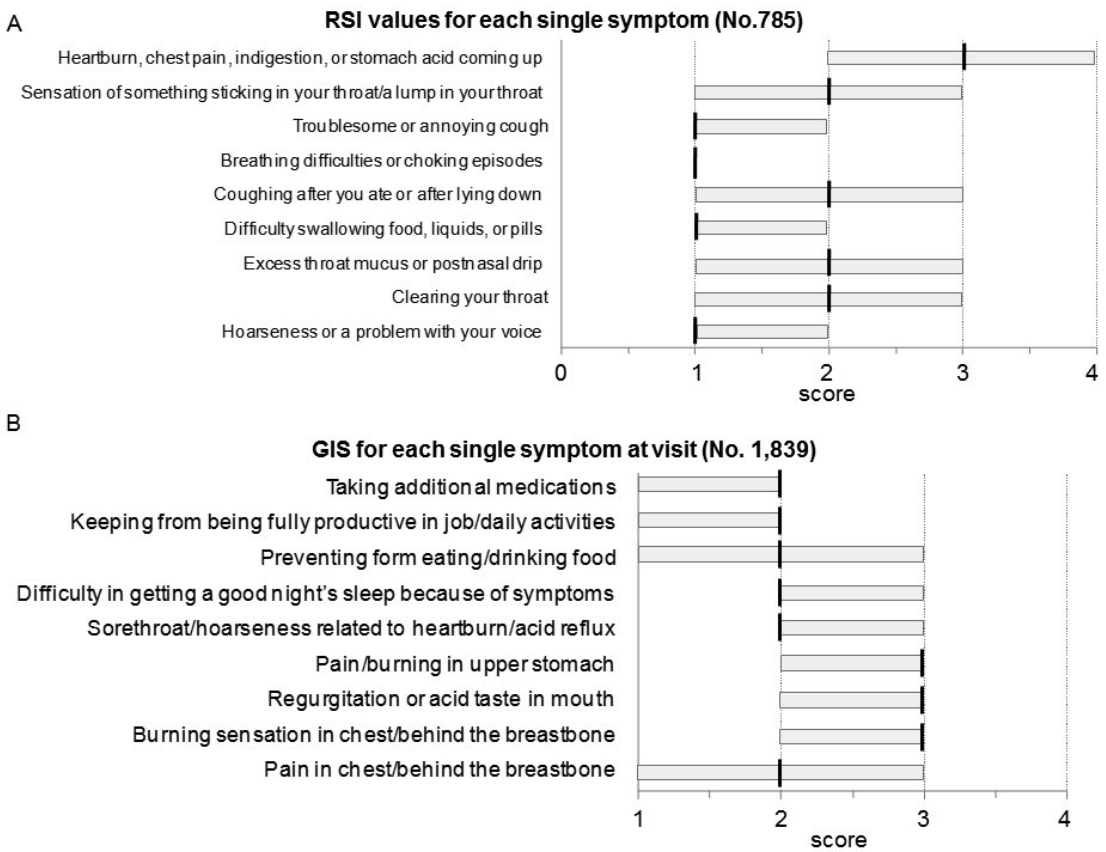

Fig. 1. ***A)*** *Reflux symptom index (RSI) as median values for each single symptom in the whole population (No. 785). Scores are reported as medians (bars) with lower and upper quartiles (boxes).* ***B)*** *GERD impact scale (GIS) as median values for each single symptom in the whole population (No.1,839). Scores are reported as medians (bars) with lower and upper quartiles (boxes).*

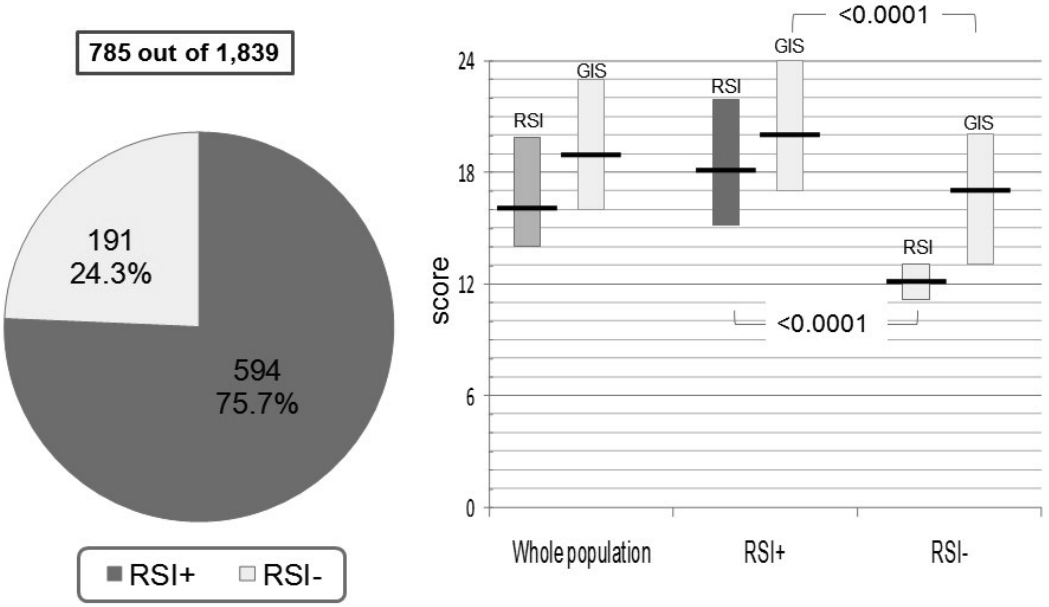

Fig. 2. *Distribution of patients according to the positivity or negativity to RSI (score >13, RSI+ and RSI-) (panel A) and median values of total RSI and total GIS in the whole population and in RSI+ and RSI- patients. Scores are reported as medians (bars) with lower and upper quartiles (boxes).*

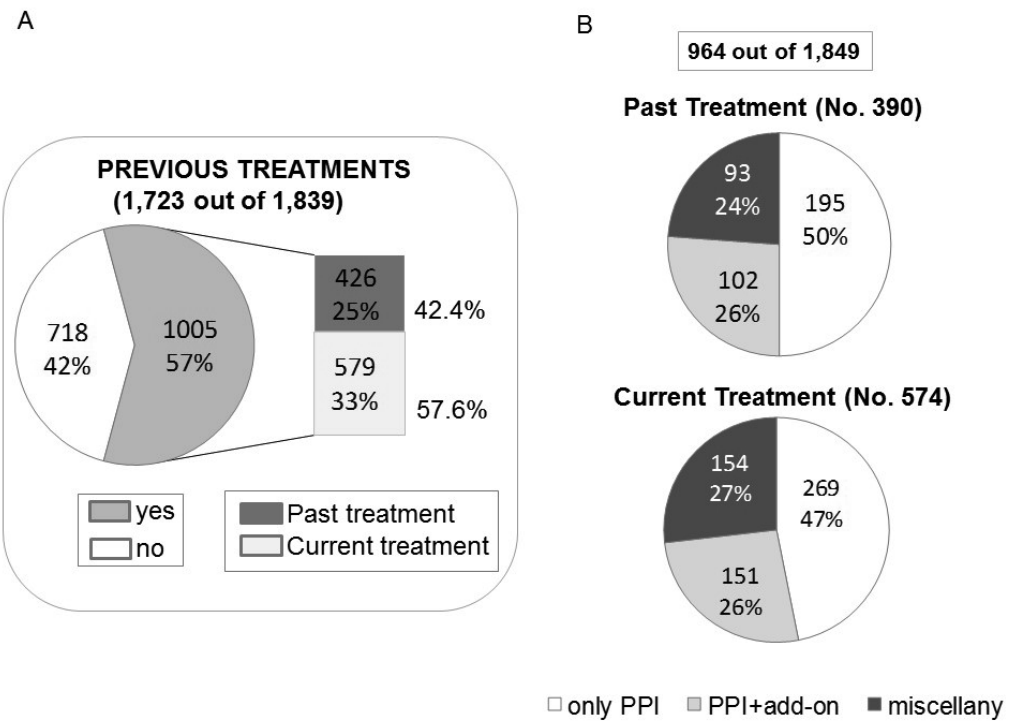

Fig. 3. ***A****) Distribution of the 1,723 patients according to the treatments: past, current or never.* ***B****) Distribution of different types of treatments prescribed in the past (panel A) or currently used (panel B): monotherapy with PPI, PPI in add-on, and Miscellany.*

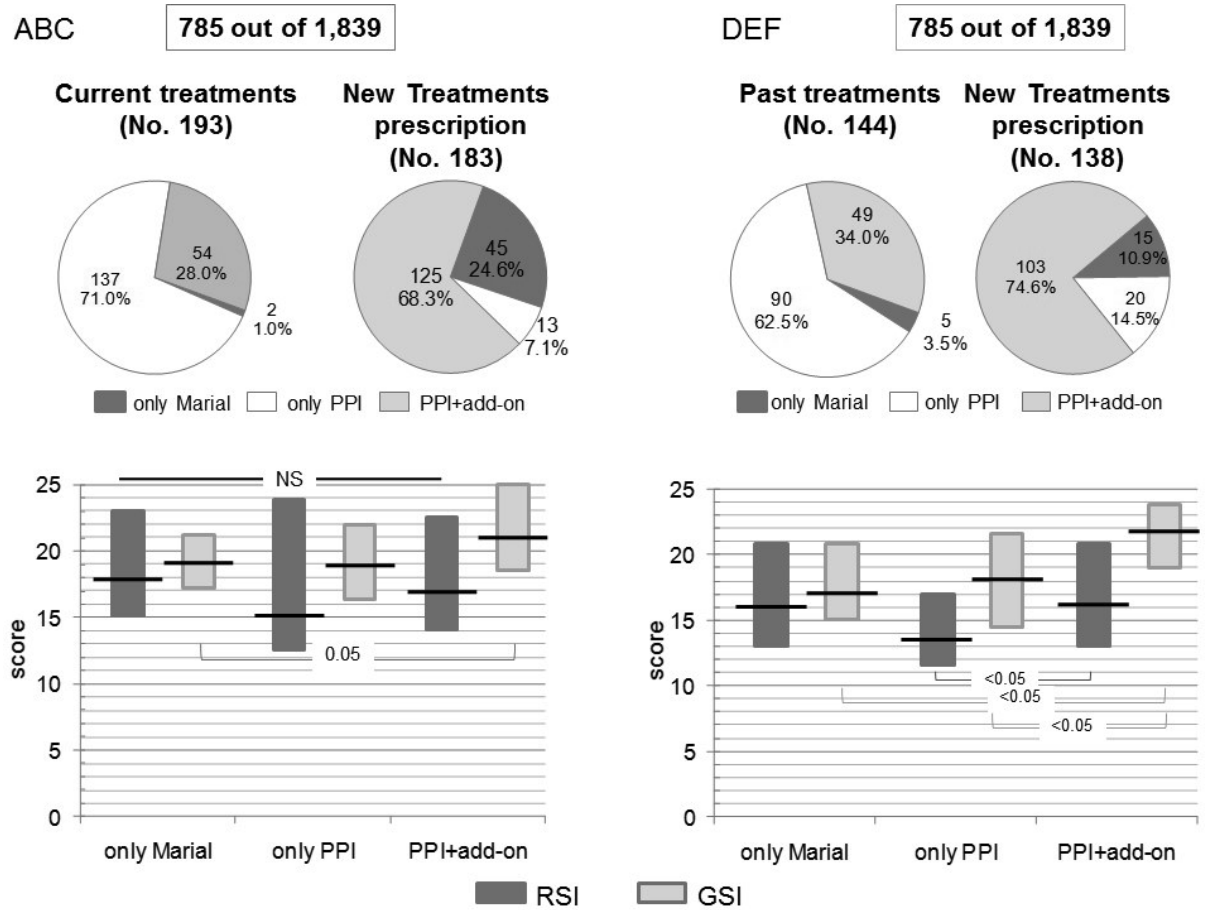

Fig. 4. *Changes in the distribution of Marial as monotherapy, PPI as monotherapy or PPI in add-on in current treatments (panel **A**) and in new prescribed treatments (i.e. prescription during the visit) (panel **B**). Panel **C** reports median RSI and GIS values in the 3 subgroups of treatments. Changes in the distribution of Marial as monotherapy, PPI as monotherapy or PPI plus add-on in past treatments (panel **D**) and in new prescribed treatments (i.e. prescription during the visit) (panel **E**). Panel F reports median RSI and GIS values in the 3 subgroups of treatments*

been reported as factors contributing to PPI failure (13). Treatment options for incomplete response to PPI therapy are limited; therefore, physicians tend to change treatment patterns and prescribe additional medications other than PPIs, also considering the potential side effects emerging from long-term regimens. In this regard, alginates may represent a useful and effective choice. Alginates have many interesting mechanisms of action and could be properly used in GERD patients, also as monotherapy as suggested by the NICE guidelines (14, 15).

The current survey was designed to evaluate the management of GERD in a real-world setting, such as Italian outpatient gastroenterological clinics. The primary outcome was the changed prescriptive approach after the availability of Marial® on the Italian market. At present, about one- quarter of new prescriptions were for Marial® compared to about one-third for PPI plus add-on, whereas PPI monotherapy was prescribed only for 6.7% of patients. This changed strategy may depend on some aspects, including awareness of potential PPI side effects, their inefficacy in some patients, the novelty of the new medical compound, and its multiple mechanisms of action (1). It is worth noting that GSI score seemed to guide the choice of medication option: indeed, patients with lower GIS score were treated with Marial®, whereas PPI plus add-on was prescribed to patients with higher GIS score. On the contrary, RSI score did not influence the therapeutic decision. Thus,

GIS may be considered a fruitful tool to treatment orientation (14, 15).

However, the present survey has some limitations: the open design, the lack of adequate control and randomization, the lack of objective diagnostic procedures, and the cross-sectional method. Further studies should therefore be performed to confirm these unmet needs.

In conclusion, the current experience demonstrated that GERD may be managed considering a patient-centred work-up by using the GIS questionnaire. GIS score may be able to define the medication choice that includes also the new medical compound Marial®.

REFERENCES

1. Kahrilas P, Yadlapati R, Roman S. Emerging dilemmas in the diagnosis and management of gastroesophageal reflux disease. F1000Res 2017; 6:1748.
2. Iwakiri K, Kinoshita Y, Habu Y, et al. Evidence-based clinical practice guidelines for gastroesophageal reflux disease 2015. J Gastroenterol 2016; 51:751-67.
3. Belafsky PC, Postma GN, Koufman JA. Validity and reliability of the Reflux Symptom Index (RSI). J Voice 2002; 16:274-77.
4. Jones R, Coyne K, Wiklund I. The gastroesophageal reflux disease impact scale: a patient management tool for primary care. Aliment Pharmacol Ther 2007; 25:1451-59.
5. Vela MF. Medical treatments of GERD. The old and new. Gastroenterol Clin N Am 2014; 43:121-33.
6. Kung YM, Hsu WH, Wu MC, et al. Recent advances in the pharmacological management of gastroesophageal reflux disease. Dig Dis Sci 2017; 62:3298-316.
7. Woodland P, Lee C, Duraisamy Y, et al. Assessment and protection of esophageal mucosal integrity in patients with heartburn without esophagitis. Am J Gastroenterol 2013; 108:535-43.
8. Chiu CT, Hsu CM, Wang CC, et al. Randomised clinical trial: sodium alginate oral suspension is non-inferior to omeprazole in the treatment of patients with non-erosive gastroesophageal disease. Aliment Pharmacol Ther 2013; 38:1054-64.
9. McGlashan JA, Johnstone LM, Sykes J, Strugala V, Dettmar PW. The value of a liquid alginate suspension (Gaviscon Advance) in the management of laryngopharyngeal reflux. Eur Arch Otorhinolaryngol 2009; 266:243-51.
10. Manabe N, Haruma K, Ito M, et al. Efficacy of adding sodium alginate to omeprazole in patients with non-erosive reflux disease: a randomized clinical trial. Dis Esophagus 2012; 25:373-80.
11. Seo SI, Bang CS, Kang HS, et al. Evaluation of treatment pattern and symptom control in patients with gastroesophageal reflux disease: multihospital questionnaire survey on the current situation in Korea. Dis Esophagus 2017; 30:1-8
12. Yadaplati R, Kahrilas PJ. When is proton pump inhibitor use appropriate? BMC Medicine 2017; 15:36.
13. Fass R, Shapiro M, Dekel R, Sewell J. Systematic review: proton-pump inhibitor failure in gastroesophageal reflux disease–where next? Alimen Pharmacol Ther 2005; 22:7994.
14. Internal Clinical Guidelines Team (UK). Dyspepsia and Gastro-Oesophageal Reflux Disease: Investigation and Management of Dyspepsia, Symptoms Suggestive of Gastro-Oesophageal Reflux Disease, or Both. London: National Institute for Health and Care Excellence (UK); 2014 Sep.
15. Davies I, Burman-Roy S, Murphy MS. Guideline Development Group. Gastro-oesophageal reflux disease in children: NICE guidance. BMJ. 2015; 350:g7703.

LETTER TO THE EDITOR

EMERGING FROM GASTROESOPHAGEAL REFLUX (EMERGE): AN ITALIAN SURVEY - II THE VIEWPOINT OF THE PATIENT

M. BIANCHETTI[1], S. PERALTA[2], R. NICITA[3], S.E. ARAGONA[4], G. CIPRANDI[4] and the EMERGE STUDY GROUP*

[1]Gastroenterologia, Humanitas Mater Domini, Castellanza (VA), Italy; [2]Endoscopia Digestiva, Policlinico P. Giaccone, Università di Palermo, Palermo, Italy; [3]Gastroenterologia, ASP 5, Reggio Calabria, Italy; [4]Center of Regenerative Medicine, Humanitas Mater Domini, Castellanza (VA), Italy; [5]Ospedale Policlinico San Martino, Genoa, Italy

**EMERGE Study Group: A. Arrigoni, D. Artuso, M. Astegiano, C. Azzinnari, E. Battaglia, C. Belcari, E. Bendia, P. Benedicenti, M. Bianchetti, G. Brandimarte, I. Buoncompagni, M. Cabras, S. Camilleri, G. Capece, S. Caronna, C. Cassieri, F. Castaldo, T. Catalano, C. Citarella, F. D'amore, G. D'alia, F. D'arpa, A. Dattola, N. De Bortoli, A. De Medici, S. Di Marzo, R. Di Mitri, A. Di Napoli, V. D'onofrio, L. Dughera, W. Elisei, G. Errico, L. Familiari, P. Familiari, R. Frasca, A. Frunzio, M. Gatti, S. Genova, S. Grosso, R. Gullotta, D.R. Iannuzziello, G. Indennitate, G. Leonardi, C. Luigiano, B. Macchiarella, T. Maisto, M.G. Mancino, A. Mancino, G. Manes, R. Marin, G.R. Mastinu, A. Moi, L.M. Montalbano, N. Monterosso, A. Morabito Loprete, L. Morlando, R. Nicita, C. Ogliari, N. Paiano Primaldo, G. Paliani, A.P. Palieri, D. Pardocchi, A. Pati, G. Pedretti, S. Peralta, A. Pisani, P. Plomaritis, A.C. Privitera, R. Pumpo, F. Quatraro, D. Raimondo, G. Rivellini, L. Rizzo Giovanni, M. Romano, R. Salerno, E. Savarino, G. Scarpulla, E. Sinagra, M. Soncini, G. Tammaro, C. Trovato, R. Vassallo, M. Vinti, C.M.P. Virgilio*

Received April 6, 2018 – Accepted April 23, 2018

Gastroesophageal reflux disease (GERD) is a very common disease, as about a quarter of the Western population has GERD symptoms at least weekly and GERD is the most frequent reason for outpatient gastroenterology consultation. GERD treatment is based on proton pump inhibitor (PPI) use, but PPI may be ineffective in some patients and potentially unsafe if administered for very long time. A new medical compound (Marial®) has been introduced on the Italian market. This product contains magnesium alginate and a phytopolymer: it may be able to repair ulcer/erosion, protect mucosal tissue, and contrast acid contents. The current survey was conducted on a large group of GERD patients visited at 56 Italian gastroenterological offices. Patients were treated with PPI alone, PPI plus add-on, or Marial® for 4 weeks: the choice was decided by each gastroenterologist on the basis of the best practice criterion. A reflux symptoms index (RSI) questionnaire was used to weekly assess the clinical features. Marial® and PPI plus add-on significantly reduced RSI scores, from the second week. Noteworthy, Marial® was more effective than PPI plus add-on. In conclusion, the current survey demonstrated that patients with GERD perceived a significant improvement of GERD symptoms measured by the RSI questionnaire. Marial® was as effective as PPI plus add-on.

Key words: gastroesophageal reflux disease, patients, RSI, PPI, Marial®

Mailing address:
Giorgio Ciprandi, M.D.
Largo R. Benzi 10,
16132 Genoa, Italy
Phone 00 39 10 35331820
Fax 00 39 10 3538664
e-mail gio.cip@libero.it

0393-974X (2018)
Copyright © by BIOLIFE, s.a.s.
This publication and/or article is for individual use only and may not be further reproduced without written permission from the copyright holder.
Unauthorized reproduction may result in financial and other penalties
DISCLOSURE: ALL AUTHORS REPORT NO CONFLICTS OF INTEREST RELEVANT TO THIS ARTICLE.

To the Editor,

Gastroesophageal reflux disease (GERD) is very common, indeed about 25% of the Western population has GERD symptoms at least weekly (1). In addition, GERD is the most frequent reason for outpatient gastroenterology consultation (2). From a therapeutic point of view, the current guidelines recommend GERD medical management as first step with proton pump inhibitors (PPIs) that are the most effective therapy for erosive esophagitis (3-5). However, there is convincing proof that in some patients with GERD symptoms, especially those with non-erosive reflux disease (NERD), the acid suppression by PPIs may be not as effective (3). Therefore, an alternative approach for treating symptomatic GERD could be to try to impede the flow of acidic refluxate. In this regard, alginic acid derivatives, or alginates, are able to treat GERD by creating a mechanical barrier that displaces the post-prandial acid pocket (6). Their mechanism of action is based on the fact that in the presence of gastric acid, they precipitate into a gel and form a raft that localizes to the acid pocket in the proximal stomach (7). Although they have been available in many countries over-the-counter for several decades, often in combination with antacids, this class of medications has recently raised renewed research interest (8). In fact, providing an impediment to distal oesophageal acid exposure, alginates may be superior to other measures or particularly useful as an additional option for patients with GERD not responding to anti-secretory therapy (9). In other words, even though the current treatment guidelines recommend prescribing PPI for acid suppression as first line therapy in patients with chronic GERD symptoms, it is well known that many patients may have only intermittent or mild/moderate symptoms and so could need a less aggressive treatment. A recent meta-analysis provided evidence that alginates alone may provide superior benefit over antacids and therefore they could be considered as an initial treatment for patients with mild/moderate GERD symptoms for whom chronic acid suppression should be either undesirable or deemed unnecessary (9). In this context, a new medical compound has been recently launched in Italy: Marial® (manufactured by Aurora, Milan, Italy) containing magnesium alginate and E-Gastryal®. An Italian survey explored the pragmatic approach of a group of gastroenterologists in GERD management. The aim of this survey analysis was to evaluate the GERD patient's point of view during a course of therapy using the RSI score changes as primary outcome.

MATERIALS AND METHODS

The current survey was conducted in 56 gastroenterological centers, distributed in the whole of Italy, so assuring a wide and complete national coverage. The gastroenterologists endorsed to the Project EMERGE (Emerging from RGE) were asked to recruit all consecutive patients visited because of GERD.

Patients were consecutively recruited during the specialist visit. The inclusion criteria were: to have a diagnosis of GERD, both genders, and adulthood. Exclusion criteria were to have comorbidities able to interfere the evaluation of outcomes. As this survey was based on a real-world practice, the doctors had the complete liberty of choosing the preferred medications on the basis of the best practice. All subjects gave informed, signed consent to participate in the study. Three therapeutic options were prescribed: PPI as monotherapy, Marial® as monotherapy, and PPI plus add-on. The add-on options included a miscellany of medication options, including alginates, anti-acids, prokinetics, antiH2, and Marial®.

The course of treatment lasted 4 weeks. Medications were taken following the specific indications. Patients were asked to complete weekly the RSI questionnaire, therefore, 5 RSI scores were available. They were collected in the specialist's office without a new visit. RSI was evaluated according to the protocol proposed by Belafsky (10). Items are analytically reported in another article published in the present issue of JBRHA.

Demographic and clinical characteristics were described using means with SDs or SEs for normally-distributed continuous data (i.e. age or percentage of RSI reduction) or medians with lower and upper quartiles for not normally-distributed data (i.e. for RSI) or as absolute frequency and percentages for categorical data (i.e. frequency of treatments).

Difference in the median values of each continuous

variable between before and after 4 weeks' treatment was evaluated with Wilcoxon signed rank test; Mann U Whitney test was used to compare percentage of changes in RSI. When more than two groups were compared (i.e. total RSI weekly trend over time), Kruskal Wallis test, followed by Dunn's test, was used.

Statistical significance was set at $p < 0.05$, and the analyses were performed using GraphPad Prism software, GraphPad Software Inc, CA, USA.

RESULTS

A total of 771 patients (50.87% males, 49.13% females, mean age 49.8 years) took the prescribed therapy, concluded the treatment course, and completed the RSI questionnaire.

Fig. 1 shows the distribution of the different therapeutic options prescribed during the gastroenterological visit. Most patients (63%) were treated with PPI plus add-on, about a quarter with Marial® alone, 7.6% with PPI as monotherapy, and only 3.5% with a miscellany.

Considering the entire patient cohort, a time-dependent significant reduction in the RSI score after the treatment is reported in Fig. 2A ($p<0.0001$).

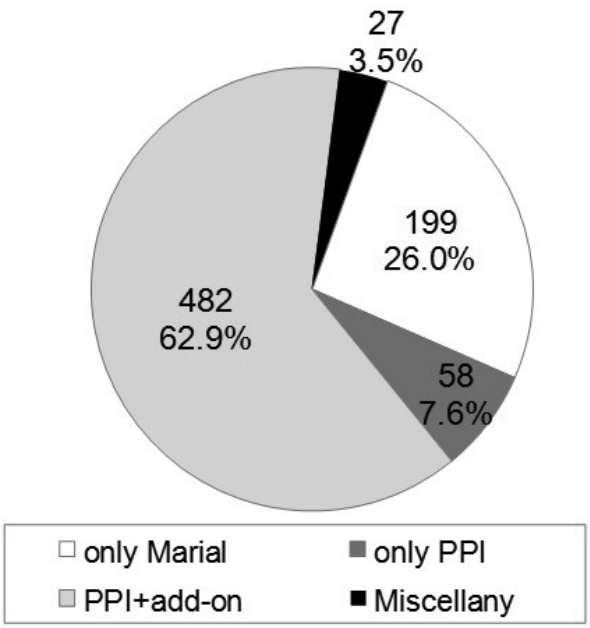

Fig. 1. *Distribution of the different treatments prescribed by the gastroenterologists.*

In particular, there was 37.8% reduction of RSI score at the end of the course.

Fig. 2B shows the trend of the total RSI values in patients treated with Marial® as monotherapy and with PPI plus add-on. A time-dependent decrease in RSI total score was observed either after Marial® as monotherapy or with PPI plus add-on. Marial® as monotherapy was able to induce a higher total RSI score reduction as compared to that observed after treatment with PPI plus add-on. This was true starting after 1 week treatment.

Changes in RSI values before and after 4 week-treatment with Marial® as monotherapy was statistically significant for each single symptom (Fig. 3A) ($p<0.001$, each comparison). A similar result was found evaluating PPI plus add-on treatment (Fig. 3B) ($p<0.001$, each comparison).

The percentage of RSI reduction in i) breathing difficulties or choking episodes, ii) difficulty swallowing food, liquids, or pills, iii) clearing throat or iv) hoarseness or a problem with voice was significantly higher in patients treated with Marial® as monotherapy as compared to those treated with PPI plus add-on (Fig. 4).

DISCUSSION

GERD is one of the most common diseases encountered in both the outpatient and inpatient settings (10, 11). The first-line treatment of gastroesophageal reflux disease continues to be the anti-secretory drugs, most commonly proton pump inhibitors (PPIs). Of course, dietary and lifestyle modifications, including avoidance of acidic foods, carbonated beverages, alcohol, spicy food, and tobacco, in any case continue to be recommended. Weight loss for patients with recent weight gain or BMI >25, avoiding lying down within 2–3 h of meals, and bedhead elevation to improve nocturnal symptoms are also effective interventions that can be recommended (12). Recently, long-term safety of PPIs has been called into question with some evidence of increased infectious complications and nutritional deficiencies, leading some to advocate caution with long-term use of PPIs in elderly,

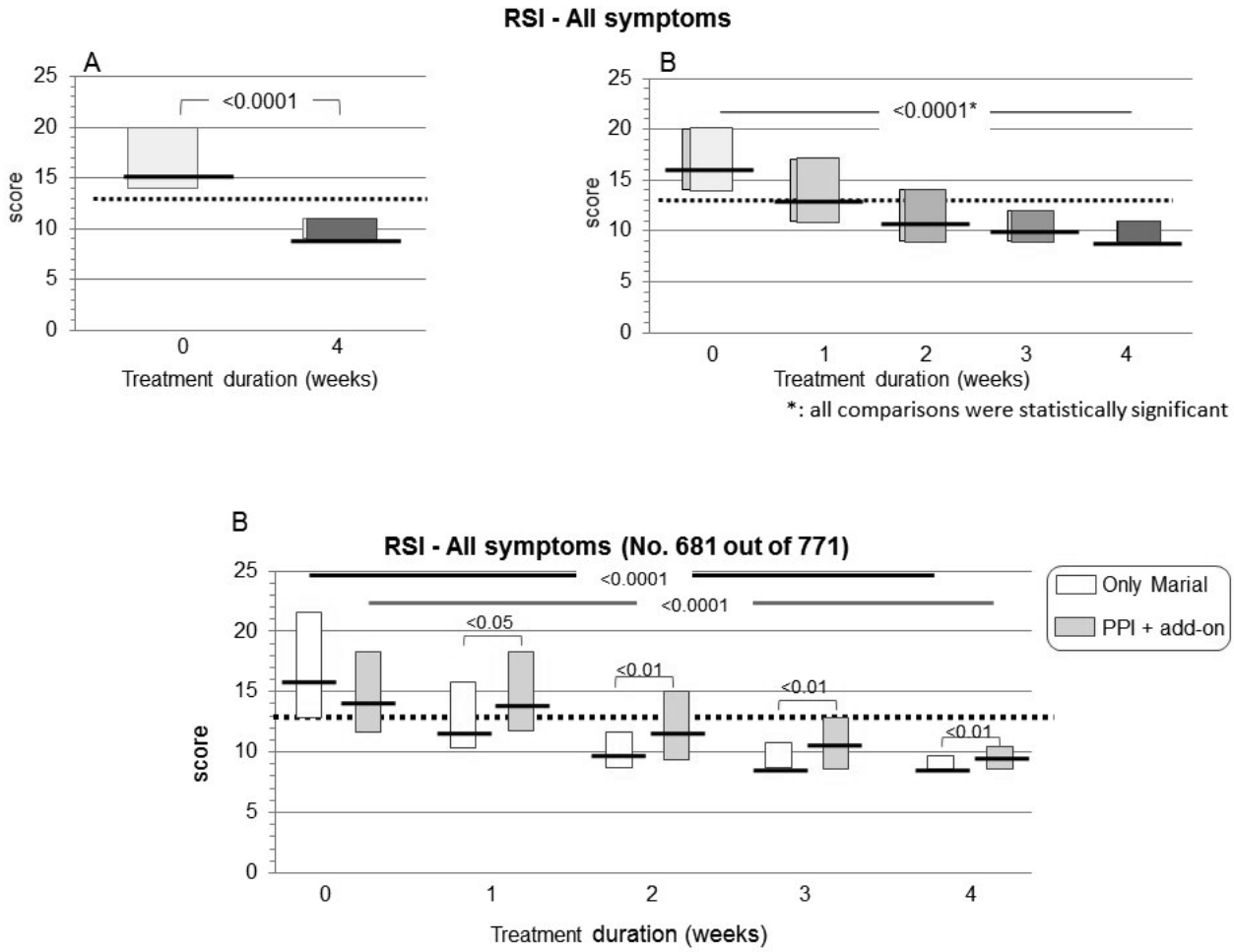

Fig. 2. ***A)*** *Total RSI value in all patients at baseline and after 4 weeks (i.e. end of the therapy) (panel A) and total RSI weekly trend over time (panel B).* ***B)*** *Trend of the total RSI values in patients treated with Marial as monotherapy and with PPI plus add-on.*

malnourished, immune-compromised, chronically ill, and osteoporotic patient populations (13, 14).

Very recently, a new medical compound has been presented on the Italian market: Marial®. This novelty has suggested the importance of evaluating its positioning in the therapeutic options for GERD. The current survey was conducted in a real-world setting, such as outpatients visited at 56 Italian gastroenterological clinics.

The primary outcome demonstrated that Marial® was prescribed in about a quarter of the visited patients, whereas PPI plus add-on remained the preferred option as prescribed in about one third of patients. Both Marial® and PPI plus add-on were able to significantly reduce RSI score; interestingly, a significant RSI diminution was remarkable from the first week. Noteworthy, Marial® induced a more significant RSI reduction than PPI plus add-on considering both the total RSI score and some single symptoms. This finding is surprising, even though partially depending on relatively lower RSI values at baseline (but without significant difference). Instead, to support this difference, Marial®-treated patients had lower GIS scores than PPI-plus-add-on-treated patients as evidenced during the visits.

The present survey has some limitations: the open

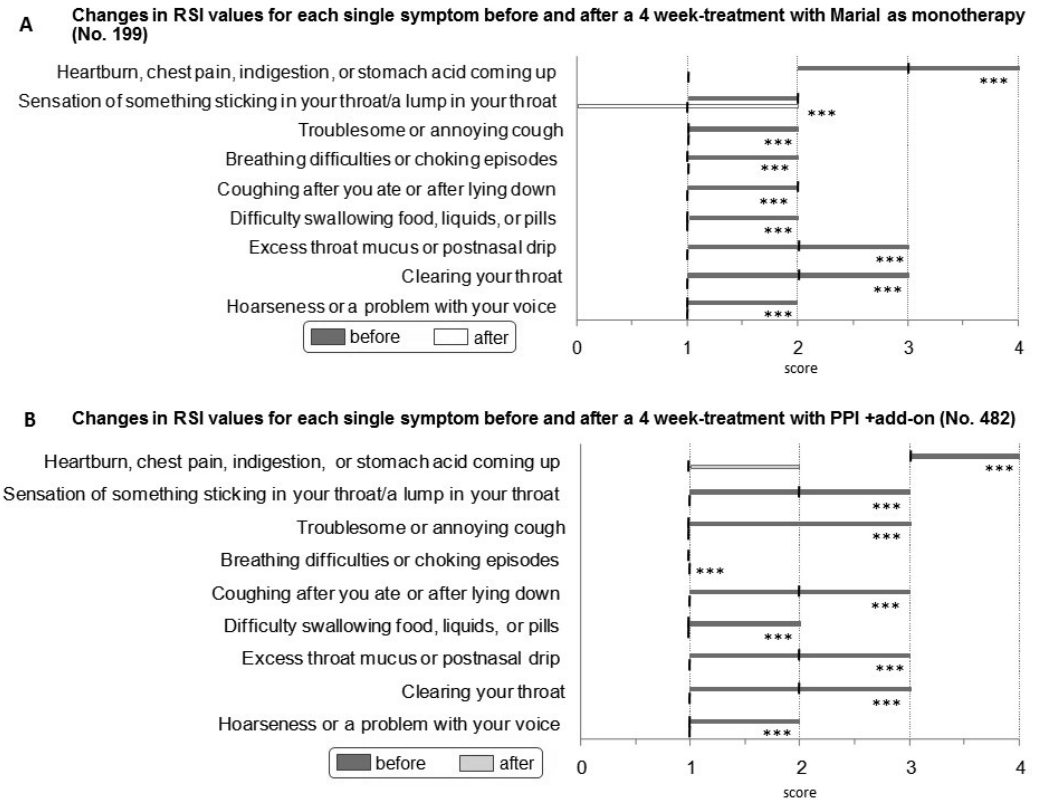

Fig. 3. ***A)*** *Changes in RSI scores for each single symptom evaluated before and after the 4-week treatment with Marial®.* ***B)*** *Changes in RSI scores for each single symptom evaluated before and after the 4-week treatment with PPI plus add-on.*

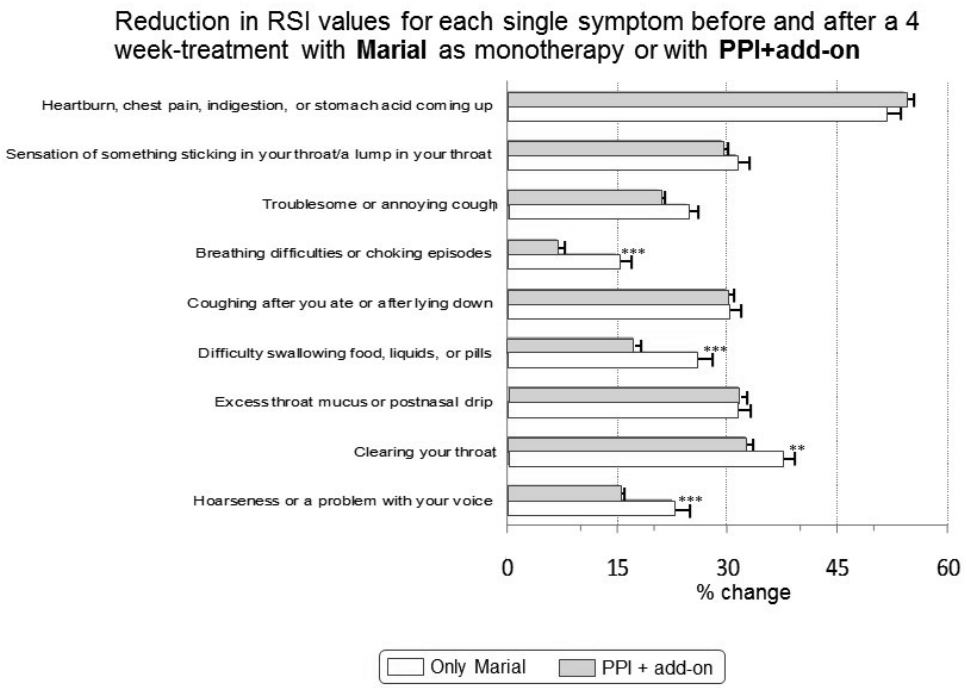

Fig. 4. *Percentages of RSI reduction for each single symptom in patients treated with Marial® as monotherapy and with PPI plus add-on.*

design, the lack of randomization and placebo-group, the lack of objective evaluation and biomarkers. Therefore, further studies should be conducted to adequately fill these shortcomings.

In conclusion, the current survey demonstrated that patients with GERD perceived a significant improvement of GERD symptoms as measured by the RSI questionnaire. Marial® was as effective and rapid as PPI plus add-on. So, Marial® could be considered a reasonable option in the management of GERD.

REFERENCES

1. El-Serag H, Sweet S, Winchester C, Dent J. Update on the epidemiology of gastrooesophageal reflux disease: a systematic review. Gut 2014; 63:871-80.
2. Hershcovici T, Fass R. Management of gastroesophageal reflux disease that does not respond well to proton pump inhibitors. Curr Opin Gastroenterol 2010; 26:367-78.
3. Katz P, Gerson L, Vela M. Guidelines for the diagnosis and management of gastroesophageal reflux disease. Am J Gastroenterol 2013; 108:308-28.
4. Kahrilas P, Shaheen N, Vaezi M. American Gastroenterological Association Medical Position Statement on the management of gastroesophageal reflux disease. Gastroenterology 2008; 135:1383-91.
5. Fass R. Proton pump inhibitor failure–what are the therapeutic options? Am J Gastroenterol 2009; 104(S2):S33-38.
6. de Ruigh Roman S, Chen J, Pandolfino J, Kahrilas P. Gaviscon double action liquid (antacid and alginate) is more effective than antacid in controlling post-prandial oesophageal acid exposure in GERD patients: a double-blind crossover-study. Aliment Pharmacol Ther 2014; 40:531-37.
7. Rohof W, Bennink R, Smout A, Thomas E, Boeckxstaens G. An alginate-antacid formulation localizes to the acid pocket to reduce acid reflux in patients with gastroesophageal reflux dis- ease. Clin Gastroenterol Hepatol 2013; 11:1585-91.
8. Sifrim D, Penagini R. Capping the gastric acid pocket to reduce postprandial acid gastroesophageal reflux. Clin Gastroenterol Hepatol 2013; 11:1592-94.
9. Leiman DA, Riff BP, Morgan S, et al. Alginate therapy is effective treatment for gastroesophageal reflux disease symptoms: a systematic review and meta-analysis. Dis Esophagus. 2017; 30:1-9.
10. Kahrilas P, Yadlapati R, Roman S. Emerging dilemmas in the diagnosis and management of gastroesophageal reflux disease. F1000Res 2017; 6:1748.
11. Kethman W, Hawn M. New approaches to gastroesophageal reflux disease. J Gastroenterol Surg 2017; 21:1544-52.
12. Subramanian CR, Triadafilopoulos G. Refractory gastroesophageal reflux disease. Gastroenterol Rep 2015; 3:41-53.
13. Ali T, Roberts DN, Tierney WM. Long-term safety concerns with proton pump inhibitors. Am J Med. 2009; 122(10):896-903.
14. Sheen E, Triadafilopoulos G. Adverse effects of long-term proton pump inhibitor therapy. Dig Dis Sci. 2011; 56(4):931-50.
15. Pandit S, Boktor M, Alexander JS, Becker F, Morris J. Gastroesophageal reflux disease: a clinical overview for primary care physicians. Pathophysiology 2018 (in press).

LETTER TO THE EDITOR

CORRELATION BETWEEN THE REFLUX FINDING SCORE AND THE GERD IMPACT SCALE IN PATIENTS WITH GASTROESOPHAGEAL REFLUX DISEASE

M. BIANCHETTI[1], S. PERALTA[2], R. NICITA[3], S.E. ARAGONA[4], G. CIPRANDI[4] and the EMERGE STUDY GROUP*

[1]Gastroenterologia - Humanitas Mater Domini, Castellanza (VA), Italy; [2]Endoscopia Digestiva - Policlinico P. Giaccone, Università di Palermo, Palermo, Italy; [3]Gastroenterologia - ASP 5, Reggio Calabria, Italy; [4]Center of Regenerative Medicine - Humanitas Mater Domini, Castellanza (VA), Italy; [5]Ospedale Policlinico San Martino, Genoa, Italy

**EMERGE Study Group: A. Arrigoni, D. Artuso, M. Astegiano, C. Azzinnari, E. Battaglia, C. Belcari, E. Bendia, P. Benedicenti, M. Bianchetti, G. Brandimarte, I. Buoncompagni, M. Cabras, S. Camilleri, G. Capece, S. Caronna, C. Cassieri, F. Castaldo, T. Catalano, C. Citarella, F. D'amore, G. D'alia, F. D'arpa, A. Dattola, N. De Bortoli, A. De Medici, S. Di Marzo, R. Di Mitri, A. Di Napoli, V. D'onofrio, L. Dughera, W. Elisei, G. Errico, L. Familiari, P. Familiari, R. Frasca, A. Frunzio, M. Gatti, S. Genova, S. Grosso, R. Gullotta, D.R. Iannuzziello, G. Indennitate, G. Leonardi, C. Luigiano, B. Macchiarella, T. Maisto, M.G. Mancino, A. Mancino, G. Manes, R. Marin, G.R. Mastinu, A. Moi, L.M. Montalbano, N. Monterosso, A. Morabito Loprete, L. Morlando, R. Nicita, C. Ogliari, N. Paiano Primaldo, G. Paliani, A.P. Palieri, D. Pardocchi, A. Pati, G. Pedretti, S. Peralta, A. Pisani, P. Plomaritis, A.C. Privitera, R. Pumpo, F. Quatraro, D. Raimondo, G. Rivellini, L. Rizzo Giovanni, M. Romano, R. Salerno, E. Savarino, G. Scarpulla, E. Sinagra, M. Soncini, G. Tammaro, C. Trovato, R. Vassallo, M. Vinti, C.M.P. Virgilio*

Received April 6, 2018 - Accepted April 23, 2018

Gastroesophageal reflux disease (GERD) is a very common disorder. As there is no gold standard diagnostic tool, patient-based strategy is adopted in clinical practice. In this regard, there are questionnaires able to easily and rapidly assess symptom severity directly by the patient. The GERD Impact Scale (GIS) and the Reflux Symptom Index (RSI) have been validated as diagnostic tools in routine clinical care. The present study aimed to correlate RIS values with GIS scores in a large cohort of GERD patients visited at gastroenterological clinics. Globally, 785 subjects (51.2% males, 48.8% females, mean age: 49.59 years) were visited in 56 Italian gastroenterological offices. The current study demonstrates that a GIS value >19 may be a reliable cut-off to define the positivity of the test, and GIS and RSI were significantly correlated. Therefore, both tests may be recommended for GERD patients in clinical practice.

To the Editor,

At present, there is no gold standard diagnostic test for the diagnosis of gastroesophageal reflux disease (GERD), considering both symptom assessment and objective measurements, such as digestive endoscopy and pH-metry (1). In particular, endoscopy has high specificity but moderate sensitivity for untreated GERD since many of these patients do not have reflux esophagitis. In these patients, esophageal pH-metry has high diagnostic specificity, but moderate

Key words: gastroesophageal reflux disease, RSI, GIS, real world study

Mailing address:
Giorgio Ciprandi, M.D.
Largo R. Benzi 10, 16132 Genoa, Italy
Te.: +39 10 35331820
Fax: +39 10 3538664
e-mail gio.cip@libero.it

0393-974X (2018)
Copyright © by BIOLIFE, s.a.s.
This publication and/or article is for individual use only and may not be further reproduced without written permission from the copyright holder.
Unauthorized reproduction may result in financial and other penalties
DISCLOSURE: ALL AUTHORS REPORT NO CONFLICTS OF INTEREST RELEVANT TO THIS ARTICLE.

sensitivity (2). For these reasons, in clinical practice both digestive endoscopy and pH-metry have limited availability, are unpleasant for the patients, and are resource-demanding and costly (3). In addition, the protonic pump inhibitor (PPI) test, such as a short course with *ex juvantibus* criteria to diagnose GERD, has questionable diagnostic relevance value (4-8). On the basis of these concepts, the current guidelines recommend a symptom-based approach for the diagnosis and treatment in primary care (8-11). In particular, patients who are young, have a short GERD duration, and mild/moderate symptoms could be empirically and immediately treated also with alternative options (8-11). In addition, some questionnaires were developed to permit symptom-based diagnosis and management of GERD. In this context, the GERD Impact Scale (GIS) and the Reflux Symptom Index (RSI) have been validated as diagnostic tools in routine clinical care (7, 12). Recently, some studies investigated the validity and reliability of both RSI and GSI in real-world settings (1, 13, 14). However, no study compared RSI with GIS in GERD patients in a real-world setting. Therefore, the present study aimed to correlate RIS values with GIS scores in a large cohort of GERD patients visited at gastroenterological clinics.

MATERIALS AND METHODS

Globally, 785 patients were consecutively visited and enrolled in 56 gastroenterological Italian centers. The inclusion criteria were GERD diagnosis, adulthood, and both genders. Exclusion criteria were other digestive disorders and/or diseases able to interfere with interpretation of the findings. All subjects gave informed, signed consent to participate in the study. Patients were visited by the gastroenterologist and completed the RSI and GSI questionnaires during the visit.

RSI was evaluated according to the protocol proposed by Belafsky (7); a total score >13 was considered positive. GSI was evaluated according to the protocol proposed by Jones (12).

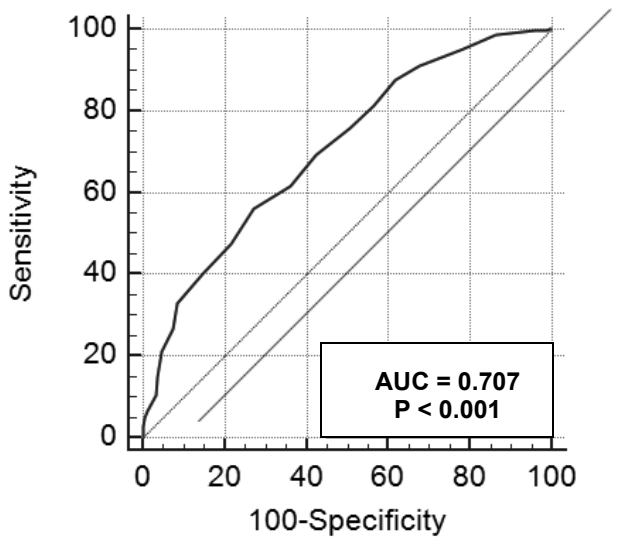

Criterion	Sensitivity (95%CI)	Specificity (95%CI)	+LR	-LR
>19	56.06 (52.0-60.1)	72.77 (65.9 - 79.0)	2.06	0.60

Fig. 1. *Receiver operator characteristic (ROC) curve analysis to identify the best cut off-point of overall GIS score able to discriminate between patients with a positive or a negative RSI.*

Demographic and clinical characteristics were described using means with SDs for normally-distributed continuous data (i.e. age) or medians with lower and upper quartiles for not normally-distributed data (i.e. for RSI and GSI). The best cut off-point of overall GIS score able to discriminate between patients with a positive or a negative RSI was estimated on the basis of the receiver operator characteristic (ROC) curve analysis. AUC was reported with 95% Confidence Intervals. Difference in the median values of RSI or GIS was evaluated with Mann U Whitney. Correlation between the RSI score and the GIS score was evaluated with Spearman rank-order correlation coefficient. Statistical significance was set at $p < 0.05$, and the analyses were performed using GraphPad Prism software, GraphPad Software Inc, CA, USA and MedCalc, MedCalc Software bvba, Ostend, Belgium.

RESULTS

A total of 785 subjects (51.2% males, 48.8% females, mean age: 49.59 (15.76) years) were visited in 56 Italian gastroenterological surgeries. All subjects completed the RSI and GIS questionnaire.

The best cut off-point of overall GIS score able to discriminate between patients with a positive or a negative RSI was 19 as estimated on the basis of the ROC curve analysis [AUC: 0.707 (0.674-0.739)]: patients with an overall GIS score >19 were considered as "RSI positive" patients (patients with GERD), whereas patients with an overall GIS score 19 were considered "RSI negative" patients (patients without GERD), as shown in Fig. 1. Therefore, 333 patients were $GIS^{+}RSI^{+}$, and 139 were $GIS^{-}RSI^{-}$.

Fig. 2 shows the median GIS and RSI values in the 2 subgroups: there was a significant difference both concerning GIS and RSI ($p<0.0001$ for both). Fig. 3 shows the relationship between GIS and RSI in the whole population: a weak-to-moderate correlation was found between RSI and GIS (r

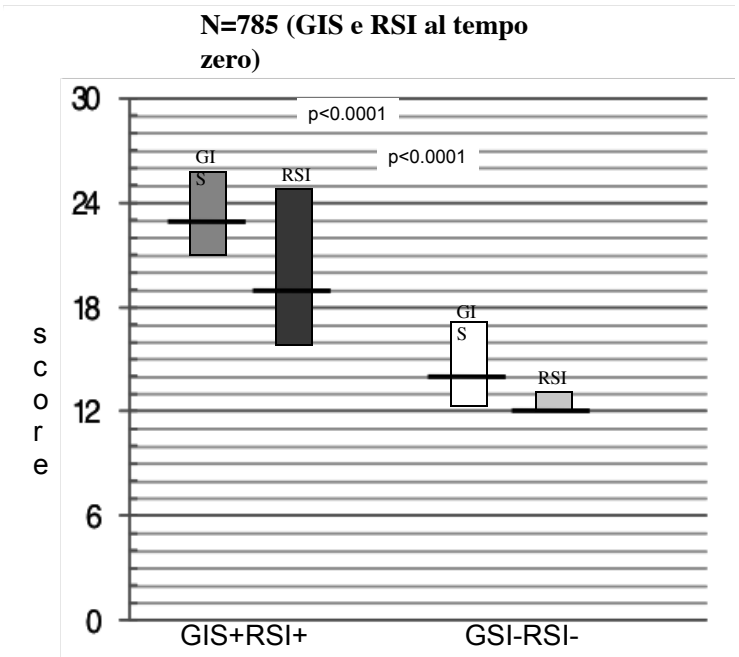

Fig. 2. *GIS and RSI values in patients with positive scores of GIS and RSI ($GIS^{+}RSI^{+}$) and in patients with negative scores of GIS and RSI ($GIS^{-}RSI^{-}$).*

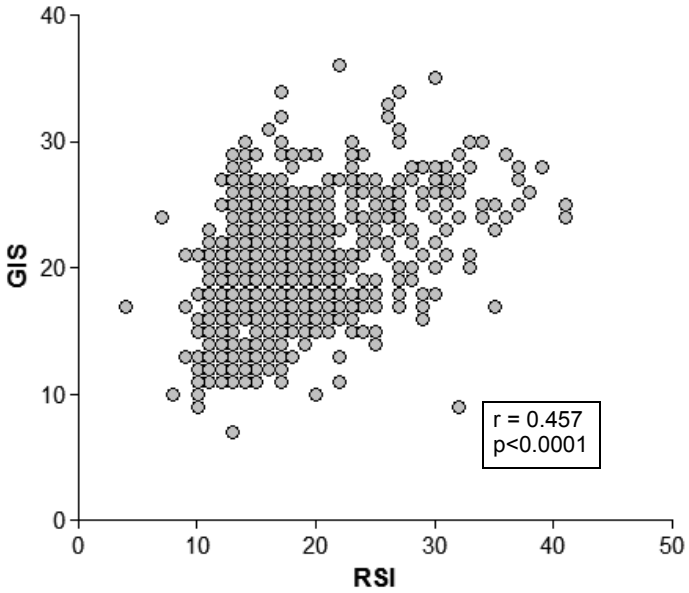

Fig. 3. *Correlation between the RSI score and the GIS score in the whole population.*

= 0.457, p <0.0001). On the contrary, a lack in the association between RSI and GIS was found when $GIS^{+}RSI$ patients and $GIS^{-}RSI^{-}$ patients were analyzed separately (data not shown).

DISCUSSION

Upper gastrointestinal symptoms, including GERD complaints, constitute one of the most common reasons for primary care visits (14). Reliable diagnostic methods for management and referral of these patients are clinically relevant to optimize care and improve cost efficiency (15, 16). A properly validated questionnaire, such as GIS, is therefore a valuable tool for facilitating the symptom-based diagnosis of GERD (8). Furthermore, RSI could positively contribute to improve the diagnostic work-up (7). Moreover, they are useful to underline the most relevant clinical features fruitful for GERD diagnosis and remark the importance of considering the patient's symptom perception. As both tests are easy, self-completed, and quick, both GIS and RSI can be used in primary care settings as well as in specialist clinics. The present study therefore aimed to compare GIS and RSI in a wide cohort of patients with GERD visited in a real-world setting, such as 56 Italian gastroenterological clinics. In addition, it has to be noted that curiously no cut-off able to define positive GIS has been calculated to date.

The current study demonstrated that a reliable cut-off for GIS correspond to a value >19: this number differentiates reasonably RSI^{+} from RSI^{-} patients. In addition, patients with both questionnaires positive showed the highest scores. The primary outcome of the current study was the moderate relationship between GIS and RSI in GERD patients. This finding underlines the clinical relevance of both tests.

Therefore, as both questionnaires are easy and rapid, their use is very fruitful in clinical practice. Indeed, they may be administered both in a specialist setting and in primary care office.

In conclusion, the current experience demonstrated that a GIS value >19 may be a reliable cut-off to define the positivity of the test, and GIS and RSI are significantly correlated. Therefore, both tests are recommended for the management of GERD patients in clinical practice.

REFERENCES

1. Jonasson C, Wernersson B, Hoff DAL, Hatlebakk JG. Validation of the GerdQ questionnaire for the diagnosis of gastro-oesophageal reflux disease. Aliment Phrmacol Ther 2013; 37:564-72.
2. Moraes-Filho JP, Chinzon D, Eisig JN, Hashimoto CL, Zaterka S. Prevalence of heartburn and gastroesophageal reflux disease in the urban Brazilian population. Arch Gastroenterol 2005; 42:122-27.
3. Mearin F, Ponce J, Ponce M, Balboa A, Gónzalez MA, Zapardiel J. Frequency and clinical implications of supraesophageal and dyspeptic symptoms in gastroesophageal reflux disease. Eur J Gastroenterol Hepatol 2012; 24:665-74.
4. Koufman J, Sataloff RT, Toohill R. Laryngopharyngeal reflux: consensus conference report. J Voice 1996; 10:215-16.
5. Eckley CA, Costa HO. Comparative study of salivary pH and volume in adults with chronic laryngopharyngitis by gastroesophageal reflux disease before and after treatment. Braz J Otorhinolaryngol 2006; 72:55-60.
6. Belafsky PC, Postma GN, Koufman JA. The validity and reliability of the reflux finding score (RFS). Laryngoscope 2001; 111:1313-17.
7. Belafsky PC, Postma GN, Koufman JA. Validity and reliability of the reflux symptom index (RSI). J Voice 2002; 16:274-77.
8. Koufman JA, Aviv JE, Casiano RR, Shaw GY. Laryngopharyngeal reflux: position statement of the committee on speech, voice, and swallowing disorders of the American Academy of Otolaryngology-Head and Neck Surgery. Otolaryngol Head Neck Surg 2002; 127:32-35.
9. Morrison MD, Nichol H, Rammage LA. Diagnostic criteria in functional dysphonia. Laryngoscope 1986; 96:1-8.
10. Koufman JÁ. The otolaryngologic manifestations of gastroesophageal reflux disease (GERD): a clinical investigation of 225 patients using ambulatory 24-hour pH monitoring and an experimental investigation of the role of acid and pepsin in the development of laryngeal injury. Laryngoscope 1991; 101(Suppl 53):1-78.
11. Mesallam TA, Stemple JC, Sobeih TM, Elluru RG. Reflux symptom index versus reflux finding score. Ann Otol Rhinol Laryngol 2007; 116:436-40.
12. Jones R, Coyne K, Wiklund I. The gastroesophageal reflux disease impact scale: a patient management tool for primary care. Aliment Pharmacol Ther 2007: 25:1451-59.
13. Nunes HS, Pinto JA, Zavanela AR, Cavallini AF, Freitas CS, Garcia FE. Comparison between the Reflux Finding Score and the Reflux Symptom Index in the practice of Otorhinolaryngology. Int Arch Otolaryngol 2016; 20:218-21.
14. Gisbert JP, Cooper A, Karagiannis D. Consultation rates and characteristics of gastro-oesophageal reflux disease in primary care: a European observational study. Eur J Gen Pract 2009; 15:154-60.
15. Internal Clinical Guidelines Team (UK). Dyspepsia and Gastro-Oesophageal Reflux Disease: Investigation and Management of Dyspepsia, Symptoms Suggestive of Gastro-Oesophageal Reflux Disease, or Both. London: National Institute for Health and Care Excellence (UK); 2014 Sep.
16. Davies I, Burman-Roy S, Murphy MS; Guideline Development Group. Gastro-oesophageal reflux disease in children: NICE guidance. BMJ 2015; 350:g7703.

LETTER TO THE EDITOR

FROM NEW SCIENTIFIC KNOWLEDGE ON ROSACEA TO ITS POSSIBLE MEDICO-LEGAL CONSEQUENCES

P. VELLANTE[1], M. AURIEMMA[2], P. AMERIO[2], A. CARNEVALE[1] and C. D'OVIDIO[1]

[1]Section of Legal Medicine, Department of Medicine and Aging Sciences, "G. d'Annunzio" University of Chieti–Pescara, Italy; [2]Department of Dermatology, and Centre for Aging Studies (CeSI), University of Chieti–Pescara, Chieti, Italy

Received March 19, 2018 – Accepted May 10, 2018

New scientific knowledge of rosacea hides possible medico-legal consequences. Indeed, the solid molecular basis surrounding rosacea exacerbation and progression has been shown among genetically prone people who are exposed to trigger factors, such as moderately hot temperatures associated with employment. If this is ignored in the phase of prevention, then progression of rosacea might lead to medico-legal consequences.

To the Editor,

Dermatological occupational diseases can reduce quality of life of employees, and sometimes induce them to change their job. As well as common dermatological diseases due to contact with chemical substances, moderately hot temperatures are also known to favour dermatological diseases (i.e., folliculitis, tinea, miliaria, psoriasis, atopic dermatitis). For rosacea, it has also been shown that moderately hot temperatures can elicit specific receptor activation. Hence, there is interest in the study of this triggering, to consider rosacea as an occupational disease and to stop its progression in order to avoid medico-legal consequences.

Tables I and II give the definitions of the old and new classification systems of rosacea, respectively. The new classification system also considers the simultaneous occurrence of more than one rosacea subtype, and the potential progression from one subtype to another (1, 2). One of the diagnostic cutaneous signs or the presence of two or more major features can be considered diagnostic (Table II).

WHAT IS NEW ON ROSACEA?

Rosacea has a complex pathogenesis, as has been reported previously (3,4). For the message of the present study, it can be noted that both innate and adaptive immune activation have been linked to rosacea, with coordinated activities of multiple cell types, including: keratinocytes, macrophages, mast cells, fibroblasts, neutrophils, TH1 and TH17 cells, B cells, and vascular endothelium. These cells produce primary effector molecules, such as cathelicidin antimicrobial peptides, reactive oxygen species, matrix metalloproteinases and cytokines, including interleukin (IL)-1β, tumour necrosis factor, interferon-γ, and IL-17, which drive rosacea inflammation (5).

In terms of possible medico-legal consequences, it has to be highlighted that the release of these various vasoactive peptides from nerve fibres in a sensitive skin, along with the release of some immunoactive molecules, can be elicited by physical stimuli, which

Key words: rosacea, moderately hot temperatures, employment, medico-legal consequences

Mailing address:
Dr Cristian D'Ovidio,
Section of Legal Medicine,
Department of Medicine and Aging Sciences,
"G. d'Annunzio" University of Chieti–Pescara,
Via dei Vestini n. 31, 66100 Chieti (CH), Italy
Tel.: +39 0871 3556724 - Fax: +39 0871 3556779
e-mail: cridov@yahoo.it

0393-974X (2018)
Copyright © by BIOLIFE, s.a.s.
This publication and/or article is for individual use only and may not be further reproduced without written permission from the copyright holder.
Unauthorized reproduction may result in financial and other penalties
DISCLOSURE: ALL AUTHORS REPORT NO CONFLICTS OF INTEREST RELEVANT TO THIS ARTICLE.

include moderately hot temperatures and UVB radiation. This happens through the actions of LL-37, an antimicrobial peptide that is highly expressed in patients with rosacea (6).

Moderately hot temperatures (>43°C) can activate transient receptor potential (TRP) cation channels, including TRP subfamily V member 1, or TRPV1 (also known as the capsaicin receptor and vanilloid receptor 1), and TRP ankyrin receptor 1 (TRPA1), as can ethanol, spicy food, cold, formalin and other chemicals (i.e., the well-established trigger factors for rosacea) (7, 8). For this reason, moderately hot temperatures are now also recognized as a trigger factor for rosacea, and hence they might contribute to its pathogenesis. Indeed, TRPV1-positive nerve fibres have been shown to be highly expressed in samples from rosacea patients compared to control patients, and this activation induces the release of substance P. In addition, increased expression of TRPV1 contributes to the lower threshold for temperature and chemicals observed in rosacea-affected skin (9).

Activation of TRPV1 in rosacea patients is indicated by persistent flushing and more prolonged burning sensations (i.e., a neurogenic inflammation reaction). This can be explained by TRPV dimerisation with TRPV3 (a vanilloid receptor that is overexpressed in fibroblasts and immune cells in rosacea). TRPV3 can be activated by lower temperatures (39°C), although in a slower fashion (2 s) compared to TRPV1 (500 ms). TRPV1 and 3 dimerisation in the same nerve fibres or cells might be responsible for differences in temperature sensitivities among patients with rosacea. These phenomena might have a feedback or loop mechanisms, which makes rosacea a chronic condition (10).

In this scenario, neuropeptides activate mast cells and fibroblasts, where their fibrosing activities have been shown prior to the clinical presentation of

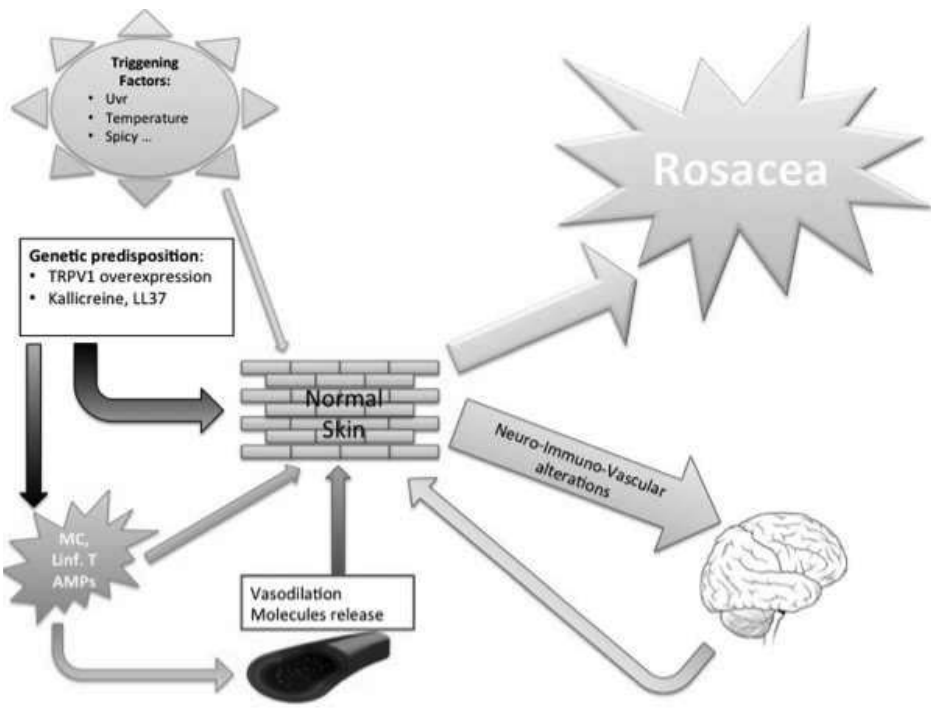

Fig. 1. *Genetic background and different triggers that can elicit sensory nerve responses. TRPV1 is highly expressed in perivascular sensitive nerve endings and can be elicited by different factors, including temperature. In rosacea patients, hyper-expression or hyper-activity of TRPV1 induces chronic neurogenic inflammation. In the downstream cascade, oedema, vasodilation and a burning and stinging sensation are often present. Vasodilation can lead to chronic erythema, and eventually to phyma, through the actions of mast cells and T lymphocytes, especially of the Th17 lineage.*

phyma itself. Mast cells produce not only LL-37, but also metalloproteinases (i.e., MMP2, 9), and they can recruit other immune cells to induce vasodilatation, and to favour remodelling processes in the skin (11).

DISCUSSION

The possibility of the development of phyma in the course of rosacea suggests the need for an early intervention campaign in both medical and employment settings. The therapeutic goal should consist of blockade of the activation of TPRV and the vessels, and thus the neuro-inflammatory cascade. In the hope of new therapeutical strategies and agents, it appears that it is worth promoting prevention through better informed employees and company doctors, noting the importance of assessing skin conditions for employees exposed to moderately hot temperatures (Fig. 1).

Not promoting prevention of an occupational disease can lead to medico-legal consequences. Many employees around the world might be exposed to the risk of this occupational disease, therefore the effects of repetitive exposure to moderately hot temperatures (i.e., 39-42°C) during employment in genetically prone people suggest the need for better evaluation of employees to ensure comfort in the workplace.

However, reality can unfortunately often be distant from what science would suggest. The situation in Italy, in particular, is reported here as an example, in the hope that it will stimulate more debate in the scientific community. Legislation in Italy (D.Lgs. 81/2008) deals only with the exposure

Table I. *Previous classification system for rosacea.*

Aspect	Classification	Details
Rosacea subtypes	I	Erythematotelangiectatic rosacea
	II	Papulopustular rosacea
	III	Phymatous rosacea
	IV	Ocular Rosacea
Rosacea diagnostic criteria	Primary	Flushing (transient erythema)
		Nontransient erythema
		Papules and pustules
		Telangiectases
	Secondary	Burning or stinging
		Plaque
		Dry appearance
		Edema
		Ocular manifestations
		Phymatous changes

Adapted from Two AM, Wu W, Gallo RL, Hata TR. Rosacea: part I. Introduction, categorization, histology, pathogenesis, and risk factors. J Am Acad Dermatol 2015; 72(5):749-58.

to very high temperatures, with reference to the European norm defined by UNI EN ISO 12894:2002 and to the 'Guidelines on Microclimate, Ventilation and Lighting in the Workplace' drafted by the Coordination of Regions and the '*Istituto Superiore per la Prevenzione e la Sicurezza del Lavoro*', and approved by the Conference of Presidents of Regions. Italian legislation, however, stops in 1956 on this subject (D.P.R. 303/1956). Later, D.Lvi. 626/94 and 242/96 only provided some general further indications on this. Thus, according to Italian law, the aim is always to protect employees from very high temperatures.

Furthermore, according to legislation in Italy, social insurance for occupational diseases or injuries (*Istituto Nazionale per l'Assicurazione contro gli Infortuni sul Lavoro e le Malattie Professionali; INAIL*) does not consider 'minor' occupational diseases. Moreover, when the supposed occupational disease is due to many factors, as for rosacea, the employee needs to demonstrate that their workplace specifically includes the casual or con-casual factors that can produce the specific disease. This is not always easy to achieve.

Dermatologists in particular hope that they will be able to act in terms of prevention and reduction of the exposure to the triggering factors for rosacea, as it is a chronic disease that is not easy to manage, and the therapies available at present are only symptomatic, and do not provide any 'cure' for the disease at all. Progression of rosacea in the phymatous phase might also interfere with organ function, therefore it deserves much more aggressive therapies. Overall, as well as dermatologists, ophthalmologists and otorhinolaryngologists can also be involved, with the consideration of surgical therapies.

Examples of employees being exposed to moderately hot temperatures are many, and the wide spread of rosacea in the general population indicates the need to consider this disease more seriously,

Table II. *The new classification system for rosacea.*

Diagnostic features (diagnostic of rosacea by themselves)	**Major features** (two or more can be considered diagnostic)	**Secondary features**
Fixed centrofacial erythema in a characteristic pattern that may periodically intensify	Flushing	Burning sensation
Phymatous changes	Papules and pustules	Stinging sensations
	Teleangectasia	Oedema
	Ocular manifestations: lid margin telangiectasia, interpalpebral conjunctival injection, spade-shaped infiltrates in the cornea, scleritis and sclerokeratitis.	Dryness
		Ocular manifestations: 'honey crust' and collarette accumulation at the base of lashes, irregularity of lid margin, evaporative tear dysfunction (rapid tear breaking time).

This system also considers simultaneous occurrence of more than one rosacea subtype, and potential progression from one subtype to another, as adapted from Gallo et al. (4).

particularly with lack of dedicated legislation. Indeed, once an employee asks a dermatologist to solve or attenuate their rosacea problem, the dermatologist cannot manage this basically genetic disease easily if the employee continues to be exposed on a daily basis to a microclimate that is not fitting to their high skin reactivity.

Thus further research is urgently warranted and should deal with the concept of a test method for the hypothesis here proposed.

REFERENCES

1. Wilkin J, Dahl M, Detmar M, Drake L, Feinstein A, Odom R, Powell F. Standard classification of rosacea: report of the National Rosacea Society expert committee on the classification and staging of rosacea. J Am Acad Dermatol 2002; 46(4):584-87.
2. Tan J, Almeida LM, Bewley A, et al. Updating the diagnosis, classification and assessment of rosacea: recommendations from the global ROSacea COnsensus (ROSCO) panel. Br J Dermatol 2017; 176:431-38.
3. Holmes AD, Steinhoff M. Integrative concepts of rosacea pathophysiology, clinical presentation and new therapeutics. Exp Dermatol 2017; 26:659-67.
4. Gallo RL, Granstein RD, Kang S, Mannis M, Steinhoff M, Tan J, Thiboutot D. Standard classification and pathophysiology of rosacea: the 2017 update by the National Rosacea Society Expert Committee. J Am Acad Dermatol 2018; 78(1):148-55.
5. Holmes AD, Spoendlin J, Chien AL, Baldwin H, Chang ALS. Evidence-based update on rosacea comorbidities and their common physiologic pathways. J Am Acad Dermatol 2018; 78(1):156-66.
6. Salzer S, Kresse S, Hirai Y, Koglin S, Reinholz M, Ruzicka T, Schauber J. Cathelicidin peptide LL-37 increases UVB-triggered inflammasome activation: possible implications for rosacea. J Dermatol Sci 2014; 76(3):173-79.
7. Brito R, Sheth S, Mukherjea D, Rybak LP, Ramkumar V. TRPV1: a potential drug target for treating various diseases. Cells 2014; 3(2):517-45.
8. Steinhoff M, Schauber J, Leyden JJ. New insights into rosacea pathophysiology: a review of recent findings. J Am Acad Dermatol 2013; 69(6 Suppl 1):S15-26.
9. Sulk M, Seeliger S, Aubert J, et al. Distribution and expression of non-neuronal transient receptor potential (TRPV) ion channels in rosacea. J Invest Dermatol 2012; 132(4):1253-62.
10. Steinhoff M, Buddenkotte J, Aubert J, et al. Clinical, cellular, and molecular aspects in the pathophysiology of rosacea. J Investig Dermatol Symp Proc 2011; 15(1):2-11.
11. Muto Y, Wang Z, Vanderberghe M, Two A, Gallo RL, Di Nardo A. Mast cells are key mediators of cathelicidin-initiated skin inflammation in rosacea. J Invest Dermatol 2014; 134(11):2728-36.

JOURNAL OF BIOLOGICAL REGULATORS & HOMEOSTATIC AGENTS Vol. 32, no. 4, 1001-1005 (2018)

LETTER TO THE EDITOR

AN INNOVATIVE PICK-UP IMPRESSION TECHNIQUE

G. DE MARCO*, A. LANZA* and F. DI FRANCESCO

Multidisciplinary Department of Medical, Surgical and Dental Sciences, Campania University Luigi Vanvitelli, Naples, Italy

Rerceived February 27, 2018 – Accepted May 8, 2018

* These Authors contributed equally to this work

Precision of impression is one of the keys for the success of implant-prosthetic rehabilitation. The choice of correct techniques, performance materials, and operator skills, can improve the accuracy of impression. The proposed technique describes a modified pick-up impression technique, both for single and multiple implants, aiming to combine the advantages of direct technique (open-tray or pick-up impression) with those of indirect technique (closed-tray or transfer type impression technique) in order to improve the accuracy of implant impression.

To the Editor,

As far as implant-prosthodontic rehabilitations are concerned, implant impression technique is one of the most delicate phases, determining the precision and accuracy of the future prostheses (1). Nowadays, new impression systems have been developed such as digital impression techniques (2) which represent a clinically acceptable alternative to conventional impression methods (3). Nevertheless, there is a lack of evidence on the accuracy of intraoral scanners compared with conventional techniques, and clinical trial studies are recommended to investigate the accuracy of intraoral scanners (4). The aim of implant impression is to register the three-dimensional positioning of the implant and to transfer the implant position to the working cast (5). Implant impression should be neither distorted nor stretched, and should be deficit-free and bubble-free. In addition, the employed materials should present an almost complete elastic return. These objectives may be achieved if specific conditions have been successfully satisfied, i.e. the implant is osteointegrated and the trans-mucosal route is stable and bleeding-free. Overall, impression techniques in oral implantology can be divided into two types, open tray or closed tray, and metal or plastic impression copings can be adopted(5-7). Metal impression copings are more accurate than plastic copings (6).

The first impression technique corresponds to the direct technique, i.e open tray impression, where the impression coping, prior to unscrewing and decoupling from the fixture, remains inside the material during the displacement of the impression. In order to achieve this, the impression coping must be sufficiently long to connect the screw and to reach the outer side of the tray. After the polymerization of impression material, the impression coping must be unscrewed in order to allow the displacement of the tray. The second impression technique is indirect, i.e closed tray impression, where the transfer coping is not removed with the impression but remains attached to the implant. Once the tray has been removed, the transfer coping is unhooked to be screwed to the lab analog. Whichever technique is

Key words: implant-prosthodontics rehabilitation, impression technique, open tray technique

Mailing address:
Prof. Alessandro Lanza,
Department of Prosthodontics,
Multidisciplinary Department of Medical,
Surgical and Dental Sciences,
Campania University Luigi Vanvitelli
Via Luigi De Crecchio 7, 80138 Naples, Italy
e-mail: alessandro.lanza@unicampania.it

0393-974X (2018)
Copyright © by BIOLIFE, s.a.s.
This publication and/or article is for individual use only and may not be further reproduced without written permission from the copyright holder.
Unauthorized reproduction may result in financial and other penalties
DISCLOSURE: ALL AUTHORS REPORT NO CONFLICTS OF INTEREST RELEVANT TO THIS ARTICLE.

employed, it is important that the implant impression shows a number of requirements:

• The implant impression should provide the three-dimensional positioning of the implant shoulder and the trans-mucous route, in order to design the abutment in relation to the finishing margin, the transition line from the trans-mucosal zone to the above-gingival zone, and to the emergency profile.

• The implant impression should be accurate, free of tearing, bubbles or other types of imperfections, including the occlusal surfaces of the other teeth in the arch, in order to allow proper jointing and occlusion of definitive restoration.

Furthermore, there are different types of impression materials, each with its own advantages and disadvantages (9). The most commonly used impression materials are polyether (PE) and vinyl polysiloxane (VPS). The choice of material must be conducted on the basis of an assessment of its physical, mechanical, biological and economic characteristics. In addition, the mixing mode of the material is crucial for the precision of the impression. Di Felice et al. reported that mechanically mixed impression materials show better performances compared to those of manually mixed impression materials (9).

This article describes a modified direct technique, single-phase and mono-component, employing polyether material, aiming to combine the advantages of the open tray technique with those of the closed tray technique.

MATERIALS AND METHODS

An individual acrylic-resin tray is necessary to allow the impression materials be a thin uniform layer. Before taking implant impression, the healing abutment is removed from the implant employing a hexagonal screwdriver and the specific impression coping is placed (Fig. 1A). At this point, an intraoral radiography through parallel technique is recommended in order to verify the correct coupling between the impression coping and the implant head (Fig. 1B). This method is defined as the parallelism between the plane of the film and object to be studied while the central axis of the X-ray is perpendicular to both planes. If these parameters are not respected, the image may result distorted and the thread of the implant may appear unspecified. Furthermore, intraoral radiography may also be used as a basis for monitoring the health of the implant in the long-term follow-up. It is important to verify in occlusal vision that the individual tray does not interfere with the mesio-distal and the bucco-lingual pick-up profile (Fig. 2A). Furthermore, the impression coping should be at least 1 mm higher than the tray in the apico-coronal axis (Fig. 2B). If the relationship between the impression coping and the individual tray should not correspond to those above-mentioned, the individual window should be increased in size. The window on the tray is then closed with tenasyle pink wax (Fig. 2C) which is a rigid and thermoplastic wax. At this point, a heated spatula should be used in order to shape the wax on the window of the tray in order to close it carefully. The central part of the wax is pushed towards the inside of the tray, in order to produce a depression on the wax (Fig. 2C). This recommendation helps the contact between the impression coping and the impression material, during impression taking. Next, a specific adhesive is applied on the inside of the tray, in order to create an adhesion between the impression material and the tray during impression taking. Moreover, while the tray is filled with the mechanically mixed material, a dedicated syringe is filled with the same impression material. Before placing the tray in the mouth, the impression material is injected around the pickup and adjacent teeth, both mesial and distal, in order to increase the precision of impression (Fig. 3A). During the leakage of the material, the tip of the syringe is constantly inside the material to reduce the formation of air bubbles. Consequently, the tray is placed in the mouth, pushed to the end of the occlusal surfaces of adjacent teeth, proving that the head of the transfer coping intercepts the wax of the tray (Fig. 3B). Waiting for the polymerization of the material, excesses of the wax are removed, allowing a proper connection between the hand screw and the transfer coping (Fig. 3C). Consequently, the impression coping can be unscrewed from the fixture, allowing the removal of the tray. Therefore, the quality of the impression can be evaluated (Fig. 4). Finally, the healing abutment is connected to fixture in order to support the stable trans-mucous route. In case of multiple implants placement, the proposed protocol remains also valid (Fig. 5 A, B).

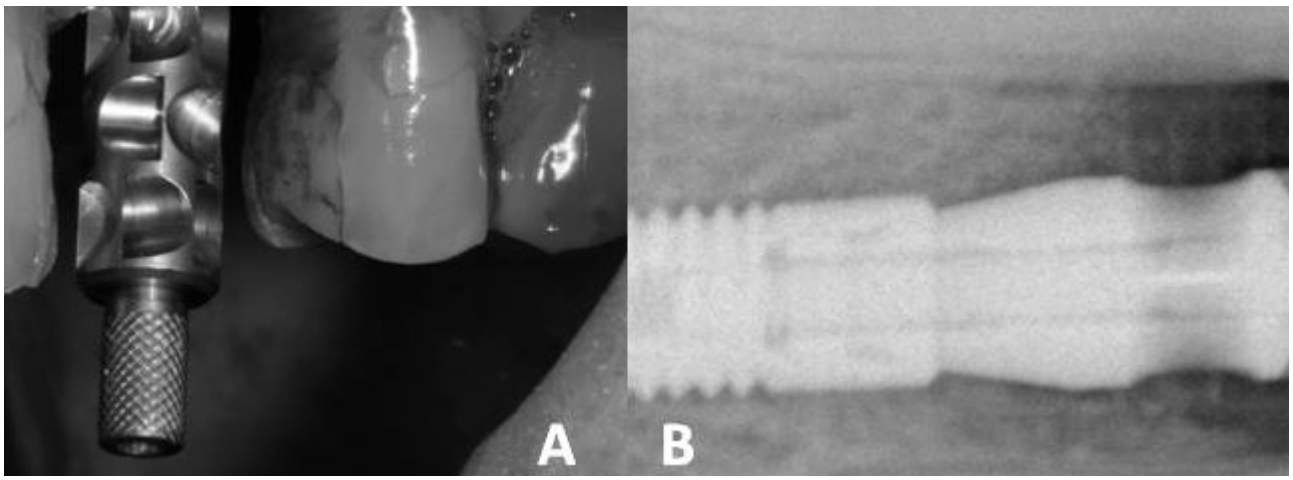

Fig. 1. ***A)*** *The specific impression coping is screwed to the implant.* ***B)*** *An intraoral radiography is employed in order to verify the correct coupling between the impression coping and the implant head.*

Fig. 2. ***A)*** *The impression coping does not interfere with the mesio-distal and the bucco-lingual pick-up profile.* ***B)*** *The impression coping is at least 1 mm higher than the tray in the apico-coronal axis.* ***C)*** *The window on the tray is closed with pink wax.*

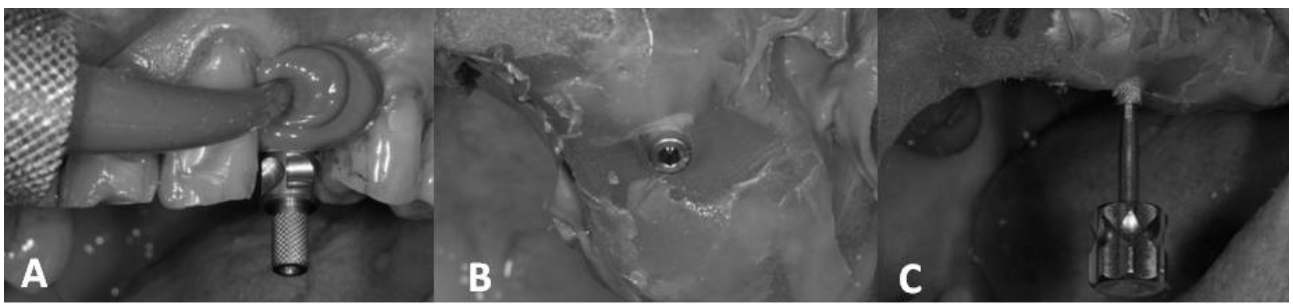

Fig. 3. ***A)*** *The material is injected around the pickup and adjacent teeth.* ***B)*** *The head of the impression coping intercepts the wax of the tray.* ***C)*** *Connection between the hand screw and the impression coping.*

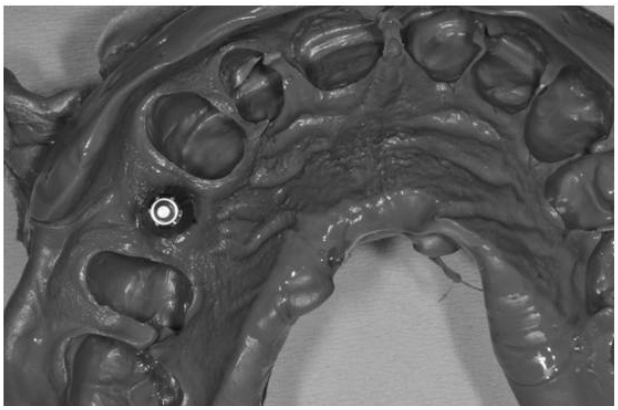

Fig. 4. *Evaluation of the impression quality.*

DISCUSSION

In implant dentistry, accuracy during the impression procedure is a crucial step in order to achieve long-term success of the implant prosthesis (5-8). The accuracy of the impression is affected by factors such as the impression material, implant position, angulation and depth (7, 8, 10, 12). Despite the presence of other studies investigating the accuracy of impression techniques, no consensus has been reached among them, and the different works present heterogeneous outcomes (5, 11, 12). Two recent systematic reviews have shown greater precision in the open tray technique compared to closed tray technique (1, 5). In particular, one of them, analyzing 32 articles between 2009 and 2013, showed that the most consistent and accurate impressions were obtained with the direct technique, followed by the indirect technique (5). In the direct technique, unscrewing the transfer coping decreases the deformation of the impression material and favors its elastic return. In the indirect technique, the tearing that occurs when the tray is removed may increase the deformation of the impression material. Furthermore, the repositioning of the transfer coping inside impression material may be difficult to manage. However, the closed tray allows a greater and more uniform push of the material reaching the transfer coping, thus obtaining greater precision. In the light of these considerations, careful placing of the pink thermoplastic wax on the window of the open tray can increase the uniformity of the material around the transfer coping. The aim of the wax is to give the right thrust to the material in a very delicate area of the tray. The thermoplastic characteristic of the wax allows both its correct adaptability to the window of the tray and an optimal support to the impression material. It is important that the head of the impression coping is visible through the wax in order to unscrew the connecting screw of the impression coping. If the screw is not visible, once the impression material is polymerized, the impression coping could be complicated to unscrew, increasing the probability of cutting the impression material. An unsuccessful procedure may lead to the repetition of the impression taking.

In conclusion, the proposed technique describes an innovative pick-up impression technique which can be employed for single and multiple implants. The aim of this technique is to combine the advantages of

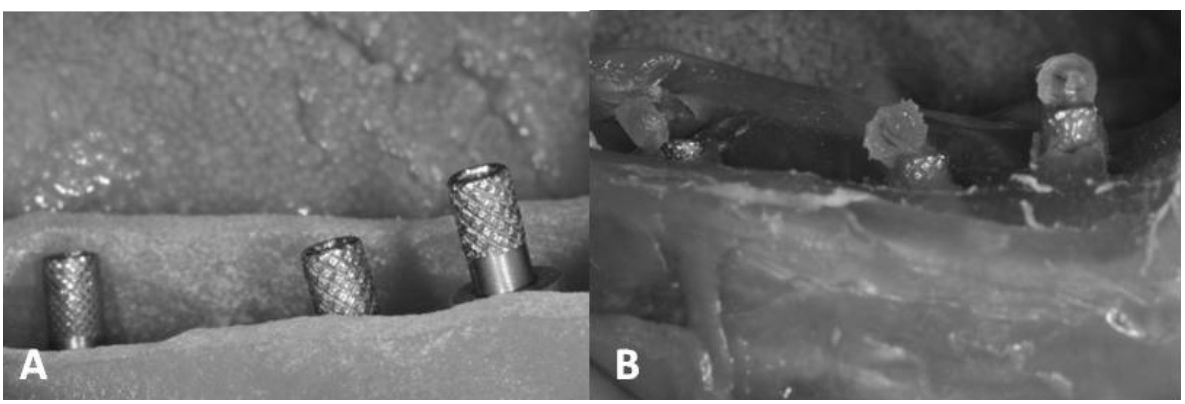

Fig. 5. ***A)*** *In the case of multiple implants, all transfer coping are at least 1 mm higher than the tray in the apico-coronal axis.* ***B)*** *The heads of all transfer coping intercept the wax of the tray.*

the direct and the indirect techniques. Modifying an individual open tray, temporarily, into a closed tray can increase the uniformity of the material reaching the transfer coping. This suggestion, together with techniques and materials already accredited in literature, can further improve the accuracy of the implant impression, and the precision of the final implant-prosthodontic rehabilitation.

REFERENCES

1. Kim JH, Kim KR, Kim S. Critical appraisal of implant impression accuracies: A systematic review. J Prosthet Dent 2015; 114:185-92.
2. Marghalani A, Weber HP, Finkelman M, Kudara Y, El Rafie K, Papaspyridakos P. Digital versus conventional implant impressions for partially edentulous arches: An evaluation of accuracy. J Prosthet Dent 2018; 119:574-57.
3. Ahlholm P, Sipilä K, Vallittu P, Jakonen M, Kotiranta U. Digital versus conventional impressions in fixed prosthodontics: a review. J Prosthodont 2018; 27:35-41.
4. Alikhasi M, Alsharbaty MHM, Moharrami M. Digital implant impression technique accuracy: a systematic review. Implant Dent 2017; 26:929-35.
5. Moreira AHJ , Rodrigues NF, Pinho ACM, Fonseca JC, Vilaça JL. Accuracy comparison of implant impression techniques: a systematic review. Clin Implant Dent Relat Res 2015; 17:e751-e764.
6. Fernandez MA, Paez de Mendoza CY, Platt JA, Levon JA, Hovijitra ST, Nimmo A. A comparative study of the accuracy between plastic and metal impression transfer copings for implant restorations. J Prosthodontics 2013; 22:367-76.
7. Bramanti E, Cervino G, Lauritano F, et al. FEM and Von Mises analysis on prosthetic crowns structural elements: evaluation of different applied materials. Sci World J 2017; 2017:1029574
8. Cicciù M, Cervino G, Bramanti E, et al. FEM Analysis of mandibular prosthetic overdenture supported by dental implants: evaluation of different retention methods. Comput Math Methods Med 2015; 2015:943839.
9. Di Felice R, Scotti R, Belser UC. The influence of the mixing technique on the content of voids in two polyether impression materials. Schweiz Monatsschr Zahnmed 2002; 112:12-6.
10. Rashidan N, Alikhasi M, Samadizadeh S, Beyabanaki E, Kharazifard MJ. Accuracy of implant impressions with different impression coping types and shapes. Clin Implant Dent Relat Res 2012; 14:218-25.
11. Hoods-Moonsammy VJ, Owen P, Howes DG. A comparison of the accuracy of polyether, polyvinyl siloxane, and plaster impressions for long-span implant-supported prostheses. Int J Prosthodont 2014; 27:433-38.
12. Gökçen-Rohlig B, Ongül D, Sancakli E, Sermet B. Comparative evaluation of the effects of implant position, impression material, and tray type on implant impression accuracy. Implant Dent 2014; 23:283-88.

JOURNAL OF BIOLOGICAL REGULATORS & HOMEOSTATIC AGENTS Vol. 32, no. 4, 1007-1013 (2018)

LETTER TO THE EDITOR

PLASMA FATTY ACID PROFILE AS BIOMARKER OF CORONARY ARTERY DISEASE: A PILOT STUDY USING FOURTH GENERATION ARTIFICIAL NEURAL NETWORKS

E. DOZIO[1*], E. VIANELLO[1*], E. GROSSI[2], L. MENICANTI[3], G. SCHMITZ[4] and M.M. CORSI ROMANELLI[1,5]

[1]Department of Biomedical Sciences for Health, Università degli Studi di Milano, Milan, Italy; [2]Villa Santa Maria Institute, Tavernerio, Como, Italy; [3]Department of Cardiac Surgery, I.R.C.C.S. Policlinico San Donato, San Donato Milanese, Milan, Italy; [4]Institute for Clinical Chemistry and Laboratory Medicine, University of Regensburg, Regensburg, Germany; [5]Service of Laboratory Medicine 1-Clinical Pathology, I.R.C.C.S. Policlinico San Donato, San Donato Milanese, Milan, Italy

Received March 8, 2018 – Accepted April 27, 2018

[*]These authors contributed equally to this work

Many studies, focused on identifying new biomarkers for coronary artery disease (CAD) risk computation and monitoring, suggested a potential diagnostic role for fatty acids (FA). In the present study, we explored the potential diagnostic role of FA by using a data mining approach based on fourth generation artificial neural networks (ANN). Forty-one male subjects were enrolled. According to coronary angiography, 31 displayed CAD and 10 did not (non-CAD, control group). FA analysis was performed on plasma samples using a gas chromatography-mass spectrometry system and analyses were performed by an ANN method. The variables most closely related to CAD were low levels of alpha-linolenic acid, eicosapentaenoic acid, eicosatetraenoic and docosahexaenoic acids. High levels of 1,1-dimethoxyhexadecane, total dimethyl acetals and docosatetraenoic acid were related to non-CAD condition. This subset of variables, which were most closely correlated to the target diagnosis, achieved a consistent predictive rate. The average accuracy obtained was 76.5%, with 93% of sensitivity and 60% of specificity. The area under the ROC curve was equal to 0.79. In conclusion, our study highlighted the association between different plasma FA species, CAD and non-CAD conditions. The specific subset of variables could be of interest as a new diagnostic tool for CAD management.

To the Editor,

Coronary artery disease (CAD) is the most common form of cardiovascular diseases (CVD). Over many years, atherosclerotic plaques may build up on coronary artery walls, but their existence may remain undiagnosed until the onset of specific symptoms that occur when the blood flow supplying the heart is severely reduced or completely cut off. Dyslipidemia, diabetes mellitus, hypertension and smoking are the main markers used in clinical practice for CAD risk computation and monitoring. However, they seem insufficient to describe all cases of CAD because a great percentage of events may occur also in people with a low risk profile (1). New tools are thus necessary to improve CAD risk discrimination and classification.

Many studies suggested a potential diagnostic role for fatty acids (FA), mainly due to their ability to induce atherosclerosis by promoting endothelial dysfunction, oxidative stress and inflammation

Mailing address:
Elena Dozio, PhD
Department of Biomedical Sciences for Health,
Università degli Studi di Milano,
Via Mangiagalli 31, 20133, Milan, Italy
Tel.: +39 02 50315342 - Fax: +39 02 50315338
e-mail: elena.dozio@unimi.it

0393-974X (2018)
Copyright © by BIOLIFE, s.a.s.
This publication and/or article is for individual use only and may not be further reproduced without written permission from the copyright holder.
Unauthorized reproduction may result in financial and other penalties
DISCLOSURE: ALL AUTHORS REPORT NO CONFLICTS OF INTEREST RELEVANT TO THIS ARTICLE.

(2). Indeed, FA levels well correlate with the Gensini score in CAD (3). Previous studies tried to describe how the FA profile may change in different pathological conditions and which species could be considered as disease biomarkers. However, in the field of CAD results seem far from being conclusive (4, 5). Indeed, all these studies have been performed using a traditional statistical (TS) approach to explore potential relationships between FA and CAD.

In the present study we focused on the potential diagnostic role of FA by using a data mining approach based on fourth generation artificial neural networks (ANN) to unravel the connections between circulating FA species and CAD. Our final aim is to create a connection map which could offer a more integrated and accessible way for CAD diagnosis and monitoring.

MATERIALS AND METHODS

Patients

Eighty male subjects referring to the I.R.C.C.S Policlinico San Donato hospital and undergoing coronary angiography and routine biochemical assays were enrolled (6, 7). Subjects aged <18 and >70 years, with recent myocardial infarction, malignant disease, major abdominal surgery, renal, liver and endocrine diseases, diabetes, more than 3% variation in body weight in the previous 3 months, incomplete clinical history and missing written informed consent were excluded. The final group included 41 subjects, of whom 31 displayed CAD and 10 did not (non-CAD). All patients gave written informed consent to participate in the study. The examination protocol, conducted in accordance with the Declaration of Helsinki was approved by the local Ethics Committee (ASL Milano Due, n. 2516).

FA analysis

Acetyl-chloride and methanol were used to generate fatty acid methyl esters which were further extracted with hexane. A BPX70 column from SGE (10 m length, 0.10 mm diameter, 0.20 μm film thickness) was used to separate FA methyl esters with helium as a carrier gas. The Shimadzu 2010 GC-MS system was used to perform the analyses. The initial oven temperature was 50°C which was programmed to increase with 40°C/min to 155°C, with 6°C/min to 210°C, to finally reach with 15°C/min to 250°C. The different species and their cis/trans isomers were characterized in the scan mode. The specific fragments of saturated and unsaturated FA (saturated: m/z 74; monounsaturated: m/z 55; diunsaturated: m/z 67; polyunsaturated: m/z 79) were quantified in the single-ion monitoring mode. As an internal standard, non-naturally occurring C13:0 was used. The fatty acid quantitative composition is expressed as concentration and percentage of total FA .

Basic statistics

Quantitative variables are expressed as mean with standard deviation (SD) or median and interquartile range. Qualitative variables are summarized as numbers and percentages. The normality of data distribution was assessed by the Kolmogorov-Smirnoff test. Groups were compared using *t*-test (normal variables) or Mann Whitney U-test (non-normal variables). Fisher exact test was used to compare the categorical variables. Analyses were performed with GraphPad Prism 5.0 (GraphPad Software, San Diego, CA, USA). A p value < 0.05 was considered significant.

Artificial neural networks

Auto-contractive map. The Auto Contractive Map (AutoCM)-system (8) finds, by a specific learning algorithm, a square matrix of "similarities" among the variables. Once the AutoCM weight matrix is obtained, it is then filtered by a Minimum Spanning Tree algorithm (MST). MST shows, among the huge number of possible ways to connect the variables, the shortest possible combination with assumption that all biological systems tend naturally to the minimal energetic states. The ultimate goal is to discover hidden trends and associations among variables with an algorithm able to create a semantic connectivity map in which non-linear associations are preserved. Map of the relevant connections and the principal hubs of the system (variables with the maximum amount of connections) are shown. The AutoCM-systems do not have initial weights posed at random. They start always from the same value. Therefore the resulting graph is perfectly reproducible along many possible runs. In simple words AutoCM 'spatialises' the correlation among different variables ('closeness'), converts it

into a compelling graph that identifies only the relevant associations and organizes them into a coherent picture, building a complex global picture of the whole pattern of variation. We transformed the 29 continuous input variables into 58 input variables constructing for each two classes: high (H) and low (L). To do this, we used a particular complement transformation by scaling original variables values from 0 to 1 and creating a complement variable by subtracting the scaled value from 1 (9). In this way, the system was allowed to project and point out the fuzzy position of each variable according to its low values.

Supervised neural networks. To assess the predictive value of the subset of variables correlated to the target diagnosis, we assembled a data set with six variables as input and two variables, CAD and non-CAD, as output. Supervised ANN with four hidden units equipped with back-propagation algorithm were trained and tested on this data set split into two random subsets. Classical training-testing protocol was applied with two experiments. During the training phase, a back propagation ANN model with four hidden units is submitted to the training sub-set containing 15 records of the CAD class and 5 records of the non-CAD class in order to learn the linear and non-linear relations existing between all the variables and between the input variables and the target variables. In this way, a classification task, *i.e.* the correct recognition of patients with and without CAD, was performed. At the end of the training phase, the ANN models showing the best performance on the classification task were submitted to the second sub-sample of patients (the testing set), made up of 16 records of CAD class and 5 records of non-CAD class not previously exposed to the networks, in order to ensure an unbiased evaluation of the classification capability of the ANN. During the so-called "testing phase", the target variable (presence/absence of CAD) was excluded and the network made its own evaluation based on the previously carried out training. In the cross validation protocol, the pairs of sub-sets are inverted during the elaboration procedure: each sub-set is used once for training and once for testing to obtain a non-polarized classification tool. Predictive results were expressed with sensitivity, specificity and accuracy rates. The receiver-operating characteristic (ROC) curve was calculated.

RESULTS

Clinical parameters

Table I shows demographic, anthropometric and biochemical characteristics of patients included in the study. In CAD, waist circumference, waist-to-hip ratio (WHR) and ALT levels were statistically higher, whereas total and LDL cholesterol were lower than non-CAD. The two groups did not differ in any other evaluated parameter. The percentages of CAD patients under aspirin, statin and antihypertensive therapies were also higher than non-CAD.

FA profile according to basic statistical methods

Circulating FA, expressed both as concentration (mM) and percentage, were compared between CAD and non-CAD. Total FA levels were the same in the two groups. Diunsaturated FA (DI-UNSAT), linoleic acid (18:2) and arachidonic acid (20:4) concentrations were lower in CAD than non-CAD ($p<0.05$) (Table II). When FA are expressed as percentages, CAD patients displayed lower DI-UNSAT ($p=0.028$) and higher monounsaturated fatty acids (MUFA) ($p=0.041$) compared to non-CAD (Table II). Oleic acid (18:1) and linoleic acid (18:2) were respectively higher ($p=0.003$) and lower ($p=0.028$) in CAD than non-CAD (Table II). The activities of Stearyl-CoA, Δ6 and Δ5 desaturases, estimated as product-precursor ratio of individual fatty acids in plasma (16:1/16:0 for Stearyl-CoA desaturase; 18:3 n-6/18:2 n-6 for Δ6 desaturase; 20:4 n-6/20:3 n-6 for Δ5 desaturase) were the same in the two groups ($p>0.05$).

Semantic connectivity map

Fig. 1 shows the structure of the semantic connectivity map obtained with the Auto-CM system. CAD and non-CAD conditions are included in two different and well separated areas of the map, with CAD belonging to the lower part together with the low variables and non-CAD to the upper part together with the high variables. The variables most closely related to the presence of CAD are low levels of alpha-linolenic acid, eicosapentaenoic acid, eicosatetraenoic, and docosahexaenoic acid. High levels of 1,1-dimethoxyhexadecane, total dimethyl

Table I. *Demographic, anthropometric and biochemical characteristics of patients included in the study.*

	CAD (n=31)	non-CAD (n=10)	*p*
Age (years)	64.84 ± 8.53	63.20 ± 11.73	0.633
BMI (kg/m^2)	27.60 ± 2.82	27.41 ± 3.88	0.869
Waist (cm)	104 (102-108)	100 (92.25-104.50)	**0.034**
Hip (cm)	103 (100-106)	105 (102-106)	0.344
WHR	1.02 (1.02-1.05)	0.95 (0.88-0.99)	**0.0003**
Fasting glucose (mg/dL)	85.00 (77.00-106.00)	89.00 (79.75-98.25)	0.585
Fasting insulin (mU/mL)	9.03 ± 5.64	7.87 ± 3.91	0.543
Total cholesterol (mg/dL)	136.50 (123.30-171.50)	184.00 (159.30-250.50)	**0.023**
HDL cholesterol (mg/dL)	36.50 (29.75-42.00)	44.50 (32.25-47.75)	0.123
LDL cholesterol (mg/dL)	86.07 ±35.47	125.90 ± 40.40	**0.030**
Triglycerides (mg/dL)	88.4 ± 32.9	119.7 ± 64.5	0.985
HOMA-IR	2.16 ± 1.85	1.80 ± 1.02	0.509
CRP (mg/dL)	0.2 (0.1-0.5)	0.3 (0.1-0.4)	0.816
SBP (mmHg)	120 (120-120)	120 (120-130)	0.348
DBP (mmHg)	70 (70-70)	70 (70-70)	0.177
ALT (U/L)	33.00 (19-52)	18.00 (11.75-21.75)	**0.0052**
AST (U/L)	24.00 (18.00-32.00)	20.00 (11.75-23.25)	0.140
Aspirin (n, %)	28 (90.32%)	3 (30.00%)	**0.0005**
ACEI/ARB (n, %)	20 (64.52%)	2 (20.00%)	**0.027**
β-Blockers (n, %)	22 (70.97%)	0 (0.00%)	**<0.0001**
Calcium channel blockers (n, %)	12 (38.71%)	1 (10.00%)	0.237
Statins (n, %)	26 (83.87%)	3 (30.00%)	**0.016**

Data are expressed as mean ± SD, median (25th-75th percentiles) or number and proportions. ACEI: angiotensinogen-converting enzyme inhibitor; ALT: alanine aminotransferase; ARB: angiotensin receptor blockade; AST: aspartate aminotransferase; BMI: body mass index; CAD: coronary artery disease; CRP: C reactive protein; DBP: diastolic blood pressure; WHR: waist to hip ratio; HOMA-IR: homeostatic model assessment of insulin resistance; SBP: systolic blood pressure. Comparison between groups was performed by t-test or Mann Whitney U-test or Fisher exact test. p values < 0.05 are indicated in bold.

acetals and docosatetraenoic acid are related to the condition of non-CAD, instead.

Prediction of diagnostic class on the basis of variables most closely related

Table III shows the results obtained in the two experiments carried out with supervised ANNs to assess the predictive value of the subset of variables most closely correlated to target diagnosis. The average accuracy obtained in the two independent experiments was 76.5% with 93% of sensitivity and 60% of specificity. The area under the ROC curve was equal to 0.79.

DISCUSSION

The present study highlighted the existence of a specific plasma FA profile related both to the presence and the absence of CAD potentially useful as a new diagnostic tool for CAD management. The novelty

Table II. *Fatty acid species measured in plasma of CAD and non-CAD patients.*

	CAD (n=31)		non-CAD (n=10)		p^a	p^b
	mM	%	mM	%		
Total	6.14 (5.05-7.40)		6.83 (6.06-9.06)		0.14	
SAT	1.90 (1.70-2.40)	32.20 (31.10-33.30)	2.15 (2.00-2.78)	31.40 (30.18-33.40)	0.17	0.63
FA12:0 (Lauric acid)	0.01 (0.006-0.01)	0.14 (0.11-0.16)	0.01 (0.007-0.012)	0.14 (0.10-0.16)	0.65	0.89
FA14:0 (Myristic acid)	0.06 (0.04-0.08)	0.95 (0.86-1.12)	0.05 (0.04-0.09)	0.75 (0.64-1.20)	0.72	0.28
FA15:0 (Pentadecylic acid)	0.01 (0.01-0.02)	0.24 (0.20-0.30)	0.02 (0.01-0.02)	0.20 (0.19-0.27)	0.41	0.51
FA16:0 (Palmitic acid)	1.49 (1.28-1.87)	24.88 (23.54-25.87)	1.70 (1.50-2.17)	24.12 (23.51-25.76)	0.18	0.88
FA17:0 (Margaric acid)	0.02 (0.01-0.02)	0.26 (0.23-0.27)	0.02 (0.02-0.02)	0.21 (0.18-0.27)	0.91	0.30
FA18:0 (Stearic acid)	0.34 (0.30-0.42)	5.49 (5.28-6.16)	0.39 (0.34-0.51)	5.64 (4.96-5.80)	0.23	0.95
MUFA	2.00 (1.60-2.90)	32.70 (28.90-35.40)	1.95 (1.80-2.63)	28.80 (28.08-30.68)	0.81	**0.04**
FA16:1-c9 (n-7) (Palmitoleic acid)	0.16 (0.11-0.21)	2.58 (2.00-3.30)	0.16 (0.12-0.29)	2.57 (1.96-3.51)	0.72	0.69
FA18:1-c9 (n-9) (Oleic acid)	1.80 (1.34-2.51)	28.79 (25.09-30.87)	1.73 (1.57-2.28)	25.03 (24.02-26.77)	0.96	**0.003**
FA18:1-c11 (n-7) (Vaccenic acid)	0.09 (0.08-0.11)	1.59 (1.32-1.76)	0.10 (0.09-0.15)	1.48 (1.31-1.93)	0.36	0.98
FA20:1-c11 (n-9) (Gondoic acid)	0 (0-0.01)	0 (0-0.17)	0 (0-0.10)	0 (0-0.12)	0.66	0.31
DI-UNSAT	1.20 (1.10-1.60)	21.10 (18.30-22.60)	1.75 (1.38-2.25)	24.700(19.30-27.03)	**0.03**	**0.03**
FA18:2-c9,c12 (n-6) (Linoleic acid)	1.20 (1.10-1.62)	21.13 (19.28-22.57)	1.76 (1.35-2.24)	24.69 (19.35-37.04)	**0.03**	**0.03**
POLI-UNSAT (>2)	0.90 (0.70-1.00)	13.50 (12.10-15.10)	1.00 (0.98-1.35)	13.90 (13.08-16.35)	**0.03**	0.43
FA18:3-c6,c9,c12 (n-6) (γ-Linolenic acid)	0.02 (0.01-0.03)	0.29 (0.25-0.42)	0.02 (0.02-0.03)	0.31 (0.26-0.41)	0.86	0.93
FA18:3-c9,c12,c15 (n-3) (α-Linolenic acid)	0.01 (0.01-0.02)	0.22 (0.18-0.26)	0.02 (0.01-0.02)	0.18 (0.16-0.27)	0.80	0.56
FA20:3-c8,c11,c14 (n-6) (Dihomo-γ-linolenic acid)	0.08 (0.06-0.11)	1.33 (1.01-1.49)	0.09 (0.00-0.12)	1.25 (1.03-1.44)	0.76	0.57
FA20:4-c5,c8,c11,c14 (n-6) (Arachidonic acid)	0.58 (0.49-0.70)	9.25 (8.22-10.95)	0.73 (0.65-0.96)	10.01 (8.65-11.50)	**0.03**	0.26
FA20:4-c8,c11,c14,c17 (n-3) (Eicosatetraenoic acid)	0.00	0.00	0 (0-0.10*10-2)	0 (0-6,57*10^{-5})	1.00	0,98
FA20:5-c5,c8,c11,c14,c17 (n-3) (Eicosapentaenoic acid)	0.02 (0.01-0.03)	0.27 (0.20-0.31)	0.02 (0.01-0.04)	0.23 (0.15-0.38)	0.94	0.48
FA22:4-7c,10c,13c,16c (n-6) (Docosatetraenoic acid)	0.01 (0.01-0.02)	0.18 (0.15-0.21)	0.01 (0.01-0.02)	0.18 (0.13-0.22)	0.58	0.48
FA22:5-7c,10c,13c,16c,19c (n-3) (Docosapentaenoic acid)	0.01 (0.01-0.02)	0.22 (0.21-0.27)	0.02 (0.02-0.03)	0.25 (0.22-0.27)	0.11	0.36
FA22:6-c4,c7,c10,c13,c16,c19 (n-3) (Docosahexaenoic acid)	0.10 (0.09-0.12)	1.56 (1.25-1.75)	0.10 (0.08-0.18)	1.37 (1.23-1.74)	0.57	0.48
DM	0.06 (0.05-0.07)	0.90 (0.70-1.10)	0.06 (0.04-0.07)	0.70 (0.60-0.90)	0.21	0.98
DM16:0 (1,1-Dimethoxyhexadecane)	0.04 (0.03-0.05)	0.62 (0.46-0.69)	0.05(0.04-0.05)	0.62 (0.44-0.79)	0.11	0.84
DM18:0 (1,1-Dimethoxyoctadecane)	0.02 (0.01-0.02)	0.26 (0.22-0.35)	0.02 (0.02-0.02)	0.23 (0.21-0.35)	0.46	0.67
DM16:1 ((9Z)-1,1-Dimethoxy-9-Hexadecene)	0.003 (0.002-0.003)	0.04 (0.03-0.05)	0.003 (0.002-0.004)	0.03 (0.03-0.05)	0.99	0.48

DM: dimethylacetals; DIUNSAT: di-unsaturated fatty acids; FA: fatty acids; MUFA: mono-unsaturated fatty acids; POLI-UNSAT: unsaturated fatty acids with > 2 double bonds; SAT: saturated fatty acids. Concentration of individual species/families and percentages relative to total FA amount are indicated. Data are expressed as median (25th-75th percentiles). Comparison between groups was performed by t-test or Mann Whitney U-test. Significant p values are in bold letters.

p^a: for data expressed as concentration (mM); p^b: for data expressed as percentage (%).

of this study mainly lies in applying a data mining approach based on fourth generation ANN to identify associations of FA species with CAD and non-CAD conditions. This analytical approach offers the possibility to discover hidden trends and associations among variables by describing, also on few samples, non linear associations that are usually not explained by TS methods (10). Besides the application of the ANN system, FA profile in CAD and non-CAD was studied also with a TS approach. By comparing results obtained with the two methods, it can be observed that variables identified by the ANN as discriminators of CAD and non-CAD conditions were not the same identified by the TS. Of course, this does not mean that these latter are not related to CAD, as described in previous studies (5, 11), but considering the complexity of the pathology and the existence of non linear relationships between variables, it seems that variables identified by TS are not useful markers for discriminating CAD from non-CAD condition.

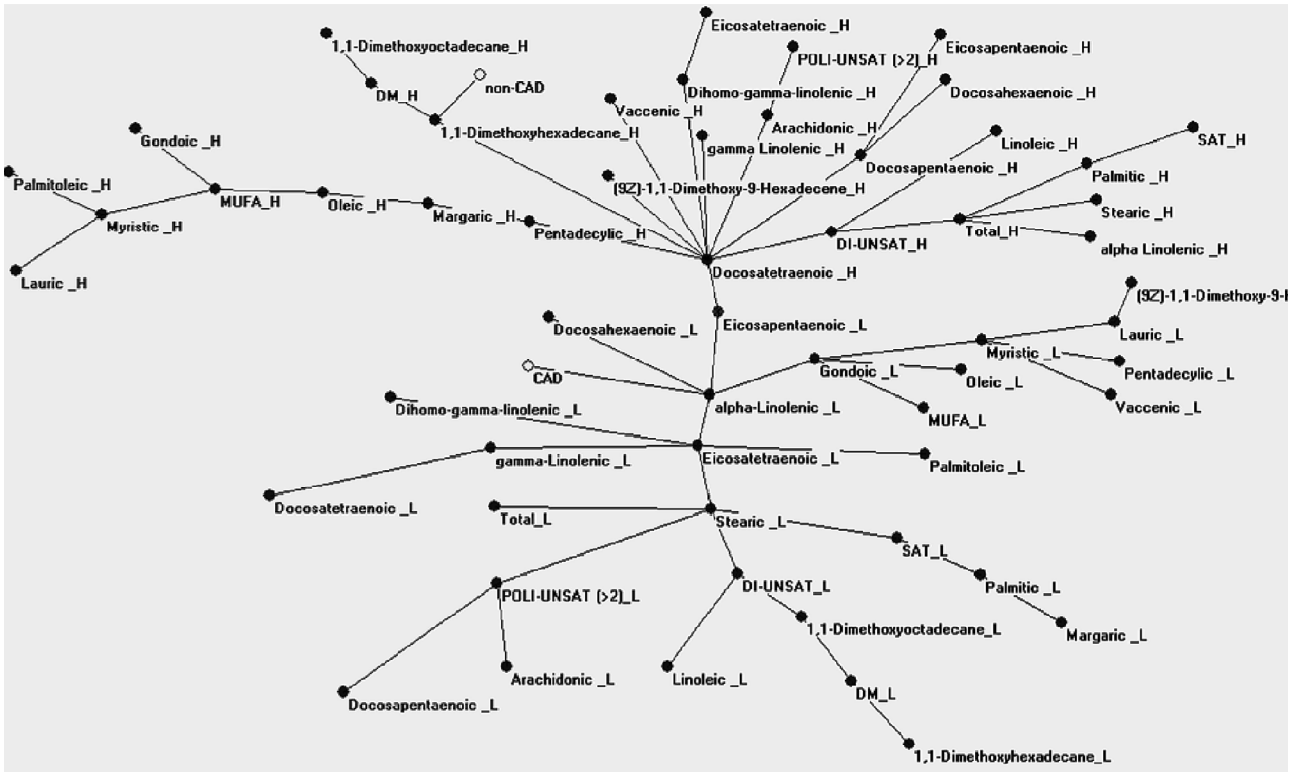

Fig. 1. *Semantic connectivity map. CAD and non-CAD conditions are included in two different and well separated areas of the map, with CAD belonging to the lower part together with the low variables and non-CAD to the upper part together with the high variables. The variables closely related to CAD are low levels of alpha-linolenic acid, eicosapentaenoic acid, eicosatetraenoic, docosahexaenoic acid. High levels of 1,1-dimethoxyhexadecane, total dimethyl acetals and docosatetraenoic acid are related to non-CAD.*

Table III. *Prediction of diagnostic class on the basis of variables most related to CAD and non-CAD.*

ANN	Records in testings	CAD	non-CAD	Sensitivity (%)	Specificity (%)	Overall accuracy (%)
FF_Bp 4 ab	20	15	5	93.33	80	86.67
FF_Bp 4 ba	21	16	5	93.00	40	66.5
Mean				**93.16**	**60**	**76.5**

ab: training on subset a and testing on subset b; ANN: artificial neural network; ba: training on subset b and testing on subset a; FF_Bp: feed-forward back-propagation architecture.

Considering both the role and the levels (H or L) of all the evaluated species, we may confirm that the map generated by the ANN approach well discriminated CAD from non-CAD. One might expect to find a perfect symmetry around CAD and non-CAD, that means that the species related to the two conditions are the same but at different levels. Differently, species related to non-CAD were not the counterpart at high levels of variables connected to CAD. They are different species with a known protective role and, not by chance, herein present at high level. This reinforces the idea of the complexity of our biological system and the need of approaches able to integrate and elaborate at the same time multiple information.

Using the ANN tool we had also the possibility to test the ability of the selected variables to discriminate between CAD and non-CAD. Although we achieved a consistent predictive rate with an area under the ROC curve equal to 0.79, the ability of these markers to really identify CAD and predict its development needs to be further tested by large-scale and longitudinal studies. Some of the drugs used in CAD patients, mainly aspirin and statins, might modify FA levels but it is not really clear whether they may modify also FA composition. Although our data seems to exclude this – *i.e*. we did not observe any change in the activity of desaturases as potential targets of statin therapy (12) – future studies will help us to clarify also this issue.

In conclusion, our study highlighted the association between different plasma FA species, CAD and non-CAD conditions. This specific subset of identified variables could be of interest as a new diagnostic tool for CAD management.

ACKNOWLEDGEMENTS

This work was supported by funds from the Italian Ministry for Health (9.12.1) "Ricerca Corrente" I.R.C.C.S. Policlinico San Donato and the EU Framework 7 (202272) project "LipidomicNet".

The authors wish to thank J.D. Baggott for language editing.

REFERENCES

1. Ansell BJ, Navab M, Hama S et al. Inflammatory/antiinflammatory properties of high-density lipoprotein distinguish patients from control subjects better than high-density lipoprotein cholesterol levels and are favorably affected by simvastatin treatment. Circulation 2003; 108:2751-56.
2. Ishiyama J, Taguchi R, Yamamoto A, Murakami K. Palmitic acid enhances lectin-like oxidized LDL receptor (LOX-1) expression and promotes uptake of oxidized LDL in macrophage cells. Atherosclerosis 2010; 209:118-24.
3. He LY, Zhao JF, Han JL, Shen SS, Chen XJ. Correlation between serum free fatty acids levels and Gensini score in elderly patients with coronary heart disease. J Geriatr Cardiol 2014; 11:57-62.
4. Luan H, Chen X, Zhong S, et al. Serum metabolomics reveals lipid metabolism variation between coronary artery disease and congestive heart failure: a pilot study. Biomarkers 2013; 18:314-21.
5. Chowdhury R, Warnakula S, Kunutsor S, et al. Association of dietary, circulating, and supplement fatty acids with coronary risk: a systematic review and meta-analysis. Ann Intern Med 2014; 160:398-406.
6. Dozio E, Malavazos AE, Vianello E, et al. Interleukin-15 and soluble interleukin-15 receptor alpha in coronary artery disease patients: association with epicardial fat and indices of adipose tissue distribution. PLoS One 2014; 9:e90960.
7. Dozio E, Briganti S, Vianello E, et al. Epicardial adipose tissue inflammation is related to vitamin D deficiency in patients affected by coronary artery disease. Nutr Metab Cardiovasc Dis 2015; 25:267-73.
8. Buscema M, Sacco PL. Auto-contractive Maps, the H Function, and the Maximally Regular Graph (MRG): A New Methodology for Data Mining. In: Capecchi V, Buscema M, Contucci P, D'Amore B, editors. Applications of Mathematics in Models, Artificial Neural Networks and Arts: Mathematics and Society. Dordrecht: Springer Netherlands 2010; 227-75.
9. Gironi M, Saresella M, Rovaris M, Vaghi M, Nemni R, Clerici M, Grossi E. A novel data mining system points out hidden relationships between immunological markers in multiple sclerosis. Immun Ageing 2013; 10:1.
10. Gallucci M, Spagnolo P, Arico M, Grossi E. Predictors of response to cholinesterase inhibitors treatment of Alzheimer's disease: date mining from the TREDEM Registry. J Alzheimers Dis 2016; 50:969-79.
11. Zong G, Li Y, Wanders AJ, et al. Intake of individual saturated fatty acids and risk of coronary heart disease in US men and women: two prospective longitudinal cohort studies. BMJ 2016; 355:i5796.
12. Jula A, Marniemi J, Ronnemaa T, Virtanen A, Huupponen R. Effects of diet and simvastatin on fatty acid composition in hypercholesterolemic men: a randomized controlled trial. Arterioscler Thromb Vasc Biol 2005; 25:1952-59.

LETTER TO THE EDITOR

MINIMALLY-INVASIVE OSTEOTOME SINUS FLOOR ELEVATION COMBINED WITH SHORT IMPLANTS AND PLATELET-RICH PLASMA FOR EDENTULOUS ATROPHIC POSTERIOR MAXILLA: A FIVE-YEAR FOLLOW-UP PROSPECTIVE STUDY

S. TASCHIERI[1,2], L. KARANXHA[1,2], L. FRANCETTI[1,2], R. WEINSTEIN[3], A.B. GIANNÌ[1,4] and M. DEL FABBRO[1,2]

[1]Department of Biomedical, Surgical and Dental Sciences, Università degli Studi di Milano, Milan, Italy; [2]Dental Clinic, IRCCS Galeazzi Orthopaedic Institute, Milan, Italy; [3]Scientific Director D&S ICH Humanitas Dental Center, Rozzano, Milan, Italy; [4]Division of Maxillofacial Surgery, Fondazione Ca' Granda IRCCS Ospedale Maggiore Policlinico, Milan, Italy

Received October 24, 2017 – Accepted November 23, 2017

The aim of this study was to investigate the success of the combination of short implants, osteotome sinus floor elevation technique (OSFE) and pure platelet rich plasma (P-PRP), for the rehabilitation of atrophic posterior maxilla. Fifty-one patients were included in this study, receiving a total of 88 short implants in three different lengths (6.5 mm, 7.5 mm, 8.5 mm), depending on the residual bone height level. A total of 39 standard implants were also inserted when judged necessary, and splinted with one or more short implants in order to support a fixed prosthesis. Data were recorded in a one-year and five-year follow-ups. No statistically significant difference was found between short implants with different length, nor between short and standard length implants in terms of both bone level change and bone height. Based on the present results, the use of short implants combined with OSFE technique for the rehabilitation of atrophic posterior maxilla can be recommended.

To the Editor,

An edentulous atrophic posterior maxilla is a commonly encountered clinical situation. Based on the residual bone height (RBH), the atrophy of the posterior region of the maxilla can be classified as severe (RBH < 4 mm) or mild to moderate (4 mm ≤ RBH ≤ 8 mm) (1). In cases of severe atrophy, bone augmentation through lateral sinus floor elevation is considered the gold standard treatment with numerous reports on its predictability and high success rate (2). Alternative treatment options for severely atrophic posterior maxilla include zygomatic and pterygoid implants.

When it comes to mild to moderate atrophy, the above approaches are considered as being excessively invasive because of a high patient discomfort and elevated treatment cost and duration (3). Therefore, attempts have been made to propose less traumatic options such as osteotome sinus floor elevation (OSFE), short implants and tilted implants. A crestal approach for sinus lifting using osteotomes (4) is a technique that aims to provide an adequate bone height for implant insertion, by avoiding a more traumatic lateral approach. Even though it is not recommended for cases of extreme atrophy, as the bone gain achievable with this technique is

Key words: dental implants, maxillary sinus augmentation, pure platelet-rich plasma, short implants, summers techniaue. transcrestal approach

Mailing address:
Prof. Massimo Del Fabbro,
Department of Biomedical, Surgical and Dental Sciences,
Università degli Studi di Milano,
IRCCS Istituto Ortopedico Galeazzi,
Via Riccardo Galeazzi 4, 20161 Milano, Italy
Tel.: +39 02 50319950 - Fax: +39 02 50319960
e-mail: massimo.delfabbro@unimi.it

0393-974X (2018)

This publication and/or article is for individual use only and may not be further reproduced without written permission from the copyright holder. Unauthorized reproduction may result in financial and other penalties
DISCLOSURE: ALL AUTHORS REPORT NO CONFLICTS OF INTEREST RELEVANT TO THIS ARTICLE.

Table I. *Demographics of patients and implants.*

	Short implants, length			Total short implants	Standard implants	Total short+standard
	6.5 mm	7.5 mm	8.5 mm			
No. patients	6	21	24	51	28	51
No. implants placed	10	50	28	88	39	127
No. implants failed	1	1	0	2	1	3
Dropout patients/implants	0/0	3/6	2/2	5/8	2/4	5
Implant survival at 5y	90%	98%	100%	97.7%	97.4%	97.6%
No. patients/implants at 5y	6/9	18/43	22/26	46/78	26/34	46/112

Table II. *Bone level measurements and comparison tests for short and standard implants.*

	Short implants, length			Total short implants	Standard implants	Short *vs* standard implants (unpaired *t*-test)
	6.5 mm	7.5 mm	8.5 mm			
Bone level change 1y, mm	0.36±0.24	0.38±0.35	0.60±0.40	0.45±0.35	0.46±0.38	0.89
Bone level change 5y, mm	0.40±0.21	0.34±0.71	0.63±0.33	0.48±0.48	0.52±0.40	0.65
p-value 1y vs 5y (paired *t*-test)	0.58	0.71	0.65	0.52	0.25	
Bone height change 1y *vs* 5y	-0.08±0.13	-0.06±0.59	0.11±1.16	0.02±0.80	0.05±0.65	0.84
p-value 1y *vs* 5y (paired *t*-test)	0.83	0.40	0.50	0.97	0.66	

limited, it represents an efficient solution for most cases having an RBH of at least 4 mm (5). An even less invasive approach for moderate atrophic maxilla is represented by short implants (6). Defined as implants no longer than 10 mm, short implants have emerged as a valuable alternative to bone augmentation procedures. They can be utilised alone in residual bone height of at least 6 mm with a similar success rate of standard implants associated with maxillary sinus augmentation (7, 8). Additionally, they can be combined with OSFE in cases of a residual bone height of at least 4 mm.

While few studies have shown the feasibility of such an approach, with excellent results over the short term, no studies have reported the long-term outcome of short implants combined with osteotome sinus floor elevation. We previously reported the one-year follow-up results for the rehabilitation of atrophic posterior maxilla through a fixed prosthesis supported by short implants splinted with standard implants (9). Short implants were inserted in combination with OSFE and platelet concentrates (P-PRP). The current study followed the same protocol with the aim to investigate more in depth the performance of short implants combined with OSFE, extending the follow-up to a five-year period. To our knowledge, no other studies have reported a five-year follow-up on the success rate of short implants combined with PRP and OSFE.

MATERIALS AND METHODS

Ethical approval was obtained from the Institutional Review Board of the IRCCS Istituto Ortopedico Galeazzi

and all patients were treated according to the principles enunciated in the Helsinki Declaration of 1980 for biomedical research involving human subjects, as revised in 2013. All subjects signed an informed consent form before being enrolled in the study. Each patient received at least one short implant and one standard implant at the same side of the posterior maxilla. Patients were recruited at the same clinical centre and one experienced surgeon performed all interventions. The inclusion criteria were: adult patients with good general health (American Society of Anaesthesiologists classification ASA-1 or ASA-2) with unilateral or bilateral atrophic edentulous posterior maxilla; a mild to moderate atrophy with an RBH of 4 to 7 mm in the region intended for the placement of one or more short implants. The exclusion criteria were: severe atrophy of implant site (less than 4 mm height), radiotherapy to the head/neck within the previous 24 months; treatment with intravenous bisphosphonates or other antiresorptive drugs.

Short implants of three different lengths were used: 6.5 mm, 7.5 mm and 8.5 mm. The choice of the most appropriate length was based on the RBH: patients with an RBH of 4-5 mm received implants with a 6.5 mm length; patients with an RBH of 5-6 mm received implants of 7.5 mm in length; patients with an RBH of more than 6 mm received implants of 8.5 mm in length (Table I). The RBH was evaluated with a cone beam CT scan. Depending on the clinical situation, one or more standard length implants (≥10 mm long) could be placed in an adjacent site with an RBH of at least 10 mm, and splinted with the short implants in the same restoration.

Surgical procedure:

As pre-surgical preparation, a professional oral hygiene session was performed three days prior to surgery and 2 g of amoxicillin and clavulanic acid (Augmentin, Roche, Milan, Italy) was administered as prophylaxis one hour prior to surgery. Additionally, the preparation of P-PRP was carried out by collecting 10 mL of peripheral blood in two citrated tubes and centrifuging for 8 min at 580 *g* at room temperature (PRGF System®, BTI Biotechnology Institute, Vitoria, Alava, Spain). After centrifugation, the deeper fraction representing the plasma rich in growth factors and the upper fraction representing the plasma poor in growth factors, were stored in a specific container until activation.

Four percent of articaine chlorhydrate and epinephrine (1:100,000) was used as local anaesthesia and a full-thickness mucoperiosteal flap was raised. A standard procedure for implant site preparation was performed using a 2-mm bur, and the implant site was underprepared in order to achieve primary stability. Attention was paid in order to keep 1 mm of intact bone immediately below the sinus floor. The P-PRP clot was inserted at the implant site and a series of osteotomes were used in order to carefully elevate the sinus floor. Intra-operative radiographs were taken in order to ensure a vertical dimension gain of at least 2 mm. Finally, the implants (Interna, Universal Platform and Universal Plus Platform, BTI Biotechnology Institute) were inserted with the aid of a handpiece that delivered a controlled torque of 25 Ncm. One or more short implants were inserted, according to each patient's need. Conversely, standard implants were used only if indicated by the clinical situation, as a better support for the prosthesis. The standard length implant(s) were inserted immediately after the short implant(s), using a traditional implant site preparation technique. Once all implants were positioned, the flap was sutured with 5-0 non-resorbable sutures (Ethicon Inc., Johnson & Johnson, Piscataway, NJ, USA).

Prosthetic phase

A surgical re-entry procedure was performed 5-6 months after implant insertion. Elevation of full thickness flaps allowed access to the marginal portion of the implant sites in order to replace the healing caps with a healing abutment. An impression was made and sent to the laboratory for prosthesis preparation. Standard prosthetic procedures were then performed and a composite resin-based provisional prosthesis restoration was delivered. The provisional restoration was not placed in the occlusion. During the following three months, progressive loading was applied through monthly apposition of composite resin on the occlusal surface, achieving contact with the opposite occlusal surfaces after two months. After 3-4 months, the provisional prosthesis was substituted by the final prosthesis, made of metal-reinforced composite or metal-ceramic crowns.

Radiographic examination

An intraoral radiograph was taken at entry, immediately after implant surgery (baseline), at the prosthetic phase,

and at each follow-up visit (12, 36, 60 months of prosthesis function). Radiographs were taken using a long-cone paralleling technique and individual trays to ensure reproducibility. Specific image analysis software (ImageJ version 1.46, National Institutes of Health, Bethesda, MD, USA; http://rsb.info.nih.gov/ij/) was used to perform measurements of marginal bone level around implants at the mesial and distal aspects. The implant neck was the reference for each measurement. Implant length was used for calibration. All the radiographs were analysed by a trained independent evaluator.

Outcome variables

i. Prosthesis success, defined as a functioning prosthesis without mobility.
ii. Implant survival, defined as the implant still present in the patient's jaw, supporting the functional prosthesis.
iii. Implant success, defined by the following parameters: no mobility, no pain, no recurrent or persistent peri-implant infection, no evidence of peri-implant radiolucency, peri-implant bone loss smaller than 1 mm in the first year and 0.2 mm per year subsequently.
iv. Peri-implant bone level changes and bone height changes were measured as described above.

Statistical analysis

The comparison of bone level changes and bone height at the different time frames (between one and five year follow-ups) within the groups of implants was made using paired Student's *t*-test. For comparisons between short and standard implants we used the unpaired Student's *t*-test. The normality of the distributions was assessed by means of the D'Agostino and Pearson omnibus normality test. The significance level was set at p=0.05.

RESULTS

A total of 51 patients were included in this prospective study and a total of 127 implants (88 short implants and 39 standard implants) were inserted between February 2010 and March 2012. Implant distribution according to implant length is reported in Table I. A total of 58 prostheses, each supported by 1 to 6 implants, was delivered as planned. Five patients, accounting for 8 short and 4 standard implants, failed to attend the five-year follow-up. These patients were contacted to make sure that their implants and prostheses were still in function, and were accounted for implant survival assessment. Two short implants and one standard length implant failed in three patients. One 7.5-mm long implant did not osseo-integrate and was removed at the prosthetic phase. One standard length implant failed after two months of function. Both implants were replaced and successfully integrated without compromising prosthetic function. One 6.5-

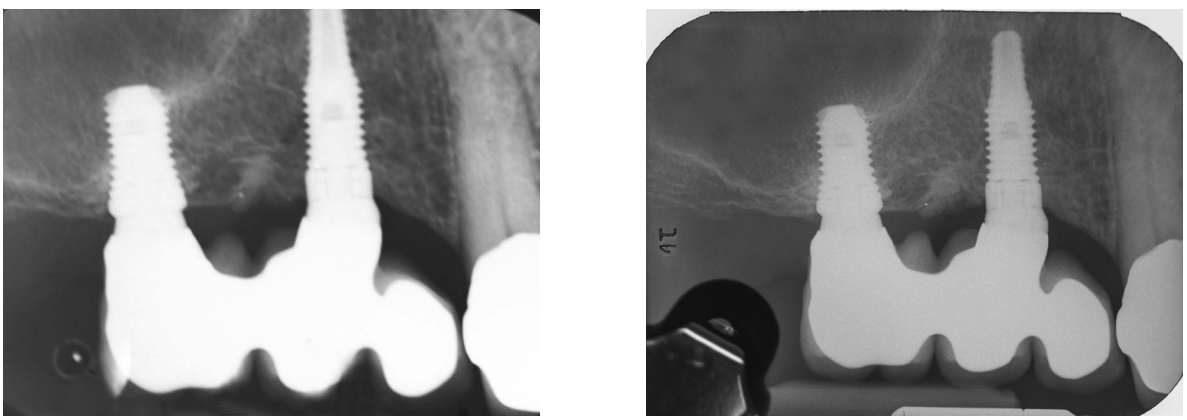

A B

Fig. 1. ***A)*** *A case of a fixed prosthesis supported by a standard implant in position 15 and a 6.5 mm-short implant in position 16, inserted with the OSFE technique.* ***B)*** *At the 5-year follow-up the marginal bone level appears well preserved.*

mm long implant failed after two years of function due to perimplantitis. In this case also the prosthesis was considered as failed. At the five-year follow-up check, overall implant survival and success was 97.6% and 97.4%, respectively (Table I). Seven prosthetic complications occurred. They consisted of one fractured crown (in the same patient experiencing failure of the 7.5-mm long implant at the prosthetic phase), one chipping and five screw loosenings of the provisional prosthesis, that required tightening at the dental office. Prosthesis survival and success was, respectively, 98.3% and 89.7%.

The results of peri-implant bone loss measurements at the 1 and 5 year follow-ups and of the comparison tests are reported in Table II. At each time frame, there was no statistically significant difference in bone level change among short implants of different lengths, nor between short and standard length implants. There was no significant difference within groups of implants of different lengths between one- and five-year follow-ups. Fig. 1 shows periapical radiographs of a fixed prosthesis taken at baseline and at the 5-year follow-up.

The mean change in bone height between one and five years of follow-up and the significances of the comparisons are also reported in Table II. There was no significant difference between groups at each follow-up nor within groups between the one-year and the five-year follow-up.

DISCUSSION

This study reports the results of a five-year follow-up for the rehabilitation of atrophic posterior maxilla with the combination of osteotome-mediated sinus floor elevation, short implants and poor platelet-rich plasma. We documented excellent 5-year survival and success rates for both implants and prostheses with no significant difference in bone loss between short and standard implants and with very few intra- or post-operative complications. Moreover, a good maintenance of peri-implant bone levels and bone height was observed. Based on the outcome of this study, the use of short implants combined with OSFE technique for the rehabilitation of atrophic posterior maxilla can be recommended.

Even though the lateral approach for sinus lifting has shown high success rates for implant insertion in grafted atrophic maxilla, it is a demanding procedure that comes with several shortcomings (10).

In this study we used a trans-alveolar approach for sinus lifting, a technique first described by Tatum (11) and later modified by Summers into the current OSFE (4). Several systematic reviews evaluated the outcome of implants inserted with this technique, reporting overall survival rates ranging between 92.7 and 96% in a one- to five-year follow-up (5).

However, the OSFE technique has some drawbacks that we tried to address during our study. The first disadvantage is the incapability to produce a significant amount of bone gain, which we overcame by using short implants instead of standard ones. Another disadvantage of OSFE technique is the low intra-operative visibility which can lead to a higher risk of complications, even though this concern is not supported by the literature. In fact, studies have demonstrated an actual lower risk for such complications during the OSFE technique (12). By including P-PRP in our protocol, we take advantage of its mechanical properties in order to ensure a safer sinus lifting procedure (13). Additionally, P-PRP has the ability to induce local biological processes like chemotaxis, proliferation, differentiation etc. which can enhance the regeneration of soft and hard tissue (14). Lastly, P-PRP is proven to bring substantial advantages in terms of accelerating soft tissue healing and reducing post-operative symptoms with an overall improvement in the patient's quality of life (15). Conclusively, short implants inserted with OSFE technique and splinted with standard implants for supporting a fixed prosthesis can serve as a valuable and predictable treatment for atrophic posterior maxilla. The adjunct of P-PRP can result in potential mechanical and biological benefits.

REFERENCES

1. Cawood JL, Howell RA. A classification of the edentulous jaws. Int J Oral Maxillofac Surg 1988; 17:232-6.
2. Del Fabbro M, Rosano G, Taschieri S. Implant survival rates after maxillary sinus augmentation. Eur J Oral Sci

2008; 116:497-506.
3. Boffano P, Forouzanfar T. Current concepts on complications associated with sinus augmentation procedures. J Craniofac Surg 2014; 25(2):e210-12.
4. Summers RB. A new concept in maxillary implant surgery: the osteotome technique. Compendium 1994; 15:1525-8.
5. Emmerich D, Att W, Stappert C. Sinus floor elevation using osteotomes: a systematic review and meta-analysis. J Periodontol 2005; 76:1237-51.
6. Felice P, Pistilli R, Barausse C, Bruno V, Trullenque-Eriksson A, Esposito M. Short implants as an alternative to crestal sinus lift: A 1-year multicentre randomised controlled trial. Eur J Oral Implantol 2015; 8(4):375-84.
7. Pohl V, Thoma DS, Sporniak-Tutak K, Garcia-Garcia A, Taylor TD, Haas R, Hämmerle CH. Short dental implants (6 mm) versus long dental implants (11-15 mm) in combination with sinus floor elevation procedures: 3-year results from a multicentre, randomized controlled clinical trial. J Clin Periodontol 2017; 44(4):438-45.
8. Esposito M, Pistilli R, Barausse C, Felice P. Three-year results from a randomised controlled trial comparing prostheses supported by 5-mm long implants or by longer implants in augmented bone in posterior atrophic edentulous jaws. Eur J Oral Implantol 2014; 7:383-95.
9. Taschieri S, Corbella S, Del Fabbro M. Mini-invasive osteotome sinus floor elevation in partially edentulous atrophic maxilla using reduced length dental implants: interim results of a prospective study. Clin Implant Dent Relat Res 2014; 16(2):185-93.
10. Caudry S, Landzberg M. Lateral window sinus elevation technique: managing challenges and complications. J Can Dent Assoc 2013; 79:d101.
11. Tatum H Jr. Maxillary and sinus implant reconstructions. Dent Clin North Am 1986; 30:207-29.
12. Katranji A, Fotek P, Wang HL. Sinus augmentation complications: etiology and treatment. Implant Dent 2008; 17:339-49.
13. Diss A, Dohan DM, Mouhyi J, Mahler P. Osteotome sinus floor elevation using Choukroun's platelet-rich fibrin as grafting material: a 1-year prospective pilot study with microthreaded implants. Oral Surg Oral Med Oral Pathol Oral Radiol Endod 2008; 105:572-79.
14. Anitua E, Andia I, Ardanza B, et al. Autologous platelets as a source for healing and tissue regeneration. Thromb Haemost 2004; 91:4-15.
15. Carlson NE, Roach RB Jr. Platelet-rich plasma: Clinical applications in dentistry. J Am Dent Assoc 2002; 133:1383-6.

LETTER TO THE EDITOR

PROANTHOCYANIDIN MAY IMPROVE THE SHEAR BOND STRENGTH AT THE COMPOSITES/DENTINE INTERFACE

G. AUTIERI[1], F. MUSSANO[1], M. PETRUZZI[2], M. CAROSSA[1], T. GENOVA[1], M. CORSALINI[2] and S. CAROSSA[1]

[1]Department of Surgical Sciences, Dental School, Università degli Studi di Torino, Torino, Italy; [2]Interdisciplinary Department of Medicine, Dental School, Università degli Studi di Bari, Bari, Italy

Received February 25, 2018 – Accepted May 3, 2018

This study aimed at assessing whether proanthocyanidin, a collagen cross-linker, affects the adhesion strength of resin composites on the dentine surface. Freshly extracted, caries-free, human molars (N=55) were embedded in transparent resin and bisected. The halves were then assigned to either a treated or a non-treated group, where the treatment consisted of a 10 min incubation in a 6.5% proanthocyanidin solution in PBS. A resin composite cylinder was polymerized perpendicularly to the dentinal surfaces and shear tests were made, using an Instron-like machine. The fracture surfaces were characterized by optical (Picro-Sirius Red stain) and electron microscopy (FESEM EDX analysis). Mean bond strength values were 10.73 MPa (SD 3.70) for the treated group and 8.69 MPa (SD 3.20) for the non-treated group ($p<0.05$ Student's *t*-test). No constant fracture patterns could be found within the two groups. Proanthocyanidin treatment may improve the adhesion properties of the dentine-bonding interface.

To the Editor,

Modern concepts in restorative dentistry rely on the conditioning of enamel and dentine substrate, thus allowing the formation of a hybrid layer and promoting intimate adhesion between the filling material and the tooth itself (1, 2). The role played by the collagen matrix on dentinal adhesion is paramount, as the acid etching exposes the collagen fibres that will be embedded in the adhesive resin. In the past few years, several studies have focused on improving the properties of this substrate by using substances able to promote the formation of cross-links within the collagen fibres. Glutharaldeyde and proanthocyanidin (PA), a class of flavonoids contained in Grape Seed Extracts (GSE), are the most frequently investigated compounds deemed suitable for this aim. Glutharaldeyde has good cross-linking properties and has been widely used in the past as a stabilizing agent for biological tissues, but its use *in vivo* is limited due to its cytotoxicity. Instead, PA is as efficient as glutaraldehyde and is endowed with significantly superior biocompatibility (3).

Treatment with PA can promote the formation of intra- and inter-fibrillar bonds in collagen, leading to improved biochemical and biomechanical properties. The cross-linked collagen showed higher resistance to thermal and chemical degradation, and increased stiffness. Studies performed on human and bovine dentine, which is mainly composed by type I collagen, evaluated the effects of cross-linking on adhesion to dental composites, showing higher tensile bond strength values when compared to

Key words: adhesion strength, proanthocyanidin, grape seed extracts, resin composite, shear test

Mailing address:
Prof. Massimo Corsalini,
Interdisciplinary Department of Medicine, Dental School,
Università degli Studi di Bari, p.zza Giulio Cesare, 10
70125 Bari, Italy
Tel.: +39 080 5593325 - Fax: +39 080 5478743
e-mail: massimo.corsalini@uniba.it

0393-974X (2018)
Copyright © by BIOLIFE, s.a.s.
This publication and/or article is for individual use only and may not be further reproduced without written permission from the copyright holder.
Unauthorized reproduction may result in financial and other penalties
DISCLOSURE: ALL AUTHORS REPORT NO CONFLICTS OF INTEREST RELEVANT TO THIS ARTICLE.

control groups (4).

The enhancements on dentinal hybrid layer properties may be of great interest, since the adhesion achieved on dentine is less predictable than that occurring on enamel, and the stability of dentine/restoration interface affects the duration of the restoration itself. The aim of this study is to evaluate the effects of PA treatment on the Shear Bond Strength (SBS) of composite to dentine.

MATERIALS AND METHODS

Sample preparation

A final sample of 55 fresh, caries-free human molars without cracks or fractures were included in the study. During the experiment, specimens were evaluated to discard those not showing the desired characteristics, i.e. a sufficient dentine surface to be able to perform bonding without including enamel or pulp, absence of reparative dentine, absence of flaws in the bonding interface, etc. Teeth were cleaned of blood and adhering soft tissues, then rinsed and stored in Hank's Buffered Salt Solution (HBSS, HyClone, South Logan, UT, USA) at room temperature to prevent dehydration and collagen modifications. Teeth were then embedded in transparent, self-curing resin (SC-22 Cristallo, Prochima, Calcinelli -PU- IT), using a silicone mould, refined, polished and numbered. Each specimen was bisected, using a microtome (Micromet, Varna, Bulgaria) at low speed, under constant irrigation; the two halves of each bisected tooth were then randomly allocated to either a Treated (T) or a Non-Treated (NT) group. This method was used to avoid biases related to the possible individual variability of the tubular structure and/or mechanical properties that might be found in different dentine areas, as only symmetric dentine surfaces were tested.

The dentine surface was refined using abrasive paper. The specimens were acid-etched using 37% ortophosphoric acid gel (Axia® Etch, Dentalica, Milano, IT) and rinsed. The T group was immersed for 10 min in a 6.5% PA (MegaNatural Gold, Polyphenolics, Madera, CA, USA) solution in PBS at pH 7.4 (Gibco, Invitrogen, Carlsbad, CA, USA) (5). The NT group was kept for the same length of time in PBS as a control. After a quick rinse, the specimens were dried with a gentle air flow. Priming and Bonding agents (OptiBond FL, Kerr, Orange, CA, USA) were applied and polymerized according to the manufacturer's instructions, then a standard 2x2 mm composite (Tetric Evoceram, Ivoclar Vivadent AG, Schaan, Liechtenstein) cylinder was built perpendicularly to dentine surface, using a 2-mm thick Teflon disc with a 2-mm diameter hole as a mould. The samples obtained were stored in HBSS for 24 h at room temperature before testing.

Mechanical bond strength test

Shear bond strength (SBS) tests were performed using a universal testing machine (MTS Insight 2kN, Eden Prairie, MN, USA), mounting a custom-made steel blade, at a crosshead speed of 0.5 mm/min until failure occurred. The force was applied as close as possible parallel to the dentine/composite interface in order to reduce the bending moment during the test, but not in contact with the surface to avoid frictional interference. The peak load data were recorded on a dedicated software (MTS TestWorks 4) and SBS was calculated on the basis of peak load and adhesive surface, according to the formula:

$$SBS = N/m^2 = PL/A = PL/(\pi r^2)$$

where SBS is expressed in Pascal (Pa), PL represents the Peak Load expressed in Newton (N) and A is the area of the adhesive surface expressed in square meters (m^2). The symbol *r* refers to the radius of the adhesive interface, corresponding to the radius of the composite cylinder. All the procedures were carried out by a single operator to reduce the effects of operator-dependant variables.

Sirius red stain for debonding area evaluation

The samples were collected after failure to analyze the debonding areas. These areas, rich in collagen fibres, were stained with Picro-Sirius Red (Direct Red 80, Sigma-Aldrich, Carlsbad, CA, USA), following a previously published protocol (6). Briefly, Sirius Red was dissolved in a saturated aqueous solution of picric acid (0.5 g/500 ml) (Sigma-Aldrich, Carlsbad, CA, USA). The samples were kept in the staining solution for at least 1 h and then rinsed once with acidified water (0.5% acetic acid and distilled water solution) and twice with deionized water to eliminate the dye excess.

Microscope characterization and analysis

Specimens were observed by stereomicroscope at low magnification (50x) and a high-resolution picture of

the debonding area was taken by means of a dedicated software (Canon Utilities Remote Capture 2.7). Pictures were analyzed according to Dahab et al. (7), which was adapted with minor modifications to best suit the different staining method. A standard circular mask, with the exact dimensions of the adhesive area, was created and applied to the pictures, making the area clearly identifiable and circumscribed. Photoshop program was then used to quantify the amount of red-coloured pixels within the mask. The data were recorded on a Microsoft Excel table and the proportion between coloured (representing dentine) and uncoloured (representing bonding and composite) pixels was calculated.

FESEM and EDX analysis

Four samples were chosen randomly (two samples for both T and NT groups) and prepared for Scanning Electron Microscope analysis. The samples were dehydrated by means of a water/ethanol solution in increasing ethanol concentrations, then finally stored in 100% ethanol for 48 h, dried and sputtered with a 40-nm thick Ag layer. The samples were mounted on stubs and observed at different magnifications (up to 3000x) using an FESEM apparatus (FEI Quanta Inspect 200 LV). Pictures representative of the samples were taken randomly from different areas.

FESEM analysis was mainly focused on specific portions of the debonding area: exposed dentine, composite/adhesive only areas and dentine/adhesive/composite interface, to evaluate the effects of shearing on samples. Energy Dispersive Spectroscopy (EDX) was performed by a spectrometer (EDAX) connected to the FESEM apparatus, in order to evaluate differences in chemical composition of similar areas between different samples.

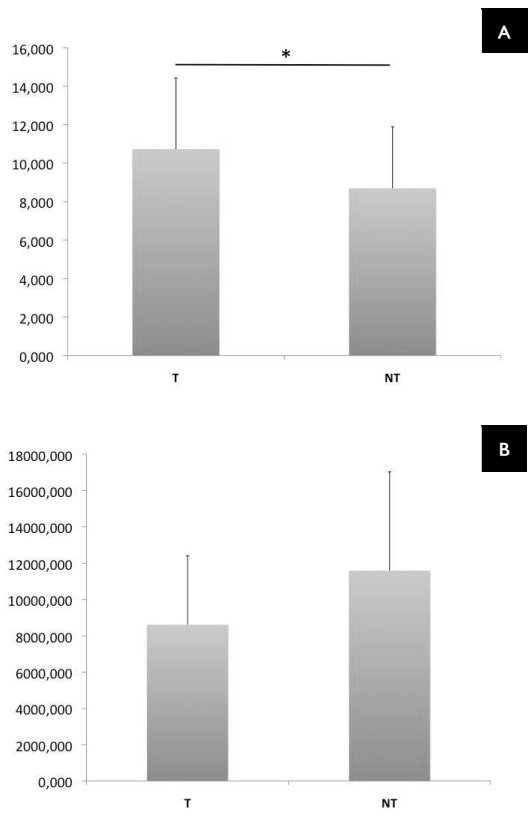

Fig. 1. ***A****) Mean SBS values of N and NT groups (bars depict the SD), t-test<0.05.* ***B****) Mean debonding areas of N and NT groups (bars depict the SD), t-test>0.05.*

RESULTS

Mechanical bond strength test

The mean SBS values were 10.73 MPa (SD 3.70) for the T group and 8.69 MPa (SD 3.20) for the NT group, the *t*-test being significant ($p<0.05$), as reported in Fig. 1A.

Debonding area

The number of coloured pixels in each picture (corresponding to the exposed collagen area, i.e. debonding area, prone to be stained with Sirius Red Stain) quantified the surface of exposed dentine in each group (Fig. 1B). A possible correlation between SBS and the extent of the debonding area was assessed. However, no significant difference could be found between T and NT samples.

FESEM and EDX analysis

Pictures taken at the dentine/adhesive/composite interface of T samples showed a rougher, less regular surface when compared to the NT group. This characteristic was more evident in the high magnification images representing exposed dentine only (Fig. 2A), with tubules appearing torn and less organized than in the pictures of similar portions in NT samples (Fig. 2B). EDX showed the presence of C and O, which could be easily anticipated owing to the composition of dentine, and higher peaks for Ca and P in T group samples (Fig. 3A) when compared to the NT groups (Fig. 3B).

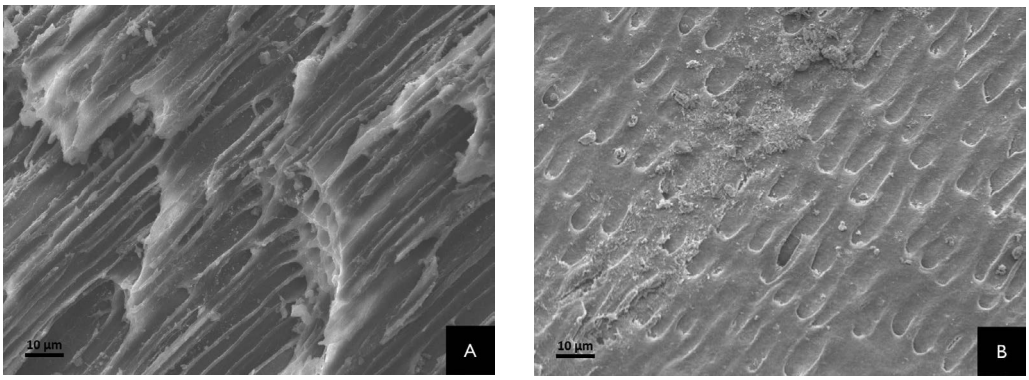

Fig. 2. *SEM image of a T sample (**A**) and NT sample (**B**).*

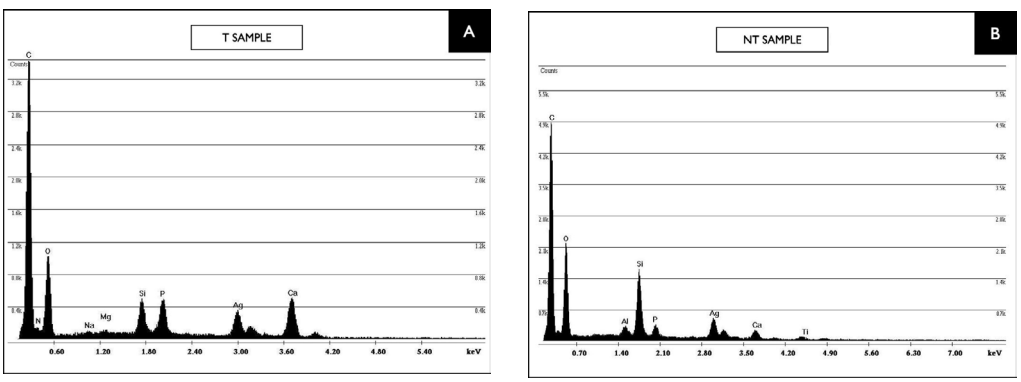

Fig. 3. *EDX analysis of a T sample (**A**) and NT sample (**B**) performed along one line randomly chosen in a putative debonding area to determine the surface elemental composition. Besides the elements C, O, P and Ca, which are major components of the dentine, Si is most likely due to traces of dental resin composite and Ag may be ascribed to the metallization process.*

DISCUSSION

A mixture of monomers, oligomers, and polymers used as natural antioxidants and free-radical scavengers, PA is known to stabilize and increase the cross-linkage of type-I collagen fibrils, due to the formation of hydrogen bonding between the protein amide carbonyl and the phenolic hydroxyl. Unsurprisingly, PA was successfully used to strengthen dentin and to enhance dentin-resin bond strength (4) in a series of studies using micro-scale evaluations. In addition, Venigalla et al. tested (8) the effect of 6.5 wt% proanthocyanidin on the immediate and long-term bond strengths of an etch and rinse adhesive system to water- versus ethanol-saturated dentin. The microtensile bond strength of cross-linked groups was higher compared to control group.

Improved strength and stability of the hybrid layer and underlying dentin was attained through proanthocyanidin after bleaching (9). Consistent with the literature (5), the stability of dentin collagen-PA complex most likely contributed to the higher values of hardness and reduced modulus of the hybrid layer and underlying dentin during the time shown in the present paper. Deep dentin surface pre-treatment with 6.5% PA resulted in a significant improvement in bond strength of resin composite to deep dentin (10). This is more or less in accordance with the data presented herein, based on a larger sample number,

where PA enhanced in a statistically significant way the mean SBS of the T specimens compared to the NT ones.

The fracture characterization entailed two different assays in this study. The former was a systematic analysis of the areas of exposed collagen within the circle of the bonded sample. However, no statistically significant difference could be found between the mean T and NT specimens, due to the high standard deviation. The latter was a qualitatively FESEM EDX analysis performed on a limited number of samples chosen randomly. Although no general trend may be inferred based on such a small sample size, the percentage of phosphorus and calcium detected by EDX analysis was higher on T specimens than on NT samples, suggesting a prevalence of the cohesive fracture within dentin for the T samples.

The PA cross-linking activity might not be the only one suitable to the enhancement of restorative material adhesion. Indeed, the elm cortex, rich in PA, showed inhibitory effects against proteases including metalloproteinases (11), the modulation of which is a major goal of conservative dentistry. Hence, the use of a natural and low cytotoxicity product, such as PA, seems to be promising during the bonding procedure (12). Further *in vitro* and *in vivo* studies may conveniently be devoted to enhancing the hybrid layer by reducing the susceptibility of the substrate to the dentin proteases.

ACKNOWLEDGEMENTS

The authors wish to thank Polyphenolics, Madera, CA, USA for kindly providing the MegaNatural Gold. Dr. Tommaso Vassallo and Dr. Salvatore Guastella (Department of Applied Sciences and Technology, Politecnico di Torino, Turin, Italy) are commended for their kind help during the SEM/EDX analyses.

REFERENCES

1. Lucchese A, Pilolli GP, Petruzzi M, Crincoli V, Scivetti M, Favia G. Analysis of collagen distribution in human crown dentin by confocal laser scanning microscopy. Ultrastruct Pathol 2008; 32:107-11.
2. Scivetti M, Pilolli GP, Corsalini M, Lucchese A, Favia G. Confocal laser scanning microscopy of human cementocytes: analysis of three-dimensional image reconstruction. Ann Anat 2007; 189:169-74.
3. Han B, Jaurequi J, Tang BW, Nimni ME. Proanthocyanidin: a natural crosslinking reagent for stabilizing collagen matrices. J Biomed Mater Res A 2003; 65:118-24.
4. Al-Ammar A, Drummond JL, Bedran-Russo AK. The use of collagen cross-linking agents to enhance dentin bond strength. J Biomed Mater Res B 2009; 91:419-24.
5. Dos Santos PH, Karol S, Bedran-Russo AK. Nanomechanical properties of biochemically modified dentin bonded interfaces. J Oral Rehab 2011; 38:541-46.
6. Dapson RW, Fagan C, Kiernan JA, Wickersham TW. Certification procedures for sirius red F3B (CI 35780, Direct red 80). Biotechnol Histochem 2011; 86:133-19.
7. Dahab GM, Kheiza MM, El-Belagi HM, Fouda AM, El-Din OA. Digital quantification of fibrosis in the liver biopsy sections: description of a new method by Photoshop software. J Gastroenterol Hepatol 2004; 19:78-85.
8. Venigalla BS, Jyothi P, Kamishetty S, Reddy S, Cherukupalli RC, Reddy DA. Resin bond strength to water versus ethanol-saturated human dentin pretreated with three different cross-linking agents. J Conserv Dent. 2016;19: 555-59.
9. Abraham S, Ghonmode WN, Saujanya KP, Jaju N, Tambe VH, Yawalikar PP. Effect of grape seed extracts on bond strength of bleached enamel using fifth and seventh generation bonding agents. J Int Oral Health. 2013; 5:101-7.
10. Srinivasulu S, Vidhya S, Sujatha M, Mahalaxmi S. shear bond strength of composite to deep dentin after treatment with two different collagen cross-linking agents at varying time intervals. Oper Dent 2012; 37:485-91.
11. Song SE, Choi BK, Kim SN, et al. Inhibitory effect of procyanidin oligomer from elm cortex on the matrix metalloproteinases and proteases of periodontopathogens. J Periodontal Res 2003; 38:282-89.
12. Epasinghe DJ, Yiu CK, Burrow MF, Tay FR, King NM. Effect of proanthocyanidin incorporation into dental adhesive resin on resin-dentine bond strength. J Dentistry 2012; 40:173-80.

JOURNAL OF BIOLOGICAL REGULATORS & HOMEOSTATIC AGENTS Vol. 32, no. 4, 1027-1031 (2018)

LETTER TO THE EDITOR

DIGITAL FLOW IN MEDICINE AND DENTISTRY: WHAT'S NEW?

L. PACIFICI and A. PACIFICI

Department of Oral and Maxillofacial Sciences, Sapienza University of Rome Italy

Received June 1, 2018 – Accepted June 8, 2018

Both Authors contributed equally to this work

The increasing requirements of standardization in medical applications have led physicians towards a deep revision of their protocols. The phenomenon of 'digital health' has revolutionized the way a patient accesses medical information, but it has also improved the way the doctor handles the surgical and clinical phases. In digital dentistry, the working steps are mainly reported as digital image acquisition, preparation and/or processing of data, device production and clinical application on patients; the new technologies have brought significant benefits to both the dentist and the patient. Digital processing of anatomical data uses virtual models, which represent a precise representation of the patient's anatomy. Recent advances in digital image acquisition technologies and the enormous complexity of modern software have made intraoral scans possible to realize digital dental arch models, however, the digital model is able to report substantial information to the clinician. Therefore, both complex surgeries and less invasive local therapies can be easily planned, with an accurate analysis of biological regulators improving the regenerative procedures, to achieve the best results in a shorter treatment.

To the Editor,

The phenomenon of 'digital health' has revolutionized the way a patient accesses medical information, but it has also improved the way the doctor handles the surgical and clinical phases.

The three cornerstones of medical progress are robotics, digital medicine and genomics, and the future is based on the integration of imaging, digital telemedicine and artificial intelligence.

In Italy, the development of dentistry as an independent branch of medicine is quite recent: only in 1980 the degree course in Dentistry and Dental Prosthetics was initiated, while specializations in Orthodontics and Oral Surgery were established in 1992. The development of new technologies in dentistry has been very rapid and is closely linked to clinical and surgical needs. Moreover, the entire field of dentistry has evolved its mission, thus starting to treat complex pathologies and moving towards the trend of aesthetics as per requests of patients (1-4).

Technology is finding more and more space in the dental work-flow, in particular in the field of the imprint the progress is constant; many manufacturers are competing to innovate this sector, for this reason we are seeing the addition of many new features, improved accuracy and greater ease of use of the intraoral scanner and other new generation of probes able to detect alteration of soft tissues (5).

The goal pursued by digital dentistry is to improve the quality of clinical examination, diagnosis and treatment of the patient. Compared to conventional workflow, the implementation of the digital workflow

Key words: digital medicine, digital dentistry, oral sciences, oral implantology

Mailing address:
Prof. Luciano Pacifici,
Department of Oral and Maxillofacial Sciences,
Sapienza University of Rome,
Rome, Italy
e-mail: prof.lucianopacifici@libero.it

0393-974X (2018)
Copyright © by BIOLIFE, s.a.s.
This publication and/or article is for individual use only and may not be further reproduced without written permission from the copyright holder.
Unauthorized reproduction may result in financial and other penalties
DISCLOSURE: ALL AUTHORS REPORT NO CONFLICTS OF INTEREST RELEVANT TO THIS ARTICLE.

in dental practice has led to data acquisition and patient assessment that is more facilitated, which increases the effectiveness in treatment planning, and better prosthesis production. The use of digital processing has also been improved with the use of "biologically guided" surgical approaches which has led dentists to perform *in-vitro* studies to investigate oral stem cells (6-9), innovative scaffolds (10) and other correlations between general medicine and oral conditions (10-12).

The introduction and dissemination of digital devices such as oral scanners, "cone-beam" computed tomography (CBCT), computer-aided design and computer-aided manufacturing (CAD/CAM) are radically transforming dentistry, improving traditional surgical planning. In this way, some fundamental processes, such as anamnesis, clinical examination, acquisition of dental impressions, planning of the implant and prosthetic interventions are improved. In the past, using radiographic data alone, without any data processing, it was difficult to obtain reliable treatment planning in all the cases treated.

Digital dentistry

In digital dentistry, the working steps are mainly reported as follows:

1. Digital image acquisition, based on classic X-ray analyses such as NMR or Orthopanoramic of dental arches;

2. Preparation/processing of data, consisting in all digital and software-guided processes to obtain reliable and useful images;

3. Device production and clinical application on patients, consisting of the finalization (treatment) of the workflow.

The evaluation of acquired digital data, obtained from computerized tomography and corroborated by the use of an optical dental arch scan, together with modern implant planning software, allow to carefully simulate the surgical and prosthetic phases.

The virtual visualization of dental arches allows to correctly evaluate a therapeutic plan and to calculate the duration of the treatment in advance.

The anatomical sites where the dental implants are to be positioned can be decided before the operation, depending on the volume, quality of the bone and position of the anatomical structures. With image analysis software, precise measurements of jaw bones that can be used for implant surgery, as well as distances and angles between implants from one side of a dental arch to another, are accurately determined, thus allowing better evaluation than the surgical protocol, positioning of the implants, and subsequent realization of the prostheses.

The computer-assisted digital design represents, therefore, a new method of in-silico reconstruction of images obtained with CT, CBCT and an intraoral scanner: this information is added together to obtain a model on which to "virtually" perform all the procedures to be subsequently performed on the patient, thus obtaining high predictability and safety in operations, with significantly reduced execution times.

These new technologies have brought significant benefits to both the dentist and the patient. With the simple scan of the study models and a subsequent scan of a custom-made model, such as waxing or a temporary element, the dentist can virtually design dental elements perfectly to insert in the surgical site, improving the performances of the temporary prosthesis and of the definitive one.

Recently, many studies evaluated the effects of a surgical guide produced by CAD/CAM technology on the precision of the implant cavities. In one study, the entrance cavities of the group in which the surgical template obtained using a digital method was used were located in correspondence with the abutments, on the other hand, the entrance cavities of the group in which the implants were positioned "hands-on", without any digital support, were performed at the prosthetic crown. It was shown that the surgical guide obtained with the CAD/CAM technology is able to facilitate the surgeon during the insertion of the fixture in the maxillary bones, for this reason, the digital technology globally improves the stability of the future prosthesis supported by implants.

Digital processing of anatomical data uses virtual models, which represents a precise representation of the patient's anatomy. Recent advances in digital image acquisition technologies and the enormous complexity of modern software have made intraoral scans possible to realize digital dental arch models

which are currently a promising alternative to traditional dental impressions.

In particular, intraoral scanners (IOS) allow the acquisition of dental impressions by analyzing the data in the form of optical analysis. The IOS act through a light beam, of the LASER type or a structured light, which is passed over the dental arches; the light is reflected towards the scanner and then it is recorded by the sensors; the obtained data are immediately processed by digital processing software. Finally, it generates a 3D model that is displayed on the computer, without making the traditional study model made of plaster.

This digital protocol allows to optimize time and reduce the steps in the therapeutic process of the patient undergoing implant and prosthetic rehabilitation. The dentist has the ability to easily send digital models to the dental technician via e-mail, reducing time and costs.

The optical impressions are much more comfortable for the patient, who feels less discomfort compared to the traditional impression that is often feared by patients; this fact is easily understandable because of the invasive procedures characterizing the process of dental impressions in the traditional technique, which often inhibits patients to proceed with the prosthetic procedures.

The use of the intraoral scanner avoids the inaccuracies that may depend on the medical operator, or the anomalies dependent on the impression material; in fact, the materials for dental impressions are subject to dimensional variations due to the continuous chemical reactions that develop between their components. These dimensional changes may lead to an inaccurate dental prosthesis, instead, digital scanning is not subjected to these variations. In the scientific literature, numerous studies have reported excellent precision of digital imprints compared to conventional imprints.

DISCUSSION

Some studies have shown that IOS is a reliable tool for acquiring images of individual as well as multiple dental abutments. For sites where a single implant is positioned, the intraoral scan of a single quadrant is more efficient than the traditional impression technique of the complete dental arch.

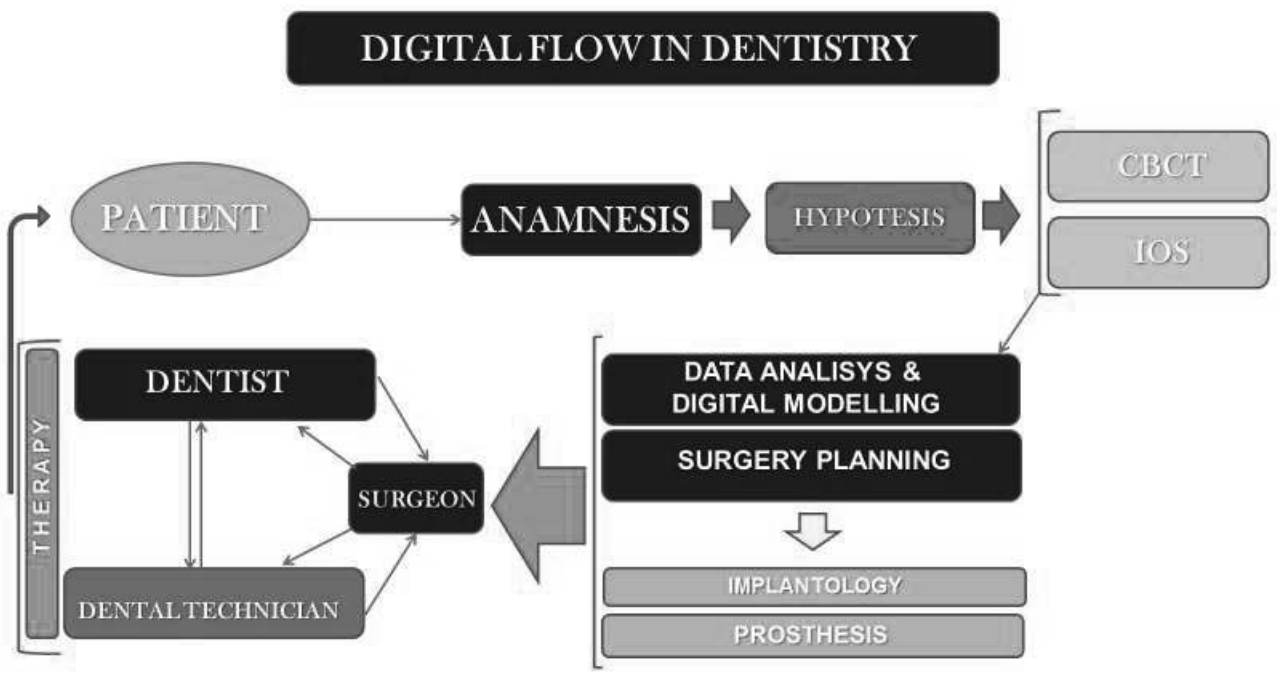

Fig. 1. *The digital workflow in dentistry.*

The accuracy and precision of the optical impressions, obtained from four different types of IOS, has been widely evaluated: in one study, the Authors used a patient model with a partial edentulism, subsequently treated with three implants. In addition, a patient model with total edentulism was also analyzed, subsequently treated with six dental implants.

After the acquisition of digital images, the Authors processed the data obtained, and a color-coded model was obtained on the anatomical scan, in order to "see" the areas where the greatest differences between the images obtained with technology were present. IOS and images were obtained with a study model. The results were excellent, both for the precision of the image and for the speed of execution of the dental impression. However, greater accuracy was noted in partially edentulous patients compared to totally edentulous patients.

The choice of an intraoral scanner in dental practice induces to modify the whole approach to the prosthetic branch. Although the clinician's learning curve is very rapid, there are many elements to consider carefully, including correct information on the technology used, so as to make it comprehensible to the patient.

The digital flow in a dental office is also based on the analysis of anatomical data that are required in case of complex surgery or implantology in areas where there is a surgical risk. Among the various devices aimed at the acquisition of digital data of the anatomical districts, "cone beam" computed tomography (CBCT) is of particular interest. This method has revolutionized diagnostic imaging in the field of dental radiology and maxillofacial; thanks to CBCT the surgeon can reconstruct in extremely accurate 3D models, all the anatomical structures that are to be investigated before surgery. The peculiarity of an analysis performed with CBCT technology is that it uses a type of data acquisition different from that used with the classic CT. In fact, CBCT does not limit itself to collect slice-by-slice data but it produces an X-ray cone that allows to capture a complex image with a single exposure. Many clinicians tried to perform and compare numerous scans performed with CT and CBCT methods; the Authors reported the obtained data in an image-analysis software, and used semi-automatic tools to measure the volumes of the maxillary sinus and sphenoid sinus. The results of this comparative and controlled study showed that the images obtained with CBCT provide more reliable volumetric information, in fact, such images are much closer to the real anatomical conditions, thus reducing volumetric distortions.

Modern dentistry currently uses CBCT computed tomography, which in recent years has allowed to reduce the exposure of patients towards ionizing radiation, as well as allowing an optimal virtual planning of the implant surgery, avoiding the possibility of the surgeon injuring the main vascular and nervous structures, and optimizing the design and construction phases of the dental prosthesis.

The digital model is able to provide substantial information for the clinician, therefore, both complex surgeries and less invasive local therapies can be easily planned. A virtuous example of the use of digital flow in dentistry is that of images obtained with CBCT applied to endodontics. The main cause of failure of root canal therapy is the difficulty in correctly visualizing all the channels present in the root region of the element to be treated. It is often not easy to obtain correct information and a thorough knowledge of root canal anatomy using traditional radiographic investigations.

In conclusion, the most important clinical advantages of digital data analysis, whether acquired through intraoral scanners or computed tomography, is that the digital process is repeatable, predictable and less subject to operator error, although it involves all the main participants of the therapeutic process: dentists, surgeons, implants surgeons, prosthetists, dental technicians and, above all, the patient (Fig. 1).

In the case of impression materials, the digital process has proven not to be vulnerable to errors associated with dimensional variations of the materials, instead these errors are very frequent in traditional impressions.

In our literature analysis, the results have clearly suggested that digitization of processes in dentistry, from digital dental impression to morphology analysis of dental canals, offers a higher success rate compared to conventional techniques, and

this advantage is all independent of the operator's clinical experience or the patient's oral condition. Therefore, the future of dentistry will be increasingly oriented towards new technologies, in order to have a predictable and minimally invasive diagnostic and therapeutic pathway, with strategic attention to the biomedical processes that will guide the new era of dental sciences.

REFERENCES

1. Tatullo M, Marrelli M, Scacco S, et al. Relationship between oxidative stress and "burning mouth syndrome" in female patients: a scientific hypothesis. Eur Rev Med Pharmacol Sci 2012; 16(9):1218-21.
2. Inchingolo F, Tatullo M, Abenavoli FM, Marrelli M, Inchingolo AD, Inchingolo AM, Dipalma G. Non-Hodgkin lymphoma affecting the tongue: unusual intra-oral location. Head Neck Oncol 2011; 3:1. doi: 10.1186/1758-3284-3-1.
3. Inchingolo F, Tatullo M, Abenavoli FM, Marrelli M, Inchingolo AD, Gentile M, Inchingolo AM, Dipalma G. Non-syndromic multiple supernumerary teeth in a family unit with a normal karyotype: case report. Int J Med Sci 2010; 7(6):378-84 doi:10.7150/ijms.7.378
4. Marrelli M, Tatullo M, Dipalma G, Inchingolo F. Oral infection by Staphylococcus aureus in patients affected by White Sponge Nevus: a description of two cases occurred in the same family. Int J Med Sci 2012; 9(1):47-50.
5. Marrelli M, Falisi G, Apicella A, et al. Behaviour of dental pulp stem cells on different types of innovative mesoporous and nanoporous silicon scaffolds with different functionalizations of the surfaces. J Biol Regul Homeost Agents 2015; 29(4):991-7.
6. Tatullo M, Falisi G, Amantea M, Rastelli C, Paduano F, Marrelli M. Dental pulp stem cells and human periapical cyst mesenchymal stem cells in bone tissue regeneration: comparison of basal and osteogenic differentiated gene expression of a newly discovered mesenchymal stem cell lineage. J Biol Regul Homeost Agents 2015; 29(3):713-8.
7. Paduano F, Marrelli M, Palmieri F, Tatullo M. CD146 Expression Influences Periapical Cyst Mesenchymal Stem Cell Properties. Stem Cell Rev 2016; 12(5):592-603.
8. Perniconi B, Coletti D, Aulino P, et al. Muscle acellular scaffold as a biomaterial: effects on C2C12 cell differentiation and interaction with the murine host environment. Front Physiol 2014; 5:354.
9. Marrelli M, Pujia A, Palmieri F, et al. Innovative approach for the in vitro research on biomedical scaffolds designed and customized with CAD-CAM technology. Int J Immunopathol Pharmacol 2016; 29(4):778-83.
10. Marrelli M, Gentile S, Palmieri F, Paduano F, Tatullo M. Correlation between Surgeon's experience, surgery complexity and the alteration of stress related physiological parameters. PLoS One 2014; 9(11):e112444.
11. Tatullo M, Simone GM, Tarullo F, et al. Antioxidant and antitumor activity of a bioactive polyphenolic fraction isolated from the brewing process. Sci Rep 2016; 6:36042.
12. Tatullo M, Gentile S, Paduano F, Santacroce L, Marrelli M. Crosstalk between oral and general health status in e-smokers. Medicine (Baltimore) 2016; 95(49):e5589.

LETTER TO THE EDITOR

IMMUNOHISTOCHEMICAL STUDY OF OSTEOPONTIN IN ORAL SQUAMOUS CELL CARCINOMA ALLIED TO FRACTAL DIMENSION

G. D'ADDAZIO[1], L. ARTESE[1], T. TRAINI[1], C. RUBINI[2], S. CAPUTI[1] and B. SINJARI[1]

[1]Department of Medical, Oral and Biotechnological Sciences, University "G. d'Annunzio" Chieti-Pescara, Chieti, Italy; [2]Department of Pathology, Polytechnic University of the Marche, Ancona, Italy

Received January 9, 2018 – Accepted June 6, 2018

The aim of the study was to consider a possible correlation between the intensity of expression of osteopontin and grading established by the pathologist. Furthermore, a correlation was investigated between the increase of fractal dimension and osteopontin in order to use this marker as an early and reliable diagnostic tool for the degree of cell transformation in oral squamous carcinoma. Ten histologically healthy oral samples and sixty-four primary oral squamous cell carcinomas specimens were analysed by a single pathologist. Immunohistochemical analysis and Fulgen stain were performed in order to evaluate intensity of expression of osteopontin and fractal dimension. Data obtained were presented as mean and standard deviation and processed for the statistical analysis. Ostepontin expression revealed a statistical significance between groups ($P < 0.001$). Fractal dimension in oral squamous cell carcinoma groups *vs* controls revealed statistically significant differences ($P < 0.001$). The fractal dimension value and the osteopontin expression were compared, using two-dimensional scatter. The correlation was relevant in the G3 group. The results demonstrated a correlation between the growths of osteopontin expression and nuclear abnormality measured by fractal dimension. These results support the hypothesis that the level of osteopontin expression might be used as a marker for the evaluation of oral squamous cell carcinoma differentiation. Osteopontin and fractal dimension could support the histological grading to increase the predictability of the diagnosis, choices of treatment procedure and long-term prognosis.

To the Editor,

Oral squamous cell carcinoma (OSCC) is the most common type of oral malignancy and represents more than 90% of oral carcinomas (1). OSCC is diagnosed by the means of histological observation that represents only a measure of morphological alterations in a specific area visualized by the pathologist. A prognostic factor based on cellular pleomorphism or immunohistochemical biomarkers could therefore be necessary (2). During the past decade, emerging evidence underlined the importance of osteopontin (OPN) as a candidate biomarker and target for cancer therapy (3). OPN is a protein of extracellular matrix (ECM) that play a critical role in several normal and pathological processes, including cell proliferation, attachment, invasion, migration, bone formation and remodelling, inflammation, cellular transformation and metastasis (4). OPN is synthesized by various cell types and acts by binding specific receptors, mainly integrins containing the alpha subunit V. OPN is a sialoprotein, chemokine-like part of the family of the small integrin binding ligand N-linked glycoprotein (SIBLING) which contains several members used as markers of early

Key words: *oral squamous cell carcinoma, osteopontin, fractal dimension, immunohistochemistry, early diagnosis*

Mailing address:
Dr. Gianmaria D'Addazio DDS,
Via Dei Vestini, 31
66100 Chieti (CH), Italy
Tel.: +39 3208058797
Fax: +39 08713554148
e-mail: gianmariad@gmail.com

0393-974X (2018)
Copyright © by BIOLIFE, s.a.s.
This publication and/or article is for individual use only and may not be further reproduced without written permission from the copyright holder.
Unauthorized reproduction may result in financial and other penalties
DISCLOSURE: ALL AUTHORS REPORT NO CONFLICTS OF INTEREST RELEVANT TO THIS ARTICLE.

cancer progression, according to their potentials in regulating the activity of matrix metalloproteinases (MMPs). In breast, stomach and prostate cancer, high expression levels of OPN have been associated with poor prognosis (4). In recent times, also OPN is being considered, in head and neck cancer, as one of the most investigated biomarkers. (5) Among the various methods for cancer diagnosis in medicine there is also the fractal dimension (FD) which help the pathologist in the histomorphometrical classification and morphological description of the tumour variability. Several studies have investigated FD in relation to tumour alterations in several areas (6). Therefore the objective of the present study was to establish a strict correlation between the intensity of OPN expression and grading established by the pathologist in order to use this marker as an early and reliable diagnostic tool. Also the fractal dimension, as mentioned, has been correlated with cellular alterations in OSCC. In this regard, a correlation was investigated between the increase of DF and OPN to better define the usefulness and diagnostic accuracy. Further understanding could facilitate the prognostic phases and the development of therapeutic strategies.

MATERIALS AND METHODS

Ten histologically normal oral samples and 64 primary oral squamous cell carcinomas specimens (OSCC) were obtained from biopsies of patients diagnosed and treated by the Department of Pathology, Polytechnic University of the Marche, Ancona, Italy. The experiments were undertaken with the understanding and written consent of each subject to use the tissues for research purposes and according to ethical principles, including the World Medical Association Declaration of Helsinki.

The collected samples were successively analysed by the Department of Medical, Oral and Biotechnological Sciences, University 'G. d'Annunzio' Chieti-Pescara, Chieti, Italy. All patients enrolled in this study had an OSCC clinical history and available histology paraffin material.

Of the 64 patients with OSCC (test group), 49 were males and 15 females, while in the control group 3 were male and 7 females. The mean age was 63.6±12.8 years and 50.0±21.9 years for OSCC and control groups, respectively. All available Hematoxylin-Eosin sections were reviewed by a pathologist in order to confirm the correct diagnosis, and to select the neoplastic areas. Three micron thick sections from each specimen were obtained and placed on super frost plus-coated glass slides (Menzel-Gläser, Braunschweig, Germany). One section, stained with hematoxylin–eosin, was used for pathological re-evaluation, another was stained with Feulgen stain for evaluation of the nuclei and the third was stained with immunohistochemical stain to evaluate the expression of OPN. Under light microscopy, the specimens were staged according to the tumour grading system proposed by Anneroth's criteria as: G1 (well differentiated), G2 (moderately differentiated), G3 (poorly differentiated) OSCC (4). Histological material of 10 patients randomly selected and treated for non-neoplastic lesions were used as controls.

Nuclear fractal dimension

The procedures for the evaluation of the fractal dimension have been extensively described in a previous work (7). Briefly, for standard nuclear histomorphometry, three representative high power fields (HPF) (40x) of Feulgen stains were randomly selected and photographed from each biopsy. The images were captured with a digital CCD-videocamera and were stored as high quality TIFF files. The above-mentioned image files were automatically transformed to binary images using ImageJ 1.40g (Wayne Rasband, National Institute of Health, Bethesda, MD, USA). After selecting a 4.3 x 4.3 cm area on each image, the fractal dimension (FD) was estimated by using the box-counting method by means of ImageJ 1.40g (Wayne Rasband, National Institute of Health, Bethesda, MD, USA).

Immunohistochemical expression of osteopontin

The specimens were immunohistochemically analysed. Specifically, the immunohistochemical staining of OPN was performed using the strep-ABC (Streptavidine-Biotine-Peroxidase) method. Three micron sections were cut and mounted on poly-L-lysine-coated slides. Paraffin sections were dewaxed by xylene, rehydrated and finally washed in PBS (pH 7.4) for 10 min. In order to unmask the antigens, a microwave oven and a 2.1% content of citric acid was used related to the antibodies. The subsequent steps were optimized by automatic staining (Optimax, BioGenex, San Ramon, CA, USA). Sections were incubated with

primary antibody for 30 min at room temperature. Slides were rinsed in buffer, and immunoreaction was completed with the Strep-ABC-Peroxidase method, applying the "Super sensitive immunodetection" kit by BioGenex (San Ramon, CA, USA) and utilizing a multi-link as a secondary biotinilated antibody. After incubation with a chromogen employing "liquid DAB substrate pack" (BioGenex, San Ramon, CA, USA), the specimens were counterstained with Mayer's hematoxyline and coverslipped.

The intensity of expression of OPN was evaluated in 5 random fields at 20X magnification. Two different intensity of expressions for each sample were automatically identified by the use of a dedicated software (LEICA QWIN) connected to an optical microscope (LEICA DMR). The software was set up to identify in standard and reproducible conditions (microscope light and camera set-up), two different colour ranges shown by immunohistochemical stain in order to automatically identify two different classes of intensity of expression. It was possible to quantify areas of high intensity of expression and areas of low expression of OPN. Finally, the software automatically calculated the area as percentage value.

Statistical analysis

Data were presented as means and standard deviations (SD). Analysis of variance (ANOVA) was used to evaluate differences between mean values. The Kruskal–Wallis test was used to evaluate differences between FD values and OPN values after stratification of the cases based on histological grading. Moreover, in order to investigate differences between single groups a multiple comparison procedure (Dunn's Method) was performed. Statistical significance was set to p=0.05. To consider a possible correlation between grading, fractal dimension and expression of the OPN, the Pearson product-moment correlation coefficient, using the SPSS v. 16.0 software, was carried out in the same fields. Priority, a representation of FD and intensity of expression of OPN, without considering the degree of differentiation established by the pathologist, was made. Then, it was repeated to separate the different tumor grading.

RESULTS

Analysis of hematoxylin and eosin images revealed the diagnosis and the degree of differentiation of the tumors: no alteration (controls), well-differentiated OSCC (G1), moderately differentiated OSCC (G2) and poorly differentiated OSCC (G3).

The fractal dimension presented the following mean values: 1.15 for the control group, 1.30 for the G1 group, 1.41 for the G2 group, and 1.61 for the G3 group, with statistically significant differences in FD value between the test group and controls ($p<0.01$). A statistically significant difference was found between the three groups ($P < 0.001$, Kruskal–Wallis test). For the multiple comparison procedure, Dunn's method was performed, finding statistically significant differences ($p<0.05$) (Table I).

In all samples, the intensity areas classified as low expression were: 16.94% (G1), 21.74% (G2) and 3.92 % (G3). Meanwhile the high expression of OPN

Table I. *FD and OPN multiple comparison procedure, Dunn's method.*

Comparison	**Diff of Ranks**	**Q**	**P<0.05**
FD G3 *vs* FD G1	191.372	12.312	Yes
FD G3 *vs* FD G2	112.480	7.468	Yes
FD G2 *vs* FD G1	78.892	6.968	Yes
Comparison	**Diff of Ranks**	**Q**	**P<0.05**
HIGH G3 *vs* HIGH G1	210.332	13.531	Yes
HIGH G3 *vs* HIGH G2	104.457	6.935	Yes
HIGH G2 *vs* HIGH G1	105.875	9.351	Yes
LOW G2 *vs* LOW G3	172.200	11.433	Yes
LOW G2 *vs* LOW G1	48.465	4.280	Yes
LOW G1 *vs* LOW G3	123.735	7.960	Yes

Statistical significant differences were found p<0.05

Table II. *Pearson product-moment correlation coefficient calculated between values of intensity of expression of OPN and fractal dimension in histological grading G3.*

		Fractal Dimension	**Osteopontin**
	Pearson's correlation	1	0.764
Fractal Dimension	Sig. (2-code)		0.010
	N	10	10
	Pearson's correlation	0.764	1
High Osteopontin	Sig. (2-code)	0.010	
	N	10	**10**

A statistical significant correlation was found in G3 ($P < 0.05$).

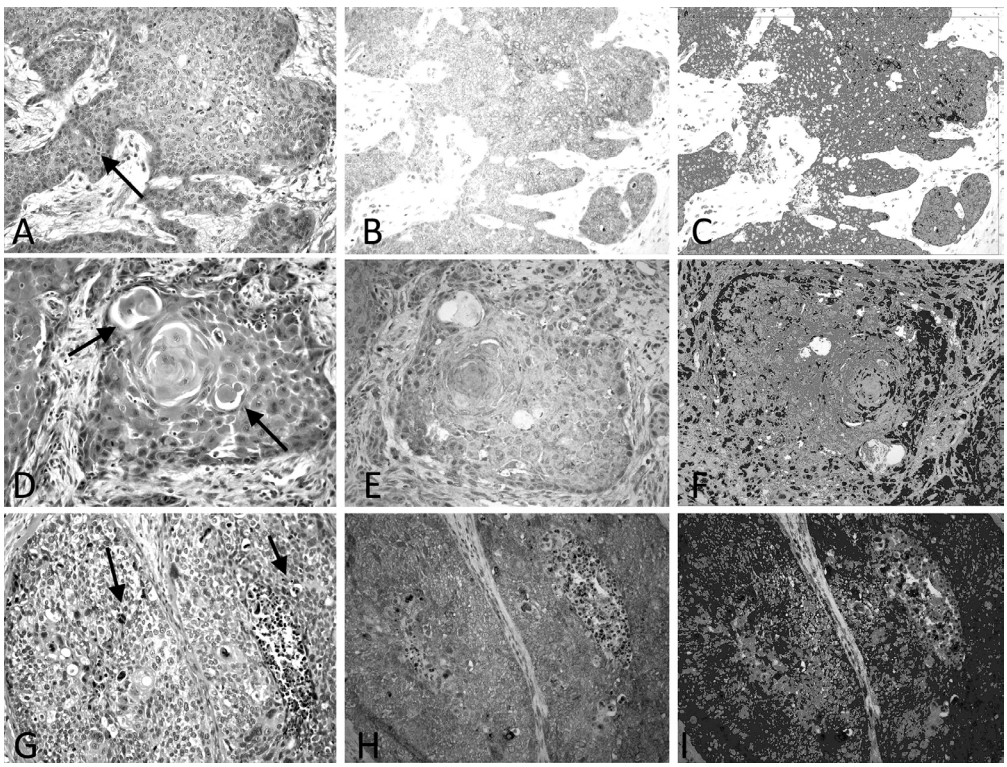

Fig. 1. ***A)*** *OSCC well differentiated, G1. Only few cellular atypia. Nuclei with elongated shape and hyperchromic. (H&E 20x magnification);* ***B)*** *OSCC well differentiated, G1 (strep-ABC 20x magnification);* ***C)*** *OSCC well differentiated, G1. In light grey, low level of OPN expression. In dark grey, high level of OPN expression (software analysis 20x magnification).* ***D)*** *OSCC moderately differentiated, G2. The cellular transformations and the number of mitoses increase. Formation of corneal pearls (H&E 20x magnification);* ***E)*** *OSCC moderately differentiated, G2 (strep-ABC 20x magnification);* ***F)*** *OSCC moderately differentiated, G2. In light grey, low level of OPN expression. In dark grey, high level of OPN expression (software analysis 20x magnification).* ***G)*** *OSCC poorly differentiated, G3, numerous cellular atypia. high number of mitosis, altered cellular architecture, numerous hyperchromic nuclei. (H&E 20x magnification);* ***H)*** *OSCC poorly differentiated, G3 (strep-ABC 20x magnification);* ***I)*** *OSCC poorly differentiated, G3. In light grey, low level of OPN expression. In dark grey, high level of OPN expression (software analysis 20x magnification).*

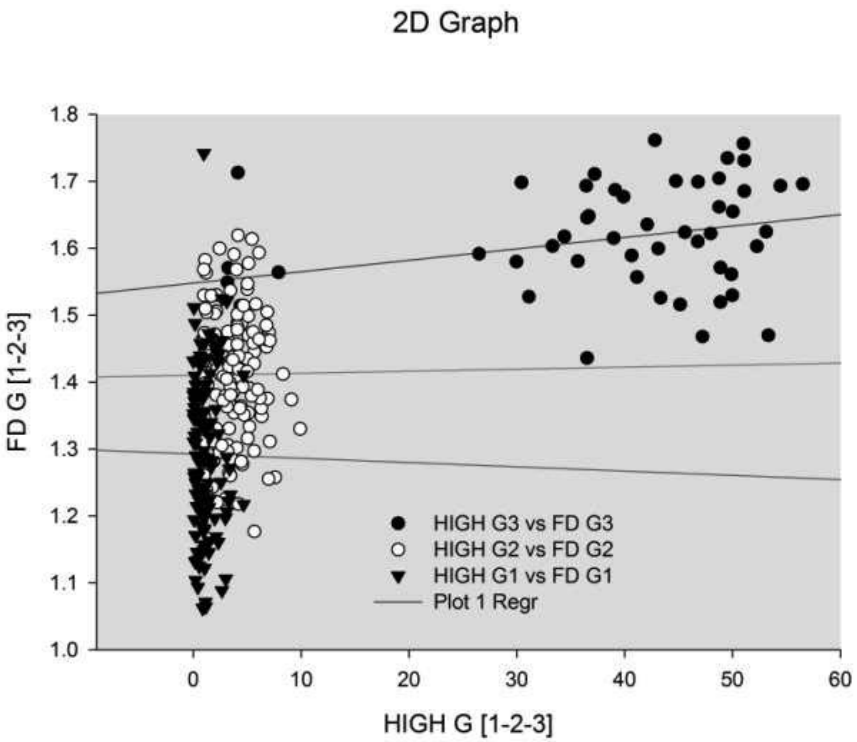

Fig. 2. *Two-dimensional graphical representation of the correlation between intensity of expression of OPN (x-axis) and the FD (y-axis).*

was: 1.30% (G1), 3.66% (G2) and 38.90% (G3). The image shows expression of OPN in different degree of differentiation (Fig. 1). Furthermore, a statistical significance between the three groups was found in both low and high intensity of expression, ($P < 0.001$, Kruskal–Wallis test). The multiple comparison procedure, Dunn's method was performed, finding statistically significant differences ($p<0.05$), as shown in Table I.

A graphical representation of FD value and the OPN expression using two-dimensional scatter was made, without considering the degree of differentiation (Fig. 2). Results were diffused, without significant relevance. The correlation between the two variables was more visually considerable when it was divided by tumor grading, especially in the G3 group, represented in Fig.2 as a black circle.

In the other two groups the data were more diffused and, therefore, the degree of correlation was not graphically evident.

For the graphical representation, Pearson product-moment correlation coefficient was calculated (Table II), and the results demonstrated that the correlation was statistically significant in the G3 group ($P<0.05$).

DISCUSSION

The main problems of the grading system were due to possible pathologist's errors. Grading could be different in different fields of analysis, or with different pathologists. Furthermore, characteristics related to the progression and the pattern of invasion may be missing. Studies indicated the correlation between OPN and systemic malignancies such as breast cancer, non-small cell lung cancer, esophageal squamous cell carcinoma (SCC), laryngeal SCC and prostate cancer (8). Furthermore Yu-Wei Chiu at al. in 2010 proposed a significant relationship between OPN expression and oral carcinogenesis (9). Other studies have investigated the role of OPN in OSCC. Subramani et al. in 2015 studied the presence of OPN in the margins of surgical resection. They showed a higher percentage of recurrence in samples where the margins showed high levels of OPN (10). Thus,

the present results suggest the direct involvement of OPN in the differentiation of neoplastic cells, in their transformation and invasion of surrounding tissues. A comparable growth in OPN expression with histological increasing grades has been reported in oral dysplasias and in laryngeal dysplasias. The high expression of OPN indicates that OPN expression may present an early event in tumor progression (11). The use of objective evaluation of OPN related to histological grading was suggested to improve clinical outcome, prognosis and survival parameters. Finally, OPN could be used in alternatives or in association with grading to clarify the pathological stage of the biopsy. In addition, a correlation between OPN and DF values was proposed. Mincione et al. in 2015, studied the correlation between the patient's survival and the value of FD (7).

Only a few other studies have identified a possible correlation between DF and OSCC (12). From our results it was possible to correlate the nuclear abnormality measured by FD with the OPN expression. Therefore, a direct correlation between the two variables allows us to state that both tools presented can be added during biopsies to the grading of OSCC, increasing the predictability of the diagnosis, choices of treatment procedure and long-term prognosis of OSCC.

However, further investigations could be necessary to better understand the correlation between the OPN expression and cell alteration.

REFERENCES

1. Choi S, Myers JN. Molecular pathogenesis of oral squamous cell carcinoma: implications for therapy. J Dent Res 2008; 87(1):14-32.
2. Sawazaki-Calone I, Rangel A, Bueno AG, et al. The prognostic value of histopathological grading systems in oral squamous cell carcinomas. Oral Dis 2015; 21(6):755-61.
3. Weber GF. The cancer biomarker osteopontin: combination with other markers. Cancer Genomics Proteomics 2011; 8(6):263-88.
4. Furger KA, Menon RK, Tuck AB, Bramwell VH, Chambers AF. The functional and clinical roles of osteopontin in cancer and metastasis. Curr Mol Med 2001; 1(5):621-32.
5. Chien CY, Su CY, Chuang HC, et al. Comprehensive study on the prognostic role of osteopontin expression in oral squamous cell carcinoma. Oral Oncol 2009; 45(9):798-802.
6. Pribic J, Vasiljevic J, Kanjer K, Konstantinovic ZN, Milosevic NT, Vukosavljevic DN, Radulovic M. Fractal dimension and lacunarity of tumor microscopic images as prognostic indicators of clinical outcome in early breast cancer. Biomark Med 2015; 9(12):1279-97.
7. Mincione G, Di Nicola M, Di Marcantonio MC, et al. Nuclear fractal dimension in oral squamous cell carcinoma: a novel method for the evaluation of grading, staging, and survival. J Oral Pathol Med 2015; 44(9):680-84.
8. Donati V, Boldrini L, Dell'Omodarme M, et al. Osteopontin expression andprognostic significance in non-small cell lung cancer. Clin Cancer Res 2005; 11(18):6459-65.
9. Chiu YW, Tu HF, Wang IK, Wu CH, Chang KW, Liu TY, Kao SY. The implication of osteopontin (OPN) expression and genetic polymorphisms of OPN promoter in oral carcinogenesis. Oral Oncol 2010; 46(4):302-6.
10. Subramani VN, Narasimhan M, Thiyagarajan M, Munuswamy BD, Jayamani L. Expression of osteopontin in oral squamous cell carcinoma and its surgical margins-an immunohistochemical study. J Clin Diagn Res 2015; 9(11):ZC66-9.
11. Staibano S, Merolla F, Testa D, et al. OPN/CD44v6 overexpression in laryngeal dysplasia and correlation with clinical outcome. Br J Cancer 2007; 97(11):1545-51.
12. Yinti SR, N S, Boaz K, Lewis AJ, Ashokkumar PJ, Kapila SN. Nuclear fractal dimensions as a tool for prognostication of oral squamous cell carcinoma. J Clin Diagn Res 2015; 9(11):EC21-5.

JOURNAL OF BIOLOGICAL REGULATORS & HOMEOSTATIC AGENTS Vol. 32, no. 4, 1039-1043 (2018)

LETTER TO THE EDITOR

PERFOMANCE ASSESSMENT OF A FULLY AUTOMATED ELECTRO-CHEMILUMINESCENCE IMMUNOASSAY SYSTEM FOR SERUM S100B PROTEIN

E. ANASTASI, G. GENNARINI, C. DEL MONTE, B. COLAPRISCA, S. TARTAGLIONE, C. DI SEGNI and A. ANGELONI

Department of Molecular Medicine, Policlinico Umberto I, Sapienza University of Rome, Rome, Italy

Received September 12, 2017 – Accepted March 6, 2018

The altered expression levels of S100 proteins can lead to four different categories of diseases: diseases of the heart and of the central nervous system, inflammatory disorders and cancer. Various studies have shown the lack of harmonization of the results obtained with different methods, mainly due to different performances and measurements of S100B. The purpose of this work was to compare quantitatively the fully automated Elecsys® immunoassay with the reference immunoenzimatic method CanAg® EIA for serum S100B protein. In the study serum samples were analyzed of 161 patients: 85 females (aged 22-83 years) and 76 males (aged 16-90 years), affected by oncological and non-oncological pathologies. Passing–Bablok regression was used to analyze the comparison between the assays; it showed a strong interassay correlation: r = 0.9350 (95% CI =0.9122 – 0.9520), with an intercept of 0.02063 (95% CI=-0.02850 – 0.01400) and a slope of 1.1125 (95% CI=1.0200 – 1.2417). Elecsys® S100 assay should be preferred to CanAg® S100 for better standardization, good reliability and precision but also with the aim to reduce costs and obtain results in a shorter time.

To the Editor,

The S100 protein family has more than 20 members and its name is due to the property of being soluble in 100% saturated ammonium sulfate at neutral pH (1).

It is known that different S100 proteins are involved in tumor growth, metastasis, angiogenesis and immune evasion, but also in tumor suppression (2). Many studies have shown that in non-small cell lung cancer, gastric cancer and lymphoma there are high levels of S100A2 (3). Regarding the role of S100 in pathologies of the central nervous system (CNS), an important function is performed by S100B. Muller published a study in which was a potential role of S100B evaluated as a marker of traumatic brain injury with the aim to improve the patient triage in the emergency room and decrease the number of cranial computed tomographies (CTs) performed (4).

Other studies, proved how serum S100B level is an important and useful marker in melanoma, especially in the late stages of the disease, and for the staging and prognosis of patients with metastatized disease (5). A meta-analysis by Mocellin propose that S100B could have a central role in the therapy and follow-up of this disease, and according to other authors it can be used to evaluate the individual risk before administration of adjuvant treatment and the response to induction therapy for nodal disease (6-7).

Various studies have shown the lack of

Key words: tumor marker, cancer, electro chemiluminescence immunoassay (ECLIA)

Mailing address:
Dr Emanuela Anastasi,
Department of Molecular Medicine,
University "Sapienza", Viale Regina Elena 324,
00161 Rome, Italy
Tel.: +39 064472347
e-mail: emanuela.anastasi@uniroma1.it

0393-974X (2018)
Copyright © by BIOLIFE, s.a.s.
This publication and/or article is for individual use only and may not be further reproduced without written permission from the copyright holder.
Unauthorized reproduction may result in financial and other penalties
DISCLOSURE: ALL AUTHORS REPORT NO CONFLICTS OF INTEREST RELEVANT TO THIS ARTICLE.

harmonization of the results obtained with different methods, mainly due to dissimilar performances and measurements of S100B (8-9). S100B can be measured by several methods such as immunoradiometric, chemiluminescence, electrochemiluminescence or enzymatic immunoassays (10).

The aim of this work was to evaluate and compare the performance and the reproducibility of two different methods used for S100B detection. We matched the manual enzyme immunoassay (EIA) (CanAg S100), already in use in our laboratory, with a fully automated analyzer based on electro-chemiluminescence immunoassay (ECLIA) (Elecsys S100) independently of the clinical condition of patients.

MATERIALS AND METHODS

For this prospective study 161 patients were selected: 85 females (aged 22-83 years), and 76 males (aged 16-90 years) affected by oncological (malignant melanoma, glioma) and non-oncological pathologies, enrolled consecutively in the period from January 2015 to February 2016. The study was approved by the institutional board. The blood samples were collected in a Red Top Vacutainer, centrifuged at 3500 rpm for 15 min and separated. Subsequently, serum aliquots were stored at -80°C until assay. Samples were thawed only once for both methods. All blood samples were analyzed in the Laboratory of Tumor Markers (Policlinico Umberto I, Sapienza University of Rome).

Serum samples were evaluated by two different methods, CanAg® S100 EIA (Fujirebio Diagnostics, AB., Göthenburg, Sweden), a manual immunoenzimatic method routinely used in our laboratory, and Elecsys® S100 (Roche Diagnostics, Penzberg, Germany) which is an ECLIA fully-automated analyzer. All assays were performed according to the manufacturers' instructions and the cut-off of normality used was 0.10 ng/mL for CanAg and 0.105 ng/mL for Elecsys, based on the 95% confidence interval.

The precision of Elecsys® S100 was evaluated by testing three serum pools routinely referred to our laboratory with respectively low, medium and high values of S100.

Assessment by EIA

The CanAg® S100 is a solid phase two-step non-competitive enzyme-immunometric assay, based on the use of two mouse monoclonal antibodies specific for two different epitopes expressed in S100B. Calibrators and patient samples are added in streptavidin-coated microstrips together with biotinylated anti-S100B monoclonal antibody (Mab S23) and incubated for two hours. Subsequently the microplate is washed and then a second monoclonal antibody labelled with horseradish peroxidase (HPR) is added.

The microplate was incubated for 1 h, and after washing, a chromogenic substrate (TMB) was added to each well; during 30 min of incubation the enzyme reaction starts with development of blue colour. After addition of a Stop Solution, the colour changes from blue to yellow, and the intensity determined by a spectrophotometer at 405 nm, is directly proportional to the concentration of antigen present in the sample. Calibration curve is constructed by plotting absorbance value *versus* the concentration for each calibrator. The manufacturer declares a detection limit (LOD) = 0.010 ng/mL and measurement range (lower end defined LOD) from 0.010 to 3.5 ng/mL .

Assessment by Elecsys®

Elecsys® S100 is a fully- automated sandwich immunoassay in ECLIA. The test begins with the incubation of the serum samples with two monoclonal S100B specific antibodies, one of which is biotinylated and the other is labeled with a ruthenium complex to make a sandwich complex. After addition of streptavidin-coated microparticles the complex binds to the solid phase through the interaction of biotin and streptavidin.

The microparticles are magnetically captured on the electrode surface and application of a voltage to the electrode induces chemiluminescent emission which is measured by a photomultiplier. Results are determined via a calibration curve which is instrument-specifically generated by 2-point calibration and a master curve provided through the reagent barcode. The light signal is directly proportional to the concentration of antigen S100B present in the sample**.** The manufacturer declares a detection limit (LOD) = < 0.005 ng/mL and mesurament range (lower end defined LOD) from 0.005 to 39 ng/mL

Statistical analysis

All analyses were performed using MedCalc® statistical software version 15.8. (MedCalc Software bvba, Ostend, Belgium).

Comparison between CanAg® S100 and Elecsys® S100

was performed evaluating Passing-Bablok regression, which is a robust, non-parametric statistical method and is not sensitive to outliers or the distribution of errors (11).

Comparison studies were also carried out using Bland-Altman and Mountain plot. Bland-Altman shows the difference in measurement between the two methods, allowing estimates of bias with corresponding confidence interval (CI); Mountain plot is a complementary representation of the difference plot and shows distribution of the differences in measurement between two methods.

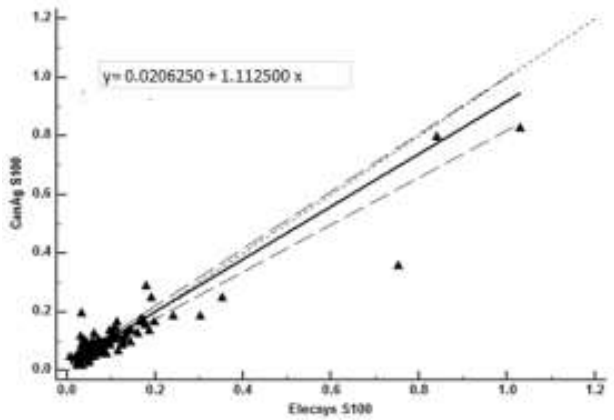

Fig. 1. *Passing-Bablok regression analysis shows the value of slope of 1. 1125 (95% CI=1.0200 to 1.2417) and intercept of 0.02063 (95% CI=-0.02850 to 0.01400). The formula for the regression line of the relation among CanAg and Elecsys is Y = -0.0206250 + 1.112500 X.*

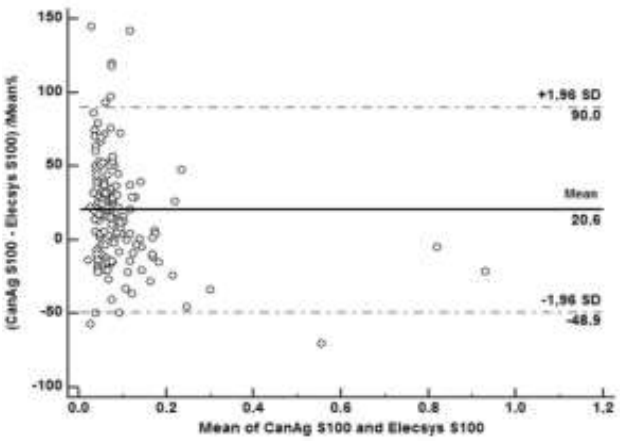

Fig. 2. *Bland-Altman difference plot of the relative differences between the Elecsys and CanAg methods for the determination of S100 protein. The x–axis represents the average of measures as the best estimate of the true value, while the y-axis the difference of these measures.*

RESULTS

The range values of protein S100B obtained with CanAg is between 0.020 – 0.83 ng/mL and with Elecsys is between 0.008 - 1.030 ng/mL. The two methods compared showed a strong interassay correlation: r = 0.9350 (95% CI =0.9122 – 0.9520), with an intercept of 0.02063 (95% CI=-0.02850 – 0.01400) and a slope of 1.1125 (95% CI=1.0200 – 1.2417) which respectively represent the constant and proportional systematic error with a CI based on 999 bootstrap samples. The formula for the regression line of the relationship between the two methods analyzed was: Y = -0. 0206250 + 1.112500 X where X = CanAg value (Fig. 1).

Other comparative studies were carried out with Mountain plot (Fig. 2) and Bland-Altman difference plot that showed a mean difference of 20.6% (95% limit of agreement = -48.9–90%) (Fig. 3).

In this study the precision Intra-Inter assay of Elecsys S100 testing pool of sera was also evaluated from routine samples referred to our laboratory; the results were expressed as coefficient of variation % (CV).

The Intra-assay precision was evaluated by examining, in a same session, three levels of pool of sera (low, intermediate, high S100B) in three duplicates each. The mean results were: 0.077 (SD= 0.006, CV=8.3%); 0.098 (SD= 0.0062, CV=6.4%); 0.254 (SD= 0.0442, CV=17.4%), respectively.

The Inter-assay precision was obtained by assaying three serum pool replicates (low, intermediate, high S100B) in three different runs. The mean results were: 0.074 (SD=0.0054, CV=7.3%); 0.098 (SD=0.0050, CV=0.5%); 0.253 (SD=0.0352, CV=12.9%), respectively.

DISCUSSION

Protein S100B is a member of the S100 family of EF-hand calcium-binding proteins involved in several pathologies, such as neurological and

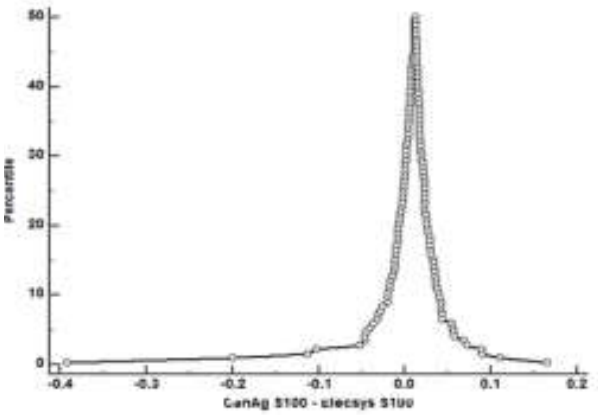

Fig. 3. *Mountain plot shows the distribution of measurement differences for the determination of S-100 protein; between the electro-chemiluminescent immunoassay Elecsys and CanAg immunoenzimatic assay, our reference method.*

oncological diseases (1). Many studies have shown a prognostic value of S100B protein in patients with ischemic stroke or brain tumors (12-13). According to several authors, this protein can be helpful also in mild brain injuries, therefore S100 B serum detection could decrease the number of cranial CTs performed on adult patients (14-15).

The main relevance of S100B, however, is in oncological diseases, such as melanoma and glioma, in particular it is largely used in the prognosis and follow up of malignant melanoma (5). The S100B protein in the post-surgical follow-up is considered the most reliable serum marker to date to improve melanoma staging and shows a prognostic significance for the survival of the patient (5) .

Due to the lack of harmonization of the results obtained with different methods, the current work was conceived to compare Elecsys® assay with the gold standard CanAg® EIA. The Elecsys® S100 (Roche Diagnostics, Penzberg, Germany) is a fully automated analyzer based on ECLIA while our reference method CanAg® S100 (Fujirebio Diagnostics, AB, Göthenburg, Sweden) is a manual immunoenzimatic method.

This comparison study performed with Passing and Bablok regression showed a strong agreement between Elecsys® and CanAg® (r= 0.9350).

This study also showed that Elecsys® S100 allows a better standardization and has good reliability, also due to its precision observed in the analysis of serum pool.

In conclusion Elecsys® S100 assay should be preferred to CanAg® S100 with the aim to reduce costs due its capacity to determinate a great number of samples with small amount of reagents, and with the intent to obtain more rapid and standardized results in a shorter time, indeed Elecsys® S100 provides results in just 18 minutes.

ACKNOWLEDGEMENTS

This study was supported by the University of Rome Sapienza. The authors are grateful to Valentina Viggiani, Lorenzo Fagiolo and Silvestra Tudini for their excellent technical assistance.

REFERENCES

1. Moore BW. A soluble protein characteristic of the nervous system. Biochem Biophys Res Commun 1965; 19:739-44.
2. Bresnick AR, Weber DJ, Zimmer DB. S100 proteins in cancer. Nat Rev Cancer 2015; 15:96-109.
3. Hsieh H-L, Schäfer BW, Sasaki N, Heizmann CW. Expression analysis of S100 proteins and RAGE in human tumors using tissue microarrays. Biochem Biophys Res Commun 2003; 307:375-81.
4. Muller K, Elverland A, Waterloo K, Langbakk. Analysis of protein S-100B in serum?: a methodological study. Clin Chem Lab Med 2006; 44:1111-14.
5. Kruijff S, Hoekstra HJ. The current status of S-100B as a biomarker in melanoma. Eur J Surg Oncol 2012; 38:281-85.
6. Mocellin S, Zavagno G, Nitti D. The prognostic value of serum S100B in patients with cutaneous melanoma: a meta-analysis. Int J cancer 2008; 123:2370-76.
7. Kruijff S, Bastiaannet E, Kobold AC van Ginkel RJ, Suurmeijer AJ, Hoekstra HJ. S-100B concentrations predict disease-free survival in stage III melanoma patients. Ann Surg Oncol 2009; 16(12):3455-62.

8. Laribi S, Kansao J, Borderie D, et al. S100B blood level measurement to exclude cerebral lesions after minor head injury?: the multicenter STIC-S100 French study. Clin Chem Lab Med 2014; 52:527-36.
9. McLawhon RW. Patient safety and clinical effectiveness as imperatives for achieving harmonization inside and outside the clinical laboratory. Clin Chem 2011; 57:936-38.
10. Ingebrigtsen T, Romner B and Trumpy JH. Management of minor head injury: the value of early computed tomography and serum protein S-100 measurements. J Clin Neurosci 1997; 4:29-33.
11. Bablok W, Passing H, Bender R, Schneider B. A general regression procedure for method transformation. Application of linear regression procedures for method comparison studies in clinical chemistry, Part III. J Clin Chem Clin Biochem 1988; 26:783-90.
12. Chełstowski K, Siennicka A, Grzelec H, Bajer-Czajkowska A, Rybicka M, Clark J, Nowacki P. The character of haemostatic disorders and level of protein S-100 in acute ischaemic stroke can affect survival in the first week of follow-up: a pilot study. Blood Coagul Fibrinolysis 2011; 22:388-95.
13. Andrés R, Mayordomo JI, Visus C, et al. Prognostic significance and diagnostic value of protein S-100 and tyrosinase in patients with malignant melanoma. Am J Clin Oncol 2008; 31:335-39.
14. Astrand R, Undén J, Romner B. Clinical use of the calcium-binding S100B protein. Methods Mol Biol 2013; 963:373-84.
15. Lippi G, Cervellin G. Diagnostic approach to the mild head trauma of the adult in Emergency Medicine: between biomarkers and imaging. Recenti Prog Med 2013; 104:120-32.

JOURNAL OF BIOLOGICAL REGULATORS & HOMEOSTATIC AGENTS Vol. 32, no. 4, 1045-1049 (2018)

LETTER TO THE EDITOR

THE USE OF CASEIN IN SPORT MOUTHGUARDS: MICROBIOLOGICAL AND ECOLOGICAL VARIATIONS IN ORAL CAVITY

D. TRIPODI, D. MARTINELLI, C. CIARAVINO, D. FULCO, M. TIERI and S. D'ERCOLE

Department of Medical, Oral and Biotechnological Sciences, University "G. D'Annunzio" of Chieti-Pescara, Chieti, Italy

Received January 25, 2018 – Accepted June 8, 2018

Sport mouthguards have the potential to become a microbial reservoir, produce oral and systemic diseases and cause negative changes in the oral cavity. The aim of this study was to monitor oral environmental changes caused by casein and sport-mouthguard *in vivo*, through clinical, salivary and bacterial markers of young athletes. Forty-eight active young athletes in different disciplines were selected and analysed at different times: baseline (T0); after three months of casein application on the mouthguard (T1); and after six months of application (T2). The product used was GC Tooth Mousse®. At T0, clinical monitoring was performed and the following parameters were recorded: Decay-Missing-Filled Teeth (DMFT) index, Plaque index (PL+) and Gingival Bleeding (BOP+). Saliva-Check Buffer GC® and Saliva-CheckMutans GC® salivary tests were then performed. At T0 the athletes demonstrated DMFT 0.03±0.01. PL value was positive in 100% of subjects at T0, T1, and T2. The BI value was always negative. At the three time-points, a significant change in baseline hydration values was observed; baseline viscosity was normal in 50% of cases while it increased in the remaining 50% at T0; it was normal and constant at T1 and T2. The value of the baseline pH underwent an not statistically significant increase at T1 (7.6±0.08) while remaining constant at T2. The amount of saliva produced after 5-min stimulation ranged significantly and gradually from T0 to T1 and T2, with a statistically significant difference. Plaque indicator tests highlighted that at T0 a plaque with a pH of 6.0±0.5 prevailed; at T1 it was 6.25±0.75 while at T2, pH was equal to 6. Tests for the detection of *S. mutans* resulted constant in all subjects at the various observation times, resulting in 67% of patients in whom *S. mutans* was present. The application of casein, within custom-made ethylene-vinyl acetate (EVA) mouthguards, positively influences salivary flow, the increase of pH values, the amount of stimulated saliva and the buffering capacity of the athlete, improving their state of oral health, which is negatively affected by the use of common mouthguards.

To the Editor,

The individual mouthguard is a soft intra-oral device made of plastic and covers the whole palate and occlusal surfaces of the teeth. It is manufactured in ethylene vinyl acetate (EVA) (1).

A factor of poor compliance by the patient is the difficult storage and cleaning of the mouthguard, which tends to accumulate plaque and debris, giving it a bad smell. Glass et al. (2) reported that "boil and bite" mouthguards harboured a range of pathogenic, opportunistic bacteria, yeasts, moulds, etc., and had the propensity to become a microbial reservoir,

Key words: mouthguards, saliva, casein, EVA material, biofilm

Mailing address:
Dr Simonetta D'Ercole,
Department of Medical, Oral
and Biotechnological Sciences
University "G. d'Annunzio" Chieti- Pescara,
Via dei Vestini, 31, 66100 Chieti, Italy
Tel.: +39 0871 3554809 - Fax: +39 0871 3554392
e-mail: simonetta.dercole@virgilio.it

0393-974X (2018)
Copyright © by BIOLIFE, s.a.s.
This publication and/or article is for individual use only and may not be further reproduced without written permission from the copyright holder.
Unauthorized reproduction may result in financial and other penalties
DISCLOSURE: ALL AUTHORS REPORT NO CONFLICTS OF INTEREST RELEVANT TO THIS ARTICLE.

and some commercially available devices were contaminated before use. Sport-mouthguards have the potential to produce oral and systemic diseases as the jagged and sharp areas of the posterior regions of typical mouthguards are in close proximity to the pterygoid plexus of veins and therefore near the entire circulatory system. D'Ercole et al. reported that custom-made mouthguards cause changes in environmental oral factors, because they increase Full Mouth Plaque Score (FMPS) and Full Mouth Bleeding Score (FMBS) and reduce the salivary buffering capacity and pH, thus inhibiting the protective effect of saliva (3). Microbiological control of saliva is easy nowadays, even in dental practice with the use of the salivary "chair-side" test (4, 5). It has been demonstrated that a mouthguard is not only a means of trauma prevention but also a vehicle for preventive substances in order to maintain oral health. Different strategies to prevent ecological changes in the oral cavity caused by the use of mouthguards are possible, as demonstrated in a study conducted with the use of chlorhexidine (6).

In the present study, it was decided to use casein inside the mouthguard, due to its many useful properties, as confirmed by the widespread use in dental practice (7, 8).

The purpose of this study was to monitor the possible ecological changes of the oral cavity by the determination of salivary and bacterial clinical markers at baseline, 3 months and 6 months after treatment, where casein was applied in the mouthguard, making use of salivary chair-side tests.

MATERIALS AND METHODS

Patient selection

Forty-eight young male athletes aged between 10 and 14 years, were selected. Twenty-four soccer players, 12 rugby players and 12 athletes were referred to the Department of Paediatric Dentistry, Department of Medical, Oral and Biotechnological Sciences, University "G. D'Annunzio" Chieti-Pescara in the period 2015-17.

Inclusion criteria were absence of any active caries and mouthguard requirement. Exclusion criteria were periodontitis, partial or total removable prosthesis, poor medical conditions (diabetes, asthma), use of systemic antibiotics or local antimicrobials during the 3 months preceding the sport treatment placement and patients under medication that could affect the saliva flow rate.

The selected subjects participated voluntarily in the study. Patients and their parents were first given oral and written information on the study's purpose. Informed consent was given by signing a protocol. (Privacy Law DL 196/2003). In this study, the approval from the Ethics Committee is not reported, as it is not required for works that are based on research protocol on medical devices already used in the clinical protocols approved by the Department.

Clinical monitoring

The study was divided into three periods of screening: baseline, before the application of the mouthguard-baseline (T0); after three months of casein application on mouthguard during training (T1) and after six months of application (T2). The mouthguard used was custom made with EVA and multilayered. The product used was GC Tooth Mousse (GC Dental Co. Ltd. Suzhou, China). Training was carried out for the selected subjects for the application of casein according to the guidelines of the manufacturer, i.e., cleaning their teeth before applying and distributing the casein, both on the teeth and the mouthguard. Patients avoided eating and drinking and brushing the teeth at least 2 h prior to taking the samples at all stages.

During the first visit the cleaning procedure of the sport mouthguard was explained to each patient, i.e., washing for 5 min with hydrogen peroxide, and storing in perforated containers after blotting the mouthguard with a napkin to eliminate liquid residues.

A dental examination was performed at T0 and the data obtained were later collected in the appropriate Medical Records along with personal data and complete medical history. In addition, an examination of intraoral mucosal was performed to assess the presence/absence of bad habits and/or parafunctional habits and to evaluate the level of oral hygiene of the individual patients. Information (according to WHO criteria) was later collected for indices in regards to eating habits and decayed missing filled teeth (DMF-T) to assess prevalence of caries, plaque (Plaque Index) and gingival bleeding (Bleeding Index) to evaluate the oral hygiene and periodontal status. Patients avoided eating or drinking and stopped tooth

brushing at least 2 hours before taking the samples at all stages. All procedures were carried out by a calibrated researcher, and commercial kits were used according to the manufacturer's instructions.

Prior to treatment, extra and intraoral photos of the athletes followed by dental impressions were taken to create the gypsum study models.

At all three observation times, the "Saliva-Check Buffer GC" and "Saliva-Check Mutans GC" salivary tests were performed on each athlete in order to obtain the following information: visual inspection of the hydration level (test 1); consistency of saliva (test 2); salivary pH (not stimulated; test 3); amount of saliva (stimulated; test 4); salivary pH (stimulated; test 5); saliva check mutans (GC; test 6); GC plaque indicator kit (test 7).

Test 1 was used to visually evaluate the secretion of the labial gland on the lower lip.

Test 2 was used to visually assess the consistency of basal saliva in the oral cavity. If the saliva was dense and foamy the viscosity was considered increased, if the saliva was watery and transparent then viscosity was considered normal.

In Test 3, the patients were asked to deposit their saliva in a container. A pH test strip was then inserted into the collected saliva sample for 10 seconds. Then the colour of the strip was verified and statically compared with the reference graph included in the package: - red: very acidic (pH 5.0 to 5.8); yellow: moderately acidic (pH 6.0 to 6.6); - green: normal (pH 6.8 to 7.8).

For Test 4 the patient chewed a paraffin gum (included in the kit) to stimulate salivary flow. After 5 min, the amount of saliva was measured with the notches on the side of the pan: - <3.5 ml: very little; between 5.0 and 3.5 ml: little; - > 5.0 ml: normal

Test 5 was carried out by placing a buffer strip on an absorbent tissue with the test side facing upwards. Using a pipette, a sufficient amount of saliva was sucked out of the collection pan and a drop was deposited on each of the three test blocks. After 2 min it was possible to calculate the final result by evaluating the colour toning of the strips and summing up the points based on the colour of each block: green: 4 points; green/blue: 3 points; blue: 2 points; red/blue: 1 point; red: 0 points. By evaluating the total sum of the three scores, saliva buffer capacity was evaluated: 0 - 5: very low; 6 - 9: low; 10 - 12: normal/high.

The Saliva-Check Mutans GC test was used for rapid detection of the concentration of *Streptococcus mutans* in the saliva and the evaluation of the patient's susceptibility to caries. To perform this test, the patients were asked not to eat or drink or clean their teeth with toothpaste and a mouthwash within 2 hours prior to the test. Each patient then chewed the paraffin gum contained in the pack for 1 min to stimulate saliva secretion. After this time, the saliva sample was collected in the mixing container, and the analysis was carried out as indicated by the instructions provided, waiting 15 min before checking the results. The result was positive if a thin red line appeared in the test window.

The GC plaque indicator kit test was performed by collecting a sample of plaque and reacting it with the solution included in the kit, or with the plaque indicator solution. The reaction was fermented for 5 min and the colour chromaticity was compared: Green: pH = 7; Yellow: pH = 6.5; Orange: pH = 6.0; Red: pH = 5.5. From red to yellow, the acidity of dental plaque decreases, therefore a yellow sample indicates plaque in which there is an equilibrium of microorganisms and less susceptibility to the onset of dental caries. To the contrary, a red sample demonstrates a major risk of dental caries due to the low level of salivary ph.

Statistical analysis

For statistical analysis, the Matched-Pairs Signed-Wilcoxon-rank test was used. Data are shown as Mean values±Standard Deviation (SD), and for all analyses a P-value of less than 0.05 was considered significant.

RESULTS

From the information obtained, none of the children suffered from food or drug allergies. Data from eating habits showed that most of the subjects regularly took carbohydrates in their diet (pasta, breads, sweets, candies, etc.), although not excessively. In addition, none of the patients had abnormalities, erosions or recessions. Twelve (25%) of the sample had widespread discoloration and 25% showed oral breathing (data not shown).

One patient stopped wearing the mouthguard for more than a month at T2 control and was excluded from the study.

As shown in Table I, concerning clinical indices,

Table I. *Clinical indices of sample.*

	T0	T1	T2
DMFT	0.03±0.01		
Plaque Index (Y/N)	100%	100%	100%
BOP +	0%	0%	0%

T0 = before mouthguard use; T1 = mouthguard plus casein after 3 months; T2 = mouthguard plus casein after 6 months

the young athletes demonstrated the following values: DMFT was 0.03±0.01; PL was positive in 100% of the subjects examined in T0, T1 and T2; BI was negative at all the time-points examined. The results of saliva and bacteria analyses are shown in Table II.

Within the three observation times, there was no significant variation in basal hydration level and salivary flow. The saliva consistency at T0 was normal in 50% of cases and increased in the remaining 50%. It appeared to be normal and constant in T1 and T2.

The pH value was increased significantly at T1 (7.6±0.08) to remain constant at T2. The amount of saliva produced under stimulation varied significantly and gradually from T0 to T1 and T2 (therefore, after application of casein), with a statistically significant difference between observation times. The buffering capacity increased at T1 and T2. This value was statistically significant.

The plaque detector test emphasized that a plaque with pH 6.0±0.5 (orange/red in Plaque Indicator) prevailed at T0; 6.25±0.75 (green) at T1, while at T2 it had a pH equal to 6 (orange), therefore casein had not varied the plaque pH in a statistically significant way.

The tests for the detection of *S. mutans* resulted constant in all subjects at the various observation time-points.

DISCUSSION

Mouthguards represent the best solution to protect teeth in traumatic accidents. A good oral hygiene is essential for the patient and for the good preservation of the mouthguard, as demonstrated by D'Ercole and Tripodi (1).

The application of casein within the custom-made mouthguard in EVA material influences the

Table II. *Data from salivary test.*

	T0	T1	T2
Basal flow	Normal	Normal	Normal
Consistency	50%Normal 50% Increased	Normal	Normal
Basal pH	7.42±0.27	7.6±0.08*	7.6±0.2*
mL of stimulated saliva	4.64±0.62	7.5±2.12§	10±0.2§**
Buffer capacity	29% normal 57% high 14% low	75% high 25% low	75% high 25% low
Plaque Indicator	75% orange/red	50% green	75% orange
S. mutans	67%positive 33%negative	67%positive 33%negative	67%positive 33%negative

T0 = before mouthguard use; T1 = mouthguard plus casein after 3 months; T2 = mouthguard plus casein after 6 months
** NS, p>0.05; § S, p<0.05 vs T0; ** S, p<0.05 vs T1*

increase of pH values, the amount of stimulated saliva and the buffering capacity of the athlete, improving the state of oral health that was negatively affected by the use of simple mouthguards. These actions are enhanced by the use of casein due to a part of the casein protein called casein phosphopeptide (or CPP), to which calcium and phosphate ions are "tied" in the form of amorphous calcium phosphate (or ACP). CPP-ACFP is superior to fluoride varnish for remineralizing smooth-surface white spot lesions (9). The increase of salivary flow, buffering capacity and pH, due to the use of casein is referred by Hegde and Thakkar (10), through the use of casein-chewing gums.

Contrary to what was expected by the Authors and already demonstrated by several studies (7, 11, 12), in this work, the casein used did not show any efficacy on *S. mutans*. The results of the bacteria tests carried out in this study can be justified in that the test in question presented low sensitivity and low quantitative discrimination.

Several further preventive strategies for the changes that occur in the oral cavity of athletes should be implemented, even if this field is in continuous development.

The application of casein as an oral protector represents a new strategy to fight ecological variations in athletes' mouths, helping the salivary buffering capacity and increasing the salivary pH, avoiding all negative effects on oral health and sport performance. The present study demonstrates for the first time in literature that casein can be useful as a preventive means in the use of sport mouthguards.

Further studies will be carried out to confirm the positive effects of casein application in mouthguards.

REFERENCES

1. D'Ercole S, Tripodi D. I protettori orali nello sport. Sport & Medicina 2017; 1:43-9.
2. Glass RT, Conrad RS, Köhler GA, Warren AJ, Bullard JW. Microbiota found in protective athletic mouthguards. Sports Health 2011; 3(3):244-48.
3. D'Ercole S, Martinelli D, Tripodi D. Influence of sport mouthguards on the ecological factors of the children oral cavity. BMC Oral Health 2014; 5:14-97.
4. D'Ercole S, Tripodi D. The effect of swimming on oral ecological factors. J Biol Regul Homeost Agents 2013; 27(2):551-58.
5. D'Ercole S, Tieri M, Martinelli D, Tripodi D. The effect of swimming on oral health status: competitive versus non-competitive athletes. J Appl Oral Sci 2016; 24(2):107-13.
6. D'Ercole S, Tieri M, Fulco D, Martinelli D, Tripodi D. The use of chlorexidine in mouthguards. J Biol Regul Homeost Agents 2017; 31(2):487-93.
7. Paglia L, Scaglioni S, Torchia V, De Cosmi V, Moretti M, Marzo G, Giuca MR. Familial and dietary risk factors in early childhood caries. Eur J Paediatr Dent. 2016; 17(2):93-99.
8. Esenlik E, Uzer Çelik E, Bolat E. Efficacy of a casein phosphopeptide amorphous calcium phosphate (CPP-ACP) paste in preventing white spot lesions in patients with fixed orthodontic appliances: A prospective clinical trial. Eur J Paediatr Dent 2016; 17(4):274-80.
9. Dashper SG, Catmull DV, Liu SW, et al. Casein phosphopeptide-amorphous calcium phosphate reduces Streptococcus mutans biofilm development on glass ionomer cement and disrupts established biofilms. PLoS One 2016; 11(9):e0162322.
10. Hegde RJ, Thakkar JB. Comparative evaluation of the effects of casein phosphopeptide-amorphous calcium phosphate (CPP-ACP) and xylitol-containing chewing gum on salivary flow rate, pH and buffering capacity in children: An in vivo study. J Indian Soc Pedod Prev Dent 2017; 35(4):332-37.
11. Mummolo S, Tieri M, Tecco S, Mattei A, Albani F, Giuca MR, Marzo G. Clinical evaluation of salivary indices and levels of Streptococcus mutans and Lactobacillus in patients treated with Occlus-o-Guide. Eur J Paediatr Dent 2014; 15(4):367-70.
12. Pasquantonio G, Condò S, Cerroni L, L.Bikiqu L, Nicoletti M, Prenna M, Ripa S. Antibacterial activity of various antibiotics against oral Streptocci isolated in the oral cavity. Int J Immunopathol Pharmacol 2012; 25(3):805-9.

LETTER TO THE EDITOR

THE RELEVANCE OF THE MOMETASONE FUROATE NASAL SPRAY IN CLINICAL PRACTICE

G. CIPRANDI and A. VARRICCHIO

Associazione Italiana Vie Aeree Superiori, Frattamaggiore, Naples, Italy

Received March 9, 2018 – Accepted June 19, 2018

Allergic rhinitis (AR) is characterized by mucosal inflammation, therefore anti-inflammatory drugs are indicated for its treatment, mainly concerning intranasal administration. Mometasone furoate nasal spray (MFNS) has been on the market under the brand Nasonex® for 20 years and has high effectiveness and an excellent safety profile. From a clinical point of view, an ideal topical medication should respect a series of requirements, including handy device, good sensory characteristics, aptitude to the reach posterior nasal cavity, long residence time, and optimal pharmacokinetic and pharmacodynamic activities. MFNS fully satisfies these claims, as underlined by 20 years of worldwide prescriptions.

To the Editor,

Allergic rhinitis (AR) is the most frequent immune-mediated disorder (1) and is characterized by a mucosal inflammation closely dependent on allergen exposure (2). Allergic inflammation sustains symptom occurrence, including nasal itching, sneezing, watery rhinorrea, and congestion. The last mirrors the level of allergic inflammation and negatively correlates with quality of life (3).

AR treatment needs an active medication that should be able to efficaciously improve symptoms, including sleep quality, fatigue, mood, and also sexuality (4). Inflammation control is the goal of AR therapy, thus, intranasal corticosteroids (INCs) are the most effective available medication. INCs are indicated both for seasonal and perennial AR. Mometasone fluroate nasal spray (MFNS) is a topical corticosteroid widely used for the past 20 years. Many studies have been conducted regarding this molecule. It has to be noted that all studies were carried out considering the Merck Sharp & Dohme (MSD) device (branded as Nasonex®). This device was realized thanks to an innovative and peculiar technology as will be discussed in the present paper. In particular, some characteristics should be considered necessary requirements: handiness, convenience, easy to use, quick effectiveness, and safety. In addition, effectiveness depends on physical, chemical, and pharmacological properties, as further discussed. The current manuscript aims to review the most recent publications concerning the relevant characteristics of this device.

Easy to use

Adherence to treatment is a fundamental requisite for any successful cure. This concept is particular compelling for INCs as they need regular and constant administration to be efficacious. Therefore, it is necessary for the patient to accept the proposed therapy and be satisfied. Recently, it was reported that product sensitivity, easy to use, and comfort are qualities appreciated by the patient (6, 7). In

Key words: allergic rhinitis, intranasal corticosteroids, mometasone furoate, nasal spray, device

Mailing address:
Giorgio Ciprandi,
Via Boselli 5,
16146 Genoa, Italy
Tel.: +39 010 3629786
e-mail: gio.cip@libero.it

0393-974X (2018)
Copyright © by BIOLIFE, s.a.s.
This publication and/or article is for individual use only and may not be further reproduced without written permission from the copyright holder.
Unauthorized reproduction may result in financial and other penalties

particular, the patient's preference closely relates with treatment compliance, so the choice of an INC should depend on patient acceptability. In this regard, a survey was conducted on 1,544 subjects (506 children and 355 elderly patients); the 11 questions asked were: do you find MFNS easy to use? Do you find MFNS easy to store? Would you say MFNS is easy to keep clean/maintain? Would you say MFNS is easy to pump/press? Do you find the mist from MFNS easy to administer? Do you feel that MFNS fits comfortably in the hand? Do you find MFNS comfortable to hold while administering a dose (or mist in the nose)? Would you say MFNS fits well in the hand when administering a dose (or mist in the nose)? Would you say the MFNS applicator fits comfortably in the nostril? Would you say you like using the MFNS pump bottle? Would you say the nozzle is appropriately sized to administer the medicine? (8). Ninety-eight percent of respondents reported that MFNS is easy to use, and 96% said that the applicator is easy to administer. Nearly all elderly users and users with arthritis said that the applicator fits comfortably in the nostril (96% and 97%, respectively) and is appropriately sized (97% and 96%, respectively); 96% of paediatric users agreed that the applicator fits comfortably. All users said the applicator's ease of use and comfortable fit were its most important attributes. The authors thereby concluded that the perceived ease of use of MFNS may help providers to appropriately treat patients with AR and may improve patient adherence to INS use (8).

Thixotropy

Thyxotropy is a rheological property that defines the capability of fluids to change their physical characteristics in terms of plasticity and viscosity: for example, a fluid may move from gel to liquid state. This property is very important for nasal spray devices as it allows an optimal distribution into the nasal cavity. Actually, when an aqueous suspension is shaken before being sprayed, it reduces its viscosity which successively returns viscous, so guaranteeing an optimal distribution and permanence into the nose. In this regard, it has been reported that the thixotropy of MFNS was 3.4 to 21.4 times greater and the final viscosity was 3.2 to 17.4 times greater than the values of other tested INC products (9). This outcome confirmed that MFNS has an optimal distribution capability during use.

Viscosity

Viscosity means the fluid resistance to flow. For a nasal device, viscosity is important as it allows an optimal deposition of the compound. Some studies investigated the viscosity of MFNS. As previously reported, MFNS exhibited the highest initial and final viscosity and highest thixotropy in three different sample preparation protocols, including one that considered the patient use. High final viscosity and thixotropy may support good retention in the nasal cavity. The nasal residence time is a relevant issue as it allows an adequate permanence of the compound in the nose so maximal efficacy may be achieved as reported (10).

Lipophilicity

Lipophilicity means the solubility in an apolar solvent, such as ether or chloroform, in water. This characteristic is important for an INC as it increases the nasal residence time. It may be affected by slowing the dissolution time, modifying the original corticosteroid molecule, such as increasing lipophilicity (11). A lipophilic INC persists longer in the nose than a hydrophilic INC.

Intranasal deposition

The rate of mucociliar clearance depends on the specific anatomic nasal area. In this regard, the most important nasal area is the posterior nasal cavity as it is associated with different disorders, including rhinosinusitis, otitis, adenoiditis, allergic rhinitis, and nasal polyps. A scintigraphic study on humans showed that MFNS delivered 86% of the metered dose to the nasal cavity, and approximately 60% of the metered dose to the posterior nasal cavity (12). After 15 minutes, mucociliary clearance removed 59% of the initial radiolabel in the nasal cavity, consistent with clearance rates from the ciliated posterior surface. MFNS deposited significant drug into the posterior nasal cavity. Both nasal cast validation and mucociliary clearance confirmed that the

radiolabel deposition distribution method accurately represented corticosteroid nasal deposition.

Preservatives

Currently, available INCs contain necessary additives and preservatives that prevent bacterial growth, absorb extra water, and maintain appropriate moisture levels. Benzalkonium chloride (BKC) is a cationic surfactant commonly used as a preservative in nasal solutions. BKC is an irritant, and a recent review showed a number of studies have reported adverse effects that involve the nasal mucosa as a result of contact with BKC (12). Usually, BKC diminished the mucociliary clearance. At present, MFNS contains BKC. However, this fact might be useful as it prolongs the nasal residence time.

Sensory attributes

Because the efficacies of INCs are largely comparable, sensory attributes are an important factor in patient preference and adherence to INC treatment. According to a recent survey, the most important sensory attribute to patients treated with INCs is aftertaste (13). Patients also ranked taste, nose runout, throat rundown, smell, and feel of the spray as important in deciding on INC treatment choice. The higher the intensity of an unfavorable sensory attribute, the less preference a patient will have for that INC. Different aspects of the formulation confer potentially unpalatable attributes to an INC. Most patients (80%) reported an increased likelihood of compliance if treated with their preferred INC. Increased preference and likelihood of compliance with unscented MFSN were also reported *vs* fluticasone propionate in patients with symptomatic AR (14). These data support the development of tasteless and odorless INCs (15).

Tonicity

Tonicity refers to the effective osmolarity of a solution and, therefore, reflects the difference between the osmolarity of a cell or tissue and the solution/suspension. An isotonic (or physiologic) solution has an equivalent osmolarity to the cell or tissue to which it is exposed. Solutions that are more dilute than the physiologic cell or tissue are hypotonic; solutions that are more concentrated are hypertonic. Tonicity is an important consideration for drug formulation and can affect its uptake, retention, and consequent efficacy and safety. Tonicity can even affect the disposition of inhaled medication. Isotonicity, such as the physiological tonicity, is preferred for topical medication. MFSN has isotonicity, so there is no interference in drug delivery.

Spray volume

The ideal INC would have a balance between an adequate spray volume to achieve optimum nasal distribution and minimal throat rundown and nose runout. The ideal volume is 100 λ: one puff of MFNS releases 100 λ of the corticosteroid compound.

CONCLUSION

An ideal medication for the topical anti-inflammatory treatment of AR (and also nasal polyps) should have high effectiveness and excellent safety profile. In addition, a series of requirements should be respected, including a handy device, good sensory characteristics, aptitude to reach the posterior nasal cavity, long residence time, and optimal pharmacokinetic and pharmacodynamic activities. MFNS fully satisfies these claims, as also underlined by 20 years of prescriptions.

ACKNOWLEDGEMENTS

Disclosure: This paper has been produced thanks to an unconditioned grant by MSD Italy.

REFERENCES

1. Gieseck RL 3rd, Wilson MS, Wynn TA. Type 2 immunity in tissue repair and fibrosis. Nat Rev Immunol 2018; 18:62-76.
2. Scadding GK, Kariyawasam HH, Scadding G, et al. BSACI guideline for the diagnosis and management of allergic and non-allergic rhinitis (Revised Edition 2017; First edition 2007). Clin Exp Allergy 2017; 47:856-89.
3. Ciprandi, G, Klersy C, Cirillo I, Marseglia GL.

Quality of life in allergic rhinitis: relationship with clinical, immunological, and functional aspects. Clin Exp Allergy 2007; 37:1528-35.
4. Brożek JL, Bousquet J, Agache I, et al. Allergic Rhinitis and its Impact on Asthma (ARIA) guidelines-2016 revision. J Allergy Clin Immunol 2017; 140:950-58.
5. Bachert C, El-Akkad T. Patients preferences and sensory comparisons of three intranasal corticosteroids for the treatment of allergic rhinitis. Ann Allergy Asthma Immunol 2002; 89:292-97.
6. Storms WW. Introduction: patient preference of inhaled corticosteroids. Allergy Asthma Proc 2001; 22(Suppl 1):S1-S3.
7. Blaiss SS. Efficacy, safety, and patient preference of inhaled nasal corticosteroids: a review of pertinent published data. Allergy Asthma Proc 2001; 22(Suppl 1):S5-S10.
8. Fromen LM, Ortiz GR, Dowdee AM. Assessment of patient attitudes about mometasone furoate nasal spray. WAO Journal 2008; 1(9):156-59.
9. Sharpe Sa, Sandweiss V, Tuazon J, Giordano M, Witchey-Laksmanan L, Hart J. Comparison of the flow properties of aqueous suspension corticosteroid nasal sprays under differing sampling conditions. Drug Develop Ind Pharm 2003; 29:1005-12.
10. Hochhaus G. Pharmacokinetic/pharmacodynamic profile of mometasone furoate nasal spray: potential effects on clinical safety and efficacy. Clin Therap 2008; 30:1-13.
11. Meltzer EO. Formulation considerations of intranasal corticosteroids for the treatment of allergic rhinitis. Ann Allergy Asthma Immunol 2007; 98:12-21.
12. Shah SA, Beger RL, McDermott J, Gupta P, Monteith D, Connor A, Lin W. Regional deposition of mometasone furoate nasal spray suspension in humans. Allergy Asthma Proc 2015; 36:48-57.
13. Naclerio RM, Barrody FM, Bidani N, De Tineo M, Penney BC. A comparison of nasal clearance after treatment of perennial allergic rhinitis with budesoni and mometasone. Otolaryngol Head Neck Surg 2003; 128:220-27.
14. Mahadevia PJ, Shaha S, Leibman C, Kleinman L, O'Dowd L. Patient preferences for sensory attributes of intranasal corticosteroids and willingness to adhere to prescribed therapy for allergic rhinitis: a conjoint analysis. Ann Allergy Asthma Immunol 2004; 93:345-50.
15. Meltzer EO, Bardelas J, Goldsobel A, Kaiser H. A preference evaluation study comparing the sensory attributes of mometasone furoate and fluticasone propionate nasal sprays by patients with allergic rhinitis. Treat Respir Med 2005; 4:289-96.